CURSO: "INGENIERIA DE YACIMIENTOS GEOTERMICOS"
13 DE MARZO AL 18 DE MAYO DE 1984

SIMULACION NUMERICA DE YACIMIENTOS GEOTERMICOS

DR. GUILLERMO DOMINGUEZ
2-13 de abril.

P R E F A C I O.

En febrero de 1979 se firmó un convenio de colaboración entre la UNAM, PEMEX, IMP y el CIPM (Colegio de Ingenieros Petroleros de México). El objeto del convenio ha sido elevar el nivel académico de los alumnos del área de Ingeniería Petrolera en la Facultad de Ingeniería, tanto de licenciatura como de posgrado, así como crear el Doctorado, y promover la superación de un mayor número de profesionales que laboran en la industria petrolera, por medio de cursos de actualización y especialización.

Uno de los programas que se están llevando a cabo a nivel de licenciatura, dentro del marco del Convenio, es la elaboración y actualización de apuntes de las materias de la carrera de Ingeniero Petrolero. Con esto se pretende dotar al alumno de más y mejores medios para elevar su nivel académico, a la vez que proporcionar al profesor material didáctico que lo auxilie en el proceso enseñanza-aprendizaje.

La elaboración de estos apuntes fué realizada por los Ingenieros Luis Ayala Gómez y José Serrano Lozano, bajo la dirección del Dr. José Luis Bashbush. El Ing. Francisco Garaicochea y el Dr. Guillermo Domínguez V., colaboraron en su revisión. La señorita Angélica Serrano Lozano se encargo de la mecanografía.

DEPARTAMENTO DE EXPLOTACION DEL PETROLEO.

I N D I C E G E N E R A L

LISTA DE FIGURAS

LISTA DE TABLAS

P R O L O G O

La evolución y desarrollo de la industria petrolera, ha traído como consecuencia la aplicación de técnicas cada vez más depuradas y sofisticadas, orientadas a maximizar la producción de hidrocarburos, pero al mismo tiempo, llevando a cabo una explotación racional de los mismos; entre dichas técnicas, se encuentra la simulación numérica de yacimientos, la cuál, "es una herramienta" sumamente útil, para predecir el comportamiento de los yacimientos.

Debe tenerse en cuenta, que si la información proviene de fuentes fidedignas, los resultados que se obtendrán serán confiables. Si por el contrario no se cuenta con buena información, los resultados obtenidos serán un elemento indicativo para determinar que parámetros deben obtenerse con precisión.

Dada la importancia que tiene la ingeniería de yacimientos en la explotación de los hidrocarburos y teniendo en cuenta las necesidades de los estudiantes de ingeniería petrolera, se elaboraron estos apuntes con la intención de brindar una fuente de información escrita en castellano, ya que en la mayoría de los casos dicha información está escrita en otro idioma. A través de los mismos se pretende despertar el interés del alumnado, motivándolo para su mejor preparación.

C O N T E N I D O

CAPITULO 1

CAPITULO 1

1.1 INTRODUCCION

El objetivo primordial al hacer uso de la simulación numérica, es predecir el comportamiento de un yacimiento en cuestión y encontrar la manera de optimizar ciertas condiciones para aumentar la recuperación.

En la ingeniería de yacimientos tradicional se trata al yacimiento en forma burda, considerándolo como un tanque con propiedades promedio, mientras que la simulación de yacimientos por medio de computadoras, permite un estudio más detallado, al poder dividir virtualmente a dicho yacimiento en un número finito de celdas o bloques y aplicar las ecuaciones fundamentales de flujo de fluidos en medios porosos para cada celda conjugadas a la ecuación de balance de materia.

Es importante señalar que la utilidad de los resultados obtenidos de una simulación, estará en función de la destreza y experiencia que el ingeniero tenga para interpretarlos, dependiendo de las condiciones de explotación de un yacimiento, ya sea en su etapa inicial o en una etapa de ajuste a través de la historia del yacimiento.

1.2 DEFINICION

La simulación numérica de yacimientos, es un proceso mediante el cuál el ingeniero, con la ayuda de un modelo matemático, inte-

-gra un conjunto de factores para describir con cierta precisión- el comportamiento de procesos físicos que ocurren en un yacimiento.

1.3 OBJETIVO

Lo que se pretende al hacer uso de la simulación es predecir- el comportamiento de los yacimientos sujetos a diferentes políticas de explotación y en base a resultados obtenidos de dicha simulación, poder seleccionar la manera más adecuada de explotarlos.- Dependiendo de la política de la empresa, la manera más adecuada- de explotar un yacimiento puede requerir; maximizar el gasto, -maximizar la recuperación, maximizar la ganancia, etc.

También en muchas ocasiones, con ayuda de la simulación, se - puede llevar a cabo el desarrollo de un campo en base a una información limitada, pudiéndose determinar donde perforar nuevos po-- zos o establecer un esquema para comparar el agotamiento por recuperación primaria y la que se tendría con una recuperación secundaria o recuperación mejorada.

La enorme ventaja que se tiene al hacer uso de la simulación- es que permite "producir" un yacimiento varias veces y en muy diferentes maneras, con lo cuál se pueden analizar diferentes alternativas y seleccionar una de ellas; en la que se obtenga por ejemplo, la máxima recuperación, mientras que físicamente el yacimiento puede producirse una sola vez, y lo más probable es que no sea en la forma más adecuada, dado que un error cometido en el proceso afectará cualquier cambio subsecuente.

1.4 DEFINICION DE UN MODELO MATEMATICO DE SIMULACION

Básicamente un modelo matemático de simulación de yacimientos, consiste en un número determinado de ecuaciones diferenciales parciales, que expresan el principio de conservación de masa y/o energía acopladas con ecuaciones representativas de flujo de fluidos, temperatura y/o la concentración de dichos fluidos a través de medios porosos.

Las ecuaciones resultantes, son ecuaciones diferenciales parciales "no lineales" y su solución es posible únicamente de una manera discreta, es decir, en un número de puntos preseleccionados en tiempo y espacio y no de una manera continua; por lo cual es indispensable el uso de un programa de cómputo.

1.5 INFORMACION REQUERIDA

Para llevar a cabo una simulación se requiere la información siguiente:

a) Propiedades petrofísicas.

- Porosidad (ϕ)
- Permeabilidad (k)
- Saturaciones de agua, aceite y gas (S_w, S_o, S_g)
- Presión capilar entre diferentes interfases

  (Pc_{w-o}, Pc_{o-g}, Pc_{g-w})
- Permeabilidades relativas; al agua, al aceite y al gas

  (k_{rw}, k_{ro}, k_{rg})

b) Propiedades pVT de los fluidos del yacimiento

-Factores de volumen (B_w, B_o, B_g)

-Relación de solubilidad (Rs)

-Viscosidades (μ_w, μ_o, μ_g)

-Compresibilidades (c_f, c_w, c_o, c_g)

c) Límites del yacimiento.

d) Características del acuífero que rodea al yacimiento

e) Cuando se trata de hacer un ajuste de la historia del yacimiento, se requieren; ritmos de producción, declinación de la presión, etc.

Tanto las propiedades petrofísicas como las propiedades PVT, se determinan en el laboratorio a través de muestras del yacimiento, que se procura sean representativas. Registros eléctricos obtenidos durante la perforación proporcionan información complementaria, necesaria en la correcta evaluación de las propiedades petrofísicas.

Los límites del yacimiento y las características del acuífero, se determinan con estudios geológicos ayudados de métodos indirectos como son los registros geofísicos, etc.

De suma importancia en un estudio de yacimientos por medio de simulación, es la determinación de las permeabilidades relativas y las presiones capilares. Las permeabilidades relativas determinan el flujo fraccional de las fases y por ende los resultados del simulador. Obviamente las curvas obtenidas en el laboratorio en pequeños nucleos, cuyas dimensiones se miden en centímetros, deben ser ajustadas antes de poder usarse en un simulador cuyas celdas se miden normalmente en centenares de metros. La evaluación oportuna y sistemática de un conjunto de "pseudo permeabilidades relati-

-vas" es un proceso indispensable y a menudo olvidado en la simulación matemática de yacimientos.

Las curvas de presión capilar son necesarias para poder describir la distribución de saturaciones y el tamaño de la zona de transición, los contactos agua-aceite y gas-aceite.

1.6 RESULTADOS

Los resultados típicos que se obtienen de un programa de simulación, consisten en la distribución de presiones, saturaciones en cada una de las celdas en las que se ha dividido al yacimiento, -- así como relaciones agua-aceite y gas-aceite para los pozos productores.

Si hay inyección de fluidos, se obtiene; o el ritmo de inyec-- ción de los pozos inyectores, o las presiones necesarias para in-- yectar los volumenes establecidos.

1.7 UTILIDAD DE LA SIMULACION

Un modelo matemático de simulación calibrado adecuadamente, es la herramienta más poderosa con la que cuenta un ingeniero para poder predecir con cierto grado de precisión el comportamiento de un yacimiento sujeto a diferentes políticas de explotación.

Aún cuando en ocasiones no se conozcan las características petrofísicas de un yacimiento la simulación puede ser útil en obte-- ner la sensibilidad de los resultados a variaciones en la descripción en el yacimiento. Por ejemplo si se tiene una propiedad "x" y

se sabe que dicha propiedad puede variar en un rango de x_1 a x_2, - es decir, $x_1 \leq x \leq x_2$ y se efectúan 2 ó 3 corridas de simulación, - si los resultados no varían mucho se puede:

1) Tomar como buena una de las predicciones.
2) Relegar a segundo término esfuerzos especiales para medir con - precisión dicha propiedad.

Si por el contrario los resultados de simular el yacimiento -- con diferentes valores de la propiedad "x" varían considerablemente, entonces se debe tener especial cuidado en la obtención de la- distribución de la propiedad "x" en diferentes áreas del yacimiento para mejorar la descripción del mismo, ya que su distribución - afectará considerablemente la recuperación.

Aún si hay diferencia en los resultados al variar las propiedades, se puede tratar de buscar ciertas invariantes en la recuperación por medio de diferentes formas de explotación del yacimiento.

Ejemplo:

Si el valor asignado a una propiedad, digamos porosidad es - (ϕ_1), y los resultados de una simulación indican las siguientes recuperaciones:

- Por agotamiento natural 20%
- Por un método de inyección A 30%
- Por un método de inyección B 40%

El incremento en la recuperación al aplicar el método de inyección A es de 50% y el incremento al aplicar el método de inyección- B es 100 %

Ahora, si el valor asignado a la porosidad es ϕ_2 y los resultados indican que la recuperación es:

- Por agotamiento natural 23%
- Por un método de inyección A 35%
- Por un método de inyección B 47%

En este caso el incremento en la recuperación al aplicar el método de inyección A es de 52% y el incremento corresponde al método de inyección B es de 104%.

De lo anterior se observa, que aún habiendo variaciones en las propiedades de ϕ_1 a ϕ_2, los incrementos calculados para ambos métodos de inyección son practicamente los mismos por lo que se deduce en este caso no es necesario conocer toda la información en forma precisa. En una forma más realista, la precisión de la información debe ser proporcional a la sensibilidad de los resultados a variaciones de dicha información.

1.8 CONSECUENCIA DE UNA INFORMACION DEFICIENTE

Lo anterior no significa que la simulación de yacimientos deba aplicarse en cualquier ocasión. Dada la complejidad y sofisticación de la simulación numérica de yacimientos, carece de sentido su utilización sino se trata previamente de obtener buena información, debido a que la confiabilidad de los resultados de una simulación, está en función de la información proporcionada.

Para usar la simulación apropiadamente, se citan a continuación ciertas consideraciones fundamentales.

- Se debe hacer un muestreo adecuado y suficiente, para asegurar que la información sea representativa del yacimiento.

- Al determinar las propiedades petrofísicas y pVT de las muestras se debe tratar de aproximar al máximo las condiciones que realmente prevalecerán en el yacimiento.
- Es importante, tratar de reproducir en el laboratorio, los mecanismos de desplazamiento que operarán en el yacimiento para determinar las permeabilidades relativas que tanta trascendencia tienen en la recuperación. Además, en el caso de simulaciones areales o tridimensionales, es indispensable efectuar primero estudios en secciones transversales que permitan determinar las curvas de pseudo permeabilidad relativa que permitan calibrar los resultados de un modelo burdo con celdas relativamente grandes a los resultados obtenidos al utilizar una mejor definición del número de capas y con celdas más pequeñas.

Si por el contrario la información disponible es insuficiente y además no representativa, la utilización de un modelo simplificado tal como las ecuaciones de balance de materia, aplicadas con buen criterio ingenieril pueden utilizarse con ventaja sobre un modelo de simulación.

Indiscutiblemente, un modelo matemático adecuadamente ajustado que ha permitido reproducir la historia de un yacimiento, es el instrumento más poderoso para predecir, con el mayor grado de confianza, el comportamiento de dicho yacimiento.

1.9 TIPOS DE SIMULADORES

1.9.1 MODELO DE CERO DIMENSIONES O MODELO DE TANQUE

(Por considerar al yacimiento como un tanque)

Este modelo, supone que el yacimiento se comporta como un tanque con propiedades promedio, además supone que las propiedades - PVT son función de la presión media y que la permeabilidad relativa es únicamente función de la saturación media.

A este modelo comunmente se le llama balance de materia (Fig. 1).

1.9.2. MODELOS DE UNA DIMENSION

Dicho modelo fue generado por BUCKLEY-LEVERETT, para dar una - solución analítica al comportamiento por recuperación secundaria. En simulación de yacimientos dicho modelo se puede aplicar, si se tiene un yacimiento en el que el flujo en una dirección es predominante. Por ejemplo en los casos de inyección de gas en la cresta de un yacimiento o en la inyección de agua (o entrada natural de - agua) por el flanco de otro yacimiento (Fig. 2).

En una dimensión también se puede utilizar un modelo en forma radial. Este modelo es útil para pruebas de formación y pruebas de incremento o decremento de presión. En cada celda se pueden variar propiedades tales como porosidad y permeabilidad (Fig. 2a).

1.9.3. MODELOS DE DOS DIMENSIONES

1.9.3.1. MODELO AREAL

Se tiene variaciones de las propiedades en dos direcciones, pudiéndose considerar además, los efectos gravitacionales al asignar diferentes profundidades a las celdas del modelo, el cual puede --

ser representado por una malla. Este modelo se aplica a yacimientos donde generalmente los espesores son pequeños con respecto a su área y no existe efecto muy marcado de estratificación o se ha generado un conjunto adecuado de pseudo permeabilidades relativas (Fig. 3a).

1.9.3.2 MODELO DE SECCION TRANSVERSAL

Otro tipo de modelo de dos dimensiones se tiene en la representación de secciones transversales en donde las propiedades de las capas varían. La utilidad de estos modelos estriba en su versatilidad en la descripción de la distribución vertical de saturaciones de avance de un frente (gas y/o agua) además de ser los instrumentos para la obtención de las mencionadas curvas de pseudo permeabilidad relativa (Fig. 3b).

1.9.3.3 MODELO AREAL DE DOS DIMENSIONES EN FORMA RADIAL

Incluyen algunas de las consideraciones del modelo anterior -- además de la ventaja de poder analizar con mayor detalle los cambios bruscos de presión y saturación que ocurren en la cercanía de los pozos (Fig. 3c).

1.9.4 MODELOS TRIDIMENSIONALES

Existen yacimientos con espesores muy grandes, por lo que es necesario considerar variaciones tanto horizontales como verticales

(Fig. 4). Otro tipo de modelo de tres dimensiones, se puede representar en forma radial (Fig. 4a).

1.10 TIPOS DE FLUJO

Hasta aquí se han mostrado solamente variaciones en la geometría o sea las dimensiones; sin embargo, en el yacimiento se pueden considerar también varios tipos de flujo, como son el monofásico, bifásico y trifásico.

1.10.1 FLUJO MONOFASICO

El flujo monofásico está dado por el flujo de un sólo fluido en particular. Por ejemplo en los acuíferos el agua; aceite en un yacimiento bajo saturado o gas en un yacimiento de gas volumétrico.

1.10.2 FLUJO BIFASICO

Se presenta cuando dos fluidos diferentes fluyen al mismo tiempo por ejemplo:

Gas y Aceite:	En un yacimiento que produce por empuje de gas disuelto liberado.
Agua y Aceite:	En un yacimiento bajo saturado con entrada de agua, cuya presión se mantiene arriba de la presión de burbujeo.
Agua y Gas:	En un yacimiento de gas con entrada de agua o cuya saturación de agua congénita es mayor

que la saturación crítica.

1.10.3 FLUJO TRIFASICO

Se presenta cuando hay flujo de tres fluidos a la vez: agua, aceite y gas. Este caso se contempla en yacimientos que producen por empuje combinado, en los que la entrada de agua, el empuje de gas disuelto y/o el empuje de un casquete original o secundario tiene influencia en la producción.

Por todo lo anterior se puede tener combinaciones entre modelos y tipos de flujo; es decir, se puede tener un modelo de una dimensión con 3 fases o bién uno en 2 dimensiones con 2 fases o generalizando un modelo de 3 dimensiones con 1, 2 ó 3 fases.

1.11 MODELOS COMPOSICIONALES

Existen otros tipos de modelos, donde no sólo se toma en cuenta la variación de la geometría y el tipo de flujo, sino también la variación de la composición de los fluidos del yacimiento al explotarlos. En esta categoría se incluyen los yacimientos de aceite-volátil y los yacimientos de gas y condensado con condensación retrógrada, para los cuales se debe tomar en cuenta la composición de los fluidos originales. Consecuentemente, este tipo de simuladores permite predecir variaciones en la composición de los fluidos producidos, así como variaciones en los gastos y presiones del yacimiento.

1.12 MODELOS TERMICOS

Cuando se somete un yacimiento a un proceso de recuperación mejorada por medio de un método térmico, como por ejemplo la inyección de vapor o la combustión in-situ, independientemente de existir flujo de fluidos en el medio poroso a causa de gradientes de presión, se genera un intercambio de energía en el yacimiento, variaciones de temperatura y viscosidad de los fluidos, efectos de destilación y/o craqueo, etc. Estos generan una serie de modificaciones en las propiedades de los fluidos.

Teniendo en cuenta lo anterior se pueden elaborar modelos que involucren tanto las variaciones de flujo, como las variaciones en las propiedades de los fluidos del yacimiento en función de los efectos composicionales y/o variaciones en las temperaturas.

" Diagrama Indicativo para la selección de un Simulador "

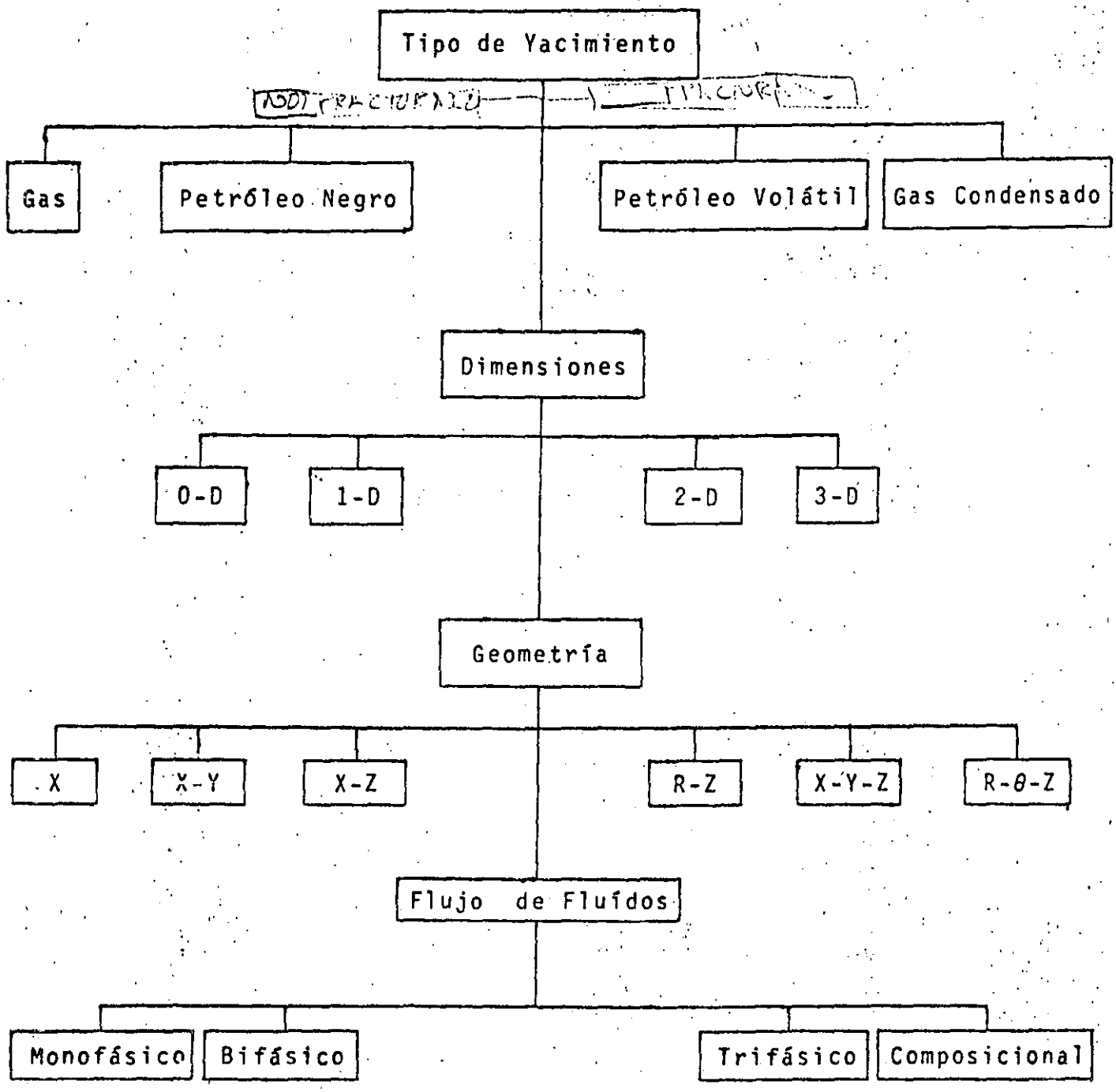

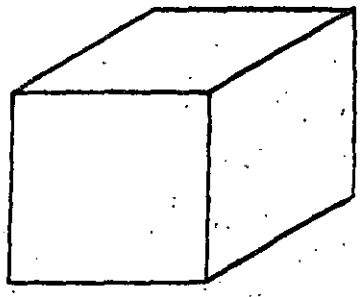

FIG. 1 MODELO DE CERO DIMENSIONES

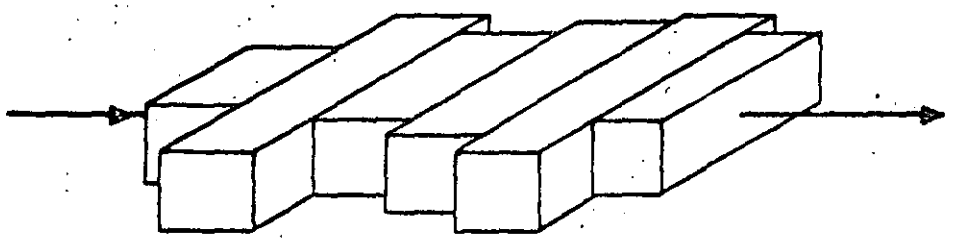

HORIZONTAL

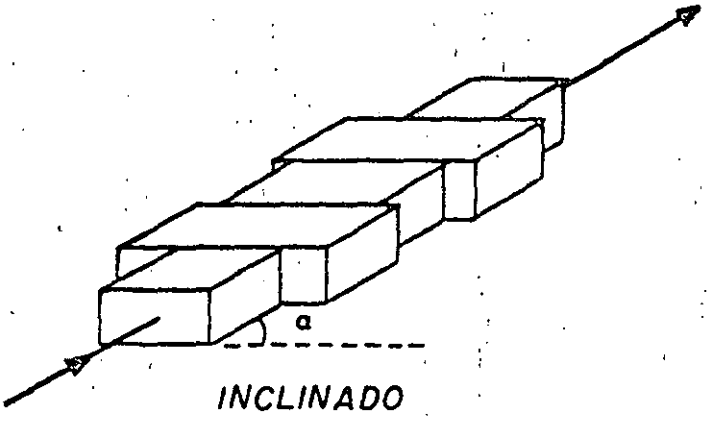

INCLINADO

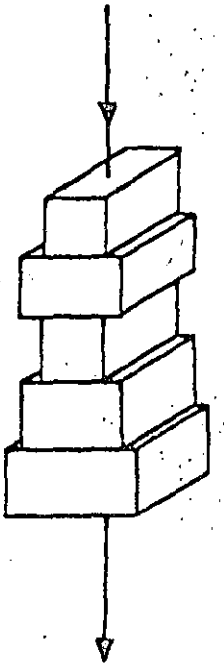

VERTICAL

FIG. 2 MODELO DE UNA DIMENSION

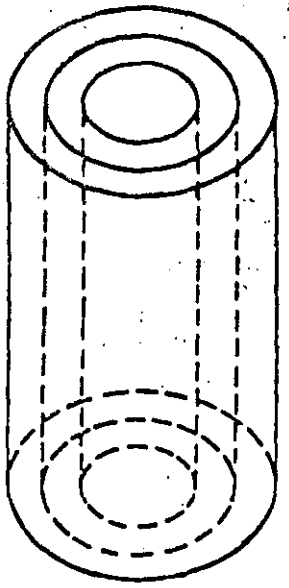

FIG 2a MODELO DE UNA DIMENSION
FORMA RADIAL

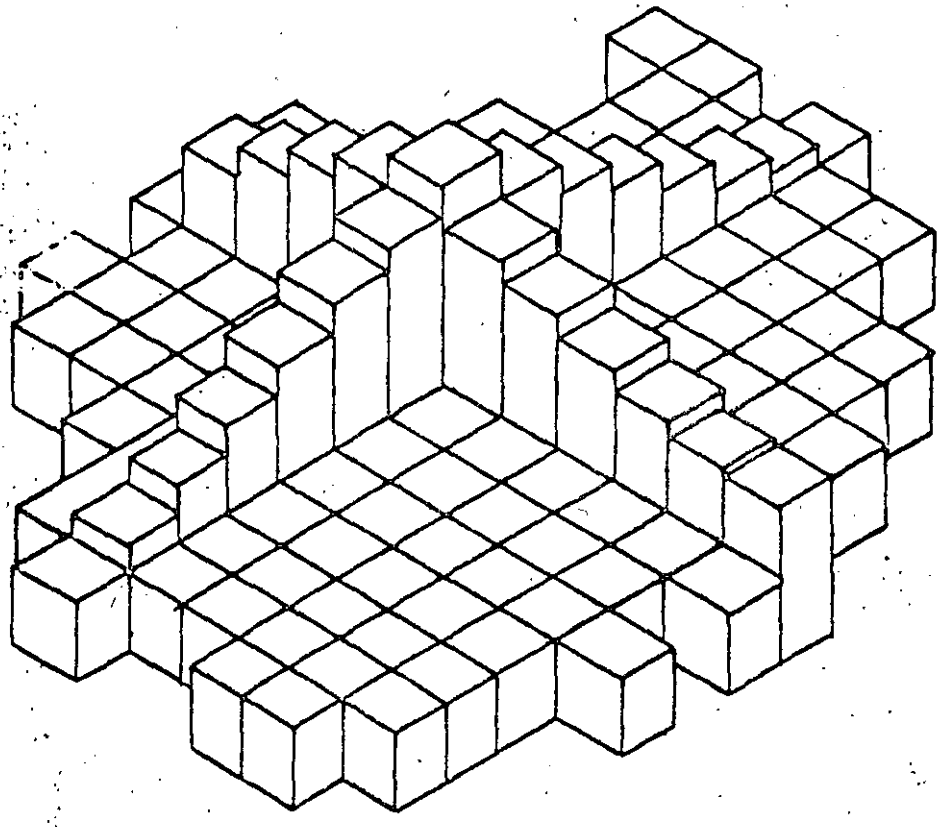

FIG 3a MODELO AREAL DE DOS DIMENSIONES

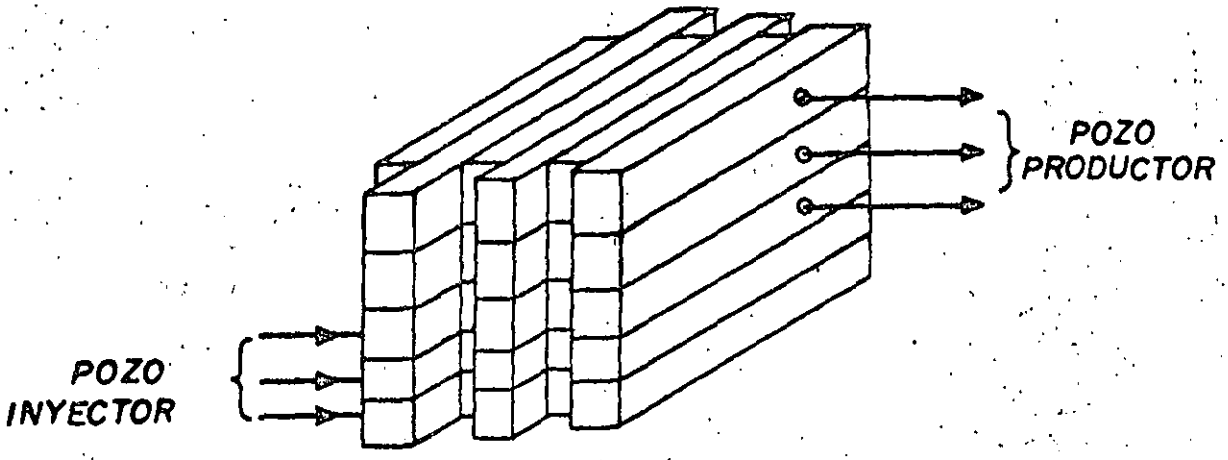

FIG. 3b DE SECCION TRANSVERSAL

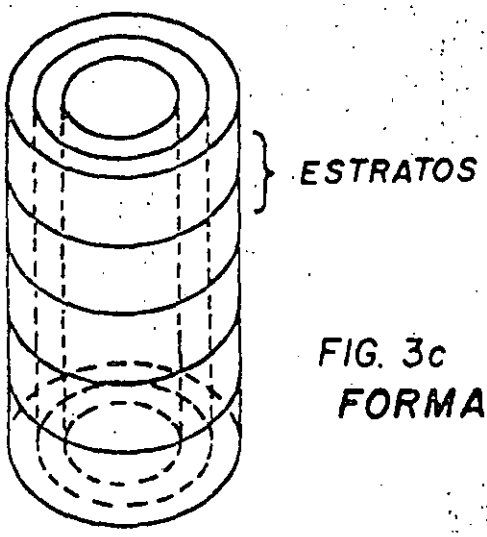

FIG. 3c
FORMA RADIAL

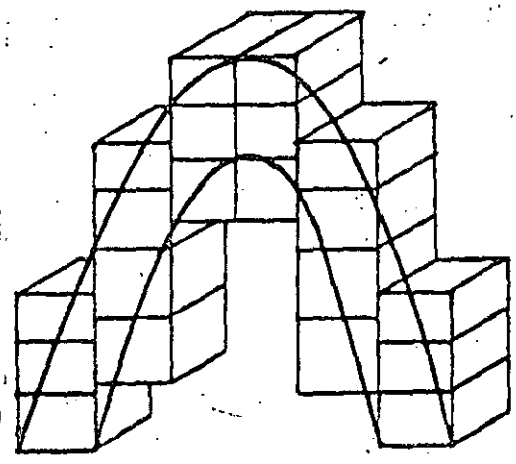

MODELOS DE DOS DIMENSIONES

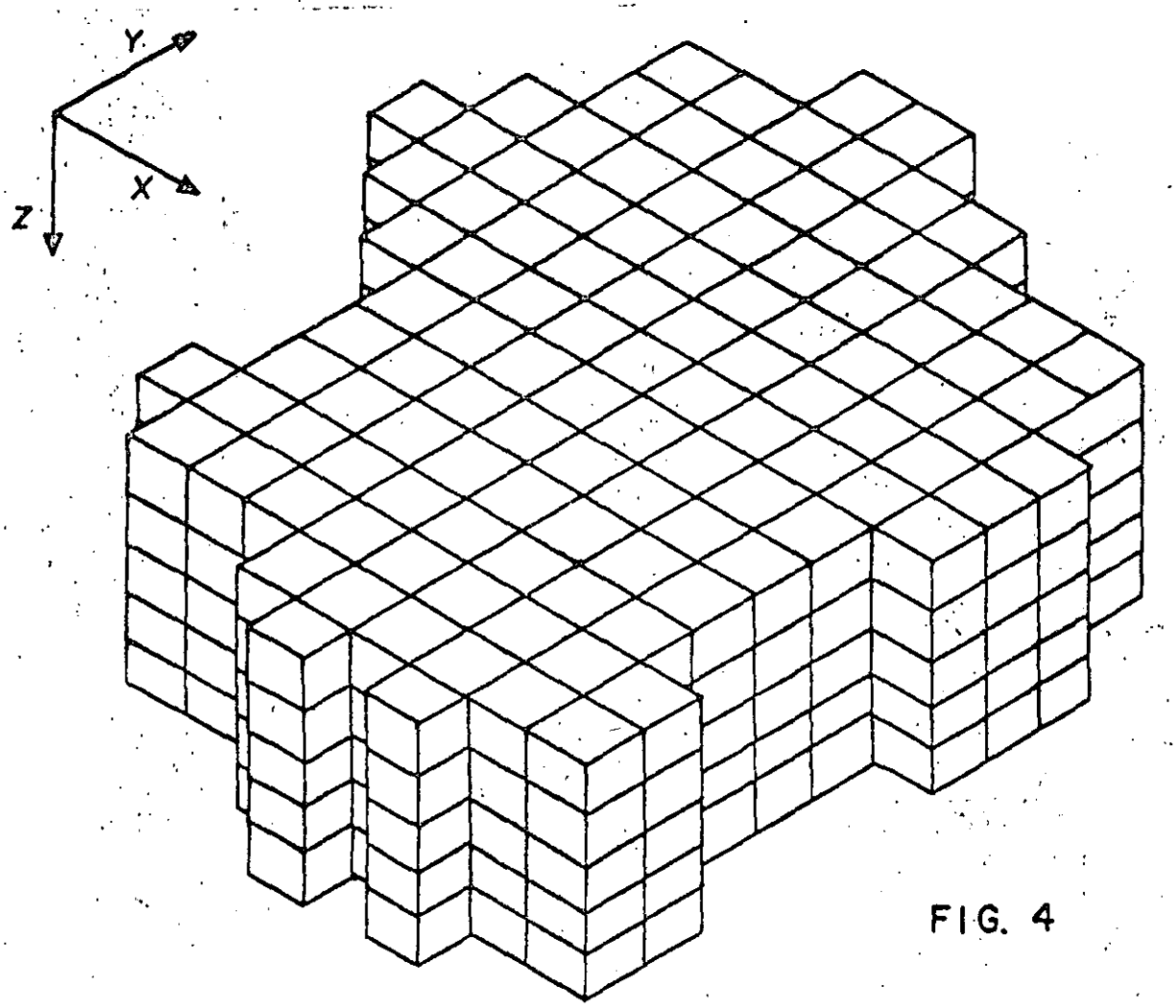

FIG. 4

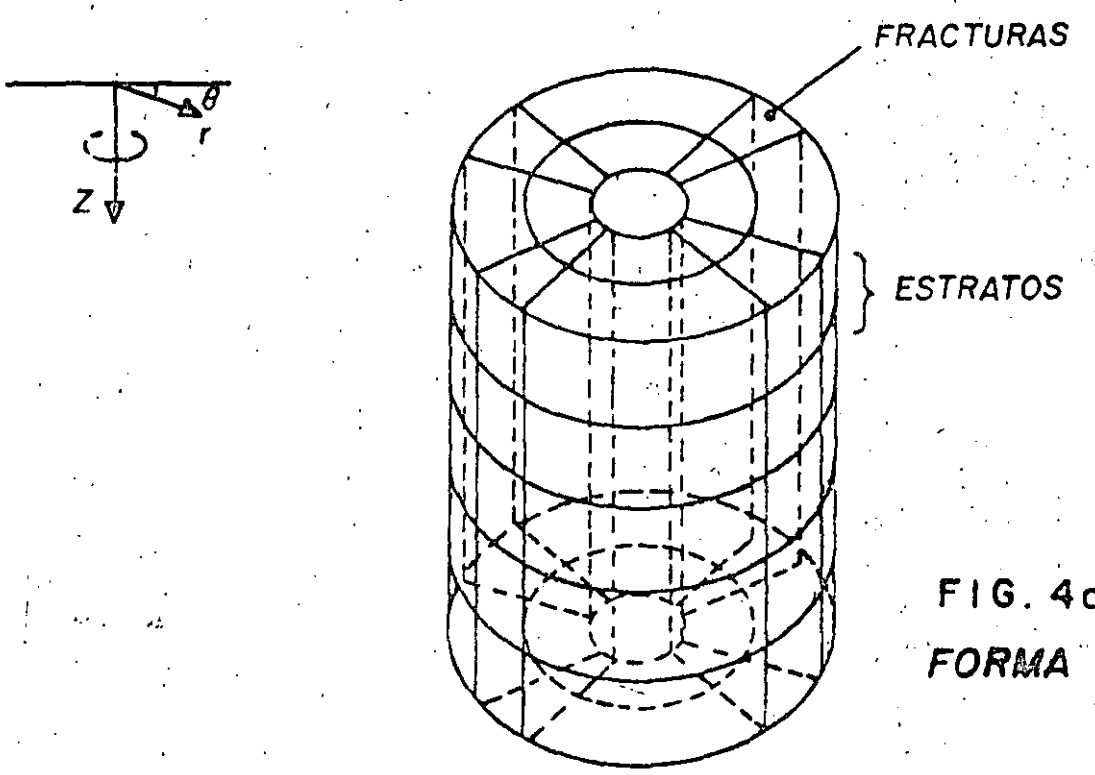

FIG. 4a
FORMA RADIAL

MODELOS DE TRES DIMENSIONES

C O N T E N I D O

C A P I T U L O 2

PRINCIPIOS BASICOS Y ECUACIONES FUNDAMENTALES

2.1 INTRODUCCION

El flujo de fluidos en medios porosos es un fenómeno muy complejo y como tal no puede ser descrito explicitamente.

En flujo a través de tuberías o conductos, es posible medir la longitud y el diámetro y calcular la capacidad de flujo como función de la caída de presión; sin embargo, el flujo en medios porosos es diferente, ya que se tienen que considerar ecuaciones que describán el flujo de los fluidos en una, dos o tres fases, a través de "canales de flujo" que presentan variaciones de uno o varios ordenes de magnitud en donde los fluidos pueden ser tratados como incompresibles, ligeramente incompresibles o compresibles. Además para representar el sistema de flujo pueden considerarse una, dos o tres dimensiones, incluyendo, si se desea, heterogeneidad en las propiedades petrofísicas, efectos gravitacionales, efectos capilares y transferencia de masa entre las fases.

2.2 POTENCIAL DE FLUJO (Φ)

El potencial de flujo combina los efectos de presión con los efectos gravitacionales y se define por:

$$\Phi = p - \rho g D \qquad (2.1)$$

en donde:

$\Phi = (p, \rho)$

ρg = es el peso específico

D = es la profundidad (positiva hacia abajo) medida a - partir de un plano conveniente de referencia.

De acuerdo a las unidades comunmente usadas en ingeniería petrolera, el potencial puede ser expresado como:

$$\Phi = p + \frac{1}{144} \frac{g}{g_c} \rho h \qquad (2.2)$$

$$\Phi = p - \frac{1}{144} \frac{g}{g_c} \rho D \qquad (2.3)$$

en donde

p = presión (lb/pg^2)

ρ = densidad ($lb/pies^3$)

h = altura medida hacia arriba de un plano dado (pies)

D = profundidad medida hacia abajo de un plano dado - (pies)

g = aceleración de la gravedad en el lugar que se está trabajando.

g_c = constante gravitacional condiciones normales y es - igual a 32.2 $pies/seg^2$.

La variación del potencial en una dirección horizontal es equivalente al cambio de presión en esa dirección.

$$\frac{d\Phi}{dx} = \frac{dp}{dx} + 0 \qquad (2.4)$$

Sin embargo, la variación del potencial en la dirección vertical incluye también el efecto gravitacional:

$$\frac{d\Phi}{dz} = \frac{dp}{dz} - \frac{1}{144} \frac{g}{g_c} \rho \qquad (2.5)$$

2.3 LEY DE DARCY

La ley de Darcy establece la proporcionalidad de la velocidad de flujo de un fluido homogéneo en medio poroso con el gradiente de presión.

$$\frac{q}{A} \sim \text{gradiente de presión} \qquad (2.6)$$

en donde

$$q = vA \qquad (2.7)$$

Para cambiar el signo de proporcionalidad por el signo igual es necesario tomar en cuenta tanto las características del medio poroso (permeabilidad) como las del fluido (viscosidad); así para flujo horizontal la ecuación de Darcy se expresa como:

$$\frac{q}{A} = -\frac{k}{\mu}\frac{dp}{dl} \qquad (2.8)$$

La validez de la ecuación anterior presupone las siguientes condiciones:

a) Fluido homogéneo (una sola fase)

b) No existen reacciones químicas entre el fluido y el medio poroso.

c) La permeabilidad es independiente del fluido, de la temperatura, de la presión y de la localización.

d) Régimen laminar.

e) No existe efecto de Klinkenberg.

f) Flujo permanente e incompresible.

g) El fluido satura 100% al medio poroso.

El signo (-) de la ecuación anterior, surge al considerar que - la presión disminuye cuando la longitud aumente y se requiere para- compensar el signo negativo del gradiente.

Para flujo inclinado es necesario considerar tanto la variación en la presión como la variación en la carga gravitacional.

$$v = \frac{q}{A} = -\frac{k}{\mu}\left(\frac{dp}{d\ell} \pm \rho g\right) \qquad (2.9)$$

La razón del signo ($\pm$) se relaciona con la dirección que se le- de a "ℓ", la cual puede ser positiva hacia arriba o viceversa.

Ahora bien, la velocidad a la que se refiere la ecuación de - - Darcy es la velocidad aparente, por lo que si se desea evaluar la - velocidad real habrá que dividir la velocidad aparente por la poro- sidad efectiva del medio, o sea:

$$v_{med.} = \frac{u}{\phi_e} \qquad (2.10)$$

donde

$v_{med.}$ = velocidad real o media.

u = velocidad aparente.

ϕ_e = porosidad efectiva.

La ecuación de Darcy en forma vectorial se expresa como:

$$\vec{v} = \frac{\vec{u}}{\phi} = -\frac{\vec{k}}{\mu\phi}\frac{\partial\phi}{\partial s} \qquad (2.11)$$

Haciendo un análisis de cada una de las variables que intervie- nen en la ecuación (2.11) :

- La viscosidad (μ) es un escalar.
- La porosidad (ϕ) es un escalar.
- La velocidad ($\vec{v}$) por tener magnitud, dirección y sentido es un vector.
- El potencial ($\frac{\partial \vec{\Phi}}{\partial s}$) también es un vector.
- La permeabilidad ($\vec{k}$) es un tensor, capaz de influir en la dirección de flujo, la cual no siempre es gobernada exclusivamente por el gradiente de presión.

Dados los ejes x, y, z no necesariamente ortogonales, las componentes de la velocidad $\vec{v}$ ($\bar{u}_x, \bar{u}_y, \bar{u}_z$) se expresan, de acuerdo a la ley de Darcy, como:

$$\bar{u}_x = -\frac{1}{\mu}\left(k_{xx}\frac{\partial \Phi}{\partial x} + k_{xy}\frac{\partial \Phi}{\partial y} + k_{xz}\frac{\partial \Phi}{\partial z} \right) \qquad (2.12)$$

$$\bar{u}_y = -\frac{1}{\mu}\left(k_{yx}\frac{\partial \Phi}{\partial x} + k_{yy}\frac{\partial \Phi}{\partial y} + k_{yz}\frac{\partial \Phi}{\partial z} \right) \qquad (2.13)$$

$$\bar{u}_z = -\frac{1}{\mu}\left(k_{zx}\frac{\partial \Phi}{\partial x} + k_{zy}\frac{\partial \Phi}{\partial y} + k_{zz}\frac{\partial \Phi}{\partial z} \right) \qquad (2.14)$$

La matriz tensor de permeabilidad tiene nueve componentes:

$$k_{i,j} = \begin{bmatrix} k_{xx} & k_{xy} & k_{xz} \\ k_{yx} & k_{yy} & k_{yz} \\ k_{zx} & k_{zy} & k_{zz} \end{bmatrix}$$

mientras que la velocidad y el potencial, siendo vectores tienen -- tres componentes solamente:

$$\vec{v} = (u_x, u_y, u_z) \qquad \frac{\partial \vec{\Phi}}{\partial s} = \left(\frac{\partial \Phi}{\partial x}, \frac{\partial \Phi}{\partial y}, \frac{\partial \Phi}{\partial z} \right)$$

Debido a la laboriosidad de trabajar con tensores, se hacen comunmente las siguientes suposiciones, para simplificar las ecuaciones :

1) La matriz tensorial es simétrica, o sea:

$k_{xy} = k_{yx}, k_{xz} = k_{zx}, k_{yz} = k_{zy}$

$$\begin{bmatrix} k_{xx} & k_{xy} & k_{xz} \\ k_{xy} & k_{yy} & k_{yz} \\ k_{xz} & k_{yz} & k_{zz} \end{bmatrix}$$

2) Al rotar los ejes de una matriz simétrica se obtiene una matriz diagonal.

$$\begin{bmatrix} k_{xx} & 0 & 0 \\ 0 & k_{yy} & 0 \\ 0 & 0 & k_{zz} \end{bmatrix}$$

En donde los ejes son ortogonales y están alineados con las direcciones principales de flujo. Por lo que las componentes de la velocidad se reducen a :

$$\bar{u}_x = - \frac{k_{xx}}{\mu} \frac{\partial \phi}{\partial x} \qquad (2.15)$$

$$\bar{u}_y = - \frac{k_{yy}}{\mu} \frac{\partial \phi}{\partial y} \qquad (2.16)$$

$$\bar{u}_z = - \frac{k_{zz}}{\mu} \frac{\partial \phi}{\partial z} \qquad (2.17)$$

En general las direcciones principales de flujo son:

S; La dirección máxima, paralela a los planos de sedimentación.

s; La dirección mínima perpendicular a los planos de sedimentación.

Si el medio es isotrópico ($k_x = k_y = k_z$), entonces la dirección del flujo es igual a la dirección del gradiente aplicado.

Si el medio es anisotrópico sin embargo ($k_x \neq k_y \neq k_z$), la dirección del flujo es diferente a la dirección del gradiente aplicado.

EJEMPLO:

Sea un medio poroso bidimensional donde $k_x = 4k_y$, si se aplica un gradiente con un ángulo de 45° (o sea $\frac{\partial \Phi}{\partial x} = \frac{\partial \Phi}{\partial y}$) encontrar la dirección del flujo.

SOLUCION

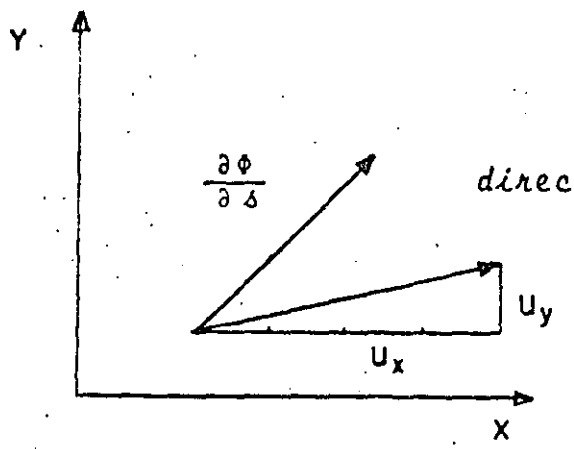

dirección del gradiente de presión

dirección de flujo

$$\bar{u}_x = -\frac{4}{\mu}\frac{\partial \Phi}{\partial x}$$

$$\bar{u}_y = -\frac{1}{\mu}\frac{\partial \Phi}{\partial y}$$

$$\bar{u}_{xy} = -\frac{4}{\mu}\left(\frac{\partial \Phi}{\partial x}\right) - \frac{1}{\mu}\left(\frac{\partial \Phi}{\partial y}\right)$$

$$|\vec{u}| = \sqrt{\left[-\frac{4}{\mu}\left(\frac{\partial \Phi}{\partial x}\right)\right]^2 - \left[\frac{1}{\mu}\left(\frac{\partial \Phi}{\partial y}\right)\right]^2}$$

$$|\vec{u}| = \frac{1}{\mu}\sqrt{17}\left(\frac{\partial \Phi}{\partial x}\right)$$

La magnitud del vector normal está dada por:

$$|\vec{u}| = \frac{1}{\mu}\sqrt{17}\left(\frac{\partial \Phi}{\partial x}\right)$$

La dirección del vector unitario está dada por:

$$\vec{e}_u = -\frac{kx}{\mu\sqrt{17}}\frac{\partial \Phi}{\partial x} - \frac{ky}{\mu\sqrt{17}}\frac{\partial \Phi}{\partial y}$$

o sea la aplicación de un gradiente a 45°a este medio, resulta en - un vector velocidad cuya dirección principal tiene un ángulo $\theta = \tan^{-1} 1/4$, $\theta = 14°02$

2.4 ECUACION DE CONTINUIDAD Y DIFUSIVIDAD

La descripción matemática del flujo de fluidos en medios poro-- sos esta basada en la ley de la conservación de la masa.

2.4.1 ECUACION DE CONTINUIDAD PARA UN SOLO FLUIDO

La ecuación de continuidad es consecuencia de la aplicación del principio de conservación de la masa, el cual establece que la masa dentro de un sistema permanece constante con el tiempo, es decir, - $dm/dt = 0$. La ecuación de continuidad para un cierto elemento de me

-dio poroso establece que la rapidez de crecimiento de la masa dentro del elemento es exactamente igual al flujo neto de masa hacia el mismo elemento.

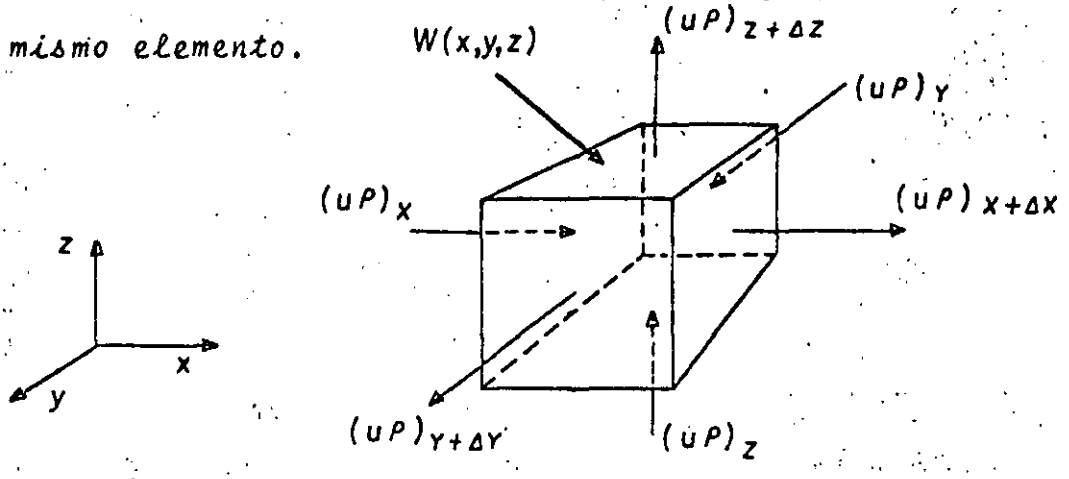

Considerese un pequeño paralelepipedo de un medio poroso de dimensiones Δx, Δy, Δz; a través del cual existe flujo en todas las caras.

Haciendo un balance de materia durante un intervalo pequeño de tiempo Δt.

Se puede considerar que:

El flujo de masa por unidad de superficie es igual a la velocidad multiplicada por la densidad

$$u\,\rho \qquad (2.18)$$

Dimensionalmente

$$\frac{L}{T}\,\frac{M}{L^3} = \frac{M}{TL^2}$$

Ahora bien si el flujo de masa se multiplica por el área transversal al flujo, se obtiene como resultado, el flujo másico.

$$u\rho A = \rho q \qquad (2.19)$$

donde

A= área

M= masa

T= tiempo

u= velocidad

ρ= densidad

Por otra parte se puede considerar que la entrada de masa al elemento considerado es positiva (inyección), mientras que la salida de masa se considera negativa (producción). El término fuente (o sumidero) se representa por $W(x,y,z)$, el cual tiene unidades de masa por unidad de volúmen de roca.

$$W(x,y,z)\left[\frac{\text{Masa}}{\text{unidad de vol. de roca}}\right]$$

$W(x,y,z)$ (+) Inyección

$W(x,y,z)$ (-) Producción

Por otra parte:

Masa de fluido en el elemento,

en el tiempo t: $\Delta x\,\Delta y\,\Delta z\,(\phi\rho)_t$ (inicial)

en el tiempo $t+\Delta t$: $\Delta x\,\Delta y\,\Delta z\,(\phi\rho)_{t+\Delta t}$ (final)

Del principio de conservación de masa:

(Masa que entra) - (Masa que sale) = Acumulación,

Acumulación = (Masa final) - (Masa inicial)

La cara Δy, Δz es perpendicular al flujo en la dirección x, con lo cual la cantidad de masa neta que entra en la dirección x se expresa como:

$$\Delta t \left[(\rho u)_x - (\rho u)_{x+\Delta x} \right] \Delta y \, \Delta z \qquad (2.20)$$

Para las direcciones "y", y "z" se obtienen expresiones similares. Ahora la acumulación se escribe como:

$$\text{Acumulación} = \Delta x \, \Delta y \, \Delta z (\phi \rho)_{t+\Delta t} - \Delta x \, \Delta y \, \Delta z (\phi \rho)_t \qquad (2.21)$$

tomando en cuenta las expresiones anteriores

$$\Delta t \left[(\rho u)_x - (\rho u)_{x+\Delta x} \right] \Delta y \, \Delta z + \Delta t \left[(\rho u)_y - (\rho u)_{y+\Delta y} \right] \Delta x \, \Delta z$$

$$+ \Delta t \left[(\rho u)_z - (\rho u)_{z+\Delta z} \right] \Delta y \, \Delta x + W(x,y,z) = \Delta x \Delta y \Delta z \left[(\phi \rho)_{t+\Delta t} - (\phi \rho)_t \right]$$

dividiendo entre $\Delta x \, \Delta y \, \Delta z \, \Delta t$ se obtiene:

$$- \frac{(\rho u)_{x+\Delta x} - (\rho u)_x}{\Delta x} - \frac{(\rho u)_{y+\Delta y} - (\rho u)_y}{\Delta y} - \frac{(\rho u)_{z+\Delta z} - (\rho u)_z}{\Delta z}$$

$$+ \frac{W(x,y,z)}{\Delta x \, \Delta y \, \Delta z \, \Delta t} = \frac{(\phi \rho)_{t+\Delta t} - (\phi \rho)_t}{\Delta t} \qquad (2.23)$$

tomando límites cuando $\Delta x \to 0$, $\Delta y \to 0$, $\Delta z \to 0$ y $\Delta t \to 0$ y recordando la definición de derivada de una función:

$$\frac{dy}{dx} = \lim_{\Delta x \to 0} \frac{y(x + \Delta x) - y(x)}{\Delta x}$$

se tiene que:

$$- \frac{\partial (\rho u x)}{\partial x} - \frac{\partial (\rho u y)}{\partial y} - \frac{\partial (\rho u z)}{\partial z} + W(x,y,z) = \frac{\partial (\phi \rho)}{\partial t} \qquad (2.24)$$

Esta ecuación es la forma general de la ecuación de continuidad en un medio poroso.

2.4.2 ECUACION DE DIFUSIVIDAD

Substituyendo las componentes de la velocidad por la ley de Darcy en la ecuación de continuidad se tiene:

$$\frac{\partial}{\partial x}\left(\rho\frac{kx}{\mu}\frac{\partial\Phi}{\partial x}\right)+\frac{\partial}{\partial y}\left(\rho\frac{ky}{\mu}\frac{\partial\Phi}{\partial y}\right)+\frac{\partial}{\partial z}\left(\rho\frac{kz}{\mu}\frac{\partial\Phi}{\partial z}\right)+W(x,y,z)=\frac{\partial(\phi\rho)}{\partial t} \qquad (2.25)$$

Esta es la ecuación general de difusividad que representa el flujo de un solo fluido a través de un medio poroso.

Para el flujo de varios fluidos, es necesario considerar también que el medio poroso estará sujeto a variaciones en la saturación por lo tanto, después de proceder en forma similar a la anterior, la ecuación de difusividad para flujo multifásico en donde k_f representa la permeabilidad efectiva al flujo en cuestión, se tiene:

$$\frac{\partial}{\partial x}\left(\rho\frac{kfx}{\mu}\frac{\partial\Phi}{\partial x}\right)+\frac{\partial}{\partial y}\left(\rho\frac{kfy}{\mu}\frac{\partial\Phi}{\partial y}\right)+\frac{\partial}{\partial z}\left(\rho\frac{kfz}{\mu}\frac{\partial\Phi}{\partial z}\right)+W(x,y,z)=\frac{\partial(Sf\phi\rho)}{\partial t} \qquad (2.26)$$

Para la solución de ésta ecuación es necesario utilizar una ecuación de estado que relacione la densidad con la presión.

2.4.3. TIPOS DE FLUIDOS

Los fluidos de un yacimiento son clasificados dentro de tres grupos, dependiendo de su compresibilidad.

a) Fluidos incompresibles.

b) Fluidos ligeramente compresibles.

c) Fluidos compresibles.

En un fluido incompresible, la densidad de los fluidos se considera constante.

Un fluido se denomina ligeramente compresible si su densidad se puede considerar como una función lineal de presión (por ejemplo compresibilidad constante).

Finalmente un fluido compresible es aquel que presenta un cambio significante de densidad con la presión.

Gráficamente se tiene lo siguiente:

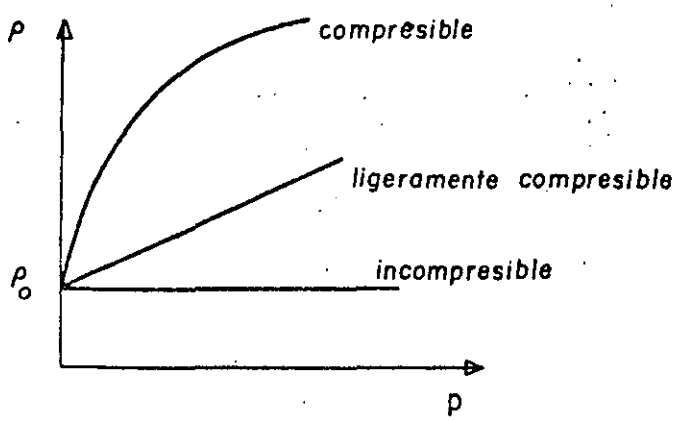

2.4.4 ECUACIONES DE ESTADO

Dependiendo del fluido que se este manejando, existen varias ecuaciones de estado.

a) Si el fluido es incompresible quiere decir que la densidad será constante.

$$\rho = ctte. \tag{2.27}$$

b) Si el fluido es ligeramente compresible (líquido) la ecuación de estado será:

$$c = \frac{1}{\rho}\left(\frac{\partial \rho}{\partial p}\right)_{T=ctte.} \tag{2.28}$$

c) Para un gas ideal

$$pV = nRT \tag{2.29}$$

d) Para un gas real

$$pV = ZnRT \tag{2.30}$$

Antes de introducir las ecuaciones de estado a la ecuación de difusividad, se definen algunos términos.

$$Bo = \text{Factor de volúmen en } \left[\frac{\text{vol. @ c.y.}}{\text{vol. @ c.s.}}\right]$$

$$q_{vol.} = \text{Ritmo de inyección en } \left[\frac{\text{vol. @ c.s./día}}{\text{pie}^3 \text{ de roca}}\right]$$

por lo que

$W(x,y,z)$ = Ritmo de inyección de masa por unidad de volúmen.

$$W(x,y,z) = Bo\ q_{vol.}\ \rho \tag{2.31}$$

$$W(x,y,z) = \left[\frac{\text{vol. @c.y.}}{\text{vol. @c.s.}}\right]\left[\frac{\text{vol.@ c.s.}}{\text{día} \cdot \text{pie}^3}\right]\left[\frac{\text{masa}}{\text{vol. @c.y}}\right]$$

2.5 DESARROLLO DE ECUACIONES PARA LOS DIFERENTES TIPOS DE FLUIDOS

2.5.1 ECUACION PARA FLUJO INCOMPRESIBLE

$$si\ \rho = ctte.\ , \quad \frac{\partial \rho}{\partial t} = 0 \tag{2.32}$$

y además la viscosidad es constante. De la ecuación de difusividad

$$\frac{\partial}{\partial x}\left(\rho\frac{kx}{\mu}\frac{\partial\Phi}{\partial x}\right) + \frac{\partial}{\partial y}\left(\rho\frac{ky}{\mu}\frac{\partial\Phi}{\partial y}\right) + \frac{\partial}{\partial z}\left(\rho\frac{kz}{\mu}\frac{\partial\Phi}{\partial z}\right) + W(x,y,z) = \frac{\partial(\phi\rho)}{\partial t}$$

substituyendo el valor de W, sabiendo que $\frac{\partial\rho}{\partial t} = 0$, multiplicando por μ y dividiendo por ρ (ambas constantes):

$$\frac{\partial}{\partial x}\left(kx\frac{\partial\Phi}{\partial x}\right) + \frac{\partial}{\partial y}\left(ky\frac{\partial\Phi}{\partial y}\right) + \frac{\partial}{\partial z}\left(kz\frac{\partial\Phi}{\partial z}\right) + q_{vol.}B = 0 \qquad (2.33)$$

En la ecuación anterior las permeabilidades pueden variar en x, y, z; es decir

$$kx = kx(x,y,z)$$

$$ky = ky(x,y,z)$$

$$kz = kz(x,y,z)$$

Si el medio es isotrópico y homogéneo

$$kx = ky = kz \equiv k$$

Dividiendo la ecuación (2.33) por k

$$\frac{\partial}{\partial x}\left(\frac{\partial\Phi}{\partial x}\right) + \frac{\partial}{\partial y}\left(\frac{\partial\Phi}{\partial y}\right) + \frac{\partial}{\partial z}\left(\frac{\partial\Phi}{\partial z}\right) + \frac{\mu q_{vol}B}{k} = 0$$

$$\frac{\partial^2\Phi}{\partial x^2} + \frac{\partial^2\Phi}{\partial y^2} + \frac{\partial^2\Phi}{\partial z^2} + \frac{\mu q_{vol}B}{k} = 0$$

la cual se puede expresar como

$$\nabla^2 \phi + \frac{q_{vol.} B}{k} = 0 \qquad \text{Ecuación de Poisson} \qquad (2.35)$$

Si no existe inyección la ecuación anterior se simplifica a:

$$\nabla^2 \phi = 0 \qquad \text{Ecuación de Laplace} \qquad (2.36)$$

Las unidades que comunmente se usan en ingeniería petrolera son las siguientes:

$$B \left[\frac{vol.\ @c.y.}{vol.\ @c.s.} \right]$$

$$q_{vol.} \left[\frac{stb}{día} \right]$$

$$\frac{}{pie^3}$$

x, y, z (pies)

ϕ (lb/pg^2)

μ (cp)

por lo que

$$\frac{\partial \phi}{\partial x} \left\{ \begin{array}{l} \dfrac{\partial p}{\partial x} + \dfrac{1}{144} \rho \dfrac{g}{g_c} \dfrac{\partial h}{\partial x} \\ \dfrac{\partial p}{\partial x} - \dfrac{1}{144} \rho \dfrac{g}{g_c} \dfrac{\partial D}{\partial x} \end{array} \right. \qquad (2.37)$$

$$\frac{\partial \phi}{\partial y} \left\{ \begin{array}{l} \dfrac{\partial p}{\partial y} + \dfrac{1}{144} \rho \dfrac{g}{g_c} \dfrac{\partial h}{\partial y} \\ \dfrac{\partial p}{\partial y} - \dfrac{1}{144} \rho \dfrac{g}{g_c} \dfrac{\partial D}{\partial y} \end{array} \right. \qquad (2.38)$$

sustituyendo en la ecuación (2.40) las expresiones (2.41) y (2.42).

$$c = \frac{-1}{m/\rho}\left(\frac{-m\partial\rho}{\rho^2\partial p}\right)$$

$$c = \frac{1}{\rho}\frac{\partial\rho}{\partial p} \qquad (2.43)$$

La ecuación anterior nos representa la relación de la densidad de un líquido con su compresibilidad. Para obtener la variación de la presión en las direcciones " x,y,z ", bastará con despejar " dp " de la ecuación (2.43) y derivar respecto a cada una de las direcciones correspondientes.

despejando "dp":

$$dp = \frac{1}{c\rho}\frac{d\rho}{1}$$

derivando respecto a "x,y,z"

$$\frac{dp}{dx} = \frac{1}{c\rho}\frac{d\rho}{dx} \qquad (2.44)$$

$$\frac{dp}{dy} = \frac{1}{c\rho}\frac{d\rho}{dy} \qquad (2.45)$$

$$\frac{dp}{dz} = \frac{1}{c\rho}\frac{d\rho}{dz} \qquad (2.46),$$

Si el espesor del yacimiento es pequeño y de bajo relieve estructural, es decir para flujo horizontal, se puede hacer la considera--

-ción de que el potencial de flujo es aproximadamente igual a la -- presión.

$$\phi \cong p \qquad (2.47)$$

Ahora bien, si no se tiene inyección en ningún pozo ($W(x,y,z)=0$), tomando en cuenta la consideración anterior y recordando la ecuación de difusividad dada por la siguiente expresión:

$$\frac{\partial}{\partial x}\left(\rho \frac{k_x}{\mu}\frac{\partial \phi}{\partial x}\right) + \frac{\partial}{\partial y}\left(\rho \frac{k_y}{\mu}\frac{\partial \phi}{\partial y}\right) + \frac{\partial}{\partial z}\left(\rho \frac{k_z}{\mu}\frac{\partial \phi}{\partial z}\right) + W(x,y,z) = \frac{\partial (S_{F\phi\rho})}{\partial t}$$

sustituyendo en la ecuación anterior las ecuaciones (2.44), (2.45), (2.46), y (2.47) se tiene:

$$\frac{\partial}{\partial x}\left(\rho \frac{k_x}{\mu}\frac{1}{c\rho}\frac{\partial \rho}{\partial x}\right) + \frac{\partial}{\partial y}\left(\rho \frac{k_y}{\mu}\frac{1}{c\rho}\frac{\partial \rho}{\partial y}\right) + \frac{\partial}{\partial z}\left(\rho \frac{k_z}{\mu}\frac{1}{c\rho}\frac{\partial \rho}{\partial z}\right) = \frac{\partial (\phi\rho)}{\partial t}$$

simplificando la ecuación anterior:

$$\frac{\partial}{\partial x}\left(\frac{k_x}{\mu}\frac{1}{c}\frac{\partial \rho}{\partial x}\right) + \frac{\partial}{\partial y}\left(\frac{k_y}{\mu}\frac{1}{c}\frac{\partial \rho}{\partial y}\right) + \frac{\partial}{\partial z}\left(\frac{k_z}{\mu}\frac{1}{c}\frac{\partial \rho}{\partial z}\right) = \frac{\partial (\phi\rho)}{\partial t} \qquad (2.48)$$

Considerando un medio isotrópico ($kx=ky=kz\equiv k$), la viscosidad - constante ($\mu=c$He), multiplicando por μc y dividiendo entre k, se -

obtiene:

$$\frac{\partial}{\partial x}\left(\frac{\partial \rho}{\partial x}\right) + \frac{\partial}{\partial y}\left(\frac{\partial \rho}{\partial y}\right) + \frac{\partial}{\partial z}\left(\frac{\partial \rho}{\partial z}\right) = \frac{\phi \mu c}{k}\frac{\partial \rho}{\partial t}$$

o sea:

$$\frac{\partial^2 \rho}{\partial x^2} + \frac{\partial^2 \rho}{\partial y^2} + \frac{\partial^2 \rho}{\partial z^2} = \frac{\phi \mu c}{k}\frac{\partial \rho}{\partial t}$$

siendo equivalente a :

$$" \nabla^2 \rho = \frac{\phi \mu c}{k}\frac{\partial \rho}{\partial t} " \qquad (2.49)$$

La ecuación obtenida anteriormente es la representativa para el-flujo de un fluido ligeramente compresible de compresibilidad cons--tante, la cual puede ser aplicada para líquidos y para gases en in--tervalos pequeños.

La ecuación (2.49) no es muy práctica para su utilización en la-forma obtenida, debido a la dificultad que presenta la evaluación de las densidades, por lo que es conveniente expresar la ecuación (2.49) en función de la presión.

De la ecuación (2.45)

$$c = \frac{1}{\rho}\frac{\partial \rho}{\partial p} = \frac{1}{\rho}\frac{d\rho}{dp}$$

despejando "cdp" se tiene:

$$c\,dp = \frac{1}{\rho}\,d\rho$$

integrando de p_o *a* p

$$\int_{p_o}^{p} c\,dp = \int_{p_o}^{p} \frac{d\rho}{\rho}$$

se obtiene:

$$c\,(p - p_o) = ln\,\frac{\rho}{\rho_o}$$

despejando " ρ*"*

$$\rho = \rho_o e^{c(\,p-p_o\,)} \qquad (2.50)$$

ρ_o = *densidad inicial del fluido valuada a una presión inicial --* $(\,p_o\,)$

p = *presión medida a cualquier tiempo.*

Recordando que la fórmula de expansión de una función "$f(z)$*", -- en las cercanías del valor conocido de la función por medio de la serie de Taylor, siendo "a" el punto conocido:*

$$f(z) = f(a) + \frac{f'(a)(z-a)}{1!} + \frac{f''(a)(z-a)^2}{2!} + \cdots\cdots + \frac{f^n(a)(z-a)^n}{n!}$$

por lo tanto se puede expandir la función $f(x)$ *alrededor del punto* $x=0$*, entonces:*

$$f(x) = 1 + \frac{x}{1!} + \frac{x^2}{2!} + \frac{x^3}{3!} + \cdots\cdots + \frac{x^n}{n!}$$

por lo tanto:

$$e^{cp} = 1 + \frac{cp}{1!} + \frac{c^2p^2}{2!} + \frac{c^3p^3}{3!} + \ldots\ldots\ldots + \frac{c^np^n}{n!} \qquad (2.51)$$

En la mayoría de los casos en ingeniería petrolera (para líquidos), se cumple que:

$$cp < 0.01$$

$$\therefore \quad c^2p^2 < 0.0001$$

por lo que la expresión (2.51) se puede simplificar a:

$$e^{cp} \doteq 1 + cp \qquad (2.52)$$

sustituyendo la ecuación (2.52) en la ecuación (2.50) se tiene:

$$\rho = \rho_o \ (\ 1 + cp \ ) \qquad (2.53)$$

teniendo la densidad como función de la presión, se podrá obtener la ecuación de flujo representativa.

Sustituyendo la ecuación (2.53) en la ecuación (2.49)

$$\frac{\partial}{\partial x}\left[\frac{\partial\left[\rho_o(1+cp)\right]}{\partial x}\right] + \frac{\partial}{\partial y}\left[\frac{\partial\left[\rho_o(1+cp)\right]}{\partial y}\right] + \frac{\partial}{\partial z}\left[\frac{\partial\left[\rho_o(1+cp)\right]}{\partial z}\right] = \frac{\phi\mu c}{k}\frac{\partial\left[\rho_o(1+cp)\right]}{\partial t} \qquad (2.54)$$

siendo "ρ_o" la densidad inicial del fluido (constante), entonces:

$$\frac{\partial \rho_o}{\partial t} = 0$$

por lo que, en la dirección "x" se tiene:

$$\frac{\partial}{\partial x}\left(0 + c\,\rho_o \frac{\partial p}{\partial x} \right)$$

reduciéndose la ecuación (2.54) a:

$$c\,\rho_o \left[\frac{\partial^2 p}{\partial x^2} + \frac{\partial^2 p}{\partial y^2} + \frac{\partial^2 p}{\partial z^2} \right] = \frac{\phi \mu c}{k}\, c\,\rho_o \frac{\partial p}{\partial t}$$

dividiendo entre $c\rho_o$

$$\frac{\partial^2 p}{\partial x^2} + \frac{\partial^2 p}{\partial y^2} + \frac{\partial^2 p}{\partial z^2} = \frac{\phi \mu c}{k} \frac{\partial p}{\partial t}$$

o sea:

$$" \nabla^2 p = \frac{\phi \mu c}{k} \frac{\partial p}{\partial t} " \qquad (2.55)$$

que es la ecuación de difusión para un fluido ligeramente compresible habiendo hecho las siguientes consideraciones:

- medio isotrópico
- medio homogéneo
- viscosidad constante
- compresibilidad constante

La importancia que reviste dicha ecuación es trascendente, debido a su múltiple utilidad. Entre otras aplicaciones se tienen:

- pruebas de presión (incremento, decremento, interferencia, etc.)
- pruebas de límite de yacimientos
- simulación de yacimientos.

2.5.3 ECUACION DE FLUJO PARA UN GAS REAL

Para poder obtener la ecuación representativa de flujo de gas, es necesario introducir la ecuación general de los gases.

Recordando la ecuación general de los gases dada por:

$$p\,V = Z\,n\,R\,T \tag{2.56}$$

$$\therefore\ n = n^{o}\ de\ moles = \frac{m}{M} = \frac{masa}{peso\ molecular} \tag{2.57}$$

sustituyendo la ecuación (2.57) en la ecuación (2.56).

$$p\,V = Z\,\frac{m}{M}\,R\,T \tag{2.58}$$

de la ecuación (2.40) $\rho = \frac{m}{V}$

sustituyendo la ecuación (2.40) en la ecuación (2.58) y despejando "ρ" se tiene:

$$\rho = \frac{m}{V} = \frac{pM}{ZRT} \tag{2.59}$$

involucrando el valor de la densidad de un gas dada por la ecuación (2.59), en la ecuación de difusividad.

$$\frac{\partial}{\partial x}\left(\frac{pM}{ZRT}\,\frac{k_x}{\mu}\,\frac{\partial p}{\partial x}\right) + \frac{\partial}{\partial y}\left(\frac{pM}{ZRT}\,\frac{k_y}{\mu}\,\frac{\partial p}{\partial y}\right) + \frac{\partial}{\partial z}\left(\frac{pM}{ZRT}\,\frac{k_z}{\mu}\,\frac{\partial p}{\partial z}\right) + \frac{pM}{ZRT}\,q.\ vol.\ (x,y,z) = \phi\,\frac{\partial}{\partial t}\left(\frac{pM}{ZRT}\right) \tag{2.60}$$

Si se llama 1 a las condiciones de yacimiento y 2 a las condiciones de superficie

$$\frac{p_1 V_1}{Z_1 T_1} = \frac{p_2 V_2}{Z_2 T_2}$$

como $V_1 = q\ vol.\ (x,y,z)$

$$\frac{p_1\ q\ vol.\ (x,y,z)}{Z_1 T_1} = \frac{p_2\ q\ vol.\ (scf)/d}{Z_2 T_2} \qquad (2.61)$$

sabiendo que las condiciones estandar son:

$T_2 = 60°F = 60+460 = 520\ °R$

$Z_2 = 1$

$p_2 = 14.7\ lb/pg^2$

$d = día$

despejando q vol. (x,y,z) de la ecuación (2.61) y sustituyendo los valores de las condiciones estandar:

$$q\ vol.\ (x,y,z) = \frac{14.7 \times q\ vol.\ (scf/d)}{520} \frac{Z_1 T_1}{p_1}$$

sustituyendo la ecuación (2.62) en la ecuación (2.60)

$$\frac{\partial}{\partial x}\left(\frac{pM}{ZRT}\frac{kx}{\mu}\frac{\partial p}{\partial x}\right) + \frac{\partial}{\partial y}\left(\frac{pM}{ZRT}\frac{ky}{\mu}\frac{\partial p}{\partial y}\right) + \frac{\partial}{\partial z}\left(\frac{pM}{ZRT}\frac{kz}{\mu}\frac{\partial p}{\partial z}\right) +$$

$$\frac{p\ (14.7)\ q\ vol.\ (scf/d)}{Z\ T \cdot p \times 520} = \phi \frac{\partial}{\partial t}\left(\frac{pM}{ZRT}\right)$$

como M, R y T son constantes; multiplicando por R T y dividiendo --- entre M resulta lo siguiente:

$$\frac{\partial}{\partial x}\left(\frac{p}{\mu}\frac{kx}{Z}\frac{\partial p}{\partial x}\right)+\frac{\partial}{\partial y}\left(\frac{p}{\mu}\frac{ky}{Z}\frac{\partial p}{\partial y}\right)+\frac{\partial}{\partial z}\left(\frac{p}{\mu}\frac{kz}{Z}\frac{\partial p}{\partial z}\right)+$$

$$\frac{14.7\ q\ vol.\ (scf/d)}{520 \times 5.615}=\frac{1}{5.615}\frac{\partial}{\partial t}\left(\phi\frac{p}{Z}\right) \qquad (2.63)$$

que es la ecuación de difusión para un gas real, en donde:

$$q.\ vol.\ \left[\frac{scf/d}{pie^3\ \ roca}\right]$$

T $[°R]$

p $[lb/pg^2]$

5.615 factor de conversión (1 bl = 5.615 pie^3)

La ecuación anterior es una ecuación no lineal.

Para reducir la no linealidad de la ecuación se utilizará un artificio.

Defínase al potencial de un gas real como (p^*):

$$p^* = \int_{p_o}^{p} \frac{\zeta}{\mu(\zeta)\ Z\ (\zeta)}\, d\varepsilon$$

la integral anterior se puede calcular a través del método de Simpson para funciones discretas. El método consiste en elaborar una tabla de valores y una gráfica de "p" VS "$p/\mu Z$", donde a partir de la unión de los puntos se obtendrá una curva, por medio de la cual se -

podrá obtener el valor de la integral en un intervalo, que representa el área bajo la curva.

La función anterior permite transformar la ecuación no lineal - de la siguiente manera:

si

$$\frac{\partial p^*}{\partial p} = \frac{p}{\mu z} \qquad y \qquad \frac{\partial p^*}{\partial x} = \frac{\partial p^*}{\partial p} \cdot \frac{\partial p}{\partial x}$$

se tendrá que:

$$" \quad \frac{\partial p^*}{\partial x} = \frac{\partial p^*}{\partial p} \cdot \frac{\partial p}{\partial x} = \frac{p}{\mu z} \frac{\partial p}{\partial x} \quad " \qquad (2.64)$$

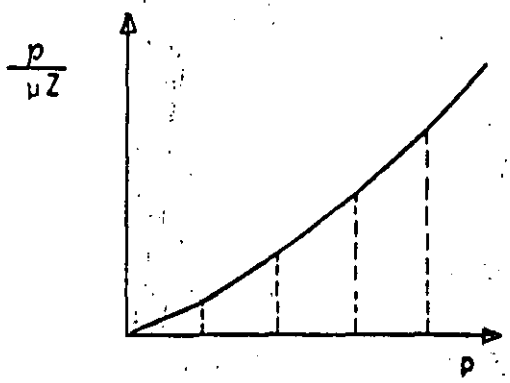

sustituyendo el valor de la ecuación (2.64) en la ecuación para un- gas real se tendrá:

$$\frac{\partial}{\partial x}\left(k_x \frac{\partial p^*}{\partial x}\right) + \frac{\partial}{\partial y}\left(k_y \frac{\partial p^*}{\partial y}\right) + \frac{\partial}{\partial z}\left(k_z \frac{\partial p^*}{\partial z}\right) +$$

$$\frac{14.7 \text{ q. vol. (scf/d)}}{520 \times 5.615} = \frac{1}{5.615} \frac{\partial}{\partial t}\left(\phi \frac{p}{z}\right) \qquad (2.65)$$

además de la expresión anterior se pueden obtener otras 2 expresio-

-nes: de la ley de los gases reales:

$$V = \frac{Zm}{M}\,\frac{R\,T}{p} \qquad (2.66)$$

derivando respecto a "p" la ecuación anterior

$$\frac{\partial V}{\partial p} = \frac{mRT}{M}\left(\frac{1}{Zp^2} + \frac{1}{p}\,\frac{\partial z}{\partial p}\right)$$

$$\frac{\partial V}{\partial p} = \frac{mRT}{M}\left(\frac{1}{p}\,\frac{\partial z}{\partial p} - \frac{Z}{p^2}\right) \qquad (2.67)$$

sustituyendo la ecuación (2.66) y la (2.67) en la ecuación de compresibilidad ecuación (2.40).

$$c = -\frac{1}{V}\left(\frac{\partial V}{\partial p}\right)_T$$

$$c = -\frac{p\,M}{Zm\,RT}\cdot\frac{mRT}{M}\left(\frac{1}{p}\,\frac{\partial z}{\partial p} - \frac{Z}{p^2}\right)$$

simplificando

$$c = -\frac{p}{Z}\left(\frac{1}{p}\,\frac{\partial z}{\partial p} - \frac{Z}{p^2}\right)$$

$$c = \frac{1}{p} - \frac{1}{Z}\,\frac{\partial z}{\partial p} \qquad (2.68)$$

que representa la ecuación de compresibilidad para gases.

Del término $\frac{\partial}{\partial t}\left(\frac{\phi p}{Z}\right)$ de la ecuación (2.65), si se considera la porosidad (ϕ) como una constante, se tiene:

$$\frac{\partial}{\partial t}\left(\frac{p}{Z}\right) = \frac{\partial}{\partial p}\left(\frac{p}{Z}\right)\frac{\partial p}{\partial t} = \left(\frac{-p}{Z^2}\frac{\partial z}{\partial p} + \frac{1}{Z}\right)\frac{\partial p}{\partial t} =$$

$$\frac{p}{Z}\left(\frac{1}{p} - \frac{1}{Z}\frac{\partial z}{\partial p}\right)\frac{\partial p}{\partial t}$$

como $$c = \frac{1}{p} - \frac{1}{Z}\frac{\partial z}{\partial p}$$

entonces:

$$" \quad \frac{\partial}{\partial t}\left(\frac{p}{Z}\right) = \frac{pc}{Z}\frac{\partial p}{\partial p^*}\frac{\partial p^*}{\partial t} \quad "$$

Si se tiene una diferencial total, es decir que "p*" es función de "p" entonces:

$$\frac{\partial p}{\partial p^*} = \frac{1}{\partial p^*/\partial p}$$

o sea:

$$\frac{dp}{dp^*} = \frac{1}{dp^*/dp} = \frac{1}{p/\mu Z}$$

por lo que:

$$" \quad \frac{\partial}{\partial t}\left(\frac{p}{Z}\right) = \frac{pc}{Z}\,\frac{\mu Z}{p}\,\frac{\partial p^*}{\partial t} = c\mu\,\frac{\partial p^*}{\partial t} \quad "$$

quedando finalmente la ecuación para un gas real en tres formas diferentes:

1a) $$\frac{\partial}{\partial x}\left(kx\,\frac{\partial p^*}{\partial x}\right) + \frac{\partial}{\partial y}\left(ky\,\frac{\partial p^*}{\partial y}\right) + \frac{\partial}{\partial z}\left(kz\,\frac{\partial p^*}{\partial z}\right) +$$

$$\frac{14.7\ q.\ vol.\ (scf/d)}{520 \times 5.615} = \frac{\phi pc}{5.615}\left(\frac{\partial p}{\partial t}\right) \qquad (2.70)$$

2a) $$\frac{\partial}{\partial x}\left(kx\,\frac{\partial p^*}{\partial x}\right) + \frac{\partial}{\partial y}\left(ky\,\frac{\partial p^*}{\partial y}\right) + \frac{\partial}{\partial z}\left(kz\,\frac{\partial p^*}{\partial z}\right) +$$

$$\frac{14.7\ q.\ vol.\ (scf/d)}{520 \times 5.615} = \frac{\phi\mu c}{5.615}\left(\frac{\partial p^*}{\partial t}\right) \qquad (2.71)$$

3a) $$\frac{\partial}{\partial x}\left(kx\,\frac{\partial p^*}{\partial x}\right) + \frac{\partial}{\partial y}\left(ky\,\frac{\partial p^*}{\partial y}\right) + \frac{\partial}{\partial z}\left(kz\,\frac{\partial p^*}{\partial z}\right) +$$

$$\frac{14.7\ q.\ vol.\ (scf/d)}{520 \times 5.615} = \frac{\phi}{5.615}\,\frac{\partial}{\partial t}\left(\frac{p}{Z}\right) \qquad (2.72)$$

NOTA: La consideración de que la porosidad es constante, es aceptable debido a que la compresibilidad de la roca es mucho menor que la compresibilidad del gas.

2.6 FORMULACION INTEGRAL DE UN PROBLEMA TRIFASICO

Para formular las ecuaciones de flujo trifásico, se tomaron encuenta las propiedades de cada fluido en particular. Procediendo en forma similar a la utilizada para deducir la ecuación de flujo monofásico, se llega a las siguientes ecuaciones de flujo de tres fases.

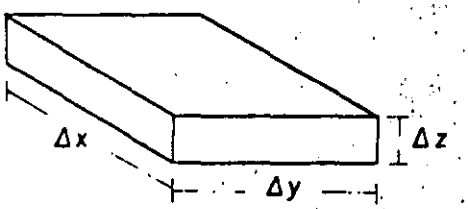

Aceite:

$$\nabla\left(\frac{Kkro A}{\mu_o B_o}\nabla\Phi_o\right)\Delta + q_o \; stb/d = \frac{Vb}{5.615}\frac{\partial}{\partial t}\left(\frac{\phi S_o}{B_o}\right) \qquad (2.73)$$

Agua:

$$\nabla\left(\frac{Kkrw\ A}{\mu_w B_w}\nabla\Phi_w\right)\Delta + q_w \; stb/d = \frac{Vb}{5.615}\frac{\partial}{\partial t}\left(\frac{\phi S_w}{B_w}\right) \qquad (2.74)$$

Gas:

$$\nabla\left(\frac{Kkrg\ A}{\mu_g B_g}\nabla\Phi_g + \frac{Rs\ Kkro A}{\mu_o B_o}\nabla\Phi_o\right)\Delta + q_g \; stb/d = \frac{Vb}{5.615}\frac{\partial}{\partial t} \qquad (2.75)$$

$$\left(\frac{\phi S_g}{B_g} + \frac{\phi S_o\ Rs}{B_o}\right)$$

donde

$$A = \Delta x \Delta z, \qquad V = \Delta x \Delta y \Delta z$$

Además del flujo de cada fase se tienen las siguientes ecuaciones auxiliares que corresponden a la presión capilar, ecuación de -

saturación y las ecuaciones del potencial.

$$- p_{c_{o-w}} = p_o - p_w \qquad (2.76)$$

$$- p_{c_{g-o}} = p_g - p_o \qquad (2.77)$$

$$- \quad 1 = So + Sw + Sg \qquad (2.78)$$

* Medio mojado por agua, donde generalmente $p_g > p_o > p_w$

Como se menciono anteriormente el comportamiento de la presión-capilar, se obtiene por medio del análisis petrofísico llevado a cabo en el laboratorio.

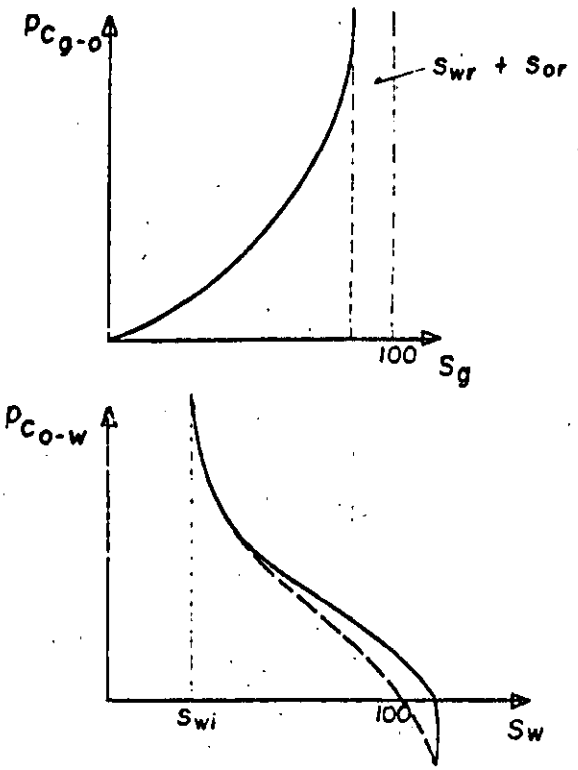

En algunas rocas $p_{c_{o-w}}$ se vuelve negativa, implicando un cambio de mojabilidad.

Relaciones de potencial.

$$\Phi_o = p_o - \frac{1}{144}\frac{g}{g_c}\rho_o D \qquad (2.79)$$

$$\Phi_w = p_w - \frac{1}{144}\frac{g}{g_c}\rho_w D \qquad (2.80)$$

$$\Phi_g = p_g - \frac{1}{144}\frac{g}{g_c}\rho_g D \qquad (2.81)$$

Con lo cual se tendrán 6 ecuaciones con 6 incógnitas y por lo tanto el sistema será compatible. Los parámetros que se deben determinar son: p_o, p_w, p_g, S_o, S_w y S_g.

2.7 CONDICIONES INICIALES Y CONDICIONES DE FRONTERA

a).- Condiciones iniciales.

Cuando una de las variables independientes en una ecuación diferencial parcial es el tiempo, se necesita conocer entre otras cosas, la variable dependiente a un tiempo t_o para obtener la solución de la ecuación a otros tiempos. A ésta se le llama condición inicial.

En simulación de yacimientos, generalmente la variable dependiente es la presión.

Las presiones y saturaciones deben ser conocidas al tiempo $t=t_o$.

Para determinar las condiciones anteriores, éstas se determinan a través de un ejemplo ilustrativo. Dadas las presiones del aceite, la saturación de agua y la saturación de gas.

$$S_g = 1 - S_o - S_w$$

$$p_w = p_o - p_{c_{o-w}} (Sw)$$

$$p_g = p_o - p_{c_{g-o}} (Sg)$$

En la práctica se debe proceder de la siguiente manera:

1.- Conocer el plano estructural y estratigráfico

2.- Conocer las profundidades de los contactos (g-o, w-o)

3.- Existencia y tamaño del acuífero (si es que existe)

4.- Propiedades pVT de los fluidos en función de la presión

5.- Curvas de presión capilar ($p_{c_{g-o}}$, $p_{c_{w-o}}$)

6.- Curvas de permabilidades relativas.

$$k_{rg} = k_{rg} (S_g)$$

$$k_{rw} = k_{rw} (S_w)$$

$$k_{ro} = k_{ro} (S_w, S_g)$$

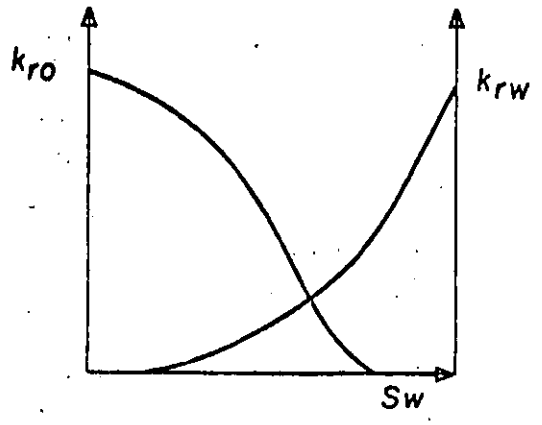

agua – aceite

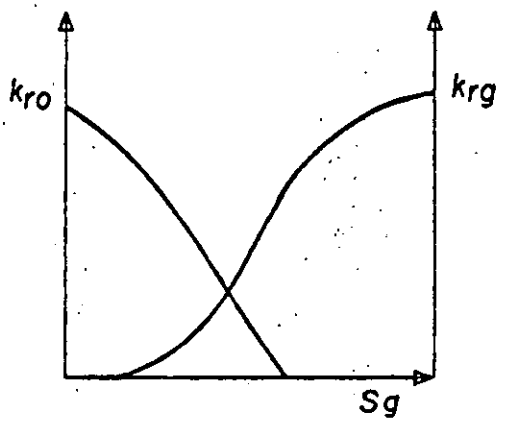

aceite - gas

En la actualidad no existe un equipo efectivo para determinar las permeabilidades relativas de 3 fases, lo que se hace es elaborar 2 gráficas utilizando 2 fluidos para cada una (g-o y w-o).

7.- Como último dato se requiere definir la presión en un plano de referencia.

Antes de entrar al análisis de fronteras, defínase algunos términos necesarios para su entendimiento.

+ Transmisividad (T)

La transmisividad se define como la capacidad de transmitir, dada por la siguiente ecuación:

$$q = T\, p,$$

de la ecuación de Darcy

$$q = - \frac{K}{\mu} \frac{A\, p}{L}$$

entonces

$$T = \frac{K}{\mu} \frac{A}{L}$$

b).- Condiciones de frontera.

Si se conoce la presión, y/o las primeras derivadas espaciales de la misma, en determinadas regiones de un yacimiento para todo valor del tiempo, a éstas se les conoce como condiciones de frontera.

Las fronteras son límites del yacimiento, que pueden estar abiertas o cerradas al flujo. De acuerdo a los problemas que se presentan en simulación de yacimientos, se consideran fronteras cerradas.

Frontera cerrada._ Frontera caracterizada por la inexistencia de flujo. Su cualidad fundamental esta dada por:

$\left(\frac{\partial p}{\partial \bar{n}} \neq 0 \right)$ = Condiciones de frontera de presión y/o gastos constantes.

$\bar{n}$ = Vector perpendicular a todas las superficies equipotenciales.

¿ Cómo cerrar las fronteras ?

Básicamente existen 2 formas de cerrar las fronteras cuando se utiliza una malla de bloques, y éstas son las siguientes:

1).- Evitar el flujo a través de toda la periferia, haciendo las transmisividades en dicha periferia igual a cero.

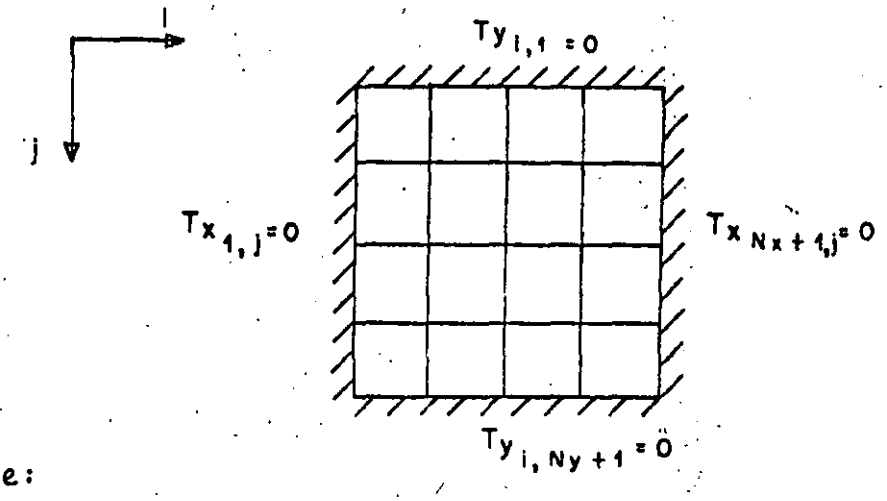

donde:

Nx = Número de bloques en la dirección "x"

Ny = Número de bloques en la dirección "y"

2).- La segunda forma se puede hacer a través de extender la malla agregando bloques virtuales externos a dicha frontera y haciendo los potenciales, permeabilidades, presiones, etc. de cada bloque agregado iguales a los del bloque interior inmediato adyacente. De tal forma que no haya cambio de bloque a bloque adyacente y el flujo sea cero.

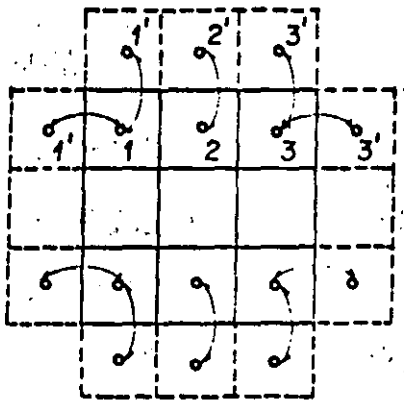

1 y 1' tienen las mismas caracterísiticas del bloque adyacente, es - decir:

$$\Phi_1 = \Phi_{1'}$$

$$k_1 = k_{1'}$$

por lo tanto el flujo de 1 a 1' es igual a cero.

La deficiencia de ésta segunda forma es que se genera una nueva- red o sea:

de $(Nx)\ (Ny)$ *a* $(Nx + 2)\ (Ny + 2) - 4$

$\therefore\ (Nx + 2)\ (Ny + 2) - 4 = 2(Ny + Nx) + Nx\,Ny - Nx\,Ny$

por lo que se agregaría un número considerable de ecuaciones.

POZOS INYECTORES O PRODUCTORES (término fuente)

+ Para un modelo areal

Si el ritmo de inyección es dato, se incluye como término fuente (sumidero) en la ecuación y se determinan las presiones y saturacio-- nes como en cualquier otro bloque.

Si se quiere determinar el gasto en función de formaciones se - - tendrá que relacionar la presión en el fondo con la presión de fondo-

fluyendo.

+ Para un modelo vertical o tridimensional.

Se debe dividir el gasto entre las capas "disparadas". Hay va--- rias formas de hacerlo, la más simple es dividir el ritmo total de - acuerdo al producto kh de cada bloque.

Por ejemplo.- Para 3 bloques (capas y un ritmo de inyección dado)

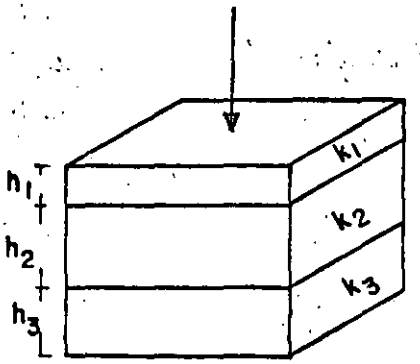

$$q_1 = \frac{K_1 \ h_1}{K_1 \ h_1 + K_2 \ h_2 + K_3 \ h_3} Q_T$$

$$q_2 = \frac{K2 \ h_2}{K_1 \ h_1 + K_2 \ h_2 + K_3 \ h_3} Q_T$$

$$q_3 = \frac{K_3 \ h_3}{K_1 \ h_1 + K_2 \ h_2 + K_3 \ h_3} Q_T$$

se puede presentar el caso de que Kx ≠ Ky ≠ Kz (anisotrópia).

Para propósito de dividir los gastos, solo se toma Kx y Ky.

Por lo que se puede calcular "K" de diferentes formas.

1.- Promedio aritmético

$$K_1 = 1/2\ (Kx_1 + Ky_1\ )$$

2.- Promedio geométrico

$$K_1 = \sqrt{\frac{Kx_1 \cdot Ky_1}{1}}$$

2.a

$$K_1 = \sqrt{\frac{Kx_1^2 + Ky_1^2}{2}}$$

3.- Promedio armónico

$$\frac{1}{K_1} = \frac{1}{2Kx_1} + \frac{1}{2Ky_1}$$

Ejemplo:

Dada K(150, 180, 10), calcular K_1

Solución:

1.- $K_1 = 1/2\ (150 + 180) = 165$

2.- $K_1 = \sqrt{150 \times 180} = 164.32$

2.a.- $K_1 = \sqrt{\frac{(150)^2 + (180)^2}{2}} = 165.68$

3.- $K_1 = \frac{1}{\frac{1}{2 \times 150} + \frac{1}{2 \times 180}} = 163.64$

Ejemplo No. 2: K (150,15,10)

Solución:

1.- $K_1 = 1/2\ (150 + 15) = 82.5$

2.- $K_1 = \sqrt{150 \times 15} = 47.43$

2.a.- $K_1 = \sqrt{\frac{(150)^2 + (15)^2}{2}} = 106.6$

3.- $K_1 = \frac{1}{\frac{1}{300} + \frac{1}{30}}$

De los ejemplos anteriores se puede concluir:

a).- Se puede utilizar cualquier forma cuando se tiene anisotropía.

b).- A través de experiencias se ha determinado que en anisotropías considerables, es recomendable el promedio geométrico para la permeabilidad horizontal del bloque.

2.8 REQUERIMIENTOS, DATOS GENERALES Y PREPARACION DE UN SIMULADOR

1).- Mapas básicos requeridos:

1.a.- Mapa estructural.- Sirve para determinar a través de las curvas de nivel, las profundidades de los pozos, efectos geológicos de subsuelo como fallas, así como la vista en planta del yacimiento, límites del mismo, contactos agua-aceite, gas-aceite y/o gas-agua.

1.b.- Mapa de isopacas.- Líneas que unen puntos en el yacimiento de igual espesor. Entre otras cosas, sirve para cuantificar volumétricamente ya sea el volúmen original de aceite y/o volúmen original de gas etc.

1.c.- Mapa de isoporosidades.- Por medio de núcleos y de registros geofísicos se determina la porosidad en ciertos puntos, los cua

-les son referidos a un plano. Posteriormente se interpola entre dichos valores para asignar un valor de porosidad a cada celda.

1.d.- Mapa de isopermeabilidades.- Igual al de isoporosidades, - la diferencia entre ellos es que en éste último se utilizan permeabilidades.

2).- Sistema de cuadricula de la malla.

Un sistema de cuadricula o sistema de celdas es sobrepuesto al -- plano estructural del yacimiento, siendo cada celda una unidad básica usada en el simulador de flujo de fluidos y calculos de balance - de materia para cada celda.

Algunos puntos básicos a considerar en la selección del sistema- de celdas es el siguiente:

a).- El sistema de la malla en toda su forma será rectangular.

b).- La malla contendrá la menor cantidad de bloques como sea posi-- ble, dependiendo de la heterogeneidad del yacimiento.

c).- La malla será correctamente orientada, clasificada según su tamaño y su forma para permitir una buena aproximación de los límites del yacimiento.

d).- Si existe permeabilidad direccional u orientada, un eje de la - malla estará en la dirección de máxima permeabilidad. Dicha permeabilidad podrá ser determinada por medio de pruebas de presión pruebas de pulso, etc.

e).- Tratar de colocar un pozo por bloque y en el centro del mismo.

f).- Si la existencia de un acuífero es conocida o si el flujo de -- agua es sospechado, el sistema de malla incluirá hileras extras de celdas a cubrir el acuífero para simular el flujo del agua.

C O N T E N I D O

CAPITULO 3 METODO DE DIFERENCIAS FINITAS

C A P I T U L O 3

3.1 INTRODUCCION

Las ecuaciones que representan el flujo de fluidos en medios porosos son en general ecuaciones diferenciales parciales no lineales, las cuales relacionan cambios de presión y saturación con el tiempo a través del medio. Esas ecuaciones son extremadamente complejas; y la obtención de una solución se complica por la presencia de condiciones de límite (de frontera) especializadas.

La solución de esas ecuaciones por medios analíticos, es generalmente imposible, excepto para casos triviales. La solución numérica de esas ecuaciones es generalmente el único camino para que una solución pueda ser obtenida en la mayoría de las aplicaciones. Para resolver numéricamente estas ecuaciones se procede a usar algunos de los métodos de solución, entre los cuales se encuentran los siguientes:

a).- Métodos de diferencias finitas.

La solución numérica de las ecuaciones presenta respuestas a puntos discretos dentro del sistema. La transformación de una ecuación diferencial (continua) a una forma discreta se hace por el uso de diferencias finitas.

b).- Métodos variacionales.

Estos métodos no tan solo resuelven las ecuaciones en puntos discretos, sino además aproximan las soluciones por medio de un conjunto de polinomios de diversos grados. Dentro de estos métodos se encuentra el método de Galerkin.

Estos métodos son muy utilizados en la solución de problemas que consideran flujo de calor, esfuerzos generados por cambios de temperatura, etc.

3.2 SERIE DE TAYLOR

La serie de Taylor es el principio básico usado en la derivación de las fórmulas de aproximación en diferencias finitas.

Sea una función $f(x)$, el valor de esta función expandida alrededor de un punto A cualquiera, está dado por:

$$f(x) = a_o + a_1 (x-a) + a_2 (x-a)^2 + a_3 (x-a)^3 + \ldots\ldots \qquad (3.1)$$

en donde las incognitas son las constantes $a_0, a_1, a_2, \ldots\ldots a_n$. La obtención de estos valores se logra derivando sucesivamente la función original:

$$f'(x) = a_1 + 2a_2 (x-a)^1 + 3a_3 (x-a)^2 + 4a_4 (x-a)^3 + \ldots$$

$$f''(x) = 2a_2 + 3.2a_3 (x-a)^1 + 4.3a_4 (x-a)^2 + 5.4a_5 (x-a)^3 + \ldots$$

$$f'''(x) = 3.2.1a_3 + 4.3.2a_4 (x-a)^1 + 5.4.3a_5 (x-a)^2 + \ldots\ldots$$

$$\vdots$$

$$f^n(x) = n!\, a_n + (n-1)!\, a_{n-1} (x-a) + \ldots\ldots\ldots\ldots\ldots$$

Ahora, evaluando las derivadas en el punto $x=a$ y despejando se obtendrán los valores de los coeficientes a_i :

$$a_0 = f(x)$$

$$a_1 = \frac{f'(a)}{1!}$$

$$a_2 = \frac{f''(a)}{2!}$$

$$a_3 = \frac{f'''(a)}{3.2.1} = \frac{f'''(a)}{3!}$$

$$\vdots$$

$$a_n = \frac{f^n(a)}{n!}$$

Sustituyendo en la ecuación (3-1) el valor de los coeficientes encontrados, se tendrá:

$$f(x) = f(a) + \frac{f'(a)}{1!}(x-a) + \frac{f''(a)}{2!}(x-a)^2 + \frac{f'''(a)}{3!}(x-a)^3 \ldots$$

$$+ \frac{f^n(a)}{n!}(x-a)^n$$

Para obtener una aproximación adecuada evaluando el menor número posible de términos de la serie es necesario que, para el enésimo término $(x-a)^n < n!$ (y/o que la enésima derivada sea pequeña).

Por lo tanto si se quieren considerar un número reducido de términos es necesario que $(x-a)$ sea pequeña.

3.3 SERIES DE MC. LAURIN

La serie de Mc. Laurin de una función se genera expandiendo la misma alrededor del punto $a = 0$.

$$f(x) = f(0) + f'(0)\,x + f''(0)\,\frac{x^2}{2!} + f'''(0)\,\frac{x^3}{3!} + \cdots + f^{n}(0)\,\frac{x^n}{n!} \qquad (3.3)$$

Ejemplo:

$$y = f(x) = \operatorname{sen} 18^\circ$$

Evaluando la función y sus derivadas en el punto a=0, y tomando en consideración que 18° son π/10 radianes:

$$\begin{aligned}
y &= \operatorname{sen} x = 0\\
y' &= \cos x = 1\\
y'' &= -\operatorname{sen} x = 0\\
y''' &= -\cos x = -1\\
y'''' &= \operatorname{sen} x = 0\\
y''''' &= \cos x = 1\\
y'''''' &= -\operatorname{sen} x = 0\\
y''''''' &= -\cos x = -1\\
y'''''''' &= \operatorname{sen} x = 0
\end{aligned}$$

Entonces

$$f(\pi/10) = 0 + \frac{\pi}{10} + 0 - \frac{1}{6}(\pi/10)^3 + 0 + \frac{1}{120}(\pi/10)^5 + 0 - \frac{1}{7!}(\pi/10)^7$$

$$f(\pi/10) = 0.314159265 - 0.005167713 + 0.00002502$$

$$f(\pi/10) = 0.309016994$$

3.4. APLICACION DE LA SERIE DE TAYLOR EN LA EVALUACION DE DERIVADAS

Considérese el intervalo 0,1 dividiendo en R subintervalos de longitud x.

$$x = \frac{1}{R}$$

En un punto cualquiera x_i :

$x_i = i\,\Delta x$, y obviamente

$$x_{i+1} = x_i + \Delta x$$

$$x_{i-1} = x_i - \Delta x$$

La distancia entre dos puntos consecutivos es la "Diferencia finita x.

En el método de "Diferencias Finitas" la evaluación de las funciones, y sus derivadas se efectúa solamente en los puntos x_i, $i = 0,1,2,\ldots\ldots R$.

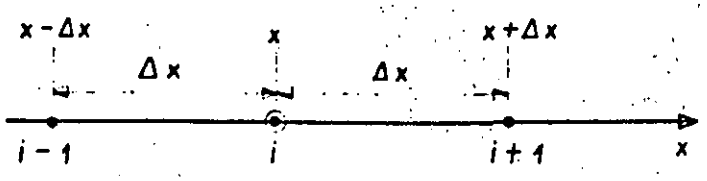

$$\therefore R = \frac{1}{\Delta x}$$

$$x - \Delta x \approx i - 1$$

$$x + \Delta x \approx i + 1$$

3.4.1 SERIES DE TAYLOR EN UNA DIMENSION

Utilizando la notación anterior las expansiones en serie de Taylor para una función $f(x)$, *en los puntos* x_{i+1} *y* x_{i-1} *se escriben como:*

$$f_{i+1} = f_i + \Delta x \left.\frac{\partial f}{\partial x}\right|_i + \frac{(\Delta x)^2}{2!}\left.\frac{\partial^2 f}{\partial x^2}\right|_i + \frac{(\Delta x)^3}{3!}\left.\frac{\partial^3 f}{\partial x^3}\right|_i + \ldots + \frac{(\Delta x)^n}{n!}\left.\frac{\partial^n f}{\partial x^n}\right|_i \qquad (3.4)$$

$$f_{i-1} = f_i - \Delta x \left.\frac{\partial f}{\partial x}\right|_i + \frac{(\Delta x)^2}{2!}\left.\frac{\partial^2 f}{\partial x^2}\right|_i - \frac{(\Delta x)^3}{3!}\left.\frac{\partial^3 f}{\partial x^3}\right|_i + \ldots + \frac{(\Delta x)^n}{n!}\left.\frac{\partial^n f}{\partial x^n}\right|_i \qquad (3.5)$$

3.4.1.1 PRIMERA DERIVADA

La expresión de la primera derivada, se obtiene despejando la ecuación (3.4) en términos de dicha derivada:

$$\left.\frac{\partial f}{\partial x}\right|_i = \frac{f_{i+1} - f_i}{\Delta x} - \frac{\Delta x}{2!}\left.\frac{\partial^2 f}{\partial x^2}\right|_i - \frac{(\Delta x)^2}{3!}\left.\frac{\partial^3 f}{\partial x^3}\right|_i + \ldots \qquad (3.6)$$

la cual tiene un error de truncamiento de segundo orden,

$$\left.\frac{\partial f}{\partial x}\right|_i = \frac{f_{i+1} - f_{i-1}}{2\Delta x} + O(\Delta x^2) \qquad (3.11)$$

Procediendo en forma análoga se pueden obtener fórmulas de mayor precisión para la primera derivada, expandiendo la función en otros puntos cercanos al punto x, por ejemplo:

$$f_{i+2} = f_i + (2\Delta x)\left.\frac{\partial f}{\partial x}\right|_i + \frac{(2\Delta x)^2}{2!}\left.\frac{\partial^2 f}{\partial x^2}\right|_i + \frac{(2\Delta x)^3}{3!}\left.\frac{\partial^3 f}{\partial x^3}\right|_i + \frac{(2\Delta x)^4}{4!}\left.\frac{\partial^4 f}{\partial x^4}\right|_i \cdots\cdots\cdots \qquad (3.12)$$

$$f_{i-2} = f_i - (2\Delta x)\left.\frac{\partial f}{\partial x}\right|_i + \frac{(2\Delta x)^2}{2!}\frac{\partial^2 f}{\partial x^2} - \frac{(2\Delta x)^3}{3!}\frac{\partial^3 f}{\partial x^3} + \frac{(2\Delta x)^4}{4!}\frac{\partial^4 f}{\partial x^4} \qquad (3.13)$$

3.4.1.2 SEGUNDA DERIVADA

Una expresión de la segunda derivada se obtiene sumando las ecuaciones (3.4) y (3.5) :

$$f_{i+1} + f_{i-1} = 2f_i + (\Delta x)^2\left.\frac{\partial^2 f}{\partial x^2}\right|_i + \frac{(\Delta x)^4}{12}\left.\frac{\partial^4 f}{\partial x^4}\right|_i + \cdots\cdots \qquad (3.14)$$

en donde el término del error es de segundo orden

$$\left.\frac{\partial^2 f}{\partial x^2}\right|_i = \frac{f_{i+1} - 2f_i + f_{i-1}}{(\Delta x)^2} - \frac{(\Delta x)^2}{12}\left.\frac{\partial^4 f}{\partial x^4}\right|_i + \ldots = \frac{f_{i+1} - 2f_i + f_{i-1}}{(\Delta x)^2}$$

$$+ \Theta(\Delta x)^2 \qquad (3.15)$$

3.4.2 SERIE DE TAYLOR EN DOS DIMENSIONES

Para la obtención de fórmulas en diferencias finitas que involucren dos dimensiones, se puede utilizar la expansión de la serie de Taylor, en dos dimensiones:

$$f_{i\pm1,j\pm1} = f_{i,j} + (\pm\Delta x)\left.\frac{\partial f}{\partial x}\right|_{i,j} + (\pm\Delta y)\left.\frac{\partial f}{\partial y}\right|_{i,j} +$$

$$\frac{(\pm\Delta x)^2}{2!}\left.\frac{\partial^2 f}{\partial x^2}\right|_{i,j} + (\pm\Delta x)(\pm\Delta y)\left.\frac{\partial^2 f}{\partial x\,\partial y}\right|_{i,j} + \frac{(\pm\Delta y)^2}{2!}\left.\frac{\partial^2 f}{\partial y^2}\right|_{i,j}$$

$$+ \ldots\ldots \qquad (3.16)$$

Otra alternativa, generalmente más sencilla se logra utilizando las fórmulas de una dimensión, haciendo variar la función en una dirección y manteniendo los subíndices de las otras direcciones constantes, por ejemplo; la expansión de la función $f(x,y)$ en el punto $(i+1,j+1)$ se puede obtener por ejemplo expandiendo primero en la en la dirección "x", manteniendo constantes los índices de la dirección "y", ejemplo:

$$f_{i+1,j+1} = \underset{(1)}{f_{i,j+1}} + \underset{(2)}{\Delta x\left.\frac{\partial f}{\partial x}\right|_{i,j+1}} + \underset{(3)}{\frac{(\Delta x)^2}{2!}\left.\frac{\partial^2 f}{\partial x^2}\right|_{i,j+1}} +$$

$$\underset{(4)}{\frac{(\Delta x)^3}{3!}\left.\frac{\partial^3 f}{\partial x^3}\right|_{i,j+1}} + \ldots\ldots\ldots \qquad (3.17)$$

Nótese que la función y las derivadas están evaluadas en (i+1, j) es decir en el punto $(x, y+\Delta y)$, por lo tanto es necesario expandir nuevamente cada uno de los términos numerados, manteniendo ahora constantes los índices en la dirección "x" y variar los índices en la dirección "y";

$$(1)\quad \delta_{i,j+1} = \delta_{i,j} + \Delta y \left.\frac{\partial \delta}{\partial y}\right|_{i,j} + \frac{(\Delta y)^2}{2!} \left.\frac{\partial^2 \delta}{\partial y^2}\right|_{i,j} + \qquad (3.18)$$

$$(2)\quad \left.\frac{\partial \delta}{\partial x}\right|_{i,j+1} = \left.\frac{\partial \delta}{\partial x}\right|_{i,j} + \Delta y \left.\frac{\partial^2 \delta}{\partial x \partial y}\right. + \frac{(\Delta y)^3}{3!} \left.\frac{\partial^3 \delta}{\partial x \partial y^2}\right|_{i,j} + \ldots$$

$$\ldots\ldots\ldots \qquad (3.19)$$

$$(3)\quad \left.\frac{\partial \delta}{\partial x}\right|_{i,j+1} = \left.\frac{\partial^2 \delta}{\partial x^2}\right|_{i,j} + \Delta y \left.\frac{\partial^3 \delta}{\partial x^2 \partial y}\right. + \frac{(\Delta y)^3}{2!} \left.\frac{\partial^4 \delta}{\partial x^2 \partial y^2}\right|_{i,j} + .$$

$$\ldots\ldots\ldots \qquad (3.20)$$

La expresión final se obtiene cuando los índices de la función y sus derivadas son precisamente (i,j), en este caso:

$$\delta_{i\pm1,j\pm1} = \delta_{i,j} \pm (\pm\Delta x)\frac{\partial \delta}{\partial x} + (\pm\Delta y)\frac{\partial \delta}{\partial y} + \frac{(\Delta x)^2}{2!}\frac{\partial^2 \delta}{\partial x^2} + \ldots\ldots \qquad (3.21)$$

3.4.3 SERIE DE TAYLOR EN TRES DIMENSIONES

La expansión de una función en tres dimensiones se logra en una forma análoga a la anterior o mediante la expansión de la serie de-

Taylor en tres direcciones i, j, k:

$$\phi_{i\pm1,j\pm1,k\pm1} = \phi_{i,j,k} + \left(\pm \Delta x \frac{\partial}{\partial x} \pm \Delta y \frac{\partial}{\partial y} \pm \Delta z \frac{\partial}{\partial z}\right) \phi_{i,j,k}$$

$$+ \frac{1}{2!} \left(\pm \Delta x \frac{\partial}{\partial x} \pm \Delta y \frac{\partial}{\partial y} \pm \Delta z \frac{\partial}{\partial z}\right)^2 \phi_{i,j,k}$$

$$+ \frac{1}{3!} \left(\pm \Delta x \frac{\partial}{\partial x} \pm \Delta y \frac{\partial}{\partial y} \pm \Delta z \frac{\partial}{\partial z}\right)^3 \phi_{i,j,k}$$

$$+ \ldots\ldots\ldots \qquad (3.22)$$

3.5 METODO DE GREENSPAN

Este método es útil para encontrar expresiones de cualquier derivada en términos de valores de la función, en los puntos cercanos en-cuestión. El método consiste en asociar a cada uno de los puntos se--leccionados una constante, la cual se valua posteriormente.

A continuación se presentan varios ejemplos para ilustrar la aplicación del método.

73

3.5.1 INTERVALOS IGUALES

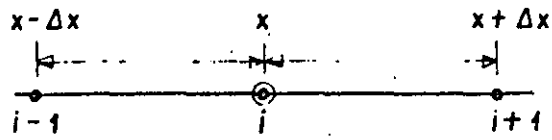

Ejemplo No. 1

Encontrar la expresión para la primera derivada de la función u en términos de los valores de la función en los puntos i, c, i + 1.

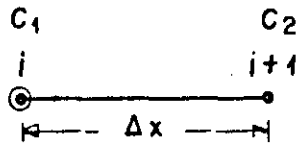

PROCEDIMIENTO.

1) *Asignar las constantes a los puntos i, e, i + 1.*

$$\left.\frac{\partial u}{\partial x}\right|_i = C_1 u_i + C_2 u_{i+1} + e_t$$

2) *Para valuar* C_1 *y* C_2, *expandimos por series de Taylor.*

$$\left.\frac{\partial u}{\partial x}\right|_i = C_1 u_i + C_2 \left[u_i + \Delta x \left.\frac{\partial u}{\partial x}\right|_i + \frac{(\Delta x)^2}{2!} \left.\frac{\partial^2 u}{\partial x^2}\right|_i \right] + e_t$$

$$\left.\frac{\partial u}{\partial x}\right|_i = (C_1 + C_2)\, u_i + C_2\, \Delta x \left.\frac{\partial u}{\partial x}\right|_i + C_2 \frac{(\Delta x)^2}{2!} \left.\frac{\partial^2 u}{\partial x^2}\right|_i + e_t$$

3) *Igualar coeficientes para obtener los valores de las constantes y del error de truncamiento. (lado izquierdo y lado derecho de la ecuación).*

$$C_1 + C_2 = 0, \quad \Delta x C_2 = 1 \qquad C_1 = -C_2 = -\frac{1}{\Delta x}, \quad C_2 = \frac{1}{\Delta x}$$

$$C_2 \frac{(\Delta x)^2}{2!} \frac{\partial^2 u}{\partial x^2}\bigg|_i + e_t = 0 \quad \therefore \quad e_t = -C_2 \frac{(\Delta x)^2}{2!} \frac{\partial^2 u}{\partial x^2}\bigg|_i$$

$$e_t = -\frac{1}{\Delta x} \frac{(\Delta x)^2}{2!} \frac{\partial^2 u}{\partial x^2}\bigg|_i = -\frac{\Delta x}{2} \frac{\partial^2 u}{\partial x^2}\bigg|_i \quad \therefore e_t = \text{término del error.}$$

4) *Substituir los valores obtenidos en la ecuación en donde aparezcan las constantes.*

$$\frac{\partial u}{\partial x}\bigg|_i = -\frac{u_i}{\Delta x} + \frac{u_{i+1}}{\Delta x} - \frac{\Delta x}{2} \frac{\partial^2 u}{\partial x^2}\bigg|_i$$

$$\frac{\partial u}{\partial x}\bigg|_i = \frac{u_{i+1} - u_i}{\Delta x} + O(\Delta x)$$

EJEMPLO No. 2

Expresar la segunda derivada mixta de una función en términos de los valores de la función en los puntos $i + 1$,

$j + 1$; $i + 1$, $j - 1$; $i - 1$, $j - 1$; $i - 1$, $j + 1$.

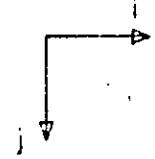

C_3 $i-1, j-1$ $\qquad$ C_2 $i+1, j-1$

i, j

C_4 $i-1, j+1$ $\qquad$ C_1 $i+1, j+1$

1er paso. Expresar lo anterior matemáticamente:

$$\frac{\partial^2 u}{\partial x \partial y} = C_1 \left[u_{i,j} + (\Delta x) \left.\frac{\partial u}{\partial x}\right|_{i,j} + (\Delta y) \left.\frac{\partial u}{\partial y}\right|_{i,j} + \frac{(\Delta x)^2}{2!} \left.\frac{\partial^2 u}{\partial x^2}\right|_{i,j} \right.$$

$$+ (\Delta x)(\Delta y) \left.\frac{\partial^2 u}{\partial x \partial y}\right|_{i,j} + \frac{(\Delta y)^2}{2!} \left.\frac{\partial^2 u}{\partial y^2}\right|_{i,j} + \frac{(\Delta x)^3}{3!} \left.\frac{\partial^3 u}{\partial x^3}\right|_{i,j}$$

$$\left. + \frac{3(\Delta x)^2 (\Delta y)}{3!} \left.\frac{\partial^3 u}{\partial x^2 \partial y}\right|_{i,j} + \frac{3(\Delta x)(\Delta y)^2}{3!} \left.\frac{\partial^3 u}{\partial x \partial y^2}\right|_{i,j} + \frac{(\Delta y)^3}{3!} \left.\frac{\partial^3 u}{\partial y^3}\right|_{i,j} \right]$$

$$+ C_2 \left[u_{i,j} + (\Delta x) \left.\frac{\partial u}{\partial x}\right|_{i,j} - (\Delta y) \left.\frac{\partial u}{\partial y}\right|_{i,j} + \frac{(\Delta x)^2}{2!} \left.\frac{\partial^2 u}{\partial x^2}\right|_{i,j} \right.$$

$$- (\Delta x)(\Delta y) \left.\frac{\partial^2 u}{\partial x \partial y}\right|_{i,j} - \frac{(\Delta y)^2}{2!} \left.\frac{\partial^2 u}{\partial y^2}\right|_{i,j} + \frac{(\Delta x)^3}{3!} \left.\frac{\partial^3 u}{\partial x^3}\right|_{i,j}$$

$$\left. - \frac{3(\Delta x)^2 (\Delta y)}{3!} \left.\frac{\partial^3 u}{\partial x^2 \partial y}\right|_{i,j} + \frac{3(\Delta x)(\Delta y)^2}{3!} \left.\frac{\partial^3 u}{\partial x \partial y^2}\right|_{i,j} - \frac{(\Delta y)^3}{3!} \left.\frac{\partial^3 u}{\partial y^3}\right|_{i,j} \right]$$

$$+ C_3 \left[u_{i,j} - (\Delta x) \left.\frac{\partial u}{\partial x}\right|_{i,j} - (\Delta y) \left.\frac{\partial u}{\partial y}\right|_{i,j} + \frac{(\Delta x)^2}{2!} \left.\frac{\partial^2 u}{\partial x^2}\right|_{i,j} \right.$$

$$- (\Delta x)(\Delta y) \left.\frac{\partial^2 u}{\partial x \partial y}\right|_{i,j} + \frac{(\Delta y)^2}{2!} \left.\frac{\partial^2 u}{\partial y^2}\right|_{i,j} - \frac{(\Delta x)^3}{3!} \left.\frac{\partial^3 u}{\partial x^3}\right|_{i,j}$$

$$\left. - \frac{3(\Delta x)^2 (\Delta y)}{3!} \left.\frac{\partial^3 u}{\partial x^2 \partial y}\right|_{i,j} - \frac{3(\Delta x)(\Delta y)^2}{3!} \left.\frac{\partial^3 u}{\partial x \partial y^2}\right|_{i,j} - \frac{(\Delta y)^3}{3!} \left.\frac{\partial^3 u}{\partial y^3}\right|_{i,j} \right]$$

$$+ C_4 \left[u_{i,j} - (\Delta x) \left.\frac{\partial u}{\partial x}\right|_{i,j} + (\Delta y) \left.\frac{\partial u}{\partial y}\right|_{i,j} + \frac{(\Delta x)^2}{2!} \left.\frac{\partial^2 u}{\partial x^2}\right|_{i,j} \right.$$

$$- (\Delta x)(\Delta y) \left.\frac{\partial^2 u}{\partial x \partial y}\right|_{i,j} + \frac{(\Delta y)^2}{2!} \left.\frac{\partial^2 u}{\partial y^2}\right|_{i,j} - \frac{(\Delta x)^3}{3!} \left.\frac{\partial^3 u}{\partial x^3}\right|_{i,j}$$

$$+ \frac{3(\Delta x)^2\,(\Delta y)}{3!}\left.\frac{\partial^3 u}{\partial x^2 \partial y}\right|_{i,j} - \frac{3(\Delta x)\,(\Delta y)^2}{3!}\left.\frac{\partial^3 u}{\partial x \partial y^2}\right|_{i,j} + \frac{(\Delta y)^3}{3!}\left.\frac{\partial^3 u}{\partial y^3}\right|_{i,j} \Big]$$

$$\frac{\partial^2 u}{\partial x \partial y} = u_{i,j}\,\underset{(1)}{(C_1+C_2+C_3+C_4)} + \left.\frac{\partial u}{\partial x}\right|_{i,j}\,\underset{(2)}{\{\Delta x\,(C_1+C_2-C_3-C_4)\}}$$

$$+ \left.\frac{\partial u}{\partial x}\right|_{i,j}\,\underset{(3)}{\{\Delta y\,(C_1-C_2-C_3+C_4)\}} + \frac{\partial^2 u}{\partial x^2}\,\underset{(1)}{\left\{\frac{(\Delta x)^2}{2!}\,(C_1+C_2+C_3+C_4)\right\}}$$

$$+ \left.\frac{\partial^2 u}{\partial x \partial y}\right|_{i,j}\,\underset{(4)}{\{(\Delta x)\,(\Delta y)\,(C_1-C_2+C_3-C_4)\}} + \frac{\partial^2 u}{\partial y^2}\,\underset{(1)}{\left\{\frac{(\Delta y)^2}{2}\,(C_1+C_2+C_3+C_4)\right\}}$$

$$+ \left.\frac{\partial^3 u}{\partial x^3}\right|_{i,j}\,\underset{(2)}{\left\{\frac{(\Delta x)^3}{3!}\,(C_1+C_2-C_3-C_4)\right\}} + \frac{\partial^3 u}{\partial x^2 \partial y}\,\underset{(3)}{\left\{\frac{(\Delta x)^2\,(\Delta y)}{2!}\,(C_1-C_2-C_3+C_4)\right\}}$$

$$+ \left.\frac{\partial^3 u}{\partial x^2 \partial y}\right|_{i,j}\,\underset{(2)}{\left\{\frac{(\Delta x)\,(\Delta y)^2}{2!}\,(C_1+C_2-C_3-C_4)\right\}} + \left.\frac{\partial^3 u}{\partial y^3}\right|_{i,j}\,\underset{(3)}{\left\{\frac{(\Delta y)^3}{3!}\,(C_1-C_2-C_3+C_4)\right\}} + e_t$$

Igualando los coeficientes de los términos análogos en ambos lados de la ecuación, se tiene:

$$C_1 + C_2 + C_3 + C_4 = 0 \qquad (1)$$

$$C_1 + C_2 - C_3 - C_4 = 0 \qquad (2)$$

$$C_1 - C_2 - C_3 + C_4 = 0 \qquad (3)$$

$$\Delta x\ \Delta y (C_1 - C_2 + C_3 - C_4) = 1 \qquad (4)$$

- Sumando (1) y (2)

$$2\ C_1 + 2\ C_2 = 0$$

donde $C_1 + C_2 = 0$ por lo que $C_1 = - C_2$

- Sumando (2) + (3)

$$2\ C_1 - 2\ C_3 = 0$$

por lo que $C_1 = C_3$

- Sumando (1) + (3)

$$2\ C_1 + 2\ C_4 = 0$$

por lo que $C_1 = - C_4$

- Sustituyendo en (4)

$$C_1 + C_1 + C_1 + C_1 = \frac{1}{\Delta x \Delta y}$$

$$\therefore \quad 4\ C_1 = \frac{1}{\Delta x \Delta y}$$

por lo que $C_1 = \dfrac{1}{4 \Delta x \Delta y}$

$$C_2 = - \frac{1}{4 \Delta x \Delta y}\ ,\ C_3 = \frac{1}{4 \Delta x \Delta y}\ y\ C_4 = - \frac{1}{4 \Delta x \Delta y}$$

Sustituyendo en la ecuación inicial y reduciendo términos:

$$\frac{\partial^2 u}{\partial x \partial y} = \frac{u_{i+1,j+1} - u_{i+1,j-1} + u_{i-1,j-1} - u_{i-1,j+1}}{4\ \Delta x\ \Delta y} + O(\Delta x \Delta y)$$

3.5.2 INTERVALOS DESIGUALES

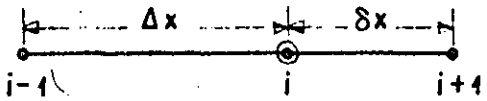

Otra aplicación de las series de Taylor es para intervalos desiguales.

EJEMPLO No. 3

Expresar la primera derivada de la función "u" en el punto "i" en términos de los valores de la función en los puntos "i + 1", "i - 1" (nótese que $\Delta x \neq \delta x$).

Expresando el problema en forma matemática

$$\left.\frac{\partial u}{\partial x}\right|_i = C_1 u_{i-1} + C_2 u_i + C_3 u_{i+1} + e_t$$

expandiendo la función "u" por medio de las series de Taylor, valuada en los puntos "i + 1" , "i - 1"

$$\left.\frac{\partial u}{\partial x}\right| = C_1 \left[u_i - \Delta x \left.\frac{\partial u}{\partial x}\right|_i + \frac{(\Delta x)^2}{2!} \left.\frac{\partial^2 u}{\partial x^2}\right|_i - \frac{(\Delta x)^3}{3!} \left.\frac{\partial^3 u}{\partial x^3}\right|_i \cdots \right]$$

$$+ C_2 u_i$$

$$+ C_3 \left[u_i + \delta x \left.\frac{\partial u}{\partial x}\right|_i + \frac{(\delta x)^2}{2!} \left.\frac{\partial^2 u}{\partial x^2}\right|_i + \frac{(\delta x)^3}{3!} \left.\frac{\partial^3 u}{\partial x^3}\right|_i + \cdots \right]$$

$$+ e_t$$

$$\left.\frac{\partial u}{\partial x}\right|_i = (C_1+C_2+C_3)\,u_i + (C_3\,\delta x - C_1\Delta x)\left.\frac{\partial u}{\partial x}\right|_i + \left(C_1\frac{(\Delta x)^2}{2} + C_3\frac{(\delta x)^2}{2}\right)$$

$$\left.\frac{\partial^2 u}{\partial x^2}\right|_i + \left(C_3\frac{(\delta x)^3}{3!} - C_1\frac{(\Delta x)^3}{3!}\right)\frac{\partial^3 u}{\partial x^3} + e_t$$

Igualando los coeficientes de los términos análogos en ambos lados de la ecuación:

$$C_1 + C_2 + C_3 = 0 \qquad (1)$$

$$C_3\,\delta x - C_1\,\Delta x = 1 \qquad (2)$$

$$C_1\frac{(\Delta x)^2}{2} + C_3\frac{(\delta x)^2}{2} = 0 \qquad (3)$$

De la ecuación (1) :

$$C_2 = -C_1 - C_3 \qquad (4)$$

De la ecuación (3) :

$$C_1 = -C_3\frac{(\delta x)^2}{(\Delta x)^2} \qquad (5)$$

Sustituyendo (5) en (4)

$$C_2 = C_3\frac{(\delta x)^2}{(\Delta x)^2} - C_3 \qquad (6)$$

Sustituyendo (5) en (2)

$$C_3\delta x + C_3\frac{(\delta x)^2}{(\Delta x)^2}\Delta x = 1 \qquad (7)$$

Despejando C_3

$$C_3\left[\frac{\Delta x\,\delta x + (\delta x)^2}{\Delta x}\right] = 1$$

$$C_3 = \frac{\Delta x}{\delta x\ \Delta x + (\delta x)^2}$$

Consecuentemente

$$C_2 = \frac{\delta x - \Delta x}{(\Delta x)\ (\delta x)} \qquad y \qquad C_1 = \frac{-\delta x}{\Delta x\ \delta x + (\Delta x)^2}$$

nótese que para el caso en que $\Delta x = \delta x$, las constantes se simplifican a:

$$C_1 = \frac{1}{-2\Delta x}\ ,\ C_3 = \frac{1}{2\Delta x}$$

y la fórmula para la primera derivada para el caso de intervalos uniformes se escribe como:

$$\left.\frac{\partial u}{\partial x}\right|_i = \frac{u_{i+1} - u_i + u_{i-1}}{2\Delta x} + O(\Delta x)^2$$

por lo tanto la fórmula buscada se expresa como:

$$\left.\frac{\partial u}{\partial x}\right|_i = \frac{(\Delta x)^2 u_{i+1} - (\delta x)^2 u_{i-1} + \{(\delta x)^2 - (\Delta x)^2\} u_i}{(\delta x + \Delta x)\Delta x \delta x} + e_t$$

3.6 RESOLUCION POR TABLA (Fórmulas de Bickley)

En las ecuaciones (3.4.1.1) y (3.4.1.2) se obtuvieron las aproximaciones de la primera y segunda derivada. En aquellos casos en que se desee incrementar el grado de aproximación (disminuir el término del error) se deben usar más puntos. El manejo de un mayor número de

términos y expansiones en series de Taylor, incrementa la posibilidad de errores algebraicos.

Para obviar las posibilidades de error, Bickley compiló una tabla con los coeficientes de la fórmula siguiente:

$$\left.\frac{d^k f(x)}{dx^k}\right|_{x=x_n} = \frac{k!}{m!h^k} \sum_{j=0}^{m} A_j f(x_j) \qquad (3.23)$$

A_j = coeficientes dados en la tabla siguiente

$h = \Delta x$

k = orden de la derivada

m = número de puntos que se desea usar en la aproximación, menos uno

n = número del punto en el que evalua la derivada

$f(x_j)$ = función evaluada en cada punto.

EJEMPLO No. 4

Obtener una aproximación en la primera derivada, en el punto i, usando 3 puntos por medio de la tabla de Bickley.

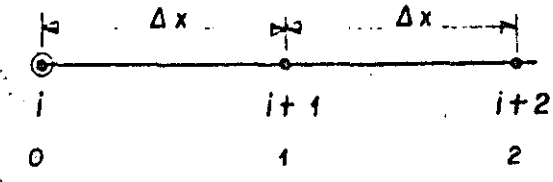

Nótese que los puntos en cuestión se numeran de izquierda a derecha comenzando con cero. Así, el punto "i" le corresponde el cero, al punto "$i + 1$" el número uno y al punto "$i + 2$" el número dos.

Por lo tanto en este caso el orden de la derivada el primero $k=1$.

El valor de "m" es "2" ya que es igual al número de puntos a usar (3) menos uno. Finalmente, ya que se desea evaluar la derivada en el punto "i" "n" es cero.

Aplicando la fórmula :

$$\left.\frac{df}{dx}\right|_{x = x_i} = \frac{1!}{2!(\Delta x)^1} \left[A_0 f_0 + A_1 f_1 + A_2 f_2 + e_t \right]$$

de la tabla I

Con los datos de primera derivada ($k = 1$), $m = 2$ y $n = 0$ se obtienen los valores de los coeficientes A_0, A_1, A_2 y el término del error.

$$A_0 = -3,\ A_1 = 4 \quad A_2 = -1 \quad y \quad e_t = \frac{1}{3}(\Delta x)^3 \left.\frac{d^3 f}{dx^3}\right|_\zeta$$

Sustituyendo estos valores en la ecuación se tiene:

$$\left.\frac{df}{dx}\right|_{x = x_i} = \frac{1}{2\Delta x}\left[-3f_0 + 4f_1 - f_2 + \frac{1}{3}(\Delta x)^3 \left.\frac{d^3 f}{dx^3}\right|_\zeta \right]$$

y en la notación original la fórmula para la primera derivada se expresa como:

$$\left.\frac{df}{dx}\right|_{x = x_i} = \frac{-3f_i + 4f_{i+1} - f_{i+2}}{2\Delta x} + \frac{1}{6}(\Delta x) \left.\frac{d^3 f}{dx^3}\right|_\zeta$$

Nota:

la $\frac{d^3 f}{dx^3}$ del término del error se evalua en el intervalo i, $i + 2$,-

es decir $x_1 \leq \zeta \leq x_{i+2}$, no se evalua en i.

EJEMPLO No. 5

Obtener una expresión para la segunda derivada de f evaluada en el punto $x = x_i$ utilizando 6 puntos. ($x_i = 2$)

Asignando primero el orden a los puntos

0	1	2	3	4	5
.	.	⊙	.	.	.
i-2	i-1	i	i+1	i+2	i+3

evaluando los parámetros k, m y n:

$k = 2$

$m = 6 - 1 = 5$

$n = 2$

De la tabla de Bickley se obtiene:

$$A_0 = -5,\ A_1 = 80,\ A_2 = -150,\ A_3 = 80,\ A_4 = -5,\ A_5 = 0$$

Expandiendo la fórmula para este caso en particular:

$$\left.\frac{\partial^2 f}{\partial x^2}\right|_{x=x_{i-2}} = \frac{2!}{5!\ (\Delta x)^2}\left[A_0 f_0 + A_1 f_1 + A_2 f_2 + A_3 f_3 + A_4 f_4 + A_5 f_5 + e_t\right]$$

$$e_t = \frac{1}{180}(\Delta x)^6 \left.\frac{d^6 f}{dx^6}\right|_{\zeta}$$

Sustituyendo los coeficientes:

$$\frac{d^2 f}{dx^2} = \frac{2!}{5!\ (\Delta x)^2}\left[-5f_0 + 80f_1 - 150f_2 + 80f_3 - 5f_4 + 0 + \frac{1}{180}(\Delta x)^6\right.$$

$$\left.\frac{\partial^6 f}{\partial x^6}\right|_\zeta \Big]$$

Simplificando:

$$\frac{\partial^2 f}{\partial x^2} = \frac{-f_{i-2} + 16 f_{i-1} - 30 f_i + 16 f_{i+1} - f_{i+2}}{12 (\Delta x)^2} + \frac{1}{10800} (\Delta x)^4 \left.\frac{\partial^6 f}{\partial x^6}\right|_\zeta$$

Obsérvese que puede darse el caso que uno más de los coeficientes sea cero. Esto quiere decir que para expresar la derivada en cuestión, no es necesario el valor de la función en todos los puntos del intervalo. Además observe que la suma de los coeficientes de la fórmula de Bickley es cero.

COEFFICIENTS FOR DIFFERENTIATION

Differentiation Formula: $\left.\frac{d^k f(x)}{dx^k}\right|_{x=x_j} = \frac{k!}{m! h^k} \sum_{i=0}^{m} A_i f(x_i)$

FIRST DERIVATIVE ($k=1$)

j	A_0	A_1	A_2	A_3	A_4	A_5	$\frac{h^k}{k!}$ Error
			Three Point ($m=2$)				
0	−3	4	−1				1/3
1	−1	0	1				$-1/6\, h^3 f^{(3)}$
2	1	−4	3				1/3
			Four Point ($m=3$)				
0	−11	18	−9	2			−1/4
1	−2	−3	6	−1			$1/12\, h^4 f^{(4)}$
2	1	−6	3	2			$-1/12\, h^4 f^{(4)}$
3	−2	9	−18	11			1/4
			Five Point ($m=4$)				
0	−50	96	−72	32	−6		1/5
1	−6	−20	36	−12	2		−1/20
2	2	−16	0	16	−2		$1/30\, h^5 f^{(5)}$
3	−2	12	−36	20	6		−1/20
4	6	−32	72	−96	50		1/5
			Six Point ($m=5$)				
0	−274	600	−600	400	−150	24	−1/6
1	−24	−130	240	−120	40	−6	1/30
2	6	−60	−40	120	−30	4	$-1/60\, h^6 f^{(6)}$
3	−4	30	−120	40	60	−6	1/60
4	6	−40	120	−240	130	24	−1/30
5	−24	150	−400	600	−600	274	1/6

SECOND DERIVATIVE ($k=2$)

j	A_0	A_1	A_2	A_3	A_4	A_5	$\frac{h^k}{k!}$ Error
			Three Point ($m=2$)				
0	1	−2	1				$-1/2\, h^3 f^{(3)}$
1	1	−2	1				$-1/24\, h^4 f^{(4)}$
2	1	−2	1				$1/2\, h^3 f^{(3)}$
			Four Point ($m=3$)				
0	6	−15	12	−3			11/24
1	3	−6	3	0			$-1/24\, h^4 f^{(4)}$
2	0	3	−6	3			$-1/24\, h^4 f^{(4)}$
3	−3	12	−15	6			11/24
			Five Point ($m=4$)				
0	35	−104	114	−56	11		$-5/12\, h^5 f^{(5)}$
1	11	−20	6	4	−1		$1/24\, h^5 f^{(5)}$
2	−1	16	−30	16	−1		$1/180\, h^6 f^{(6)}$
3	−1	4	6	−20	11		$-1/24\, h^5 f^{(5)}$
4	11	−56	114	−104	35		$5/12\, h^5 f^{(5)}$
			Six Point ($m=5$)				
0	225	−770	1070	−780	305	−50	137/360
1	50	−75	−20	70	−30	5	−13/360
2	−5	80	−150	80	−5	0	$1/180\, h^6 f^{(6)}$
3	0	−5	80	−150	80	−5	$1/180\, h^6 f^{(6)}$
4	5	−50	70	−20	−75	50	−13/360
5	−50	305	−780	1070	−770	225	137/360

THIRD DERIVATIVE ($k=3$)

j	A_0	A_1	A_2	A_3	A_4	A_5	$\frac{h^k}{k!}$ Error
			Four Point ($m=3$)				
0	−1	3	−3	1			−1/4
1	−1	3	−3	1			$-1/12\, h^4 f^{(4)}$
2	−1	3	−3	1			$1/12\, h^4 f^{(4)}$
3	−1	3	−3	1			1/4
			Five Point ($m=4$)				
0	−10	36	−48	28	−6		7/24
1	−6	20	−24	12	−2		$1/24\, h^5 f^{(5)}$
2	−2	4	0	−4	2		$-1/24\, h^5 f^{(5)}$
3	2	−12	24	−20	6		1/24
4	6	−28	48	−36	10		7/24
			Six Point ($m=5$)				
0	−85	355	−590	490	−205	35	−5/16
1	−35	125	−170	110	−35	5	−1/48
2	−5	−5	50	−70	35	−5	$1/48\, h^6 f^{(6)}$
3	5	−35	70	−50	5	5	$-1/48\, h^6 f^{(6)}$
4	−5	35	−110	170	−125	35	1/48
5	−35	205	−490	590	−355	85	5/16

FOURTH DERIVATIVE ($k=4$)

j	A_0	A_1	A_2	A_3	A_4	A_5	$\frac{h^k}{k!}$ Error
			Five Point ($m=4$)				
0	1	−4	6	−4	1		$-1/12\, h^5 f^{(5)}$
1	1	−4	6	−4	1		$-1/24\, h^5 f^{(5)}$
2	1	−4	6	−4	1		$-1/144\, h^6 f^{(6)}$
3	1	−4	6	−4	1		$1/24\, h^5 f^{(5)}$
4	1	−4	6	−4	1		$1/12\, h^5 f^{(5)}$
			Six Point ($m=5$)				
0	15	−70	130	−120	55	−10	17/144
1	10	−45	80	−70	30	−5	5/144
2	5	−20	30	−20	5	0	$-1/144\, h^6 f^{(6)}$
3	0	5	−20	30	−20	5	$-1/144\, h^6 f^{(6)}$
4	−5	30	−70	80	−45	10	5/144
5	−10	55	−120	130	−70	15	17/144

FIFTH DERIVATIVE ($k=5$)

j	A_0	A_1	A_2	A_3	A_4	A_5	$\frac{h^k}{k!}$ Error
			Six Point ($m=5$)				
0	−1	5	−10	10	−5	1	−1/48
1	−1	5	−10	10	−5	1	−1/80
2	−1	5	−10	10	−5	1	$-1/240\, h^6 f^{(6)}$
3	−1	5	−10	10	−5	1	$1/240\, h^6 f^{(6)}$
4	−1	5	−10	10	−5	1	1/60
5	−1	5	−10	10	−5	1	1/48

Compiled from W. G. Bickley, Formulae for numerical differentiation, Math. Gaz. 25, 19-27, 1941 (with permission).

TABLA I

C O N T E N I D O

CAPITULO 4

SOLUCION DE ECUACIONES DIFERENCIALES EN DERIVADAS PARCIALES POR EL METODO DE DIFERENCIAS FINITAS.

4.1 INTRODUCCION

Las ecuaciones obtenidas para la simulación de yacimientos son generalmente ecuaciones diferenciales en derivadas parciales no lineales para las cuales, salvo en algunas excepciones, no se han encontrado soluciones analíticas. Por esta razón es necesario utilizar métodos numéricos para llegar a una solución.

Anteriormente se presentaron las bases del Método de Diferencias Finitas que es la técnica más comunmente utilizada para este tipo de problemas. Ahora se presentará una breve clasificación de las ecuaciones diferenciales en derivadas parciales, algunas consideraciones sobre la forma de expandir el lado derecho de las ecuaciones de flujo (el término de acumulación) y los diversos procedimientos propuestos para resolver las ecuaciones de flujo de fluidos a través de médios procesos.

4.2 CLASIFICACION DE LAS ECUACIONES DIFERENCIALES EN DERIVADAS PARCIALES.

En general las ecuaciones diferenciales en derivadas parciales pueden ser clasificadas como elípticas, parabólicas, hiperbólicas o mixtas. Cada una de estas clases pueden ser lineal o no lineal. La mayoría de las ecuaciones resultantes de problemas prácticas de simulación son ecuaciones no lineales, es decir, los coeficientes de las derivadas par-

-ciales son funciones tanto de las variables dependientes como de -- las variables independientes.

Por esta razón, y en especial las ecuaciones resultantes en problemas de flujo en dos o tres fases pueden ser muy difíciles de clasificar, ya que además de las no linealidades de las ecuaciones, estas aparecen como sistemas de ecuaciones y no como una sola ecuación.

Una ecuación diferencial parcial de segundo orden es una ecua- ción que contiene derivadas hasta de segundo orden y más de una variable independiente. La forma más general de una ecuación diferencial parcial de segundo orden con dos variables independientes es:

$$A(x,y)\frac{\partial^2 u}{\partial x^2} + B(x,y)\frac{\partial^2 u}{\partial x \partial y} + C(x,y)\frac{\partial^2 u}{\partial y^2} = f\left(x,y,u,\frac{du}{dx},\frac{du}{dy}\right) \qquad \ldots\ldots\ldots \quad (4.1)$$

en donde "x" e "y" son las variables independientes y "u" es la variable dependiente. Normalmente "x" e "y" se refieren a posición pero en problemas en los que una de las variables sea el tiempo "y", - se puede referir a tiempo. Si los coeficientes A, B y C son funciones únicamente de las variables independientes, son constantes o son cero, la ecuación es lineal. Esta ecuación es no lineal si cualquiera A, B o C es función de la variable dependiente. Por ejemplo la - ecuación (4.2) es lineal.

$$\frac{\partial}{\partial x}\left(\frac{kx}{\mu}\frac{\partial p}{\partial x}\right) + \frac{\partial}{\partial y}\left(\frac{ky}{\mu}\frac{\partial p}{\partial y}\right) + \frac{(qsth)\ x,y,t}{\Delta x\ \Delta y} = cc\frac{\partial p}{\partial t} \qquad \ldots\ldots\ldots \quad (4.2)$$

y la ecuación (4.3) es no lineal.

$$\frac{\partial}{\partial x}\left(\frac{kx}{\mu}\frac{p}{Z}\frac{\partial p}{\partial x}\right)+\frac{\partial}{\partial y}\left(\frac{ky}{\mu}\frac{p}{Z}\frac{\partial p}{\partial y}\right)+\left(\frac{p}{T}\right)_{c.s.}+\frac{(q_{srb})_{xyt}}{\Delta x\,\Delta y}=\phi\frac{\partial}{\partial t}\left(\frac{p}{Z}\right) \qquad (4.3)$$

La ecuación (4.1) se clasificará como elíptica, parabólica o hiperbólica dependiendo del valor del discriminante $B^2 - 4AC$, para un punto dado (x,y)

si	$B^2 - 4AC$	$<$	0	Elíptica	(4.4)
si	$B^2 - 4AC$	$=$	0	Parabólica	(4.5)
si	$B^2 - 4AC$	$>$	0	Hiperbólica	(4.6)

Esta delimitación involucra que la ecuación pueda cambiar de clasificación dependiendo de los valores de "x" e "y" bajo consideración (valores de los coeficientes A y B).

Así por ejemplo la ecuación

$$\frac{\partial^2 u}{\partial x^2} = \frac{\partial^2 u}{\partial y^2}$$ es siempre hiperbólica;

la ecuación $$\frac{\partial^2 u}{\partial x^2} + \frac{\partial^2 u}{\partial y^2} = 0$$ es siempre elíptica, (ecuación de Laplace)

y la ecuación $$\frac{\partial^2 u}{\partial x^2} = \frac{1}{\alpha}\frac{\partial u}{\partial t}$$ es siempre parabólica, (ecuación de onda)

Sin embargo, la ecuación

$$(1-y)\frac{\partial^2 u}{\partial x^2} + 2x\frac{\partial^2 u}{\partial x \partial y} + (1+y)\frac{\partial^2 u}{\partial y^2} = 0$$

cuyo discriminante es:

$$D = (2x)^2 - 4(1-y)(1+y)$$

$$D = 4x^2 - 4(1-y^2)$$

$$D = 4x^2 - 4 + 4y^2$$

$$D = x^2 + y^2 - 1$$

es elíptica dentro del círculo $x^2 + y^2 = 1$ (ejemplo: discriminante negativo), hiperbólica fuera del círculo (ejemplo discriminante positivo) y parabólica en la frontera. (ejemplo: discriminante cero).

Los problemas en los que el signo del discriminante depende de la solución pueden presentar dificultades especiales ya que el tipo de ecuación gobierna el número y la naturaleza de las condiciones iniciales y/o de frontera.

Es decir, un problema complejo puede tener en un cierto rango una solución única y bien determinada mientras que en otro rango las soluciones pueden ser múltiples y no determinadas o aún no existir.

Sin embargo las ecuaciones netamente elípticas, parabólicas o hiperbólicas se mantienen como tales, independientemente de las dimensiones y del sistema de coordenadas que se considere. Así, por ejemplo, las ecuaciones

$$\frac{\partial^2 p}{\partial x^2} + \frac{\partial^2 p}{\partial y^2} + \frac{\partial^2 p}{\partial z^2} = \frac{1}{\eta}\frac{\partial p}{\partial t}$$

y

$$\frac{\partial^2 p}{\partial r^2} + \frac{1}{r}\frac{\partial p}{\partial r} = \frac{1}{\eta}\frac{\partial p}{\partial t}$$

son también parabólicas.

4.3 ESQUEMAS DE SOLUCION DE LAS ECUACIONES DE FLUJO

La formulación de un esquema adecuado de solución a las ecuaciones diferenciales parciales es de suma importancia ya que de él dependen la estabilidad y precisión de las soluciones. En general se puede decir que entre más implícito sea el esquema de solución, se logrará una mayor esta—bilidad, y se podrán utilizar intervalos de tiempos mayores. Desafortunadamente, entre más implícito sea un esquema mayor será el grado de dificultad para resolverlo (o avanzar la solución del tiempo t al tiempo $t+\delta t$).

Por esta razón es necesario encontrar un equilibrio entre un esquema simple que permita intervalos de tiempo pequeños y requiera poco tiempo de cómputo para avanzar la solución y un esquema muy complicado que sea estable aún para intervalos de tiempo grandes pero que requiera un tiempo de cómputo considerablemente mayor.

Determinante en la formulación de estos esquemas es el nivel de tiempo al cual los términos de flujo, o sea las derivadas espaciales, se evalúan. Tres de los esquemas más comunmente utilizados son el esquema explícito, el esquema mixto y el esquema implícito. Su ilustración se hará mediante la ecuación simplificada de flujo monofásico:

$$\frac{\partial}{\partial x}\left(\frac{k}{\mu B}\frac{\partial p}{\partial x}\right) = \frac{\partial p}{\partial t} \qquad (4.7)$$

la cual se aproxima en diferencias finitas como:

$$Tx_{i+1/2}\,(p_{i+1}-p_i)-Tx_{i-1/2}\,(p_i-p_{i-1})=\frac{V_{bi}}{\Delta t}\,(p_i^{n+1}-p_i^n) \qquad (4.8)$$

en donde, Tx es la transmisividad entre las celdas y V_{bi} es el volúmen total del bloque i.

4.3.1 ESQUEMA EXPLICITO.

En este esquema, las presiones y transmisividades de los términos de flujo se evaluan al nivel de tiempo conocido "n".

Por esta razón es el esquema más sencillo. Su expresión en diferencias finitas se escribe como:

$$Tx^n_{i+1/2}\,(p^n_{i+1}-p^n_i)-Tx^n_{i-1/2}\,(p^n_i-p^n_{i-1})=\frac{V_{bi}}{\Delta t}\,(p_i^{n+1}-p_i^n) \qquad (4.9)$$

Como en este esquema la única incógnita es p_i^{n+1}, para avanzar la solución de "n" a "n + 1" lo que se requiere es aplicar la ecuación (4.9) a cada uno de los puntos de la malla. Por su sencillez este esquema presenta limitaciones fuertes de estabilidad lo que implica tener que usar intervalos pequeños de tiempo al avanzar la solución. Esta limitación hace que su aplicación sea impráctica en la mayoría de los problemas de simulación.

4.3.2 ESQUEMA MIXTO.

Este es el esquema que se utiliza con mayor frecuencia y consiste en evaluar las presiones al nivel nuevo de tiempo "n + 1", mientras que las transmisividades se evaluan al nivel de tiempo conocido "n". Así, la ecuación en diferencias finitas se expresa como:

$$Tx^{n}_{i+1/2}\left(p^{n+1}_{i+1} - p^{n+1}_{i}\right) - Tx^{n}_{i-1/2}\left(p^{n+1}_{i} - p^{n+1}_{i-1}\right) = \frac{V_{bi}}{\Delta t}\left(p^{n+1}_{i} - p^{n}_{i}\right) \quad \ldots\ldots \quad (4.10)$$

Para cada celda para la que se escribe la ecuación (4.10) se tienen ahora tres incógnitas p^{n+1}_{i-1} , p^{n+1}_{i} , p^{n+1}_{i+1} por lo tanto para avanzar la solución del tiempo "n" al tiempo "n + 1" se requiere escribir las ecuaciones para todas las celdas y posteriormente resolver un sistema de ecuaciones algebraicas lineales.

Este tipo de esquema se utiliza con éxito en simuladores areales y tridimensionales en los cuales, en general, no se dan cambios bruscos de presiones y/o saturaciones de un intervalo de tiempo al otro. Sin embargo pueden presentar serias limitaciones de estabilidad y consecuentemente requerir intervalos de tiempo muy pequeños en simuladores de flujo convergente tales como simuladores de conificación y algunos simuladores de secciones transversales.

Es de mucha importancia la forma en que se manejan los términos fuente en este esquema, especialmente en modelos tridimensionales y de secciones transversales en donde existen pozos terminados en varias capas. Una formulación inadecuada de los términos fuente puede disminuir la estabilidad del modelo y reducir en mucho el máximo incremento de tiempo (Δt) permisible para obtener resultados aceptables.

4.3.3 ESQUEMA IMPLICITO.

Este esquema consiste en evaluar tanto las presiones como las transmisividades al nuevo nivel de tiempo "n + 1" quedando la ecuación en diferencias finitas como:

$$Tx^{n+1}_{i+1/2}\,(p^{n+1}_{i+1}-p^{n+1}_{i})-Tx^{n+1}_{i-1/2}\,(p^{n+1}_{i}-p^{n+1}_{i-1})=\frac{V_{bi}}{\Delta t}\,(p^{n+1}_{i}-p^{n}_{i}) \qquad \ldots\ldots (4.11)$$

Nuevamente, al escribir la ecuación para cada celda las incógnitas resultantes son p^{n+1}_{i-1}, p^{n+1}_{i}, p^{n+1}_{i+1}, por lo tanto para avanzar la solución hay que escribir las ecuaciones para todas las celdas. El sistema resultante no puede evaluarse directamente ya que los coeficientes $Tx^{n+1}_{i-1/2}$ dependen de presiones al nivel "n + 1", o sea que se tiene un sistema de ecuaciones no-lineales. La solución se logra mediante técnicas iterativas tales como la de Newton-Raphson extendida al caso de variables múltiples.

Por esta razón el esquema implícito es el que involucra mayor esfuerzo de cómputo para avanzar la solución de un nivel a otro (tres o cuatro veces mayor que el esquema mixto) sin embargo esta formulación permite utilizar incrementos de tiempo mucho mayores que el esquema mixto y aún permenecer estable.

Para flujo multifásico, las técnicas de solución utilizadas normalmente combinan los dos últimos esquemas presentados.

La figura adjunta presenta una comparación esquemática de los tres esquemas en la cual los círculos representan los puntos en los cuales se evaluan las presiones y los triángulos los puntos en donde

se evaluan las transmisividades.

ESQUEMA EXPLICITO.

NIVEL DE TIEMPO

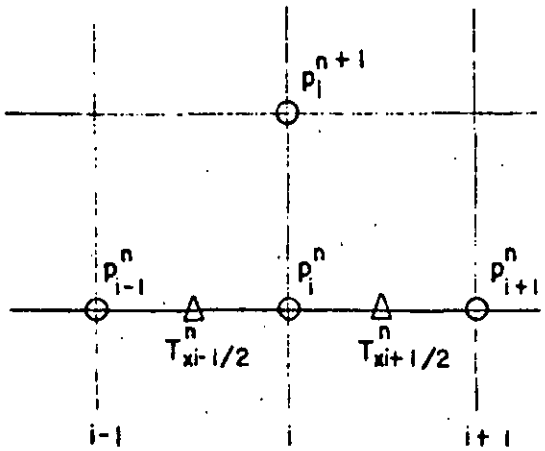

n + 1

n

ESQUEMA MIXTO.

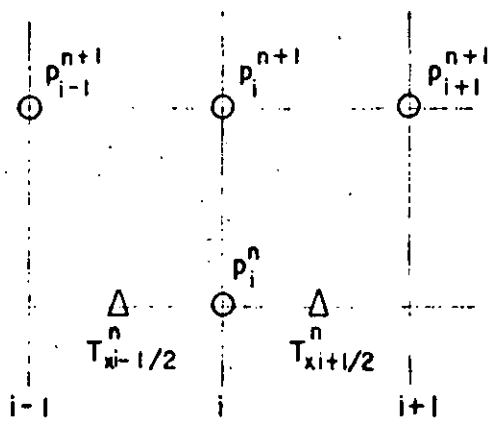

n + 1

n

ESQUEMA IMPLICITO.

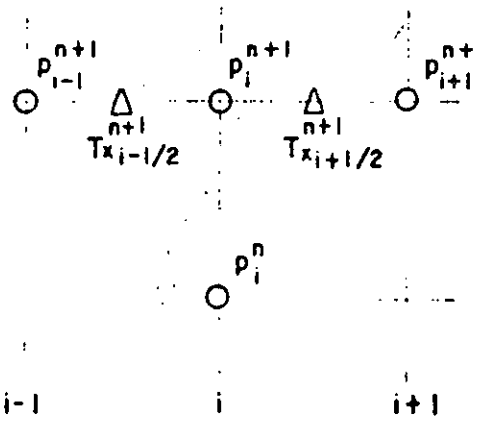

n + 1

n

De acuerdo a la discusión anterior, las ecuaciones en diferencias finitas presentadas en las secciones previas pueden ser resueltas utilizando dos procedimientos diferentes para problemas multifásicos:

El primer procedimiento es implícito en presión y explícito en saturación (IMPES) y el segundo es implícito en presión y saturación (IMPIS).

En la mayoría de los estudios de yacimientos se puede utilizar ventajosamente el procedimiento IMPES, sin embargo, en problemas tales como conificación en donde se utilizan celdas muy pequeñas cerca del pozo es necesario usar un procedimiento ---- IMPIS o una de sus variaciones.

En problemas monofásicos la presión en líquidos, o el potencial real del gas para gases son las únicas variables dependientes y es conveniente calcularlas implícitamente. Por esto para problemas monofásicos no hay limitaciones en el tamaño del intervalo de tiempo a utilizar, en cuanto a estabilidad se refiere.

C O N T E N I D O

C A P I T U L O 5

SOLUCION DE SISTEMAS DE ECUACIONES ALGEBRAICAS.

5.1 INTRODUCCION.

El objetivo de esta sección es presentar maneras de resolver las ecuaciones de presión, las cuales forman un sistema lineal de ecuaciones simultaneas. Dichas ecuaciones pueden ser escritas con la siguiente notación matricial:

$$A\,p = b \qquad (5.1)$$

La ecuación (5.1) puede ser llamada ecuación vectorial o ecuación matricial y representa un número de ecuaciones lineales simultaneas, debido a que las ecuaciones son lineales, por que la matriz A contiene solo coeficientes que son constantes. El vector "p" representa las incógnitas de presión en todos los puntos del sistema considerado.

La solución de la ecuación de presión puede ser en todo caso muy simple o muy compleja, dependiendo del problema físico. Cuando la solución es relativamente fácil, como en el caso de problemas de una dimensión y muchos problemas de dos dimensiones, la solución de la ecuación de presión constituye solo una fracción del tiempo total computación y del costo de la simulación del yacimiento. En problemas difíciles como algunos de dos y la mayoría de tres dimensiones, el esfuerzo requerido para resolver la ecuación de presión tiene un-

mayor significado en relación al resto del problema de la simulación del yacimiento.

Existe un número de técnicas para resolver la ecuación (5.1), la mayor parte de éstas estan orientadas hacia problemas de dos dimensiones puesto que estos ocurren mas frecuentemente en simulación de yacimientos. A continuación se explica un número de técnicas de solución comunmente usadas para la simulación de yacimientos.

5.2 PROBLEMAS EN UNA DIMENSION.

Para el problema de una dimensión, se puede ser más especifico acerca de la interpretación de la ecuación vectorial A p = b. Para principiar considérese el siguiente diagrama esquemático (Fig. 5) usando un número de celdas Nx las cuales se encuentran numeradas de izquierda a derecha. Cualquier celda puede ser referida a la celda "i" con el propósito de escribir una ecuación general. De la ecuación de simulación de yacimientos, se sabe que una ecuación escrita para la celda "i" involucra también los valores de las dos celdas continuas próximas, desde las cuales puede ocurrir el flujo de fluidos. Una ecuación para la celda "i" presenta el siguiente aspecto:

$$a_i\, p_{i-1} + b_i\, p_i + c_i\, p_{i+1} = d_i \qquad (5.2)$$

Para la celda 1 c I, solamente una celda esta próxima, y esto representa la condición límite de no flujo en el final de la celda. Sus ecuaciones estan dadas por:

$$b_{i1}\, p_1 + c_i\, p_2 = d_1 \qquad (5.3)$$

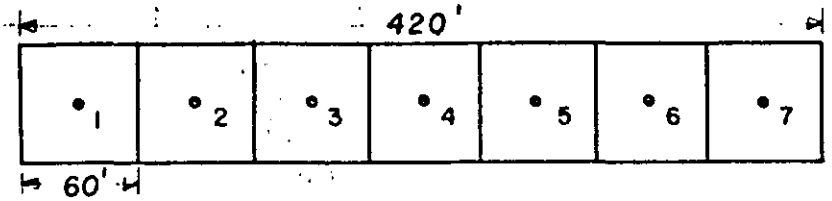

FIG. 5.1y5.2

$kx = 200\ mD$

$\mu = 1\ cp$

$A = 200\ pies^2$

$p_1 = 600\ lb/pg^2$

$p_7 = 100\ lb/pg^2$

Se tiene un sistema lineal, medio homogéneo, hay un pozo inyector en la celda 1 y un pozo productor en la celda 7.

SOLUCION:

Los gastos se pueden calcular con la ecuación de Darcy

$$q = \frac{kA}{\mu}\frac{\Delta p}{\Delta x} = \frac{(0.2)\ (1.127)\ (200)}{(1.0)} \times \frac{(600-100)}{(360)}$$

$q = 62.61\ bls/dia.$

En este caso particular las presiones se pueden calcular en una forma muy sencilla. Considerando que se trata de un sistema lineal, la presión varía en forma lineal para cada celda y el gradiente permanece constante en el sistema, se puede hacer una gráfica de x vs p tomando en cuenta los datos proporcionados, de tal manera que para cada distancia se pueda tener un valor de presión.

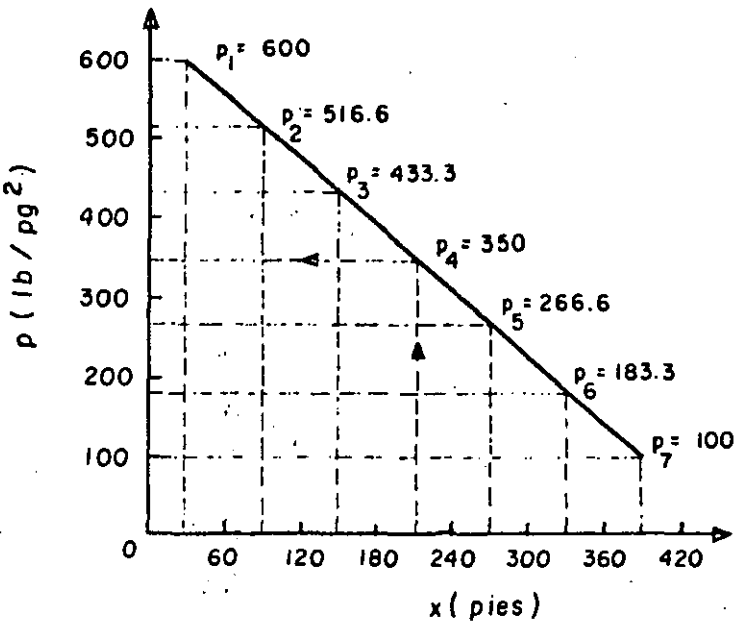

Otra forma de resolver el problema es utilizando la formulación en diferencias finitas. Escribiendo la ecuación general para cada nodo en el cual no se conoce la presión, se tiene lo siguiente:

$$\frac{p_{i-1} - 2\,p_i + p_{i+1}}{(\Delta x)^2} + \frac{\mu\, Bo}{kx\ (Vol.\ del\ nodo\ i)}\left[q\ stb\right] = 0$$

sustituyendo los valores correspondientes en la ecuación anterior:

$$\frac{p_{i-1} - 2\,p_i + p_{i+1}}{(60)^2} + \frac{(1.0)\ (1.0)\ (q\ stb/d)i}{(0.2)\ (1.127)\ (200x60)} = 0$$

donde para $(q\ stb/d)_1 = 62.61$, $(q\ stb/d)_7 = -62.61$. Los gastos son iguales en valor absoluto debido a que el flujo es incompresible -- por lo que se dice que el gasto que se inyecta (+) es igual al gasto que se produce (-). En las celdas 2,3,4,5,6 existe flujo pero no hay fuentes ni sumideros por lo tanto:

$(q\ stb/d)_{i=2,3,4,5,6} = 0$; las incógnitas son las $p_{i=2,3,4,5,6}$, para lo cual se tiene que escribir la ecuación en diferencias para cada uno de los nodos en donde no se conoce la presión. Para esto se tiene lo siguiente:

Nodo

$i=2 \quad p_1 - 2p_2 + p_3 + 0 + 0 + 0 + 0 = 0$

$i=3 \quad 0 + p_2 - 2p_3 + p_4 + 0 + 0 + 0 = 0$

$i=4 \quad 0 + 0 + p_3 - 2p_4 + p_5 + 0 + 0 = 0$

$i=5 \quad 0 + 0 + 0 + p_4 - 2p_5 + p_6 + 0 = 0$

$i=6 \quad 0 + 0 + 0 + 0 + p_5 - 2p_6 + p_7 = 0$

pasando las presiones conocidas al lado derecho de las ecuaciones

$$-2p_2 + p_3 + 0 + 0 + 0 = -600$$

$$p_2 - 2p_3 + p_4 + 0 + 0 = 0$$

$$0 + p_3 - 2p_4 + p_5 + 0 = 0$$

$$0 + 0 + p_4 - 2p_5 + p_6 = 0$$

$$0 + 0 + 0 + p_5 - 2p_6 = -100$$

Este sistema de ecuaciones lineales se puede escribir en notación matricial como:

$$\begin{bmatrix} -2 & 1 & 0 & 0 & 0 \\ 1 & -2 & 1 & 0 & 0 \\ 0 & 1 & -2 & 1 & 0 \\ 0 & 0 & 1 & -2 & 1 \\ 0 & 0 & 0 & 1 & -2 \end{bmatrix} \begin{bmatrix} p_2 \\ p_3 \\ p_4 \\ p_5 \\ p_6 \end{bmatrix} = \begin{bmatrix} -600 \\ 0 \\ 0 \\ 0 \\ -100 \end{bmatrix}$$

El arreglo de los coeficientes puede ser llamado matriz de coeficientes (A), el arreglo de las presiones p (s) como vector de incógnitas ($\vec{p}$) y el arreglo de coeficientes del lado derecho de la igualdad como lado derecho (D). La ecuación vectorial del arreglo es la siguiente:

$$A\,\vec{p} = D$$

premultiplicando a la ecuación vectorial por la inversa de A, con el objeto de tener el vector de incógnitas en función de (A^{-1}) y (D)

$$A^{-1} A\, p = A^{-1} D \quad , \quad p = A^{-1} D$$

Este sistema podrá resolverse por inversión matricial solamente si es posible obtener la inversión de A (A^{-1}) en otras palabras sólo si $det \neq 0$.

Para sistemas pequeños es relativamente sencillo obtener la inversa de la matriz de coeficientes, pero para sistemas grandes puede ser ventajoso utilizar en la solución métodos iterativos.
Una ilustración de los métodos mas comunes se presenta a continuación.

5.3.1 METODO DIRECTO.

Antes de presentar el método directo se recordará el teorema fundamental de equivalencia, el cual es la base para el desarrollo de la eliminación de Gauss. Este teorema se expresa de la siguiente forma: Si en un sistema de ecuaciones se sustituye una de ellas por una combinación lineal de las ecuaciones del sistema, se obtiene un nuevo -- sistema que es equivalente al anterior.

5.3.1.1 METODO DE ELIMINACION DE GAUSS.

Este método es un método exacto para resolver sistemas lineales,- el cual básicamente consiste en sistematizar el teorema fundamental - de equivalencia.

El método consiste en aplicar a una matriz ampliada (la cual se forma con la matriz de coeficientes y el lado derecho de la ecuación- vectorial (5.4), un número determinado de operaciones, las cuales - son llamadas operaciones elementales sobre los renglones de una ma- - triz, con el fin de obtener un sistema equivalente al anterior en donde se pueden obtener facilmente las incógnitas.

Tomando el sistema original, el objetivo es transformar a la ma-- triz de coeficientes A, en una matriz tridiagonal superior.

$$\begin{bmatrix} -2 & 1 & 0 & 0 & 0 \\ 0 & -2 & 1 & 0 & 0 \\ 0 & 1 & -2 & 1 & 0 \\ 0 & 0 & 1 & -2 & 1 \\ 0 & 0 & 0 & 1 & -2 \end{bmatrix} \begin{bmatrix} p_2 \\ p_3 \\ p_4 \\ p_5 \\ p_6 \end{bmatrix} = \begin{bmatrix} -600 \\ 0 \\ 0 \\ 0 \\ -100 \end{bmatrix}$$

formando la matriz ampliada, se obtiene:

$$\left[\begin{array}{ccccc|c} -2 & 1 & 0 & 0 & 0 & -600 \\ 0 & -2 & 1 & 0 & 0 & 0 \\ 0 & 1 & -2 & 1 & 0 & 0 \\ 0 & 0 & 1 & -2 & 1 & 0 \\ 0 & 0 & 0 & 1 & -2 & -100 \end{array}\right]$$

$$\left[\begin{array}{ccccc|c} -2 & 1 & 0 & 0 & 0 & -600 \\ 0 & -3/2 & 1 & 0 & 0 & -300 \\ 0 & 1 & -2 & 1 & 0 & 0 \\ 0 & 0 & 1 & -2 & 1 & 0 \\ 0 & 0 & 0 & 1 & 2 & -100 \end{array}\right]$$

1º multiplique el primer renglón por 1/2 y súmese al segundo renglón.

$$\left[\begin{array}{ccccc|c} -2 & 1 & 0 & 0 & 0 & -600 \\ 0 & -3/2 & 1 & 0 & 0 & -300 \\ 0 & 0 & -4/3 & 1 & 0 & -200 \\ 0 & 0 & 1 & -2 & 1 & 0 \\ 0 & 0 & 0 & 1 & 2 & -100 \end{array}\right]$$

2º multiplique el segundo renglón por 2/3 y súmese al tercero.

$$\left[\begin{array}{ccccc|c} -2 & 1 & 0 & 0 & 0 & -600 \\ 0 & -3/2 & 1 & 0 & 0 & -300 \\ 0 & 0 & -4/3 & 1 & 0 & -200 \\ 0 & 0 & 0 & -5/4 & 1 & -150 \\ 0 & 0 & 0 & 1 & -2 & -100 \end{array}\right]$$

3º multiplique el tercer renglón por 3/4 y súmese al cuarto renglón.

$$\left[\begin{array}{ccccc|c} -2 & 1 & 0 & 0 & 0 & -600 \\ 0 & -3/2 & 1 & 0 & 0 & -300 \\ 0 & 0 & -4/3 & 1 & 0 & -200 \\ 0 & 0 & 0 & -5/4 & 1 & -150 \\ 0 & 0 & 0 & 0 & -6/5 & -220 \end{array}\right]$$

4º multiplique el cuarto renglón por 4/5 y súmese al quinto.

Por lo que $p_6 = \frac{-(220)(5)}{-6} = 183.33 lb/pg^2$, sustituyendo este valor en el cuarto renglón

$$-5/4\ p_5 + p_6 = -150$$

$$\therefore \quad p_5 = \frac{(-150 - 183.33)(4)}{-5} = 266.67\ lb/PG^2$$

y a la vez sustituyendo p_5 en el 3er renglón

$$-4/3\ p_4 = -200 - 266.67$$

$$p_4 = 350\ lb/pg^2$$

ahora p_4 en el 2do renglón

$$-3/2\ p_3 = -300 - 350$$

$$p_3 = 433.33\ lb/pg^2$$

y por último, sustituyendo p_3 en el 1er renglón

$$-2\ p_2 = -600 - 433.33$$

$$p_2 = 516.67\ lb/pg^2$$

obteniendose la siguiente distribución de presiones:

$p_1 = 600$ psi, $p_2 = 516.67$ psi, $p_3 = 433.33$ psi, $p_4 = 350$ psi, $p_5 = 266.67$ $p_6 = 183.33$ psi y $p_7 = 100$ psi.

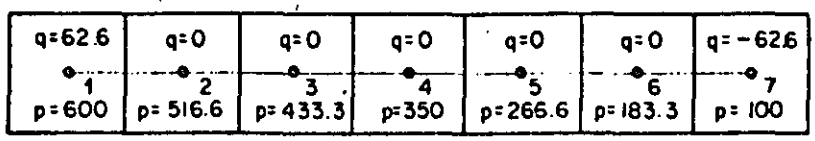

$\therefore$ q (bl/día), p (lb/pg^2)

5.3.2 METODOS ITERATIVOS.

5.3.2.1 METODO DE JACOBI. (DE PUNTO JACOBI)

Escribanse las ecuaciones de tal manera que cada ecuación contenga una incógnita en función de las otras cantidades, la incógnita corresponderá con el orden de la ecuación. Por el ordenamiento de estas ecuaciones la incógnita tiene generalmente el coeficiente más grande. Este método converge siempre que por lo menos un elemento diagonal - sea, en valor absoluto, mayor que la suma del resto de los elementos- del mismo renglón. Aplicando el método el ejemplo anterior.

$i = 2$ $\qquad p_1 - 2p_2 + p_3 = 0$

$$-2p_2 = -p_1 - p_3$$

$$2p_2 = p_1 + p_3$$

$$p_2 = 1/2 \left(p_1 + p_3 \right)$$

$i = 2$ $\qquad p_2^{m+1} = 1/2 \left(p_3^m + p_1 \right) = 1/2 \left(p_3^m + 600 \right)$

Haciendo lo mismo para los siguientes nodos se tiene:

$i = 3$ $\qquad p_3^{m+1} = 1/2 \left(p_2^m + p_4 \right)$

$i = 4$ $\qquad p_4^{m+1} = 1/2 \left(p_3^m + p_5 \right)$

$i = 5$ $\qquad p_5^{m+1} = 1/2 \left(p_4^m + p_6 \right)$

$i = 6$ $\qquad p_6^{m+1} = 1/2 \left(p_5^m + p_7 \right) = 1/2 \left(p_5^m + 100 \right)$

En las ecuaciones anteriores la incógnita está en el lado izquierdo de la igualdad y se le asigna el nivel de iteración "m+1", la parte conocida se encuentra en el lado derecho y se le asigna el nivel de iteración "m".

El proceso iterativo consiste en suponer valores para cada una de las incógnitas, resolviendo las ecuaciones del método y mediante éste proceso mejorar los valores supuestos por medio de iteraciones.
El proceso se continua hasta que dos valores consecutivos de todas las variables presentan una variación a una tolerancia predeterminada.

EJEMPLO:

1era Iteración

suponer: $\qquad p_2^0 = p_3^0 = p_4^0 = p_5^0 = p_6^0 = 0$

$m = 0$

$m + 1 = 0 + 1 = 1$

entonces:

$$p_2^1 = 1/2(p_1^0 + p_3^0) = 1/2\ (600 + 0) = 300$$

$$p_3^1 = 1/2(p_2^0 + p_4^0) = 1/2\ (0 + 0) = 0$$

$$p_4^1 = 1/2(p_3^0 + p_5^0) = 1/2\ (0 + 0) = 0$$

$$p_5^1 = 1/2(p_4^0 + p_6^0) = 1/2\ (0 + 0) = 0$$

$$p_6^1 = 1/2(p_5^0 + p_7^0) = 1/2\ (0 + 100) = 50$$

2da Iteración

$$p_2^2 = 1/2\ (0 + 600) = 300$$

$$p_3^2 = 1/2\ (300 + 0) = 150$$

$$p_4^2 = 1/2\ (0 + 0) = 0$$

$$p_6^2 = 1/2\ (0 + 100) = 50$$

Para las demás iteraciones el procedimiento será el mismo, hasta el número de iteraciones requeridas. Para éste ejemplo el número de iteraciones pedidas es de nueve. Los resultados son presentados en la tabla (5.1).

5.3.2.2 METODO DE GAUSS SEIDEL.

Este método es similar al de Jacobi, pero permite acelerar la convergencia del método iterativo, al tomar ventaja del hecho de que cuando se calculan variables posteriores a la segunda, las incógnitas de menor subíndice se conocen a un nivel de iteración más avanzado. Este es el método de Gauss-Seidel también llamado de iteraciones parciales o desplazamientos sucesivos.

3ra Iteración

$p_1^2 = 600,\ p_2^2 = 375,\ p_3^2 = 225,\ p_4^2 = 131.25,\ p_5^2 = 100,\ p_6^2 = 100$

$p_7^2 = 100$ psi

$$p_2^3 = 1/2\ (225 + 600) = 412.5$$

$$p_3^3 = 1/2\ (412.5 + 131.25) = 271.87$$

$$p_4^3 = 1/2\ (271.87 + 100.00) = 185.93$$

$$p_5^3 = 1/2\ (185.94 + 100.00) = 142.97$$

$$p_6^3 = 1/2\ (142.97 + 100.00) = 121.48$$

Iterando sucesivamente se obtienen los valores presentados en la tabla (5.2).

5.3.2.3 METODO DE SOBRERELAJACION PUNTUAL SUCESIVA (PSOR)

El concepto de sobrerelajación es un método de aceleramiento en la convergencia de los anteriores procesos iterativos. En este caso el nuevo valor de iteración p^{m+1} se obtiene con parte del nuevo y parte de la iteración anterior p^m.

Para el ejemplo anterior, las ecuaciones del método PSOR se escriben de la siguiente manera:

$$p_2^{m+1} = \omega(1/2\ (p_3^m + 600)\ ) + (1-\omega)\ p_2^m$$

$$p_3^{m+1} = \omega(1/2\ (p_2^{m+1} + p_4^m)\ ) + (1-\omega)\ p_3^m$$

$$p_4^{m+1} = \omega(1/2\ (p_3^{m+1} + p_5^m)\ ) + (1-\omega)\ p_4^m$$

$$p_5^{m+1} = \omega(1/2\ (p_4^{m+1} + p_6^m)\ ) + (1-\omega)\ p_5^m$$

$$p_6^{m+1} = \omega\{1/2\ (p_5^{m+1} + 100)\ \} + (1-\omega)\ p_6^m$$

$$1 \leq \omega \leq 2$$

durante la sobrerelajación, se amplifica la magnitud del cambio de presión durante cada iteración multiplicando éste cambio de presión por un parámetro de relajación, $\omega > 1.0$.

Si ω estuviese comprendido entre cero y uno, se tendría bajorelajación. Este procedimiento no es efectivo para el tipo de problemas de yacimientos.

Si $\omega = 1$, el PSOR se reduce al método de Gauss-Seidel. Ahora usando un valor de 1.334 para ω se tiene:

1era Iteración

suponiendo $p_2^0 = p_3^0 = p_4^0 = p_5^0 = p_6^0 = 0$

$$p_2^1 = 1.334\ \{1/2\ (0 + 600)\} + (1-1.334)\ (0) = 400.2$$

$$p_3^1 = 1.334\ \{1/2\ (400.2 + 0)\} + (1-1.334)\ (0) = 266.93$$

$$p_4^1 = 1.334\ \{1/2(266.9 + 0)\} + (1-1.334)\ (0) = 178.04$$

$$p_5^1 = 1.334\ \{1/2\ (178.0 + 0)\} + (1-1.334)\ (0) = 118.75$$

$$p_6^1 = 1.334\ \{1/2\ (118.7 + 100)\} + (1-1.334)\ (0) = 145.91$$

2da Iteración

$p_2^1 = 400.2$, $p_3^1 = 266.9$, $p_4^1 = 178$, $p_5^1 = 118.7$, $p_6^1 = 145.91$

$p_7^1 = 100$

$$p_2^2 = 1.334\ \{1/2\ (266.9 + 600) + (1-1.334)\ (400.2) = 444.57$$

$$p_3^2 = 1.334\ \{1/2\ (444.5 + 178.0) + (1-1\ 334)\ (266.93) = 326.13$$

$$p_4^2 = 1.334\ \{1/2\ (326.13 + 118.7) + (1-1.334)\ (178.00) = 237.27$$

$$p_5^2 = 1.334\ (1/2\ (237.27 + 145.9) + (1-1.334)\ (118.7) = 215.91$$

$$p_6^2 = 1.334\ (1/2\ (215.91 + 100) + (1-1.334)\ (145.91) = 161.98$$

iterando sucesivamente se obtienen los valores presentados en la tabla (5.3).

TABLA. 5.1

Inc	Valor Inicial	Iteraciones										
		1a	2a	3a	4a	5a	6a	7a	8a	9a	10a	11a
p	0	300	300.00	375.00	375.00	415.625	415.625	442.1875	442.1875	461.13	461.13	475.09
p	0	0	150.00	150.00	231.25	231.250	284.375	284.3750	322.2600	322.26	350.19	350.19
p	0	0	0	87.50	87.50	153.125	153.125	202.3440	202.3440	239.26	239.25	266.94
p	0	0	25	25.00	75.00	75.000	120.313	120.3130	156.2500	156.25	183.69	183.69
p	0	50	50	62.50	62.50	87.500	87.500	110.1563	110.1563	128.12	128.12	141.84

TABLA. 5.1 (continuación)

Iteración							
12a	13a	14a	15a	16a	17a	18a	19a
475.09	485.31	485.51	493.304	493.30	499.14	499.14	503.52
371.02	371.22	386.61	386.610	398.29	398.29	407.05	407.05
266.94	287.72	287.70	303.280	303.28	314.96	314.96	323.72
204.39	204.39	219.95	219.950	231.63	231.63	240.38	240.38
141.84	152.19	152.19	159.980	159.98	165.81	165.81	170.19

TABLA. 5.2

Inc	Valor Inicial	Iteración										
		1a	2a	3a	4a	5a	6a	7a	8a	9a	10a	11a
p	0	300	375.00	412.50	435.94	455.670	470.600	482.0800	490.7100	497.27	502.26	505.72
p	0	150	225.00	271.87	310.94	341.210	364.160	381.4300	394.4000	404.13	411.43	416.91
p	0	75	131.25	185.94	226.95	257.710	280.760	298.0800	311.0600	320.80	328.10	333.57
p	0	37.5	100.00	142.97	174.22	197.400	214.746	227.7000	237.4600	244.76	250.24	254.35
p	0	68.7	100.00	121.48	137.11	148.710	157.370	163.8600	168.7300	172.38	175.12	177.17

TABLA. 5.2 (continuación)

Iteración							
12a	13a	14a	15a	16a	17a	18a	19a
508.45	510.33	512.04	513.200	514.06	514.71	515.20	515.57
421.01	424.34	426.40	428.136	429.43	430.41	431.14	431.68
337.68	340.71	343.07	344.800	346.10	347.07	347.80	348.35
257.43	259.73	261.47	262.768	263.74	264.47	265.02	265.43
178.71	179.83	180.73	181.380	181.87	182.22	182.20	182.72

TABLA. 5.3

Inc.	Valor inicial	iteración									
		1a	2a	3a	4a	5a	6a	7a	8a	9a	10a
p	0	400.2	444.57	469.24	485.13	509.60	512.58	515.580	516.0800	516.48	516.57
p	0	265.9	326.13	362.31	406.96	423.68	428.83	431.63	432.7600	433.10	433.24
p	0	178.04	237.27	306.43	329.39	342.50	346.84	348.88	349.5500	349.84	349.94
p	0	118.75	215.91	240.31	274.75	262.67	265.10	266.01	266.4400	266.58	266.63
p	0	145.91	161.98	172.88	178.87	182.15	182.68	183.11	183.2500	183.31	183.32

120

TABLA. 5.3 (continuación)

iteración								
11a	12a	13a	14a	15a	16a	17a	18a	19a
516.63	516.66	516.57	516.63	516.66	516.66	516.66	516.66	516.66
433.30	433.30	433.24	433.30	433.32	433.33	433.33	433.33	433.33
349.98	349.99	349.94	349.98	349.99	349.99	349.99	349.99	349.99
266.65	266.66	266.63	266.65	266.66	266.66	266.66	266.66	266.66
183.33	183.33	183.32	183.32	183.33	183.33	183.33	183.33	183.33

121

$p_6 = 183.329$ "

$p_7 = 100.000$ "

c).- Al sobrerelajar el método de Gauss-Seidel, es decir, aplicando-PSOR únicamente se necesitaron 10 iteraciones para que se llegara a - la convergencia con la misma tolerancia de 0.001 de presión, obte--- niendose la siguiente distribución de presiones:

$p_1 = 600.000$ lb/pg^2

$p_2 = 516.666$ "

$p_3 = 433.320$ "

$p_4 = 349.980$ "

$p_5 = 266.650$ "

$p_6 = 183.329$ "

$p_7 = 100.000$ "

En forma breve e ilustrativa se ejemplifico la eficiencia de 3 - métodos iterativos, siendo el PSOR el de mayor utilidad. Aplicado - ya a una simulación en computadora la disminución de tiempo es sumamente notable aunada a una disminución en los costos.

5.3.2.4 CRITERIOS DE CONVERGENCIA.

El criterio para que el PSOR converja es:

1).- La matriz sea diagonalmente dominante.

2).- El valor de ω sea menor que 2.

Diagonal dominante quiere decir que el valor absoluto de la diagonal principal será mayor o igual a la suma de los valores absolutos

de los otros coeficientes para algún nodo. Físicamente en simulación de yacimientos, esta condición es siempre satisfactoria si se tiene formulado un sistema físico propio. Los requerimientos para que esto ocurra es que la compresibilidad del sistema físico sea positiva, el transcurso del tiempo positivo, y la transmisividad positiva. Si el PSOR no converge, es posible que haya un error en el sistema físico, probablemente ocurra una compresibilidad negativa en algún nodo.

$$\left\| d \right\|_{max}^{m+1} = \max_{i} \left| p_i^{m+1} - p^m \right|$$

La proposición de convergencia puede ser analizada por el término llamado factor de reducción, ρ , primero se definirá una medida de convergencia referida a una variable a cada máximo residual. Si se observa el máximo residual a cada iteración y se traza este valor vs el número de iteraciones se tendrá la Fig. (5a)

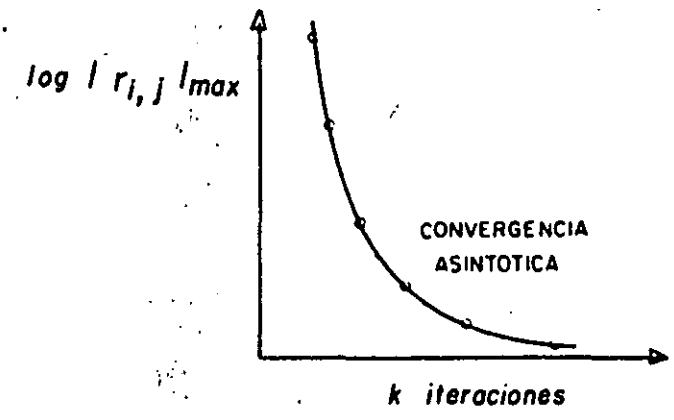

FIG. 5a

Durante esta convergencia asintónica, el máximo residual y todos los otros residuales en las celdas estan gobernadas por la relación siguiente:

$$r_{i,j}^{k+1} = \rho r_{i,j}^{k}$$

donde ρ es llamado el factor de reducción y es igual al radio espectral de la matriz formada durante el proceso PSOR, ρ depende del valor de ω y la velocidad y razón de convergencia.

EJEMPLO:

Calcule $\| d \|$ y ρ, en donde $\rho = \dfrac{\| d \|^{m+1}_{max}}{\| d \|^{m}_{max}}$

por el método de Gauss-Seidel

Solución

De la tabla 5.2 se tiene lo siguiente:

	7a iteración	8a iteración	9a iteración
p_2 =	482.0800781	490.7165527	497.2015381
p_3 =	381.4331055	394.4030762	404.1343689
p_4 =	298.0959960	311.0671997	320.8003998
p_5 =	227.7313232	237.4664307	244.7668076
p_6 =	163.8656616	168.7332153	172.3834038

diferencia máxima entre la 7a y 8a iteración

12.9712037

diferencia máxima entre la 8a y 9a iteración

9.7332001

de la fórmula $\rho = \dfrac{\| d \|^{m+1}_{max}}{\| d \|^{m}_{max}}$

entonces

$$\rho = \frac{9.7332001}{12.9712037} = 0.7503698442$$

COMPORTAMIENTO DE ω

En general, se puede obtener un valor de ω que optimize el proceso iterativo. Una manera práctica de obtener $\omega_{opt.}$, consiste en efectuar unas 10 iteraciones con $\omega = 1$. Entre la 7a, 8a, 9a, y 10a se obtiene ρ. Por ejemplo para el problema de Gauss-Seidel $\rho = 0.75037$

$$\omega_{opt.} = \frac{2}{1 + \sqrt{1 - 0.7507}} = 1.334$$

El parámetro de relajamiento ω es mayor para problemas mas complicados, por ejemplo; grandes contrastes en permeabilidad y su comportamiento esquemático es similar al presentarlo en la siguiente figura.

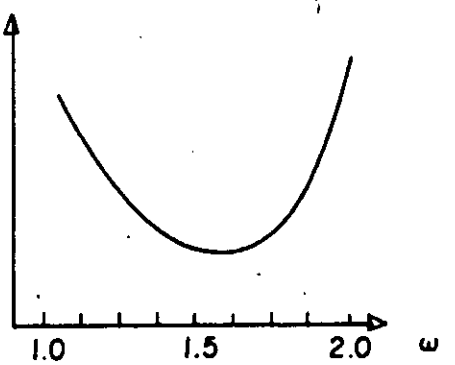

5.4 EJEMPLO DE FLUJO MONOFASICO BIDIMENSIONAL INCOMPRESIBLE.

De la ecuación para flujo monofásico incompresible en 2 dimensio-

-nes, se tiene:

$$\frac{\partial}{\partial x}\left(\frac{kx}{\mu_o B_o}\frac{\partial p}{\partial x}\right)+\frac{\partial}{\partial y}\left(\frac{ky}{\mu_o B_o}\frac{\partial p}{\partial y}\right)+q=0$$

Expandiendo en diferencias finitas, suponiendo k_x, k_y, y Bo como constantes

$$\frac{kx}{B_o}\frac{p_{i-1,j}-2p_{i,j}+p_{i+1,j}}{(\Delta x)^2}+\frac{ky}{B_o}\frac{p_{i,j-1}-2p_{i,j}+p_{i,j+1}}{(\Delta y)^2}+$$

$$\frac{q_{stb}}{(vol.\ del\ nodo)_i}=0$$

Datos

k_x = 200 mD.

k_y = 50 mD.

μ_o = 1.5 cp.

B_o = 1.2

h = 20 pies

x = 100 pies

y = 120 "

q_1 = 500 bl/dia

q_9 = -500 "

p_9 = 1000 lb/pg^2

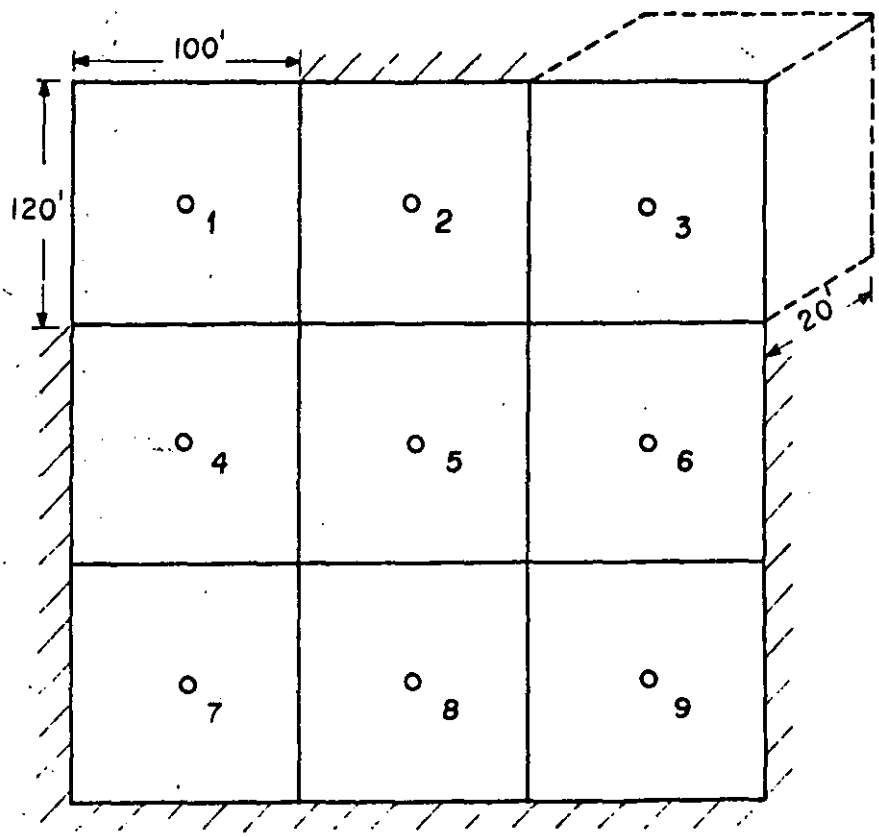

Es importante notar que el sistema es cerrado, es decir, que no hay flujo en la frontera externa. Para hacer esto, recordando la - - ecuación de Darcy, en donde el gasto es proporcional a la caída de -

presión:

$$q = \text{ctte.}\ p$$

Si el flujo es cero en la frontera p tiene que ser cero. Por lo tanto hay que aumentar nodos ficticios alrededor del sistema cuyas presiones son identicas a las de los nodos inmediatamente contiguos dentro del sistema.

Escribiendo las ecuaciones correspondientes a cada uno de los nodos se tiene lo siguiente:

Nodo

1) $$\frac{0.2 \times 1.127}{(1.5)\ (1.2)} \times \frac{p_1 - 2p_1 - p_2}{(100)^2} + \frac{0.05 \times 1.127}{(1.5)\ (1.2)} \times \frac{p_1 - 2p_1 + p_4}{(120)^2} +$$

$$\frac{500}{(100 \times 120 \times 20)} = 0$$

2) $$\frac{0.2 \times 1.127}{1.8} \times \frac{p_1 - 2p_2 + p_3}{(100)^2} + \frac{0.05 \times 1.127}{1.8} \times \frac{p_2 - 2p_2 + p_5}{(120)^2} +$$

$$0 = 0$$

3) $$\frac{0.2 \times 1.127}{1.8} \times \frac{p_2 - 2p_3 + p_3}{(100)^2} + \frac{0.05 \times 1.127}{1.8} \times \frac{p_3 - 2p_3 + p_6}{(120)^2} +$$

$$0 = 0$$

4) $$\frac{0.2 \times 1.127}{1.8} \times \frac{p_4 - 2p_4 + p_5}{(100)^2} + \frac{0.05 \times 1.127}{1.8} \times \frac{p_1 - 2p_4 + p_7}{(120)^2} +$$

$$0 = 0$$

5) $$\frac{0.2 \times 1.127}{1.8} \times \frac{p_4 - 2p_5 + p_6}{(100)^2} + \frac{0.05 \times 1.127}{1.8} \times \frac{p_2 - 2p_5 + p_8}{(120)^2} +$$

$$0 = 0$$

6) $$\frac{0.2 \times 1.127}{1.8} \times \frac{p_5 - 2p_6 + p_6}{(100)^2} + \frac{0.05 \times 1.127}{1.8} \times \frac{p_3 - 2p_6 + 1000}{(120)^2} +$$

$$0 = 0$$

7) $$\frac{0.2 \times 1.127}{1.8} \times \frac{p_7 - 2p_7 + p_8}{(100)^2} + \frac{0.05 \times 1.127}{1.8} \times \frac{p_4 - 2p_7 + p_7}{(120)^2} +$$

$$0 = 0$$

8) $$\frac{0.2 \times 1.127}{1.8} \times \frac{p_7 - 2p_8 + 1000}{(100)^2} + \frac{0.05 \times 1.127}{1.8} \times \frac{p_5 - 2p_8 + p_8}{(120)^2} +$$

$$0 = 0$$

$$\begin{bmatrix} a_{11} + a_{12} & & + a_{18} \\ a_{31} + a_{32} & & + a_{38} \\ & & \\ & & \\ & & \\ a_{81} + a_{82} & & + a_{88} \end{bmatrix} \begin{bmatrix} p_1 \\ p_2 \\ p_3 \\ p_4 \\ p_5 \\ p_6 \\ p_7 \\ p_8 \end{bmatrix} = \begin{bmatrix} q_1 \\ q_2 \\ q_3 \\ q_4 \\ q_5 \\ q_6 \\ q_7 \\ q_8 \end{bmatrix}$$

$$
\begin{aligned}
3055.42\,p_1 + 1803.2\,p_2 + 0\,p_3 + 1252.22\,p_4 + 0\,p_5 + 0\,p_6 + 0\,p_7 + 0\,p_8 &= -3\times10^{} \\
1803.2\,p_1 - 4858.6\,p_2 + 1803.2\,p_3 + 0\,p_4 + 1252.22\,p_5 + 0\,p_6 + 0\,p_7 + 0\,p_8 &= 0 \\
0\,p_1 + 1803.2\,p_2 - 3055.42\,p_3 + 0\,p_4 + 0\,p_5 + 1252.22\,p_6 + 0\,p_7 + 0\,p_8 &= 0 \\
1252.22\,p_1 + 0\,p_2 + 0\,p_3 - 4307.64\,p_4 + 1803.2\,p_5 + 0\,p_6 + 1252.22\,p_7 + 0\,p_8 &= 0 \\
0\,p_1 + 1252.2\,p_2 + 0\,p_3 + 1803.2\,p_4 - 6110.84\,p_5 + 1803.2\,p_6 + 0\,p_7 + 1252.2\,p_8 &= 0 \\
0\,p_1 + 0\,p_2 + 1252.22\,p_3 + 0\,p_4 + 1803.2\,p_5 - 4307.6\,p_6 + 0\,p_7 + 0\,p_8 &= -1252222 \\
0\,p_1 + 0\,p_2 + 0\,p_3 + 1252.22\,p_4 + 0\,p_5 + 0\,p_6 - 3055.42\,p_7 + 1803.2\,p_8 &= 0 \\
0\,p_1 + 0\,p_2 + 0\,p_3 + 0\,p_4 + 1252.22\,p_5 + 0\,p_6 + 1803.2\,p_7 - 4858.6\,p_8 &= -1803200
\end{aligned}
$$

Resolviendo el sistema de ecuaciones por eliminación de Gauss - (método directo), se obtiene la siguiente distribución de presiones:

$p_1 = 1303.6270$ lb/pg^2

$p_2 = 1216.6606$ "

$p_3 = 1174.7270$ "

$p_4 = 1189.2844$ "

$p_5 = 1151.8139$ "

$p_6 = 1114.3426$ "

$p_7 = 1128.9000$ "

$p_8 = 1086.9664$ "

q = 500 o_1 p = 1303.6	q = 0 o_2 p = 1216.6	q = 0 o_3 p = 1174.7
q = 0 o_4 p = 1189.2	q = 0 o_5 p = 1151.8	q = 0 o_6 p = 1114.3
q = 0 o_7 p = 1128.9	q = 0 o_8 p = 1086.9	q = - 500 o_9 p = 1000

∴ q(bl/día), p(lb/pg^2)

5.5 ARREGLOS CARACTERISTICOS RESULTANTES DE FLUJO MONOFASICO.

a).- Una dimensión

Ecuación:

$$\frac{p_{i-1}^{n+1} - 2p_i^{n+1} + p_{i+1}^{n+1}}{(\Delta x)^2} = \frac{1}{\alpha} \frac{p_i^{n+1} - p_i^{n}}{\Delta t}$$

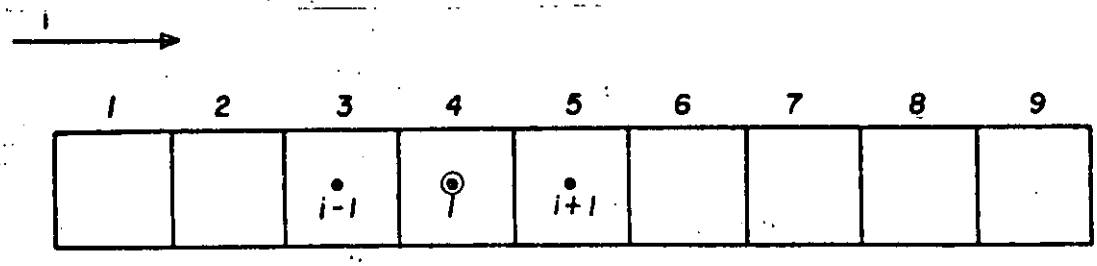

$$\begin{bmatrix} xx & & & & & & & & \\ xxx & & & & & & & & \\ xxx & & & & & & & & \\ xxx & & & & & & & & \\ xxx & & & & & & & & \\ xxx & & & & & & & & \\ xxx & & & & & & & & \\ xxx & & & & & & & & \\ xx & & & & & & & & \end{bmatrix} \begin{bmatrix} p_1 \\ p_2 \\ p_3 \\ p_4 \\ p_5 \\ p_6 \\ p_7 \\ p_8 \\ p_9 \end{bmatrix} = \begin{bmatrix} q_1 \\ q_2 \\ q_3 \\ q_4 \\ q_5 \\ q_6 \\ q_7 \\ q_8 \\ q_9 \end{bmatrix}$$

Obteniendose una matriz tridiagonal

b).- *Dos dimensiones*

Ecuación

$$\frac{p^{n+1}_{i-1} - 2p^{n+1}_{i,j} + p^{n+1}_{i+1,j}}{(\Delta x)^2} + \frac{p^{n+1}_{i,j-1} - 2p^{n+1}_{i,j} + p^{n+1}_{i,j+1}}{(\Delta y)^2} = \frac{1}{\alpha}$$

$$\frac{p^{n+1}_{i,j} - p^{n}_{i,j}}{\Delta t}$$

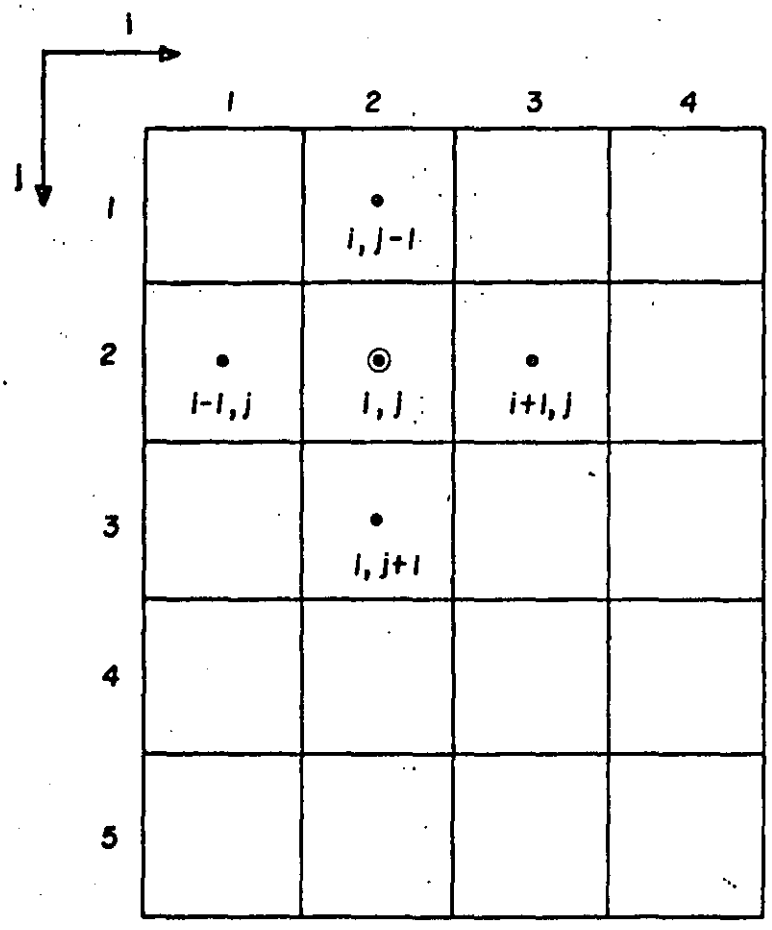

Suponiendo que se tiene una malla de cuatro por cinco, se obtendrá una matriz pentadiagonal, diagonalmente dominante, en donde la parte - central de la matriz, esta formada por cinco matrices de 4 x 4, que corresponderá al flujo en la dirección "x".

Las diagonales adyacentes a la parte central corresponderán al flujo en la dirección "y".

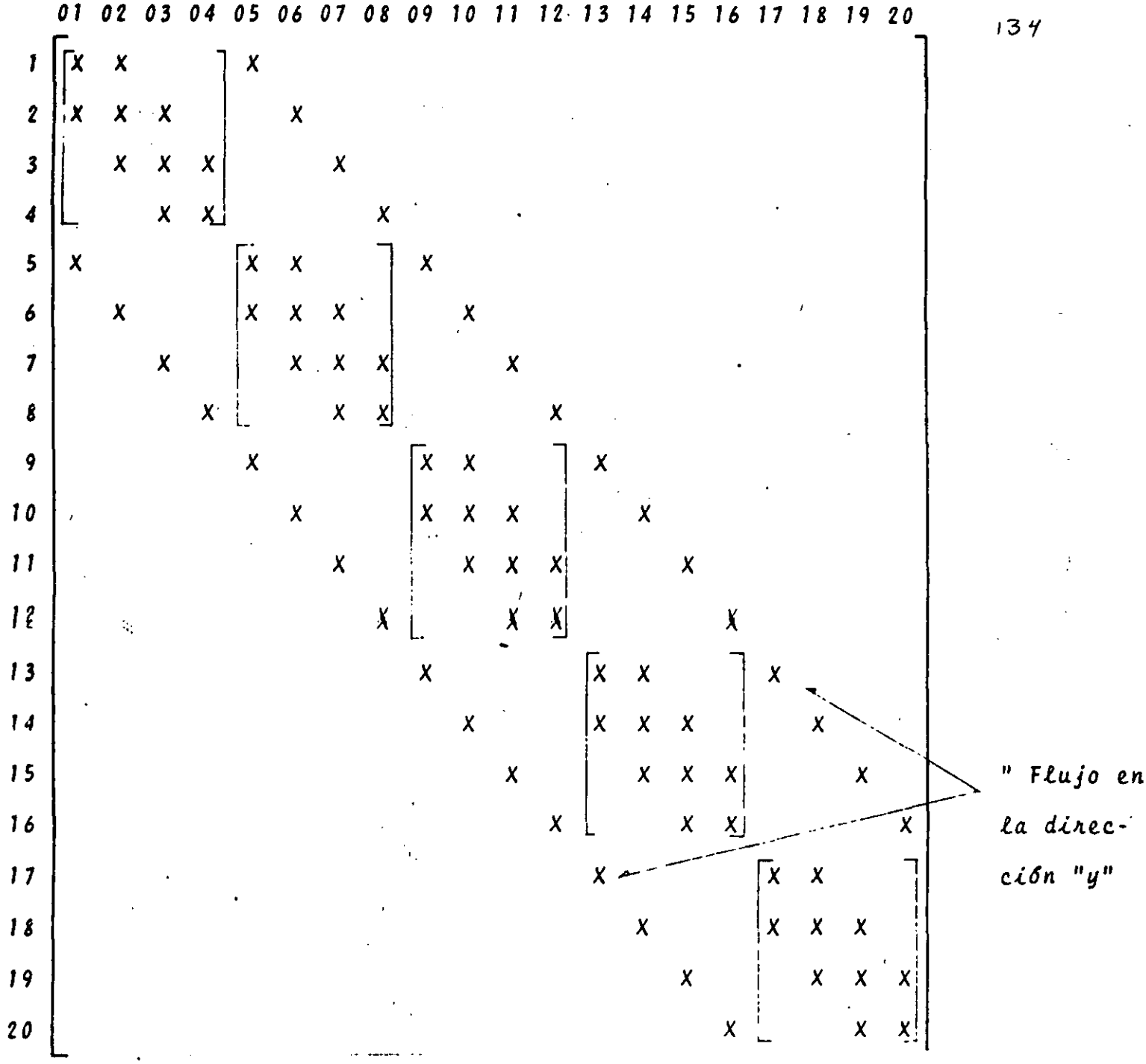

e) Tres dimensiones (flujo monofásico)

Ecuación

término en x + término en y +

$$+\frac{p_{i,j,k-1}^{n+1} - 2p_{i,j,k}^{n+1} + p_{i,j,k+1}^{n+1}}{(\Delta z)^2} = \frac{1}{\alpha}\,\frac{p_{i,j,k}^{n+1} - p_{i,j,k}^{n}}{\Delta t}$$

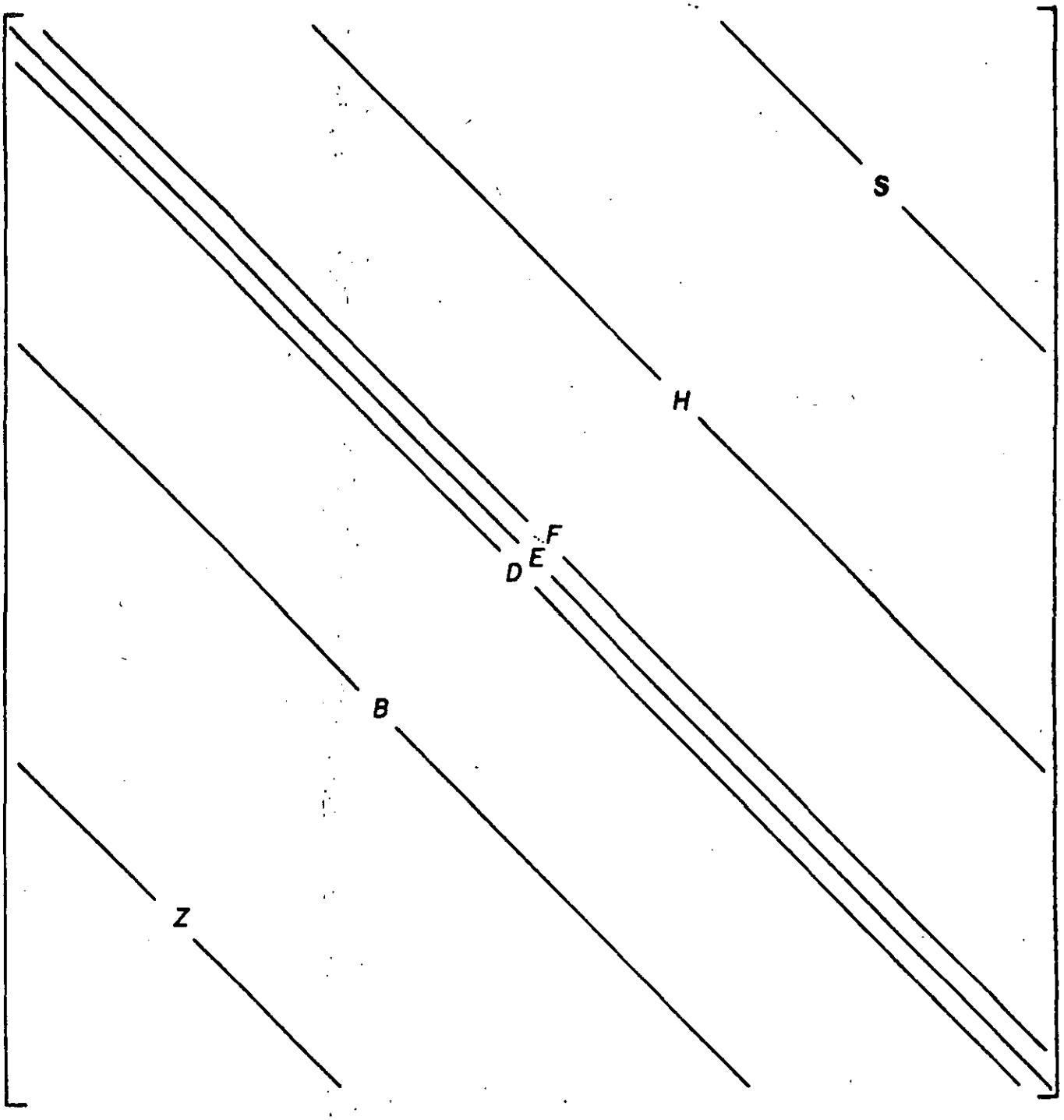

D, E y F —— FLUJO EN LA DIRECCION "X"
B y H —— FLUJO EN LA DIRECCION "Y"
Z y S —— FLUJO EN LA DIRECCION "Z"

5.6 ALGORITMO DE THOMAS PARA UN SISTEMA DE ECUACIONES TRIDIAGONAL.

El algoritmo de Thomas es esencialmente una variación de la eliminación Gaussiana y con el cual se evita el crecimiento del error asociado con la solución de las ecuaciones y se disminuyen los problemas en cuanto a capacidad de computadora.

Supongase que se tiene un sistema de n ecuaciones con las incógnitas $x_1, x_2, \ldots\ldots\ldots x_n$ *en donde:*

$$\begin{bmatrix} b_1 & c_1 & 0 & 0 & 0 & 0 \\ a_2 & b_2 & c_2 & 0 & 0 & 0 \\ 0 & a_3 & b_3 & c_3 & 0 & 0 \\ 0 & 0 & a_4 & b_4 & c_4 & 0 \\ & & & \cdot & \cdot & \cdot \\ & & & \cdot & \cdot & \cdot \\ & & & \cdot & \cdot & \cdot \\ & & & a_{n-1} & b_{n-1} & c_{n-1} \\ & & & & a_n & b_n \end{bmatrix} \begin{bmatrix} x_1 \\ x_2 \\ x_3 \\ x_4 \\ \cdot \\ \cdot \\ \cdot \\ x_{n-1} \\ x_n \end{bmatrix} = \begin{bmatrix} d_1 \\ d_2 \\ d_3 \\ d_4 \\ \cdot \\ \cdot \\ \cdot \\ d_{n-1} \\ d_n \end{bmatrix}$$

$$b_1x_1 + c_1x_2 + \qquad\qquad = d_1$$

$$a_2x_1 + b_2x_2 + c_2x_3 + \qquad = d_2$$

$$+ a_3x_2 + b_3x_3 + c_3x_4 \qquad = d_3$$

$$+ a_4x_3 + b_4x_4 + c_4x_5 \qquad = d_4$$

$$\cdot \qquad \cdot$$

$$\cdot \qquad \cdot$$

$$a_{n-1}x_{n-2} + b_{n-1}x_{n-1} + c_{n-1}x_n = d_{n-1}$$

$$a_n x_{n-1} + b_n x_n = d_n$$

Por definición

$$\gamma_1 = \frac{d_1}{b_1} \quad \ldots\ldots \quad (1)$$

$$\omega_1 = \frac{c_1}{b_1} \quad \ldots\ldots \quad (2)$$

despejando x_1 de la primera ecuación y sustituyendo las expresiones anteriores se tiene lo siguiente:

$$x_1 = \frac{d_1}{b_1} - \frac{c_1}{b_1} x_2$$

entonces

$$x_1 = \gamma_1 - \omega_1 x_2 \ldots\ldots\ldots \quad (3)$$

sustituyendo la ecuación (3) en la segunda ecuación del sistema se tiene

$$a_2 (\gamma_1 - \omega_1 x_2) + b_2 x_2 + c_3 x_3 = d_2$$

factorizando x_2

$$(b_2 - a_2\omega_1) x_2 + c_3 x_3 = d_2 - a_2\gamma_1$$

definiendo a

$$\beta_2 = b_2 - a_2\omega_1$$

$$x_2 = \frac{d_2 - a_2\gamma_1}{\beta_2} - \frac{c_2 x_3}{\beta_2}$$

ahora

$$\gamma_2 = \frac{d_2 - a_2\gamma_1}{\beta_2}, \quad \omega_2 = \frac{c_2}{\beta_2}$$

$$x_2 = \gamma_2 - \omega_2 x_3 \ldots\ldots\ldots\ldots\ldots\ldots \quad (4)$$

continuando el proceso hasta n-1, ya que hasta n-1 habrán 3 ecuaciones por lo tanto

$$\beta_i = b_i - a_i \omega_{i-1}$$

$$\gamma_i = \frac{d_i - a_i \gamma_{i-1}}{\beta_i}$$

$$\omega_i = \frac{c_i}{\beta_i}$$

.

.

.

$$x_{n-1} = \gamma_{n-1} - \omega_{n-1} x_n$$

sustituyendo las expresiones anteriores en la última ecuación del sistema se tiene,

$$a_n (\gamma_{n-1} - \omega_{n-1} x_n) + b_n x_n = d_n$$

$$(b_n - a_n \omega_{n-1}) x_n = d_n - a_n \gamma_{n-1}$$

$$x_n = \gamma_n$$

$$x_i = \gamma_i - \omega_i x_{i+1}$$

como ya se conoce el valor de x_n, *ahora se conocerán los valores de-* x_{n-1}, x_{n-2}, x_{n-3}, *etc. El algoritmo de Thomas consiste en dos secuencias:*

1).- *Primera secuencia progresiva:*

$$\beta_1 = b_1$$

$$\omega_i = \frac{c_i}{\beta_i} \quad , \qquad i = 1, 2, 3, \ldots\ldots n-1$$

$$\beta_i = b_i - a_i \omega_{i-1} \qquad i = 2, 3, 4, \ldots\ldots n$$

$$\gamma_1 = \frac{d_1}{\beta_1} \, , \gamma_i = \frac{d_i - a_i \gamma_{i-1}}{\beta_i} \qquad i = 2, 3, 4, \ldots\ldots n$$

2).- *Segunda secuencia regresiva*

$$x_n = \gamma_n$$

$$x_i = \gamma_i - \omega_i \, x_{i+1} \, , \; i = n-1, \; n-2, \; n-3, \; \ldots\ldots \; 1$$

5.7 FLUJO POCO COMPRESIBLE, HORIZONTAL, EN DOS DIMENSIONES.

La ecuación para este tipo de flujo es la siguiente:

$$\frac{\partial}{\partial x}\left(\frac{Ax\,Kx}{\mu_o\,Bo}\frac{\partial p}{\partial x}\right)\Delta x + \frac{\partial}{\partial y}\left(\frac{Ay\,Ky}{\mu_o Bo}\frac{\partial p}{\partial y}\right)\Delta y + q_{stb/d} = \frac{\phi\, c\, V_b}{5.615}\frac{\partial p}{\partial t}$$

En donde:

A	*Area transversal total*	$[pie^2]$
K	*Permeabilidad absoluta (1.127 x Darcy)*	[Darcy]
μ_o	*Viscosidad del fluido*	[cp]
Bo	*Factor de volúmen*	[vol. cy./vol.@c.s.]
p	*Presión*	$[lb/pg^2]$
x, y	*Distancia*	[pie]
$\Delta x, \Delta y$	*Longitudes de las celdas*	[pie]
ϕ	*Porosidad*	[fracción]
c	*Compresibilidad del fluido*	$[vol./vol.\,lb/pg^2]$
t	*Tiempo*	[días]
V_b	*Volúmen total de la celda*	$[pie^3]$

$A = h\,\Delta y$

$A = h\,\Delta x$

$V = h\,\Delta x\,\Delta y$

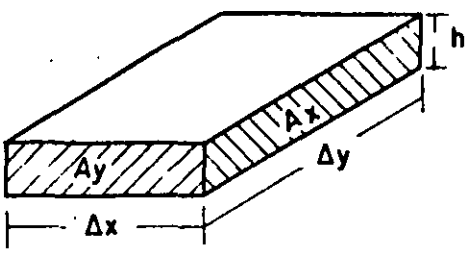

La expansión en diferencias finitas será:

$$\frac{\partial^2 p}{\partial x^2} = \frac{p_{i-1,j} - 2p_{i,j} + p_{i+1,j}}{(\Delta x)^2}$$

$$\frac{\partial^2 p}{\partial y^2} = \frac{p_{i,j-1} - 2p_{i,j} + p_{i,j+1}}{(\Delta y)^2}$$

* 1.127 ctte. de transformación para que el gasto de directamente en b1/día

Formulando la expresión en la dirección "x" se tiene:

$$\left(\frac{A_x K_x \Delta x}{\mu_o B_o}\right)\left(\frac{p_{i-1,j} - 2p_{i,j} + p_{i+1,j}}{(\Delta x)^2}\right) = \left(\frac{A_x K_x}{\mu_o B_o \Delta x}\right)$$

$$(p_{i-1,j} - 2p_{i,j} + p_{i+1,j})$$

$$\left(\frac{A_x K_x}{\mu_o B_o \Delta x}\right)(p_{i-1,j} - p_{i,j} - p_{i,j} + p_{i+1,j})$$

$$\left(\frac{A_x K_x}{\mu_o B_o \Delta x}\right)\Big|_{i+1/2,j}(p^{n+1}_{i+1,j} - p^{n+1}_{i,j}) - \left(\frac{A_x K_x}{\mu_o B_o \Delta x}\right)\Big|_{i-1/2,j}(p^{n+1}_{i,j} - p^{n+1}_{i-1,j})$$

en la dirección "y"

$$\left(\frac{A_y K_y}{\mu_o B_o \Delta y}\right)\Big|_{i,j+1/2}(p^{n+1}_{i,j+1} - p^{n+1}_{i,j}) - \left(\frac{A_y K_y}{\mu_o B_o \Delta y}\right)\Big|_{i,j-1/2}(p^{n+1}_{i,j} - p^{n+1}_{i,j-1})$$

obteniendose la siguiente expresión:

$$\left(\frac{Ax\ Kx}{\mu_o B_o \Delta x}\right)\Big|_{i+1/2,j}\left(p^{n+1}_{i+1,j} - p^{n+1}_{i,j}\right) - \left(\frac{Ax\ Kx}{\mu_o B_o \Delta x}\right)\Big|_{i-1/2,j}\left(p^{n+1}_{i,j} - p^{n+1}_{i-1,j}\right) +$$

$$+ Tx_{i+1/2,j} \qquad - Tx_{i-1/2,j}$$

$$\therefore \quad \frac{Ax\ Kx}{\mu_o B_o \Delta x} = Tx_{i\pm1/2,j}$$

$$\left(\frac{Ay\ Ky}{\mu_o B_o \Delta y}\right)\Big|_{i,j+1/2}\left(p^{n+1}_{i,j+1} - p^{n+1}_{i,j}\right) - \left(\frac{Ay\ Ky}{\mu\ B\ \Delta y}\right)\Big|_{i,j-1/2}\left(p^{n+1}_{i,j} - p^{n+1}_{i,j-1}\right) +$$

$$+ Ty_{i,j+1/2} \qquad - Ty_{i,j-1/2}$$

$$q_{i,j}\ stb/dia = \frac{\phi\ c\ V_{b\,i,j}}{5.615\ \Delta t}\left(p^{n+1}_{i,j} - p^{n}_{i,j}\right)$$

esta ecuación se puede escribir en la notación SIP:

$$B_{i,j}\ p_{i,j-1} + D_{i,j} p_{i-1,j} + E_{i,j}\ p_{i,j} + F_{i,j}\ p_{i+1,j} + H_{i,j}\ p_{i,j+1} = q_{i,j}$$

en donde:

$$B_{i,j} = \left(\frac{Ay\ Ky}{\mu_o\ B_o \Delta y}\right)_{i,j-1/2} \qquad D_{i,j} = \left(\frac{Ax\ Kx}{\mu o\ B_o \Delta x}\right)_{i-1/2,j}$$

$$\Gamma_{i,j} = \frac{V_{b\,i,j}\ \phi\ c}{5.615} \qquad H_{i,j} = \left(\frac{Ay\ Ky}{\mu_o\ B_o \Delta y}\right)_{i,j+1/2}$$

$$F_{i,j} = \left(\frac{Ax\ Kx}{\mu_o B_o \Delta x}\right)_{i+1/2,j} \qquad q_{i,j} = -\,q\,stb/dia_{i,j} - \frac{\Gamma_{i,j}}{\Delta t}\,p^{n}_{i,j}$$

$$E_{i,j} = Ex_{i,j} + Et_{i,j} + Ey_{i,j} \qquad Ex_{i,j} = -\left(\frac{Ax\ Kx}{\mu_o\ B_o \Delta x}\right)_{i+1/2,j} - \left(\frac{Ax\ Kx}{\mu o\ B_o \Delta x}\right)_{i-1/2j}$$

$$Et_{i,j} = -\frac{\Gamma_{i,j}}{\Delta t} \qquad Ey_{i,j} = -\left(\frac{Ay\,Ky}{\mu o\,Bo\Delta y}\right)_{i,j+1/2} -$$

$$\left(\frac{Ay\,Ky}{\mu o,Bo\Delta y}\right)_{i,j-1/2}$$

$$Ex_{i,j} = -(D + F) \qquad Ey_{i,j} = -(B + H)$$

5.8 ESQUEMAS DE SOLUCION.

1.- DIFERENCIAS PROGRESIVAS

- Nivel de tiempo (n) en el LIE*
- Condicionalmente estable:

$$\alpha\frac{\Delta t}{(\Delta x)^2} + \alpha\frac{\Delta t}{(\Delta y)^2} \leq 1/2$$

- Error $O(\Delta x)^2 + O(\Delta t) + O(\Delta y)^2$

2.- DIFERENCIAS REGRESIVAS

- Nivel de tiempo (n+1) en el LIE
- Incondicionalmente estable
- Error $O(\Delta x)^2 + O(\Delta t) + O(\Delta y)^2$

3.- CRANK - NICHOLSON

- Nivel de tiempo 1/2 (n+1) y 1/2 (n) en el LIE
- Incondicionalmente estable
- Error $O(\Delta x)^2 + O(\Delta t)^2 + O(\Delta y)^2$

4.- PROMEDIOS PONDERADOS

- Nivel de tiempo θ(n+1) y (1- θ) (n) en el LIE
- Incondicionalmente estable si $1/2 \leq \theta \leq 1$

* LIE LADO IZQUIERDO DE LA ECUACION

- Condicionalmente estable si $0 \leq \theta \leq 1/2$

5.- DUFORT - FRANKEL

- Tres niveles de tiempo (n-1), (n), (n+1)
- Explícito en (n+1)
- Puede ser inconsistente .'. no es recomendable

6.- ADEP (PROCEDIMIENTO EXPLICITO DE DIRECCION ALTERNANTE)

versión de BARAKAT - CLARK

- Explícito
- Incondicionalmente estable
- Error $\theta(\Delta x)^2 + \theta(\Delta y)^2 + \theta(\Delta t)^2$

PRIMER PASO

$$\frac{U^{n+1}_{i-1,j} - U^{n+1}_{i,j} - U^{n}_{i,j} + U^{n}_{i+1,j}}{(\Delta x)^2} + \frac{U^{n+1}_{i,j-1} - U^{n+1}_{i,j} - U^{n}_{i,j} - U^{n}_{i,j+1}}{(\Delta y)^2} =$$

$$\frac{1}{\alpha} \frac{U^{n+1}_{i,j} - U^{n}_{i,j}}{\Delta t}$$

si $a = \frac{\alpha \Delta t}{(\Delta x)^2}$ y $b = \frac{\alpha \Delta t}{(\Delta y)^2}$

$$aU^{n+1}_{i-1,j} - aU^{n+1}_{i,j} - aU^{n}_{i,j} + aU^{n}_{i+1,j} + bU^{n+1}_{i,j-1} - bU^{n+1}_{i,j} - bU^{n}_{i,j} - bU^{n}_{i,j+1} = U^{n+1}_{i,j} - U^{n}_{i,j}$$

despejando

$$U^{n+1}_{i,j} = \frac{1-a-b}{1+a+b} U^{n}_{i,j} + \frac{aU^{n+1}_{i-1,j} + aU^{n}_{i+1,j} + bU^{n+1}_{i,j-1} + bU^{n}_{i,j+1}}{1+a+b}$$

Ahora, se barre la malla en el siguiente orden:

$j = 1$; $i = 1, 2, 3, \ldots\ldots Nx$

$j = 2$; $i = 1, 2, 3, \ldots\ldots Nx$

$j = 3$; $i = 1, 2, 3, \ldots\ldots Nx$

. .

$j = Ny$; $i = 1, 2, 3, \ldots\ldots Nx$

SEGUNDO PASO

$$\frac{u^{n}_{i-1,j} - u^{n}_{i,j} - u^{n+1}_{i,j} - u^{n+1}_{i+1,j}}{(\Delta x)^2} + \frac{u^{n}_{i,j-1} - u^{n}_{i,j} - u^{n+1}_{i,j} - u^{n+1}_{i,j+1}}{(\Delta y)^2} =$$

$$\frac{1}{\alpha}\ \frac{u^{n+1}_{i,j} - u^{n}_{i,j}}{\Delta t}$$

$$aU^{n}_{i-1,j} - aU^{n}_{i,j} - aU^{n+1}_{i,j} + aU^{n+1}_{i+1,j} + bU^{n}_{i,j-1} - bU^{n}_{i,j} - bU^{n+1}_{i,j} + bU^{n+1}_{i,j+1}$$

$$u^{n+1}_{i,j} - u^{n}_{i,j}$$

despejando

$$u^{n+1}_{i,j} = \frac{1-a-b}{1+a+b}\, u^{n}_{i,j} + \frac{aU^{n}_{i-1,j} + aU^{n+1}_{i+1,j} + bU^{n}_{i,j-1} + bU^{n+1}_{i,j+1}}{1+a+b}$$

ahora; se barre la malla en el siguiente orden:

$j = Ny$; $i = Nx, Nx-1, Nx-2, \ldots, 1$

$j = Ny-1$; $i = Nx, Nx-1, Nx-2, \ldots, 1$

$j = Ny-2$; $i = Nx, Nx-1, Nx-2, \ldots, 1$

. .

. .

. .

$j = 1$; $i = Nx, Nx-1, Nx-2 \ldots, 1$

TERCER PASO

$$U^{n+1}_{i,j} = \frac{U^{(1)\,n+1}_{i,j} + U^{(2)\,n+1}_{i,j}}{2}$$

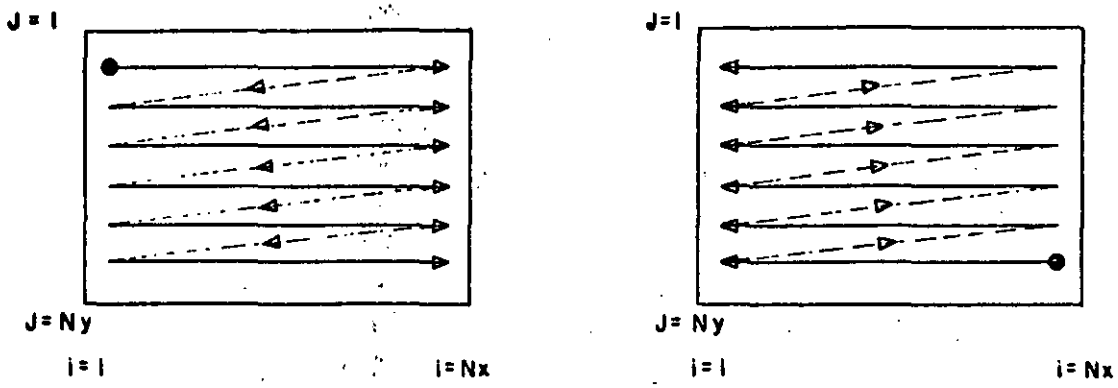

7.- ADIP (No iterativo)

(PROCEDIMIENTO IMPLICITO DE DIRECCION ALTERNANTE)

Peaceman y Rachford, Trans.AIME 1959.

PROPOSITO: Avanzar la solución del tiempo "n" al tiempo "n+1"

PRIMER PASO

Se consideran implícitas las incógnitas en la dirección "x" y explícitas las incógnitas en la dirección "y". Además en los términos - $q_{i,j}$, $E\,t$, se usa un intervalo de tiempo de $\Delta t/2$. (por ejemplo - $r_{i,j}/\Delta t/2$). En el primer paso se avanza la solución del nivel "n" - al nivel "*".

$$D\,P^{*}_{i-1,j} + (Ex+Et)P^{*}_{i,j} + F\,P^{*}_{i+1,j} = -\,(B\,P^{n}_{i,j-1} + Ey\,P^{n}_{i,j} + H\,P^{n}_{i,j+1}) + q^{n}_{i,j}$$

Para cada (i, j) se tiene una ecuación con tres incógnitas, por -

lo tanto para poder resolver el sistema es necesario escribir Nx ecuaciones para toda "i" y una "j" dada. Las Nx ecuaciones con Nx incógnitas resultan en un sistema tridiagonal que se puede resolver eficientemente con el algoritmo de Thomas.

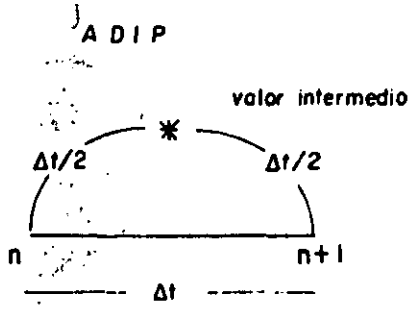

SEGUNDO PASO

Ahora se consideran implícitas las incógnitas en la dirección "y" y explícitas las incógnitas en la dirección "x":

$$B\,P^{n+1}_{i,j-1} + (Ey+Et)\,P^{n+1}_{i,j} + H\,P^{n+1}_{i,j+1} = -\,(D\,P^{*}_{i-1,j} + Ex\,P^{*}_{i,j} + F\,P^{*}_{i+1,j}) + q^{n}_{i,j}$$

Similarmente se analizan simultaneamente Ny ecuaciones con Ny incógnitas escribiendo las ecuaciones para toda "j" y una "i" dada. La solución se obtiene por medio del algoritmo de Thomas.

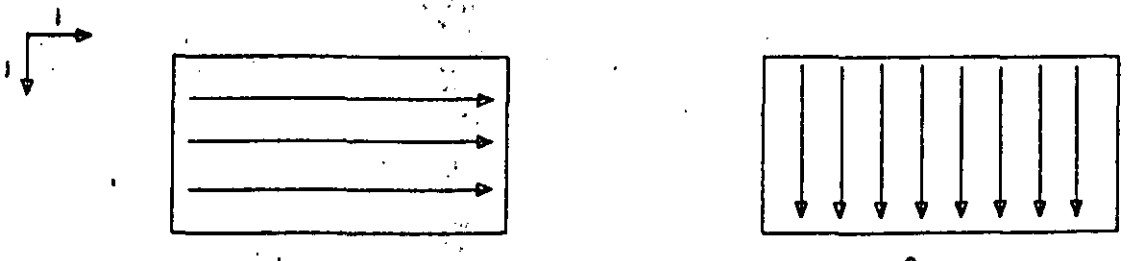

Comparativamente, para una malla de 10 x 20 el esquema regresivo genera 200 ecuaciones con 200 incógnitas, dando lugar a una estructura pentadiagonal. Por lo tanto, para avanzar la solución de "n" a "n+1" se necesita resolver este sistema. El esquema ADIP requiere resolver 10 ecuaciones veinte veces más 20 ecuaciones diez veces, todas ellas

PASO 2

$$\frac{U^{(m+1/2)}_{i-1,j} - 2\,U^{(m+1/2)}_{i,j} + U^{(m+1/2)}_{i+1,j}}{(\Delta x)^2} + \frac{U^{(m+1)}_{i,j-1} - 2\,U^{(m+1)}_{i,j} + U^{(m+1)}_{i,j+1}}{(\Delta y)^2} +$$

$$q_{i,j} = \alpha_L\left(U^{(m+1)}_{i,j} - U^{(m+1/2)}_{i,j}\right)$$

Los α_L son PARAMETROS DE ITERACION. Su empleo acelera la convergencia del proceso. Normalmente se utilizan de 4 a 8 parámetros de iteración en forma cíclica. Por ejemplo, si se seleccionan cuatro parámetros $\alpha_1 = 4$, $\alpha_2 = 2$, $\alpha_3 = 1$, $\alpha_4 = 0.5$ se usaría α_1 para la primera iteración, α_2 para la segunda, α_3 para la tercera, α_4 para la cuarta, α_1 para la quinta, α_2 para la sexta, etc. El método converge para cualquier valor positivo de α.

En todos los métodos iterativos hay que investigar si ya se alcanzó la convergencia despuls de cada iteración, por ejemplo

$$\text{¿ Max}_{i,j} \left| U^{(m+1)}_{i,j} - U^{(m)}_{i,j} \right| < \varepsilon \text{ ?}$$

METODOS ITERATIVOS PARA FLUJO TRANSITORIO

9.- METODO DE JACOBI

$$P^{(m+1)}_{i,j} = -\frac{1}{E_{i,j}}\left[\left(-q^{n}_{i,j} + B_{i,j}\,P^{n+1\,(m)}_{i,j-1} + D_{i,j}\,P^{n+1\,(m)}_{i-1,j} + F_{i,j}\,P^{n+1\,(m)}_{i+1,j} + H_{i,j}\,P^{n+1\,(m)}_{i,j+1}\right)\right]$$

Este método es muy lento y por lo tanto no es recomendable utilizarlo

10.- METODO DE GAUSS-SEIDEL

$$P_{i,j}^{(m+1)\,n+1} = -\frac{1}{E_{i,j}}\left(-q_{i,j}^{n} + B_{i,j}P_{i,j-1}^{(m+1)\,n+1} + D_{i,j}P_{i-1,j}^{(m+1)\,n+1} + F_{i,j}P_{i+1,j}^{(m)\,n+1} + H_{i,j}P_{i,j+1}^{(m)\,n+1} \right)$$

11.- PSOR (SOBRERELAJACION PUNTUAL SUCESIVA)

$$P_{i,j}^{(m+1)\,n+1} = (1-\omega)\,P_{i,j}^{(m)\,n+1} + \omega\left\{ -\frac{1}{E_{i,j}}\left(-q_{i,j}^{n} + B_{i,j}P_{i,j-1}^{(m+1)\,n+1} + D_{i,j}P_{i-1,j}^{(m+1)\,n+1} + F_{i,j}P_{i+1,j}^{(m)\,n+1} + H_{i,j}P_{i,j+1}^{(m)\,n+1} \right)\right\}$$

12.- LSR (RELAJACION LINEAL SUCESIVA) : $\omega = 1$

En este método se tienen dos opciones, considerar la dirección "x" implícita, o considerar la dirección "y" implícita. Para la primera - iteración se tiene lo siguiente:

$$P_{i,j}^{(m+1)\,n+1} = -\frac{1}{E_{i,j}}\left(-q_{i,j}^{n} + B_{i,j}P_{i,j-1}^{(m)\,n+1} + D_{i,j}P_{i-1,j}^{(m+1)\,n+1} + F_{i,j}P_{i+1,j}^{(m+1)\,n+1} + H_{i,j}P_{i,j+1}^{(m)\,n+1} \right)$$

despejando:

$$D_{i,j}P_{i-1,j}^{(m+1)\,n+1} + E_{i,j}P_{i,j}^{(m+1)\,n+1} + F_{i,j}P_{i+1,j}^{(m+1)\,n+1} =$$

---------- *incógnitas* ----------

$$= \frac{1}{1} \left(- q_{i,j} + B_{i,j} P^{n+1}_{i,j-1(m)} + H_{i,j} P^{n+1}_{i,j+1(m)} \right)$$

--------- términos conocidos ----------

Por lo tanto se tiene que para:

j= 1 se generan Nx ecuaciones

j= 2 " " " "

j= 3 " " " "

j= 4 " " " "

. . . . .

. . . . .

j= Ny se generan Nx ecuaciones

Estos sistemas de ecuaciones se deben resolver M veces hasta que- se obtiene convergencia.

13.- LSOR (SOBRERELAJACION LINEAL SUCESIVA)

Nuevamente, para este método se tienen las dos opciones del LSR. Ilustrando ahora la forma de las ecuaciones al considerar la dirección "y" implícita.

$$P^{n+1}_{i,j(m+1)} = (1 - \omega) P^{n+1}_{i,j(m)} +$$

$$\omega \left\{ - \frac{1}{E_{i,j}} \left(- q^{n}_{i,j} + B_{i,j} P^{n+1}_{i,j-1(m+1)} + D_{i,j} P^{n+1}_{i-1,j(m)} + F_{i,j} P^{n+1}_{i+1,j(m)} + H_{i,j} P^{n+1}_{i,j+1(m+1)} \right) \right\}$$

Despejando:

$$\frac{Bi,j}{1}\ {}^{n+1}_{(m+1)}P_{i,j-1} + E_{i,j}\ {}^{n+1}_{(m+1)}P_{i,j} + H_{i,j}\ {}^{n+1}_{(m+1)}P_{i,j+1} =$$

términos desconocidos o incógnitas

$$(1-\omega)\ {}^{n+1}_{(m)}P_{i,j} + -\frac{1}{E_{i,j}} - {}^{n}q_{i,j} + D_{i,j}\ {}^{n+1}_{(m)}P_{i-1,j} + F_{i,j}\ {}^{n+1}_{(m)}P_{i+1,j}$$

-términos conocidos

En este caso, se tiene que para:

i= 1 se generan Ny ecuaciones

i= 2 se generan Ny ecuaciones

i= 3 " " "

. .

. .

i= Nx se generan Ny ecuaciones

Estos sistemas de ecuaciones se deben resolver M veces hasta obtener convergencia.

Para obtener ω optima en LSOR se procede en forma similar al caso de PSOR, por ejemplo se efectúan varias iteraciones con ω = 1 (LSOR) - obteniéndose el radio espectral (ρ). Con este valor se calcula ωopt.
ADIP (iterativo) PROCEDIMIENTO IMPLICITO DE DIRECCION ALTERNANTE Peaceman-Rachford, Douglas-Rachford (no usarlo ni en problemas en tres dimensiones ni en flujo multifásico)

PRIMER PASO

Considerando implícitas las incógnitas en la dirección "x" y explícitas las incógnitas en la dirección "y":

$$D\,P^{(*)}_{i-1,j} + (Ex+Et - hk\Sigma T)\,P^{(*)}_{i,j} + F\,P^{(*)}_{i+1,j} = q_{i,j} - \left[B\,P^{(m)}_{i,j-1} + (Ey + hk\Sigma T)\,P^{(m)}_{i,j} + HP^{(m)}_{i,j+1}\right]$$

SEGUNDO PASO

Considerando ahora implícitas las incógnitas en la dirección "y" y explícitas las incógnitas en la dirección "x":

$$B\,P^{(m+1)}_{i,j-1} + (Ey+Et- hk\Sigma T)\,P^{(m+1)}_{i,j} + H\,P^{(m+1)}_{i,j+1} = q_{i,j} - \left[D\,P^{(*)}_{i-1,j} + (Ex+ hk\Sigma T)\,P^{(*)}_{i,j} + F\,P^{(*)}_{i+1,j}\right]$$

PEACEMAN-RACHFORD

$$= q_{i,j} - \left[D\,P^{(*)}_{i-1,j} + Ex\,P^{(*)}_{i,j} + hk\Sigma TP^{(m)}_{j,j} + F\,P^{(*)}_{i+1,j}\right]$$

DOUGLAS-RACHFORD

Nótese que la única diferencia entre los dos esquemas iterativos - es que P-R le suma al LDE: $hk\Sigma T\,(P^{(m+1)}_{i,j} - P^{(*)}_{i,j})$ mientras que D-R le suma al LDE: $hk\Sigma T\,(P^{(m+1)}_{i,j} - P^{(m)}_{i,j})$ en el segundo paso de la iteración.

El procedimiento D-R en 3 dimensiones es similar usando niveles de iteración, $^{(*)}$, $^{(**)}$ y $^{(m+1)}$ y sumando $hk\Sigma T\,(P^{(**)}_{(m+1)} - P^{(m)})$ al LDE - respectivamente.

5.9 CONSISTENCIA, CONVERGENCIA, Y ESTABILIDAD.

En esta sección se verán formas de analizar las expansiones en diferencias finitas y determinar que tan representativas son para las -

ecuaciones diferenciales parciales originales, así como bajo que condiciones el esquema propuesto es estable.

Se dice que una ecuación en diferencias finitas es CONSISTENTE O-COMPATIBLE si tiende a ser idéntico a la ecuación diferencial parcial original a medida que $\Delta x \to 0$ y $\Delta t \to 0$.

Se dice que una ecuación en diferencias finitas es CONVERGENTE si la solución exacta a las ecuaciones en diferencias (u) tiende a la solución exacta a las ecuaciones diferenciales (u) para todo valor de x a medida que $\Delta x \to 0$ y $\Delta t \to 0$.

Se dice que un sistema de ecuaciones en diferencias finitas es - ESTABLE si un error en la solución (introducido por cualquier forma)- tiende a desvanecerse a medida que avanza la solución y si los errores de truncamiento en las operaciones aritméticas no se acumulan con el tiempo.

CONSISTENCIA O COMPATIBILIDAD

El análisis de consistencia de un esquema en diferencias finitas- se lleva a cabo en una forma similar a la desarrollada para analizar - el término del error, es decir, se expanden los términos en función - de series de Taylor y se analiza el comportamiento de la expresión resultante a medida que Δx y Δt tienden a cero.

Ejemplo: Analizar la consistencia del esquema de Dufort-Frankel.

ecuación diferencial parcial:

$$\frac{\partial^2 u}{\partial x^2} - \frac{1}{\alpha} \frac{\partial u}{\partial t} = 0$$

ecuación en diferencias finitas:

$$\frac{2\alpha \Delta t}{(\Delta x)^2} \left[U_{i+1}^{n} - U_{i}^{n+1} - U_{i}^{n} + U_{i-1}^{n} \right] = U_{i}^{n+1} - U_{i}^{n}$$

expandiendo en series de Taylor:

$$\frac{2\alpha\Delta t}{(\Delta x)^2}\left[U_i^n + (\Delta x)\left.\frac{\partial u}{\partial x}\right|_i^n + \frac{(\Delta x)^2}{2!}\frac{\partial^2 u}{\partial x^2} + \frac{(\Delta x)^3}{3!}\frac{\partial^3 u}{\partial x^3} + \frac{(\Delta x)^4}{4!}\frac{\partial^4 u}{\partial x^4} + \cdots\cdots\right.$$

$$- U_i^n - (\Delta t)\left.\frac{\partial u}{\partial t}\right|_i^n - \frac{(\Delta t)^2}{2!}\frac{\partial^2 u}{\partial t^2} - \frac{(\Delta t)^3}{3!}\frac{\partial^3 u}{\partial t^3} - \frac{(\Delta t)^4}{4!}\frac{\partial^4 u}{\partial t^4} - \cdots\cdots$$

$$- U_i^n + (\Delta t)\left.\frac{\partial u}{\partial t}\right|_i^n - \frac{(\Delta t)}{2!}\frac{\partial^2 u}{\partial t^2} + \frac{(\Delta t)}{3!}\frac{\partial^3 u}{\partial t^3} - \frac{(\Delta t)}{4!}\frac{\partial^4 u}{\partial t^4} + \cdots\cdots$$

$$\left. + U_i^n - (\Delta x)\frac{\partial u}{\partial x} + \frac{(\Delta x)^2}{2!}\frac{\partial^2 u}{\partial x^2} - \frac{(\Delta x)^3}{3!}\frac{\partial^3 u}{\partial x^3} + \frac{(\Delta x)^4}{4!}\frac{\partial^4 u}{\partial x^4}\cdots\right] =$$

$$= U_i^n + (\Delta t)\left.\frac{\partial u}{\partial t}\right|_i^n + \frac{(\Delta t)}{2!}\frac{\partial^2 u}{\partial t^2} + \frac{(\Delta t)}{3!}\frac{\partial^3 u}{\partial t^3} + \frac{(\Delta t)}{4!}\frac{\partial^4 u}{\partial t^4} + \cdots\cdots$$

$$- U_i^n + (\Delta t)\left.\frac{\partial u}{\partial t}\right|_i^n - \frac{(\Delta t)^2}{2!}\frac{\partial^2 u}{\partial t^2} + \frac{(\Delta t)^3}{3!}\frac{\partial^3 u}{\partial t^2} - \frac{(\Delta t)^4}{4!}\frac{\partial^4 u}{\partial t^4} + \cdots\cdots$$

simplificando términos, la ecuación se reduce a:

$$\frac{2\alpha\Delta t}{(\Delta x)^2}\left[(\Delta x)^2\left.\frac{\partial^2 u}{\partial x^2}\right|_i^n - (\Delta t)^2\left.\frac{\partial^2 u}{\partial t^2}\right|_i^n + \left.\frac{\partial^2 u}{\partial t^2}\right|_i^n + \frac{(\Delta x)^4}{12}\left.\frac{\partial^4 u}{\partial x^4}\right|_i^n - \right.$$

$$\left.\frac{(\Delta t)^4}{12}\left.\frac{\partial^4 u}{\partial t^4}\right|_i^n\right] = 2(\Delta t)\left.\frac{\partial u}{\partial t}\right|_i^n + \frac{(\Delta t)^3}{3}\left.\frac{\partial^3 u}{\partial t^3}\right|_i^n$$

dividiendo por $2\alpha\Delta t$

$$\frac{\partial^2 u}{\partial x^2} - \frac{(\Delta t)^2}{(\Delta x)^2}\frac{\partial^2 u}{\partial t^2} + \frac{(\Delta x)^2}{12}\frac{\partial^4 u}{\partial x^4} - \frac{(\Delta t)^4}{12(\Delta x)^2}\frac{\partial^4 u}{\partial t^4} = \frac{1}{\alpha}\frac{\partial u}{\partial t} + \frac{(\Delta t)^2}{6\alpha}\frac{\partial^3 u}{\partial t^3}$$

$$\frac{\partial^2 u}{\partial x^2} - \frac{1}{\alpha}\frac{\partial u}{\partial t} + \left[\frac{(\Delta x)^2}{12}\frac{\partial^4 u}{\partial x^4} - \frac{(\Delta t)^2}{6\alpha}\frac{\partial^3 u}{\partial t^3} - \left(\frac{(\Delta t)^2}{(\Delta x)}\right)^2 \frac{\partial^2 u}{\partial t^2} - \frac{1}{12}\left(\frac{(\Delta t)^2}{(\Delta x)}\right)^2 \frac{\partial^4 u}{\partial t^4}\right] = 0$$

Ahora la pregunta a contestar para analizar la consistencia de esta última ecuación es si tiende a la ecuación diferencial parcial a medida que $\Delta x \to 0$ *y que* $\Delta t \to 0$.

Como se puede comprobar el primero, segundo y cuarto término del parentesis tienden a cero a medida que $\Delta x \to 0$ *y* $\Delta t \to 0$ *(el término* $\frac{(\Delta t)^2}{\Delta x}$ *probablemente se acerca a cero) pero el cociente* $\frac{\Delta t}{\Delta x}$ *que aparece en el tercer término puede ser un número finito, digamos* β *por lo tanto el esquema Dufort-Frankel representa mas bién una ecuación del tipo de la ecuación de onda, por ejemplo:*

$$\frac{\partial^2 u}{\partial x^2} - \beta^2\frac{\partial^2 u}{\partial t^2} - \frac{1}{\alpha}\frac{\partial u}{\partial t} = 0$$

Una vez asegurada la consistencia de un esquema iterativo y para poder tener una aproximación válida, ésta debe arrojar resultados que esten más o menos cerca de la solución del problema original. Esta consideración se puede analizar en dos formas diferentes:

Primero se puede considerar un punto fijo x_i^n *y preguntar acerca de la diferencia entre* u_i^n *y* U_i^n *a medida que la malla (espacio-tiempo) se -*

hace cada vez más fina. Se espera que en el límite, a medida que $\Delta x \to 0$ y $\Delta t \to 0$, el error tienda también a cero. (CONVERGENCIA)

El segundo aspecto del comportamiento de la aproximación en diferencias finitas puede estudiarse manteniendo fijas Δx y Δt y examinando que pasa a medida que la solación se avanza en tiempo. Se espera - en este caso que los errores no se amplifiquen a tal grado que los resultados obtenidos no sean válidos (ESTABILIDAD).

CONVERGENCIA - ERROR DE TRUNCAMIENTO

En general, entre menor sea el error de truncamiento, la conver-- gencia de la ecuación en diferencias a la ecuación diferencial es más rápida. Por esto, una forma de analizar la convergencia de un esquema en diferencias finitas es analizando su error de truncamiento.

Error de truncamiento es el error incurrido al reemplazar la ecuación diferencial por una ecuación en diferencias finitas. Debido a este error, la solución exacta a la ecuación en diferencias (sin error de redondeo) es diferente a la solución de la ecuación diferencial -- parcial correspondiente.

El término "error de truncamiento" viene del hecho de que al reemplazar derivadas por cocientes de diferencias es equivalente a utilizar series de Taylor "truncadas".

El error de truncamiento local de una aproximación en diferencias finitas se define como:

$$E_L = L_D U_i^n - (Lu)_i^n$$

en donde:

E_L = error de truncamiento local

L_D = forma en diferencias finitas

Lu = forma diferencial

Por ejemplo: Para el esquema en diferencias progresivas:

$$Lu = \frac{\partial^2 u}{\partial x^2} - \frac{\partial u}{\partial t}$$

$$L_D U_i^n = \frac{U_{i-1}^n - 2 U_i^n + U_{i+1}^n}{(\Delta x)^2} - \frac{U_i^{n+1} - U_i^n}{\Delta t}$$

$$E_L = \frac{(\Delta x)^2}{12} \frac{\partial^4 u}{\partial x^4} - \frac{\Delta t}{2} \frac{\partial^2 u}{\partial t^2} \quad \acute{o} \quad E_L = \Theta(\Delta x)^2 + \Theta(\Delta t)$$

Si se tuviesen las soluciones exactas se podría definir el ERROR DE TRUNCAMIENTO GLOBAL mediante:

$$E_G = \text{Max}_{i,n} \left| U_i^n - u(x_i, t_n) \right|$$

En la mayoría de los casos, no se tiene la solución exacta $u(x_i, t_n)$ por lo tanto el problema consiste en tratar de encontrar los límites al error global. Para ecuaciones diferenciales simples normalmente se pueden encontrar pero, a medida que las ecuaciones se hacen más complejas, la estimación de estos límites se hace bastante más difícil. Afortunadamente se ha encontrado que los errores globales muestran el mismo orden de dependencia con respecto a los tamaños de malla (espacio-tiempo) que los errores locales. De aquí que los ERRORES LOCALES DE TRUNCAMIENTO que son mucho más fáciles de estimar se puedan usar por lo menos como guía para el orden de CONVERGENCIA de la solución a la ecuación en diferencias finitas a la solución de la ecuación diferencial a medida que el tamaño de la malla tiende a cero.

En la práctica, para problemas que tengan algún grado de dificultad la estimación del error se obtiene resolviendo la ecuación en diferencias utilizando diferentes tamaños de malla variando tanto los incrementos espaciales (Δx, Δy, Δz) como el incremento temporal (Δt) para encontrar sus efectos en la solución.

En muchas ocasiones, valores prácticos de Δx y Δt (para los cuales el tiempo de computación no se hace excesivo), son tan grandes que el error no parece disminuir tan rápidamente como lo predicen las fórmulas para el error local de truncamiento. La razón de esto es que las expresiones que se obtienen para el orden del error describen el comportamiento asimptótico a medida que Δx y Δt tienden a cero y no dicen mucho acerca del comportamiento del error para tamaños de malla relativamente grandes.

Por estas razones, normalmente se tienen que considerar como estimaciones empíricas del error obtenidas corriendo el mismo problema con diferentes tamaños de mallas. Una vez encontrado el tamaño de malla que equilibra el costo de usar un tamaño pequeño, contra el riesgo asociado al utilizar una malla grande y aumentar el error, se corren los siguientes casos con dicho tamaño.

ESTABILIDAD

Un esquema en diferencias finitas es ESTABLE si el efecto de un error (o perturbación) hecha en alguna de las etapas de cómputo no se propaga en errores a medida que la solución se avanza en etapas posteriores de cálculo.

Para el análisis de estabilidad no importa cual es la fuente del error por ejemplo, error de truncamiento, error de redondeo o alguna-

C A P I T U L O 6

CONSIDERACIONES GENERALES

1.- La simulación de yacimientos una herramienta útil, que aunada a otros procesos de predicción permite obtener mejores resultados en el estudio de yacimientos petroleros.

2.- La efectividad de una simulación está en función de la representatividad y de la calidad de la información que se proporcione.

3.- Los modelos matemáticos permiten simular el comportamiento de un yacimiento, bajo diferentes alternativas de producción, a fin de seleccionar la forma óptima de desarrollar y explotar un yacimiento de aceite y/o gas.

4.- En ocasiones es conveniente desarrollar un modelo matemático, de acuerdo a las características del yacimiento por estudiar.

5.- La predicción mediante una simulación, solo puede ser confiable cuando se cuente con la caracterización precisa del yacimiento y, además cuando el modelo permita simular los nuevos mecanismos de desplazamiento así como sus fenómenos asociados que posteriormente se presentarán.

6.- Ningún modelo simula los fenómenos de convención, supersaturación de aceite y el de inversión de pre—sión asociados al mecanismo de la segregación gravitacional.

7.- Un modelo matemático, una vez ajustado, es el mejor recurso para predecir el comportamiento de un yacimiento.

8.- Teniendo en cuenta las consideraciones anteriores se infiere que la aplicación de un modelo simplificado, con un buen criterio ingenieril, puede tener ventaja sobre un modelo sofisticado de simulación.

NOMENCLATURA

SIMBOLOS		UNIDADES FACTIBLES DE USARSE
A	: Area	$(pies^2)$
Bg	: Factor de volúmen del gas $(B_g < 1)$	$\frac{pies_g^3 \ @c.y}{pies_g^3 \ @c.s}$
Bo	: Factor de volúmen del aceite $(B_o > 1)$	$\frac{pies_o^3 \ @c.y + gd.@c.y}{pies_o^3 \ @c.s}$
Bw	: Factor de volúmen del agua.	$\frac{pies_w^3 \ @c.y + gd.@c.y}{pies_w^3 \ @c.s}$
c	: Compresibilidad	$(lb./pg^2)^{-1}$
c_f	: Compresibilidad de la formación	$(lb./pg^2)^{-1}$
c_g	: Compresibilidad del gas	$(lb./pg^2)^{-1}$
c_o	: Compresibilidad del aceite	$(lb./pg^2)^{-1}$
c_w	: Compresibilidad del agua	$(lb./pg^2)^{-1}$
D	: Profundidad	(pies)
E_G	: Error de truncamiento global	
E_L	: Error de truncamiento local	
e_t	: Término del error	
$f(x_i)$	: Función evaluada en cada punto	

g	: Aceleración de la gravedad.	(pies/seg.^{2})
g_c	: Constante gravitacional @ condiciones.	
	normales y es igual a 32.2 pies/seg.^{2}	(pies/seg.^{2})
h	: Altura.	(pies)
I	: Potencial de un gas real.	
K	: Permeabilidad absoluta.	(Darcy)
k_g	: Permeabilidad efectiva al gas.	(Darcy)
k_o	: Permeabilidad efectiva al aceite.	(Darcy)
k_w	: Permeabilidad efectiva al agua.	(Darcy)
kr_g	: Permeabilidad relativa al gas.	(Darcy)
kr_o	: Permeabilidad relativa al aceite.	(Darcy)
kr_w	: Permeabilidad relativa al agua.	(Darcy)
L	: Longitud.	(pies)
M	: Peso molecular +	(lb/mole-lb)
m	: Masa.	(lb $_m$)
Nx	: Número de bloques en la dirección "x"	
Ny	: Número de bloques en la dirección "y"	
Nz	: Número de bloques en la dirección "z"	
n	: Número de moles ($n = m/M$)	
$\vec{n}$	: Vector perpendicular a todas las super-	
	ficies equipotenciales.	
Θ	: Error de truncamiento.	
p	: Presión.	(lb./pg^2)
pc	: Presión capilar.	(lb./pg^2)
pc_{o-g}	: Presión capilar entre las interfases	
	gas-aceite.	(lb./pg^2)

+ En algunos capítulos se hace, M = masa, solamente para fines de análisis dimensional.

$p_{c_{w-o}}$	: Presión capilar entre las interfases agua-aceite.	(lb./pg^2)
$q_{vol.}$	: Ritmo de inyección y/o producción.	(bl.@c.s/día.pies^3)
q	: Gasto.	(bl./día)
R	: Constante universal de los gases.	(lb-pg^2/°R-mole-lb)
Rs	: Razón gas disuelto-aceite.	(pies^3_g/pies^3_o)
Sf	: Saturación de fluido en general.	(pies^3_f@c.y/pies$^3_{poros}$)
Sg	: Saturación de gas.	(pies^3_g@c.y/pies$^3_{poros}$)
So	: Saturación de aceite.	(pies^3_o@c.y/pies$^3_{poros}$)
Sw	: Saturación de agua.	(pies^3_w@c.y/pies$^3_{poros}$)
Sgr	: Saturación de gas residual.	(pies^3_g@c.y/pies$^3_{poros}$)
Sor	: Saturación de aceite residual.	(pies^3_o@c.y/pies$^3_{poros}$)
Swr	: Saturación de agua residual.	(pies^3_w@c.y/pies$^3_{poros}$)
Swi	: Saturación de agua intersticial.	(pies^3_w@c.y/pies$^3_{poros}$)
T	: Temperatura ++	(°R)
T	: Transmisividad $T = \frac{A\,k}{\mu\,B\Delta x}$	(pies^2 mD/cp pies)
t	: Tiempo.	(días)
u	: Velocidad aparente.	(pies/seg.)
$v_{med.}$	: Velocidad media.	(pies/seg.)
Vb	: Volúmen bruto de roca.	(pies^3)
V	: Volúmen.	(barriles)
W	: Término fuente o sumidero.	(Masa/volúmen de roca)
Z	: Factor de desviación de los gases reales.	
ϕ	: Porosidad.	(pies^3 poros/pies^3 roca)
ϕ_e	: Porosidad efectiva.	(pies^3 poros/pies^3 roca)
μ	: Viscosidad.	(poises)
μ_g	: Viscosidad del gas.	(poises)

++ En algunos capítulos se hace, T = tiempo, solamente para fines de análisis dimensional.

μ_o : Viscosidad del aceite. (poises)

μ_w : Viscosidad del agua. (poises)

ρ : Densidad. ($lb/pies^3$)

ρ_g : Densidad del gas. ($lb/pies^3$)

ρ_o : Densidad del aceite. ($lb/pies^3$)

ρ_w : Densidad del agua. ($lb/pies^3$)

Φ : Potencial de flujo. (lb/pg^2)

ω : Razón de convergencia.

ρ_e : Radio espectral de la matriz.

@c.s : Medido a condiciones estandar o superficiales.

@c.y : Medido a condiciones de yacimiento.

SUBINDICES

i : Irreductible.

g : Gas.

o : Aceite, inicial.

w : Agua.

x,y,z Direcciones ortogonales en los ejes x,y,z

i,j,k Direcciones ortogonales en los ejes x,y,z

TERMINOS USADOS EN TABLAS

A' . Coeficientes dados en la tabla.

m . Número de puntos usados en la aproximación menos uno.

n . Número del punto en el que se evalua la derivada.

L_D . Forma en diferencias finitas.

L_U . Forma diferencial.

FACTORES DE CONVERSION

Longitud

1 pg = 2.54 cm.

1 pie = 30.48 cm.

Volúmen

1 BL = 159 lt = 42 gal

1 BL = 5.615 $pies^3$

1 m^3 = 6.29 Bl = 35.314 $pies^3$

Presión

1 atm = 760 mm. Hg

1 atm = 14.7 lb/pg^2 abs.

CONSTANTES

Condiciones superficiales (c.s); 1 atm y 20°C ó 14.7 lb/pg^2 y 60°F

TEMPERATURA ABSOLUTA °K = °C + 273

°R = °F + 460

Peso molecular medio del aire seco = 28.97

Volúmen de 1 mole-gr de gas @c.s = 22.40 litros

Volúmen de 1 mole-lb de gas @c.s = 379.40 $pies^3$

Peso específico del agua @ c.s = 1 gr/cm^3 = 62.4 lb/pie^3

Peso específico del gas @c.s. = 0.0764 (lb/pie^3)

R = 82.05 (atm-cm) / (°K- mole-gr)

R = 10.73 (lb/pg^2- pie^3) / (°R-molc-lb)

CURSO: "INGENIERIA DE YACIMIENTOS GEOTERMICOS "
13 DE MARZO AL 18 DE MAYO DE 1984

TEMA: "GEOTHERMAL RESERVOIR SIMULATION
WITH SHAFT.

DR. GUILLERMO DOMINGUEZ
2-13 de abril

GEOTHERMAL RESERVOIR SIMULATIONS WITH SHAFT79

by Karsten Pruess and Ron C. Schroeder

Lawrence Berkeley Laboratory, Berkeley, Ca. 94720

INTRODUCTION

The rational development of geothermal resources requires an adequate knowledge of the behavior of a given reservoir under various production and injection schemes. Mathematical modeling attempts to provide such knowledge and to determine important reservoir parameters, such as formation permeabilities and reserves of fluid and heat.

Because of phase changes and because of the coupling between energy- and mass-flow, the equations describing geothermal reservoirs are strongly non-linear. This limits the applicability of analytical approximations and has motivated the development of numerical simulators. In this paper, we review the concepts and methods used in LBL's geothermal simulator SHAFT79, and illustrate its application to a variety of typical problems.

PHYSICAL MODEL AND SOLUTION METHOD

The simulator SHAFT79 was developed for computing two-phase flow phenomena in geothermal reservoirs. The program handles transient initial-value problems with prescribed boundary conditions. SHAFT79 is an improved version of the simulator SHAFT78, which was discussed in detail in ref. 1). It solves coupled equations for mass- and energy-transport, using an integrated finite difference method. This method allows a very flexible description of reservoirs because it does not distinguish between one-, two-, or three-dimensional regular or irregular geometries.

The main assumptions and approximations made in the formulation of SHAFT79 are as follows: (1) Geothermal reservoirs are approximated as systems of porous rock saturated with one-component fluid in liquid and vapor form. (2) All rock properties - porosity, density, specific heat, thermal conductivity, absolute permeability - are independent of temperature, pressure, or vapor saturation. (3) Liquid, vapor, and rock matrix are in local thermodynamic equilibrium, i.e. at the same temperature and pressure, at all times. (4) Capillary pressure is neglected.

The main new feature in SHAFT79 as compared with SHAFT78 is a completely simultaneous, iterative solution of the coupled mass- and energy-transport equations. This allows between ten and one hundred times larger time steps than the sequential method employed in SHAFT78. In particular, phase transitions can be computed accurately and efficiently. SHAFT79 offers a choice of several methods for solving the coupled non-linear equations for mass- and energy-flow. The preferred solution method is fully implicit, employs a Newton/Raphson iteration for simultaneous solution of the non-linear mass- and energy-transport equations, and uses an efficient sparse solver.[2] SHAFT79 has been applied to problems with up to 350 elements in three dimensions. Typical throughputs range from 0.1 in highly transient situations to more than 10^6 in problems approaching steady state. Here throughput is defined as ratio of the fluid mass flowing through the surface of an element in one time step, divided by the fluid mass initially in place in that element.

APPLICATIONS

Table 1 gives an overview of the types of systems and processes which have been modeled with SHAFT79. Below are presented results of selected SHAFT79-simulations which illustrate the range of applications. Parameters for the individual cases are given in the figure captions. Relative permeabilities were obtained from Corey's equations, with residual immobile steam saturation S_{sc} equal to zero, and residual immobile water saturation S_{wc} varying between 0.40 and 0.70.

DEPLETION OF A RESERVOIR WITH SHARP STEAM/WATER INTERFACE

When steam is produced from above a liquid water table, boiling commences near the top of the water zone. This gives rise to a drop in temperature and pressure, whereby a two-phase layer between water and steam zones is established. Water moves upward into the two-phase zone, releasing pressure below the boiling front and advancing it downward.[3] In

GEOMETRY	TYPE OF PROBLEM	SIMULATED PROCESSES
1-D, rectangular	depletion of two-phase geothermal reservoirs[3]	various production and injection schemes for reservoirs with uniform initial conditions or with sharp steam/water interfaces
1-D, cylindrical	two-phase flow near wells	production from two-phase zones; cold water injection into two-phase and superheated steam zones, respectively
2-D, rectangular	Krafla geothermal reservoir (Iceland)[4]	different space and time patterns of production and injection
2-D, cylindrical	high level nuclear waste repository[5]	long-term evolution of temperatures and pressures near a powerful heat source (in progress)
3-D, regular	two-phase interference test in Cerro Prieto (Mexico)	(in progress)
3-D, irregular	Serrazzano geothermal reservoir (Italy)[3]	detailed field production from 1960 to 1966

Table 1: Simulation Studies with SHAFT79.

the examples studied (see fig. 1) the top of the two-phase zone does not dry up until after the boiling front has reached the bottom of the reservoir. This occurs after 6.4 years for the "high permeability" case (A in fig. 1), and after 9.6 years for the "low permeability" case (B in fig. 1). Vapor saturation at the top of the water table then reaches 46.7 % for case A and 78.9 % for case B. Pressure at the steam/two-phase interface, at a depth of 500 m, declines very slowly during the advancing of the boiling front in case A. The reason for this is that the most rapid boiling occurs at the bottom of the two-phase zone. This provides a supply of hotter steam, which flows up from depth and tends to maintain temperature and hence pressure at the top of the two-phase zone. In case B this mechanism for pressure maintenance is much less effective because of the lower permeability.

INJECTION OF COLD WATER

Cold water injection into a steam reservoir gives rise to a hydrodynamic front and, trailing behind it, a temperature front. In the finite-difference simulation of this process subsequent elements undergo phase transitions from superheated steam to two-phase conditions to subcooled water. Fig. 2 shows the fronts at two different times. It is apparent that the fronts are propagated according to the parameter t/R^2. The volume swept by the temperature front is close to 1/4 of the volume swept by the hydrodynamic front. This reflects the fact that, at a porosity of 20 %, the volumetric heat capacity of water is about 1/4 of the volumetric heat capacity of the rock/water mixture.

SIMULATION OF KRAFLA FIELD (ICELAND)

Fig. 3 shows a vertical two-dimensional grid as used by Jonsson for simulating production and injection at Krafla.[4] The reservoir is initially almost entirely filled with liquid water close to saturated conditions. Various production and injection schemes were explored in an attempt to optimize injection, i.e. to combine pressure and temperature maintenance during production with minimal sacrifices in terms of decreasing vapor saturation S. Fig. 4 shows typical results. Jonsson finds that deep injection is preferable to shallow injection. Complete problem specifications and discussions of results are given in ref. 4).

SIMULATION OF SERRAZZANO FIELD (ITALY)

The most complex simulation effort undertaken with SHAFT79 to date is a case study (history match) of the Serrazzano reservoir. Serrazzano is one of the distinct zones of the extensive geothermal area near Larderello in central Tuscany (Italy). Detailed production data gathered since 1939 and an extensive body of geological and hydrological work make Serrazzano an attractive example for developing geothermal reservoir simulation methodology (see references given in 3). Fig. 5 gives a map of the reservoir, and fig. 6 shows the geologically accurate mesh as developed by Weres.[7] Conceptual model of the reservoir and parametrization of the problem are discussed in refs. 3) and 7).

Many parameters are only partially known, and are determined in trial-and-error fashion by comparing simulated reservoir performance with field observations. A valuable criterion for determining absolute permeabilities is that well blocks must remain very close to steady flow conditions. Our most complete simulation so far covers the period from 1960 to 1966. With the permeability distribution as indicated in fig. 5 we achieve steady flow for all wells producing since 1961 or earlier to within 2 % for the entire six year period modeled (i.e., the difference between inflow and production for any well block never exceeds 2 %).

From mass balance considerations it can be shown that most of the fluid reserves in Serrazzano are in place in liquid form. Little is known, however, about the distribution of pore water in the reservoir. Making the tentative assumption that liquid water is distributed throughout most of the reservoir, we compute a pressure decline (see fig. 7) which is slower than observed in the field by a factor of approximately 3.5. In the simulation pressure declines slowly because boiling is spread out over a large volume. We conclude that in most of the reservoir volume no liquid water is present, and we shall modify our initial conditions accordingly in subsequent simulations. We also need to correct some imbalances in initial conditions, which are apparent from the initial non-monotonic behavior of pressure in fig. 7.

CONCLUSION

The simulator SHAFT79 uses efficient methods for computing mass- and energy-transport in geothermal reservoirs, and allows for a flexible description of irregular geometric features. A broad range of applications, including idealized systems as well as large field problems, demonstrates its usefulness for geothermal reservoir studies. Further development work is presently under way to improve on some of the restrictive approximations made in the formulation of the physical model.

ACKNOWLEDGEMENT

This work was supported by the U.S. Department of Energy under contract No. W-7405-ENG-48.

REFERENCES

(1) K. Pruess, J.M. Zerzan, R.C. Schroeder, and P.A. Witherspoon, Description of the three-dimensional two-phase simulator SHAFT78 for use in geothermal reservoir studies, paper SPE-7699, presented at the Fifth Symposium on Reservoir Simulation, Denver/Colorado, 1979.

(2) I.S. Duff, MA28 - a set of Fortran subroutines for sparse unsymmetric linear equations, Report AERE - R 8730, Harwell/Oxfordshire, Great Britain (June 1977).

(3) K. Pruess, G. Bodvarsson, R.C. Schroeder, P.A. Witherspoon, R. Marconcini, G. Neri, and C. Ruffilli Simulation of the depletion of two-phase geothermal reservoirs, paper SPE-8266, presented at the 54th Annual Fall Technical Conference and Exhibition of the SPE, Las Vegas/Nevada, 1979.

(4) V. Jonsson, Lawrence Berkeley Laboratory Report LBL-10003 (in preparation).

(5) R. Eaton, private communication.

(6) S.K. Garg, Pressure transient analysis for two-phase (liquid water/steam) geothermal reservoirs, paper SPE-7479, presented at the 53rd Annual Fall Technical Conference and Exhibition of the SPE, Houston/Texas, 1978.

(7) O. Weres, A model of the Serrazzano zone, Proc. Third Stanford Workshop on Geothermal Reservoir Engineering, Stanford/California, 1977.

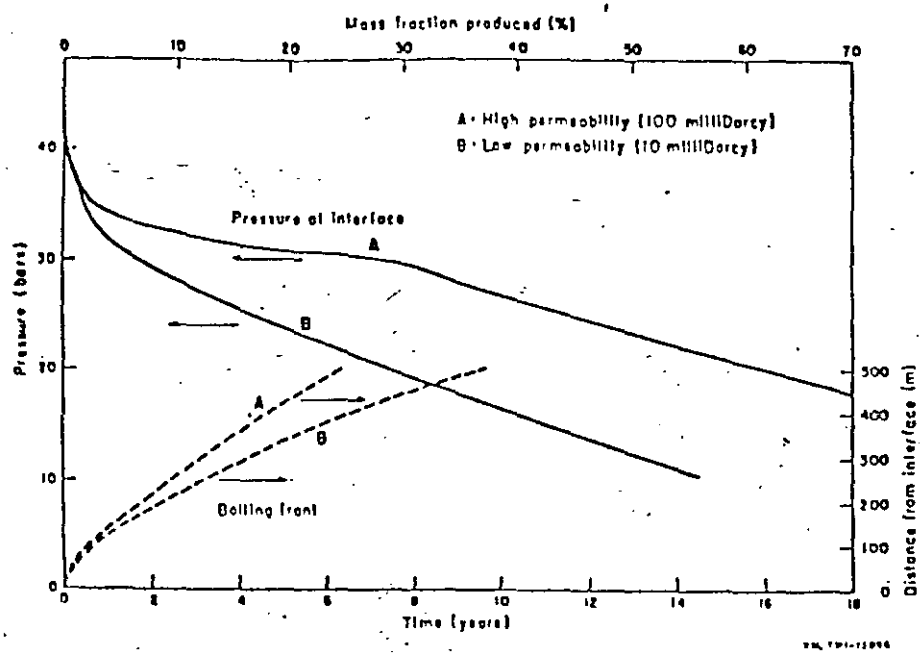

Fig.1: Depletion of a reservoir with sharp steam/water interface. The reservoir is a vertical column of 1 km depth with a volume of 1 km^3 and "no flow" boundaries. For purposes of numerical simulation it is subdivided into 44 horizontal elements. Initially, the bottom half is filled with liquid water, the top half with superheated steam, with temperature T = 252 ^{o}C and pressures carefully equilibrated under gravity. (Rock parameters: density = 2000 kg/m^3; specific heat = 1232 J/kg ^{o}C; porosity = 10 %; residual immobile water saturation = 70 %) Depletion occurs uniformly at the top with a constant rate of 50 kg/s. The curves are for a permeability of 10^{-13} m^2 (A) and 10^{-14} m^2 (B), respectively. Typical time steps in the simulation are 2 - 5 x 10^6 seconds, corresponding to throughputs of up to 250.

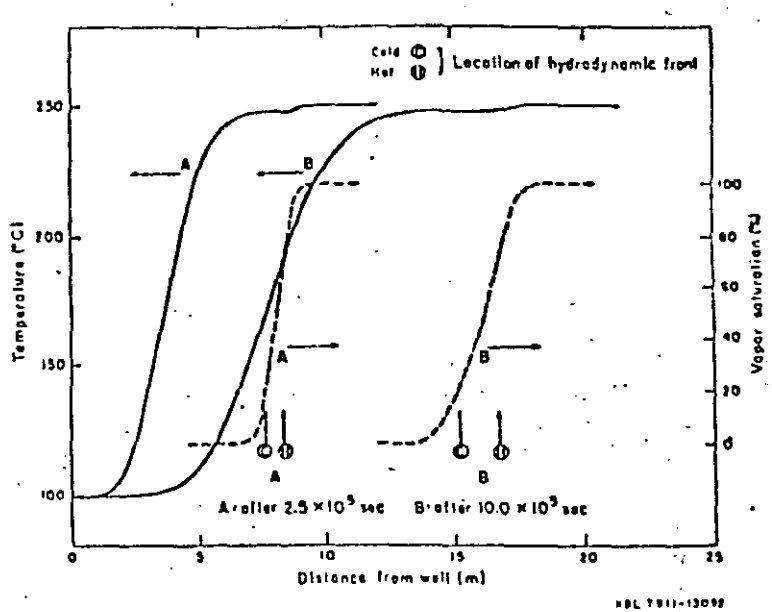

Fig. 2: Injection of cold water into a steam zone. The reservoir is a cylinder with large radius, initially filled with superheated steam at T = 250 ^{o}C, pressure = 38 bars. Water with T = 99.3 ^{o}C is injected along the center line at a constant rate of 0.14 kg/s m. The numerical simulation employs an axisymmetric grid as used by Garg.[6] (Rock parameters: density = 2650 kg/m^3; specific heat = 1000 J/kg ^{o}C; porosity = 20 %; heat conductivity = 5.25 W/m ^{o}C; permeability = 10^{-13} m^2; residual immobile water saturation = 40 %) The simulation uses time steps from 2500 to 10000 seconds, with throughputs of up to 6. The arrows labeled C and H show the locations of the hydrodynamic front if all injected water were to remain at injection temperature (C) or were heated up to initial reservoir temperature (H).

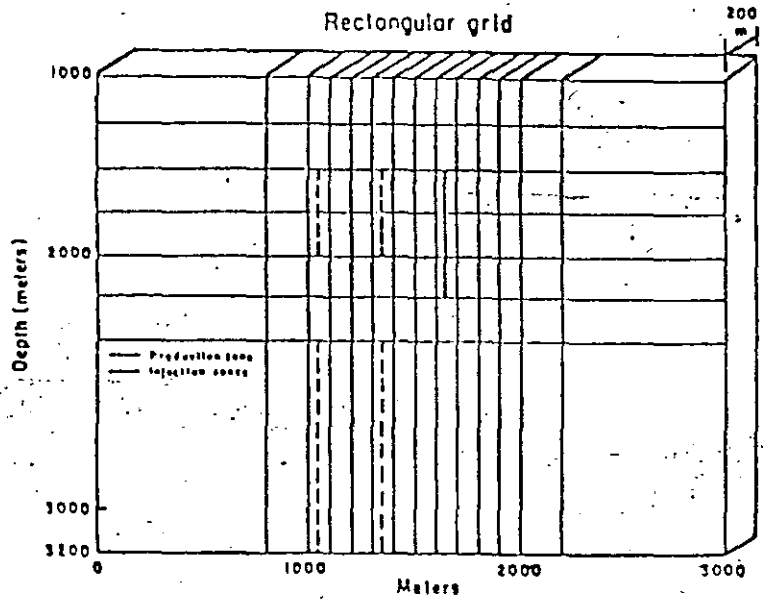

XBL 910-13062

Fig. 3: Two-dimensional grid for simulation of Krafla (Iceland). (from ref. 4)

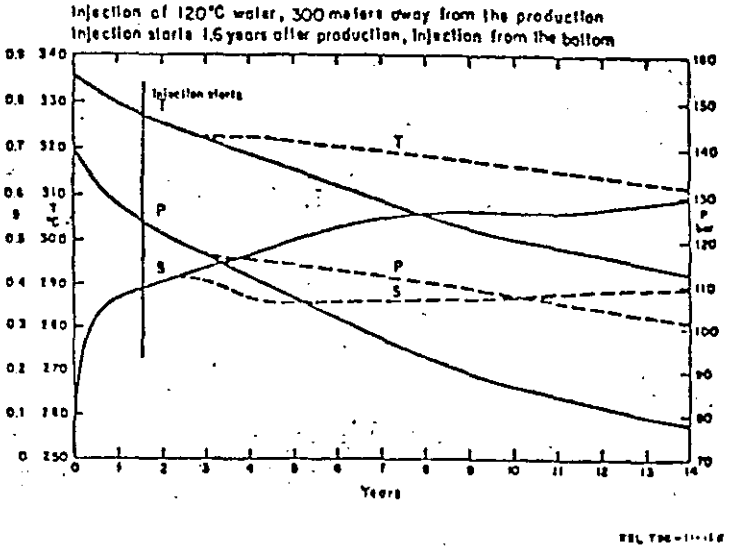

Fig. 4: Simulated performance of Krafla reservoir. Temperature, pressure and vapor saturation at the well block are given as function of time with injection (dashed lines) and without injection (solid lines). Production rate is 45 kg/s and injection rate is 22.5 kg/s. Typical time steps in the simulation are 1.25×10^6 seconds, with throughputs of about 0.1 (from ref. 4).

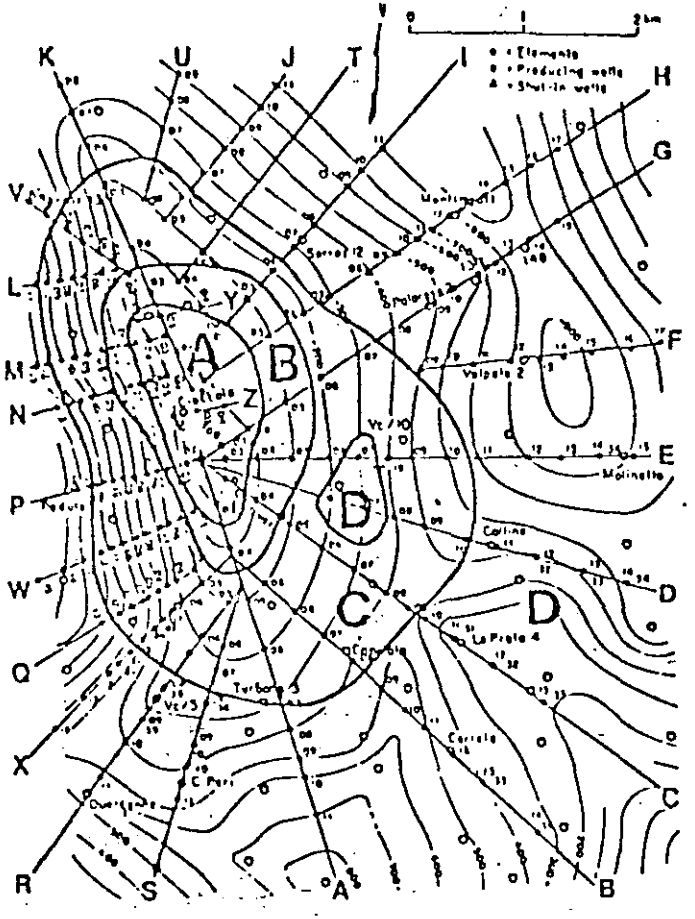

Fig. 5: Aerial map of Serrazzano geothermal reservoir. The thin contour lines show elevations of the cap rock as determined from drill logs. The straight lines labeled A to Z indicate the locations of geological cross sections used in constructing a three-dimensional finite difference grid.[7] Locations of elements (nodes) are also shown. A - D are regions of different permeability as determined in the simulation: A - 0.75×10^{-12} m^2; B - 0.25×10^{-12} m^2; C - 0.75×10^{-13} m^2; D - 0.15×10^{-13} m^2.

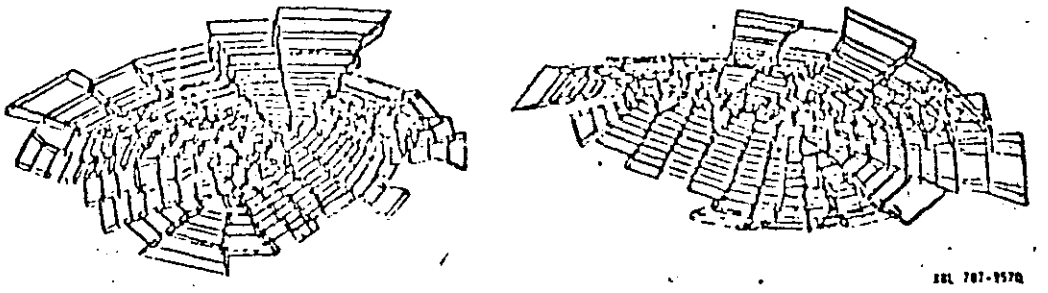

Fig. 6: Serrazzano grid. The computer-generated geologically accurate grid of the Serrazzano reservoir as developed by Weres is shown in two rotated perspective views (ref. 7). This three-dimensional grid represents a reservoir that is a curved thin sheet approximately 1 km from top to bottom, with an aerial extension of about 25 km^2. It has 234 polyhedral elements, with 679 polygonal interfaces between them. There are up to 10 interfaces per element.

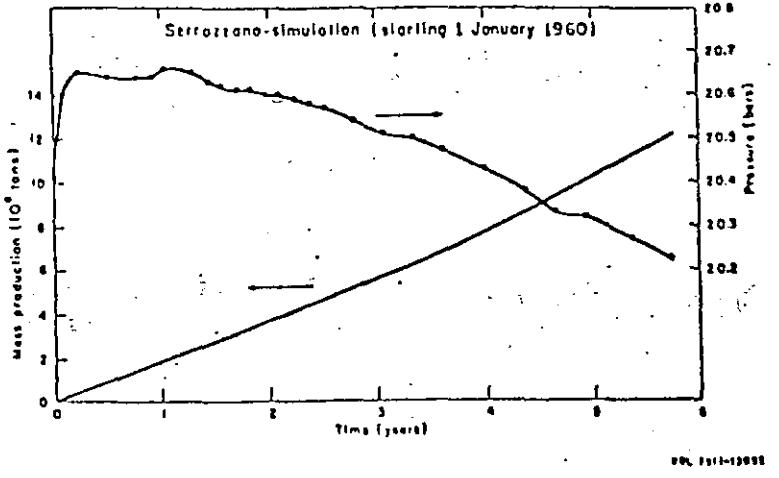

Fig. 7: Average reservoir steam pressure and cumulative fluid production as calculated in Serrazzano simulation. Typical time steps in the simulation are 10 to 50 days, with throughputs of up to 65.

CURSO: " INGENIERIA DE YACIMIENTOS GEOTERMICOS "
13 DE MARZO AL 18 DE MAYO DE 1984

TEMA: "GEOTHERMAL RESERVOIR SIMULATION"
1-MATHEMATICAL MODELS FOR LIQUID-AND VAPOR
DOMINATED HYDROTHERMAL SYSTEMS

DR. GUILLERMO DOMINGUEZ
2-13 de abril

Geothermal Reservoir Simulation 1. Mathematical Models for Liquid- and Vapor-Dominated Hydrothermal Systems

CHARLES R. FAUST AND JAMES W. MERCER

U.S. Geological Survey, Reston, Virginia 22092

Two alternative mathematical models are presented that are suitable for numerical simulation of geothermal reservoirs. The general mathematical model describes the three-dimensional flow of single-component water (both one and two phase) and the transport of heat in porous media. It is composed of two nonlinear partial differential equations, posed in terms of fluid pressure and enthalpy, and appropriate boundary conditions. An alternative quasi-three-dimensional model is derived by partial integration (in the vertical dimension) of the three-dimensional equations. The reservoir is assumed to have good vertical communication so that vertical equilibrium (gravity segregation) between steam and water is achieved. The resulting equations, posed in terms of vertically averaged pressure and enthalpy, include effects of an inclined, variable-thickness reservoir and mass and energy leakage to confining beds.

INTRODUCTION

Geothermal energy recently has received substantial attention as an alternative energy source. This has stimulated considerable research in several broad areas: exploration and identification of geothermal resources, technology for extracting energy from different types of geothermal resources, and characterization of geothermal reservoirs and hydrothermal system behavior. Geothermal reservoir simulation, one aspect of the third area, is the subject of this series of three papers. This paper, first in the series, deals with the development of the mathematical models that are the basis of our approach to geothermal reservoir simulation. The second paper introduces the numerical methods used and presents examples to verify the models as well as to demonstrate important characteristics of geothermal reservoir behavior. The final paper in the series presents an application of one of our models to the Wairakei hydrothermal system in New Zealand.

The primary objective of this paper is to provide a rational mathematical description of fluid (liquid water and steam) flow and energy transport in porous hydrothermal systems. This description begins with the balance equations for mass, momentum, and energy in porous media. These equations are combined (invoking appropriate simplifying assumptions) to yield two nonlinear partial differential equations posed in terms of fluid pressure and enthalpy. We then present the consistent boundary and initial conditions, which, along with the partial differential equations, comprise the general three-dimensional mathematical model.

Three-dimensional models are not always practical to use due to constraints imposed by data requirements and computational expense (for numerical solution). As an alternative we propose a quasi-three-dimensional areal model based on vertical integration of the three-dimensional equations. This approach, unique in geothermal simulation, leads to two nonlinear partial differential equations posed in terms of vertically averaged fluid pressures and enthalpies. The resulting areal model accounts for vertical variations in properties (such as the presence of a steam cap) as well as variations in reservoir thickness and slope.

Paper number 8W0880.

GEOTHERMAL SYSTEMS

The ultimate source of geothermal energy is heat energy generated and stored within the earth. Potential sources of geothermal energy can be divided into three major systems: hydrothermal, geopressured, and hot, dry rock (conduction dominated). In hydrothermal systems, heat from near-surface sources such as magmatic bodies is transferred to porous media and to the fluid within those media by conductive and convective processes. These systems can be further classified as being either liquid dominated or vapor dominated [*White et al.*, 1971]. In geopressured systems, fluid is trapped in geosynclinal accumulations where it is subjected to extreme pressures and high temperatures. Finally, in hot rock systems, low-permeability igneous rocks are heated by sources similar to those associated with hydrothermal systems. These systems are, by nature, fluid independent.

In this study, only geothermal energy from hydrothermal systems is considered. When such a system is utilized for its heat energy, it is called a geothermal reservoir. The best known geothermal reservoir that is liquid dominated is the Wairakei field in New Zealand. Of the vapor-dominated geothermal reservoirs the best known are the Larderello field in Italy and The Geysers field in California.

Although geothermal fluids contain impurities, many reservoirs, as a first approximation, may be treated as pure water systems. Making this assumption, consider the pressure-enthalpy diagram for pure water in Figure 1. Because all the known geothermal reservoirs exist at temperatures below the critical point of water (the temperature above which two phases cannot exist), this diagram may be divided into three regions. The first of these is the compressed-water region, which is the condition existing in liquid-dominated hydrothermal systems. The second is the two-phase (steam-water) region, in which temperature is a function of pressure only. The third region contains superheated steam. The vapor-dominated system described by *White et al.* [1971] is believed to exist in the two-phase region, although the lower part of these systems may have a water table below which the fluid exists as compressed water. In the vapor-dominated systems it is also possible, especially when influenced by production, that parts of the system may contain superheated steam.

From the above description it is apparent that any mathematical model of fluid flow and energy transport in hydro-

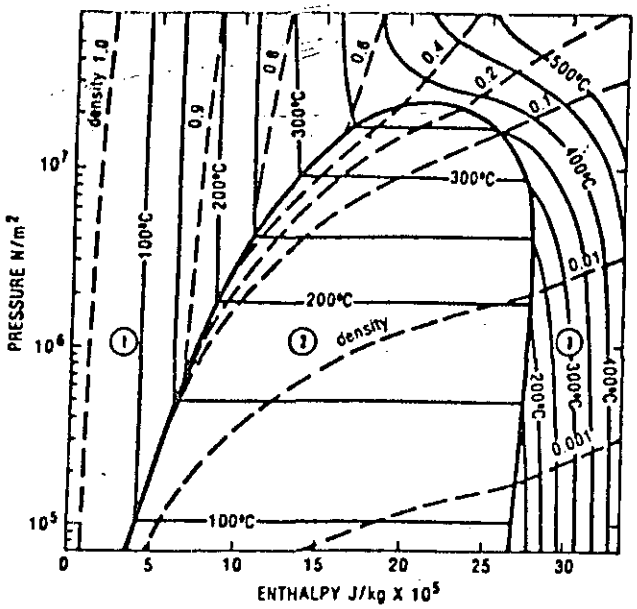

Fig. 1. Pressure-enthalpy diagram for pure water and vapor showing three states below the critical point (top of two-phase envelope): 1, compressed water; 2, two-phase steam and water; and 3, superheated steam.

thermal systems will be complex. It must account for the flow behavior of one- and two-phase fluids and heat transport in complex natural systems. The remainder of this paper is an attempt to offer a simplified yet realistic description of this behavior subject to appropriate assumptions.

General Mathematical Model

A general mathematical model of a geothermal system that describes the three-dimensional flow of water and/or steam and transport of heat in a porous medium is the basis for several numerical models developed in this study. Elsewhere, we have presented a heuristic derivation [*Mercer et al.*, 1974] and a more formal derivation [*Faust and Mercer*, 1977*a*] of this general mathematical model. Other derivations of general geothermal models may also be found in work by *Brownell et al.* [1977] and *Witherspoon et al.* [1975]. Rather than repeat the details of these lengthy derivations, in this paper we only show a brief derivation of the final equations and state major assumptions.

The conservation equations for mass, momentum, and energy must first be considered for each phase in the geothermal system. Using a set of constitutive relationships, these balance equations are reduced to two nonlinear partial differential equations in terms of the dependent variables pressure and enthalpy.

Mass Balance

The mass balance for steam s and water w may be written as

$$\frac{\partial(\phi S_s \rho_s)}{\partial t} + \nabla\cdot(\rho_s \mathbf{v}_s) - q_s' - d_s = 0 \qquad (1)$$

and

$$\frac{\partial(\phi S_w \rho_w)}{\partial t} + \nabla\cdot(\rho_w \mathbf{v}_w) - q_w' + d_s = 0 \qquad (2)$$

where boldface type indicates a vector quantity and ∇ is the vector differential operator. In the above equations, ϕ is the porosity, S is the volumetric saturation, ρ is the density, d_s is the gain of steam mass due to the vaporization (loss of liquid water), q' is a source term, and $\mathbf{v}$ is the averaged phase velocity.

Momentum Balance

It is assumed that Darcy's equations for multiphase flow may be used as simplified momentum balances. For steam and water these are as follows:

$$\mathbf{v}_s = -\frac{\mathbf{K}k_{rs}}{\mu_s}\cdot(\nabla p_s - \rho_s g \nabla D) \qquad (3)$$

and

$$\mathbf{v}_w = -\frac{\mathbf{K}k_{rw}}{\mu_w}\cdot(\nabla p_w - \rho_w g \nabla D) \qquad (4)$$

where sans serif type indicates a second-order tensor quantity. In these equations, $\mathbf{K}$ is the intrinsic permeability tensor of the porous medium, k_r is the relative permeability of the phase, μ is the dynamic viscosity, g is the gravitational constant, D is the depth, and p is phase pressure. The representation of mobility as $\mathbf{K}k_r/\mu$ is thought to be a reasonable assumption, although data on geothermal systems are not available to support it conclusively.

Energy Balance

Simplified energy equations for steam, water, and rock r may be written as

$$\frac{\partial(\phi S_s \rho_s h_s)}{\partial t} + \nabla\cdot(\rho_s h_s \mathbf{v}_s) + \nabla\cdot\boldsymbol{\lambda}_{cs} + \nabla\cdot\boldsymbol{\lambda}_{ds} - \frac{\partial(\phi S_s p_s)}{\partial t} - \mathbf{v}_s\cdot\nabla p_s - Q_s' - q_s' h_s' = 0 \qquad (5)$$

$$\frac{\partial(\phi S_w \rho_w h_w)}{\partial t} + \nabla\cdot(\rho_w h_w \mathbf{v}_w) + \nabla\cdot\boldsymbol{\lambda}_{cw} + \nabla\cdot\boldsymbol{\lambda}_{dw} - \frac{\partial(\phi S_w p_w)}{\partial t} - \mathbf{v}_w\cdot\nabla p_w + Q_w' - q_w' h_w' = 0 \qquad (6)$$

and

$$\frac{\partial[(1-\phi)\rho_r h_r]}{\partial t} + \nabla\cdot\boldsymbol{\lambda}_{cr} - Q_r' = 0 \qquad (7)$$

where h is specific enthalpy, $\boldsymbol{\lambda}_c$ is the heat conduction vector, $\boldsymbol{\lambda}_d$ is the dispersion (thermal mixing) vector, and Q_w', Q_s', and Q_r' are the interphase energy exchange terms.

In these equations, kinetic energy (viscous dissipation) and potential energy are neglected. *Garg and Pritchett* [1977] have shown that viscous dissipation has negligible effects in one-phase (water) and two-phase geothermal systems.

Constitutive Relationships

The balance equations (1)–(7) are not sufficient to describe the geothermal system, and consequently, additional equations are required. These are in the form of constitutive relationships that are based on the following assumptions:

1. Capillary pressure effects are negligible.
2. Thermal equilibrium exists among the steam, water, and rock.
3. The reservoir fluid is single-component water consisting of either one or two phases.
4. Relative permeability is a function of liquid volume saturation; hysteresis is neglected.
5. Viscosities are considered functions of temperature.
6. Porosity is a linear function of pressure, given by

$$\phi = \phi_i + \beta(p - p_i) \qquad (8)$$

where ϕ_i and p_i are the initial porosity and pressure, respectively, and β is the intergranular vertical compressibility coefficient.

7. Rock density, reservoir thickness, and intrinsic permeability are functions of space.

8. Rock enthalpy is a linear function of temperature, given by

$$h_r = c_r T \tag{9}$$

where c_r is the specific heat of the rock and T is temperature. We now consider the first three of these assumptions in detail.

Capillary pressure. An expression relating phase pressure is given by

$$p_c = p_s - p_w \tag{10}$$

where p_c is the capillary pressure. Capillary pressure has the effect of lowering the vapor pressure of water. *Ramey et al.* [1973] point out that the reason for this lowering is that vapor pressure data found in steam tables [*Meyer et al.*, 1968; *Keenan et al.*, 1969] are based on flat steam-water interfaces, whereas the interface in porous media is curved. The amount that the vapor pressure curve is lowered in a geothermal reservoir is not completely understood. The work of *Calhoun et al.* [1949] on consolidated rock does show a lowering with decreased fluid saturation. *Cady* [1969] and *Bilhartz* [1971], however, indicate no significant vapor pressure lowering in experiments using unconsolidated sands. An important difference in these results is that the experiments of Calhoun and others were made at a temperature of 36°C, while those of Cady and Bilhartz were done over a temperature range of 121°–240°C. Further work on the importance of capillary pressure in geothermal reservoirs is required. For this development the only effect of capillary pressure that is considered is the possible occurrence of a residual water saturation (disconnected water in the pore space that is immobile). Other capillary pressure effects are neglected, and capillary pressure is assumed negligible, an assumption which implies that fluid pressures in the steam and water phases are equal. With this assumption, (1) and (2) may be combined to eliminate the vaporization terms:

$$\frac{\partial(\phi\rho)}{\partial t} + \nabla\cdot(\rho_s \mathbf{v}_s) + \nabla\cdot(\rho_w \mathbf{v}_w) - q_s' - q_w' = 0 \tag{11}$$

where ρ is the density of the total steam-water mixture, defined as

$$\rho = S_w\rho_w + S_s\rho_s \tag{12}$$

the volume saturations are defined so that they sum to 1,

$$S_s + S_w = 1 \tag{13}$$

and phase velocities can now be expressed in terms of a single pressure p.

Thermal equilibrium. The movement of steam and water through porous media is sufficiently slow and the surface areas of all phases are sufficiently large that it is reasonable to assume that local thermal equilibrium among phases is achieved instantaneously. This assumption permits the energy equations for rock, steam, and water to be combined and the medium conduction-dispersion term to be expressed as a function of a single temperature. In this development the lumped conduction-dispersion term is defined by a Fourier-type equation:

$$\lambda_{cr} + \lambda_{cs} + \lambda_{cw} + \lambda_{ds} + \lambda_{dw} = -K_m\nabla T \tag{14}$$

where the medium conduction-dispersion coefficient K_m is isotropic. This simplifying assumption is made because data on the tensor nature of thermal dispersion are generally unavailable. In addition to the limitation of combining the effects of conduction and dispersion, (14) neglects the important effect of temperature on thermal conductivity. In this regard, *Somerton et al.* [1974] point out that the thermal conductivity of a porous medium is a function of temperature, porosity, and water saturation. This effect may be important in a purely conductive system; however, in this study these effects are neglected.

Invoking these assumptions concerning thermal equilibrium and dispersion, the energy balance equations may be combined, yielding

$$\frac{\partial}{\partial t}\left[\phi\rho h + (1-\phi)\rho_r h_r\right] + \nabla\cdot(\rho_s h_s \mathbf{v}_s) + \nabla\cdot(\rho_w h_w \mathbf{v}_w) - \nabla\cdot(K_m\nabla T) - q_s' h_s' - q_w' h_w' - \left[\frac{\partial\phi p}{\partial t} + (\mathbf{v}_s + \mathbf{v}_w)\cdot\nabla p\right] = 0 \tag{15}$$

in which h is the enthalpy of the steam-water mixture and is defined as

$$h = (S_s\rho_s h_s + S_w\rho_w h_w)/\rho \tag{16}$$

Note that the interphase energy exchange terms in (5), (6), and (7) have been eliminated in (15), because they sum to zero. Finally, the last term in (15) is the pressure material derivative, which in part comprises the compressible work term. *Moench* [1976] points out that the term for compressible work is negligible except for conditions of low water saturation. The same characteristics can be shown for the rest of the pressure material derivative, and for most applications this term is neglected.

Thermodynamic properties. As was previously indicated, it is assumed that the hydrothermal fluid is pure water. Just how unrestrictive this assumption can be is demonstrated by *Haas* [1976*a*, *b*], who gives thermodynamic data for an NaCl solution. These data show that in the pressure range of most geothermal reservoirs the vapor pressure curve is lowered by less than 3°C for a 5% (by weight) solution. Although the fluid in geothermal reservoirs contains other dissolved solids in addition to NaCl, in a qualitative sense the effects are similar for other impurities. For geothermal reservoirs such as those at Wairakei, New Zealand, Larderello, Italy, and The Geysers, California, in which the salinities are low [*Koenig*, 1973], the effects of dissolved solids are small.

Additional expressions are needed to relate the thermodynamic properties of pure water and steam to the dependent variables pressure and enthalpy. These expressions are functional in form, were obtained by least squares regressions applied to data from steam tables [*Meyer et al.*, 1968; *Keenan et al.*, 1969], and are described in detail by *Faust and Mercer* [1977*b*]. This approach avoids the necessity of searching for and interpolating data from tables. Also, derivatives of the functions can be easily obtained by analytical methods. The necessary relationships for this development are as follows:

1. Saturated steam enthalpy h_s and saturated water enthalpy h_w are treated as functions of pressure.

2. Temperature is treated as a function of pressure and enthalpy for the compressed-water region and the superheated-steam region and is treated as a function of pressure in the two-phase region.

3. Total density ρ and steam and water densities ρ_s and ρ_w are considered functions of pressure and enthalpy.

4. Phase saturations are functions of enthalpy and pressure in the two-phase region. Water saturation in the compressed-water region is assumed to be 1 and in the superheated-steam region is assumed to be 0. In the steam-water region, water saturation is obtained from (12), (13), and (16) as

$$S_w = \frac{\rho_s(h_s - h)}{h(\rho_w - \rho_s) - (h_w\rho_w - h_s\rho_s)} \tag{17}$$

and S_s is determined using (13).

Three-Dimensional Equations

The final equations are formulated in terms of the dependent variables pressure and enthalpy, because these two variables uniquely define the thermodynamic state of the system and because they are commonly obtained in a field situation. With the assumptions of zero capillary pressure and thermal equilibrium the number of balance equations was reduced to four (equations (3), (4), (11), and (15)). These can be reduced further by substitution of (3) and (4) into (11) and (15) and by expansion of the temperature derivative in (15) to yield

$$\frac{\partial(\phi\rho)}{\partial t} - \nabla\cdot\left[\frac{Kk_{rs}\rho_s}{\mu_s}\cdot(\nabla p - \rho_s g\nabla D)\right] - \nabla\cdot\left[\frac{Kk_{rw}\rho_w}{\mu_w}\cdot(\nabla p - \rho_w g\nabla D)\right] - q_m' = 0 \tag{18}$$

and

$$\frac{\partial}{\partial t}[\phi\rho h + (1-\phi)\rho_r h_r] - \nabla\cdot\left[\frac{Kk_{rs}\rho_s h_s}{\mu_s}\cdot(\nabla p - \rho_s g\nabla D)\right] - \nabla\cdot\left[\frac{Kk_{rw}\rho_w h_w}{\mu_w}\cdot(\nabla p - \rho_w g\nabla D)\right] - \nabla\cdot\left[K_m\left(\frac{\partial T}{\partial p}\right)_h\nabla p + K_m\left(\frac{\partial T}{\partial h}\right)_p\nabla h\right] - q_h' = 0 \tag{19}$$

where the pressure material derivative has been neglected.

These final three-dimensional equations describe the two-phase flow of heat in a steam-water-rock system; however, with minor modification they also describe the flow of heat in a water-rock or a steam-rock system. When either steam or water is absent, the saturation of the absent phase is 0 and that for the existing phase is 1. Further, it is assumed that the relative permeability of the absent phase is 0 and that for the existing phase is 1. Therefore (18) and (19) reduce to the appropriate equations for either the compressed-water region or the superheated-steam region. A solution for these equations will determine whether a specified location contains compressed water, a steam-water mixture, or superheated steam.

Source terms The mass and energy source terms q_m' and q_h', respectively, represent the amount of mass and heat lost (or gained) to source-sinks. In the two-phase region the mass rate loss to a source-sink is defined as

$$q_m' = q_s' + q_w' \tag{20}$$

and the heat rate loss to a source-sink is

$$q_h' = h_s'q_s' + h_w'q_w' \tag{21}$$

where a negative rate indicates a loss from the reservoir. The steam production rate may be determined by the fractional flow of the steam phase as follows:

$$q_s' = \alpha_s q_m' \tag{22}$$

and

$$\alpha_s = k_{rs}/[k_{rs} + (\rho_w\mu_s/\rho_s\mu_w)k_{rw}]$$

Because h_s' and h_w' are known functions of pressure and the mass flux q_m' is specified, q_s' is calculated using (22), and q_h' is calculated using (21).

Boundary conditions Equations (18) and (19) together comprise a pair of nonlinear second-order partial differential equations. Two conditions (one in terms of pressure and one in terms of enthalpy) are required at the boundaries. Perhaps the most common boundary condition is the specification of fluxes. Frequently, the flux is specified as zero, indicating a no-flow boundary. For specification of a mass flux the following equation must be satisfied:

$$q_m^* = -\left(\frac{Kk_{rs}\rho_s}{\mu_s} + \frac{Kk_{rw}\rho_w}{\mu_w}\right)\cdot\frac{\partial(p - \rho g D)}{\partial n} \tag{23}$$

where q_m^* is the specified mass flux at the boundary and $\partial/\partial n$ is the outward normal derivative. If a mass flux is specified, a convective energy flux must also be specified according to an equation analogous to (21):

$$q_h^* = q_s^* h_s^* + q_w^* h_w^* \tag{24}$$

where h_s^* and h_w^* are the pressure-dependent saturated water and saturated steam enthalpies and q_s^* and q_w^* are the fractional steam and water fluxes at the boundary. The total energy flux for the general case consists of two parts,

$$q_{rh}^* = q_h^* + q_h^{**} \tag{25}$$

where q_h^{**} represents the conductive heat flux at the boundary, determined by

$$q_h^{**} = -K_m\left.\frac{\partial T}{\partial n}\right|_{\text{boundary}} \tag{26}$$

A constant-pressure condition may also be encountered. Since this implies a mass flux at the boundary, it also implies a convective energy flux. To determine the convective energy flux, the mass flux is calculated from (23) and used in (24).

AREAL MODEL

The general equations (18) and (19) describe three-dimensional flow and heat transport. For many field problems a three-dimensional model is unnecessary and expensive. In order to obtain areal two-dimensional equations the three-dimensional equations must be partially integrated in the z dimension (vertical). The process of vertically integrating the three-dimensional equations is fairly straightforward but is lengthy and tedious. We gave a detailed derivation of the vertically integrated equations in an earlier paper [*Faust and Mercer*, 1977a]. Here, as in the previous section, we will present only the major assumptions and final equations resulting from the derivation.

To perform the averaging procedure, it is necessary to introduce the following definitions. A quantity averaged in the z dimension is given by

$$\langle\psi\rangle = \frac{1}{b}\int_{z_1}^{z_2}\psi\,dz \tag{27}$$

where $z_1 = z_1(x, y, t)$ is the bottom of the reservoir, $z_2 = z_2(x, y, t)$ is the top, $b = b(x, y, t) = z_2 - z_1$ is the thickness, and the angle brackets signify a quantity averaged in the z dimension. Leibnitz's rule is frequently used to reverse the order of in-

$$-\frac{\partial}{\partial x}\left[b\left((\omega_{cp})\left\langle\frac{\partial p}{\partial x}\right\rangle+(\omega_{ch})\left\langle\frac{\partial h}{\partial x}\right\rangle\right.\right.$$
$$\left.\left.+\left\langle\hat{\omega}_{cp}\frac{\hat{\partial p}}{\partial x}\right\rangle+\left\langle\hat{\omega}_{ch}\frac{\hat{\partial h}}{\partial x}\right\rangle\right)\right]$$
$$-\frac{\partial}{\partial y}\left[b\left((\omega_{cp})\left\langle\frac{\partial p}{\partial y}\right\rangle+(\omega_{ch})\left\langle\frac{\partial h}{\partial y}\right\rangle\right.\right.$$
$$\left.\left.+\left\langle\hat{\omega}_{cp}\frac{\hat{\partial p}}{\partial y}\right\rangle+\left\langle\hat{\omega}_{ch}\frac{\hat{\partial h}}{\partial y}\right\rangle\right)\right]-b\langle q_h'\rangle$$
$$+h\mathbf{v}|_{z_1}\cdot\nabla(z-z_1)-h\mathbf{v}|_{z_2}\cdot\nabla(z-z_2)$$
$$+\lambda_m|_{z_1}\cdot\nabla(z-z_1)$$
$$-\lambda_m|_{z_2}\cdot\nabla(z-z_2)=0 \tag{38}$$

The terms in (37) and (38) with the vertical bars are flux terms that are evaluated at either the top z_2 or the bottom z_1 of the reservoir and are defined (for the reservoir bottom) as follows:

$$\mathbf{v}\Big|_{z_1}\cdot\nabla(z-z_1)=-\left(\omega_x\frac{\partial p}{\partial x}\right)\Big|_{z_1}\frac{\partial z_1}{\partial x}$$
$$-\left(\omega_y\frac{\partial p}{\partial y}\right)\Big|_{z_1}\frac{\partial z_1}{\partial y}+\left(\omega_z\frac{\partial p}{\partial z}+\omega_{gz}\right)\Big|_{z_1} \tag{39}$$

$$h\mathbf{v}\Big|_{z_1}\cdot\nabla(z-z_1)=-\left(\omega_{hx}\frac{\partial p}{\partial x}\right)\Big|_{z_1}\frac{\partial z_1}{\partial x}$$
$$-\left(\omega_{hy}\frac{\partial p}{\partial y}\right)\Big|_{z_1}\frac{\partial z_1}{\partial y}+\left(\omega_{hz}\frac{\partial p}{\partial z}+\omega_{hgz}\right)\Big|_{z_1} \tag{40}$$

$$\lambda_m\Big|_{z_1}\cdot\nabla(z-z_1)=-\left(\omega_{cp}\frac{\partial p}{\partial x}+\omega_{ch}\frac{\partial h}{\partial x}\right)\Big|_{z_1}\frac{\partial z_1}{\partial x}$$
$$-\left(\omega_{cp}\frac{\partial p}{\partial y}+\omega_{ch}\frac{\partial h}{\partial y}\right)\Big|_{z_1}\frac{\partial z_1}{\partial y}+\left(\omega_{cp}\frac{\partial p}{\partial z}+\omega_{ch}\frac{\partial h}{\partial z}\right)\Big|_{z_1} \tag{41}$$

Similar expressions may be written for the reservoir top by exchanging z_2 for z_1 in (39)–(41). These terms account for convective and conductive fluxes at the reservoir top and bottom and include the effects caused by the slope of reservoir bedding and the spatial change in reservoir thickness.

Evaluation of Vertically Averaged Terms

Given (37) and (38), a critical problem remains in evaluating averaged quantities and averages of the pressure and enthalpy derivatives. The relationship between the vertical average of a derivative and the derivative of a vertically averaged quantity is given by (34). For pressure the x derivative becomes

$$\left\langle\frac{\partial p}{\partial x}\right\rangle=\frac{\partial\langle p\rangle}{\partial x}-\frac{1}{b}(\langle p\rangle-p|_{z_1})\frac{\partial z_1}{\partial x}+\frac{1}{b}(\langle p\rangle-p|_{z_2})\frac{\partial z_2}{\partial x} \tag{42}$$

If we assume hydrostatic equilibrium, it can be shown that

$$p|_{z_1}=\langle p\rangle+\langle(z-z_1)\rho g\rangle \tag{43}$$

and

$$p|_{z_2}=\langle p\rangle+\langle(z-z_2)\rho g\rangle-b\langle\rho g\rangle \tag{44}$$

Noting that

$$(z-z_1)=b/2 \tag{45}$$

and substituting (32), (43), and (44) into (42) lead to

$$\left\langle\frac{\hat{c}p}{\hat{c}x}\right\rangle=\frac{\hat{c}\langle p\rangle}{\partial x}+\frac{1}{2}\langle\rho g\rangle\left(\frac{\partial z_1}{\partial x}+\frac{\hat{c}z_2}{\partial x}\right)$$
$$+\frac{1}{b}\langle\hat{c}\rho\hat{g}\rangle\left(\frac{\partial z_1}{\partial x}-\frac{\hat{c}z_2}{\partial x}\right) \tag{46}$$

Further, it may be shown that the derivative of the average depth is

$$\frac{\partial\langle D\rangle}{\partial x}=-\frac{1}{2}\left(\frac{\partial z_1}{\partial x}+\frac{\partial z_2}{\partial x}\right) \tag{47}$$

so that the average of the pressure derivative becomes

$$\left\langle\frac{\hat{c}p}{\partial x}\right\rangle=\frac{\hat{c}\langle p\rangle}{\hat{c}x}-\langle\rho g\rangle\frac{\hat{c}\langle D\rangle}{\hat{c}x}-\frac{1}{b}\langle\hat{c}\hat{\rho}\rangle\frac{\hat{c}\langle D\rangle}{\partial x} \tag{48}$$

Hence this term includes the effects of a sloping reservoir of variable thickness. Equation (48) and the analogous equation for the y derivative may be used to replace the $\langle\partial p/\partial x\rangle$ and $\langle\hat{c}p/\hat{c}y\rangle$ terms in (37) and (38). For enthalpy the relationship for the x derivative is

$$\left\langle\frac{\partial h}{\partial x}\right\rangle=\frac{\partial\langle h\rangle}{\partial x}-\frac{1}{b}(\langle h\rangle-h|_{z_1})\frac{\partial z_1}{\partial x}+\frac{1}{b}(\langle h\rangle-h|_{z_2})\frac{\partial z_2}{\partial x} \tag{49}$$

which, along with the analogous expression for the y derivative, may be substituted into (38) directly.

Having considered the evaluation of averaged derivatives of pressure and enthalpy, we must now address the problem of evaluating the averaged coefficients that also appear in (37) and (38). In general, these terms may be evaluated under two conditions: the fluids are (1) unsegregated and (2) segregated.

If the fluids are not segregated, then their properties are assumed to be uniform throughout the thickness of the reservoir. For this condition, laboratory relative permeability curves may be used in the areal calculations. This leads to the easiest evaluation of the vertically integrated terms, but for two-phase systems it is also a very restrictive assumption, being limited to very thin reservoirs. For single-phase reservoirs, however, the uniform-property assumption is normally used.

A less restrictive condition (one that allows simulation of two-phase reservoirs), and one that conforms with the assumption concerning the absence of significant capillary pressure, is that of segregation. For this condition, it is common to assume vertical equilibrium, a concept that was first used in connection with areal simulation of multiphase petroleum reservoirs [*Coats et al.*, 1967, 1971; *Hearn*, 1971; *Jacks et al.*, 1973]. It is assumed in applying the concept of vertical equilibrium to petroleum reservoirs that the fluid potentials are uniform throughout the reservoir thickness. This corresponds to a gravity-segregated fluid distribution with the potential of each fluid being uniform in the part of the column occupied by that fluid. This condition requires that the reservoir have good vertical communication. Using this assumption, vertically averaged liquid saturations are related to pressure at some reference level by employing pseudo capillary pressure and pseudo relative permeability curves. Basically, the pseudofunction approach gives results similar to those that would be obtained if vertically averaged pressures were used.

Spivak [1974] has made a detailed study of gravity segregation in two-phase petroleum displacement processes. His conclusions are based on simulation runs in which the parameters

affecting gravity segregation were varied. He found that gravity segregation increases with increasing permeability, increasing fluid density difference, increasing viscosity ratio, and decreasing viscosity for a given ratio. It is obvious that in steam-water geothermal systems, conditions are favorable for gravity segregation, because the density difference and viscosity ratio for steam and water are large and the viscosities are relatively low.

For the geothermal problem, many thermodynamic properties are strongly dependent functions of pressure and enthalpy; hence the pseudofunction approach would be awkward. Instead, the concept of vertical equilibrium is used to average the terms in (37) and (38). To perform this averaging, it is necessary to make certain a priori assumptions concerning the vertical distribution of the dependent variables pressure and enthalpy. In making the following assumptions we have relied upon conceptual descriptions of vapor-dominated reservoirs such as those provided by *White et al.* [1971]. We have also relied upon the results of numerous computer experiments (second paper in this series) using three-dimensional and cross-sectional (vertical) reservoir simulators. Our basic assumption is vertical equilibrium. In the absence of significant capillary pressure, steam and water separate by gravity segregation, producing a steam cap with a water saturation equal to the residual water saturation S_{wr}; below the steam cap the water saturation is 1.0 (see Figure 3).

Because the pressure varies hydrostatically in each phase (see Figure 4), the vertically averaged pressure is

$$\langle p \rangle = [(p_w)(z_c - z_1) + \langle p_{sw} \rangle (z_2 - z_c)]/b \qquad (50)$$

Recall that vertically averaged quantities are denoted by angle brackets. In (50) the averaged pressure in the saturated region (below the interface at z_c), $\langle p_w \rangle$, is defined by

$$\langle p_w \rangle = p_{z_c} + \rho_w g(z_c - z_1)/2 \qquad (51)$$

and the averaged pressure in the two-phase region (above the interface at z_c), $\langle p_{sw} \rangle$, is defined by

$$\langle p_{sw} \rangle = p_{z_c} - \rho_z g(z_2 - z_c)/2 \qquad (52)$$

where ρ_z is the density in the two-phase region, defined by

$$\rho_z = \rho_s(1 - S_{wr}) + \rho_w S_{wr} \qquad (53)$$

Note that the steam and water densities in (51)–(53) are considered functions of the interface pressure p_{z_c}.

The assumed enthalpy distribution is also shown in Figure 4. Note that the enthalpy increases with depth in the two-phase zone because the water saturation is assumed constant and pressure increases with depth. The vertically averaged

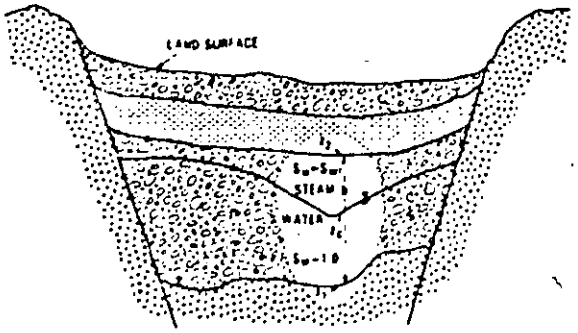

Fig. 3. Idealized cross section showing the steam cap in a confined reservoir, z_c is the steam-water contact, and S_{wr} is the residual water saturation.

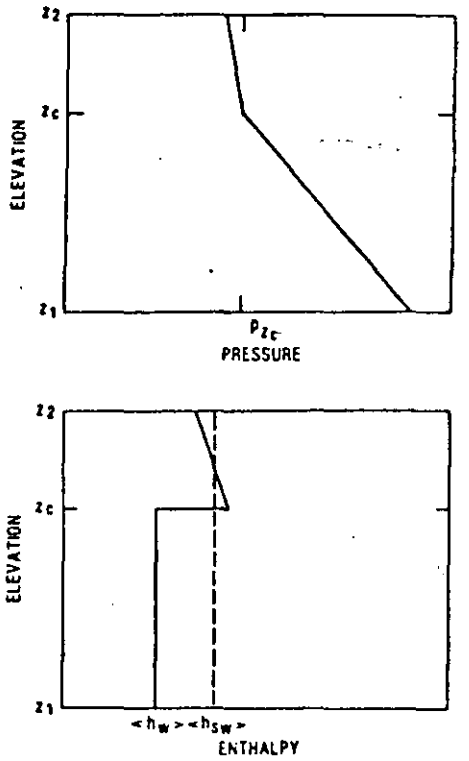

Fig. 4. Pressure and enthalpy profiles through idealized reservoir, showing the pressure at the steam-water contact, p_{z_c}; average water enthalpy $\langle h_w \rangle$; and average steam cap enthalpy $\langle h_{sw} \rangle$.

enthalpy is defined as

$$\langle h \rangle = [(h_w)(z_c - z_1) + \langle h_{sw} \rangle (z_2 - z_c)]/b \qquad (54)$$

where $\langle h_w \rangle$ is the averaged enthalpy in the saturated region and is a function of the interface pressure. The averaged enthalpy in the two-phase region above the interface is defined by

$$\langle h_{sw} \rangle = \frac{\rho_s h_s(1 - S_{wr}) + \rho_w h_w S_{wr}}{\rho_s(1 - S_{wr}) + \rho_w S_{wr}} \qquad (55)$$

where the water and steam densities and enthalpies in (55) are considered functions of $\langle p_{sw} \rangle$. As was previously noted, the assumptions concerning the vertical enthalpy distribution are based on results from numerous cross-sectional and three-dimensional simulations.

The assumptions concerning the vertical distribution of pressure and enthalpy expressed explicitly in (50)–(55) permit the determination of all pressure- and enthalpy-dependent parameters in (37) and (38). The procedure used to obtain these parameters is straightforward. Equations (50)–(55) are solved simultaneously, by Newton-Raphson iteration, to obtain the elevation of the interface contact, z_c, and the fluid pressure p_{z_c} at the contact as functions of x-y space. Required for these calculations are the vertically averaged pressure $\langle p \rangle$ and enthalpy $\langle h \rangle$ and the top z_2 and bottom z_1 elevations of the reservoir, all as functions of x-y space. With this information, $\langle p_{sw} \rangle$ is computed using (52), $\langle p_w \rangle$ is computed using (50), p_{z_c} is computed using (51), $\langle h_{sw} \rangle$ is computed using (55), and z_c is computed using (54). If steam is not present at a point (x, y), then averaged pressure and enthalpy are used to calculate the thermodynamic properties of water.

Finally, the averages of relative permeabilities can be obtained by vertical integration of any standard relative per-

meability function. For a segregated system, these averages are given by

$$\langle k_{rw} \rangle = [z_c - z_1]/b \tag{56}$$

and

$$\langle k_{rs} \rangle = (z_2 - z_c)k_{rs}(S_{wr})/b \tag{57}$$

where $k_{rs}(S_{wr})$ is the rock relative permeability of steam at residual water saturation. As may be seen, these result in linear relationships.

Given the assumptions that we have made regarding gravity segregation, it is clear that discontinuities in quantities occur at the steam cap interface z_c. Strict application of Leibnitz's rule to these discontinuities leads to additional interface terms of the form

$$\frac{1}{b}(\psi_{\text{above interface}} - \psi_{\text{below interface}})\frac{\partial z_c}{\partial x}$$

For practical applications, these are neglected because $(1/b)(\partial z_c/\partial x)$ is usually small. Furthermore, in general, the codeviation terms are also neglected. In paper 2 we outline the conditions for which the vertical equilibrium assumption, the assumption neglecting codeviation terms, and the assumption neglecting interface terms are approximately valid.

Conclusions

The mathematical development of fluid flow and energy transport in hydrothermal systems presented in this paper serves two general purposes. Mainly, it provides a better understanding of the implicit and explicit assumptions that are necessary to derive tractable governing equations that describe hydrothermal systems. As it emphasizes these assumptions, it also reveals the need for further work to eliminate restrictive approximations.

For two-phase hydrothermal systems the need for experimental data is most evident. Little suitable experimental work has been done on thermal dispersion in steam-water porous systems. Although some very limited data for relative permeability of steam and water are available, they are insufficient for general applications. Additional studies of capillary pressure effects and thermal effects on intrinsic permeability would also be useful.

From practical considerations it is necessary to keep the mathematical models as simple (yet realistic) as possible. It is apparent that general analytical solutions to the multiphase equations for hydrothermal systems are not likely to be obtained due to their complex nonlinear nature. Numerical solutions are also difficult. For three-dimensional problems the expense of numerical solutions is often excessive. A rigorous two-dimensional treatment is a reasonable alternative but also requires more study. Specifically, alternative assumptions for averaging quantities in the vertical dimension should be investigated, and the significance of codeviation terms and interface terms that arise in the partial integration should be determined.

Acknowledgments. Much of the early work for this study was done while the senior author was a Ph.D. candidate at the Pennsylvania State University. We wish to thank Richard R. Parizek and Barry Voight of the Department of Geosciences and S. M. Farouq Ali of the Department of Petroleum and Natural Gas Engineering for their help during the formulative part of this study. We would also like to thank our colleague, Nobuhiro Yotsukura, of the U.S. Geological Survey for his suggestions and advice concerning equation development.

References

Bilhartz, H. L., Jr., Fluid production from geothermal steam reservoirs, M.S. thesis, Stanford Univ., Stanford, Calif., 1971.

Brownell, D. H., S. K. Garg, and J. W. Pritchett, Governing equations of geothermal reservoirs, *Water Resour. Res.*, *13*(6), 929–935, 1977.

Cady, G. V., Model studies of geothermal fluid production, Ph.D. thesis, 82 pp., Stanford Univ., Stanford, Calif., 1969.

Calhoun, J. V., M. Lewis, Jr., and R. C. Newman, Experiments on the capillary properties of porous solids, *Trans. AIME*, *186*, 189–196, 1949.

Coats, K. H., R. L. Neilson, M. H. Terhune, and A. G. Weber, Simulation of three-dimensional, two-phase flow in oil and gas reservoirs, *Soc. Petrol. Eng. J.*, *7*(4), 377–388, 1967.

Coats, K. H., J. R. Dempsey, and J. H. Henderson, The use of vertical equilibrium in two-dimensional simulation of three-dimensional reservoir performance, *Soc. Petrol. Eng. J.*, *11*(1), 63–71, 1971.

Faust, C. R., and J. W. Mercer, Theoretical analysis of fluid flow and energy transport in hydrothermal systems, *Open File Rep. 77-60*, 85 pp., U.S. Geol. Surv., Reston, Va., 1977*a*.

Faust, C. R., and J. W. Mercer, Finite-difference model of two-dimensional single- and two-phase heat transport in a porous medium: Version 1, *Open File Rep. 77-234*, 84 pp., U.S. Geol. Surv., Reston, Va., 1977*b*.

Garg, S. K., and J. W. Pritchett, On pressure-work viscous dissipation and the energy balance relation for geothermal reservoirs, *Adv. Water Resour.*, *1*(1), 41–47, 1977.

Haas, J. L., Jr., Physical properties of the coexisting phases and thermochemical properties of the H_2O component in boiling NaCl solutions, *U.S. Geol. Surv. Bull., 1421-A*, 73 pp., 1976*a*.

Haas, J. L., Jr., Thermophysical properties of the coexisting phases and thermochemical properties of the NaCl component in boiling NaCl solutions, *U.S. Geol. Surv. Bull., 1421-B*, 71 pp., 1976*b*.

Hearn, C. L., Simulation of stratified waterflood by pseudo relative permeability curves, *J. Petrol. Technol.*, *11*(2), 805–813, 1971.

Jacks, H. H., O. J. E. Smith, and C. C. Mattax, The modeling of a three-dimensional reservoir with a two-dimensional reservoir simulator: The use of pseudo functions, *Soc. Petrol. Eng. J.*, *13*(3), 175–185, 1973.

Keenan, J. H., F. G. Keyes, P. G. Hill, and J. G. Moore, *Steam Tables*, 162 pp., John Wiley, New York, 1969.

Koenig, J. B., Worldwide status of geothermal resources, in *Geothermal Energy*, edited by P. Kruger and C. Otte, pp. 15–58, Stanford University Press, Stanford, Calif., 1973.

Korn, G. A., and T. M. Korn, *Mathematical Handbook for Scientists and Engineers*, p. 100, McGraw-Hill, New York, 1961.

Mercer, J. W., C. R. Faust, and G. F. Pinder, Geothermal reservoir simulation, Proceedings of the Conference on Research for the Development of Geothermal Energy Resources, *Rep. RA-N-74-159*, Nat. Sci. Found., Pasadena, Calif., Sept. 23–25, 1974.

Meyer, C. A., R. B. McClintock, G. J. Silvestri, and R. C. Spencer, *ASME Steam Tables*, 2nd ed., 328 pp., American Society of Mechanical Engineers, New York, 1968.

Moench, A. F., Simulation of steam transport in vapor-dominated geothermal reservoirs, *Open File Rep. 76-607*, 43 pp., U.S. Geol. Surv., Menlo Park, Calif., 1976.

Monin, A. S., and A. M. Yaglom, *Statistical Fluid Mechanics; Mechanics of Turbulence*, pp. 205–218, Massachusetts Institute of Technology Press, Cambridge, 1973.

Ramey, H. J., Jr., P. Kruger, and R. Raghaven, Explosive stimulation of hydrothermal reservoirs, in *Geothermal Energy*, edited by P. Kruger and C. Otte, pp. 231–249, Stanford University Press, Stanford, Calif., 1973.

Somerton, W. H., J. A. Keese, and S. L. Chu, Thermal behavior of unconsolidated oil sands, *Soc. Petrol. Eng. J.*, *14*(5), 513–521, 1974.

Spivak, A., Gravity segregation in two-phase displacement processes, *Soc. Petrol. Eng. J.*, *14*(6), 619–632, 1974.

White, D. E., L. P. J. Muffler, and A. H. Truesdell, Vapor-dominated hydrothermal systems compared with hot-water systems, *Econ. Geol.*, *66*, 75–97, 1971.

Witherspoon, P. A., S. P. Neuman, M. L. Sorey, and M. J. Lippmann, Modeling geothermal systems, paper presented at International Meeting on Geothermal Phenomena and Its Applications, Accad. Nat. dei Lincei, Rome, Italy, March 3–5, 1975.

(Received April 1, 1978;
revised June 21, 1978;
accepted August 14, 1978.)

CURSO: "INGENIERIA DE YACIMIENTOS GEOTERMICOS "
23 DE MARZO AL 18 DE MAYO DE 1984

TEMA: "GEOTHERMAL RESERVOIR SIMULATION"
3. APPLICATION OF LIQUID-AND VAPOR DOMINATED HYDROTHERMAL MODELING TECHNIQUES TO WAIRAKEI, NEW ZEALAND

DR. GUILLERMO DOMINGUEZ
2-13 de abril.

Geothermal Reservoir Simulation: 3. Application of Liquid- and Vapor-Dominated Hydrothermal Modeling Techniques to Wairakei, New Zealand

JAMES W. MERCER AND CHARLES R. FAUST

U.S. Geological Survey, Reston, Virginia 22092

A quasi three-dimensional, areal model based on finite-difference approximations is applied to the hydrothermal field at Wairakei, New Zealand. The model simulates heat transport associated with the flow of steam and water through porous media. An analysis is made of the production aquifer under steady-state and transient flow conditions, allowing vertical flow of heat and fluid through confining beds. Computed steady-state results correlate well with observed data and indicate that portions of the aquifer had a steam cap prior to exploitation. Computed transient results also match observed data and support the hypothesis that the production aquifer is recharged through underlying confining beds. The limiting factor on production is the amount of mass available, both from storage and leakage. Although simulation results indicate that the field can maintain production rates to the year 2000, such long range predictions are unreliable due to the lack of information on the leakage properties of the confining beds.

INTRODUCTION

This report is the third in a series of three concerned with geothermal reservoir simulation. The first report [*Faust and Mercer*, 1979*a*] dealt with a theoretical development of the equations that describe mass flow and heat transport in liquid- and vapor-dominated hydrothermal systems. Numerical solution techniques used to solve the resulting nonlinear partial differential equations were the subject of the second paper [*Faust and Mercer*, 1979*b*]. In this report, we apply a quasi three-dimensional, areal model (based on vertical integration and the assumption of vertical equilibrium) to the hydrothermal system located at Wairakei, New Zealand. Steady-state behavior is reproduced and used as initial conditions for a two-part transient simulation. The first part is a history match from 1953 to 1973; the second part represents a prediction from 1974 to 2000.

This modeling study is an attempt to bring together existing information and data on Wairakei and to develop a rational framework on how the system operates. The framework is a numerical model that incorporates: (1) a conceptual description of the physics of fluid flow and heat transport in porous media, (2) the thermodynamics of two-phase, single-component water, (3) a geometric description of the Wairakei field including boundary conditions and initial pressure and enthalpy conditions, and (4) the hydrologic and heat transport parameters that characterize the Wairakei field. Information included in the third group is based primarily on published descriptions. Many of the hydrologic and heat transport parameters are determined by comparing model computations with historical data. The model is tested and calibrated through this history matching procedure, and is used to identify data deficiencies. Once the history matching is complete, the model is used to make predictions on future reservoir performance.

Modeling studies of complex physical systems are generally unable to completely explain all details of observed behavior. In addition to uncertainties associated with interpretation of field measurements of subsurface conditions, numerical models, no matter how sophisticated, are approximations to nature. Because of these uncertainties, model calibration requires either subjective evaluation or statistical treatment. Statistical procedures for history matching of the numerical model used in this study have not been sufficiently developed. We must, therefore, set subjective guidelines. For the Wairakei field, it is required that determined parameters be physically reasonable and major aspects of the reservoir behavior be explained (or matched). For steady-state conditions, major reservoir aspects include observed initial fluid pressures and the distributed fluid and heat (convective and conductive) leakage at the surface. For transient conditions, these aspects include (1) the sharp decline in temperatures that occurred around 1962, (2) differential drop in pressure between the top and bottom of the reservoir, (3) the pressure recovery that was observed during a partial shut down of the field, and (4) changes in surface discharge characteristics during the first ten years of production.

The numerical results that are presented in this paper do meet the subjective guidelines. Obviously, these results are not a unique description of the Wairakei system. Further, this description and subsequent predictions are based on currently available data, and as additional information on Wairakei is obtained, the model should be updated. The Wairakei field application represents a validation of the numerical simulators developed in this study. This hydrothermal field was chosen for the validation of our model because abundant data covering approximately 21 years of production history were made available by the New Zealand government.

WAIRAKEI HYDROTHERMAL SYSTEM

Location and History of Development

The geology of the Wairakei field is discussed in *Grindley* [1965] and the geohydrology is described in *Studt* [1958], *Bolton* [1970], and *Mercer et al.* [1975]. The field is located north of Lake Taupo and is situated on the west bank of the Waikato River (see Figure 1), which at this location serves as a groundwater discharge area. The field is considered to occupy a surface area of approximately 15 km^2 [*Grindley*, 1965] and extends westward from the Waikato River for 5 km, where it is bordered by hills that act as a groundwater recharge area [*Studt*, 1958].

Centered in an active volcanic belt, Wairakei is one of many geothermal regions located between the Tongariro and White Island volcanoes. This volcanic belt appears to be a surface manifestation of a landward extension of the Pacific trench system found north of New Zealand. This hypothesis is supported by gravity, magnetic, and seismic studies, which indicate that this volcanic belt is a structural depression approximately 5 km deep filled with broken block structures and

Paper number 9W0202.

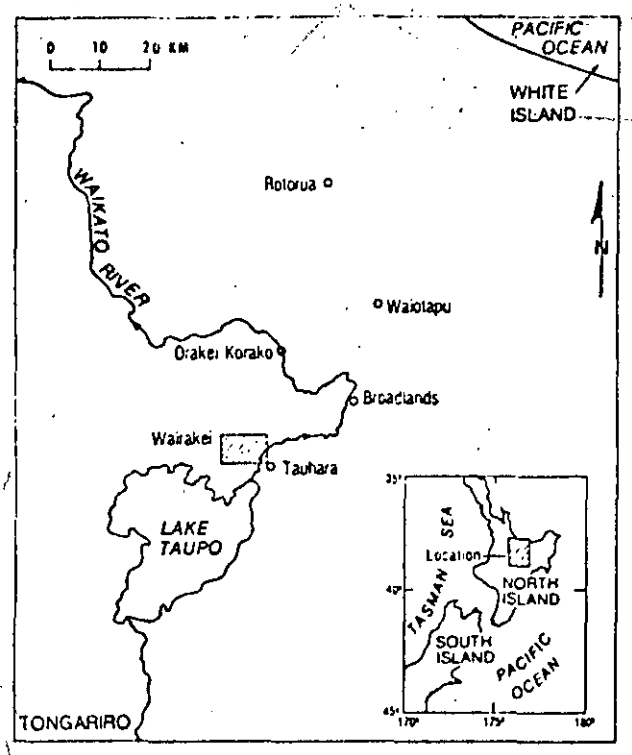

Fig. 1. Index map showing location of Wairakei, New Zealand; inset is of North Island [*Mercer et al.*, 1975].

penetrated by rhyolitic complexes [*Modriniak and Studt*, 1959].

The first wells were drilled at Wairakei in 1953, and to date, over 100 wells have been drilled, some to a maximum depth of approximately 1400 m. Power generation began in 1958, and by 1968 the power stations at Wairakei were providing approximately 172 MW (R. S. Bolton, written communication, 1978), or 18% of the total electrical requirements of New Zealand's North Island. Wairakei is considered to have been a liquid-dominated system prior to exploitation [*White et al.*, 1971; *Studt*, 1958; *Bolton*, 1970]. Utilizing steam (which flashes in the wells and discharges under pressure) to drive turbines, it became the first liquid-dominated system to be developed for the purpose of generating electricity.

Availability of water, rather than heat, appears to be the dominant factor controlling production rates. A cumulative mass discharge, amounting to approximately 6.0×10^{11} kg of steam and water by the end of 1969 [*Bolton*, 1970], has resulted in pressure drops ranging from 2.0×10^{6} to 2.4×10^{6} N/m^2 throughout the main production area. As pressures have dropped, steam has formed and accumulated in the upper parts of the reservoir. As a result, temperatures have dropped in the upper portions of the reservoir. Temperatures are stable in the deeper parts of the reservoir, possibly indicating a source for the hot water. Cold water intrusion around the field margins does not appear to be a serious problem [*Grindley*, 1965].

Fluid produced by Wairakei wells contains less than 1% weight concentration of dissolved solids, and 80% of the original geothermal fluid produced is discharged to the Waikato River, apparently without harmful effect [*Koenig*, 1973]. Even though the hot water is relatively pure, mineral deposition associated with steam separation may be an important factor limiting the performance and life of Wairakei wells [*Grindley*, 1965].

Geohydrology

The local stratigraphy consists of nearly horizontal Quaternary acidic volcanic rocks of the following formations, in descending order [*Grindley*, 1965]: Holocene pumice cover, Wairakei Breccia, Huka Falls Formation, Haparangi Rhyolite, Waiora Formation, Waiora Valley Andesite, Wairakei Ignimbrites, and the Ohakuri Group. There are at least two aquifers in the above sequence: the Wairakei Breccia and the Waiora Formation. Although a deeper third aquifer may also

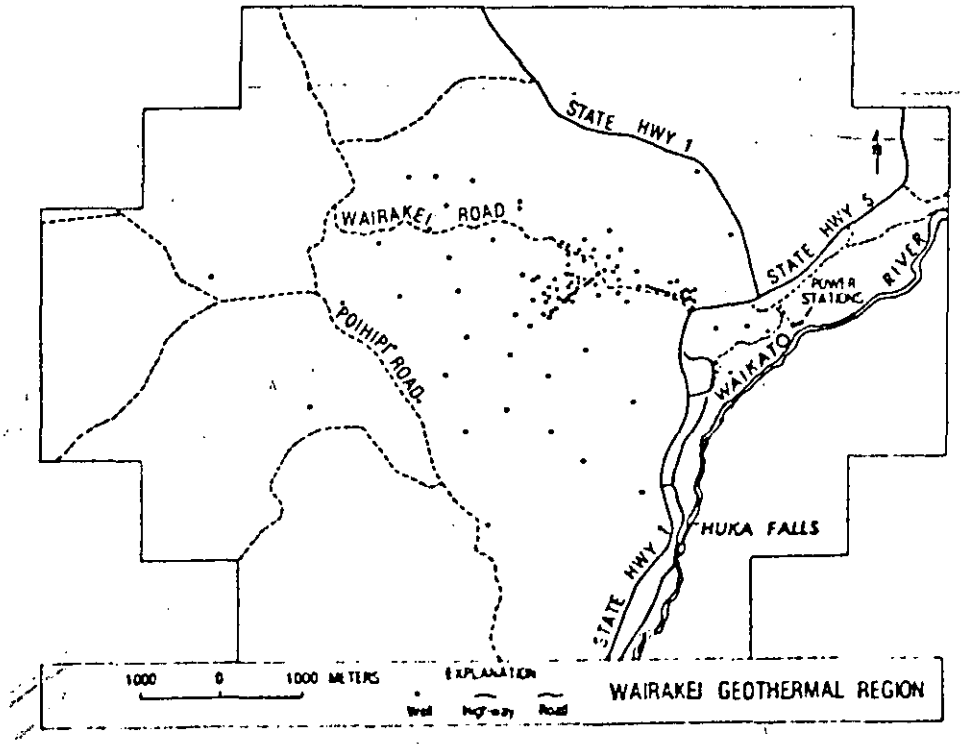

Fig. 2. Map of Wairakei geothermal region showing main production area (concentration of wells) and local features

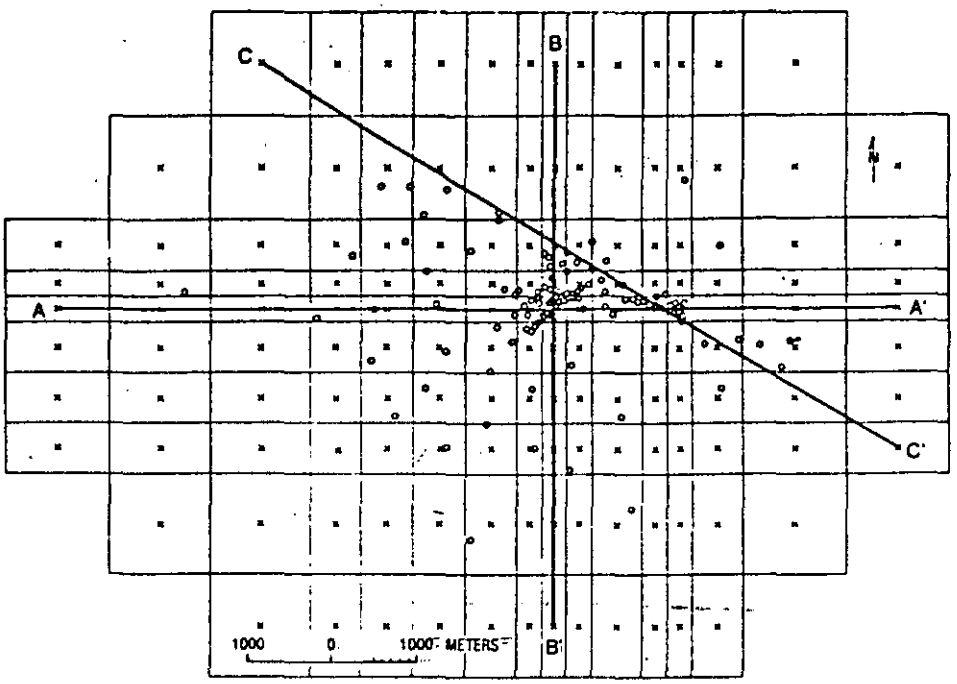

Fig. 3. Finite-difference grid used in Wairakei simulation showing well locations (circles) and block-centered nodes (crosses); also shown are three section lines, A-A', B-B', and C-C'.

exist in the Ohakuri Group, it has been found in only one well, and its lateral extent is unknown.

The bulk of steam and hot water discharged by Wairakei wells comes from the Waiora aquifer, which consists of pumice breccias and vitric tuffs. Detailed measurements are not available, however, it is believed that the permeability of the Waiora aquifer varies spatially depending on the amount of brecciation and is highest at fault zones and near a lower unconformable contact. Although productive wells at Wairakei are nearly always located in zones of locally high permeability associated with major faults, the reservoir as a whole responds as a porous medium defined in a continuum sense [*McNabb et al.*, 1975], and is treated as such in this work.

The Waiora aquifer is overlain by lacustrine shales of the Huka Falls Formation that act as confining beds. In some locations the shales are interbedded with breccia. Hydrothermal, mudflow conglomerates that are also interbedded in the Huka Falls Formation may indicate that hydrothermal activity at Wairakei is at least 500,000 years old [*Grindley*, 1965].

Underlying the Waiora aquifer are the Wairakei Ignimbrites, welded tuffs of low primary permeability. The base of the Waiora aquifer is not well defined because of secondary permeability afforded by fracture zones and the irregular surface of the contact between the ignimbrites and the aquifer. The problem of determining the base of the aquifer is further complicated in the south and southwest, where rhyolite overlies the ignimbrites and progressively cuts out the Waiora aquifer from below. The rhyolite also displays secondary permeability in its upper layers [*Studt*, 1958].

The stratified volcanic sequence at Wairakei is complexly faulted and draped over a basement horst, and thickens eastward and westward into adjoining volcano-tectonic depressions [*Grindley*, 1965]. Most of the major fault zones are well defined through drilling, and strike in a southwest-northeast direction [*Bolton*, 1970]. It is generally thought that such fault zones in the underlying ignimbrites are the source of the hot water in the Waiora aquifer.

Heat and Mass Flows and Temperatures at Wairakei

The natural heat flow at Wairakei has been measured several times, beginning in 1951. *Fisher* [1964] gives a summary of results obtained by various authors during the period 1951–1959. The values range from 3.431×10^9 to 6.820×10^9 J/s; however, Fisher concludes that the best value for natural (preexploitation) heat flow at Wairakei is approximately 4.184×10^9 J/s, where a heat flow reference temperature of 12°C is used.

One common conclusion of all the heat flow surveys is that the majority of the natural heat flow is due to convection and is thus associated with a natural mass discharge. Although some mass discharge was measured, the total initial natural mass discharge was not; however, it can be estimated from the measured heat flow. *Fisher* [1964], using a mean enthalpy of 1.025×10^6 J/kg and omitting the heat flow due to conduction, obtained a mass discharge of 440 kg/s for the 1951–1952 period. Fisher also noted that the natural heat discharge between 1951 and 1958 appears to have remained relatively uniform, whereas the natural mass discharge decreased, resulting in more steam and less water being discharged.

Temperatures at Wairakei increase rapidly with depth down to the top of the Waiora aquifer, where the temperature in the hotter regions is about 200°C. In the aquifer the temperature gradient is reduced with depth, and in the lower part of the aquifer the gradient is either very small or becomes negative. In some locations, temperatures reach approximately 250°C at 460 m depth.

WAIRAKEI MODEL

The conceptual model of the Wairakei field presented in this paper is similar to that presented by *Mercer et al.* [1975] with the exceptions that mass leakage is now allowed through the Wairakei Ignimbrites and two-phase flow is allowed in the reservoir. Thus the Waiora Formation is assumed to be the principal producing reservoir. It is overlain and underlain by leaky confining beds of the Huka Falls Formation and the Wairakei Ignimbrites.

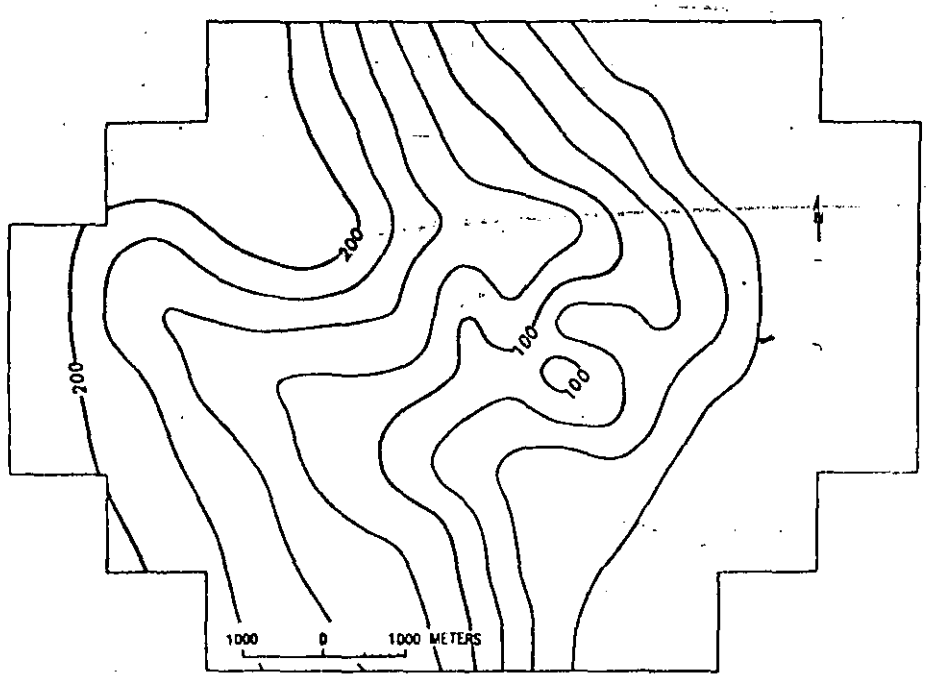

Fig. 4. Map of equal thickness for the water-table aquifer used in the finite-difference model; contour interval is 25 m.

Modeling the Wairakei field is accomplished in two steps: a steady-state simulation and a transient simulation. Briefly, in the steady-state simulation, we attempt to match single-phase flow conditions and the observed natural discharge rate of 440 kg/s through the Huka Falls Formation. This is accomplished by (1) adjusting pressure distributions on both sides of the Huka Falls Formation (this controls the direction of the spatially distributed leakage through the Huka Falls) and (2) adjusting the vertical permeability through the Huka Falls Formation (this controls the magnitude of the leakage). During this process, temperature distributions are considered known from downhole temperature measurements. Concurrently, we compute a distributed steady-state leakage through the Wairakei Ignimbrites that maintains the initial pressures and temperatures in the Waiora aquifer. Once a satisfactory match is obtained by trial and error, the steady-state solution, including the steady-state leakage from above and below (which sum to zero), is used as the initial conditions for the transient simulation. For this step, transient mass leakage through the confining beds is approximated by analytical solutions and is added to the steady-state leakage. During this part of the simulation (history match), permeabilities in the Waiora aquifer are adjusted and vertical leakage properties of the Wairakei Ignimbrites are estimated. Finally, these results are used for the predictive portion of the transient simulation.

Numerical Approach

The numerical approach is described in detail in parts 1 and 2 of this study; only a brief summary is given here. Two-phase

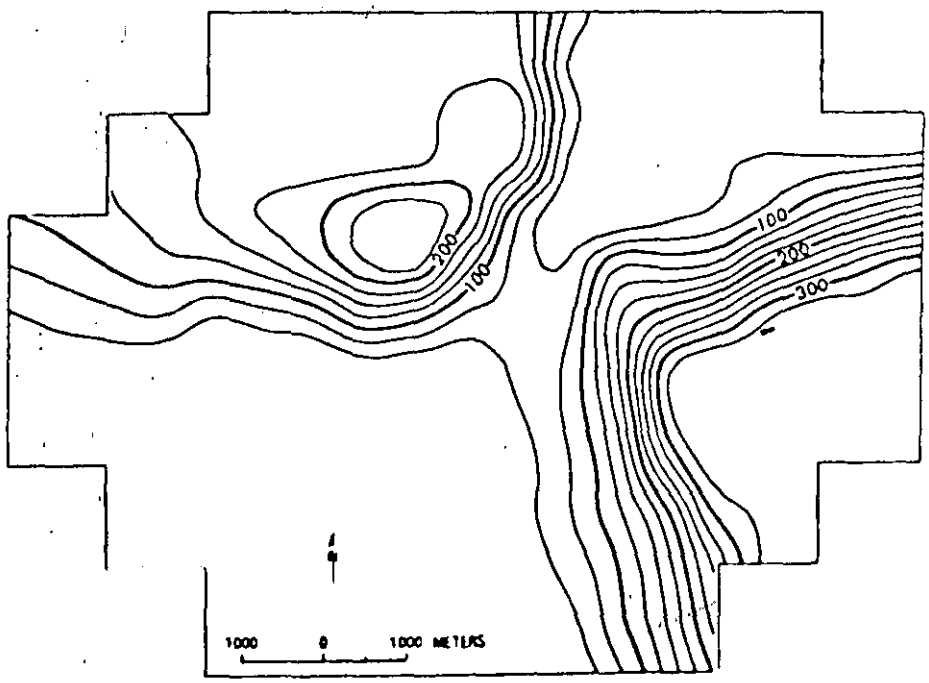

Fig. 5. Map of equal thickness for the Huk Falls confining bed used in the finite-difference model contour interval is 25 m.

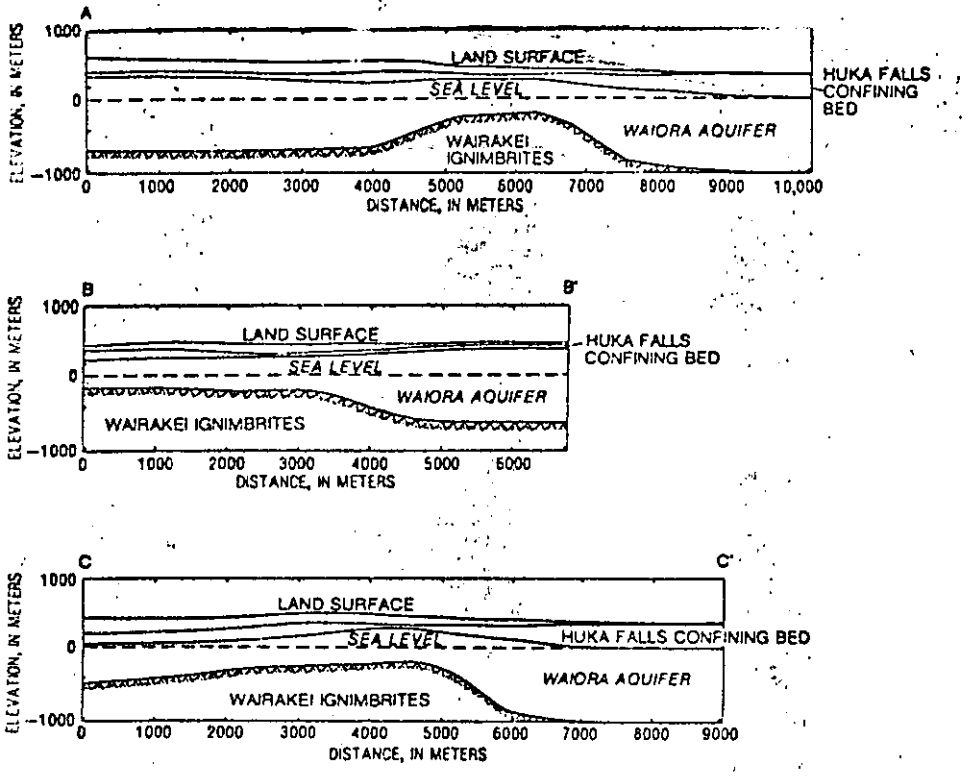

Fig. 8. Geologic cross sections from Wairakei model data showing in descending order: water-table aquifer, Huka Falls confining bed, Waiora aquifer and Wairakei Ignimbrites. Cross sections correspond to section lines shown in Figure 3 and are (A-A') west to east, (B-B') north to south, and (C-C') northwest to southeast.

Boundary Conditions

A base map of the Wairakei region showing the major geographical features is presented in Figure 2, where the cluster of wells represents the main production area. The production area is often subdivided further into an eastern and western production area, which will be used for later reference. Also, note the location of the power stations, as these will be used as a reference point in later figures. The irregular boundary of Figure 2 represents the boundary used in the finite-difference model. This boundary is essentially the same as that used by *Mercer et al.* [1975] and is similar to that described by *Bolton* [1970] except that it has been extended slightly further from the main production area. It is interesting to note that these boundaries coincide approximately with those defined by ground subsidence, gravity surveys [*Hunt*, 1970], and electrical resistivity surveys (G. E. K. Thompson, written communication, 1972).

The boundary condition for the fluid flow equation is considered to be no-flow (that is, the boundary is impermeable). As was pointed out earlier in this report, the southern boundary of the Waiora aquifer is cut off by rhyolite, which may be considered impermeable. The northern and eastern boundaries are also considered impermeable, since the pressure response in wells near these boundaries appears to be independent of production [*Bolton*, 1970]. Finally, the western boundary is extended far enough from the main production area that the transient solution is not significantly affected by it, and it too may be treated as impermeable. This western boundary may actually be no-flow if the hills near it act as a groundwater divide. Finally, it is interesting to note that the impermeable boundaries to the north and east may have resulted in part from silica deposition and self-sealing (D. E. White, oral communication, 1975) that is associated with other geothermal fields.

The boundary condition for the energy equation is also considered no-flow. In previous work [*Mercer et al.*, 1975], this boundary condition was considered constant temperature; however, numerical results were insensitive to the type of boundary condition, and no-heat-flow is chosen for convenience.

Figure 3 is the finite-difference grid used for the Wairakei simulation. The circles represent well locations and the crosses are the block-centered nodes. There are 150 blocks covering an area of approximately 74.5 km². Although the actual field only covers 15 km², the impermeable boundaries of the entire system enclose a larger area. This difference in areal coverage is important to note since some studies of Wairakei [for example, *McNabb et al.*, 1975; *Grant and Robinson*, 1976] consider the smaller area and therefore do not use impermeable boundaries. Finally, note the three section lines in Figure 3, as these will be used for future reference. Also the block where the north-south (B-B') and east-west (A-A') section lines intersect will be referred to in the modeling results as the western production block.

Reservoir Properties and Description

The thickness of the water-table aquifer, where the water-table aquifer is comprised of the Holocene pumice and Wairakei Breccia, is shown in Figure 4. The values are in meters and the contour interval is 25 m; the scale is the same as that on the finite-difference grid. This plot is based on well data from *Grindley* [1965]. The data were smoothed and extrapolated to the node points; consequently, general trends are indicated and details of local geology, such as fault locations,

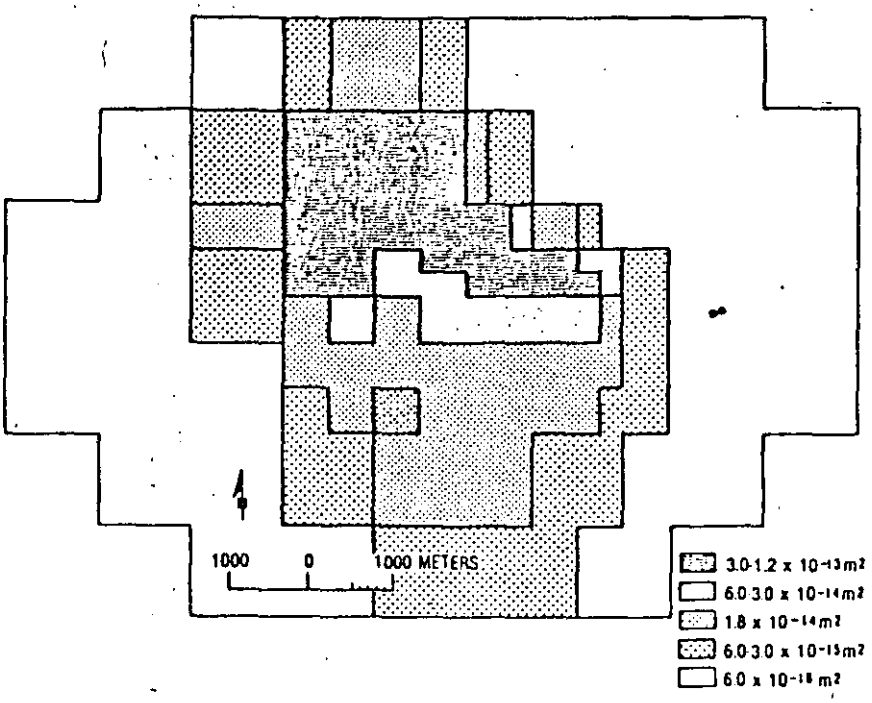

Fig. 9. Horizontal permeability distribution for the Waiora aquifer used in the finite-difference model; values are in meters squared.

are lost. Note that there is a considerable amount of uncertainty in these and other data to be presented, especially outside the main production area.

Figure 5 is a thickness map of the Huka Falls confining bed. Again the values are in meters, the contour interval is 25 m, and the plot is based on smoothed well data from *Grindley* [1965]. The thickness of the Waiora aquifer is shown in Figure 6. The aquifer thickens toward the south where it is intruded and eventually cut off by the lowly permeable rhyolite. In preparing Figure 6, the rhyolite is considered to contribute to the total reservoir thickness. An attempt is made to compensate for this by using a lower permeability in the southern region.

A structure map of the top of the Waiora aquifer in meters above mean sea level, is presented in Figure 7. The data for this are also from *Grindley* [1965] and the contour interval is 25 m. To better visualize the hydraulic units used in the model, it is helpful to construct cross sections. The finite-difference grid (Figure 3) has the locations of three section lines indicated. The corresponding cross-sections are shown in Figure 8. The units are (from top to bottom) the water-table aquifer, the Huka Falls confining bed, the Waiora aquifer, and the

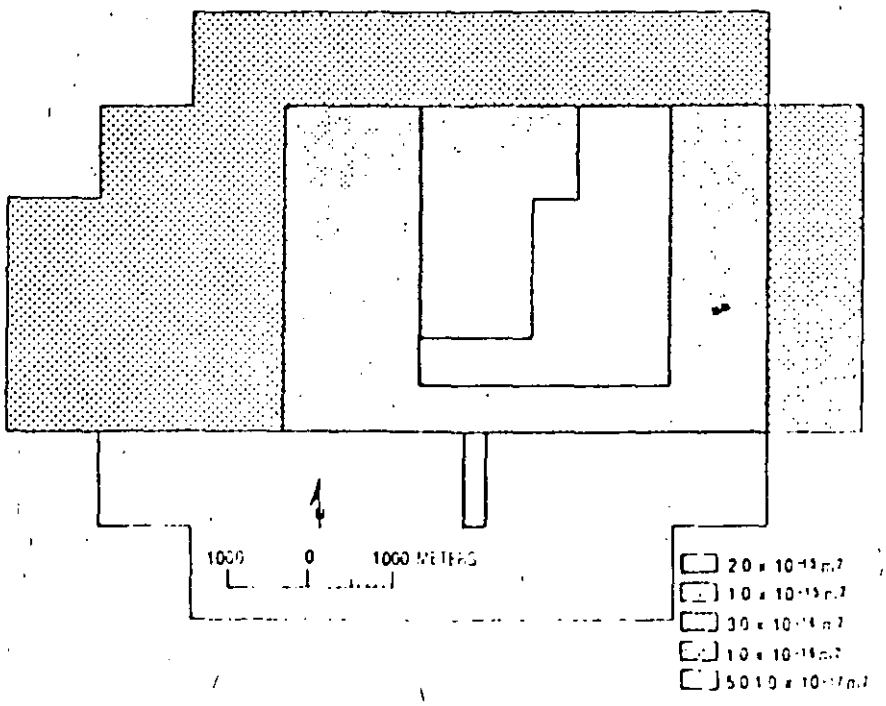

Fig. 10. Vertical permeability distribution for the Huka Falls confining bed used in the finite-difference model; values are in meters squared.

TABLE 1. Data Used in Wairakei Model

Property	Value
Initial aquifer porosity (Waiora)	0.25
Confining bed porosity (Huka Falls)	0.25
Medium thermal conductivity (Waiora)	21.80 W/(m·K)
Confining bed thermal conductivity (Huka Falls)	2.18 W/(m·K)
Rock density (Waiora)	2.187 kg/m³
Rock specific heat (Waiora)	9.2×10^3 J/(kg·k)
Rock compressibility (Waiora)	5.0×10^{-10} m²/N

Wairakei Ignimbrites. The horizontal line passing through the Waiora aquifer represents mean sea level. As indicated in the east-west cross section (A-A'), the Waiora aquifer dips steeply in the east and west. The exact depth of the Waiora Formation in these directions is unknown and, therefore, the indicated depth may be in error.

Very little is known about the permeability distribution at Wairakei. In earlier work [*Mercer et al.*, 1975], an average value of 1.0×10^{-13} m² was used for most of the Waiora aquifer and 1.0×10^{-14} m² was used for the eastern production area, which is less faulted. For the confining bed, in general, *Mercer et al.* [1975] used 1.0×10^{-16} m², which was widely criticized as being too high. *McNabb et al.* [1975], using a simplified analytical model, estimated a horizontal permeability for Wairakei of 7.0×10^{-16} m². Using the temperature profile at 1 km and early pressure measurements, they estimated a vertical permeability of 7.6×10^{-16} m². Finally, results from core analysis [*Pritchett et al.*, 1976] indicate that the Waiora aquifer has a primary permeability of approximately 5.0×10^{-17} m², which is clearly insufficient to sustain the production at Wairakei.

Based upon these limited data and on our simulation results, the permeability distribution we use for the Waiora aquifer is shown in Figure 9, where the values at each point are used for both the x- and y-directions in the model. We have assumed that the reservoir as a whole responds as a porous medium defined in a continuum sense. This assumption leads to a value of permeability that probably lies between that of the intergranular matrix and the fracture permeability. As can be seen in Figure 9, the eastern production area is assigned permeabilities that range from 3.0×10^{-13} to 3.0×10^{-14} m². Permeability in the western production area and just west and north of this area is generally assigned the higher value of 3.0×10^{-13} m² to allow for increased faulting there. As indicated earlier, to account for the rhyolitic intrusion in the southern part of the aquifer, the permeability in that direction is decreased. Also, to help account for the impermeable boundary in the east and allow for the possibility of self-sealing in this direction we have decreased the permeability eastward.

The vertical permeability distribution of the Huka Falls confining bed, shown in Figure 10, was determined by a trial and error match of the steady-state surface mass discharge. Again, this distribution represents effective permeabilities that incorporate both primary permeability and secondary permeability resulting from faulting. The values vary from 1.0×10^{-17} m² in the south to 2.0×10^{-15} m² in the main production area. In general, these values are lower than those used by *Mercer et al.* [1975]. Note the southern block with the high permeability; this is based on an attempt to reproduce the observed natural discharge at the Karapiti area, an area of relatively high discharge located south of main production area (not shown). It is interesting to note that although the permeability distribution in the Huka Falls confining bed is adjusted to match the observed natural field discharge, zones assigned high permeability generally are located in areas of known faults.

Other data used in the Wairakei model are given in Table 1. As may be seen, the initial aquifer porosity is estimated to be 0.25; this value is increased in the western production area to 0.35 to help account for the effects of the fractures there. Also note that the medium thermal conductivity is considered constant and is a lumped coefficient that includes the effects of both conduction and dispersion in the water and conduction in the rock matrix. Most of the values in Table 1 compare favorably with the core analysis results presented in *Pritchett et al.* [1976].

Vertical Flow at the Top and Base of the Reservoir

It is believed that the Waiora aquifer receives hot water through fault zones in the Wairakei Ignimbrites. Also flow occurs through the Huka Falls confining bed as evidenced by mass discharge observed at the surface. The difficulty is to describe these flow terms as functions of time and space.

The equations used in this study were obtained by integrating the three-dimensional flow and heat-transport equations over the reservoir thickness [*Faust and Mercer*, 1979*a*]. The resulting quasi three-dimensional, areal equations include terms that account for convective and conductive fluxes at the reservoir top and base (these are referred to as leakage terms). These terms need to be evaluated for both steady-state and transient conditions in order to model the Wairakei field. This is complicated by the lack of data, since only the steady-state heat flow at the surface has been measured.

Steady-state leakage. In the Wairakei model, we consider only the vertical component of convective and conductive leakage through the Huka Falls confining bed and Wairakei Ignimbrites. In general, to determine the direction and magnitude of these fluxes, pressure and temperature distributions at the top of the Huka Falls confining bed and bottom of the Wairakei Ignimbrites are required. The temperature distribution at the top of the Huka Falls confining bed is shown in Figure 11. This temperature distribution was estimated from well data in *Grindley* [1965], and is similar to that used in *Mercer et al.* [1975]. Figure 12 shows the pressure distribution at the base of the water-table aquifer (top of the Huka Falls Formation). These pressures were determined by assuming the water-table aquifer had a saturated thickness that was 80% of its total thickness. These values were used in conjunction with a density distribution, which was a function of the temperatures in Figure 11, to compute hydrostatic pressures. Using these as our initial approximation, we adjusted the water-table pressures in order to obtain the proper direction of the observed mass flow at the surface. Our final result is the pressure distribution in Figure 12. Using the distributions in Figures 11 and 12, pressure and temperature data for the Waiora aquifer, the vertical permeability distribution in Figure 10, and the confining bed thermal conductivity in Table 1, the steady-state leakage through the Huka Falls confining bed was determined by use of Darcy's equation and Fourier's equation.

Data for the base of the Wairakei Ignimbrites do not exist and steady-state leakage through the ignimbrites to the base of the Waiora aquifer was treated using distributed mass and heat source terms. These were determined from the steady-state simulation and were used to maintain the steady-state pressure and temperature distributions in the Waiora aquifer.

Transient leakage. Discharge to wells causes pressure de-

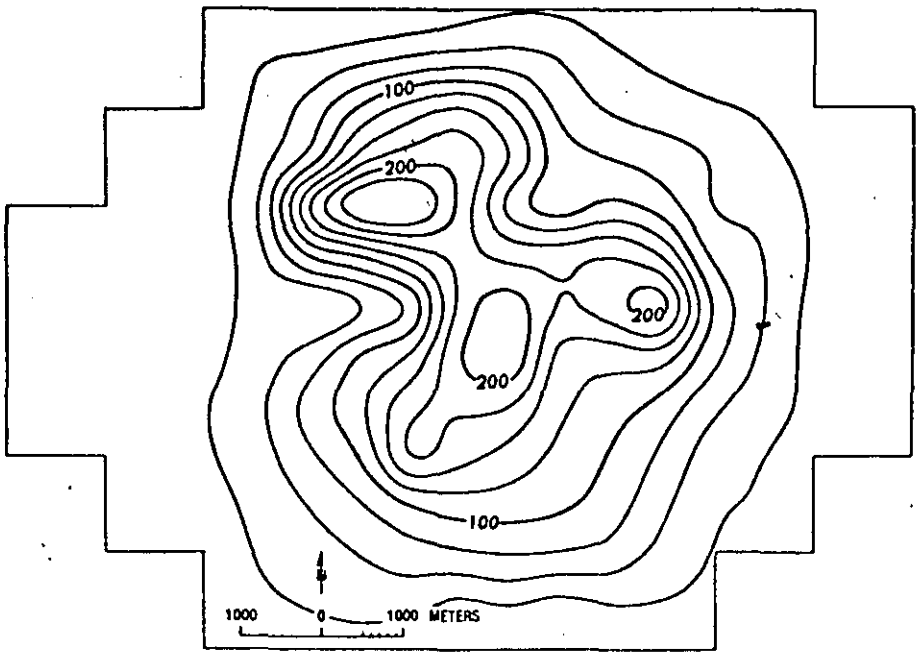

Fig. 11. Temperature distribution (degrees Celsius) at the top of the Huka Falls confining bed used in the finite-difference model; contour interval is 25°C.

clines in the Waiora aquifer. These pressure decreases cause an influx of mass (fluid) into the aquifer, that is, transient leakage. It is estimated from gravity data [*Hunt*, 1970] that 20% of the water discharged to wells from 1961 to 1967 was replaced by recharge and that between 1967 and 1968, approximately 100% replacement occurred, presumably by transient leakage from confining beds.

Transient mass leakage through the overlying Huka Falls confining bed is assumed to be the result of a stepwise change in pressure in the Waiora aquifer and may be approximated by [*Trescott et al.*, 1976] (modified for pressure):

$$q_T = (\rho_0 - p)\frac{K'}{gb'}\left\{1 + 2\sum_{n=1}^{\infty}\exp\left[-n^2\pi^2\left(\frac{K't}{3b'^2S_s'}\right)\right]\right\} \qquad (1)$$

where q_T is the mass leakage at the top of the Waiora aquifer; K' and S_s' are the hydraulic conductivity and specific storage of the Huka Falls confining bed, approximated by $K' = k'\rho g/\mu$ and $S_s' = \rho g\phi'\beta$; p_0 and p are the initial and current aquifer pressures; t is the elapsed time of the pumping period; g is the graviational constant; and b' is the thickness of the Huka Falls Formation. Finally, k' and ϕ' are the permeability and porosity of the Huka Falls Formation, respectively, ρ is fluid density, μ is fluid viscosity and β is the vertical compressibility coefficient. In this approach we have assumed that leakage through the Huka Falls confining bed is single phase (water) and recharge (rainfall) is sufficient to maintain the water table in the upper aquifer near its initial or steady-state location. Note that q_T varies spatially, and that during production simu-

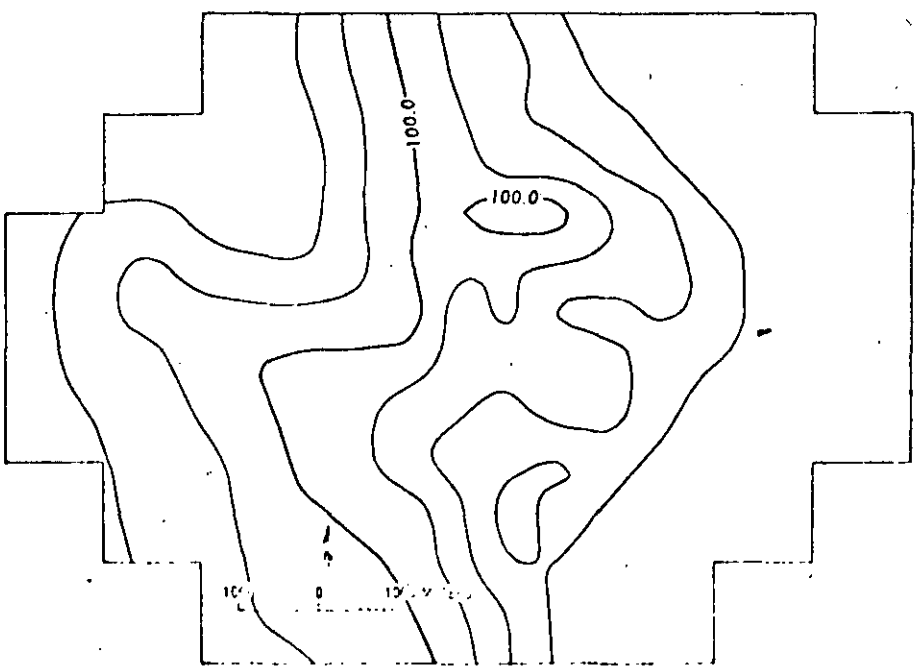

Fig. 12. Pressure distribution (N/m² × 10⁶) at the top of the Huka Falls confining bed used in the finite-difference model; pressure decreases from west to east with a contour interval of 25 × 10⁶ N/m².

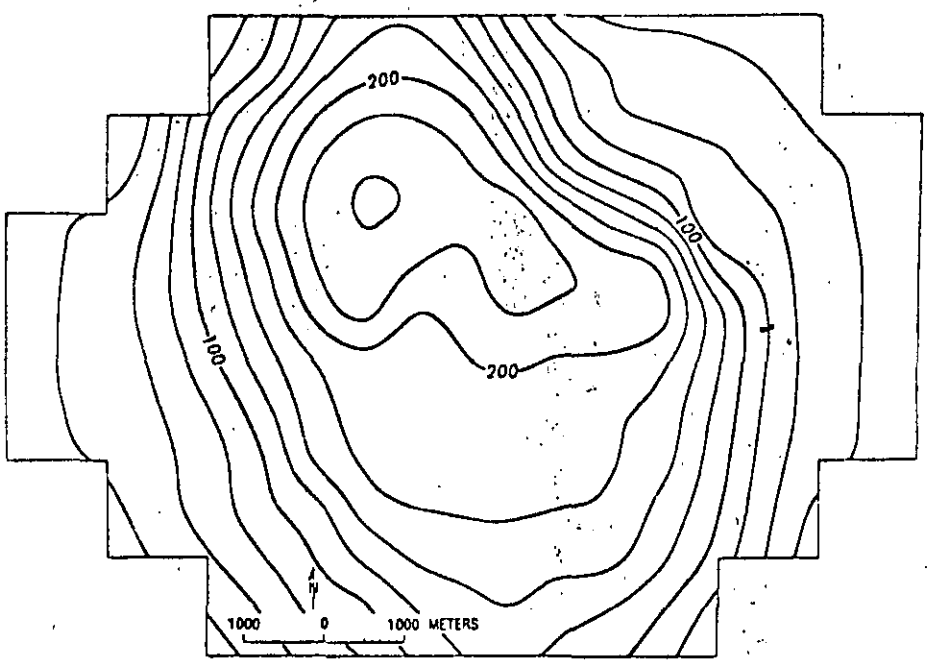

Fig. 13. Observed steady-state temperature distribution (degrees Celsius). Values have been vertically averaged through the Waiora aquifer; contour interval is 25°C.

lations, the computed transient leakage is added to the steady-state leakage.

We approximate the transient mass leakage through the underlying Wairakei Ignimbrites by using an analytical solution that describes the flow at the contact of the Waiora aquifer and the Wairakei Ignimbrites caused by a stepwise change in pressure in the aquifer. The solution assumes that the ignimbrites can be treated as a semi-infinite layer and is given by [*Ferris et al.*, 1962] (modified for pressure):

$$q_B = (p_0 - p)\frac{1}{g}\left[(KS_s)_B/\pi t\right]^{1/2} \qquad (2)$$

where q_B is the single-phase mass leakage at the base of the Waiora aquifer, $(KS_s)_B$ is the hydraulic conductivity-specific storage product for the Wairakei Ignimbrites. No data are available for this product and its value was determined by trial and error. The final distribution ranged from 7.5×10^{-8} s^{-1} in the faulted zones to 1.5×10^{-13} s^{-1} near the boundaries. Implications resulting from these high values will be discussed later.

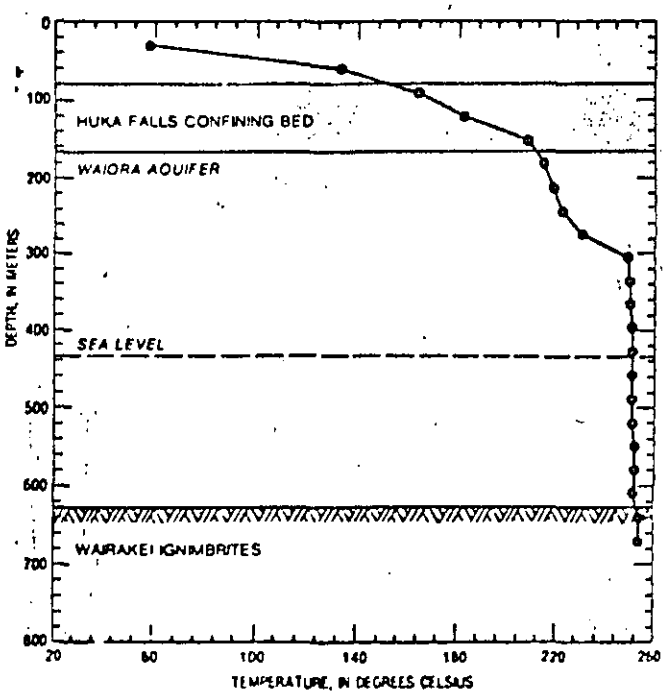

Fig. 14. Example of observed downhole temperature profile (degrees Celsius). Also indicated in descending order are water-table aquifer, Huka Falls confining bed, Waiora aquifer, and Wairakei Ignimbrites.

Transient mass leakage has an associated enthalpy, providing a transient convective heat leakage. It is assumed that flow from both above and below enters the Waiora aquifer with an enthalpy equal to the initial vertically averaged enthalpy in the Waiora. This assumption is reasonable for flow from the Wairakei Ignimbrites. It is also appropriate for the Huka Falls Formation during early stages of reservoir development, since initial temperatures in that formation were high. During later stages of development, however, there may be some reservoir cooling due to this upper leakage that our model does not take into account. Several computer runs were also made in which the vertically averaged saturated water enthalpy at the current time step was used for convective heat leakage. This change did not significantly affect the computed results.

Although the computer model is capable of computing a transient conductive heat leakage [*Faust and Mercer*, 1977], this option was not used in the Wairakei model. Because temperatures are relatively invarient with time, transient conductive heat leakage is not considered significant.

Vertical Equilibrium

The concept of vertical equilibrium as discussed in *Faust and Mercer* [1979a] incorporates the assumption that as steam forms, it migrates to the top of the aquifer, forming a two-phase zone at residual water saturation. It is believed that after production began, a steam cap formed at Wairakei. Unfortunately, no measured residual water saturation is reported in

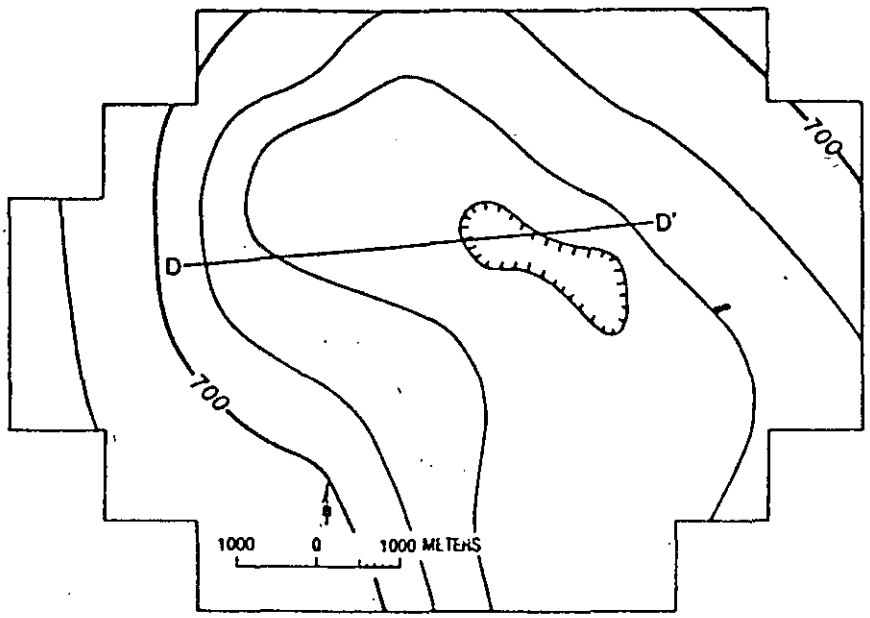

Fig. 15. Steady-state pressure distribution ($N/m^2 \times 10^6$, absolute) at a datum of 274 m below mean sea level computed from the finite-difference model; contour interval is 25×10^6 N/m^2. Also shown is a section line D-D'

the literature. *Pritchett et al.* [1976] used a residual water saturation of 0.2 in their study of Wairakei, and that same value is used here.

Averages of relative permeabilities can be obtained by vertical integration of measured rock relative permeabilities, which results in linear relationships. Measured rock relative permeabilities for Wairakei do not exist and the following averages were used in the model:

$$(k_{rw}) = \frac{S_w - S_{wr}}{1 - S_{wr}} \qquad (k_{rw}) = 1.0 \qquad S_w \le S_{wr} \qquad (3)$$

and

$$(k_{rs}) = 1.0 - S_w \qquad (4)$$

where (k_{rw}) and (k_{rs}) are averaged relative permeability for water and steam, S_w is the water saturation, and S_{wr} is residual water saturation.

Finally, recall that in the quasi three-dimensional, areal model properties and dependent variables such as pressure and enthalpy have been vertically averaged. Therefore data for the Wairakei model must also be vertically averaged.

Initial Conditions

The Wairakei hydrothermal system is considered to have been at steady state prior to exploitation. The first step in modeling Wairakei is therefore the reproduction of observed virgin or steady-state conditions. These results will be used as initial conditions for the transient model of exploitation. Inasmuch as wells drilled in the early 1950's had little discharge, temperature and pressure measurements made in these original wells are considered representative of steady-state conditions.

The steady-state (or initial) temperature distribution for the Waiora aquifer is presented in Figure 13. The temperatures have been vertically averaged over the thickness of the Waiora aquifer using well data from *Grindley* [1965]. This temperature distribution is similar to that used in *Mercer et al.* [1975], except that the temperatures in the main production area have been lowered slightly. The reason for lowering these temperatures will be discussed later. It is interesting to note that although the temperatures are vertically averaged, downhole temperatures are relatively uniform within the Waiora aquifer, as is evidenced by the downhole temperature plot in Figure 14. The data for this plot come from a well located in the western production area, and are somewhat typical of vertical temperature distributions at Wairakei. As can be seen, the temperatures at this location do not vary greatly with depth, with a maximum temperature of 254°C. Note that the confining bed and aquifer are indicated, as well as mean sea level. The temperatures at the top of the Huka Falls confining bed were used to construct Figure 11, and for the aquifer temperatures, the values between the top and bottom of the Waiora Formation were depth averaged. In the model, these temperatures are used to compute vertically averaged enthalpies, considered to be the initial conditions. The enthalpies, along with vertically averaged pressures, are used to compute thermodynamic properties, such as density.

The steady-state pressure distribution is shown in Figure 15. Although vertically averaged pressures are used in the model, for purposes of discussion, a reference level of 274 m below mean sea level is used. The general trend of the pressure

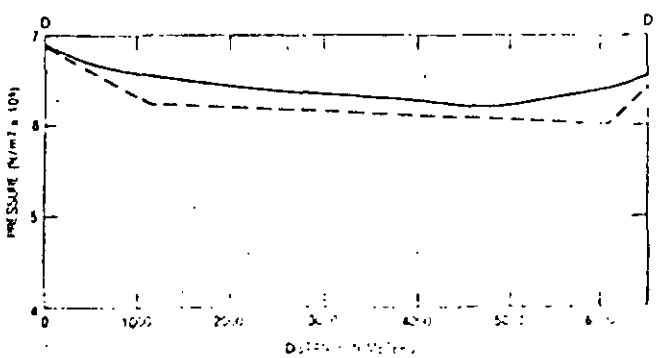

Fig. 16. Pressure profile ($N/m^2 \times 10^6$) corresponding to section line shown in Figure 15, datum is 274 m below mean sea level. Solid line was computed from Figure 15, dashed line is observed steady state data from *Bodvarsson* [1974].

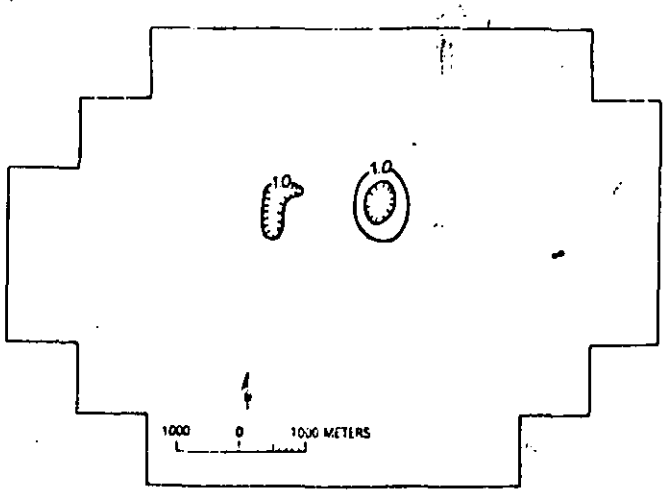

Fig. 17. Vertically averaged water saturations computed by the finite-difference model for steady-state conditions; contour interval is 0.1.

distribution was estimated from 1955 potentiometric surfaces given in *Studt* [1958]. Initial pressure data for the lower part of the aquifer are very limited, and the magnitude of the pressures computed from Studt's surfaces had to be increased to prevent substantial two-phase behavior throughout the field. Recall that prior to exploitation, Wairakei was considered to have been single phase (water). The pressure profile corresponding to the section line D-D' in Figure 15 is shown in Figure 16. The model data (solid line) is compared to an observed 1956 pressure profile (dashed line) from *Bolton* [1970]. Note that all pressures are absolute. As may be seen, the trend compares well; however, the pressures used in the model are generally higher than Bolton's. The final pressure distribution shown in Figure 15 was obtained by trial and error in an attempt to permit as much of the field as possible to be single phase (water) and to match the observed mass discharge at the surface (through the Huka Falls Formation).

Even with the higher pressures, portions of the field were two phase. Other than increase pressures, two additional data modifications could be made to reduce the size of the two-phase zone. First, the vertically averaged temperatures used by *Mercer et al.* [1975] were lowered slightly to obtain those shown in Figure 13. Second, a lower elevation of the aquifer top shown in Figure 7 was assumed. This modification causes an increase in vertically averaged water saturation as a result of the vertical-equilibrium assumption, and is believed to be justified since the lower part of the Waiora aquifer is the producing layer and its location is poorly defined. Using the downhole temperatures (see, for example, Figure 14) as a guide we lowered the aquifer top 60 m. This is the depth where the thermal gradient becomes approximately zero, which we felt indicates a zone of higher permeability.

With these data modifications, we obtained the steady-state, vertically averaged water saturations shown in Figure 17. As may be seen, our modeling results indicate that two parts of the field had a small steam cap, even before exploitation began. This could be a result of our approximations or the lack of detailed data in the early stages of development. We believe, however, that the field was two-phase prior to exploitation. It is interesting to note that most wells are cased with openings only in the lower part of the Waiora aquifer, below the steam cap shown in Figure 17. The effect of this on interpreting pressure and temperature data is unknown. It should also be noted that *Pritchett et al.* [1976] had to lower the shallow temperatures in their Wairakei simulation to ensure no vaporization. Also M. A. Grant (written communication, 1977) believes that Wairakei was two-phase prior to exploitation.

A surface mass discharge through the Huka Falls Formation was computed in the steady-state model. The calculations were made using Darcy's equation, the permeability of the Huka Falls confining bed, and the potential gradient across the confining bed. In general, recharge occurred toward the west where the Wairakei hills are located, and discharge occurred toward the east. The accepted total natural mass flow rate for Wairakei as computed by *Fisher* [1964] is 440 kg/s. The total discharge rate computed in this modeling work is 424 kg/s, with most of it occurring in the production area. Thus the match on the natural mass discharge is good except for the Karapiti area (the discharge area in the south) for which we were unable to use reasonable hydrologic parameters to reproduce its large discharge. This area is outside the main production area, and is believed not to have a large effect on the transient simulation.

The surface heat discharge computed by the steady-state model has a similar distribution to the mass discharge. The heat flow includes the effects of both convection and conduction, and is computed using the mass flux multiplied by the enthalpy of the mixture and Fourier's equation, respectively. The range of values for the total natural heat flow measured at Wairakei as given by *Fisher* [1964] is 1.172×10^7 to 5.983×10^7 J/s by conduction through the soil, and approximately 3.431×10^8 to 6.444×10^8 J/s by convection, with a heat flow reference temperature of 12°C. Heat discharge through the Huka Falls Formation computed by the model was 5.99×10^7

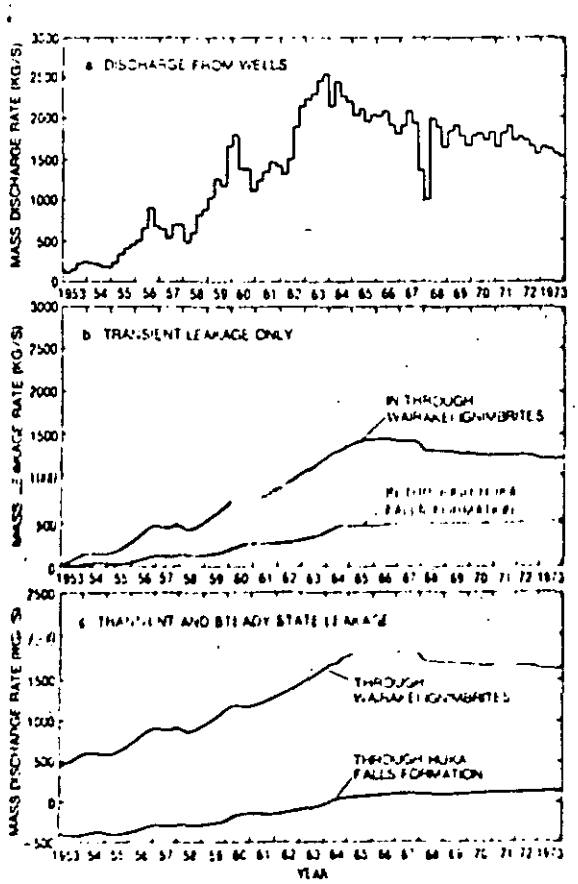

Fig. 18. (*a*) Mass discharge rate (kilograms per second) from Wairakei wells 1953-1973; (*b*) also shown is the computed transient leakage through the Wairakei Ignimbrites and Huka Falls Formation for the same time period, (*c*) and the total (steady-state and transient) leakage through both confining beds

J/s by conduction, and 3.566×10^8 J/s by convection, with a heat flow reference temperature of 0°C, giving a total calculated natural heat discharge of 4.165×10^8 J/s. The comparison with the total measured value of 4.184×10^8 J/s, which Fisher considers the best value, is reasonable.

The steady-state convective and conductive fluxes at the base of the Waiora aquifer were computed from the model by specifying aquifer pressures and enthalpies. Unfortunately, by computing the fluxes in this manner, the uncertainty in other reservoir parameters precludes meaningful interpretation of the steady-state bottom mass and heat distributions.

Transient Simulation: History Match

By using the steady-state enthalpy and pressure solutions as initial conditions, well discharge rates are incorporated into the model and transient effects of exploitation are simulated. Discharge rates were averaged for each well over 3-month intervals. The rates for each well lying within a finite-difference block were summed, and that the value was considered to be the discharge rate for that block for that time interval. The discharge for the entire field may be obtained by summing the discharge for each well and is presented in Figure 18*a*. As may be seen, little discharge took place before power generation began in 1958; it peaked at the end of 1963, after which a steady decrease occurred. The large decrease in 1968 resulted from a partial shut down of the field. At its peak, the well discharge was three to four times the steady-state (natural) mass discharge of 440 kg/s. At the time of this simulation work, we only had discharge data up to January 1974 and this period of 21 years was used to 'history match' the Wairakei data.

The mass source/sink (well) term is specified in the model; however, the heat source/sink (well) term must be computed. The vertical-equilibrium approach allows us to track the elevation of the contact between the single-phase (water) and two-phase boundary. Wells at Wairakei are cased and in general, are open in only the deeper part of the reservoir. For simulation purposes, we have assumed that the wells are fully-penetrating and are slotted (open) in the lower part of the reservoir. For wells in the eastern production area, we generally use an elevation of 60.0 m above mean sea level for the elevation of the top of the open interval and for the western production area we use 60.0 m below mean sea level. These values were estimated from drilling data. When the two-phase contact is above the elevation of the top of the open interval, mass is removed with the enthalpy of water. When the two-phase contact drops below this elevation, a mixture of steam and water is removed, and the heat sink term is determined from the phase mobilities according to [*Faust and Mercer*, 1979*a*]:

$$q_h' = \left[h_w + \frac{(h_s - h_w)k_{rs}}{k_{rs} + (\rho_w \mu_s / \rho_s \mu_w)k_{rw}} \right] q_m' \qquad (5)$$

where h_s and h_w are the saturated steam and water enthalpies, ρ_s and ρ_w are the steam and water densities, μ_s and μ_w are the steam and water viscosities, q_m' is the specified mass discharge of the well, and k_{rs} and k_{rw} are the relative permeabilities of steam and water computed using (3) and (4) and the thickness of the open interval.

Since the simulation is over an extended period of time, a time step of 91.3125 days (3 months) was utilized. This time step, in conjunction with a backward difference scheme, was found to provide a satisfactory solution.

In our first attempt at history matching we assumed that all discharge was coming from storage, that is, the Huka Falls confining bed and the Wairakei Ignimbrites provide no transient leakage. Without transient leakage the computed pressures decreased much more rapidly than did the observed pressures. Therefore some form of transient leakage is induced by production at the Wairakei field.

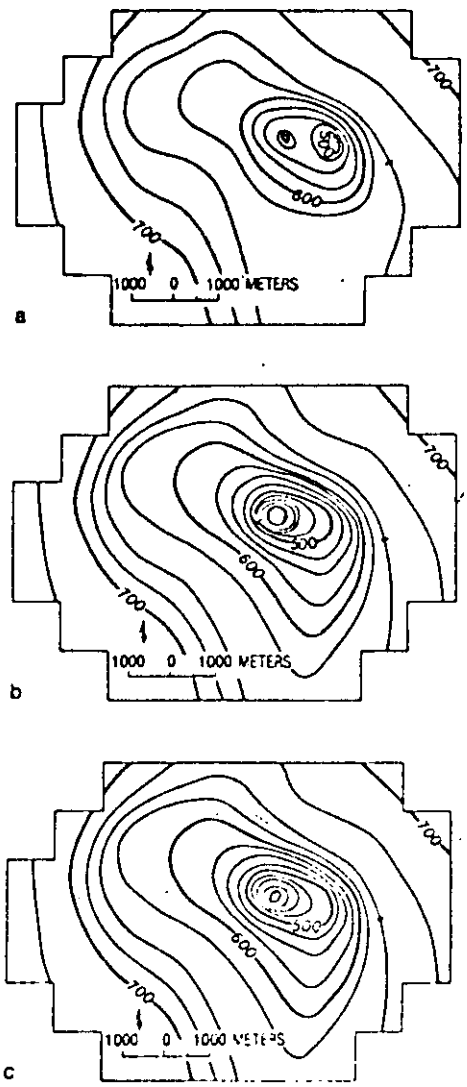

Fig. 19. Computed pressure distributions ($N/m^2 \times 10^6$) for (*a*) April 1960, (*b*) April 1965, and (*c*) April 1970. Datum is 274 m below mean sea level; contour interval is 25×10^6 N/m^2.

Next we used the transient leakage formulas presented in (1) and (2), and simulated the field to January 1974. The results are shown in Figures 18–23. Figures 19*a*, 19*b*, and 19*c* show pressure distributions for April 1960, April 1965, and April 1970, respectively. These pressure distributions are at the same datum as the initial pressures in Figure 15. In the early stages of development, the eastern production area had the larger amount of mass removed, and this area shows the larger decrease in pressure (Figure 19*a*). By 1965 the maximum production rate had shifted to the western production area and so did the modeled maximum decrease in pressure (Figure 19*b*). By 1970 the maximum decrease in pressure in the western production area amounted to approximately 2.25×10^6 N/m^2 (Figure 19*c*). This computed value compares well with the observed pressure drops reported by *Bolton* [1970] of 2.0×10^6 to 2.4×10^6 N/m^2; however, the observed maximum pressure drop occurred in the eastern production area.

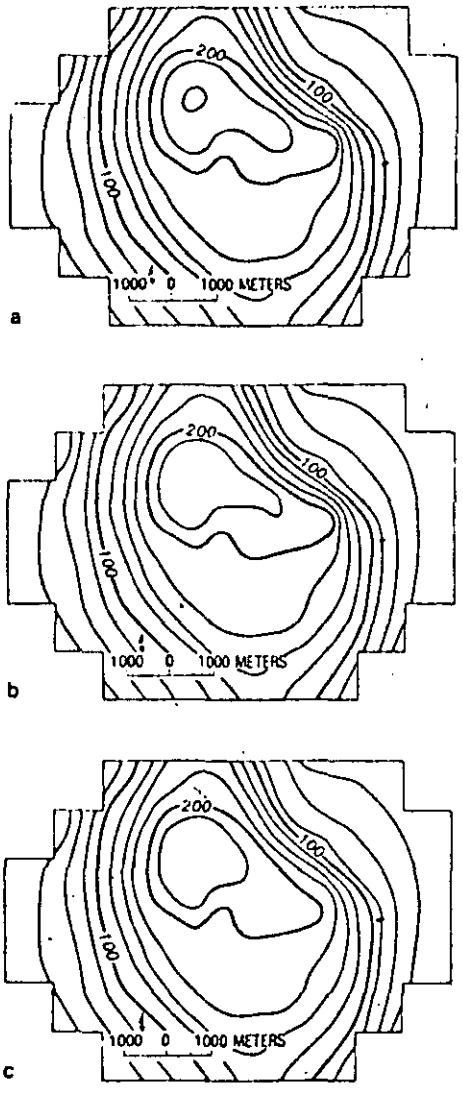

Fig. 20. Computed temperature distributions (degrees Celsius) for (*a*) April 1960, (*b*) April 1965, and (*c*) April 1970. Values are vertically averaged, and the contour interval is 25°C.

A possible explanation of this discrepancy may be related to the observation that just northeast of the eastern production area is located the region of maximum ground subsidence of approximately 4.5 m [*Stilwell* et al., 1975]. It is possible that in this location the rock units have a high compressibility. Early declines in pressure in the eastern production area caused subsidence and probably a reduction in permeability. Reducing the permeability in the eastern production area would cause greater pressure declines in that area than those shown in Figure 19. If this interpretation is correct, then modeling the permeabilities as invarient with time, as was done, might explain the difference between the location of observed and computed maximum pressure declines. Finally, note that in all the pressure plots, with the exception in the southeast, little change in pressure occurs outside the main production area, especially toward the eastern boundary. This behavior conforms with what is observed at Wairakei [*Bolton*, 1970]. The pressure declines toward the southeast may indicate that our boundary should be extended in that direction to include the undeveloped Tauhara geothermal field (see Figure 1). Wells in this field do show slight response to production at Wairakei.

Figures 20*a*, 20*b*, and 20*c* present computed vertically averaged temperatures for April 1960, April 1965, and April 1970, respectively. A comparison of Figure 20 with the initial temperatures in Figure 13 shows that very little change in temperature occurred by 1960. This conforms with field temperature data given in *Grindley* [1965]. By 1965, computed temperatures in the main production area have started to decline. In the model, the vertical-equilibrium interface between the two-phase zone and single-phase water had dropped below the top of the open interval for several wells in 1963. Therefore these simulated wells began producing a mixture of steam and water from the reservoir and a temperature drop resulted. We feel that to a large extent this is what actually occurred at Wairakei. By 1970, the temperatures had continued to decrease in the main production area and the thermal gradient to the northeast had been reduced.

The vertically averaged water saturation distributions corresponding to the same dates are presented in Figure 21. These represent vertically averaged values of a steam cap at 20% residual water saturation underlain by single-phase water. That is, the smaller values of saturation in Figure 21 correspond to the larger steam cap thickness for a given reservoir thickness. Outside the 1.0 contour, the reservoir contains no steam. Comparing Figures 17 and 21, it may be seen that by 1960 the two initial two-phase regions had merged. As pressures decline with time, the steam cap increases in both thick-

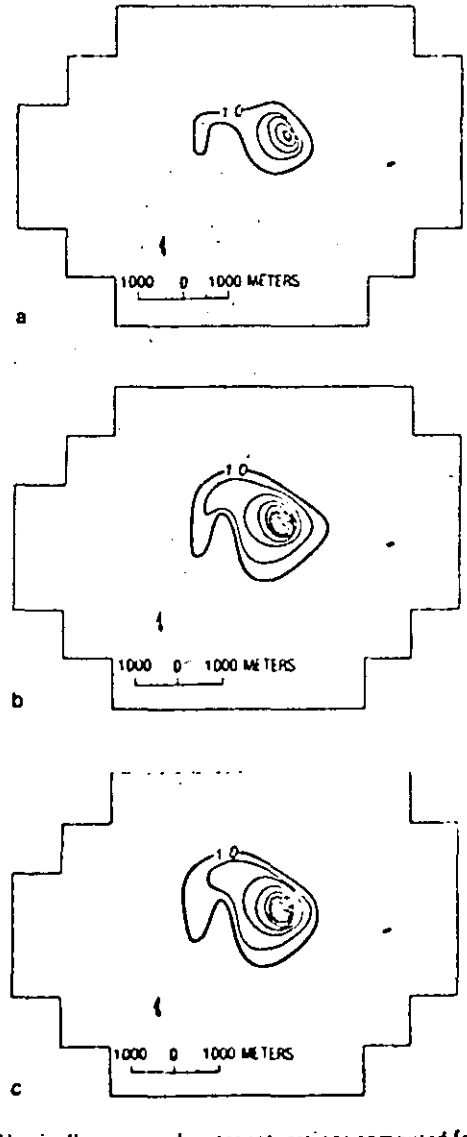

Fig. 21. Vertically averaged water saturations computed for (*a*) April 1960, (*b*) April 1965, and (*c*) April 1970; contour interval is 0.1.

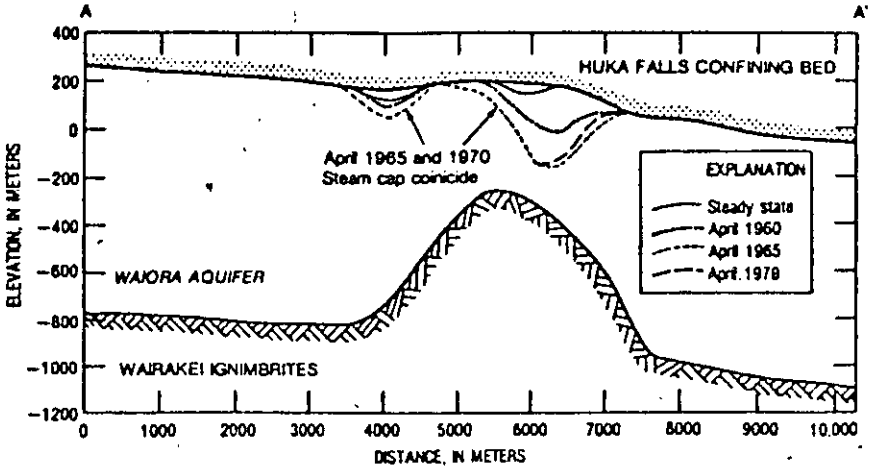

Fig. 22. Profile showing contact between steam cap and water for steady-state conditions, April 1960, April 1965, and April 1970. Only the Waiora aquifer is shown and the cross section corresponds to the west to east (A-A') section line in Figure 3.

ness and areal extent, as shown in the plots for 1965 and 1970. No observed water saturations are available for comparison.

To better visualize what the vertically averaged saturation distributions mean, a profile showing contacts between the steam cap and water is shown in Figure 22. The contacts are shown for steady-state, April 1960, April 1965, and April 1970. The profile corresponds to the west to east section line in Figure 3 and to section (A-A') in Figure 8. The vertical scale has been increased from that in Figure 8 in order to show the two-phase contact more clearly. Also the aquifer elevation is lower than that shown in Figure 8 as a result of our data modification discussed previously. As may be seen, the steady-state steam cap is very small. As production proceeds, the steam cap grows, except for some recovery between 1965 and 1970. As indicated in Figure 22, between 1953 and 1970 the computed steam cap has a maximum increase in thickness between 200 and 300 m. This compares well with calculations based on pressure and temperature measurements in wells that indicate the boiling level at Wairakei has declined about 200 m (M. L. Sorey, written communication, 1978). As a result of our quasi three-dimensional model, the steam cap is at a residual water saturation of 20%. It is possible, however, that in the field, superheated steam could form in the upper parts of the steam cap, as was demonstrated by *Faust and Mercer* [1979*b*] using a cross-sectional model.

A plot of pressure versus time is shown in Figure 23*a*. The computed values (dashed line) are for the western production block (finite-difference block in Figure 3 where the north-south, B-B', and east-west, A-A', section lines intersect). The solid line is the observed field pressures (from all wells) at a reference level of 274 m below mean sea level. The data between 1953 and 1968 are from *Bolton* [1970]; data after 1968 are from unpublished plots by the New Zealand Ministry of Works. Note that the shaded area represents the data spread. As may be seen the comparison between computed and observed data is good. Pressures decrease only slightly from 1953 to 1958, corresponding to the time period of little well discharge (see Figure 18*a*). In 1958 power production began, discharges increased, and from 1959 to 1965, pressures declined rapidly. After 1965, discharges began to decrease and in the beginning of 1968 a partial shutdown resulted in a slight increase in the pressure curve. After 1965, pressure decrease only slightly and by the end of 1972 the computed pressures show some recovery.

A plot of temperature and enthalpy versus time for the western production block is shown in Figure 23*b*. As may be seen, between 1953 and 1961, temperatures are fairly constant. At approximately 1962, two-phase behavior occurred in the lower part of the reservoir where the wells were slotted, and temperatures declined about 8°C. It is believed that this behavior is consistant with what is observed at Wairakei. It is interesting to note that in one simulation run, the wells were assumed to be slotted throughout the thickness of the Waiora aquifer, so that a mixture of steam and water was removed, beginning with the onset of two-phase flow at the top of the aquifer. These results (not shown) gave early temperature declines that reached values greater than 20°C. Returning to Figure 23, once two-phase flow occurred in the lower part of

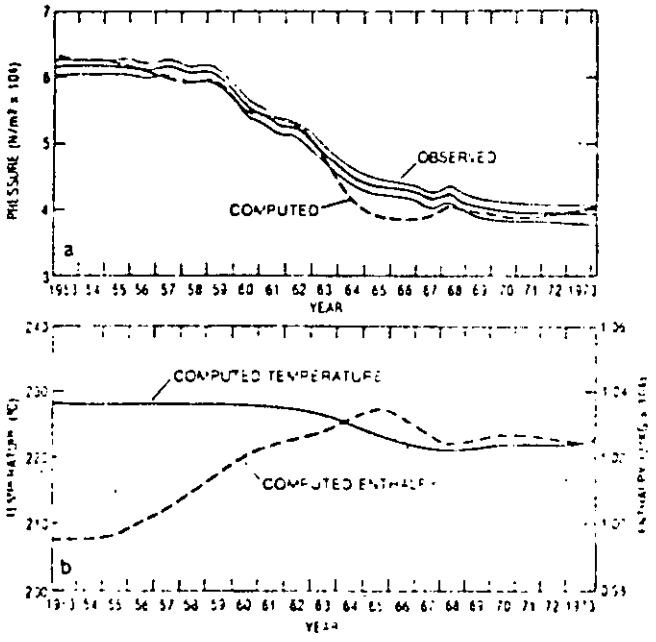

Fig. 23. (*a*) Pressure ($N/m^2 \times 10^6$) versus time, 1953-1973; datum is 274 m below mean sea level. Dashed line was computed for the western production block, and solid line is observed data for entire field (1953-1968 from *Bolton* [1970]), shaded area represents data spread. Computed temperature (degrees Celsius) versus time, 1953-1973, for the western production block is shown in Figure 23*b* as a solid line. Also shown is the computed mixture enthalpy (J/kg) versus time 1953-1973, for the western production block (dashed line).

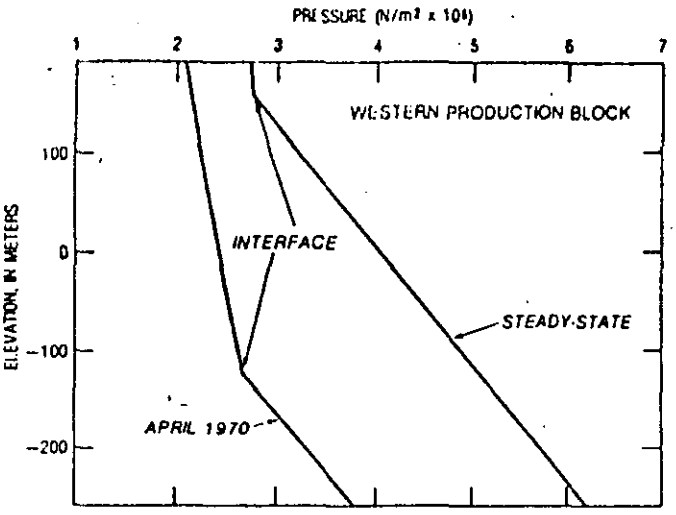

Fig. 24. Pressure profiles through the Waiora Formation for the western production block for steady-state and April 1970.

the aquifer, temperature and pressure became dependent, and therefore, toward the end of the history match, when pressures recovered slightly, temperatures did also.

As shown in Figure 23*b*, the enthalpy of the fluid mixture increases from 1953 to 1965, then decreases from 1965 to 1968. After 1968 the enthalpy remains fairly constant. The increase in vertically averaged enthalpy reflects the increase in the steam cap (or decrease in the vertically averaged water saturation). The decrease in enthalpy after 1965, in part, reflects the pressure recovery. This trend agrees qualitatively with data on total field discharge enthalpy presented in *Pritchett et al.* [1978]. Because the computed fluid enthalpy is a reservoir value, and the data in *Pritchett et al.* [1978] are for the discharge fluid, no quantitative comparison is made.

Although vertically averaged pressures are used in the model, pressures relative to a reference level of 274 m below mean sea level are presented in this paper. We are able to compute these values based on the vertical equilibium assumption that the pressure in the steam cap and underlying water zone increase hydrostatically with depth. This assumption also allows us to compute the vertical pressure distribution in the aquifer. Two computed pressure profiles through the Waiora Formation are shown in Figure 24 for the western production block at steady state and April 1970. The interesting point to note from Figure 24 is that the pressure decrease in the upper portion of the aquifer, where the steam cap is located, is less than the pressure decrease in the lower portion of the aquifer. This is caused by gravity segregation in the reservoir. For this particular block, the pressure decline in the upper portion averages about 1.0×10^6 N/m², whereas in the lower portion the pressure decline is approximately 2.4×10^6 N/m². This difference compares well with what is observed at Wairakei. According to M. L. Sorey (written communication, 1978), pressure measurements in Wairakei wells indicate that the average pressure decline with exploitation at shallow levels in the two-phase zone is about 1.0×10^6 N/m², compared with an average decline of 2.6×10^6 N/m² in the deeper liquid zone. Also, for this same block and times in Figure 24, the average computed temperature decline is 7.5°C in the upper portion, while that in the lower portion averaged only a 2.3°C drop. Qualitatively, these differences with depth in temperature declines are also observed at Wairakei.

Throughout the simulation, mass and energy balances were checked at each time step. Both balances generally had less than a 0.01% error, and convergence was obtained within 2–4 Newton-Raphson iterations. Although transient leakage is spatially distributed, the net leakage was computed for each time step. The net transient mass leakage into the Waiora aquifer computed by the model is plotted in Figure 18*b* for the period between 1953 and 1973. It is separated into two parts: that through the Wairakei Ignimbrites and that through the Huka Falls Formation. As may be seen, transient leakage from the confining beds replaced a large portion of the mass produced by wells, with most of it coming from the Wairakei Ignimbrites. In the model, transient mass leakage is added to the steady-state leakage, and this sum is shown in Figure 18*c*. It is interesting to note from the plot of leakage through the Huka Falls Formation, that the natural discharge at the surface should decrease with time, and by approximately 1964, the total natural discharge should be 'captured.' As noted by *Fisher* [1964], the observed natural mass discharge did decrease between 1951 and 1958. Information on observed natural discharge after 1958 is not available.

The amount of transient mass leakage from the Wairakei Ignimbrites is too great toward the end of the simulation, as indicated by the increase in some computed pressures at the

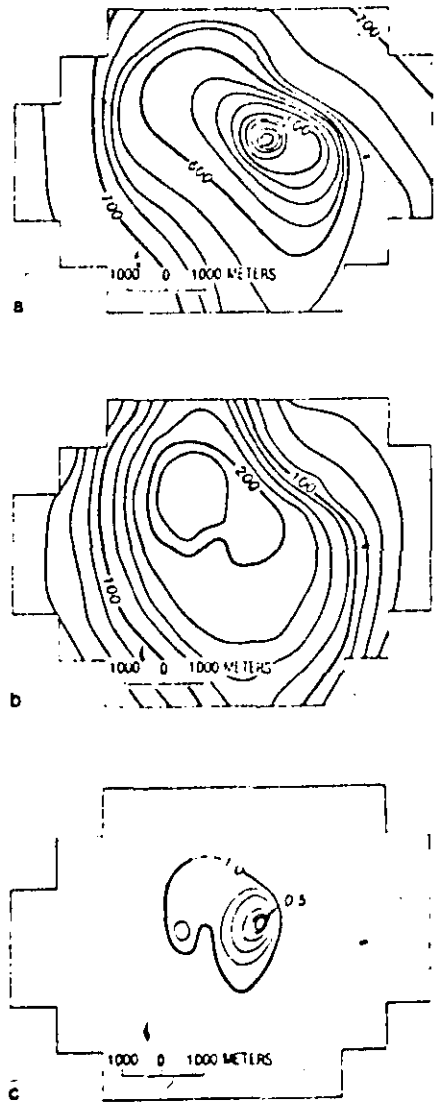

Fig. 25. Predicted results for January 2000 (*a*) pressure distribution (N/m² × 10⁶) with datum of 274 m below mean sea level and a contour interval of 25×10^6 N/m² (*b*) vertically averaged temperature distribution (degrees Celsius) with a contour interval of 25°C; and (*c*) vertically averaged water saturations with a contour interval of 0.1.

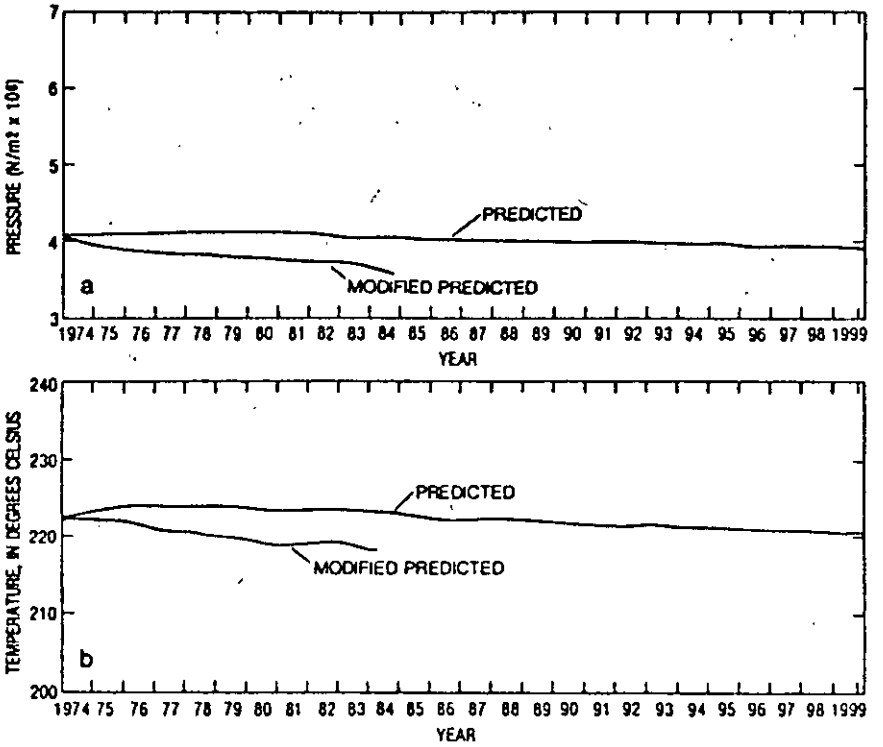

Fig. 26. Predicted (*a*) pressures ($N/m^2 \times 10^6$) versus time, 1974–1999 (datum is 274 m below mean sea level), and (*b*) vertically averaged temperatures (degrees Celsius) versus time, 1974–1999. All values are for the western production block; modified predicted refers to simulation run in which transient leakage was decreased.

end of the history match. The hydraulic properties providing this amount of leakage were required to be large in order to maintain production during the peak discharge years of 1962–1964. In fact, the hydraulic conductivity-specific storage product for some parts of the Wairakei Ignimbrites used in the simulation implies permeabilities that are of the same order of magnitude as those for the Waiora Formation. According to M. L. Sorey (written communication, 1978), preexploitation vertical pressure gradients into the ignimbrites were nearly uniform and perhaps indicate vertical permeability in the ignimbrites not much different from that of the Waiora Formation. These observations emphasize the uncertainties associated with locating the aquifer base and with the description of leakage from the Wairakei Ignimbrites.

Transient Simulation: Prediction

For this study, well discharge after January 1974 was not available. For predictive purposes, the January 1974 discharge rates were used. Production wells produced at this assigned rate or a lesser rate that the well is capable of producing against an average flowing well pressure of 1.0135×10^6 N/m². The production capability of a well is approximated by [*Craft and Hawkins*, 1959]

$$q_w = \frac{2\pi hk}{\mu \ln (r_e/r_w)}(p_e - p_w) \qquad (6)$$

where h is the thickness of the open interval, r_w is the well radius, p_w is the average flowing well pressure, p_e is the grid block pressure, and r_e is the grid block radius defined as $r_e = (\Delta x \Delta y)^{1/2}/\pi$, where Δx and Δy are the grid block spacing. The well radius used for Wairakei wells is 21.9 cm [*Grindley*, 1965]. The heat-sink term is computed as described previously, and each grid block is assumed to contain a maximum of 12 wells. Equation (6) is an approximation to account for decreased discharge associated with decreases in reservoir pressures.

During the prediction portion of this study, the Wairakei field was simulated from 1974 to January 2000 using a time step of 121.75 days (4 months). It should be emphasized that we attempt to predict only reservoir behavior, not power output. Pressures, temperatures, and water saturations are presented in Figure 25 for January 2000. The pressures are for a reference level of 274 m below mean sea level, and both temperatures and water saturations are vertically averaged. In all three distributions the same trend is present: values have decreased slightly from those obtained in the history-match portion, and the declines have spread further from the main production area.

Pressure and temperature versus time for the western production block are shown in Figure 26. Enthalpies are not shown, but follow a trend similar to that shown in the temperature plot. Again it may be seen that pressures and temperatures decrease only slightly from 1974 to January 2000.

During this predictive run, the January 1974 production rates are maintained, in large part by leakage from confining beds. The limiting factor at Wairakei is probably the amount of mass available, and not heat. More specifically, the limiting factor appears to be the mass from leakage, especially through the Wairakei Ignimbrites. It is difficult to evaluate our treatment of the leakage terms, since matching the pressure-decline history is the only method we have to determine them. As presented in Figure 23, this match appears good, except perhaps for the pressure recovery toward the end of the match. Because of the uncertainty associated with our treatment of the leakage, there is also considerable uncertainty in our prediction. In order to test the sensitivity of our prediction against different leakage properties, we decreased the hydraulic con-

ductivity-specific storage coefficient for the Wairakei Ignimbrites by half. The results of this simulation are also presented in Figure 26 and are labeled 'modified prediction.' For this run, the January 1974 production rates could not be maintained, and saturations approached the residual water saturation of 20%. As may be seen in Figure 26, this happened at approximately 1984.

It is difficult to assess the meaning of these two predictive runs. We feel that, due to the uncertainty associated with the leakage properties, long range predictions, such as the one in this paper to the year 2000, are not very reliable. Shorter range predictions of approximately five to ten years are more valid, especially if the leakage description can be continuously scrutinized as additional pressure-decline data become available.

Finally, it should be noted that other predictive simulation runs were made with expected results. Of these, one of the more interesting runs used a zero discharge rate, that is, production ceased. For this simulation, pressures and saturations recovered substantially. Simulations with reinjection were not made because, at the time of this modeling work, reinjection at Wairakei was considered unlikely. In order to help control pressure declines, however, reinjection is now being considered (R. S. Bolton, written communication, 1978).

CONCLUSIONS

Complex liquid- and vapor-dominated hydrothermal systems generally require some form of three-dimensional description. The quasi three-dimensional, areal model used in this study appears to be an economical alternative to a fully three-dimensional model. By applying the areal model to the hydrothermal field located at Wairakei, New Zealand the following may be concluded about the field's behavior.

1. After matching observed temperatures, preexploitation surface heat and mass discharges, and limited pressure data, model results indicate that prior to development, the aquifer had steam in its upper regions. Since most wells were cased through the steam cap, in the early stages of development the steam had little or no effect on reservoir performance, and the field was considered to be liquid-dominated.

2. As development progressed, the steam cap increased both areally and in thickness. When the contact between the two-phase zone and the single-phase (water) zone dropped below the slotted interval of the wells, a mixture of steam and water was removed from the reservoir, and reservoir temperatures declined. This occurred around 1963 and resulted in a drop in temperature of 8°–10°C. At this time the reservoir began to exhibit characteristics of a vapor-dominated field, and superheated steam may have begun to form in the upper parts of the steam cap. It should also be noted that part of the observed cooling in the upper portions of the reservoir may be due to leakage of cooler fluid through the Huka Falls Formation.

3. The boundaries and boundary conditions used in this study appear to be appropriate; the southeast boundary, however, perhaps could be extended to include the Tauhara geothermal field.

4. Based on model runs, some form of transient mass leakage is induced by production. In the model, most of the leakage was determined to come from below; that is, through the Wairakei Ignimbrites. Also, it was determined that complete capture of the natural surface discharge through the Huka Falls Formation should have occurred around 1964.

5. The limiting factor on production is the amount of mass available, not heat. Long range predictions are not reliable due to uncertainties inherent in the assumptions used in formulating the model, especially those regarding leakage from the Wairakei Ignimbrites. Short range predictions (5–10 years) are more reliable and indicate that production can be maintained at or near the January 1974 production rate.

The Wairakei field is a very complex system with many observations that must be explained. This modeling study is an attempt to use these observations and develop a rational framework on how the system operates. Our conceptual model of the Wairakei field does, for the most part, account for what is observed. Due to the uncertainties associated with any subsurface description, this conceptual model is obviously not unique. Numerical results, however, verify most of the assumptions that comprise our conceptual model, and reproduce many of the observed conditions.

Acknowledgments. This study was a cooperative effort of the U.S. Geological Survey and the New Zealand government. The authors wish to thank all those who helped with various aspects of the study and in particular wish to thank Richard S. Bolton of the Ministry of Works for his helpful correspondence, critical review of this manuscript, and organization of the data, and Ian G. Donaldson and Russell James of the Department of Scientific and Industrial Research for their assistance during the senior author's visit to the field area.

REFERENCES

Bolton, R. S., The behavior of the Wairakei geothermal field during exploitation, paper presented at U.N. Symposium on Development and Utilization of Geothermal Resources, United Nations, Pisa, Italy, Sept. 22–Oct. 1, 1970.

Craft, B. C., and M. F. Hawkins, Applied petroleum reservoir engineering, 437 pp., Prentice-Hall, Englewood Cliffs, N. J., 1959.

Faust, C. R., and J. W. Mercer, Finite-difference model of two-dimensional single- and two-phase heat transport in a porous medium, version 1, *Open File Rep. 77-234*, 84 pp., U.S. Geol. Surv., Reston, Va., 1977.

Faust, C. R., and J. W. Mercer, Geothermal reservoir simulation, 1, Mathematical models for liquid- and vapor-dominated hydrothermal systems, *Water Resour. Res., 15*, 23–30, 1979*a*.

Faust, C. R., and J. W. Mercer, Geothermal reservoir simulation, 2, Numerical solution techniques for liquid- and vapor-dominated hydrothermal systems, *Water Resour. Res., 15*, 31–46, 1979*b*.

Ferris, J. G., and D. B. Knowles, R. H. Brown, and R. W. Stallman, Theory of aquifer tests, *U.S. Geol. Surv. Water Supply Pap. 1536-E*, 174 pp., 1962.

Fisher, R. G., Geothermal heat flow at Wairakei during 1958, *N. Z. J. Geol. Geophys., 7*, 172–184, 1964.

Grant, M. A., and J. L. Robinson, Asymptotic solution for the one-phase field model lifetime estimate, *Rep. 47*, Dep. of Sci. and Indus. Res., Wellington, New Zealand, 1976.

Grindley, G. W., The geology, structure and exploitation of the Wairakei field, Taupo, New Zealand, *N. Z. Geol. Surv. Bull., 75*, 131 pp., 1965.

Hunt, T. M., Net mass loss from the Wairakei geothermal field, New Zealand, *Geothermics Int. J. Geothermal Res., 2*, 487–491, 1970.

Koenig, J. B., Worldwide status of geothermal resources, in *Geothermal Energy*, edited by P. Kruger and C. Otte, pp. 15–58, Stanford University Press, Stanford, Calif., 1973.

McNabb, A., M. Grant, and J. Robinson, Permeability estimates, *Rep. 34*, Dep. of Sci. and Indus. Res., Wellington, New Zealand, 1975.

Mercer, J. W., G. F. Pinder, and I. G. Donaldson, A Galerkin-finite element analysis of the hydrothermal system at Wairakei, New Zealand, *J. Geophys. Res., 80*(17), 2608–2621, 1975.

Modriniak, N., and F. E. Studt, Geological structure and volcanism in the Taupo-Tarawera District, New Zealand, *J. Geol Geophys., 2*, 654–684, 1959.

Pritchett, J. W., S. K. Garg, D. H. Brownell, Jr., L. F. Rice, M. H. Rice, T. D. Riney, and R. R. Hendrickson, Geohydrological environmental effects of geothermal power production phase IIA, *Rep. SSS-R-77-2998*, 125 pp., Systems, Science and Software, La Jolla, Calif., 1976.

Pritchett, J. W., L. F. Rice, and S. K. Garg, Reservoir engineering data: Wairakei geothermal field, New Zealand, *Rep SSS-R-78-*

3597-1, 359 pp., Systems, Science and Software, La Jolla, Calif., 1978.

Stilwell, W. B., W. K. Hall, and J. Tawhai, Ground movement in New Zealand geothermal fields, paper presented at the Second U.N. Symposium on the Development and Use of Geothermal Resources, United Nations, San Francisco, Calif., May 20–29, 1975.

Studt, F. E., The Wairakei hydrothermal field under exploitation, *N. Z. J. Geophys.*, *1*, 703–723, 1958.

Trescott, P. C., G. F. Pinder, and S. P. Larson, Finite-difference model for aquifer simulation in two dimensions with results of numerical experiments, *U.S. Geol. Surv. Tech. Water-Resour. Invest.*, *Book 7*, chap. C1, 116 pp., U.S. Geol. Surv., Reston, Va., 1976.

White, D. E., L. J. P. Muffler, and A. H. Truesdell, Vapor-dominated hydrothermal systems, *Econ. Geol.*, *55*, 75–97, 1971.

(Received January 29, 1979;
accepted January 29, 1979.)

CURSO: " INGENIERIA DE YACIMIENTOS GEOTERMICOS "
13 DE MARZO AL 18 DE MAYO DE 1984

TEMA: "GEOTHERMAL RESERVOIR SIMULATION"
2.-NUMERICAL SOLUTION TECHNIQUES FOR
LIQUID-AND VAPOR-DOMINATED
HYDROTHERMAL SYSTEMS.

DR. GUILLERMO DOMINGUEZ
2-13 de abril.

Geothermal Reservoir Simulation
2. Numerical Solution Techniques for Liquid- and Vapor-Dominated Hydrothermal Systems

CHARLES R. FAUST AND JAMES W. MERCER

U.S. Geological Survey, Reston, Virginia 22092

Two numerical models are introduced for simulating three-dimensional, two-phase fluid flow and heat transport in geothermal reservoirs. The first model is based on a three-dimensional formulation of the governing equations for geothermal reservoirs. Since the resulting two partial differential equations, posed in terms of fluid pressure and enthalpy, are highly nonlinear and inhomogeneous, they require numerical solution. The three-dimensional numerical model uses finite difference approximations, with fully implicit Newton-Raphson treatment of nonlinear terms and a block (vertical slice) successive iterative technique for matrix solution. Newton-Raphson treatment of nonlinear terms permits the use of large time steps, while the robust iterative matrix method reduces computer execution time and storage for large three-dimensional problems. An alternative model is derived by partial integration (in the vertical dimension) of the three-dimensional equations. This second model explicitly assumes vertical equilibrium (gravity segregation) between steam and water and can be applied to reservoirs with good vertical communication. The resulting equations are posed in terms of depth-averaged pressure and enthalpy and are solved by a two-dimensional finite difference model that uses a stable sequential solution technique, direct matrix methods, and Newton-Raphson iteration on accumulation and source terms. The quasi-three-dimensional areal model should be used whenever possible, because it significantly reduces computer execution time and storage and it requires less data preparation. The areal model includes effects of an inclined, variable-thickness reservoir and mass and energy leakage to confining beds. The model works best for thin (<500 m) reservoirs with high permeability. It can also be applied to problems with vertical to horizontal anisotropy when permeability is sufficiently high. Comparisons between finite difference and higher-order finite element approximations show some advantage in using finite element techniques for single-phase problems. In general, for nonlinear two-phase problems the finite element method requires use of upstream weighting and diagonal lumping of accumulation terms. These lead to lower-order approximations and tend to obviate any advantage of using the finite element method.

INTRODUCTION

This paper is the second in a series of three papers concerning geothermal reservoir simulation. In the first paper [*Faust and Mercer*, 1978] we introduced mathematical and conceptual models that serve as a basis for the numerical models (simulators) discussed here. The final paper will describe an application of our numerical models to the hydrothermal system at Wairakei, New Zealand.

In the present study we expand our previous work (summarized in the literature review section) in several areas: extension of the numerical model to three dimensions, improvement of numerical techniques, and development of a quasi-three-dimensional areal model.

The three-dimensional model differs from models discussed in the literature review in its formulation in terms of fluid pressure and enthalpy and in its numerical solution technique. The pressure-enthalpy formulation offers the advantage of being posed in terms of parameters commonly obtained from field data and of avoiding the necessity of using three unknown parameters (which is the case in the pressure-temperature-saturation formulation). The numerical model is fully implicit and is based on a Newton-Raphson finite difference approximation of the nonlinear partial differential equations describing flow in geothermal reservoirs. A reliable iterative technique, slice successive overrelaxation (SSOR), is used to solve the resulting system of linearized equations. This iterative method is more efficient than direct solution techniques for large three-dimensional problems, yet more reliable than other iterative techniques for difficult problems [*Wattenbarger and Thurnau*, 1976].

Unfortunately, three-dimensional models often are not practical due to constraints imposed by data requirements and computational expense. As an alternative approach a quasi-three-dimensional areal model (based on vertical integration of the three-dimensional mathematical model) is proposed. The areal model uses finite difference approximations and accounts for vertical variations in properties (such as the presence of a steam cap) as well as variations in reservoir thickness and slope.

To show the use of the various models, we present several examples that include one-, two-, and three-dimensional applications involving both one-phase (liquid) and two-phase geothermal systems. These examples were chosen to test the accuracy of several numerical techniques (finite difference as well as finite element), to compare model results with available data from laboratory experiments, to demonstrate the adequacy of the proposed quasi-three-dimensional approximation, and to illustrate various types of reservoir behavior.

LITERATURE REVIEW

In this study, only geothermal energy from hydrothermal systems is considered (similar models can be used for other types of geothermal resources, e.g., geopressured ones and hot, dry rock). When such a system is utilized for its heat energy, it is called a geothermal reservoir. In hydrothermal systems, heat from near-surface sources such as magmatic bodies is transferred to porous media and to the fluid within those media by conductive and convective processes. These systems are classified as being either liquid dominated or vapor dominated [*White et al.*, 1971].

Paper number 8W0851.

Most modeling work related to geothermal studies may be divided into two broad classes: (1) free convection models to examine the geothermal reservoir under natural conditions and (2) reservoir models to examine exploitation effects. In this brief review we consider only reservoir models; however, a review of free convection models is given by *Witherspoon et al.* [1975].

Geothermal reservoir models may be subdivided further into two general types: lumped parameter and distributed parameter. Although the emphasis in this paper is on distributed-parameter models, for completeness, lumped-parameter models are included in the review section.

Lumped-Parameter Models

The concept of a lumped-parameter model offers the simplest means of describing the behavior of a geothermal reservoir during exploitation. In this type of model the entire system is considered a perfect mixing cell for both mass and energy, so the spatial variation in rock and fluid properties is reduced to a single point in space. Instead of considering the internal distribution of mass and energy, attention is restricted to the total amounts generated within the system as well as to those crossing the boundaries. Since time is the only independent variable, the system can be characterized mathematically by a set of ordinary differential equations or an equivalent set of algebraic expressions representing total mass and energy [*Witherspoon et al.*, 1975].

The first reservoir model applied to a geothermal field problem was a lumped-parameter model developed by *Whiting and Ramey* [1969]. Their model allowed fluid influx from an adjacent aquifer and was used to simulate the two-phase steam-water behavior of the Wairakei hydrothermal field. This approach was also used by *Cady* [1969] to simulate a laboratory experiment. *Brigham and Morrow* [1974] applied a lumped-parameter model to vapor-dominated systems by considering three different liquid distributions. *Martin* [1975] used a lumped-parameter model to examine two-phase flow in a geothermal reservoir where the liquid and gas phases are uniformly distributed throughout the reservoir. Brigham and Morrow, and Martin, considered the reservoir to be completely closed. Finally, *Seki et al.* [1977] applied the Whiting-Ramey model to several fields and used a least squares technique to match historical data.

Distributed-Parameter Models

A model in which the properties of the rock and/or the fluid are allowed to vary in space is referred to as a distributed-parameter model. In general, these models are complex and cannot be solved analytically. An alternative approach is to replace the governing partial differential equations by an equivalent set of algebraic equations and to solve the problem numerically with the aid of a computer.

Harlow and Pracht [1972] considered the problem of extracting heat from dry rock using a distributed-parameter model which simulated rock fracturing and single-phase (compressed water) flow. The first application of a distributed-parameter model to a geothermal field problem was made by *Mercer et al.* [1975]. Using a Galerkin finite element method and solving for temperature and pressure, their areal model was restricted to liquid-dominated reservoirs and was able to reproduce historical data at Wairakei to 1962, by which time, large quantities of steam had formed in the reservoir. *Toronyi and Farouq Ali* [1975] developed a two-phase, two-dimensional reservoir model that was coupled with a well bore model. Their work was restricted to the saturated vapor pressure curve; they solved for pressure and saturation and used a finite difference technique that incorporated Newton-Raphson iteration.

At this point in the chronological development the only distributed-parameter models that exist for geothermal reservoirs are restricted either to compressed water or to the saturated vapor pressure curve. In 1975 at the Second United Nations Symposium on the Development and Use of Geothermal Resources, held in San Francisco, three independent groups presented distributed-parameter models capable of simulating both liquid- and vapor-dominated geothermal reservoirs [*Faust and Mercer*, 1975; *Garg et al.*, 1975; *Lasseter et al.*, 1975].

Faust and Mercer [1975] and, later, *Mercer and Faust* [1975] and *Faust* [1976] applied both Galerkin finite element and finite difference techniques to approximate a pressure-enthalpy formulation of the multiphase flow equations in two horizontal dimensions. Both *Garg et al.* [1975] and *Lasseter et al.* [1975] formulated their multiphase equations in terms of internal energy and density. The former used finite difference techniques to approximate their equations, whereas the latter used an integrated finite difference technique. Both of these models were capable of treating three-dimensional problems.

More recently, *Thomas and Pierson* [1976] have developed a model for simulating geothermal reservoirs containing water in either the vapor or the liquid state. Their model is three dimensional and solves for pressure, temperature, and saturation. Finite difference techniques were used in conjunction with an implicit pressure–explicit saturation formulation. *Coats* [1977] has also proposed a model based on a pressure-temperature-saturation formulation that includes flow in well bores and discrete fractures.

Finally, three field applications of distributed-parameter models for single-phase liquid reservoirs have been published recently. *Sorey et al.* [1977] applied a cross-sectional integrated finite difference model to simulate steady state conditions in the Long Valley hydrothermal system in California. Another California field, located in the East Mesa area, Imperial Valley, was simulated by *Intercomp* [1976]. Their model solved for pressure and temperature and used finite difference techniques. *Kettenacker* [1977] used a horizontal reservoir (pressure only) model and a vertical, one-dimensional heat transfer model for each well to examine the Raft River, Idaho, geothermal field.

NUMERICAL METHODOLOGY

The mathematical models developed for geothermal reservoir simulation are nonlinear and are not amenable to convenient analytical solution. Additionally, the highly nonlinear thermodynamic relationships in the model render even numerical solution a difficult task. Consequently, considerable effort has been expended in testing alternative solution procedures. In particular, we have examined (1) numerical approximations, including Galerkin finite element, collocation on finite elements, and finite difference; (2) nonlinear techniques, including Picard iteration, semiimplicit procedures, and fully implicit Newton-Raphson iteration; and (3) matrix solution methods, both direct and iterative. Some of these solution procedures are discussed by *Mercer and Faust* [1975] and *Faust and Mercer* [1977]. In this paper we describe those techniques that we found more reliable and efficient to use for geothermal reservoir simulation.

Two models are presented: one for two dimensional areal applications and the other for three-dimensional applications. The three-dimensional model uses finite difference approxima-

tions with fully implicit Newton-Raphson iteration and is capable of simulating one- and two-phase flow in geothermal reservoirs. The areal model also uses a finite difference representation. It can simulate sloping reservoirs of variable thickness, heat and mass fluxes from confining beds, and both one- and two-phase reservoir behavior. Options are provided for vertical averaging based on either uniform-property or vertical equilibrium assumptions.

Mathematical Models

Two general mathematical models are the basis of the numerical simulators introduced in this paper. Basic assumptions, derivations of the equations, and boundary conditions are presented and discussed in paper 1 of this series, to which the reader is referred for details [*Faust and Mercer*, 1978]. Major assumptions that apply to both the three-dimensional and the areal model are that (1) Darcy's equation for multiphase flow is valid, (2) capillary pressure effects are negligible, (3) thermal equilibrium exists among all phases, (4) the geothermal fluid is pure water, and (5) kinetic and potential energy are negligible.

The three-dimensional equations are formulated in terms of the dependent variables pressure and enthalpy, since these two variables uniquely define the thermodynamic state of the system and because they are commonly obtained in a field situation. These equations are

$$\frac{\partial(\phi\rho)}{\partial t} - \nabla\cdot\left[\frac{Kk_{rs}\rho_s}{\mu_s}\cdot(\nabla p - \rho_s g\nabla D)\right] - \nabla\cdot\left[\frac{Kk_{rw}\rho_w}{\mu_w}\cdot(\nabla p - \rho_w g\nabla D)\right] - q_m' = 0 \quad (1)$$

and

$$\frac{\partial}{\partial t}[\phi\rho h + (1-\phi)\rho_r h_r] - \nabla\cdot\left[\frac{Kk_{rs}\rho_s h_s}{\mu_s}\cdot(\nabla p - \rho_s g\nabla D)\right] - \nabla\cdot\left[\frac{Kk_{rw}\rho_w h_w}{\mu_w}\cdot(\nabla p - \rho_w g\nabla D)\right] - \nabla\cdot\left[K_m\left(\frac{\partial T}{\partial p}\right)_h\nabla p + K_m\left(\frac{\partial T}{\partial h}\right)_p\nabla h\right] - q_h' = 0 \quad (2)$$

In the above equations, p is fluid pressure, h is the specific enthalpy of the fluid, ρ is density, K is intrinsic permeability, k_r is relative permeability, μ is dynamic viscosity, g is the gravitational constant, D is depth, q_m' is the mass source term, q_h' is the energy source term, K_m is a combined isotropic conduction–thermal dispersion coefficient, T is temperature, and t is time. The subscripts r, w, and s refer to rock, liquid water, and steam, respectively. The enthalpy of the steam-water mixture is defined as

$$h = (S_s\rho_s h_s + S_w\rho_w h_w)/\rho \quad (3)$$

where ρ is the density of the total steam-water mixture, defined as

$$\rho = S_w\rho_w + S_s\rho_s \quad (4)$$

and the volume saturations (S_s and S_w) are defined so that they sum to 1:

$$S_s + S_w = 1 \quad (5)$$

These equations describe the two-phase flow of heat in a steam-water-rock system; however, with minor modification they also describe the flow of heat in a water-rock or a steam-rock system. When either steam or water is absent, the saturation of the absent phase is 0, and that for the existing phase is 1. Further, it is assumed that the relative permeability of the absent phase is 0 and that for the existing phase is 1. Therefore (1) and (2) reduce to the appropriate equations for either the compressed-water region or the superheated-steam region. A solution for these equations will determine whether a specified location contains compressed water, a steam-water mixture, or superheated steam. Boundary conditions for (1) and (2) represent the presence or absence of mass and energy fluxes or specified pressures and enthalpies at the reservoir boundaries. Initial conditions required are initial pressure and enthalpy distributions for the reservoir.

The equations for the areal model are posed in terms of depth-averaged fluid pressure and enthalpy. Vertically averaged quantities are denoted by angle brackets. The general equations are given by

$$b\frac{\partial}{\partial t}((\phi\rho)) - \frac{\partial}{\partial x}\left[b(\omega_x)\left(\frac{\partial}{\partial x}\langle p\rangle - \langle\rho g\rangle\frac{\partial\langle D\rangle}{\partial x}\right)\right] - \frac{\partial}{\partial y}\left[b(\omega_y)\left(\frac{\partial}{\partial y}\langle p\rangle - \langle\rho g\rangle\frac{\partial\langle D\rangle}{\partial y}\right)\right] - b(q_m') + \mathbf{v}|_{z_1}\cdot\nabla(z-z_1) - \mathbf{v}|_{z_2}\cdot\nabla(z-z_2) = 0 \quad (6)$$

and

$$b\frac{\partial}{\partial t}[(\langle\phi\rho h\rangle + \langle\rho_r h_r\rangle - \langle\phi\rho_r h_r\rangle)] - \frac{\partial}{\partial x}\left[b(\omega_{hx})\left(\frac{\partial}{\partial x}\langle p\rangle - \langle\rho g\rangle\frac{\partial\langle D\rangle}{\partial x}\right)\right] - \frac{\partial}{\partial y}\left[b(\omega_{hy})\left(\frac{\partial}{\partial y}\langle p\rangle - \langle\rho g\rangle\frac{\partial\langle D\rangle}{\partial y}\right)\right] - \frac{\partial}{\partial x}\left[b(\omega_{cp})\left(\frac{\partial}{\partial x}\langle p\rangle - \langle\rho g\rangle\frac{\partial\langle D\rangle}{\partial x}\right)\right] - \frac{\partial}{\partial y}\left[b(\omega_{cp})\left(\frac{\partial}{\partial y}\langle p\rangle - \langle\rho g\rangle\frac{\partial\langle D\rangle}{\partial y}\right)\right] - \frac{\partial}{\partial x}\left(b(\omega_{ch})\frac{\partial}{\partial x}\langle h\rangle\right) - \frac{\partial}{\partial y}\left(b(\omega_{ch})\frac{\partial}{\partial y}\langle h\rangle\right) - b(q_h') + h\mathbf{v}|_{z_1}\cdot\nabla(z-z_1) - h\mathbf{v}|_{z_2}\cdot\nabla(z-z_2) + \boldsymbol{\lambda}_m|_{z_1}\cdot\nabla(z-z_1) - \boldsymbol{\lambda}_m|_{z_2}\cdot\nabla(z-z_2) = 0 \quad (7)$$

The terms in (6) and (7) with the vertical bars are flux terms that are evaluated at either the top z_2 or the bottom z_1 of the reservoir and are defined (for the reservoir bottom) as follows:

$$\mathbf{v}\Big|_{z_1}\cdot\nabla(z-z_1) = -\left(\omega_x\frac{\partial p}{\partial x}\right)\Big|_{z_1}\frac{\partial z_1}{\partial x} - \left(\omega_y\frac{\partial p}{\partial y}\right)\Big|_{z_1}\frac{\partial z_1}{\partial y} + \left(\omega_z\frac{\partial p}{\partial z} + \omega_{gz}\right)\Big|_{z_1} \quad (8)$$

$$h\mathbf{v}\Big|_{z_1}\cdot\nabla(z-z_1) = -\left(\omega_{hx}\frac{\partial p}{\partial x}\right)\Big|_{z_1}\frac{\partial z_1}{\partial x} - \left(\omega_{hy}\frac{\partial p}{\partial y}\right)\Big|_{z_1}\frac{\partial z_1}{\partial y} + \left(\omega_{hz}\frac{\partial p}{\partial z} + \omega_{hgz}\right)\Big|_{z_1} \quad (9)$$

$$\boldsymbol{\lambda}_m\Big|_{z_1}\cdot\nabla(z-z_1) = -\left(\omega_{cp}\frac{\partial p}{\partial x} + \omega_{ch}\frac{\partial h}{\partial x}\right)\Big|_{z_1}\frac{\partial z_1}{\partial x} - \left(\omega_{cp}\frac{\partial p}{\partial y} + \omega_{ch}\frac{\partial h}{\partial y}\right)\Big|_{z_1}\frac{\partial z_1}{\partial y} + \left(\omega_{cp}\frac{\partial p}{\partial z} + \omega_{ch}\frac{\partial h}{\partial z}\right)\Big|_{z_1} \quad (10)$$

Similar terms may also be written for the reservoir top. We have also combined terms to simplify the final equations. For the x direction (terms for the y and z directions are similar) these terms are

$$\omega_x = \frac{k_x k_{rw} \rho_w}{\mu_w} + \frac{k_x k_{rs} \rho_s}{\mu_s}$$

$$\omega_{hx} = \frac{k_x k_{rw} \rho_w h_w}{\mu_w} + \frac{k_x k_{rs} \rho_s h_s}{\mu_s}$$

$$\omega_{cp} = K_m \left(\frac{\partial T}{\partial p}\right)_h$$

$$\omega_{ch} = K_m \left(\frac{\partial T}{\partial h}\right)_p$$

where k_x is the principal component of the permeability tensor in the x direction. For the z dimension, additional terms are defined as

$$\omega_{gz} = \frac{k_z k_{rw} \rho_w^2 g}{\mu_w} + \frac{k_z k_{rs} \rho_s^2 g}{\mu_s}$$

$$\omega_{hgz} = \frac{k_z k_{rw} \rho_w^2 g h_w}{\mu_w} + \frac{k_z k_{rs} \rho_s^2 g h_s}{\mu_s}$$

Equations (6) and (7) are simplified versions of the more general areal equations presented in paper 1 of this study [*Faust and Mercer*, 1978]. The simplifications involve neglecting codeviations of vertically averaged products, neglecting jump conditions at the steam cap interface, and assuming, for enthalpy, that $\langle \partial h/\partial x \rangle = \partial/\partial x \langle h \rangle$. These simplifications are not necessary but are desirable for practical applications. Evaluation of neglected terms would most likely render the areal model as cumbersome and expensive (computationally) as the fully three-dimensional model. In the applications section of this paper we consider in detail reservoir conditions under which the simplified areal model and vertical equilibrium assumption are appropriate.

Finite Difference Approximations

Both the two- and the three-dimensional models are based on a finite difference scheme using the block-centered grid commonly found in groundwater models [e.g., *Pinder and Bredehoeft*, 1968]. The grid allows variable spacing and can be used to approximate irregular reservoir geometry. For the three-dimensional model the compact, implicit finite difference representations of (1) and (2) are

$$\Delta[(T_w + T_s)\,\Delta p^{n+1}] - \Delta[(T_w \rho_w g + T_s \rho_s g)\,\Delta D] + V_b q_m' - (V_b/\Delta t)(M^{n+1} - M^n) = 0 \quad (11)$$

and

$$\Delta(T_h\,\Delta p^{n+1}) + \Delta(T_c\,\Delta h^{n+1}) - \Delta[(T_w h_w \rho_w g + T_s h_s \rho_s g)\,\Delta D] + V_b q_h' - (V_b/\Delta t)(E^{n+1} - E^n) = 0 \quad (12)$$

where the terms directly to the left of the equals signs in (11) and (12) are the accumulation terms for mass and energy, respectively. The transmissibility terms are defined as

$$T_w = (kA/l)\rho_w k_{rw}/\mu_w$$

$$T_s = (kA/l)\rho_s k_{rs}/\mu_s$$

$$T_h = T_w h_w + T_s h_s + (K_m A/l)(\partial T/\partial p)_h$$

$$T_c = (K_m A/l)(\partial T/\partial h)_p$$

and the mass and energy terms are

$$M = \phi\rho \qquad E = [\phi\rho h + (1 - \phi)\rho_r h_r]$$

where V_b, A, and l are the grid block volume, the cross-sectional area perpendicular to the flow direction, and the length increment in the flow direction, respectively. The difference operator Δ is defined for three dimensions, but, as an example, acts as follows in the x direction:

$$\Delta_x(T_w \Delta_x p^{n+1}) = T_{wx_{i+1/2,j,k}}(p_{i+1,j,k}^{n+1} - p_{i,j,k}^{n+1}) - T_{wx_{i-1/2,j,k}}(p_{i,j,k}^{n+1} - p_{i-1,j,k}^{n+1}) \quad (13)$$

where i, j, and k are indices in the x, y, and z directions, respectively, and n is the index for the time level. Interblock transmissibilities (those evaluated at $i = \pm\frac{1}{2}$, $j = \pm\frac{1}{2}$, and $k = \pm\frac{1}{2}$) require averaging or weighting of their various components. Density, viscosity, and the derivatives $(\partial T/\partial p)_h$ and $(\partial T/\partial h)_p$ are evaluated as arithmetic averages of the values in the adjacent blocks. Relative permeabilities and enthalpies are usually assigned the upstream value (that is, the value at the grid block having the higher fluid potential). Other terms, such as (kA/l) and $(K_m A/l)$, that are space dependent are determined as harmonic means of the values in the two adjacent blocks. For example,

$$(kA/l)_{i+1/2} = \frac{2k_i A_i k_{i+1} A_{i+1}}{k_i A_i l_{i+1} + k_{i+1} A_{i+1} l_i} \quad (14)$$

Finite difference approximations for the areal model, (6) and (7), are made in a manner similar to that outlined for the three-dimenisional model. In the areal model, however, the difference operator only acts in the two horizontal dimensions, and the equations include the additional terms that account for the fluxes from confining beds.

Nonlinear Techniques

The difference equations (11) and (12) are nonlinear in the transmissibility, accumulation, and source terms. These terms can lead to serious numerical instabilities if not treated properly. For isothermal, multiphase flow applications the techniques that have demonstrated the least severe stability restrictions are those that treat nonlinear terms implicitly and use upstream weighting on relative permeability terms [*Blair and Weinaug*, 1969; *Peaceman*, 1977]. For many geothermal applications we have found it necessary to use the same techniques to achieve stable solutions.

Implicit treatment of nonlinear terms in (11) and (12) requires that these terms be evaluated at the new time level $(n + 1)$. This leads to a system of $2N$ nonlinear equations (N being the number of grid blocks) for each time step. Each grid block is connected to, at most, six adjacent blocks (three-dimensional case), so that each equation has a maximum of seven unknown grid block values for both pressure and enthalpy, or 14 unknowns per equation. This set of equations is linearized using a residual formulation with Newton-Raphson iteration. Rewriting (11) and (12) in vector form,

$$\mathbf{R}(\mathbf{X}) = 0 \quad (15)$$

where $\mathbf{R}$ is the vector of nonlinear difference equations (11) and (12) written for each grid block and $\mathbf{X}$ is the vector of unknown pressure and enthalpy values at each grid block. Application of the Newton-Raphson procedure involves ap-

proximating (15) with a Taylor's series expansion about an assumed solution. This leads to the linearized matrix equation

$$\left[\frac{\partial R(X)^m}{\partial X}\right]\{\delta X\} = -\{R(X^m)\} \tag{16}$$

where m is the iteration level and $\delta X = X^{m+1} - X^m$. For the first iteration in each time step the values of p and h at the old time level are used as the initial solution. In general, this procedure converges very rapidly (within four iterations). Convergence is checked by calculating global mass and energy balance errors and comparing them to specified criteria.

The three-dimensional model is fully implicit with Newton-Raphson iteration applied to the transmissibility, accumulation, and source terms. For the areal model, stable solutions are obtained by treating only accumulation and source terms implicitly; Picard iteration is used on transmissibility terms.

Matrix Solution Techniques

Application of the Newton-Raphson procedure to the nonlinear difference equations produces a system of linear equations in the form of (16) that require a solution for each iteration. For many problems, solving this matrix equation is the most time-consuming part of the simulation process. Hence it is essential that this operation be performed as efficiently as possible.

A combination of direct and robust interative matrix techniques is used in both the areal and the three-dimensional model. The matrix equations in the areal model are solved using a sequential solution procedure coupled with Gauss-Doolittle decomposition that takes advantage of the matrix structure obtained by alternate diagonal (D4) ordering. A block successive overrelaxation method coupled with Gauss-Doolittle decomposition is used in the three-dimensional model.

Solution technique, areal model. Sequential solution of difference equations with two unknowns per grid block is an obvious alternative to simultaneous solution for the two unknowns, since the simultaneous solution results in a $2N \times 2N$ nonsymmetric matrix (for a description of a simultaneous solution, see *Faust and Mercer* [1977]). Unfortunately, a simple decoupling of (11) and (12) (or their areal equivalents) leads to an unstable iterative sequential procedure. To improve the matrix equation solution technique in the two-dimensional (vertical equilibrium) model, a sequential solution formulation outlined by *Coats et al.* [1974] is used. In this approach, Gaussian elimination is applied to the linearized Newton-Raphson equations in order to upper-triangularize the block 2×2 nodal equations.

As an example, this procedure is outlined for the two-dimensional equations for horizontal flow in a geothermal reservoir. The equations are first rewritten for each grid block in the form

$$[C]\{X\} = [I]\{Y\} + \{R\} \tag{17}$$

in which $[C]$ is the 2×2 time matrix, $[I]$ is the identity matrix, and

$$\{X\} = \begin{Bmatrix} \delta p^{n+1} \\ \delta h^{n+1} \end{Bmatrix}$$

where $\delta p = p^{n+1} - p^n$ and $\delta h = h^{n+1} - h^n$ is the iteration level;

$$\{Y\} = \begin{Bmatrix} \Delta[(T_w + T_o)\,\Delta(\delta p^{n+1})] \\ \Delta[T_h\,\Delta(\delta p^{n+1})] + \Delta[T_r\,\Delta(\delta h^{n+1})] \end{Bmatrix}$$

and

$$\{R\} = \begin{Bmatrix} \Delta[(T_w + T_o)\,\Delta p^{n+1}] + q_m' - (M^{n+1} - M^n)\dfrac{V_b}{\Delta t} \\ \Delta(T_h\,\Delta p^{n+1}) + \Delta(T_r\,\Delta h^{n+1}) + q_h^{n+1} - (E^{n+1} - E^n)\dfrac{V_b}{\Delta t} \end{Bmatrix} = \begin{Bmatrix} R_m \\ R_r \end{Bmatrix} \tag{18}$$

Applying Gaussian elimination, we obtain

$$\begin{bmatrix} C_{11} & C_{12} \\ 0 & C_{22} - \dfrac{C_{21}}{C_{11}} C_{12} \end{bmatrix} \begin{Bmatrix} \delta p^{n+1} \\ \delta h^{n+1} \end{Bmatrix} = \begin{bmatrix} 1 & 0 \\ -\dfrac{C_{21}}{C_{11}} & 1 \end{bmatrix} \{Y\} + \begin{bmatrix} R_m \\ R_r - R_m \dfrac{C_{21}}{C_{11}} \end{bmatrix} \tag{19}$$

where

$$C_{11} = \frac{\partial M}{\partial p}\frac{V_b}{\Delta t}$$

$$C_{12} = \frac{\partial M}{\partial h}\frac{V_b}{\Delta t}$$

$$C_{21} = \frac{\partial E}{\partial p}\frac{V_b}{\Delta t} - \frac{\partial q_h'}{\partial p}$$

$$C_{22} = \frac{\partial E}{\partial h}\frac{V_b}{\Delta t} - \frac{\partial q_h'}{\partial h}$$

Note that we are treating the enthalpy source term implicitly.

Solving the enthalpy equation first and using Newton-Raphson iteration on only the accumulation and source terms result in two symmetric matrix equations that are each $N \times N$. By imbedding the sequential solution in the linearized Newton-Raphson equations, decomposition of the two matrices is required only on the first 'sequential' iteration. Subsequent sequential iterations require only the formulation of a new right-hand side and backsubstitution. Each additional Newton-Raphson iteration requires the formulation of an updated left-hand side, one decomposition, and several backsubstitutions.

The work involved in solving the matrix equation includes the initial decomposition plus three to five backsubstitutions, depending on the convergence criterion. Usually, the computation time for all backsubstitutions is less than the computation time for the one decomposition. The symmetric matrix equations are solved using Gauss-Doolittle decomposition that takes advantage of D4 ordering [*Price and Coats*, 1974]. In this ordering, the finite difference blocks are numbered in alternating diagonals. This numbering scheme results in a matrix with the upper half already in upper triangular form, so that only the lower half needs to be decomposed. Overall, sequential solution and D4 ordering reduce the computational work of solving the matrix equation by a factor that ranges from one-fourth to one-sixteenth the work required for simultaneous solution and normal ordering (numbering blocks in the direction of fewest blocks).

Solution technique, three-dimensional model. The three-dimensional model is more severely nonlinear due to gravity

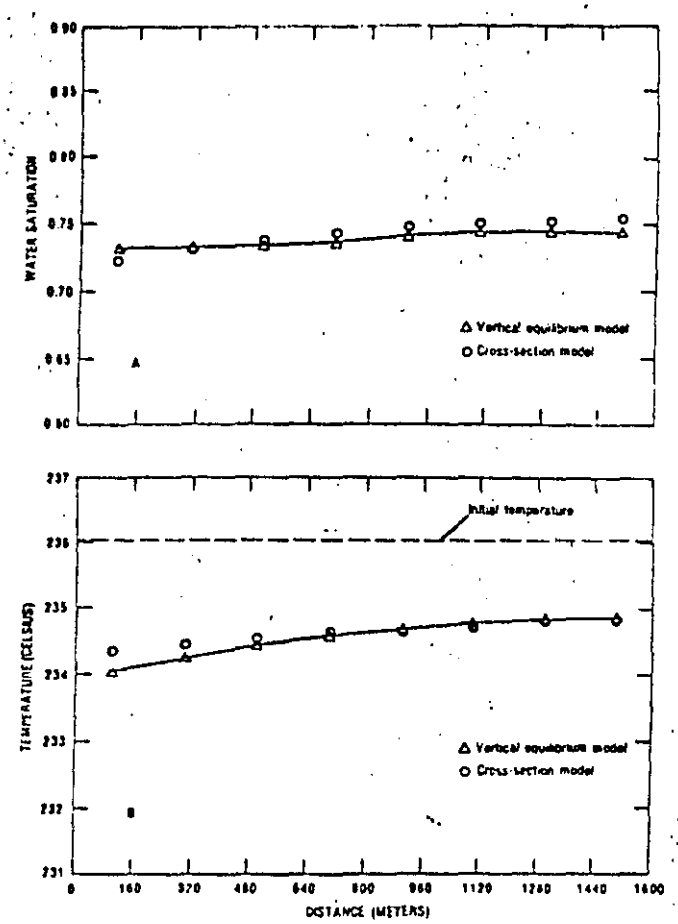

Fig. 7. High-permeability example. Depth-averaged (*a*) water saturations and (*b*) temperatures for simulated period of 5.0×10^8 s showing results from vertical equilibrium model and cross-sectional model.

cross section) calculated for the one-dimensional models and the six-layer cross-sectional model. The results of the 10-layer model are not shown because they are nearly the same as those of the six-layer model. As can be seen from the calculated time-saturation plots for the well block(s), the cross-sectional and vertical equilibrium results compare favorably. The results for the one-dimensional model assuming uniform properties are erroneous. Thus ignoring gravity segregation and vertical variations in the thermodynamic properties can lead to the incorrect prediction of early reservoir depletion for reservoirs involving two-phase flow. However, for liquid-dominated reservoirs the uniform-property assumption is adequate.

Relative permeability effects. Relative permeability can significantly affect gravity segregation and hence the validity of the vertical equilibrium assumption. Unfortunately, reliable relative permeability data for steam-water flow is limited to a few experimental studies, and these results cannot be extrapolated to field scale with confidence. It is thus important to consider the sensitivity of reservoir models to relative permeability. In the absence of reliable laboratory data for a particular reservoir rock the nonlinear equations (28) and (29), which were originally proposed for oil and gas, are commonly used. Alternatively, simpler linear expressions for relative permeability are also used:

$$k_{rs} = (S_s - S_{sr})/(1 - S_{sr}) \qquad (30)$$

and

$$k_{rw} = (S_w - S_{wr})/(1 - S_{wr}) \qquad (31)$$

These expressions are similar to the relative permeability functions that are obtained by vertical integration.

The example chosen to demonstrate the effect of relative permeability is the same as the previous one; only additional results from a cross-sectional model using the linear relative permeabilities and having an 8×10 grid are presented. The water saturation distributions after 5.4×10^8 s of production for the cross-sectional models using nonlinear and linear relative permeabilities are shown in Figure 4. The outline in the figures represents the boundary of the reservoir. The solid line is the boundary between two-phase and one-phase (water) blocks in the cross-sectional model with the calculated water saturations given at the center of each grid block. The vertical equilibrium, one-dimensional model predicts the two-phase/liquid-water contact represented by the dashed line in the figure. The results from the one-dimensional model compare much more favorably with those from the cross-sectional model using linear relative permeabilities (Figure 4*b*) in that the interface positions are similar and water saturations in the two-phase zone are much closer to the residual water saturation of 0.3. Recall that the vertical equilibrium model is based on the assumption that water above the interface is at residual water saturation. The saturations calculated using the nonlinear relative permeabilities (Figure 4*a*) show a wider variance about the residual water saturation. Also, a zone of superheated steam is formed, and the two-phase/liquid-water interface is substantially lower.

A low intrinsic permeability was chosen for this example to provide a difficult test for the vertical equilibrium model. Even with this low permeability and the deviations in Figure 4, the depth-averaged saturations agree fairly well among the alternative models (as shown in Figure 5*a*). The depth-averaged temperatures agree less favorably, especially in the grid block containing the well (Figure 5*b*). The vertical equilibrium model tends to break down when water saturations approach residual water saturation, that is, when the water table disappears. This breakdown is reflected in the depth-averaged temperatures. For this low-permeability example the vertical equilibrium model therefore provides the best results when relative permeabilities are linear and water saturations are well above the residual water saturation.

Permeability effects. On the basis of previous studies for gas-oil reservoirs we anticipate that high permeabilities will be favorable for gravity segregation. To see if this conclusion is applicable to geothermal reservoirs, an example using a higher

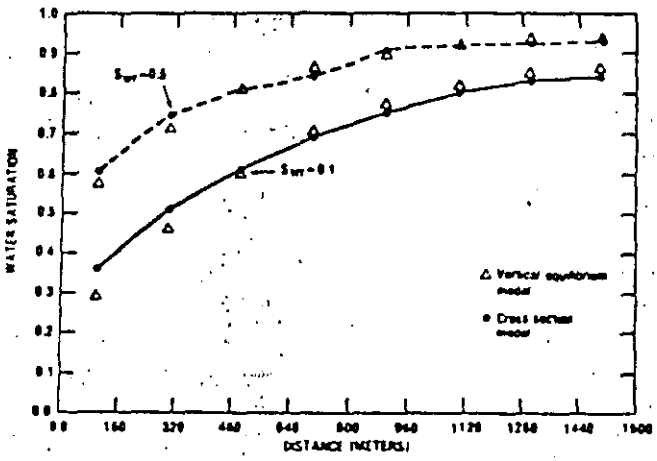

Fig. 8. Depth-averaged water saturations for vertical equilibrium and cross-sectional models using residual water saturations of 0.1 and 0.5; simulation periods equal 6.31×10^8 and 3.23×10^8 s, respectively.

Whiting, R. L., and H. J. Ramey, Jr., Application of material and energy balances to geothermal steam production, *J. Petrol. Technol.*, *21*(7), 893–900, 1969.

Witherspoon, P. A., S. P. Neuman, M. L. Sorey, and M. J. Lippmann, Modeling geothermal systems, paper presented at International Meeting on Geothermal Phenomena and Its Applications, Accad. Nat. dei Lincei, Rome, Italy, March 3–5, 1975.

Woo, P. T., and A. S. Emanuel, A block successive over-relaxation method for coupled equations, paper presented at 51st Annual Fall Meeting, Soc. of Petrol. Eng., AIME, New Orleans, La., Oct. 3–6, 1976.

(Received July 31, 1978;
accepted August 14, 1978.)

CURSO: " INGENIERIA DE YACIMIENTOS GEOTERMICOS "
23 DE MARZO AL 18 DE MAYO DE 1984

TEMA: "THREE DIMENSIONAL GEOTHERMAL RESERVOIR SIMULATION"

DR. GUILLERMO DOMINGUEZ
2-13 de abril

Society of Petroleum Engineers of AIME
6200 N. Central Expwy.
Dallas, Tex. 75206

PAPER
NUMBER SPE 6104

Three Dimensional Geothermal Reservoir Simulation

By
L. Kent Thomas, Member SPE-AIME, and Ray Pierson, Phillips Petroleum Co.

ABSTRACT

This paper presents the development of a three dimensional, finite difference model for the simulation of geothermal reservoirs. The model is designed to simulate geothermal reservoirs which contain water in any of its vapor or liquid states and provisions are included for properly treating changes of state during a time step. This logic provides for a stable calculation of state change and eliminates pressure, heat balance, and material balance errors.

Mass and energy balances are solved simultaneously using an IMPES formulation. An implicit treatment of production rates, capillary pressure, and transmissibilities is included as an option. Thus, entire field, cross-sectional, or individual well studies can be efficiently performed.

Example problems are presented to demonstrate the utility of the model and to provide insight into the nature of geothermal production under various conditions. In particular, an example of a reservoir initially containing subcooled liquid is presented where fluid conditions near the production well go from subcooled liquid to saturated steam and then to superheated steam.

References and illustrations at end of paper.

INTRODUCTION

Geothermal energy represents an essentially untapped alternate source of energy throughout the world. The exploration effort for this energy source has increased, however, and should lead to the discovery and development of new geothermal areas. Noteable producing geothermal fields include: Wairekei in New Zealand; Cero Prieto in Mexico; Matsukawa in Japan; Larderello in Italy; and The Geysers in California.

Recent publications in the literature include papers dealing with zero (one cell), one, and two dimensional geothermal reservoir simulation. Most of these papers treat steam in only one of its states or mention the difficulty of simulating blocks changing from one state to another.

Whiting and Ramey[1] presented a zero dimensional geothermal model which included water influx as an option. A thorough discussion of reservoir performance during the various states that steam can assume was given.

Their paper also included a successful match of the pressure, production performance of the Wairekei geothermal reservoir in New Zealand from 1956 to 1966.

Coats[2,3] developed a three dimensional, finite difference, steam flooding model which simultaneously solves the mass and energy equations. An IMPES formulation was used to solve for pressures implicity followed by a solution for temperatures, saturations, etc. Saturations calculated using explicit rates, capillary pressures, and transmissibilities were recalculated at the end of each time step using an implicit formulation for these variables.

Brigham and Morrow[4] presented a paper discussing the P/Z behavior of geothermal steam reservoirs. Their model was similar to Whiting and Ramey's model but they allowed for the presence of a vapor and liquid zone. Mass and energy balances were written for both zones and logic for a constant or falling liquid level was included. Martin[5] presented an analysis of internal steam drive in geothermal reservoirs which assumed that temperature, pressure, and fluid saturation gradients as well as capillary pressure and gravity were negligible.

Gould[6] presented the development of a vertical two phase pressure drop calculation for flow in geothermal wells. A discussion of the effect of heat transfer to the surrounding formation and the effect of steam quality on production was given.

Mercer and Faust[7] developed a two-dimensional (areal), two-phase geothermal model using a Galerkin finite element formulation in space and finite difference formulation for time. They chose pressure and enthalpy as independent variables and solved for these two variables simultaneously. A ten month simulation of a hypothetical hot-water reservoir with initial conditions similar to those in the Wairekei reservoir was presented. No provisions were included for changing states, for example from subcooled liquid to saturated steam, during the course of a run.

Toronyi and Farouq Ali[8] presented a two-dimensional, two-phase (saturated steam) finite difference geothermal simulator. They solved both areal and cross-sectional problems. A wellbore model was included to calculate well head quality and pressure given bottom hole conditions from the reservoir model solution. In their model pressure and water saturation were used as dependent variables and were simultaneously solved for at each block. An implicit solution scheme similar to that used in coning models was employed. Capillary pressure and heat transfer to and from the reservoir were assumed negligible.

Faust and Mercer[9] developed a two-dimensional (areal), finite difference geothermal simulator and compared results from this model with those from their Galerkin finite element model. Pressure and enthalpy were used as independent variables and were calculated using a simultaneous solution. They discussed the occurrence of material balance errors in blocks changing from one state to another during a time step. This material balance error was minimized by repeating the time step and reducing its size so that the state change occurred near the end of a time step.

This paper presents the development of a three-dimensional, finite difference model for the simulation of geothermal reservoirs. The solution technique employed simultaneously solves the mass and energy balances using an IMPES formulation.

The model is designed to simulate geothermal reservoirs which contain water in various regions of a reservoir, in any of its vapor or liquid states (subcooled liquid, saturated steam, or superheated steam). Provisions are included for properly treating changes of state during a time step. This logic provides a stable calculation of state change and eliminates material and heat balance errors.

The model is formulated with implicit production rates, capillary pressure, and transmissibilities as an option which allows entire field, cross-sectional, or individual well studies to be efficiently made.

DEVELOPMENT OF FLOW EQUATIONS

The equations describing three dimensional, two-phase flow in a geothermal reservoir include the conservation of mass for water and steam; conservation of energy; and an equation specifying the state of the system. The conservation equations written in finite difference form are:

Water

$$\Delta\left[T_w(\Delta p_w - \rho_w \frac{g}{g_c}\Delta D)\right] - q_w = \frac{V_b}{\Delta t}\,\delta(\phi\rho_w S_w) - q_c \qquad (1)$$

Steam

$$\Delta\left[T_g\left(\Delta p_g - \rho_g \frac{g}{g_c}\Delta D\right)\right] - q_g = \frac{V_b}{\Delta t}\delta(\phi\rho_g S_g) + q_c \quad (2)$$

Energy

$$\Delta(T_H\Delta p) + \Delta(T_c\Delta T) - q_L - q_H = \frac{V_b}{\Delta t}\delta\left[\phi(\rho_w S_w U_w + \rho_g S_g U_g) + (1-\phi)(\rho C_p)_f T\right] \quad (3)$$

The above mass balances on water and steam state that the net flow of mass into a grid block minus the rate of production is equal to the rate of accumulation of mass. The term q_c is the rate of water condensation. The energy balance states that the net flow of enthalpy into a grid block plus the net rate of heat conduction minus the rate of enthalpy production is equal to the change of internal energy in the block. Potential and kinetic energy terms are assumed to be negligible and have been omitted from the energy balance.

In addition to the above equations another relationship is necessary to determine the physical state of the water in a given grid block. For subcooled, saturated, and superheated conditions the following equations hold.

Subcooled Liquid

$$\delta S_g = -S_{gn} \quad (4)$$

Saturated Steam

$$p = p_{sat}(T) \quad (5)$$

Superheated Steam

$$\delta S_w = -S_{wn} \quad (6)$$

Equations 4 and 6 indicate that the change in saturation of blocks that are subcooled or superheated at the end of a time step is equal to minus their saturation at the beginning of a time step. Equation 5 represents the vapor pressure curve for water and states that pressure and temperature are uniquely related when both water and steam are present.

The condensation term in the water and steam mass balances can be eliminated by adding these two equations[2]. Writing the combined steam-water balance and equations 3 - 6 in residual form with transmissibilities, capillary pressure, and densities evaluated at time n yields

$$\Delta\left[(T_w + T_g)\Delta\delta p\right] = C_{11}\delta S_w + C_{12}\delta T + C_{13}\delta p + R_1 \quad (7)$$

$$\Delta(T_H\Delta\delta p) = C_{21}\delta S_w + C_{22}\delta T + C_{23}\delta p + R_2 \quad (8)$$

$$0 = C_{31}\delta S_w + C_{32}\delta T + C_{33}\delta p + R_3 \quad (9)$$

The coefficients on the right hand sides of equations 7 and 8 result from the expansion of the accumulation terms in equations 1, 2, and 3 in terms of δS_w, δT, and δp. For example, the expansion of $V_b/\Delta t\delta\phi(\rho_w S_w + \rho_g S_g)$ yields

$$C_{11} = \frac{V_b}{\Delta t}\left[\phi_{n+1}\rho_{wn+1} - \phi_{n+1}\rho_{gn+1}\right] \quad (10)$$

$$C_{12} = \frac{V_b}{\Delta t}\left[\phi_{n+1}(S_{wn}\rho'_{wT} + S_{gn}\rho'_{gT})\right] \quad (11)$$

$$C_{13} = \frac{V_b}{\Delta t}\left[S_{wn}(\phi_{n+1}\rho_w(T_{n+1})c_w + \rho_{wn}\phi_i c_f) + S_{gn}(\phi_{n+1}\rho'_g + \rho_{gn}\phi_i c_f)\right] \quad (12)$$

The terms ρ'_{wT} and ρ'_{gT} are the partial of water and steam densities with respect to temperature at constant pressure and ρ'_g is the partial of steam density with respect to pressure at constant temperature. This latter term, ρ'_g, is only present when superheated steam exists at time n+1 which will be discussed in a later section. All partial derivatives are evaluated as chord slopes.

The terms R_1 and R_2 are the residuals of equations 7 and 8 at time n. For instance,

$$R_1 = -\Delta T_w\left(\Delta p_{wn} - \rho_w \frac{g}{g_c}\Delta D\right) - \Delta T_g\left(\Delta p_{gn} - \rho_g \frac{g}{g_c}\Delta D\right) + q_w + q_g \quad (13)$$

The coefficients and residual in equation 9 depend on the state of a block at time n+1. For example, if saturated steam is present at time n+1

$$\delta p = p_{sat}(T_n) + p'_{sat}\delta T - p_n \quad (14)$$

where

$$p'_{sat} = \frac{p_{sat}(T_{n+1}) - p_{sat}(T_n)}{T_{n+1} - T_n}$$

and the coefficients in equation 9 are

$$C_{31} = 0 \quad (15)$$

$$C_{32} = p'_{sat} \quad (16)$$

$$C_{33} = 1 \quad (17)$$

$$R_3 = p_n - p_{sn} \quad (18)$$

TREATMENT OF FLUID AND ROCK PROPERTIES

Water density for subcooled liquid is calculated using water compressibility, c_w, and saturated water density, $\rho_w(T)$.

$$\rho_w(p,T) = \rho_w(T)\left[1 + c_w(p - p_{sat})\right] \quad (19)$$

The term p_{sat} is the vapor pressure of saturated steam corresponding to the temperature, T.

Internal energy for subcooled water varies only slightly with pressure from its saturated value and can be written as

$$U_w(p,T) = U_w(T) + U'_w(p - p_{sat}) \quad (20)$$

where $U_w(T)$ is the internal energy of saturated water and U'_w is the partial of water internal energy with respect to pressure at constant temperature.

Saturated values of p, ρ_w, ρ_g, U_w, and U_g are calculated directly from the steam tables[10] using linear interpolation. Equations 19 and 20 are used for calculating ρ_w and U_w from $\rho_w(T)$ and $U_w(T)$. Use of these equations for both subcooled and saturated steam results in a stable numerical transition from subcooled liquid to saturated steam. It should be noted that equations 19 and 20 yield

$$\rho_w = \rho_w(T) \quad (21)$$

and

$$U_w = U_w(T) \quad (22)$$

for saturated steam since pressure and saturation pressure are equal.

Properties of superheated steam from the steam tables are internally stored as a function of both temperature and pressure. Superheated steam properties are calculated using linear interpolation of both temperature and pressure. Special considerations are given to conditions near the saturation boundary to insure correct interpolates.

Transition from saturated steam at time n to superheated steam at time n+1 requires the addition of the partial of steam density and steam internal energy with respect to pressure at constant temperature to coefficients C_{13} and C_{23}, respectively. For saturated steam these variables are a function of only one variable, T or p.

Steam and water viscosities are input in tabular form as a function of temperature. Porosity is calculated as a function of pressure and formation compressibility.

$$\phi = \phi_i\left[1 + c_f(p - p_i)\right] \quad (23)$$

SOLUTION OF FLOW EQUATIONS

Equations 7, 8, and 9 represent three equations in the three unknowns δp, δT, and δS_w at each grid block. These equations can be efficiently solved using the implicit pressure explicit saturation (IMPES) method. Saturation and temperature are eliminated from equations 7-9 by multiplying equation 7 and 8 by appropriate coefficients and then adding the three equations. The reduced band-width direct solution method presented by Price and Coats[11] is used to solve for pressures.

After solving for pressure, equations 7 and 9 are used to calculate δT and δS_w. Eliminating δS_w from equations 7 and 9 yields

$$\delta T = \frac{C_{31}}{C_{12}C_{31} - C_{11}C_{32}}\left\{\Delta\left[(T_w + T_g)\,\Delta\delta p\right] - R_1 - \frac{(C_{13}C_{31} - C_{11}C_{33})}{C_{31}}\delta p + \frac{C_{11}}{C_{31}}R_3\right\} \quad (24)$$

The change in water saturation, δS_w, is calculated from equation 7.

$$\delta S_w = \frac{1}{C_{11}}\left\{\Delta\left[(T_w + T_g)\Delta\delta p\right] - R_1 - C_{12}\delta T - C_{13}\delta p\right\} \quad (25)$$

The above calculations for δp, δT, and δS_w constitute one iteration. After each iteration, temperature and pressure dependent coefficiencts are updated and another iteration is performed until convergence

is reached. Convergence can be based on maximum temperature and pressure changes or on the absolute sum of residuals divided by total production. Generally only two or three iterations are required to reach convergence on most problems.

IMPLICIT PRODUCTION RATES

Production rates vary with block pressure, water saturation, and wellbore pressure. If the effect of these variables on production rate is not considered, saturation and pressure oscillations will occur for difficult problems and the solution may become unstable. To reduce this stability condition production rates are written implicitly as

$$q_{n+1} = q_n + \frac{\partial q}{\partial p}\delta p + \frac{\partial q}{\partial S_w}\delta S_w + \frac{\partial q}{\partial p_{wf}}\delta p_{wf} \quad (26)$$

where q_n is the explicit production rate,

$$q_n = \frac{2\pi kh k_r \rho/\mu (p - p_{wf})}{\ln \frac{r_e}{r_w} + s - 1/2} \quad (27)$$

The implicit treatment of each variable is optional and in many cases the $\partial q/\partial p_w$ can be deleted. However, for problems such as near wellbore simulations of incompressible or slightly compressible systems involving production from more than one layer[12] the effect of wellbore pressure on production rate should be included.

The partial of q with respect to p is calculated holding S_w and P_{wf} constant and is equal to the well PI at time n.

$$\frac{\partial q}{\partial p} = \frac{2\pi kh k_r \rho/\mu}{\ln \frac{r_e}{r_w} + s - 1/2} \quad (28)$$

This term is included in the pressure solution and it is simply combined with coefficient C_{13}.

Nolen and Berry[12] eliminated pressure oscillations caused by variations of wellbore pressure in a water-oil coning example by adding an additional column of blocks with large vertical permeabilities to simulate the wellbore. The total production was then taken from the top block in the column. Trimble and McDonald[13] treated this problem for single well, three dimensional coning simulation by writing the production rate in the flow equations as a function of wellbore pressure. A production equation was added to their set of 3N equations and the changes in pressure, saturation, and wellbore pressure over a time step were solved simultaneously using Newtonian iteration.

The method for treating $\partial q/\partial p_{wf}$ presented here can be applied to single or multiwell simulations. Writing total well production rate implicitly with respect to pressure and wellbore pressure yields

$$q_T = \sum_{k=1}^{L} q_{ni} + \sum_{k=1}^{L} PI_k \delta P_k - \sum_{k=1}^{L} PI_k \delta p_{wf_k} \quad (29)$$

Since $\partial q/\partial p_{wf}$ is only applied to wells not on decline, the total production rate is equal to the sum of the individual layer rates at time n. Thus, assuming that $\delta p_{wf_1} = \delta p_{wf_2} \cdots \delta p_{wf_L}$,

$$\delta p_{wf} = \frac{\sum_{k=1}^{L} PI_k \delta p_k}{\sum_{k=1}^{L} PI_k} . \quad (30)$$

The $\partial q/\partial p_{wf}$ for layer k is equal to

$$\frac{\partial q_k}{\partial p_{wf}} = -PI_k . \quad (31)$$

The expression for δp_w is evaluated using pressure changes from the previous iteration. Both the $\partial q/\partial p$ and $\partial q/\partial p_{wf}$ are omitted from the first iteration when the $\partial q/\partial p_{wf}$ is included, since δp is zero prior to the first iteration. The effect on convergence of evaluating δp_{wf} using last iterate pressures is generally small for most problems. For instance, on the average about one extra iteration per time step was required for the radial problem presented later in the text.

After pressure and temperature convergence is reached and δS_w is calculated explicitly, an implicit δS_w calculation is made using implicit production rates with respect to water saturation. The difference between implicit and explicit production is given by[3]

$$-q_T f_{wn+1} + q_{wn} = \frac{V_{pn+1}}{\Delta t}(\delta S_w - \delta S_w^*) \quad (32)$$

where δS_w^* is saturation change calculated using explicit production rates and δS_w is the implicit saturation change. The term f_w is the fractional flow of water and q_T is total production rate.

$$q_T = q_w + q_g, \ ft^3/day \quad (33)$$

Fractional water flow is written at time n+1 as

$$f_{wn+1} = \frac{\lambda_{wn} + \lambda_w' \delta S_w}{\lambda_{wn} + \lambda_w' \delta S_w + \lambda_{gn} + \lambda_g' \delta S_w} \quad (34)$$

where

$$\lambda_{wn} = k_{rwn}/\mu_{wn} \quad (35)$$

$$\lambda_{gn} = k_{rgn}/\mu_{gn} \quad (36)$$

Substituting the above expressions into equation 32 yields a quadratic equation which can be solved directly for δS_w.

IMPLICIT SATURATION CALCULATION

MacDonald and Coats[14] first proposed the use of implicit transmissibilities and capillary pressures in the solution of saturations following the pressure solution. Later authors[2,3,15] presented improved versions of this treatment. The method used here closely follows the development presented by Coats[3]. For simplicity the equations are presented only for the x direction. Analogous equations hold in the y and z directions.

The flow of water and steam from block i-1 to i in ft^3 is given by

$$q_w = T_w(\Delta p_w - \rho_w \frac{g}{g_c}\Delta D) \quad (37)$$

and

$$q_g = T_g(\Delta p_w + \Delta P_c - \rho_g \frac{g}{g_c}\Delta D) . \quad (38)$$

Eliminating p_w from equations 37 and 38 yields the following fractional flow equation for water:

$$q_w = f_w q_T - f_w T_g(\Delta P_c + \rho_{wg} \frac{g}{g_c}\Delta D) \quad (39)$$

where

$$f_w = T_w/T, \quad (40)$$

$$q_T = q_w + q_g, \quad (41)$$

$$T = T_w + T_g, \quad (42)$$

and

$$\rho_{wg} = \rho_w - \rho_g . \quad (43)$$

Now writing the water flow equation explicitly and implicitly and subtracting yields (for the x-direction)

$$\delta q_{wi-1,i} - \delta q_{wi,i+1} = \frac{V_{pn+1}}{\Delta t}(\delta S_w - \delta S_w^*) . \quad (44)$$

The term $\delta q_{wi-1,i}$ represents the change in water flux at face i- 1/2 due to using implicit saturations and can be expressed as

$$\delta q_{wi-i,i} = \frac{\partial q_w}{\partial S_{wi-1}} \delta S_{wi-1} + \frac{\partial q_w}{\partial S_{wi}} \delta S_{wi} \quad (45)$$

The term $\partial q_{wi-1,i}/\partial S_{wi-1}$ can be written as

$$\frac{\partial q_{wi-1,i}}{\partial S_{wi-1}} = f_{wi-1}' \left[q_T - T_{gn} (\Delta P_c + \rho_{wg} \frac{g}{g_c} \Delta D) \right] - f_{wn}(\Delta P_c + \rho_{wg} \frac{g}{g_c}\Delta D) T_{gi-1}' - f_{wn} T_{gn} P_{ci-1}' \quad (46)$$

A similar expression can be written for $\partial q_{wi-1,i}/\partial S_{wi}$. The partial derivatives shown in equation 45 may or may not be present depending on the direction of flow potentials. For example, if both water and steam are flowing from i-1 to i then the $\partial q_{wi-1,i}/\partial S_{wi-1}$ is given by equation 46 and the

$$\frac{\partial q_{wi-1,i}}{\partial S_{wi}} = f_{wn} T_{gn} P_{ci}' . \quad (47)$$

In the above equations f_w' and T_g' are calculated as

$$f_w' = \frac{f_{wn+1} - f_{wn}}{\delta S_w} \quad (48)$$

and

$$T_g' = \frac{T_{gn+1} - T_{gn}}{\delta S_w} \quad (49)$$

where f_{wn+1} and T_{gn+1} are calculated by perturbing S_{wn} by a fixed amount.

and

$$k_{rg} = \left[1 - \frac{(S_w - S_{wc} - S_{gc})}{1 - S_{wc} - S_{gc}}\right]^2 \left[1 - \frac{(S_w - S_{wc} - S_{gc})^2}{(1 - S_{wc} - S_{gc})^2}\right] \quad (53)$$

A complete list of the data used in this example are shown in Table II.

Automatic time steps with a minimum step size of 1 second and a maximum step size of 10 seconds were used. Step size was based on a desired maximum saturation change of .03. Increase in step size from one step to the next was limited to 1.5 times Δt_n.

Saturations at 180 and 300 seconds from this simulation are presented in Figure 2. Calculated and experimental pressures at 300 seconds are shown in Figure 3 and are reasonably matched considering that hypothetical relative permeability curves and heat transfer relationships were used.

THREE DIMENSIONAL EXAMPLE

In this example, a three dimensional simulation of production from a reservoir with a 10° dip is presented. A typical slice of the reservoir representing the drainage volume of a single well is shown in Figure 4. Areally the slice was divided into three cross-sections with the well located in the center section near the top of the reservoir. The well was perforated in the top 5 layers of the model which represents 250 feet or half of the reservoir thickness. Due to the symmetry line through J = 2, only one half of the typical slice was actually modeled.

Initial reservoir temperature and pressure in the top well cell were 500°F and 1200 psia, respectively. Temperature variation with depth was 3°F/100 ft. At these conditions the reservoir is initially subcooled by approximately 67°F or in terms of pressure at 500°F, the reservoir is 519 psi above its saturation point. Additional data for this example are presented in Tables III, IV, and V.

Production from the well was set equal to a constant surface steam rate of 2 MM lb_m/day which was calculated from bottomhole rates using the following equation:

$$q_{g\ surface} = q_g + .18\ q_w \quad (54)$$

The coefficient multiplying q_w represents the amount of steam that will be generated by flashing the produced water adiabatically at a surface pressure of 150 psia.

Steam and water production rates versus time are shown in Figure 5. Water rate declined rapidly at the start of the run as the saturation pressure near the well was reached and free steam production was initiated. By the end of 4 years, the water rate has declined to a point equal to the steam rate and by the end of 12 years the ratio of steam to water flow rates is approximately 2. Total recovery of water and steam from the reservoir at the end of 12 years was equal to 42% of the original water in place. The surface steam rate was still 2 MM lb_m/day at 12 years, but the well was about to go on decline as the flowing bottomhole pressure had dropped to approximately 275 psia.

Contours of pressure, temperature, and water saturation for the cross-section containing the well are presented in Figures 6, 7, and 8. Note the superheated region at the top of the reservoir near the well. The top well cell went to superheat after about 9.5 years and by the end of 12 years it was superheated by approximately 2.5°F. The effect of water coning into the partially penetrated well is apparent in Figure 8.

This example was run using implicit rates with respect to pressure and saturation and with implicit transmissibilities. Material and heat balances at the end of 12 years were 1.0020 and .9998, respectively. The small material balance error shown here is due to the use of implicit transmissibilities and is the result of the variation in density from one cell to the next. This example was also run using explicit transmissibilities and the material and heat balances at 12 years were .9998 and 1.0003, respectively. Although minor oscillations in saturation occured near the bottom perforations using explicit transmissibilities, the results at the end of 12 years were essentially identical. The run using implicit transmissibilities required approximately 10% fewer time steps. Automatic time steps were used in both runs with desired pressure and saturation changes of 100 psi and .03 controlling step size.

RADIAL EXAMPLE

This example illustrates the use of the model for studying near wellbore problems. Radial coordinates were used to perform drawdown and buildup calculations for a well producing at a constant rate from a reservoir which initially contains subcooled water. Initial reservoir temperature and pressure were 500°F and 1000 psia, respectively. Relative permeability and viscosity data from the 3-D example were also used here. Other pertinent data are shown in Table VI.

TABLE III - THREE DIMENSIONAL EXAMPLE

Initial temperature (1,1,1) = 500°F

Initial temperature gradient, 3°F/100 ft.

Initial pressure (1,1,1) = 1200 psia

Permeability = 150 md

Porosity = .20

Vertical permeability = 15 md

Initial water saturation = 1.0

Water compressibility = 10.8 (10^{-6}) vol/vol-poi

Formation compressibility = 4 (10^{-6}) vol/vol-poi

Formation specific heat = 38. BTU/ft^3 - °F

Thermal conductivity = 35. BTU/°F - ft - day

Reservoir dip = 10°

Length of reservoir = 6000 ft

Width of reservoir = 1250 ft

NX = 12, NY = 3, NZ = 10

ΔX = 500 ft

ΔY = 500, 250, 500 ft

ΔZ = 50 ft

Wellbore radius = .4 ft

Skin = -4

Production rate = 2 (10^6) lb_m/day

= [steam rate + .18 (water rate)] bottomhole

Minimum flowing bottomhole pressure = 250 psia

TABLE IV - RELATIVE PERMEABILITY DATA FOR THREE DIMENSIONAL PROBLEM

S_w	K_{rw}	K_{rg}
.2	0.0	1.000
.3	.01	.754
.4	.025	.524
.5	.050	.336
.6	.090	.188
.7	.160	.086
.8	.315	.027
.9	.585	.01
1.0	1.000	0.0

TABLE V - WATER AND STEAM VISCOSITY DATA FOR THREE DIMENSIONAL PROBLEM

T, °F	μ_w, cps	μ_g, cps
400	.131	.0157
450	.115	.0169
500	.103	.0181
550	.094	.0193

TABLE VI - RADIAL EXAMPLE

Initial pressure = 1000 psia

Initial temperature = 500°F

Permeability = 10 md

Porosity = .20

Initial water saturation = 1.0

Water compressibility = 10.8 (10^{-6}) vol/vol-psi

Formation compressibility = 4 (10^{-6}) vol/vol-psi

Formation specific heat = 38 BTU/ft^3 °F

Thermal conductivity = 35 BTU/°F -ft-day

Wellbore radius = .4 ft

External radius = 5000 ft

Block center radius of cell 1 = 10 ft

Skin = -2.6

NX = 7, NY = 10

Production rate = 5 (10^6) lb_m/day

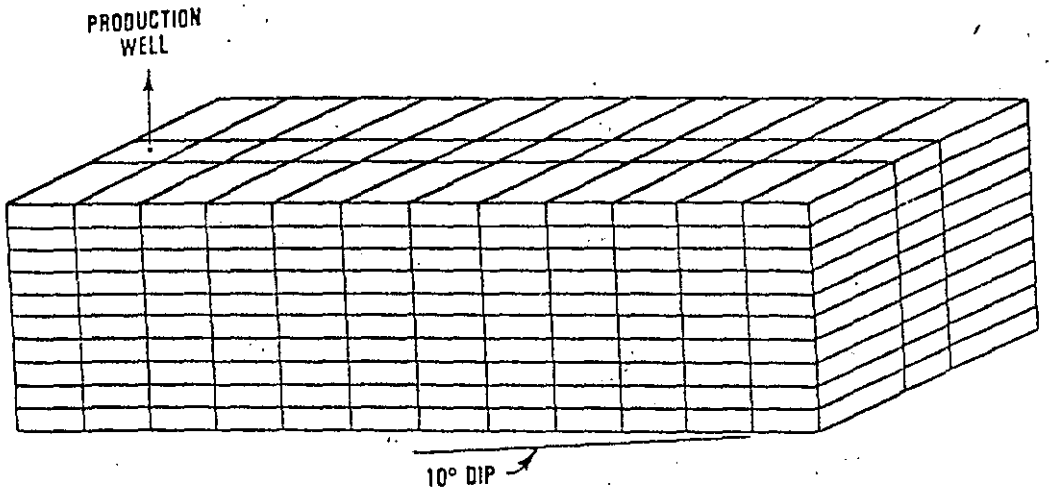

Fig. 4 - Grid for the three dimensional example.

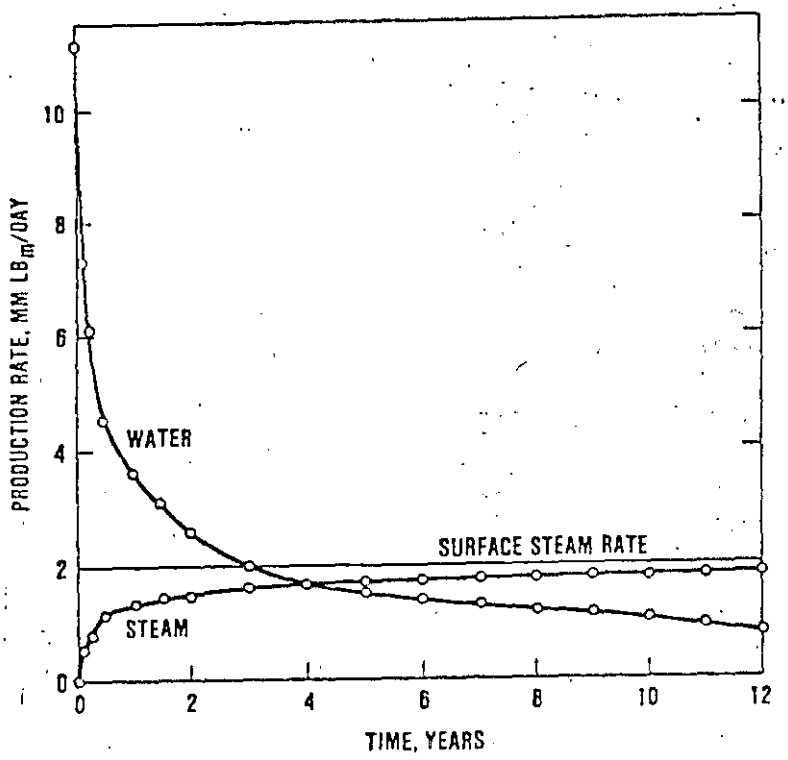

Fig. 5 - Water and steam production from 3-D example.

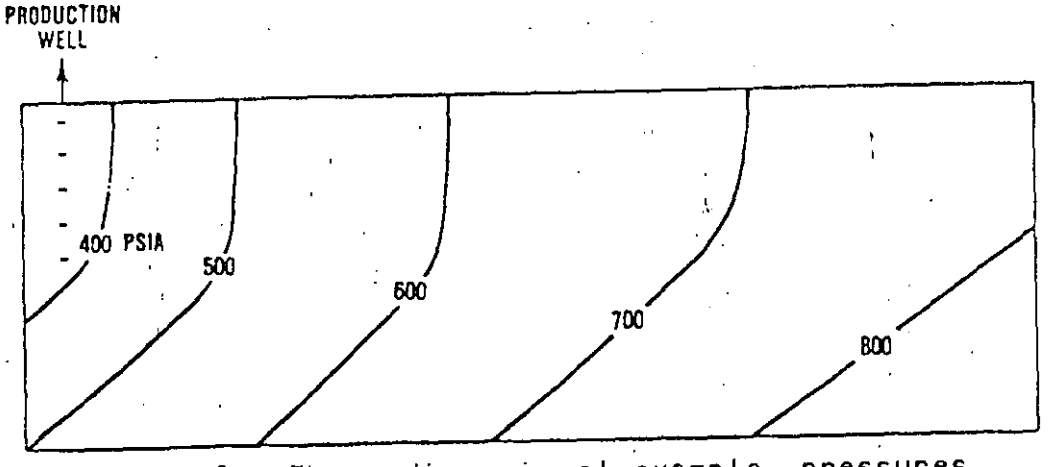

Fig. 6 - Three dimensional example, pressures at 12 years.

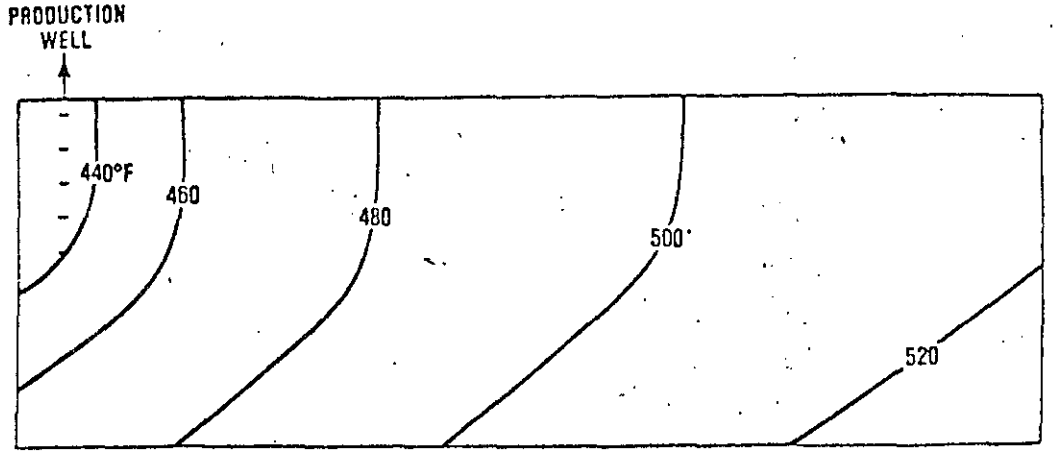

Fig. 7 - Three dimensional example, temperatures at 12 years.

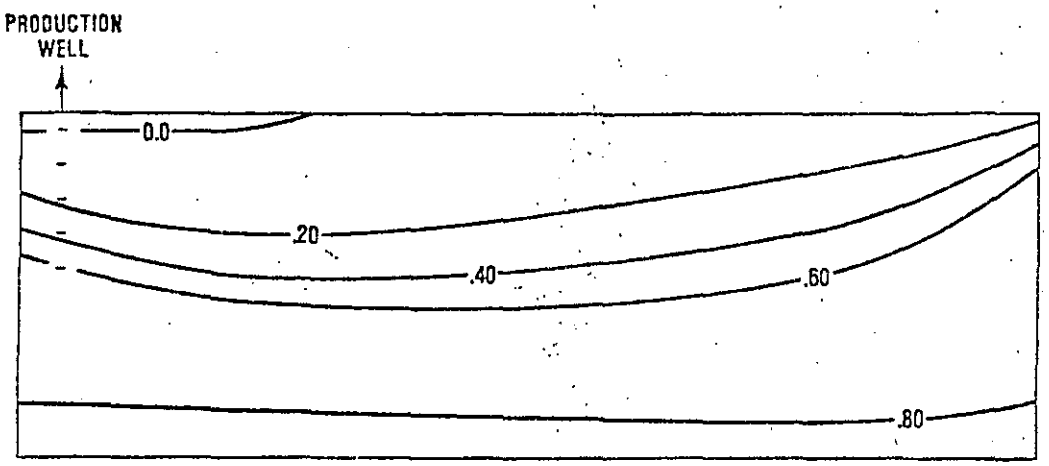

Fig. 8 - Three dimensional example, water saturations at 12 years.

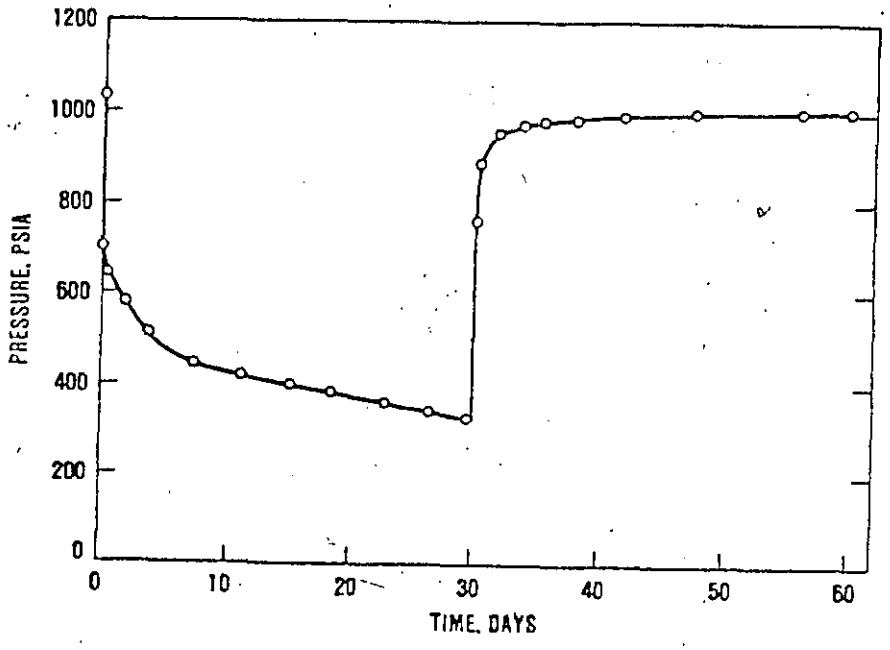

Fig. 9 - Radial example, bottom hole flowing pressure.

.735	.891	1.0	1.0	1.0	1.0	1.0
.749	.942	1.0	1.0	1.0	1.0	1.0
.764	1.0	1.0	1.0	1.0	1.0	1.0
.774	1.0	1.0	1.0	1.0	1.0	1.0
.796	1.0	1.0	1.0	1.0	1.0	1.0
1.0	1.0	1.0	1.0	1.0	1.0	1.0
1.0	1.0	1.0	1.0	1.0	1.0	1.0
1.0	1.0	1.0	1.0	1.0	1.0	1.0
1.0	1.0	1.0	1.0	1.0	1.0	1.0
1.0	1.0	1.0	1.0	1.0	1.0	1.0

Fig. 10 - Radial example, water saturations at 30 days.

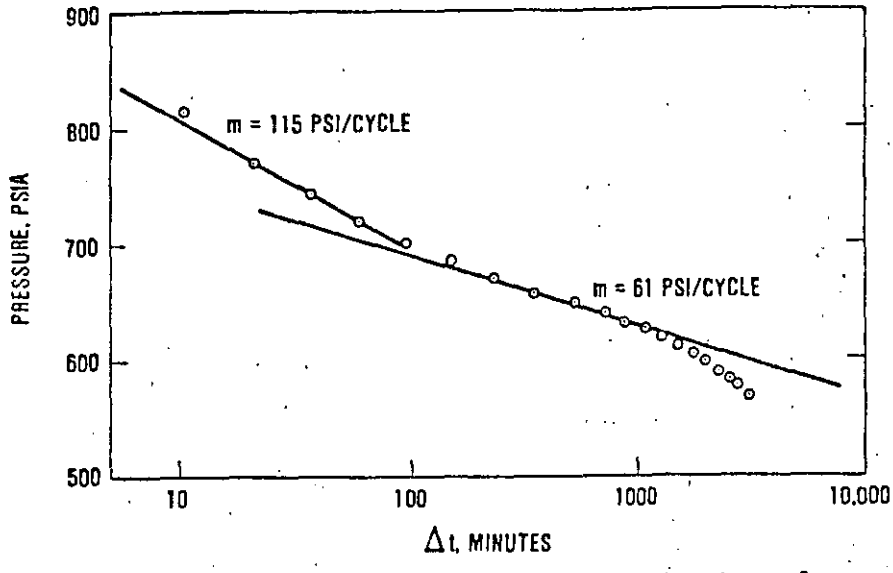

Fig. 11 - Radial example, analysis of drawdown data.

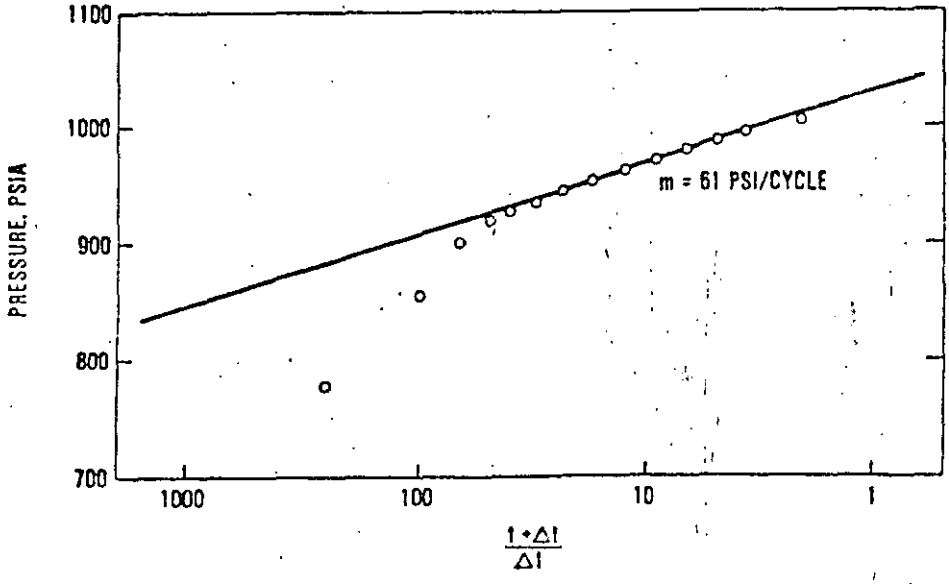

Fig. 12 - Radial example, Horner analysis of buildup data.

CURSO: "INGENIERIA DE YACIMIENTOS GEOTERMICOS"
13 DE MARZO AL 18 DE MAYO DE 1984

TEMA: "THE BEST USES OF NUMERICAL SIMULATORS"

DR. GUILLERMO DOMINGUEZ
2-13 de abril

CURSO: " INGENIERIA DE YACIMIENTOS GEOTERMICOS "
13 DE MARZO AL 18 DE MAYO DE 1984

TEMA: "GEOTHERMAL RESERVOIR ENERGY RECOVERY-
A THREE-DIMENSIONAL SIMULATION STUDY
OF THE EAST MESA FIELD".

DR. GUILLERMO DOMINGUEZ
2-13 de abril

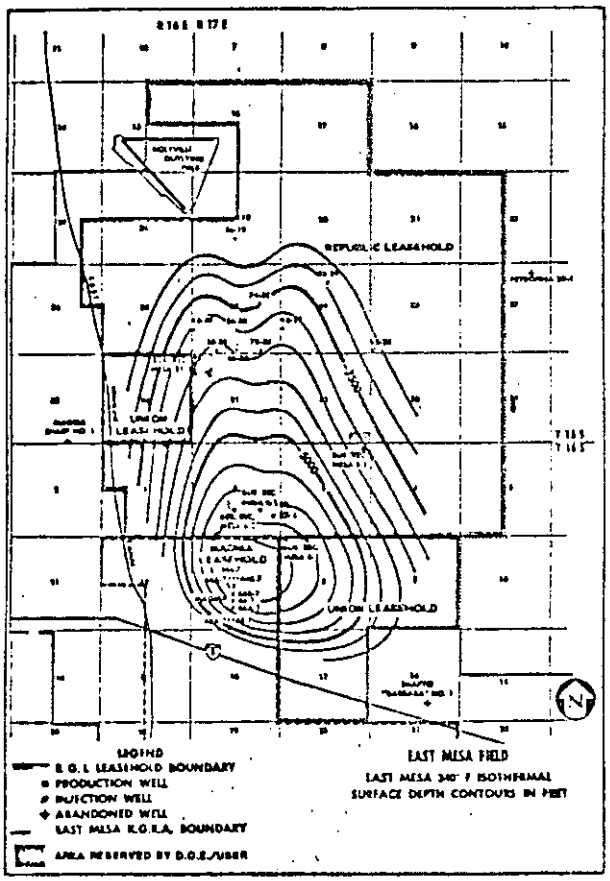

Fig. 1 – East Mesa field.

The use of average porosity values in the simulation model that are weighted to include the bulk volume of the intervening discontinuous shale layers is intended to compensate for the inability of present simulators to model discretely a great number of layers. By modeling the reservoir as all sand but including the shale rock volume with an assumed zero porosity in the average for the gross interval, it is possible to model both the correct fluid storage capacity and total heat content. This model assumes there is essentially instant temperature equilibration between the sand matrix and the adjacent shales. It has been found from layered cross-sectional model studies that shale layers of the order of 30 ft (9.1 m) or less equilibrate very rapidly with adjacent sand layers. The shales at East Mesa have a geometric mean thickness of less than 5 ft (1.5 m) and, therefore, always will be essentially in thermal equilibrium with sand layers which carry fluid.

The permeability values in Table 1 are based on the calibration of logs with laboratory core measurements using air. To relate such values to the underground flow of geothermal waters, it is normal reservoir engineering practice to apply a reduction factor based on measured performance. Recent production well tests and pressure interference tests performed by Republic and Lawrence Berkeley Laboratory[2] have shown that the average permeability-thickness (kh) in the area of the existing producers is about 30,000 md-ft (9144 md·m). In addition, the permeability-thickness appears to increase to the north, away from the center of the thermal anomaly located to the south. Results for Wells 38-30, 56-30, and 16-29 indicate good flow capacity in the producing interval with an average kh greater than 30,000 md-ft (9144 md·m). However, the two producers located on the southern edge of the currently developed area show a reduced flow capacity potential. These wells, 78-30RD and 58-30, have an average permeability-thickness of only 18,000 and 10,000 md-ft (5486 and 3048 md·m), respectively.

As field development continues to the north, it is

TABLE 1 – EAST MESA PETROPHYSICAL PROPERTIES FROM LOG AND CORE ANALYSES*

	Depth Interval (ft)											
	2,500 to 4,500			4,500 to 5,500			5,500 to 7,000			7,000 to 8,000		
Well	h (ft)	ϕ (fraction)	k (air) (md)	h (ft)	ϕ (fraction)	k (air) (md)	h (ft)	ϕ (fraction)	k (air) (md)	h (ft)	ϕ (fraction)	k (air) (md)
Producers												
16-29	N/A	N/A	N/A	606†	0.18	98	1,039	0.16	41	372†	0.10	8
16-30	740	0.10	93	586	0.16	90	952	0.16	63	507†	0.10	14
38-30**	1,044	0.14	186	620	0.18	277	1,119	0.21	353	403	0.10	23
56-30	998	0.13	49	607	0.15	85	1,014	0.17	64	136†	0.04	1
58-30	1,109	0.11	124	623	0.12	70	921	0.13	11	82†	N/A	N/A
78 30 RD	959	0.13	100	527†	0.13	38	1,268	0.21	69	206†	0.08	2
74-30	1,043	0.16	1,025	693	0.21	765	1,015	18	145	334†	0.11	3
Injectors												
18-28	N/A	N/A	N/A	342†	0.21	864	0.17	470	374	0.09	45	876
52-29	1,288	0.17	157	N/A	N/A	N/A	N/A	N/A	N/A	N/A	N/A	N/A
56-19	792	0.12	427	N/A	N/A	N/A	N/A	N/A	N/A	N/A	N/A	N/A

*Porosity and permeability values weighted to include shale content.
**k values for Well 38-30 considered to be anomalously high, not used in simulation model averages.
†Log analysis data not available for complete interval, average petrophysical properties assumed over interval.
Note: Rock properties: Thermal conductivity = 36 Btu/ft-D-°F.
Heat capacity = 35 Btu/cu ft-°F.
Compressibility = 0.000004 psi^{-1}.
Reference temperature = 60°F.

considered reasonable to use an average permeability-thickness of 30,000 md-ft (9144 md·m) for the producing interval of the model. The actual gross completion interval [5,000 to 7,500 ft (1524 to 2286 m)] in the existing wells contains about 1,500 ft (457 m) of net sand; thus, the "measured" permeability is about 20 md. This is significantly lower than the average air permeability obtained by log analyses for this interval (even after excluding the anomalously high permeability values from Well 38-30). Thus, Table 1 values for the 5,500- to 7,000-ft (1676- to 2134-m) interval in the producers (the completion interval in the model) were multiplied by a proportional correction factor to yield an average of 30,000 md-ft (9144 md·m). All other Table 1 values were "normalized" similarly using the same factor for input in the model.

The division into four porosity/permeability intervals for simulation purposes is arbitrary inasmuch as there is little vertical distinction in properties within the planned injection/production intervals between 2,500 and 7,000 ft (762 and 2134 m). Sand/shale layering is present, but layers are not generally continuous between wells and modeling as a series of discrete layers is unwarranted, even if it were feasible. Fig. 2 illustrates the complex structure with an east-west cross section through several of the wells at the northern end of the field. Marker horizons are well-defined shales which can be correlated from well to well but generally are displaced by faulting.

Good horizontal and vertical communication actually exists due to (1) the sand-dominated deltaic depositional environment which provides a primary horizontal stratigraphic continuity, with sufficient cut and fill present to interrupt the thinner shale interbeds, (2) the system of penecontemporaneous normal growth faults which vertically disturb and dislocate the sediments, thereby increasing the means for vertical fluid communication, (3) the post-depositional folding and doming in this area which promotes the propagation of vertical tensional cracks, and (4) the more recent near-vertical lateral faults which further vertically disrupt the dominantly sandstone/siltstone lithologic assemblage.

Temperature

Temperature surveys have been run in all the Republic East Mesa wells. These temperature measurements are made while the well is shut in and under conditions such that the data is as representative as possible of the static formation temperature at each depth surveyed.

Isothermal surface contour maps covering essentially all of the East Mesa field have been constructed using the static temperature surveys from shallow gradient holes, the 10 deep Republic wells, the five U.S. Bureau of Reclamation wells, and the eight wells drilled by Magma. These maps begin at a temperature of 280°F (138°C) and continue in 20°F (11°C) increments to a temperature of 360°F (182°C). Fig. 1 shows the 340°F (171°C) isothermal surface map. The shape of these surfaces is essentially dome-like, centered south of Republic's leases,

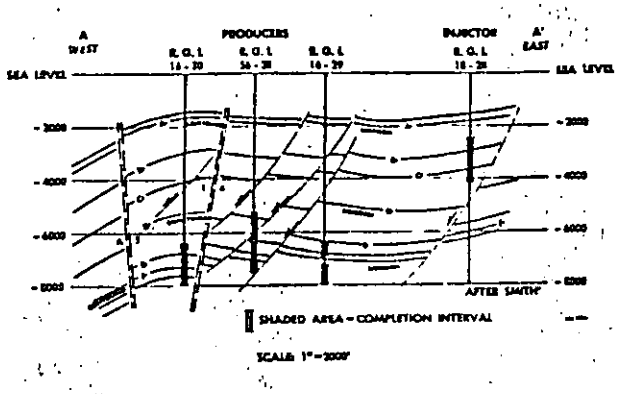

Fig. 2 – East Mesa structural cross section.

and conforms to the positive residual gravity anomaly. Note that the contours have been closed to the north for purposes of the current modeling because no deep well control exists. There is, however, some resistivity, gravity, and shallow temperature hole data that suggest that the resource may continue significantly farther north.

Rock and Fluid Thermal Properties

The thermodynamic and heat transfer properties of the formation overburden, underburden, and reservoir rock are based on typical sandstone and shale values found in the literature (Table 1). The produced water is remarkably fresh, averaging less than 2,000 ppm TDS, and is free of heavy metals which might cause environmental disposal problems. Noncondensable gas content of the fluid is also low – i.e., less than one-tenth of 1 wt% of the total fluid. Therefore, it is reasonable to assume the reservoir fluid to be initially single-phase (no free gas) and to have the physical and thermodynamic properties of pure water.

Simulation Model

The numerical simulator employed in this study was developed by Intercomp Resource Development and Engineering Inc. of Houston. It is a fully implicit, finite difference numerical scheme, coupled with an analytical wellbore model which can solve the multiphase mass flow and energy equations simultaneously for a three-dimensional matrix of several hundred grid points.[3]

Grid

The reservoir properties described in the foregoing were translated into a numerical model for a postulated field development at the northern end of the field intended to support a 64-MW power plant. The grid consists of 600 blocks in an areal pattern as shown in Fig. 3. Note that because of symmetry, only half the proposed field development model actually is simulated. The center line is determined by the center of the temperature isotherms so as to exploit the maximum energy recovery potential of the system. With a symmetric well location pattern, the center line becomes a no-flow boundary. Relatively minor heterogeneous effects on reservoir behavior can be

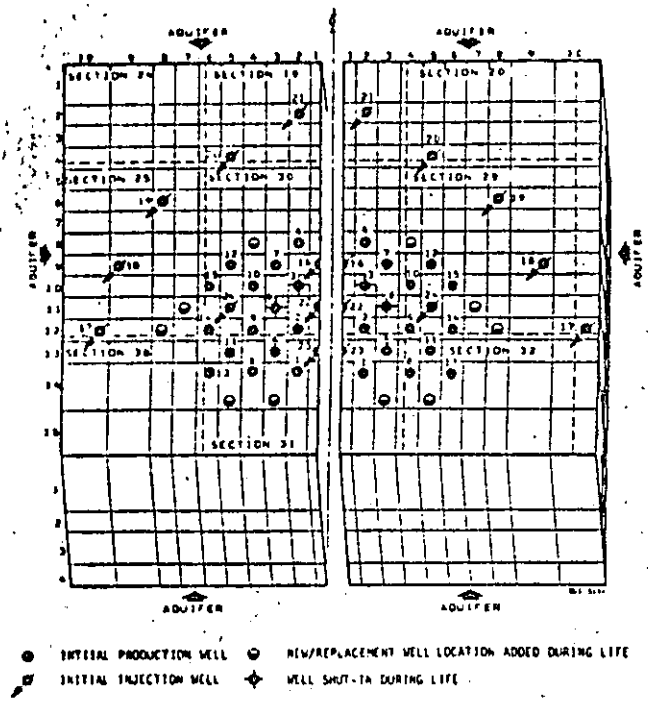

Fig. 3 – Conceptual well location plan – East Mesa reservoir model.

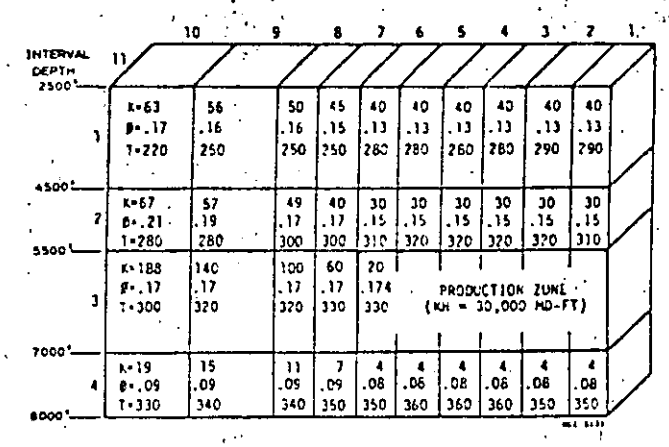

Fig. 4 – East-west cross section of East Mesa reservoir model.

investigated by simulating each half of the field separately; however, this is not now justified.

Except for the southernmost row of producers, each proposed well location is separated by at least one grid block from any adjacent well location. This reduces the numerical stability problems of the finite difference solution. As shown in Fig. 3, the grid pattern has four layers. The injection wells normally are completed in the top layer, and the production wells are completed in the third layer. Thus, a layer is used to separate the two completion intervals vertically. The five interior pattern injectors, however, are completed in both Layers 1 and 3. The production/injection zones are shown as horizontal layers (no dip) but in reality may vary with depth across the field by a few hundred feet (about 100 m).

Fig. 4 is an east/west cross section of the model extending west along the southern boundary of Sections 25 and 30 from the axis of symmetry. Note that the producing interval (Layer 3, Blocks 1 through 6) has a kh of 30,000 md-ft (9144 md·m) with $k = 20$ md and $h = 1{,}500$ ft (457 m). As previously noted, permeabilities above and below Layer 3 were determined from the average log analyses values for existing producers normalized to the value of 30,000 md-ft (9144 md·m). Permeability in Block 10 is based on normalized log analysis values for the existing injectors. Porosities and permeabilities between the core producer area and the peripheral injection area (Blocks 7, 8, and 9) are simply interpolations. Vertical permeability, based on laboratory core measurements, was assumed to be two-thirds of the horizontal permeability. The Layer 3 grid blocks along the southern edge of the production zone have been assigned kh values of 20,000 md-ft (6096 md·m). The reduced permeability in this area is consistent with the increased cementation of the rock matrix and the observed pressure interference data[4] from the U.S. Bureau of Reclamation wells.

Each grid block in the reservoir model is assigned an initial temperature based on the temperature isotherms described in the foregoing section. The specific temperature of a grid block is the temperature at the center of the block. In a production and/or injection well completion grid block, the entire interval is at one temperature. While this may produce an initial temperature distortion in the grid system, long-term production effects are slight.

At this time, the heterogeneity of the reservoir is limited to the petrophysical property and temperature distributions, and no faults or barriers are included. Only one barrier is known to exist (near Well 16-30), but its extent and degree of sealing have not yet been determined. Therefore, the production zone is modeled as being free of sealing barriers.

A final comment on the physical properties of the model involves the individual grid cells which contain the existing wells. Although the average properties of all the wells are used across the production zone, each grid cell that contains an existing well completion is assigned the actual physical characteristics of that well. These properties include production/injection rates, permeability, porosity, and wellbore radius effects. The producing interval (Layer 3) kh is adjusted further to agree with the observed productivity index of each well as determined from field tests. Thus, the productivity of each existing well accurately reflects the actual effects of completion interval and formation damage.

of 0.05 was selected arbitrarily because it provides an accuracy of 0.1 percent. This level of accuracy is easily achieved in pressures obtained by the Hewlett-Packard quartz crystal gauge. Further, it is observed from Figs. 5 and 6 and Tables 2 and 3 that the reservoir boundary starts affecting the mean pressure and drainage-boundary pressure at a dimensionless time of 0.025. A time limit of 0.05, therefore, provides a practical average.

It is stressed that many of the equations presented here, such as Eqs. 5, 7, 9, 14, 20, and 22, are obtained empirically from superposition calculations. Some of these can be derived analytically.

It is worthwhile to discuss the physical implications of f. It was stated earlier that a range of values of f corresponds to the following reservoir situations: (1) $f = 0$, closed reservoir; (2) $f = 1$, full injection or constant-pressure boundary case; (3) $0 < f \leq 0.5$, partial water drive reservoir or an enlarged drainage area; (4) $0.5 < f < 1$, partial fluid injection; and (5) $f > 1$, excess fluid injection.

These interpretations are evident in light of the superposition grid shown in Fig. 1. When f has a value between 0 and 0.5, two grids of producers generate the effect of no-flow drainage boundaries that are farther from the well than when $f = 0$. This can be caused by either a larger drainage area than is known in an otherwise closed reservoir, or a partial water drive condition resulting from a limited aquifer having the same transmissibility (kh/μ) and storage (ϕch) as the reservoir.

When $f = 0.5$, the image grid of injectors in Fig. 1 effectively vanishes because q is zero for every well in the image grid. Therefore, it generates pressures for a well in the center of a closed square that is twice the area of the drainage area assumed in calculating the dimensionless time, t_{DA}. The dimensionless pressures therefore deviate from early-time infinite reservoir, with a straight line at $t_{DA} = 0.1$ instead of 0.05 for the $f = 0$ case. Further, a given value of dimensionless pressure for the $f = 0.5$ case occurs at twice the dimensionless time of the $f = 0$ case. Therefore, a value of $f = 0.5$ implies two reservoir situations: (1) a closed reservoir with twice the area of what currently is known and (2) a water drive reservoir

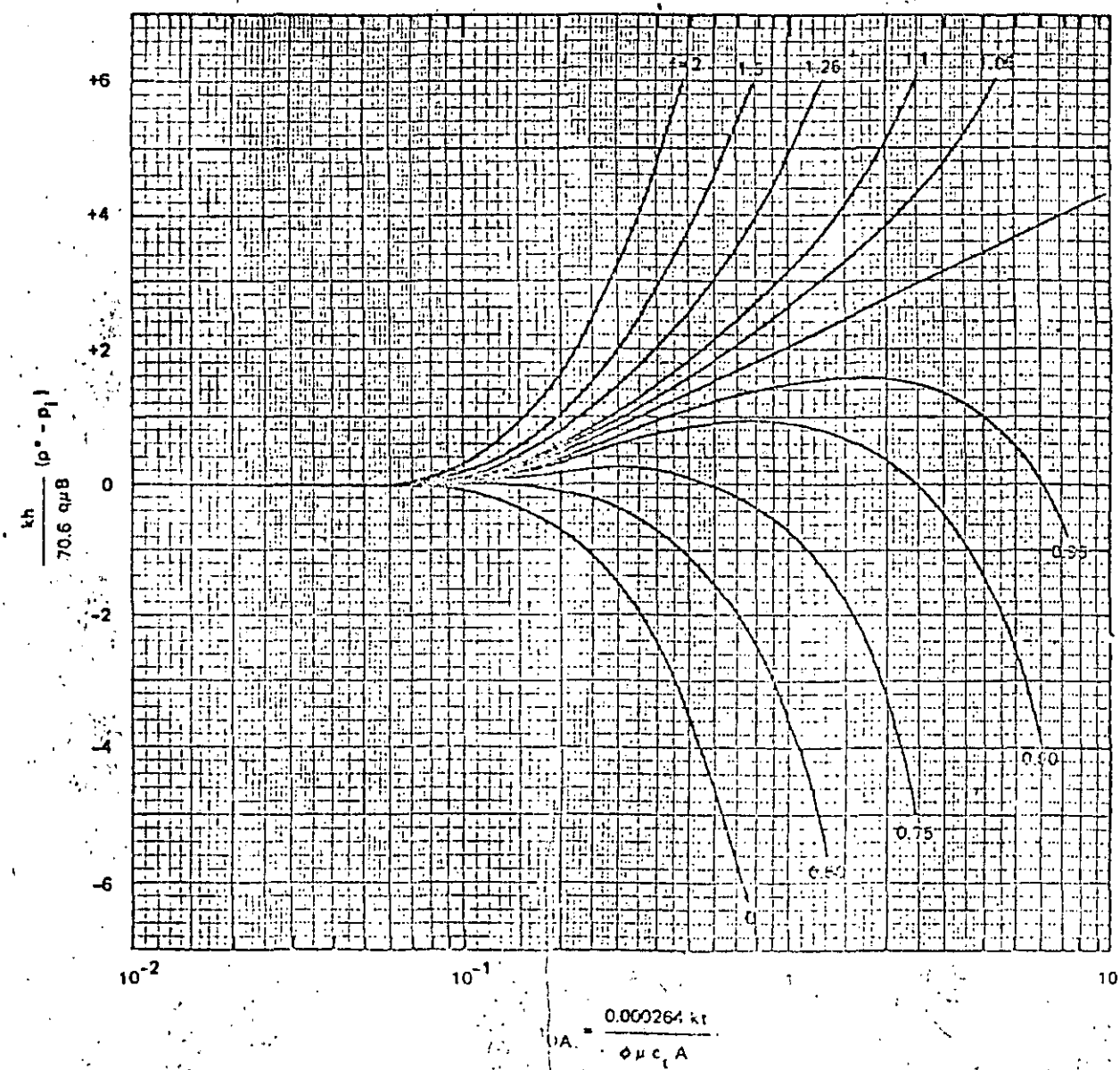

Fig. 10 – Graph of dimensionless $(p^* - p_i)$ group vs producing time for a well in the center of a square reservoir for various f.

an aquifer equal in volume to reservoir having the same transmissibility (kh/μ) and storativity (ϕch) as in the reservoir.

When $0.5 < f < 1$, wells in the image grid in Fig. 1 have a net injection rate less than the production rate. This corresponds to a partial fluid injection system. Therefore, the pressure at the drainage boundary continues to decrease with the producing life of a field.

If a natural water-drive reservoir yields $f > 0.5$, it has to be attributed to a greater transmissibility of fluids in the aquifer as compared with that in the reservoir. Further, in the absence of fluid injection, one always should obtain a value of f less than unity.

It is stressed that this discussion directs attention to only a few interpretations for various values of f, but many more are possible.

Summary and Conclusions

This study has presented a unified general scheme for characterizing well pressure behavior in closed, water drive, and partial, full, or excess fluid injection reservoir systems and the interrelationships that exist among them. Superposition in well rates was used to generate the pressure drawdown and buildup behavior at the central well in a finite square reservoir. The behavior of drainage-area mean pressure and the drainage boundary pressure are also presented as functions of time.

A parameter f is introduced to characterize the strength of water drive or fluid injection. This parameter is determined directly from a graph of the $(p^* - p_i)$ function, shown in Fig. 10. It also can be estimated from buildup pressure behavior using the Horner graph, as well as from drawdown pressure data using Eqs. 5 or 6.

Once f is known, the drainage-area mean pressure, $\bar{p}$, and the drainage boundary pressure, p_e, at any time are determined from Figs. 9 and 11, respectively.

Nomenclature

A = well drainage area, sq ft
B = oil formation volume factor, RB/STB

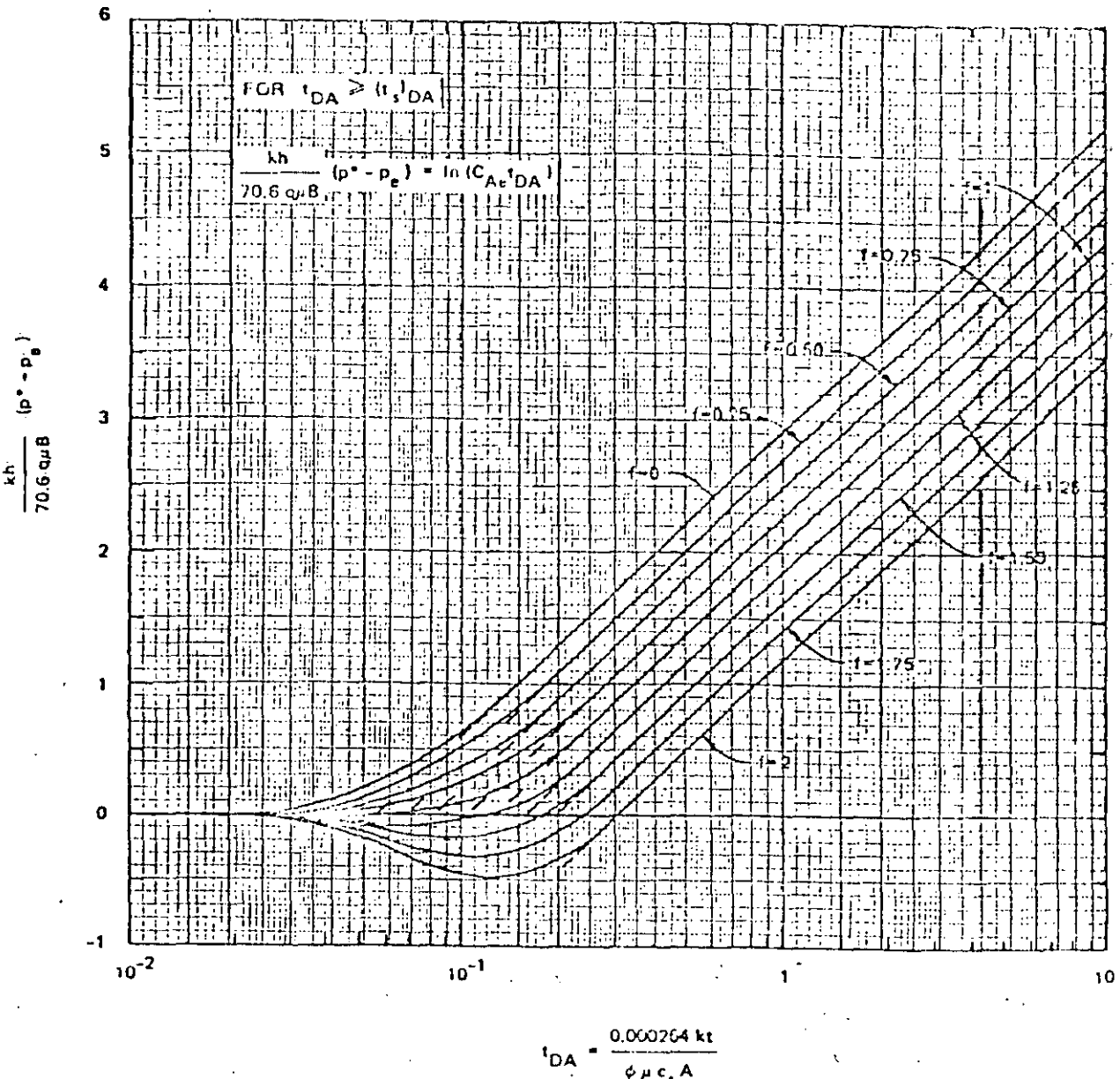

Fig. 11—Graph of dimensionless $(p^* - p_i)$ group vs producing time for a well in the center of a square reservoir for various f.

En forma general, el procedimiento a seguir en el análisis de datos de presión por medio del método de "curva tipo" es el siguiente:

1. Se selecciona la "curva tipo" (Log p_D contra Log t_D) correspondiente a la situación real del pozo.

2. Se grafican los datos de campo, Δp contra Δt en un papel transparente. Para hacer esto debe emplearse la misma escala de la "curva tipo". Es decir, el papel transparente se superpone en la "curva tipo" y se grafican los resultados de campo empleando esta gráfica. A continuación se encuentra el mejor ajuste posible entre los datos de campo y la "curva tipo", por medio de un desplazamiento en forma vertical y horizontal, manteniendo siempre paralelas las escalas de las dos gráficas. Una vez hecho esto, se elige un punto común o de ajuste a las dos gráficas. Esto se hace leyendo un punto de la "curva tipo" $(p_D)_M$, $(t_D)_M$ y el punto correspondiente en la "curva tipo de campo", $(\Delta p)_M$, $(\Delta t)_M$.

3. Se determinan los parámetros de interés del yacimiento; por ejemplo, de los datos de presión del punto común se puede determinar la permeabilidad, k, y de los datos del tiempo se puede obtener el producto de la porosidad por la compresibilidad, total, ϕc_t. La Ec. 1, para los datos del punto común puede escribirse:

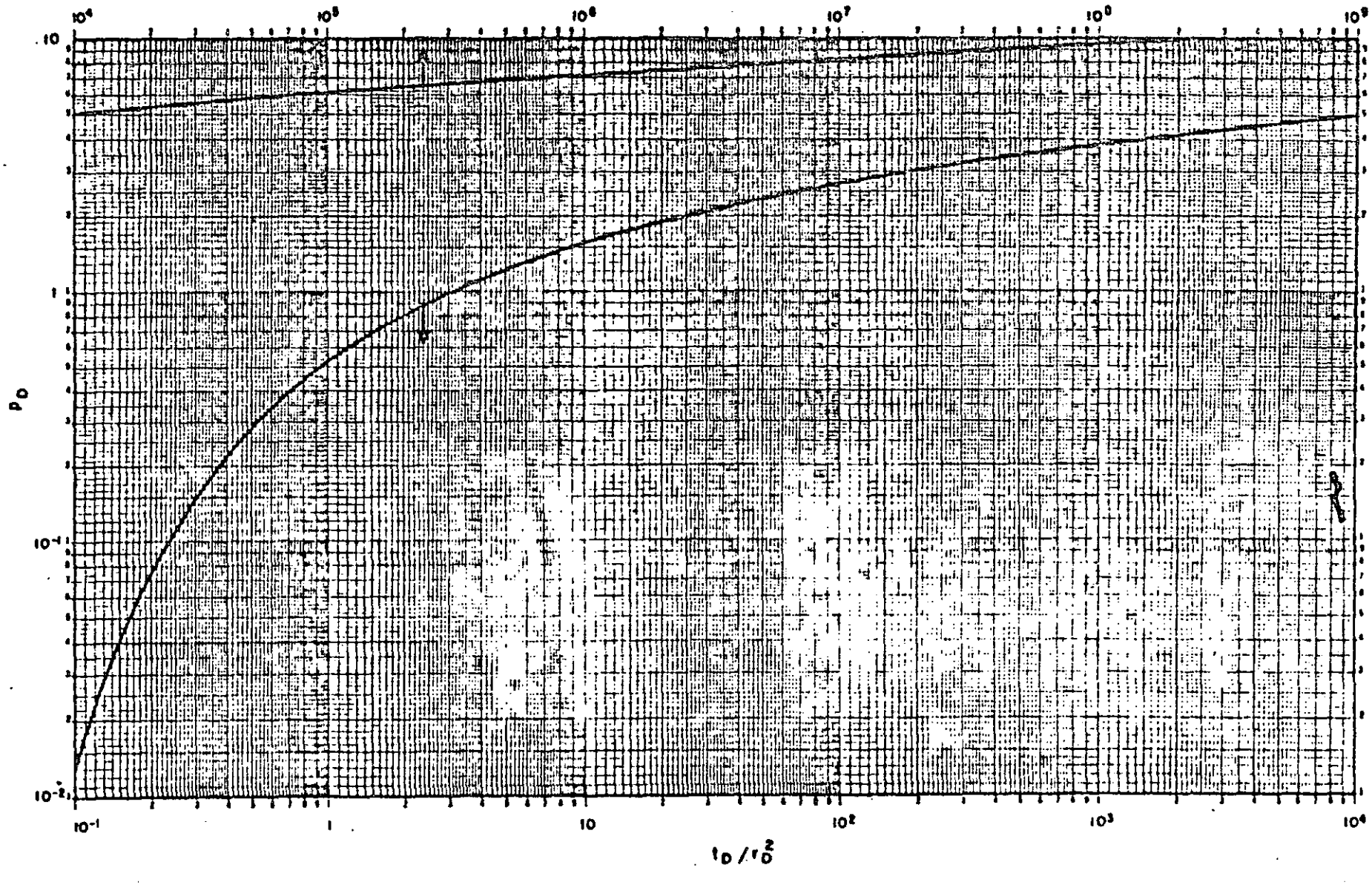

Fig. C.2 Dimensionless pressure for a single well in an infinite system, no wellbore storage, no skin. Exponential-integral solution.

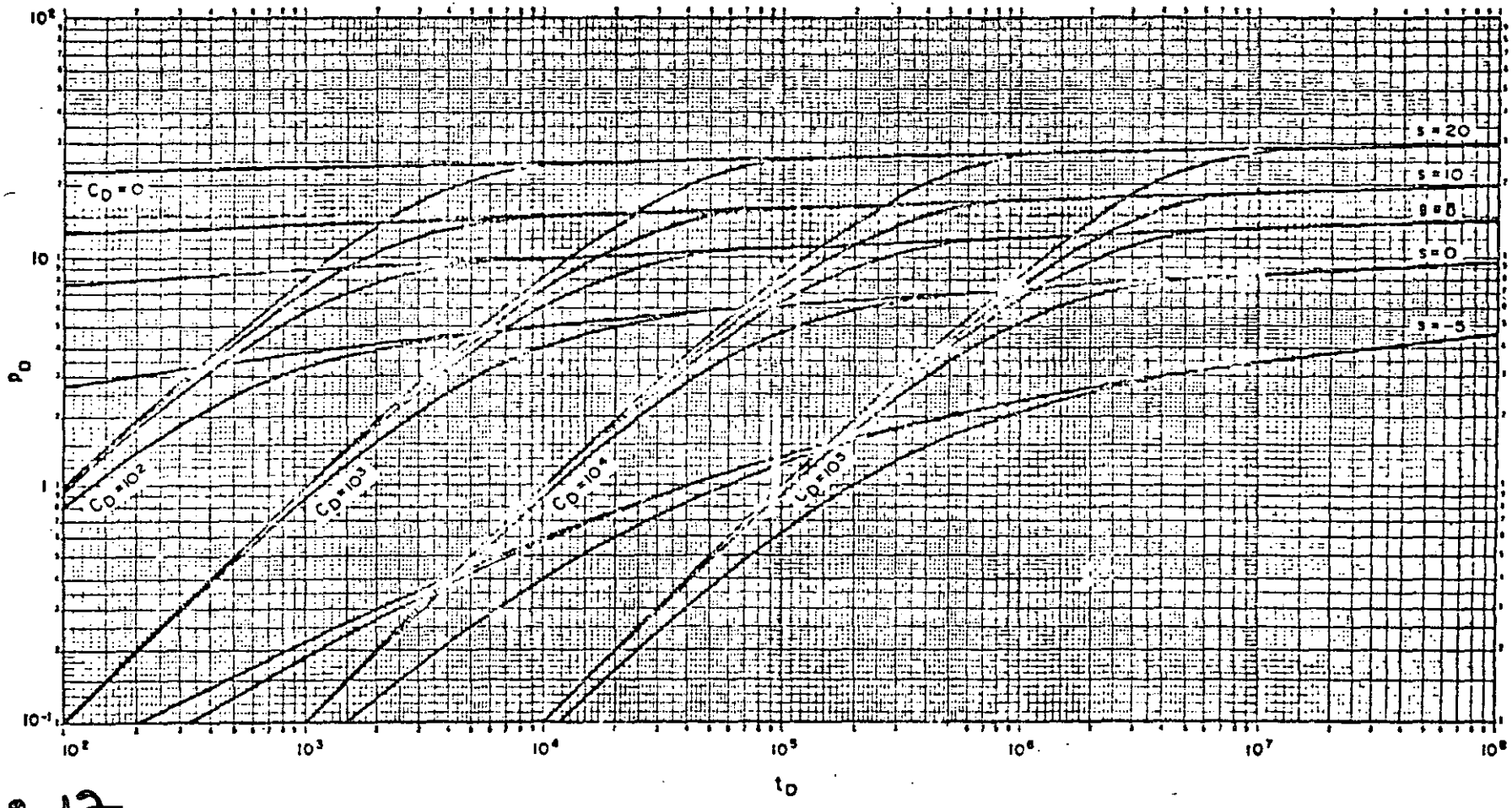

3.12

Fig. C.6 Dimensionless pressure for a single well i... ... finite system, wellbore storage and skin included. After Agarwal, Al-Hussainy, and Ramey.[10] Graph courtesy H. J. Ramey, Jr.

CURSO: INGENIERIA DE YACIMIENTOS GEOTERMICOS"

* SIMULACION NUMERICA DE YACIMIENTOS GEOTERMICOS
PROCEEDINGS SPECIAL PANEL ON GEOTHERMAL MODEL INTERCOM PARISON STUDY

PROF. DR. GUILLERMO DOMINGUEZ V.

ABRIL, 1984

STANFORD GEOTHERMAL PROGRAM
STANFORD UNIVERSITY

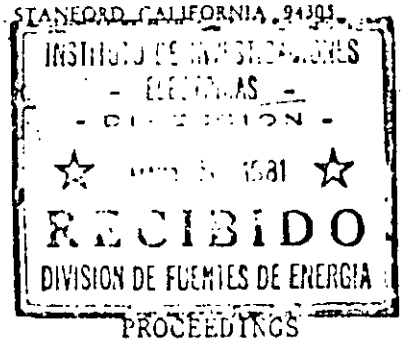

SGP-TR-42

PROCEEDINGS

SPECIAL PANEL ON GEOTHERMAL
MODEL INTERCOMPARISON STUDY

held in conjunction with
The Code Comparison Contracts
issued by
Department of Energy
Division of Geothermal Energy
San Francisco Operations Office

at the
Sixth Annual Workshop on
Geothermal Reservoir Engineering
December 16-18, 1980

Conducted under Contract No. DE-AT03-80SF11459
Department of Energy
Division of Geothermal Energy

TABLE OF CONTENTS

PREFACE

The Stanford Geothermal Program hosts an annual workshop as part of its contract with the Department of Energy to develop reservoir engineering practices for accelerating the commercial development of geothermal resources. The annual workshop has two major objectives: (1) to bring together researchers active in the various scientific and engineering disciplines involved in the study of geothermal reservoirs to review progress and exchange ideas in this rapidly developing field, and (2) to summarize the effective state of the art of geothermal reservoir engineering in a form readily useful to the many government and private agencies involved in the development of geothermal resources. Each annual workshop features a panel analysis of a problem of major interest to the geothermal energy community.

The topic for panel analysis for the Sixth Annual Workshop in Geothermal Reservoir Engineering was selected in conjunction with the Department of Energy to assess the state of development and the appropriate role of geothermal reservoir simulator models in predicting geothermal reservoir performance as it affects investment decisions. The panel analysis was planned as a cohesive session with (1) an introduction on the background of the DOE decision to issue a number of contracts to determine how well existing simulator models can evaluate problems of varying complexity; (2) a report by the authors of the respective problems on how well the existing codes appear to evaluate the problems; (3) a discussion by invited panelists representing various sectors of the geothermal community to respond on how the state of [illegible] geothermal simulators [illegible]

industry needs; and (4) a general discussion by all of the participants with summary reports by three selected rapporteurs.

The Stanford Geothermal Program is making the results of this panel session available as a separate report since the potential role of simulators in geothermal reservoir engineering is large, and the need to encourage further development of simulator models is apparent. The Stanford Geothermal Program hopes that these proceedings will assist in furthering the successful development of these simulator models.

Paul Kruger
Stanford Geothermal Program
March 31, 1981

GEOTHERMAL RESERVOIR ENGINEERING CODE COMPARISON PROJECT

Martin W. Molloy
Geothermal Energy Division
U.S. Department of Energy
1333 Broadway, Oakland, California 94612

Review of the need for geothermal reservoir simulators, begun at the 1978 Stanford Workshop, continues with the results of U.S. Department of Energy (DOE) contracts on comparison of computer codes. The fundamental issue is the appropriate role of simulators in major investment decisions on geothermal projects, such as the construction of a power plant at a specific reservoir.

WHAT

With this session at the 1980 Stanford Workshop, the Department of Energy responds to the geothermal industry's recommendation that reservoir simulators be evaluated and compared. Last year, DOE Headquarters' Division of Geothermal Energy budgeted for a code comparison project. In February 1980, a group of code developers met at DOE's San Francisco Operations Office to design a set of test problems. In the following papers, the designers of these problems will present the results of this Code Comparison Project.

In June, DOE requested proposals to run the problem set on commercially available geothermal reservoir simulators. In September, multiple awards were made to four offerors: Intercomp; Systems, Science and Software; GeoTrans; and Stanford Univ. Negotiations on a fifth contract were unsuccessful. Lawrence Berkeley Laboratory and the University of Auckland have also prepared solutions to the problem set. Final reports containing solutions, descriptions of the simulators, and approaches were delivered to my office in mid-November. Copies can be obtained from USDOE Technical Information Center, P.O. Box 62, Oak Ridge, TN 37830 (Final Report DOE/SF/11451-1).

DOE has not undertaken to evaluate these results, or to certify any of the reservoir simulators. Rather, the final reports were delivered to the problem designers to summarize and comment on the results. The Department supports the Stanford Workshop as the medium for the geothermal reservoir engineering community to become familiar with these results, and to determine their meaning and value.

WHY

Public funds were expended on this project for two reasons: the recommendation of geothermal industry advisors, and the mandate in the geothermal public law.

In May, 1979, the Technical Review Committee on Reservoir Engineering (Nielson, 1979) recommended to DOE that "Model comparison and validation should be a new initiative in the (Geothermal) Reservoir Engineering Program.

An attempt should be made to try all major codes on the same system and compare results with respect to output and efficiency of the code. It was suggested the codes should be run on an actual geothermal system where adequate data exists rather than a hypothetical situation. Suggested areas which could be used for code comparison include Cerro Prieto, Mexico; Wairakei, New Zealand; or Larderello, Italy. A workshop should then be held on the use and limitations of the various codes available..."

The mandate from Congress to the Department of Energy to support this effort is found in the Geothermal Research, Development and Demonstration Act of 1974 (Public Law 93-410, Sections 103(a) and 104(a)). "The specific goals shall include . . . the development of better methods for predicting the power potential and longevity of geothermal reservoirs; (and) . . . the development of reliable predictive methods and control techniques for the production of geothermal resources from reservoirs."

Don Campbell of Republic Geothermal, Inc. has stated the fundamental need as one of establishing the confidence of consultants to banks, utilities, etc. in computer simulation as a basis for investment decisions on major geothermal projects (e.g. power plants). As you know, computer simulation is an established technique in oil and gas investment decisions.

In summary, we seek to learn what the capabilities of geothermal reservoir simulators are, and if they are reliable bases for geothermal investment decisions.

HOW

In defining how to evaluate and compare simulators, DOE turned to code developers and industry users.

A position paper was prepared for DOE Headquarters by John Pritchett (1979) of Systems, Science and Software, to describe mathematical reservoir modeling and geothermal reservoir simulators. Pritchett pointed out that reservoir simulators are tools used in the overall reservoir modelling process whose application to real fields requires considerable engineering judgment and insight. He suggested, as a first step, testing the reservoir simulators alone by setting up a suite of idealized problems designed to fully exercise the codes, thus testing the "tools" rather than the "modellers."

A comprehensive review of geothermal reservoir simulators has been published by Pinder (1979) under the DOE-LBL subsidence research program.

At the December 1979 Stanford Workshop, differences between numerical simulations and observed data at geothermal fields were discussed by Donaldson and Sorey (1979), and several limited applications were proposed. Their paper responded to the questions posed at the 1978 Workshop: whether these simulators are of any real value, and, if so, what are their best uses.

DOE then requested code developers and industry users to validate the need for a Code Comparison Project. This they did, and recommended that a set of standard problems be defined for that purpose. And, in February, 1980, the code developers met and designed the problem set.

What Next?

In my understanding, the current situation is as follows (Fig. 1):

1) Specific Reservoir and Integrated Model

At operating and developing geothermal reservoirs, field and test data has been used to derive physical properties, their distribution and change over time. These same data form the basis for conceptual model(s) of the reservoir constructed by integrating structural geology, geochemistry and reservoir engineering analyses. Reservoir management strategies (flash, pump, inject, stimulate etc.), selected by the field operator(s), define production and injection operations used to produce the reservoir.

2) Computer Simulator

Fundamental physical processes in geothermal reservoirs have been represented by partial differential equations and assumptions. Several code developers have prepared reservoir simulators to solve these equations. A set of hypothetical reservoir problems has been designed to test the simulators.

3) Reservoir Model and Simulator

With the aid of simulator "tools", matches to actual production data may be achieved. Projections into the future, using possible reservoir management strategies, yield estimates of reserves, production/injection rates and reservoir lifetime. Together with extensive financial and other considerations, these results provide input to investment decisions on the reservoir.

Hopefully, the Code Comparison Project will establish that several reliable reservoir simulator "tools" are now available to the industry. The question remains of how best to engender industry and investment community confidence in the use of geothermal simulators. Perhaps acceptance of numerical simulation will evolve gradually, as more field studies are made which build a track record for the methodology.

Has DOE satisfied the concerns that led the geothermal industry to recommend that this effort be undertaken? Are consultants to major geothermal projects sufficiently confident to start using these "black boxes" for investment decisions?

If not, I invite you to define the tasks, the geothermal reservoir, and the sources of data that are needed. Will the next step be carried out by the industry, or do you recommend that DOE participate in a joint effort?

Acknowledgement

It is a pleasure to acknowledge the contributions of John Pritchett, Karsten Pruess, Michael Sorey, Michael O'Sullivan, Leland Mink and Marshall Reed in defining the code comparison project. Their concern with the relation between simulators and reservoir assessment has deepened my understanding, and increased the effectiveness of this effort.

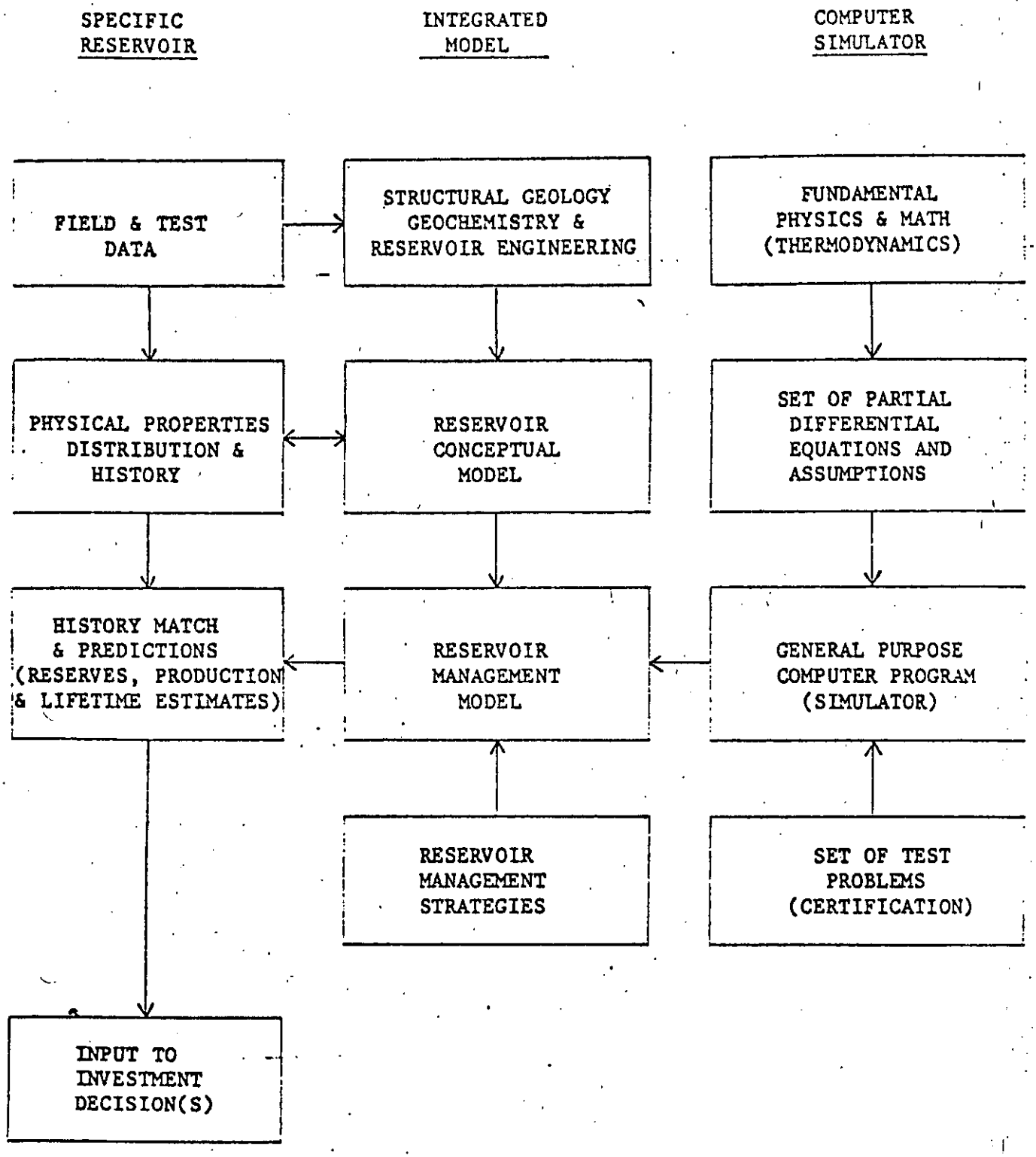

Figure 1. Design and Application of Reservoir Simulators.

References

Donaldson, Ian G., and Sorey, Michael L., "The Best Uses of Numerical Simulators", Fifth Annual Workshop on Geothermal Reservoir Engineering, Stanford Geothermal Program, Stanford Univ., Dec. 1979.

Nielson, D.L. ed., "Program Review, Geothermal Exploration and Assessment Technology Program, Including a Report of the Reservoir Engineering Technical Advisory Group", Earth Sciences Laboratory University of Utah Research Institute, Salt Lake City, Utah; Dec. 1979.

Pinder, George F. and Golder Associates, "State-of-the-Art Review of Geothermal Reservoir Modeling, Geothermal Subscience Research Management Program, Lawrence Berkeley Laboratory, LBL-9093, GSRMP-5, UC-66a, March 1979.

Pritchett, J.W., "Position Paper; Mathematical Reservoir Modeling Using Numerical Reservoir Simulators as Applied to Geothermal Systems", Aug. 1979 (unpublished).

EXHIBIT I

PROBLEM SET

The Contractor shall provide solutions to the problems included herein. Work shall be accomplished in accordance with the terms and conditions of this contract and with the Contractor's proposal submitted in response to Request for Proposal (RFP) No. DE-RP03-80SF10844.

If possible within the project budget, although not a requirement of this contract, problem set #6 will be addressed to illustrate the capabilities of the Contractor's code, but a complete solution will not be provided.

PROBLEM STATEMENT

#1. 1-D Avdonin Solution

PHYSICAL DESCRIPTION

This problem involves one-dimensional, radial, steady-state flow, and unsteady heat transport in a single-phase liquid. The purpose is to test heat conduction and convection in the single-phase compressed water region.

PROBLEM SPECIFICATIONS

Water at 160°C is injected into the fringe of a geothermal reservoir of temperature 170°C. This problem looks at one well and assumes a quasi steady-state flow field is set up very rapidly. The boundary conditions for flow are: injection rate, q - 100kg/sec, specified at the well face, and pressure = 50 bars at an outer radius of 1000m. For heat transport, the temperature at the well face is 160°C and at the outer radius is 170°C. Initial temperature is 170°C everywhere in the reservoir, and the initial pressure is 50 bars. Boundary conditions and initial conditions are shown below.

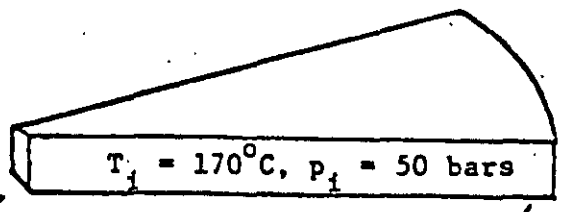

at $r = r_w = 0.0$

$T(t) = 160°C$

$q = 100$ kg/sec

at $r = R = 1000$m

$T(t) = 170°C$

$p(t) = 50$ bars

Properties

permeability = $10^{-12} m^2$

density rock = 2500 kg/m^3

specific heat of rock = 1.0 $J/g.^{\circ}C$

thermal conductivity = 20 $W/m.^{\circ}C$

reservoir thickness = 100m

porosity = .2

Thermal properties for water

provided by modeler

specify constants: specific heat, viscosity and density of water ($165^{\circ}C$, 50 bars).

Numerical grid and time step data

time steps = 1.67×10^7 sec

grid spacing = 25m

OUTPUT SPECIFICATIONS

1) Temperature versus radial distance at 10^9 sec (60 time steps)
2) Take node at r = 37.5m and give solution of temperature versus time.

COMMENTS

For constant density, viscosity, and heat capacity of water, an analytical solution is available for this problem. For example, this solution is a limiting case of the problem solved by Avdonin, 1964.

Reference

Avdonin, N.A., 1964, Some formulas for calculating the temperature field of a stratum subject to thermal injection: Meft'i Gaz, v. 3, p. 37-41.

10

PROBLEM STATEMENT

#2. 1-D Well Test Analysis

PHYSICAL DESCRIPTION

This problem involves a set of three constant discharge, transient well test cases. Each case has 1-D radial flow to a line sink (zero radius well) in a homogeneous porous media. In Case a the fluid is single-phase liquid; in Case b the fluid is a two-phase mixture with both water and steam mobile; and in Case c the fluid changes from compressed liquid to a two-phase mixture as a flash front propogates away from the well. For each case, either an exact analytical solution (Theis solution) or an accurate semi-analytical solution is available for comparison with numerical solutions. Solutions will consist of pressure, saturation, and flowing enthalpy changes as functions of t/r^2 (time/distance squared).

PROBLEM SPECIFICATIONS

The following initial and boundary conditions and parameter values are to be used:

Specification	Case a	Case b	Case c
Initial pressure (bars)	90	30	90
Initial liquid saturation	1	.65	1
Initial temperature (^{o}C)	260	233.8 1/	300
Porosity	.20	.15	.20
Permeability ($10^{-12}m^2$)	.01	.24	.01
Thickness (m)	100	100	100
Discharge (kg/s)	14.0	16.7	14.0
Rock heat capacity (kJ/m^3^{o}C)	2650	2000	2650
Rock compressibility	0	0	0
Relative permeability functions 2/	1-ph	Corey	Corey
Rock thermal conductivity	0	0	0

1/ Saturation temperature at 30 bars

2/ $k_{rw} = [S^*]^4$, $k_{rs} = [(1-S^*)^2] \cdot [1 - (S^*)^2]$, $S^* = [(S - .3)/(.65)]$,

S = liquid saturation

NUMERICAL SOLUTIONS

Analytical results for each case indicate that solutions for pressure, saturation, and flowing enthalpy are functions of t/r. To minimize computational requirements while avoiding the significant spatial discretization errors, the following nodal arrangement should be used for each case.

$$r_n = 0.5\,(\sqrt{2})^{n-1} \qquad n = 1, 26$$

Total simulation time in each case should be 1 day. For the grid specification given above, an initial time step near 10^{-4} or 10^{-5} days is suggested for accurate solutions at early times.

ONE NODE TWO-PHASE PROBLEM

To facilitate evaluation of numerical solutions for two-phase flow, an additional problem under Case b conditions should be run. It involves 1 grid block with volume = 314 m^3 and constant discharge of 16.7 kg/s for .01 days. A constant time step of 10^{-4} days should be used, and the enthalpy of the discharge fluid should be weighted according to the mobility of each fluid phase (as in Cases b and c).

OUTPUT SPECIFICATIONS

Results for each case, except for the one-node problem, should consist of plots of pressure in bars, liquid saturation (Cases b and c), and flowing enthalpy in kJ/kg (Cases b and c) as functions of log (t/r^2) in days/m^2 for nodal points at 0.5 m, 0.707 m and 1.0 m from the well. The corresponding data in tabular form should also be provided. Data covering 5 log cycles for Cases a and c, and 4 log cycles

for Case b should be included in the plots and tabulations. Specification of the computational grid and time step variation utilized should also be procided. Results for the one-node problem should consist of plots of pressure, liquid saturation, and discharge enthalpy versus time, along with the corresponding data tabulations.

PROBLEM STATEMENT

#3. 2-D Flow to a Well in Fracture/Block Media

PHYSICAL DESCRIPTION

This problem represents a simplification of the general problem of well testing in fractured geothermal reservoirs. As shown in the following sketch, a well producing at constant discharge is open to a horizontal fracture of infinite lateral extent. Vertical flow in the block and radial flow in the fracture, each obeying Darcy's law,

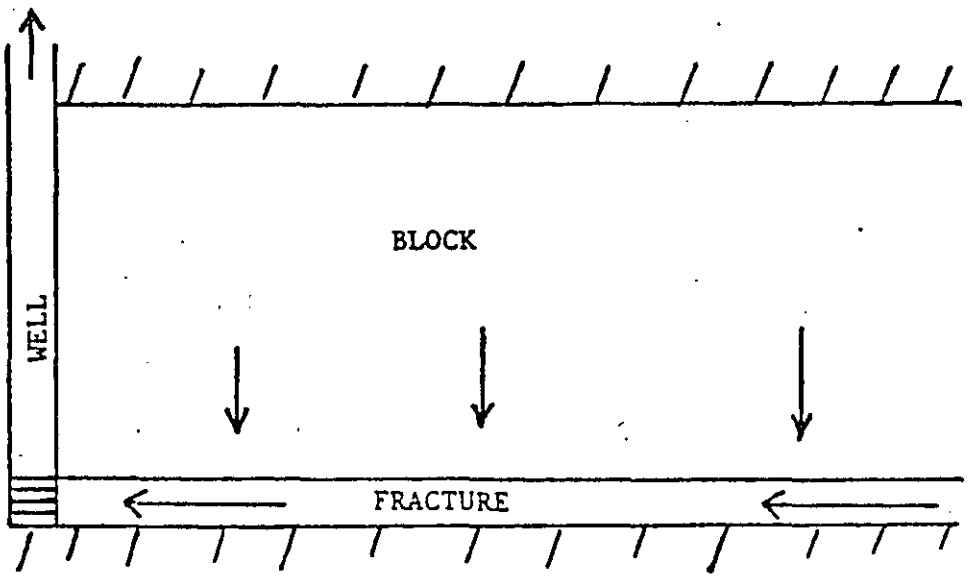

is to be simulated. The upper boundary of the block and the lower boundary of the fracture are impermeable, and the well has a finite radius with well-bore storage.

PROBLEM SPECIFICATIONS

For application to vapor-dominated reservoirs, steam flow in the block and fracture will be simulated. Parameter specifications for two cases are listed below:

Specification	Case a	Case b
Initial pressure (bars)	30.5	30.5
Initial liquid saturation (in block) 1/	0	.2
Initial temperature (^{o}C) 2/	234	234
Porosity in fracture	.1	.1
Porosity in block	.1	.1
Permeability in fracture ($10^{-12}m^2$)	.3	.3
Permeability in block ($10^{-12}m^2$) 3/	.00003	.00003
Thickness of fracture	.1	.1
Thickness of block	1.0	1.0
Well discharge (kg/s)	.028	.028
Well radius (m)	.16	.16
Rock heat capacity (kJ/m^3^{o}C)	2570	2570
Rock compressibility	0	0
Rock thermal conductivity	0	0

1/ Initial liquid saturation is zero in the fracture in both cases

2/ Saturation temperature at 30.5 bars

3/ Horizontal permeability in block is zero in both cases

In Case a, liquid saturation is zero everywhere (no boiling). In Case b, immobile liquid boils in the blocks but not in the fracture. Relative permeability to steam is 1.0 in both cases.

NUMERICAL SOLUTION

A computational grid consisting of 1 well block, 10 logarithmically-spaced nodes in the fracture, and 100 nodes of equal vertical thickness in the block should be used. For those codes using finite difference techniques, either block-centered or face-centered nodal

patterns could be used provided that nodal positions were approximately the same as those shown below. The porosity and permeability in the well block should be set to 1.0 and 30 x $10^{-12}m^2$ (or larger), respectively.

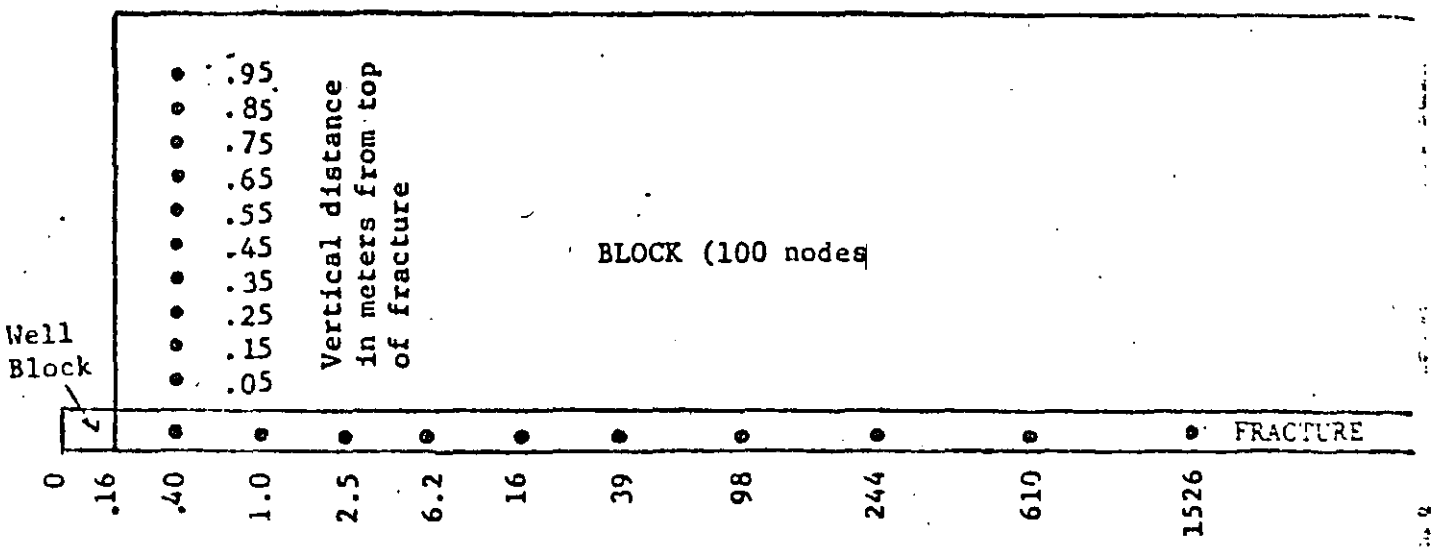

Radial distance in meters from center of well.

Total simulation time should be 10^6s or more, and to define the pressure history at the well face an initial time step of 1 s should be used. Minimum simulation time of 10^6s would be reached in about 130 time steps if a time step multiplication factor of 1.05 were used.

OUTPUT SPECIFICATIONS

Results for Cases a and b should consist of plots of pressure as a function of log (time), along with the corresponding data in tabular form. For each case, plot pressure at the well face, and pressure at a point located 2.5 m from the center line of the well and .25 m above the top of the fracture. Include a tabulation of liquid saturation versus time for this same point in the block under Case b conditions. The required data for each case should cover at least 4 log cycles in time.

PROBLEM STATEMENT

#4. Expanding 2 Phase System with Drainage

PHYSICAL DESCRIPTION

This problem involves 1-D vertical flow under both single and two phase conditions. An initially hydrostatic column of liquid is disturbed by mass withdrawal at the bottom. Boiling occurs in portions of the column, and inflow of cold water is induced at the top.

PROBLEM SPECIFICATIONS

1-D Cartesian (Vertical) Geometry

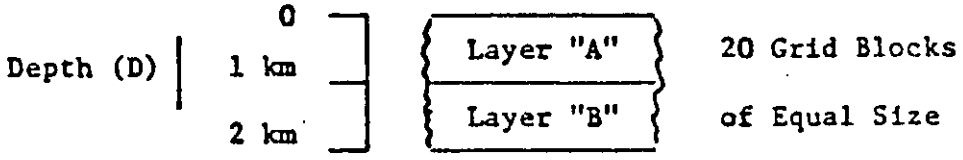

$g = 9.8$ m/s

Rock Properties

	Layer "A" ($0 \leq D \leq 1$ km)	Layer "B" ($1 \text{ km} < D \leq 2$ km)
Grain Density (g/cm^3)	2.5	2.5
Porosity	0.15	0.25
Permeability (m^2)	5×10^{-15}	100×10^{-15}
Heat Capacity ($J/g-^oC$)	1	1
Grain Thermal Conductivity ($W/m - ^oC$)	1	1

Relative Permeability Functions: Corey (as specified in Problem #2)

PROBLEM STATEMENT

#5. Flow in a 2-D Areal Reservoir

PHYSICAL DESCRIPTION

This problem involves multiphase flow in a 2-D horizontal reservoir. Mass is produced at one point in the reservoir, and recharge is induced over one of the lateral boundaries.

PROBLEM SPECIFICATIONS

2-D Areal Geometry

Region is horizontal (gravity neglected; $g_x = g_y = 0$) and of uniform thickness; extends over $0 \leq x \leq 300$ meters, $0 \leq y \leq 200$ meters

Finite - difference zoning as indicated; 12 x 8 grid (96 zones total) of uniform size $\Delta x = \Delta y = 25$ meters.

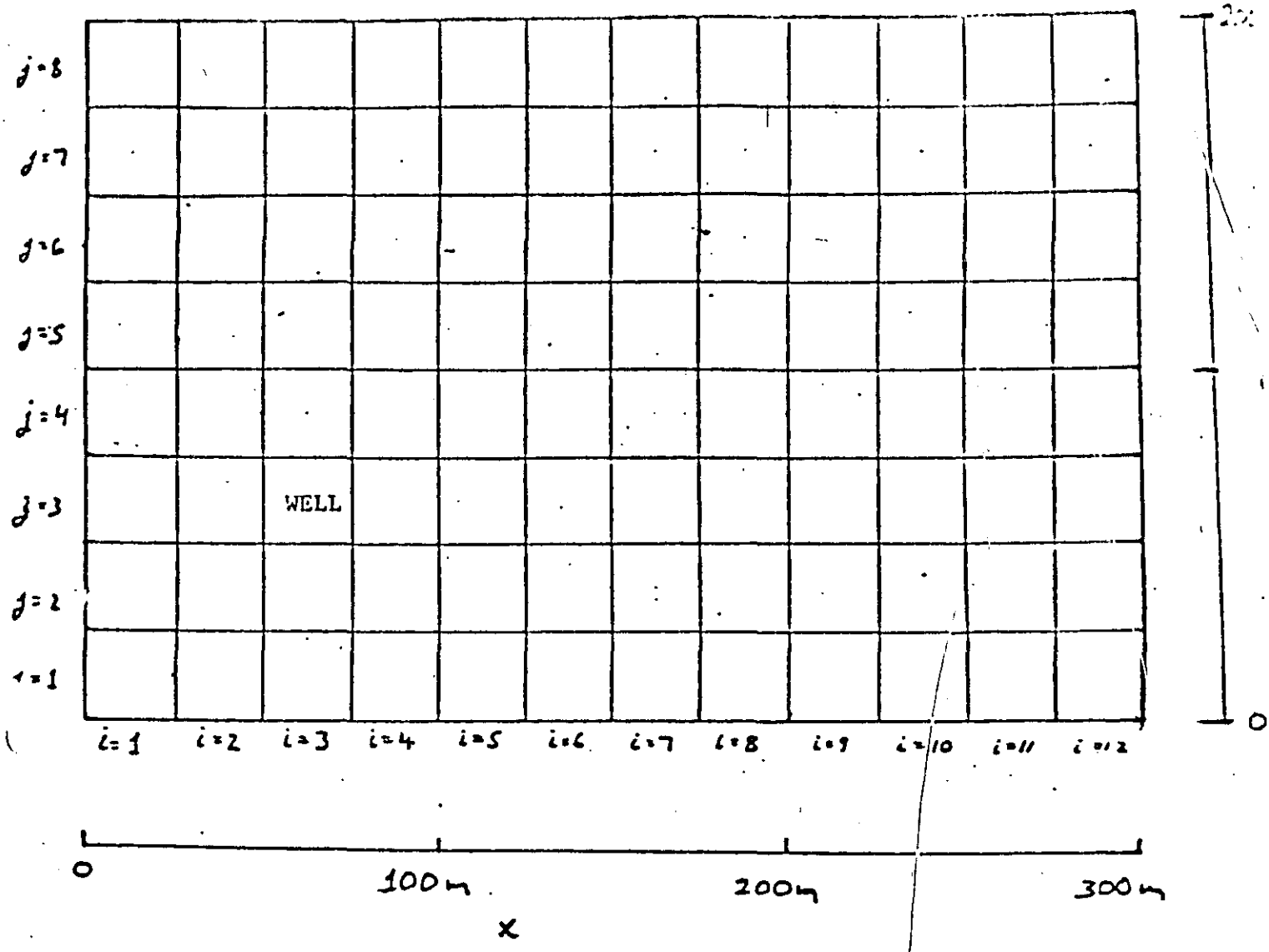

Rock Properties (Uniform over Grid):

Rock Grain Density = 2.5 g/cm^3

Porosity = 0.35

Permeability ($k_x = k_y$) = 2.5 x 10^{-14} m^2

Heat Capacity of Rock Grain = 1 J/g ^oC

Rock Thermal Conductivity = 1 W/m ^oC

Relative Permeabilities -- Corey Equations as in Problem #2 with liquid residual saturation S_{lr} = 0.3, gas residual saturation S_{gr} = 0.1

Boundary Conditions: (See Figure Below)

Impose no convection, no conduction (impermeable, insulated) along:

$y = 0m$; $y = 200m$; $x = 0m$

Maintain initial P, T along $x = 300m$, $0 \leq y \leq 200m$

($P \approx 36$ bars, $T = 160^{\circ}C$); see below

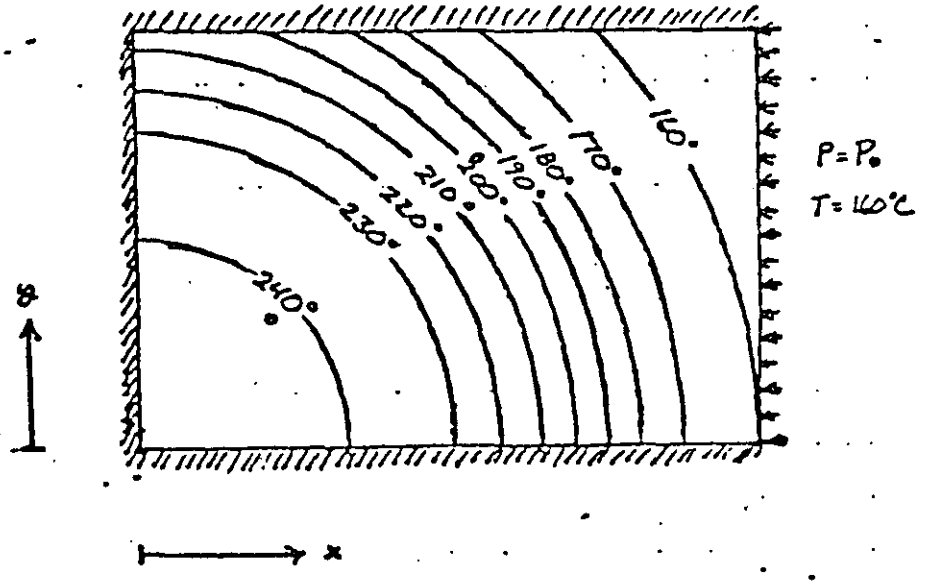

Initial Conditions:

Pressure initially uniform, and equal to saturation pressure at $240^{\circ}C$, plus 2.5 bars:

$$P(t = 0,\ 0 \leq x \leq 300m,\ 0 \leq y \leq 200m) =$$

$$P_{sat}(240^{\circ}C) + 2.5 \text{ bars}$$

Note that $P_{sat}(240^{\circ}C)$ 33.5 bars, so $P_o \approx 36$ bars

Initial temperatures for each zone are provided on the table on the next page. They are given approximately by:

$T(t=o) = 240^{\circ}C$ for $r \leq 100m$

$$= \left[240 - 160 \left(\frac{r-100m}{200m}\right)^2 + 80 \left(\frac{r-100m}{200m}\right)^4\right]^{\circ}C$$

for $100m < r < 300m$

$= 160^{\circ}C$ for $r \leq 300m$

where $r \equiv \sqrt{x^2 + y^2}$

Initial Temperatures (°C) $T_{ij}(t=0)$:

212.07	210.18	206.41	200.81	193.59	185.18	176.31	168.09	162.03	160.00	160.00	160.00
224.92	223.16	219.54	213.95	206.41	197.16	186.79	176.31	167.13	161.12	160.00	160.00
234.31	232.93	229.92	224.92	217.70	208.29	197.16	185.18	173.71	164.58	160.11	160.00
239.31	238.62	236.74	232.93	226.64	217.70	206.41	193.59	180.56	169.11	161.54	160.00
240.00	240.00	239.77	237.76	232.93	224.92	213.95	200.81	186.79	173.71	163.85	160.00
240.00	240.00	WELL 240.00	239.77	236.74	229.92	219.54	206.41	191.85	177.68	166.22	160.26
240.00	240.00	240.00	240.00	238.62	232.93	223.16	210.18	195.36	180.56	168.09	160.77
240.00	240.00	240.00	240.00	239.31	234.31	224.92	212.07	197.16	182.06	169.11	161.12
i=1	i=2	i=3	i=4	i=5	i=6	i=7	i=8	i=9	i=10	i=11	i=12

j

j

j

j

j

j

j

j

Production Strategy for Case A

A fully-penetrating production well is located at x = 62.5m, y = 62.5m (at the center of zone i=3, j=3). Starting at t=o, it produces fluid at the constant rate of 0.05 kilograms/sec-meter of thickness. The well radius is 15 cm and no skin effect is present.

Production Strategy for Case B

A production well is present, identical to Case A. In addition, an injection well is located at x = 162.5m, y = 137.5m, at the center of zone i=7, j=6. The well is fully penetrating, has no skin effect,

and is of radius 15 cm. The injection well is inoperative until $t = 1$ year (3.1536×10^7 sec). Thereafter, it begins injecting water at $T = 80^{\circ}C$ at a rate of 0.03 kilograms/sec-meter of thickness.

OUTPUT SPECIFICATIONS

In both cases, the time domain of interest is--

$$0 \leq t \leq 10 \text{ years } (3.1536 \times 10^8 \text{ sec}).$$

For cases A & B, plot and tabulate:

(1) Pressure history in zones i=3, j=3 and i=7, j=6.

(2) Temperature history in zones i=3, j=3.

(3) History of discharge (flowing) enthalpy in zone i=3, j=3.

(4) Variation with time of total mass of steam in the system per meter of thickness.

Optional (for those with subgrid well model):

(5) What is the sandface pressure history for the production well in cases A & B?

(6) What is the sandface pressure history for the injection well in Case B?

(7) What is the sandface steam saturation history at the production well in cases A & B?

PROBLEM STATEMENT

#6. Flow in a 3-D Reservoir.

PHYSICAL DESCRIPTION

This problem involves flow within a 3-D system, with production from one corner grid block, and constant pressure upper and lower surfaces. The flow is initially single phase liquid, except in one layer where an immobile steam phase exists.

PROBLEM SPECIFICATIONS

3-D geometry, five layer

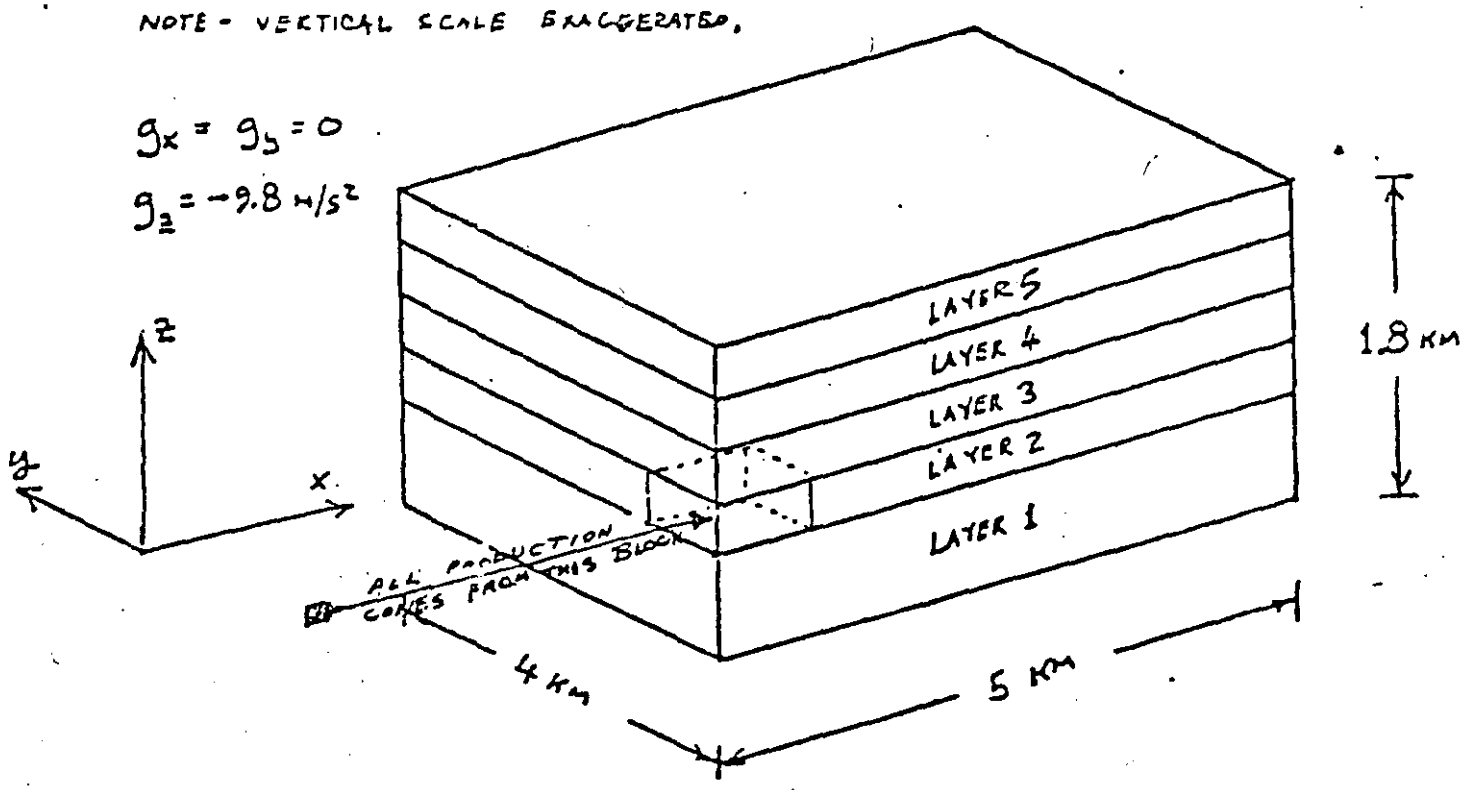

LAYER THICKNESSES:
LAYER 1, 0.6 KM
LAYERS 2-5, 0.3 KM EACH

GRID: 5 x 5 x 5
(Horizontal, uniform, 5 zones each direction

Rock Properties

	Layer 1	Layer 2	Layer 3	Layer 4	Layer 5
Grain Density (g/cm^3)	2.5	2.5	2.5	2.5	2.5
Porosity	0.2	0.25	0.25	0.25	0.2
x-Permeability (m^2)	100×10^{-15}	200×10^{-15}	200×10^{-15}	200×10^{-15}	100×10^{-15}
y-Permeability (m^2)	100×10^{-15}	200×10^{-15}	200×10^{-15}	200×10^{-15}	100×10^{-15}
z-Permeability (m^2)	2×10^{-15}	50×10^{-15}	50×10^{-15}	50×10^{-15}	2×10^{-15}
Heat Capacity ($J/g-^oC$)	1	1	1	1	1
Rock Therm. Cond.($w/m-^oC$)	1	1	1	1	1
Relative Permeability: Corey equations as in Problem #2, except:					
S_{lr} (liquid residual)	0.3	0.3	0.3	0.3	0.3
S_{gr} (gas residual)	0.1	0.1	0.1	0.1	0.1

Initial Conditions

Temperature:

Layers 1-4, 280°C everywhere

Layer 5, 160°C

Pressure:

Layer 4: $P_4^o = P_{sat}$ (280°C) $\tilde{\sim}$ 64 Bars

(Steam saturation) $S_s^o = 0.1$ (steam initially immobile)

Layer 5: $P_5^o = P_4^o - (1470\ m^2/s^2) \times (\rho_4^o\text{-liq} + \rho_5^o)$

Layer 3: $P_3^o = P_4^o + (1470\ m^2/s^2) \times (\rho_4^o\text{-liq} + \rho_3^o)$

Layer 2: $P_2^o = P_3^o + (1470\ m^2/s^2) \times (\rho_3^o + \rho_2^o)$

Layer 1: $P_1^o = P_2^o + (1470\ m/s) \times (\rho_2^o + 2\rho_1^o)$

Where ρ_4^o-liq = liquid density in Layer 4

These initial conditions (P^o, ρ^o, $S_s{}^o$) are functions of z only. Layers 1, 2, 3 and 5 are initially single-phase liquid; layer 4 is initially 2-phase with an immobile steam phase. The pressure distribution is liquid-hydrostatic throughout at zero time.

Boundary conditions

At z = 1.5 km (top surface), maintain $P_{top} = P_5{}^o - (1470\ m^2/s^2) \times \rho_5{}^o$ and $T = 100^oC$.

At z = 0, maintain $P_{bottom} = P_1{}^o + (2940\ m^2/s^2) \times \rho_1{}^o$ and $T = 280^oC$.

Along planes at x = 0 and y = 0, impose symmetry conditions.

Treat plane at y = 4 km as impermeable and insulated.

Along plane at x = 5 km, maintain initial distributions of P, T, S_s.

Production Strategy

All production is taken from a single corner cell (i=1, j=1, k=2).

$0 \leq t \leq 2$ years, $Q(t) = 1000$ kg/s

2 years $< t \leq 4$ years, $Q(t) = 2500$ kg/s

4 years $< t \leq 6$ years, $Q(t) = 4000$ kg/s

$t > 6$ years, $Q(t) = 6000$ kg/s

OUTPUT SPECIFICATIONS

For a total production time of 10 years, plot and tabulate:

Discharge enthalpy history.

Histories of P, T, S_s at x = y = o for each layer.

THE DOE CODE COMPARISON STUDY: SUMMARY OF RESULTS FOR PROBLEM 1

Charles R. Faust, James W. Mercer
William J. Miller
GeoTrans, Inc.
P.O. Box 2550
Reston, VA 22090

INTRODUCTION

The steps in developing a numerical model consist of different levels of error elimination. The first step is to compile the program to remove FORTRAN errors. Next, the numerical solution is compared with analytical solutions to remove logic errors in solving the equation. Numerical solutions are compared with laboratory and field observations to remove logic errors in equations describing the physics. Finally, it is good programming practice to include mass and energy balances as checks that the model is working properly.

Problem 1 satisfies the second step. That is, it is a problem for which there exists an analytical solution. Computed results from the numerical models are therefore compared with the exact analytical results.

PROBLEM DESCRIPTION

This problem involves one-dimensional, radial, steady-state flow and unsteady heat transport in a single-phase liquid. The purpose is to test heat conduction and convection in the single-phase compressed water region.

Water at 160°C is injected into the fringe of a geothermal reservoir of temperature 170°C. This problem looks at one well and assumes a quasi steady-state flow field is set up very repidly. The boundary conditions for flow are: injection rate, q = 10kg/s, specified at the well face, and pressure = 50 bars at an outer radius of 1000 m. For heat transport, the temperature at the well face is 160°C and at the outer radius is 170°C. Initial temperature is 170°C everywhere in the reservoir, and the initial pressure is 50 bars. These boundary and initial conditions are shown in Figure 1. Reservoir properties are given in Table 1.

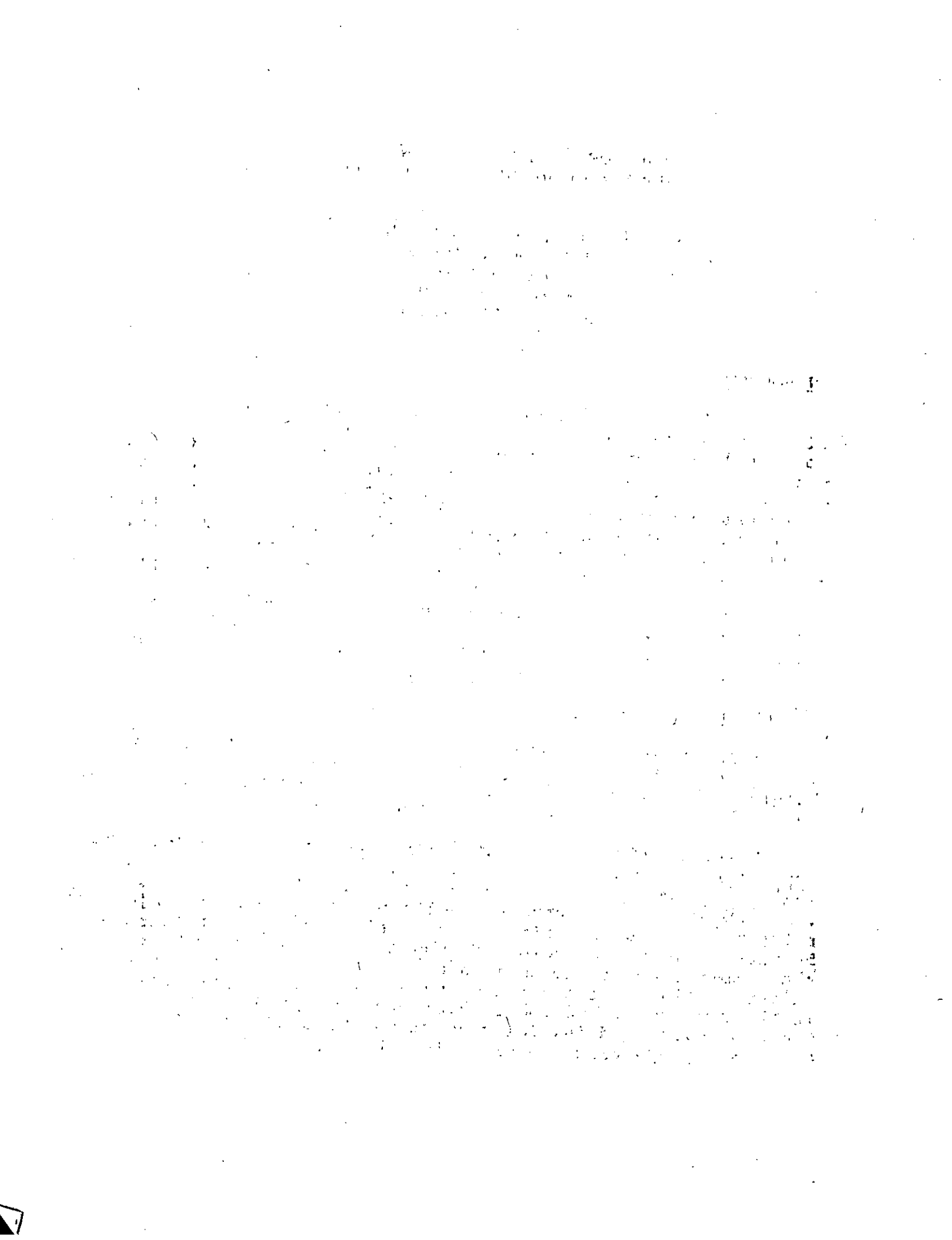

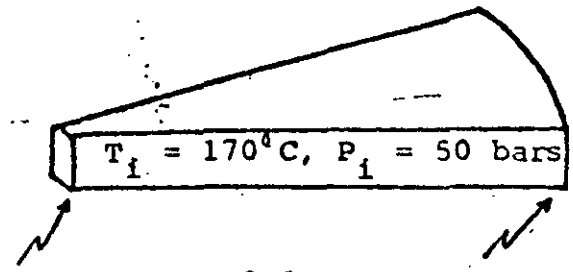

at $r = r_w = 0.0$ | at $r = R = 1000$ m

$T(t) = 160°C$ | $T(t) = 170°C$

$q = 10$ kg/sec | $p(t) = 50$ bars

Figure 1. Boundary and initial conditions for Problem 1.

Table 1. Reservoir properties and output specifications for Problem 1.

Properties

Permeability = $10^{-12}m^2$
density rock = 2500 kg/m^3
specific heat of rock = 1.0 J/g °C
thermal conductivity = 20 W/m °C
reservoir thickness = 100m
porosity = .2

Thermal properties for Water

provided by modeler
specify constants: specific heat, viscosity and density of water (165°C, 50 bars)

Numerical Grid and Time Step Data

time steps = 1.67×10^7 sec
grid spacing = 25m

Output Specifications

1) Temperature versus radial distance at 10^9 sec (60 time steps)

2) Take node at r = 37.5m and give solution of temperature versus time

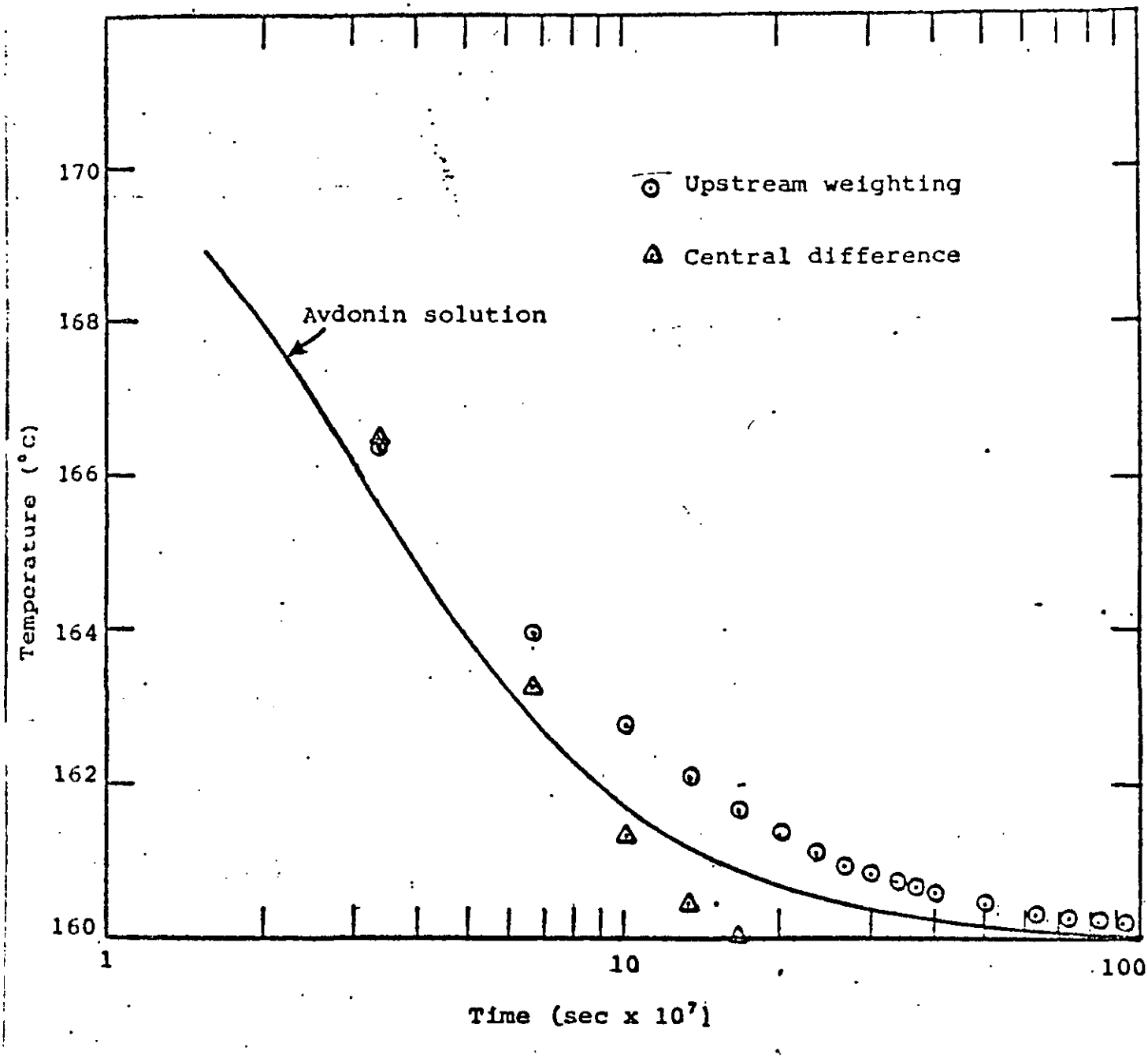

Figure 2. Problem 1, calculated results for node 2 at 37.5 m from injection well.

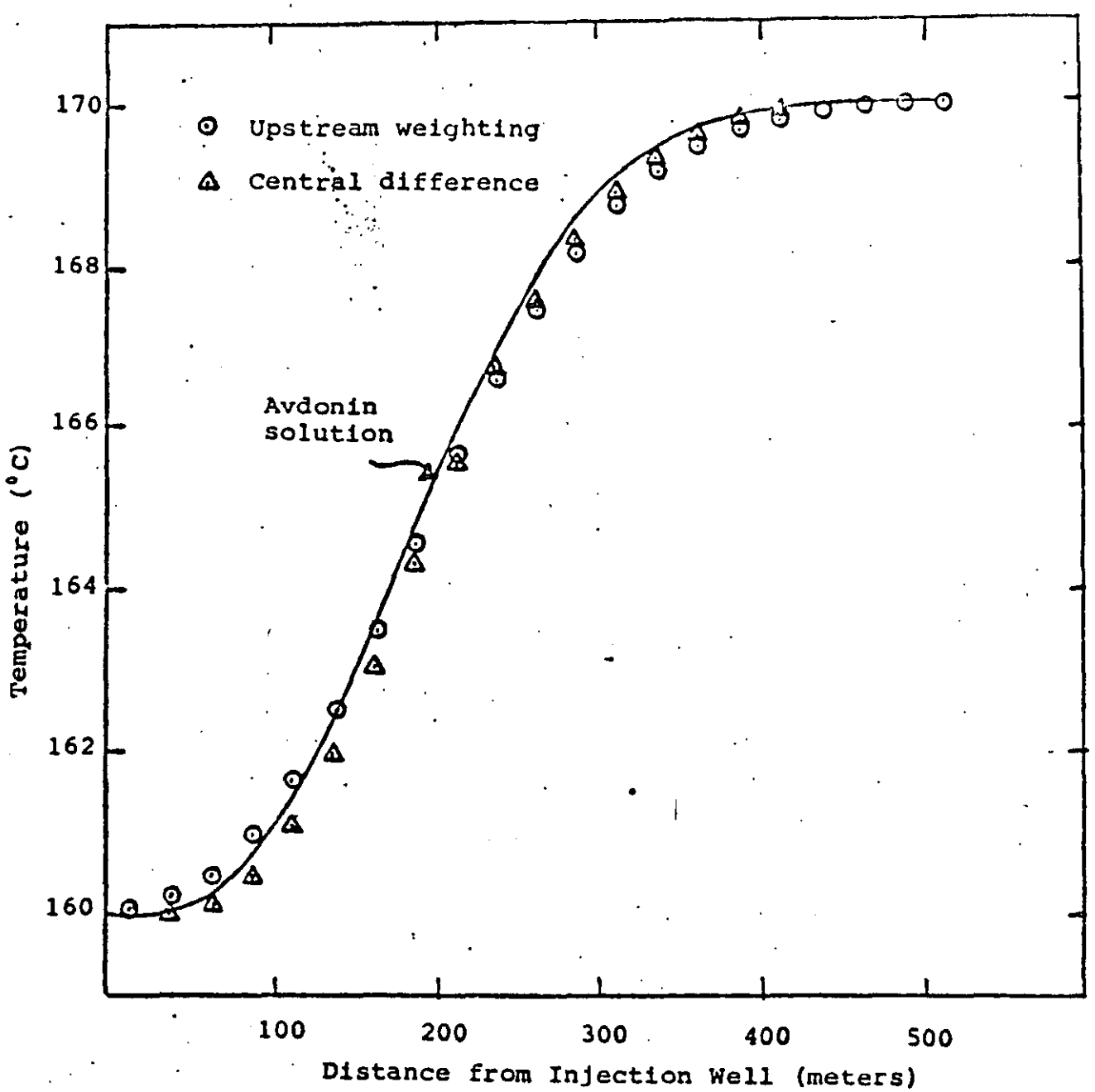

Figure 3. Problem 1, calculated results at time = 10^9 sec.

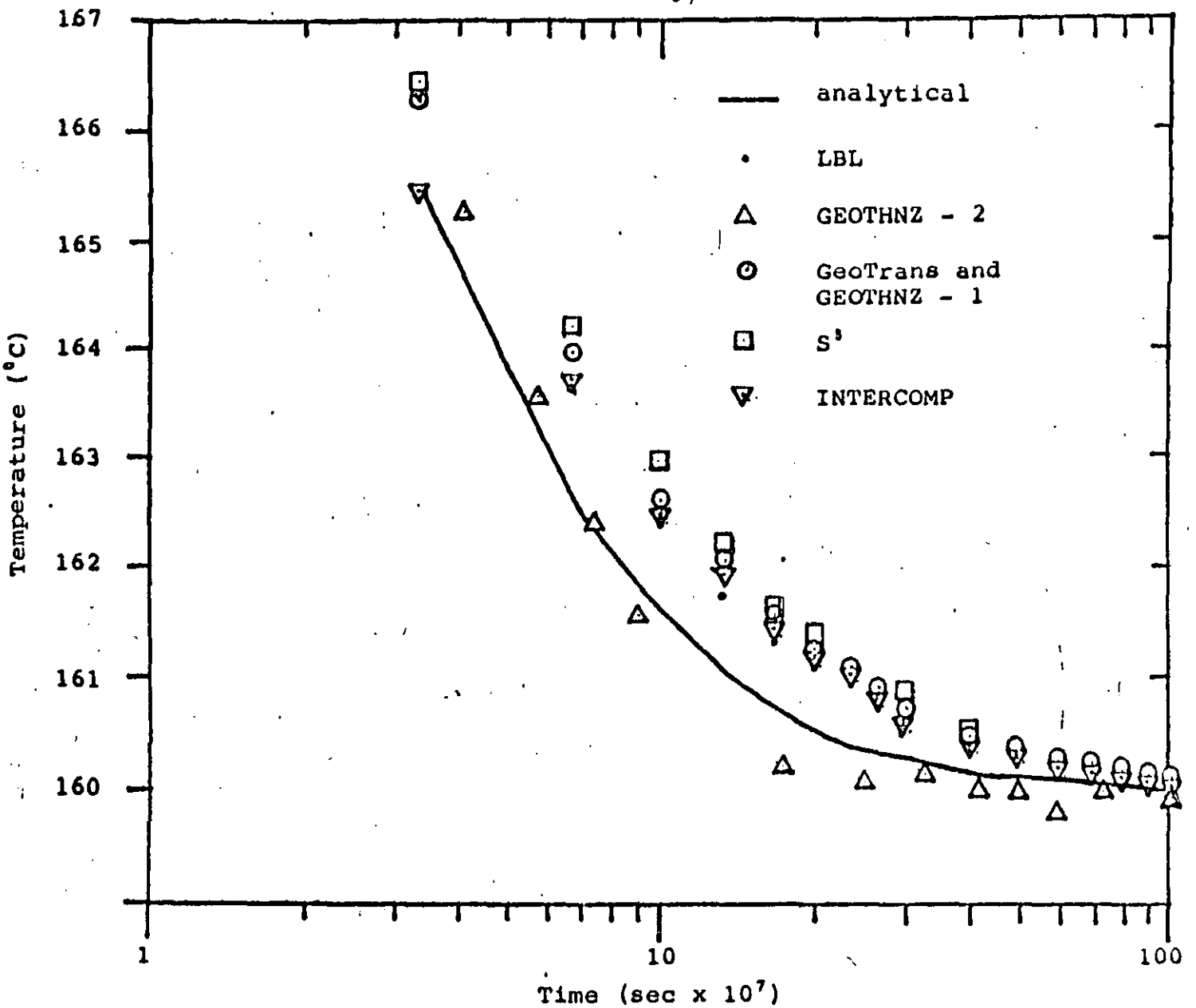

Figure 4. Problem 1, calculated results for node 2 at 37.5 m from injection well for all participants

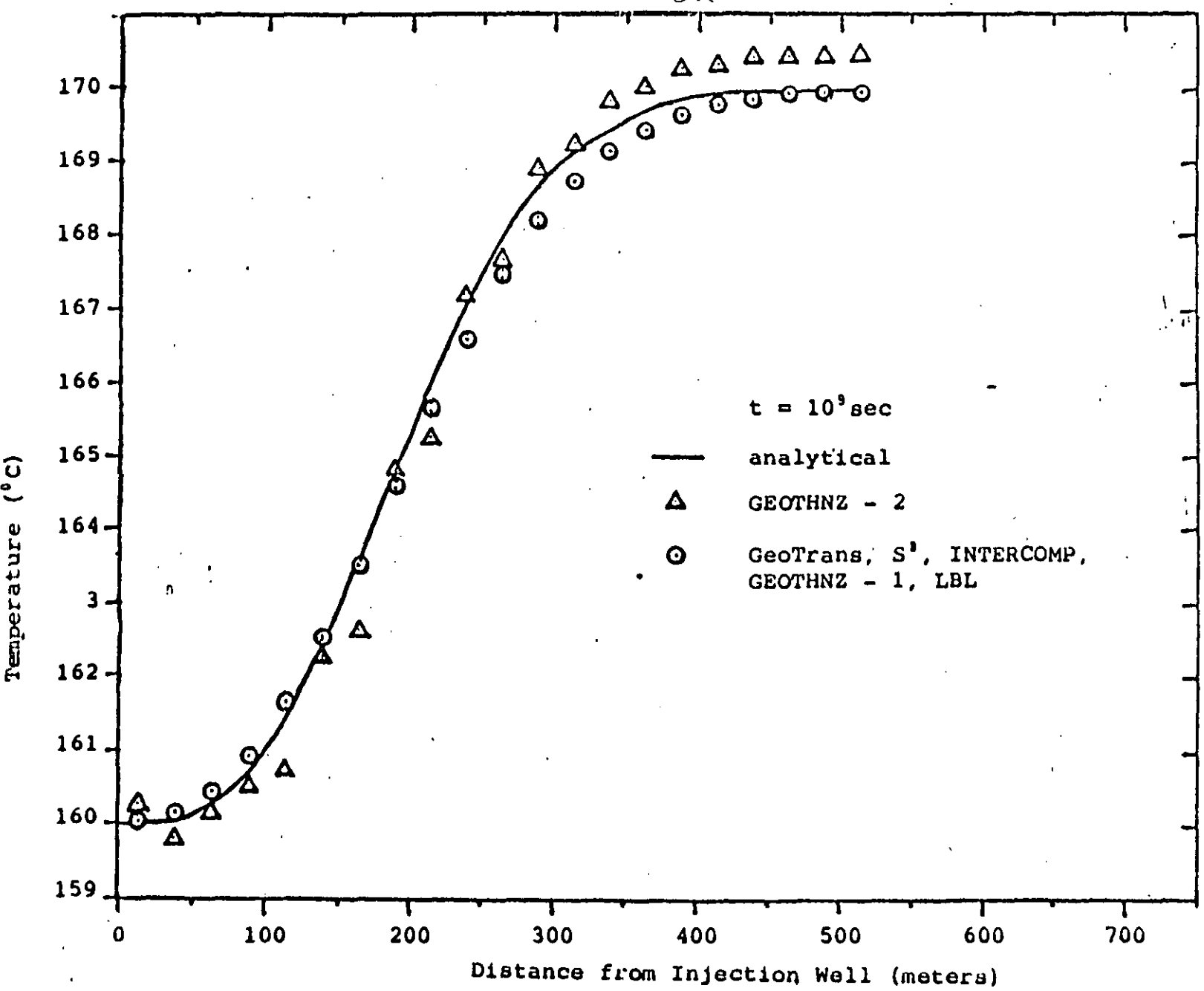

Figure 5. Problem 1, calculated results at time = 10^9 sec for all partici

GENERAL DISCUSSION

For constant density, viscosity, and heat capacity of water, an analytical solution is available for this problem. For example, this solution is a limiting case for the problem solved by Avdonin (1964).

This problem offers little difficulty in solution. The grid spacing specified leads to numerical dispersion if upstream weighting is used. To see how significant the numerical dispersion could be, the problem was run twice - once with upstream weighting and once with midpoint weighting (central difference).

The results of this problem are shown in Figures 2 and 3. In the model the specific heat, viscosity and density of water for 165°C and 50 bars are 0.44425×10^8 ergs/g-°C, 0.001636 g/cm-s, and 0.90893 g/cm^3, respectively. Both Figure 2 (temperature vs time at 37.5m) and Figure 3 (temperature vs distance at 10^9sec) show the effects of the coarse grid spacing. The upstream-weighting results show numerical dispersion, whereas the central-difference results show an overshoot.

COMPARISON OF RESULTS

Figures 4 and 5 show the simulated results of GeoTrans, S^3, LBL, INTERCOMP, and two results from a code called GEOTHNZ. As may be seen all results compare favorably (within the range of the thermodynamic parameters used in each code and within machine error), except the second results for GEOTHNZ. For these results, the thermal boundary condition at the outer radius was specified as 170.5°C. Also, central difference was used for both the space and time approximations. These differences in input specifications easily account for the differences in results.

CONCLUSION

The numerical solutions compare well with the Avdonin analytical solution. Thus, it appears that the simulators are solving the equations properly.

REFERENCE

Avdonin, N.A., 1964, Some formulas for calculating the temperature field of a stratum subject to thermal injection: Neft'i Gaz, Vol. 3, p. 37-41.

THE D.O.E. CODE COMPARISON PROJECT: SUMMARY OF RESULTS FOR PROBLEM 2 - RADIAL FLOW TO A WELL UNDER SINGLE AND TWO-PHASE CONDITIONS

Michael L. Sorey
U.S. Geological Survey
Menlo Park, California

INTRODUCTION

Problem 2 involves a set of four constant-discharge, transient well test cases. Three of the cases involve one-dimensional radial flow to a line sink (zero-radius well) in a homogeneous porous media. In case A the reservoir fluid remains single-phase liquid; in case B the fluid remains a two-phase mixture with both steam and water mobile; in case C the fluid changes from compressed liquid to a two-phase mixture as a flash-front propogates away from the well. An additional problem was run under the initial conditions used in case B, involving only one grid block with discharge but no inflow. In each of these cases analytical or semi-analytical solutions for pressure, saturation, and flowing enthalpy as functions of time/distance squared (t/r^2) are available for comparison with the numerical results.

PROBLEM SPECIFICATIONS

The initial and boundary conditions specified for this problem are listed below.

Specification	Case A	Case B	Case C
Initial pressure (bars)	90	30	90
Initial temperature (^{o}C)	260	233.8	300
Initial liquid saturation	1	0.65	1
Porosity	0.2	0.15	0.2
Permeability (10^{-12} m^2)	0.01	0.24	0.01
Thickness (m)	100	100	100
Discharge (kg/s)	14.0	16.7	14.0
Rock heat capacity (kJ/m^3 ^{o}C)	2650	2000	2650
Rock compressibility	0	0	0
Rock thermal conductivity	0	0	0

Relative permeability functions, based on the Corey equations, were used as indicated below.

$$k_{rl} = (S^*)^4$$

$$k_{rv} = ((1-S^*)^2).(1-(S^*)^2)$$

$$S^* = (S-0.3)/\ 0.65$$

where S = liquid saturation.

To minimize computational requirements while avoiding significant spacial discreetization errors, the following nodal arrangement was suggested for each radial-flow case.

$$r_n = 0.5\ m(2)^{\frac{n-1}{2}},\ n=1,26$$

For these cases a total simulation time of 1 day and an initial time step of 10^{-5} days were specified. In the one-node problem under case B conditions, a volume of 314 m^3 and 100 time steps of 10^{-4} days each were called for, with the enthalpy of the discharged fluid weighted according to the mobility of each phase.

The desired output for cases A, B, and C included pressure (in bars), liquid saturation, and flowing enthalpy (in kJ/kg) histories as functions of t/r^2 (in days/m^2) for nodal points at 0.5 m, 0.707m, and 1.0m from the well. For the one-node problem, pressure, saturation, and flowing enthalpy in the block versus time were required.

RESULTS

Case A

For this case the exponential integral solution of Theis (1935) is available for comparison. Results plotted in figure 1 show excellent agreement for each simulator solution. The fluid remains an isothermal compressed liquid as reservoir pressures remain above the saturation pressure of 47 bars during the

1-day simulation period.

One-node Problem

Results for the one-node problem are plotted in figure 2. The expected change in pressure (ΔP) and saturation (ΔS) per time step (Δt) can be hand-calculated from the equations shown in figure 2, which can be obtained from simultaneous solutions to the mass and energy balance equations as presented by Grant and Sorey (1979) and Sorey, Grant, and Bradford (1980), where

Q = discharge
V = block volume
ϕ = porosity
c_e = effective two-phase compressibility
ρ_f = density of flowing fluid mixture
ρ_w = density of water (liquid phase)

The value of $\Delta P/\Delta t$ changes with time as c_e and ρ_f vary; calculations of $\Delta P/\Delta t$ were made at $t = 0$ and $t = 70 \times 10^{-4}$ days. All the numerical results are in good agreement with the analytically-determined values for $\Delta S/\Delta t$ (which remain nearly constant) and $\Delta P/\Delta t$. Corresponding hand-calculations for changes in flowing enthalpy were not carried out. Simulator results for flowing enthalpy are self-consistent and show the characteristic rise in enthalpy to a stable value observed for radial flow to wells in two-phase reservoirs (Sorey, Grant, and Bradford, 1980).

Case B

For case B, involving radial flow with mobile liquid and steam, a semi-analytical similarity solution involving numerical integration of ordinary differential equations (O'Sullivan and Pruess, 1980) is available for comparison with numerical solutions. Results shown in figure 3 are in reasonable agreement; additional runs using the SHAFT79 simulator indicate that the numerical solutions would match the semi-analytical solution even better if a finer grid were used near the well. The scatter among the different results is probably due mainly to minor variations in the thermodynamic relationships

used in each code. Numerical results for pressure, saturation, and flowing enthalpy at each of the three nodal distances listed previously as functions of t/r^2 are essentially identical, in agreement with the similarity solution.

Case C

Case C involves the propogation of a flash front away from the well. The initial reservoir pressure is approximately 5 bars above the saturation pressure of 86 bars for T=300°C so boiling occurs near the well soon after discharge commences and extends to a distance of about 10 m after 1 day. In several respects, this case is more difficult to accurately simulate than are the other cases in Problem 2 and consequently deviations of the numerical results from the semi-analytical solution are somewhat greater in this case as shown in figure 4. Numerical solutions are sensitive to nodal spacing and some improvement in the comparison with the analytical solution would result if a finer grid near the well were used. In this case also, the choice of a logarithmically-spaced grid causes the numerical solution at large values of t/r^2 to oscillate. This is most noticeable in the plot of flowing enthalpy. Using a grid with equally-spaced nodal increments near the well greatly reduces the size of the oscillations, but does not improve the fit with the analytical solution at large t/r^2. In spite of these numerical difficulties, results from each simulator are roughly the same, and the level of agreement with the analytical result indicates that these numerical simulators can adequately handle the flashing-front problem.

REFERENCES

Grant, M.A., and Sorey, M.L.,1979, The compressibility and hydraulic diffusivity of a water-steam flow, Water Resources Research, vol. 15, No. 3, pp. 684-686.

O'Sullivan, M.J., and Pruess, K., 1980, Analysis of injection testing of geothermal reservoirs; Geothermal Resources Council, Transactions, vol. 4, pp. 401-404.

Sorey, M.L., Grant, M.A., and Bradford, E., 1980, Nonlinear effects in two-phase flow to wells in geothermal reservoirs, Water Resources Research, vol. 16, No. 4, pp.767-777.

Theis, C. V., 1935, The relation between the lowering of the piezometric surface and the rate and duration of discharge of a well using groundwater storage; Trans. Amer. Geophysical Union, Vol. 16, pp. 519-524.

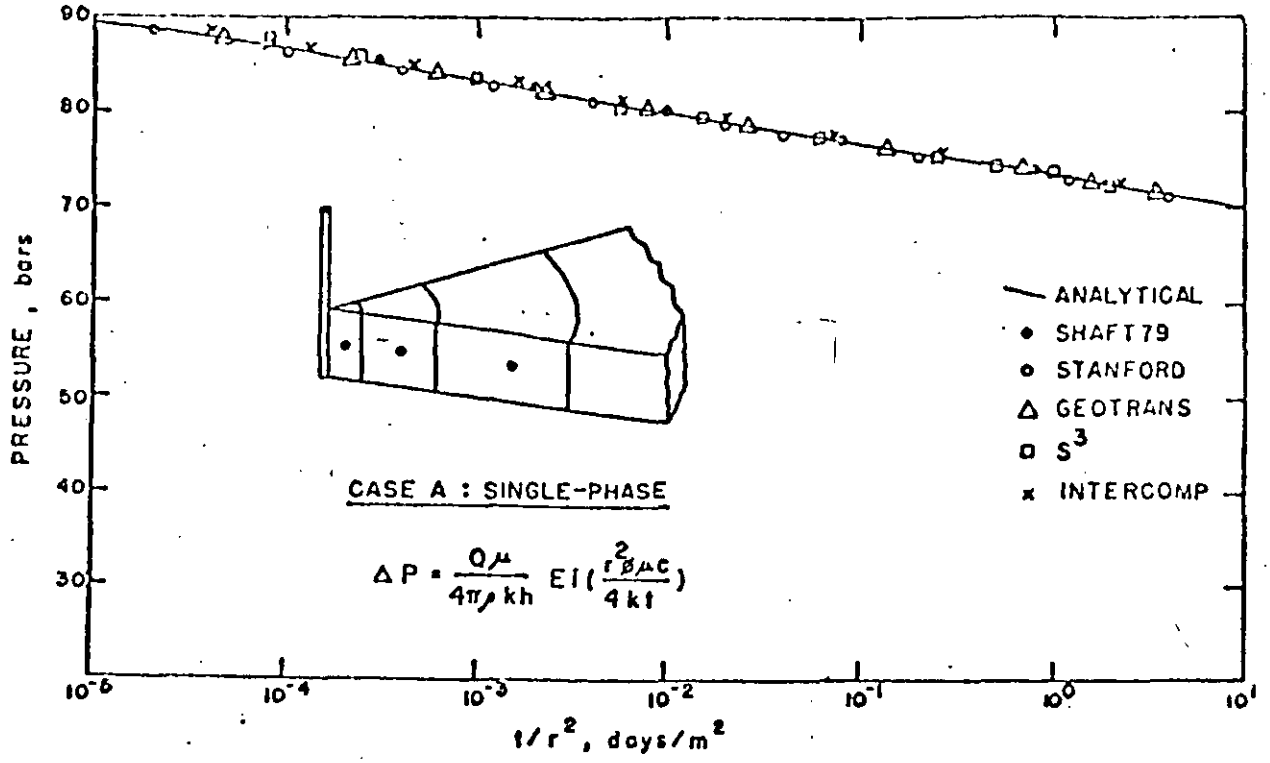

Figure 1. Solutions to Problem 2, case A.

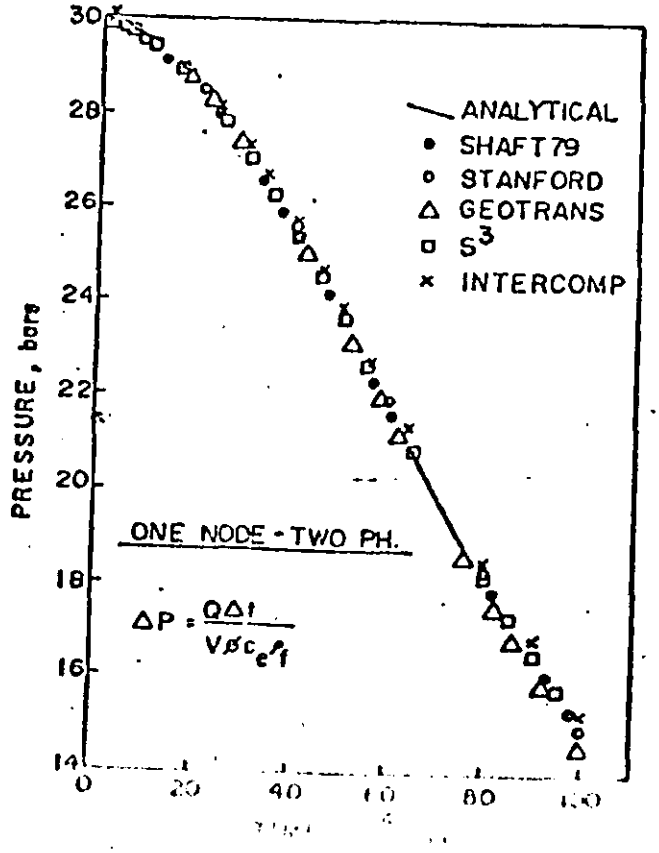

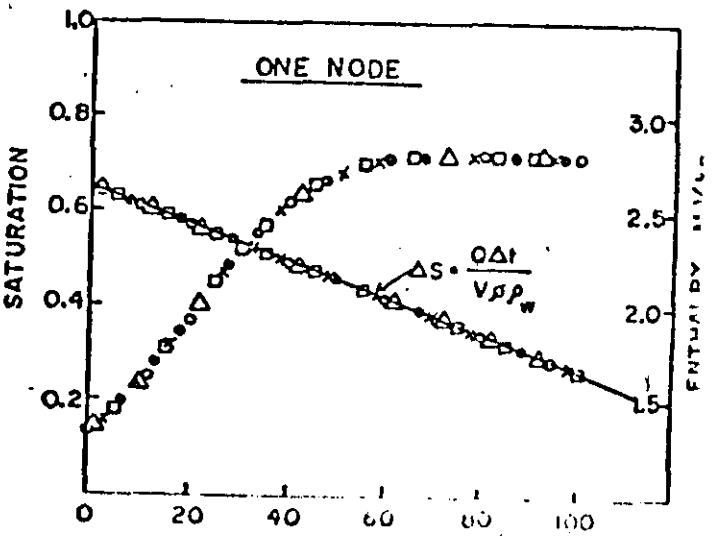

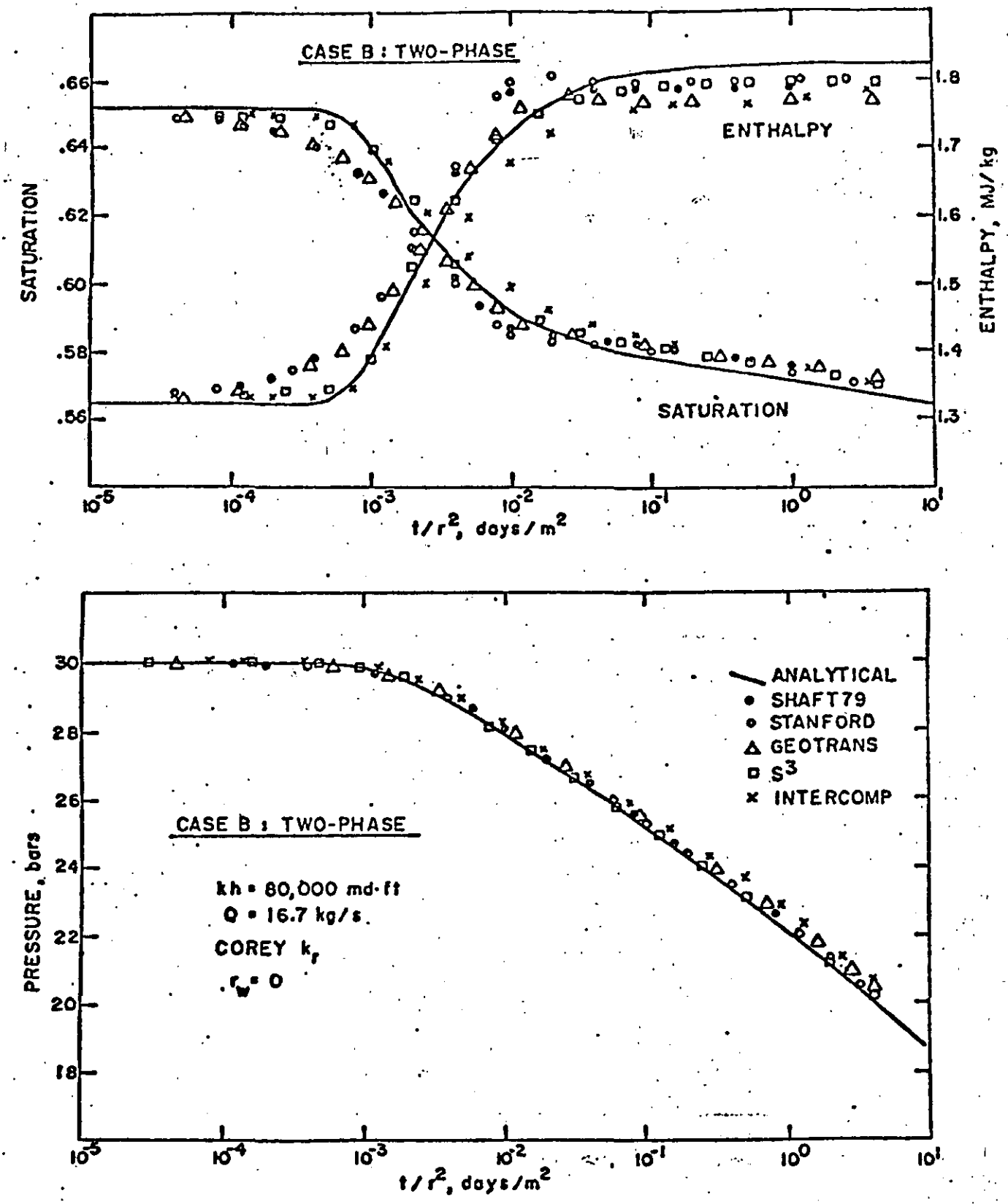

Figure 3. Solutions to Problem 2, case B.

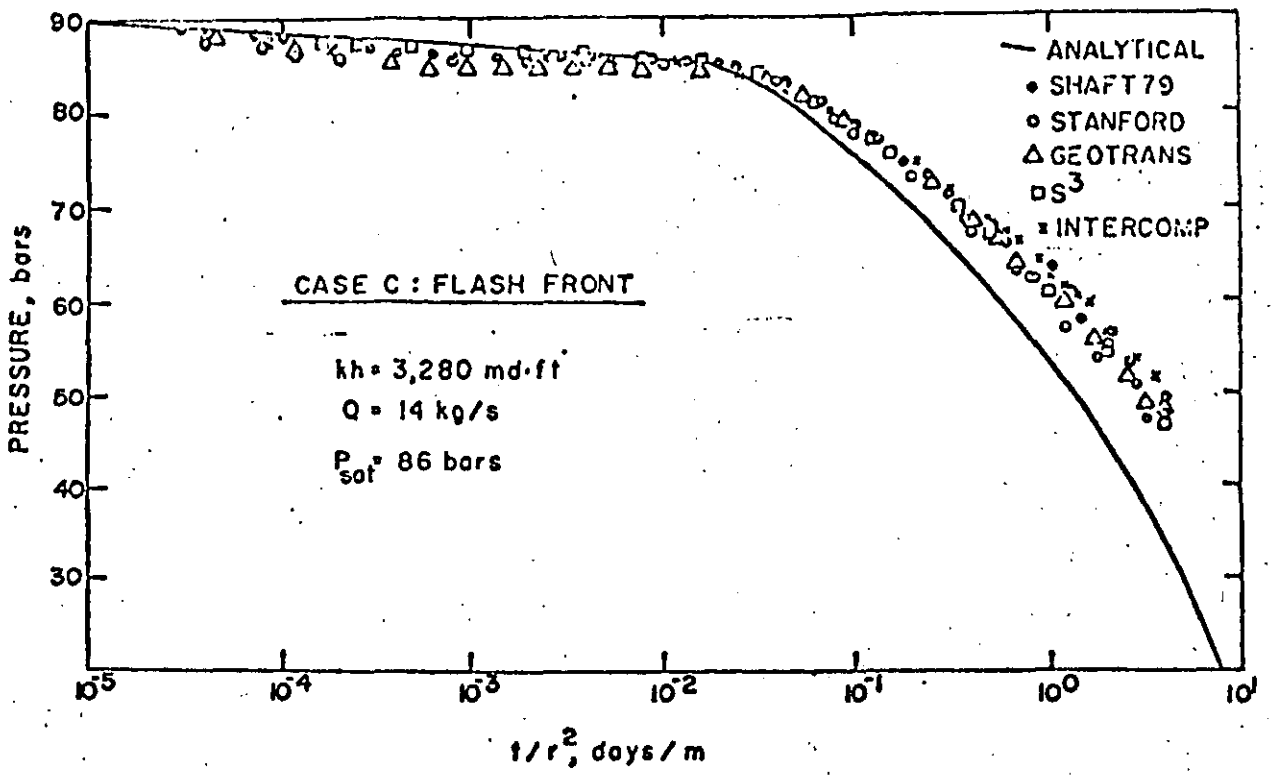

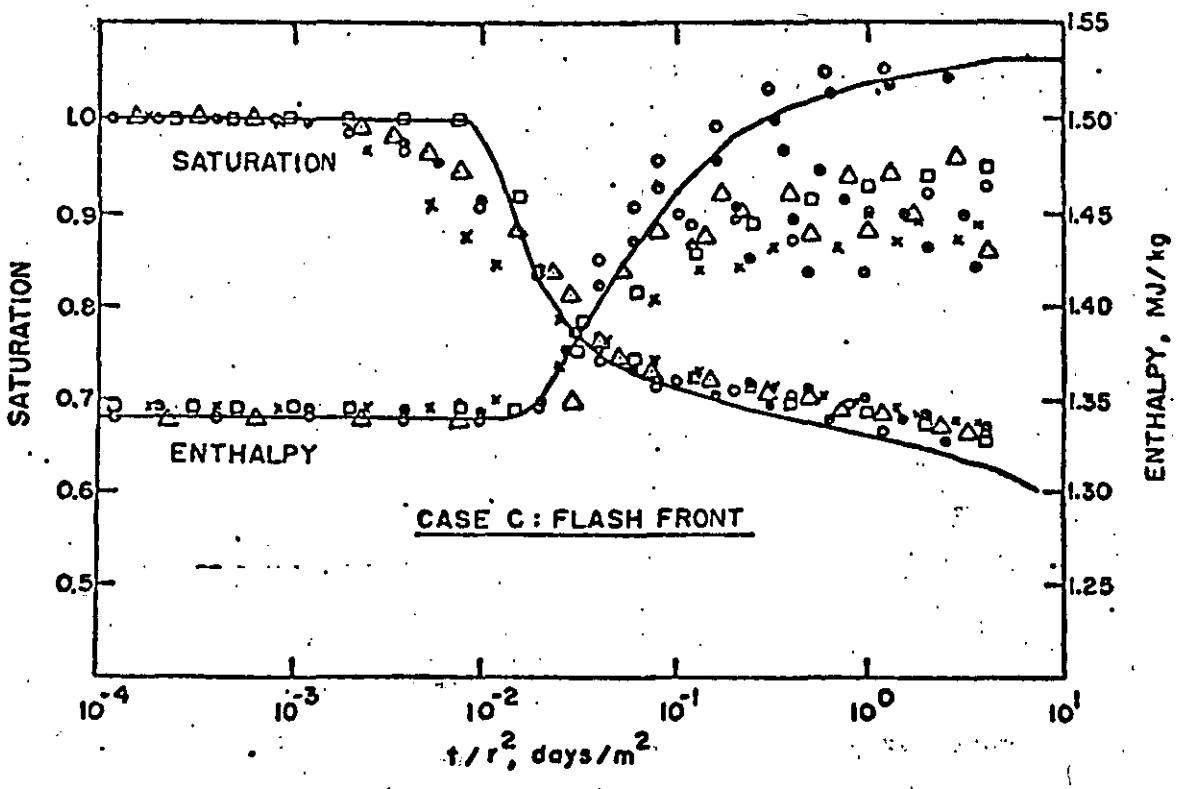

Figure 4. Solutions to Problem 2, case C.

D.O.E. Code Comparison - Problem 3
"2-D Flow to a Well in Fracture/Block Media"

A.F. Moench, U.S.G.S.

INTRODUCTION

This problem represents a simplification of the general problem of well testing in fractured geothermal reservoirs. The reservoir is idealized as a horizontal fissure of infinite lateral extent bounded on one side by a block of finite thickness. Steam flows vertically from the block to the fissure and thence radially to a well where it discharges to the atmosphere.

PROBLEM SPECIFICATION

Figure 1 shows the geometry of the reservoir and a suggested mesh design. The upper boundary of the block and the lower boundary of the fissure are impermeable. The flow of steam in the fissure and block obeys Darcy's law. The well has a finite radius and discharges steam at a constant rate.

Two cases are considered. In Case a, liquid saturation is zero everywhere. In Case b, liquid water partially saturates the block but not the fissure. The relative permeability to steam is 1.0 and the relative permeability to liquid water is 0.0. Rock compressibility and thermal conductivity are zero. The remaining parameters are listed in Table 1.

A computational grid consisting of one well block, ten logarithmically-spaced nodes in the fissure, and ten equally spaced nodes in the block, as partially illustrated in figure 1, is suggested. The node in the fissure furthest from the well block will be located a distance of about 1½ km from the well if the spacing from one node to the next is increased by a factor of 2.5. A large fictional permeability at least 100x the permeability of the fissure should be assigned to the well block node. Total simulation time should be 10^4 seconds and the initial time step should be 1 second. A time step multiplication factor of 1.05 is suggested. This would result in achieving the required simulation time in about 130 time steps.

Results for Cases a and b should consist of plots of pressure as a function of the logarithm of time, along with the corresponding data in tabular form. Pressure at the well face and at a point in the block located 2.5 m from the center line of the well and 0.25 m from the top of the fissure should be presented. Also, for Case b liquid saturation versus time for the above specified point in the block should be tabulated.

COMPARISON OF RESULTS

Figures 2a and 2b show the results obtained by the various participants for the single phase flow of steam (Case A). The solid lines represent the results deemed by this author to be most accurate. This conclusion is based in part upon comparisons with an analytical solution and in part upon comparisons with yet another finite-difference model designed specifically for this problem. Pressure declines in the block are about the same for all the participants but there is considerable discrepancy in the pressure declines at the well face. Upon discussing the results with several of the participants it was found that these discrepancies were due primarily to the manner in which the transmissive characteristic was obtained for the flow between the well block node, which was assigned a very large permeability, and the node in the fissure adjacent to the well block node. In all but the results obtained by LBL and S[3] this procedure effectively increased the well diameter so that computed pressure drawdowns were less than they should have been[1]. Results obtained by Stanford are in error for the additional reason that the wrong well radius was specified.

Figures 3a and 3b show the results obtained when immobile liquid water is present in the block (Case B). As in Case A the solid lines represent the results deemed by this author to be most accurate. Pressure declines in the block are nearly the same for all participants. Unfortunately the parameters defined in the problem were such that little change occurred in the specified block node so a good test of the code is not possible at this location. As in case A there is considerable discrepancy in the pressure declines at the well face. In the case of Geo Trans[2] and New Zealand this can be attributed to permeabilities in the vicinity of the well block node as in Case A. The discrepancy is enhanced in Intercomp's results because of unduly large time steps early in the simulation and in Stanford's results because of recognized errors in the thermodynamics at the saturated steam-superheated steam interface.

Figure 4 shows the changes in saturations that occur in the block in Case B. Differences in the results can be attributed to the reasons already given for discrepancies in figures 3a and 3b.

---

[1]After the Workshop Geo Trans submitted revised results, correcting this error, which agree closely with S[3] and LBL.

[2]Ibid.

CONCLUSIONS

The results presented in figures 2-4 show considerable variations from one participant to another. It was found that these variations could be explained by operator errors and misunderstanding of the specified problem. Unfortunately the problem was not posed in a manner which eliminated ambiguity. Variations obtained by the different participants were not due to errors inherent in any of the computer codes.

Table 1

Specification	Case a	Case b
Initial pressure (bars)	30.5	30.5
Initial liquid saturation in block 1/	0	.2
Initial temperature (°C) 2/	234.8	234.8
Porosity in fracture	.1	.1
Porosity in block	.1	.1
Permeability in fracture ($10^{-12}m^2$)	.3	.3
Permeability in block ($10^{-12}m^2$) 3/	.00003	.00003
Thickness of fracture (m)	.1	.1
Thickness of block (m)	1.0	1.0
Well discharge (kg/s)	.028	.028
Well radius (m)	.16	.16
Rock heat capacity ($kJ/m^3°C$)	2570.	2570.

1/ Initial liquid saturation is zero in the fracture in both cases.

2/ Saturation temperature at 30.5 bars.

3/ Horizontal permeability in block is zero in both cases.

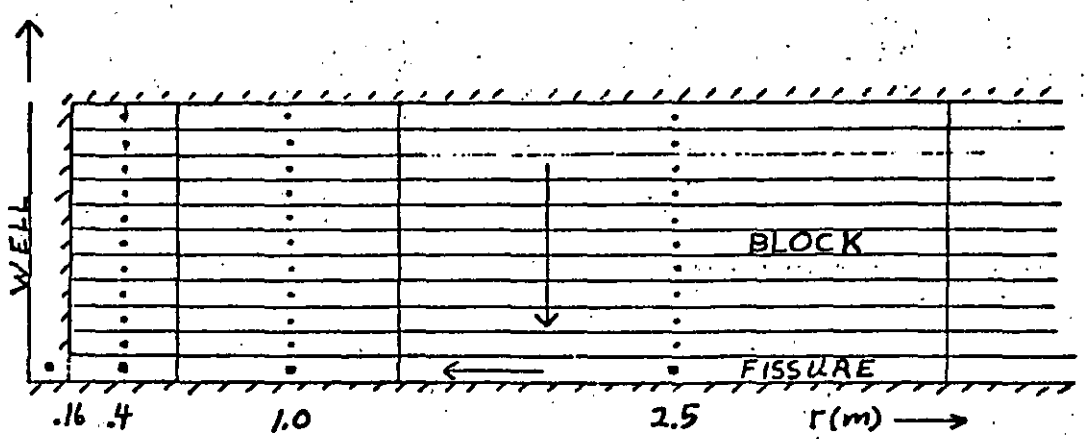

Figure 1. Reservoir geometry and possible mesh design

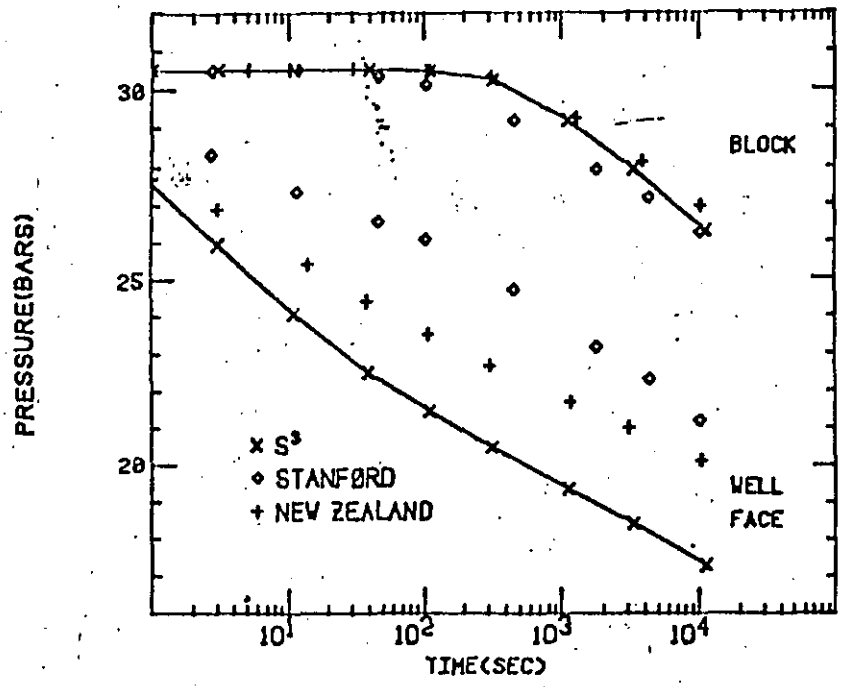

Figure 2a.--Pressure versus time at well face and in reservoir block for Case A.

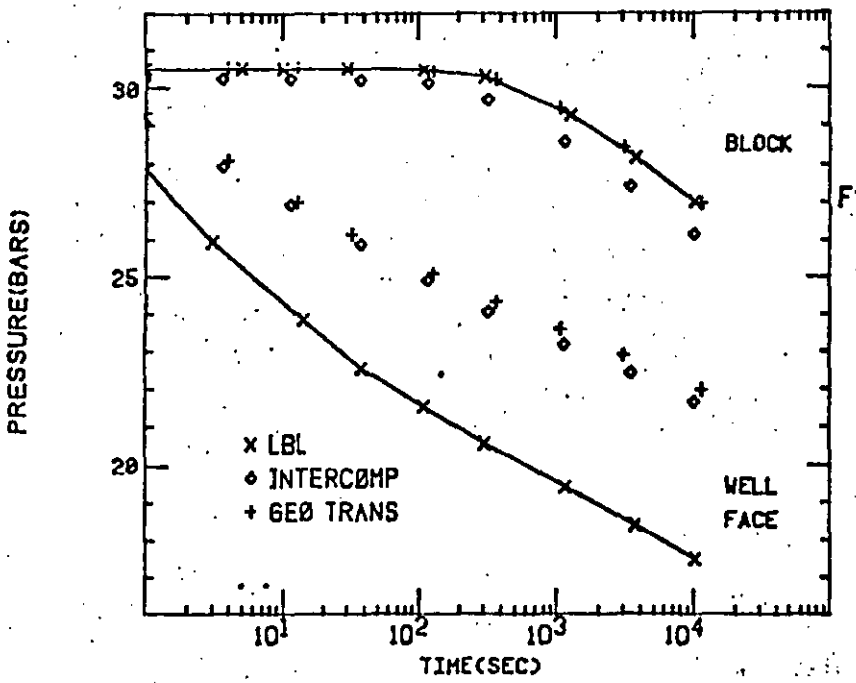

Figure 2b.--Pressure versus time at well face and in reservoir block for Case A.

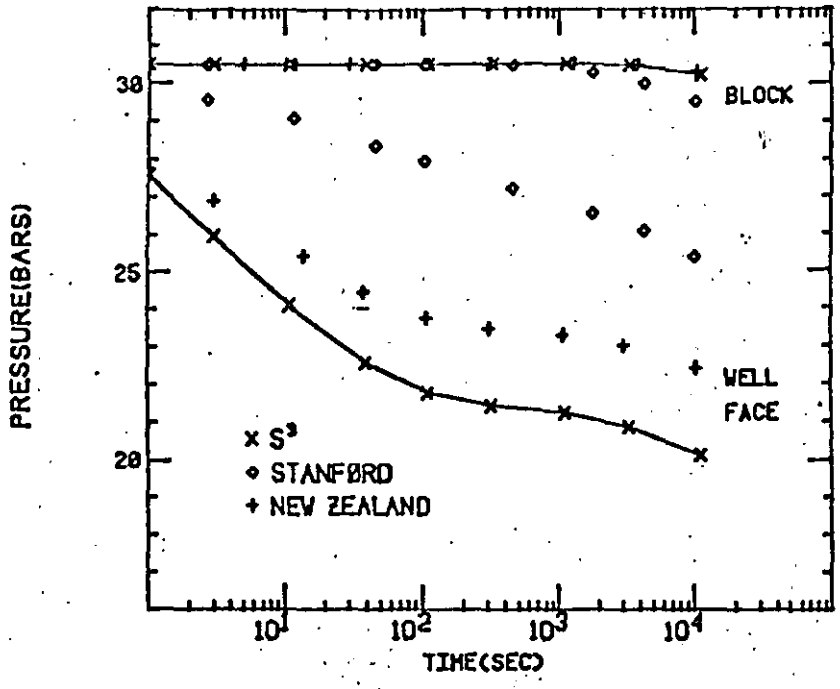

Figure 3a.--Pressure versus time at well face and in reservoir block for Case B.

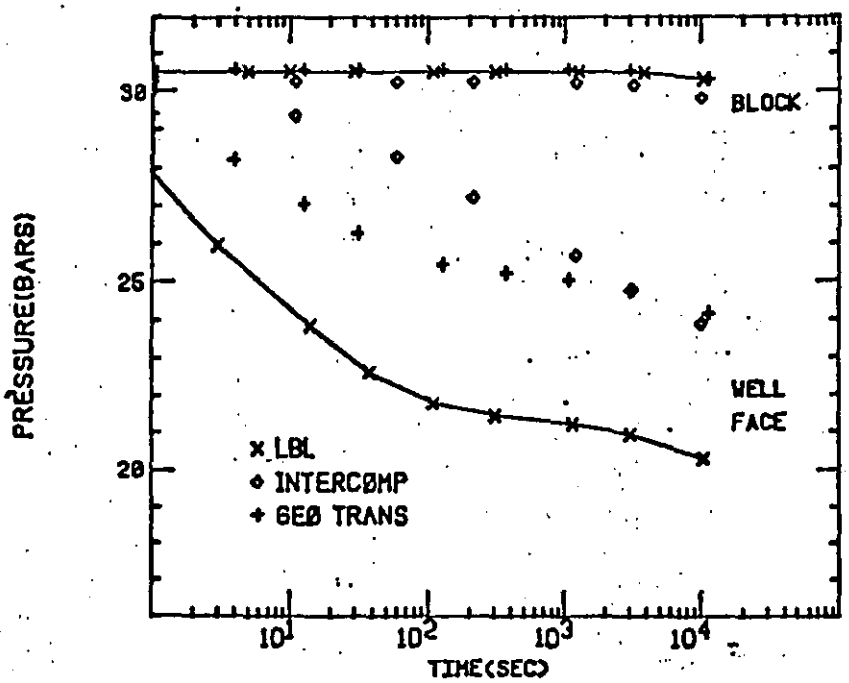

Figure 3b.--Pressure versus time at well face and in reservoir block for Case B.

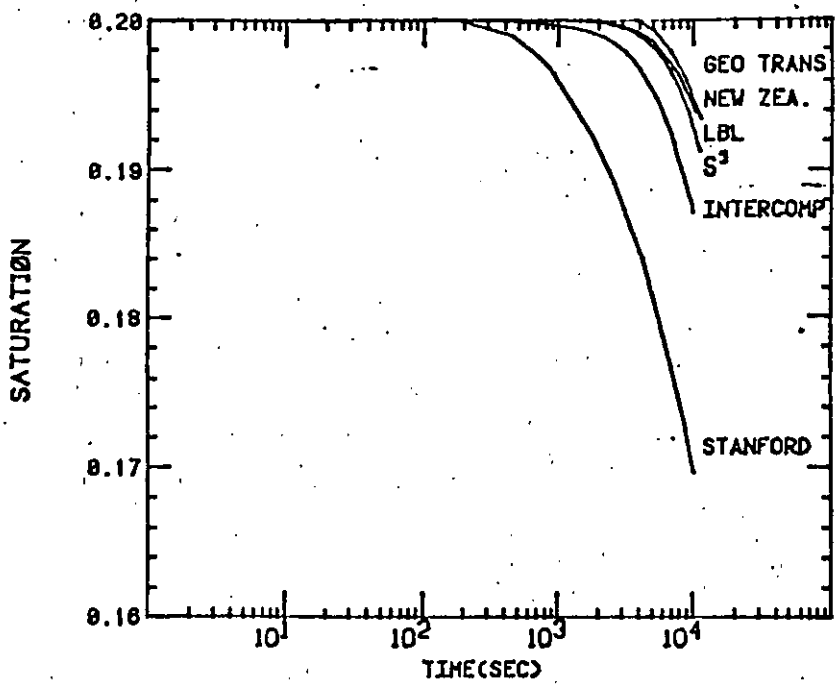

Figure 4.--Saturation versus time in reservoir block for Case B.

THE D.O.E. CODE COMPARISON STUDY : SUMMARY OF RESULTS FOR PROBLEM 4 - EXPANDING TWO-PHASE SYSTEM WITH DRAINAGE

M.J. O'Sullivan, Lawrence Berkeley Laboratory

INTRODUCTION

The reservoir in this problem consists of two layers each 1km thick with the top layer less permeable than the bottom (detailed properties are given in Table 1). The initial temperature in the reservoir drops linearly from 310°C at the bottom of the reservoir to 290°C at the interface between the two layers and then drops more steeply, but still linearly to 10°C at the ground surface. The initial pressure distribution is the hydrostatic profile corresponding to this temperature distribution.

The reservoir is produced at the bottom of the system at a rate of 100kg/s.km^2. It is assumed that the system and the production are uniform in the horizontal directions so that flow occurs in the vertical direction only.

A calculation grid of 20 equal sized blocks is specified and results are required for a 40 year period.

The anticipated behavior of the reservoir is that a boiling zone will develop near the top of the more permeable layer and spread downwards, also spreading a short distance into the upper layer. As the pressure drops in the lower layer, down flow through the top layer and recharge at the ground surface will be induced.

DIFFICULTIES

The vertical flow of a boiling fluid driven by a combination of gravity and production related pressure gradients is one of the most difficult flow problems for a numerical simulator to handle. Initially the pressure in the reservoir increases rapidly with depth. After production begins the slope of the pressure profile decreases and a liquid/vapor counter-flow develops after about one year when the reservoir starts boiling. That is, water flows downwards to the production well while steam rises and recondenses at a higher level. The numerical analysis required to simulate these physical processes is quite complex. Separate treatment of the vapor flow and the liquid flow is required with upstream weighting of pressure gradient terms in opposite directions for each phase.

At a more elementary level this problem also tests the ability of simulators to handle vigorous boiling (several nodes changing from liquid to two-phase) and the implementation of a constant pressure, constant temperature recharge condition at the ground surface.

RESULTS

The pressure profiles given in Figure 1 show the processes involved clearly. The flow in the top layer does not change very significantly with time and at a rate of approximately 30kg/s.km^2 is not sufficient to supply all the production. Therefore the fluid from the bottom layer is progressively mined. The steeper part of the pressure profile in the lower layer corresponds to the boiling zone. At about 30 years this extends throughout the lower layer and after about 37 years the liquid saturation has dropped sufficiently to inhibit the flow of water and then the pressure gradient steepens to induce an adequate additional downward flow of steam. The steam flow-rate profiles given in Figure 2 show the upward flow of steam changing to a later downward flow at around 37 years.

COMPARISON OF RESULTS

A selection of the required results for problem four are shown in Figures 3,4,5 and 6. The surface recharge results shown in Figure 3 all agree well except for those of Intercomp. Even the Intercomp results are not significantly different. The surface recharge rate is very strongly dependent on the viscosity of water and other parameters at temperatures close to the recharge temperature of 10°C. Therefore, the differences between Intercomp's results and the other results could be explained by minor inaccuracies in their low temperature thermodynamic properties of water. A more detailed comparison of temperatures and pressures at nodes near the surface would be required to fully explain the differences. The production enthalpies shown in Figure 4 are all similar except for those submitted by Intercomp. Their results predict a later rise in the enthalpy, that is a later boiling of the production node. This result is to be expected because of their higher surface recharge rate. Since more cold water flows into the Intercomp reservoir it takes longer for the bottom layer to completely boil.

The pressure and saturation histories at various depths shown in Figures 5 and 6 all agree well (with Intercomp results showing some variation).

CONCLUSIONS

All the simulators compared in this study came through the severe test represented by problem four very well. Clearly they are capable of handling the counter-flow of steam and water, the expansion of a boiling zone and the vertical drainage of cold surface water into a reservoir. As all these processes occur in real geothermal reservoirs such as Wairakei, the results for this problem have considerable practical significance. The simulators tested all appear to be satisfactory tools for analyzing models of this type of geothermal reservoir.

TABLE 1. RESERVOIR PROPERTIES

	Top Layer	Bottom Layer
Porosity	0.15	0.25
Permeability ($10^{-15}m^2$)	5.0	100.0
Rock density (kg/m^3)	2500.	2500.
Rock heat capacity (kJ/kg.K)	1.0	1.0
Thermal conductivity (W/m.K)	1.0	1.0

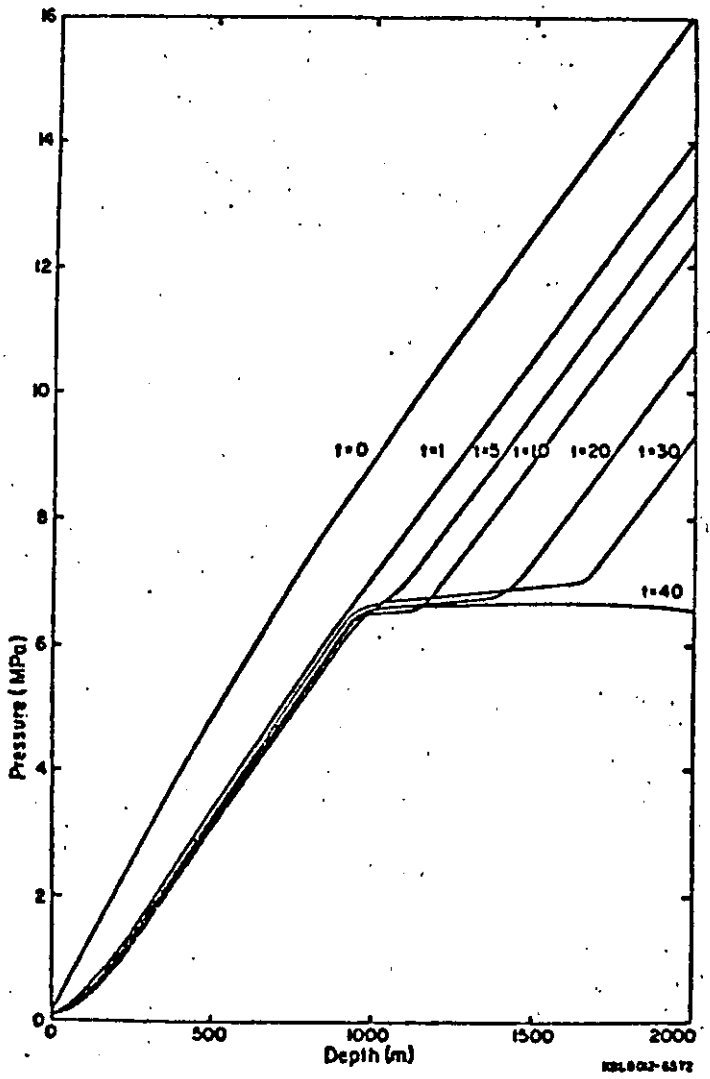

Figure 1. Pressure profiles in the reservoir at various times.

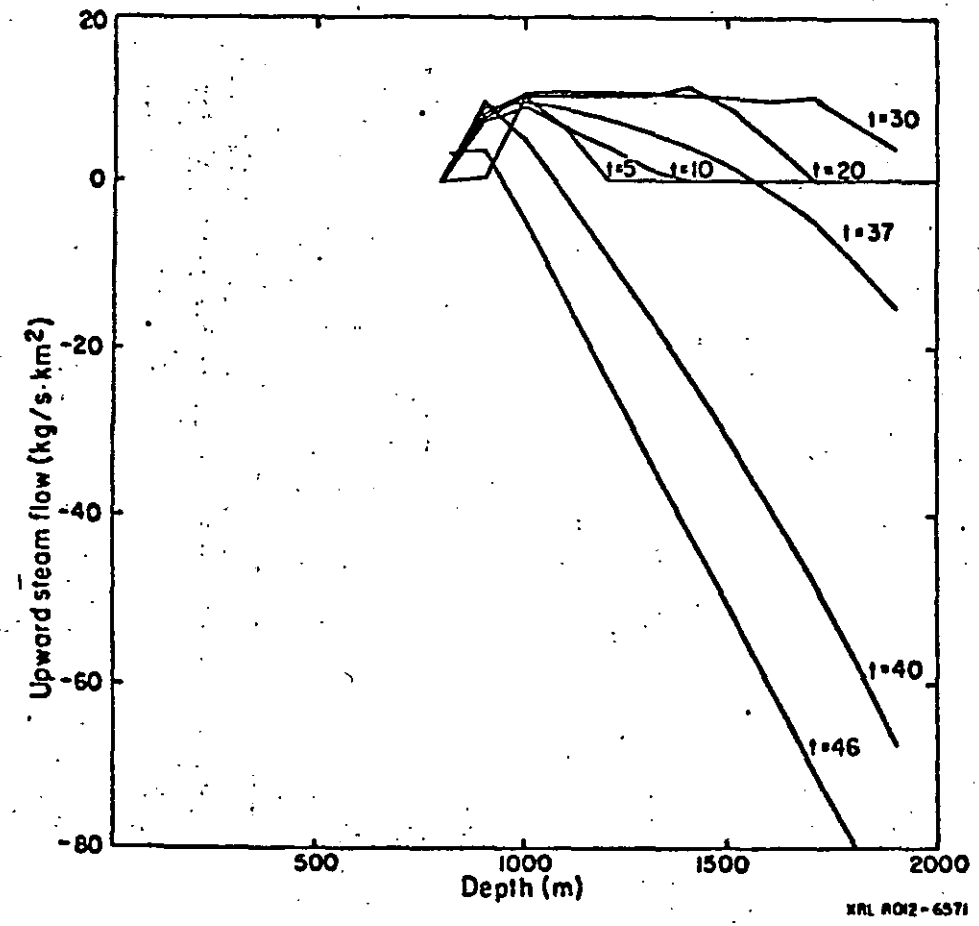

Figure 2. Steam flow in the reservoir at various times.

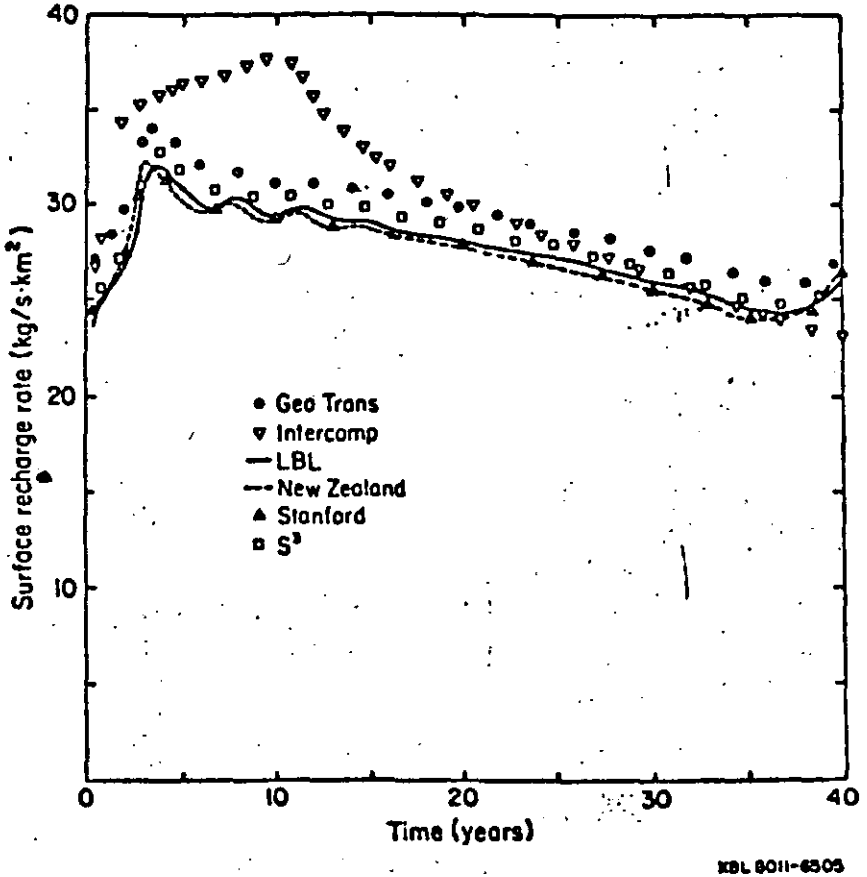

Figure 3. Surface recharge rate.

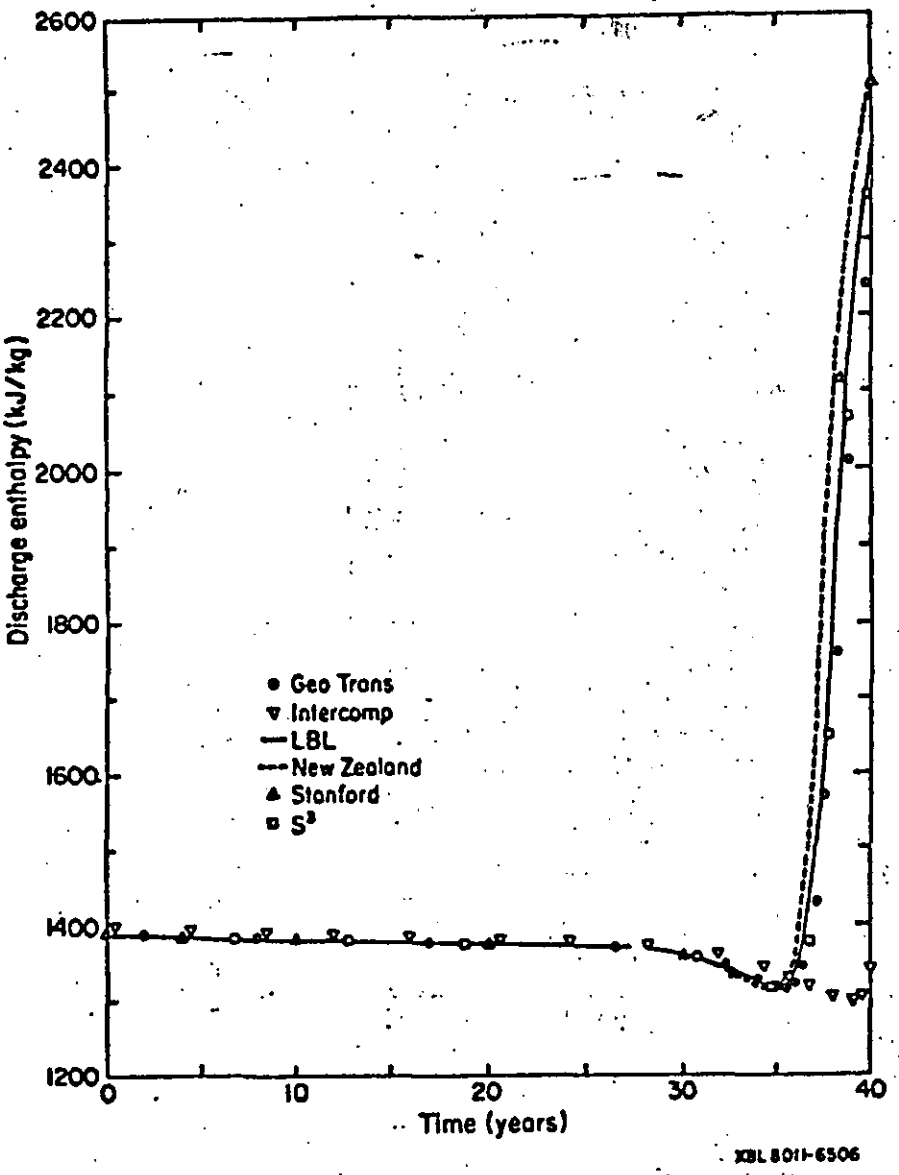

Figure 4. Production enthalpy.

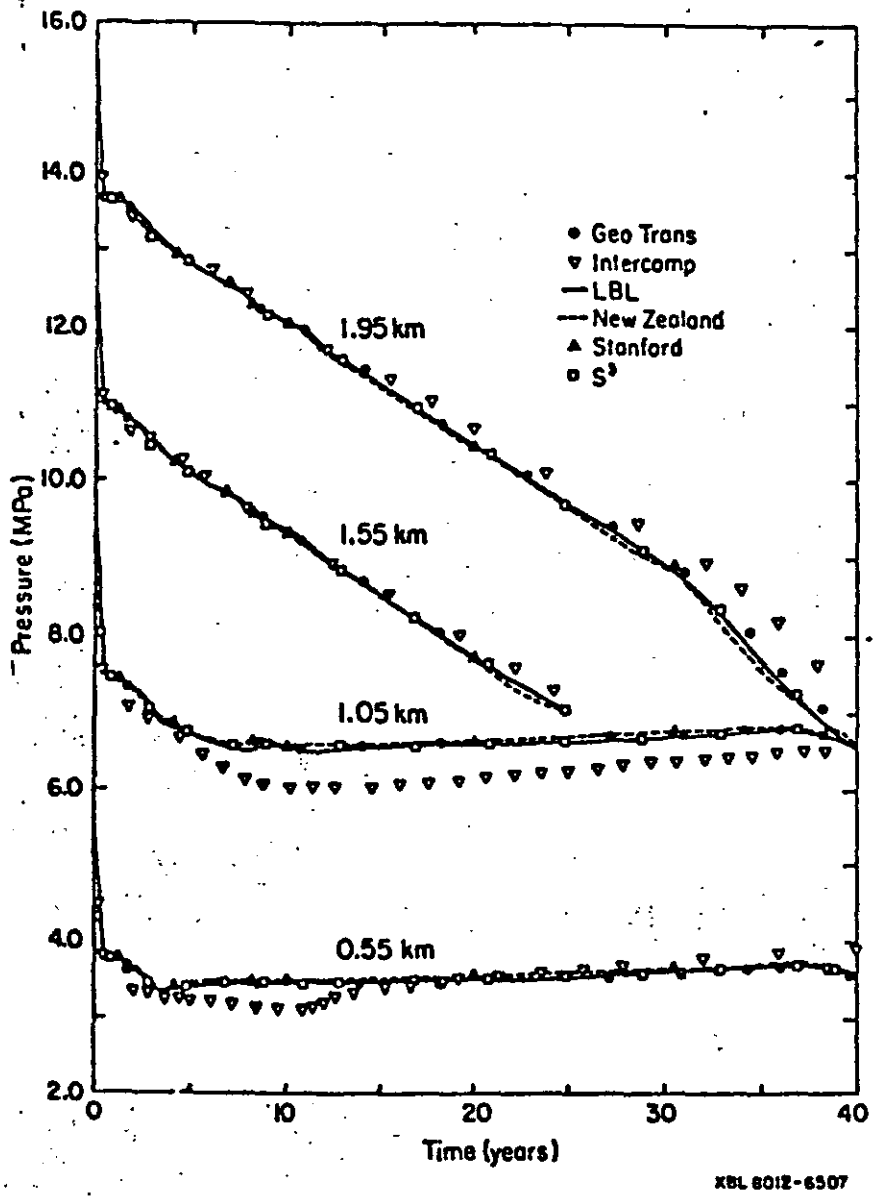

Figure 5.— Pressure histories at various depths

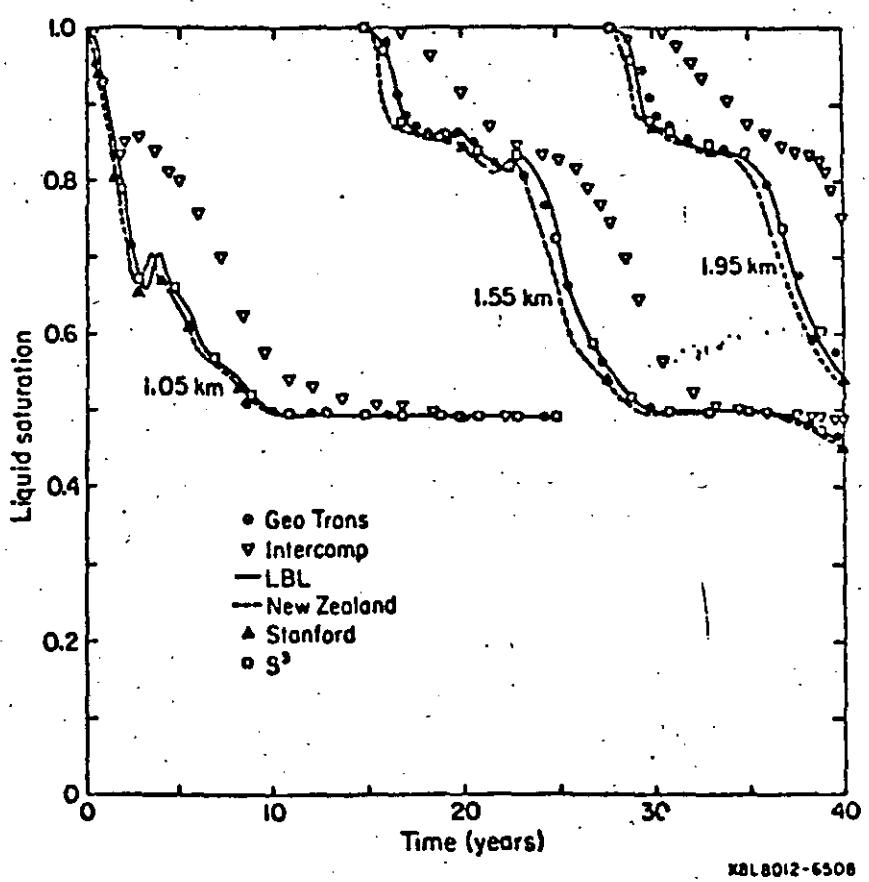

Figure 6. Liquid saturation histories at various depths.

THE DOE CODE COMPARISON PROJECT:

-SUMMARY OF RESULTS FOR PROBLEM 5-

John W. Pritchett
Systems, Science and Software
P. O. Box 1620
La Jolla, CA 92038

INTRODUCTION

Problem 5 is a two-dimensional areal case involving both single-phase (water) and two-phase (water/steam) flow in a system in which lateral cold-water recharge occurs; the initial temperature distribution is non-uniform. Thus, convective heat transfer and water/steam phase transitions play important roles. The first case (Problem 5A) considers the effect of a single production well; the second (5B) treats the combined effects of fluid production and reinjection.

PROBLEM DESCRIPTION

Consider a horizontal region extending over $0 \leq x \leq 300$ meters, $0 \leq y \leq 200$ meters (see Figure 1). The rock properties within the region are uniform (see Table 1). Initially, temperatures are distributed in a non-uniform manner. For $r \leq 100$ meters, the initial temperature is 240°C ($r^2 = x^2 + y^2$). For $r \geq 300$ meters, the initial temperature is 160°C. For intermediate values of r, the initial temperature varies smoothly between 160°C and 240°C according to:

$$T = (240°C) - (160°C)\ \nu^2 + (80°C)\ \nu^4;\ \nu = \frac{r-100\ m}{200\ m}$$

The initial pressure in the system is uniform, and is sufficient to maintain an all-liquid state throughout. The initial pressure (P_o) is taken to be equal to the water/steam saturation pressure associated with a temperature of 240°C (P_{sat} (240°C) = 33.48 bars according to the ASME Steam Tables), plus 2.5 bars. Thus, the initial pressure (P_o) is about 36 bars, so that a pressure drop of at least 2.5 bars will be required to cause boiling in the region within r = 100 meters, and even more pressure decline will be required to cause phase changes at greater radii. The boundaries along x = 0, along y = 0, and along y = 200 meters are all taken as impermeable and insulated. Along x = 300 meters, the pressure and temperature are maintained at their initial values (T = 160°C, $P = P_o \approx 36$ bars), so that recharge fluid may enter the system.

The first case (Problem 5A) involves a single production well located at x = 62.5 meters, y = 62.5 meters which starts producing fluid at zero time at a constant rate of 50 grams per second per meter of thickness. In Problem 5B, in addition to the production well, an injection well is located at x = 162.5 m, y = 137.5 m. Starting at t = 1 year, this well injects fluid at a temperature of 80°C at a constant rate of 30 grams per second per meter of thickness (60 percent of the production rate). In both cases, the time domain of interest is $0 \leq t \leq 10$ years. The problem is to be subdivided, for numerical purposes, into 8 x 12 = 96 square zones measuring 25 meters on a side, as indicated in Figure 1. The time-step to be used is left to the discretion of the engineer.

THE NUMERICAL CALCULATIONS

Six different organizations used five different numerical reservoir simulators to solve this problem during the DOE Code Comparison Project. Geotrans, Inc., Intercomp, and Lawrence Berkeley Laboratory (LBL), Systems, Science and Software (S-Cubed) and the University of Auckland in New Zealand each used their own internally-developed simulators. In addition, Stanford University undertook the problem using the University of Auckland's simulator. In all of these calculations, the prescribed spatial zoning was employed. The time-resolution employed by the various investigators varied significantly, however, as shown in Table 2. Intercomp used by far the crudest time-resolution ($\Delta t \approx 4$ months), followed by Geotrans ($\Delta t \approx 6$ weeks), LBL ($\Delta t \approx 5$ weeks), S-Cubed ($\Delta t \approx 18$ days), the University of Auckland ($\Delta t \approx 4$ days) and Stanford University ($\Delta t \approx 2$ days). The very small time-steps used by the last two groups were required for computational stability by the University of Auckland simulator. As will be seen, the crude time-step used by Intercomp adversely influenced accuracy at early times.

EFFECTS OF THE SATURATION CURVE

At very early times, the pressure in the production well-block (zone i = 3, j = 3 centered at x = 62.5 m, y = 62.5 m) drops very rapidly in response to production. Very quickly, pressures in this zone reach saturation conditions. Thereafter, the well-block pressure drops more slowly, accompanied by a decline in temperature and the evolution of steam. Thus, the temperature and pressure histories in the production well-block may be cross-correlated; the resulting relationship between pressure and temperature coincides with the water/steam saturation curve $P_{sat}(T)$.

Results of this type are shown in Figure 2, along with data points taken from the ASME Steam Tables. Figure 2 illustrates the accuracy of the fit to the water/steam saturation curve employed by each simulator. Both the LBL and S-Cubed codes use interpolation between tabulated steam-table points to establish $P_{sat}(T)$; the

other three simulators use analytic fits. Thus, the LBL and S-Cubed saturation curves are essentially exact. The Intercomp code uses a fit that is high by about 0.2 bar in the vicinity of 240°C; the University of Auckland simulator is high by 0.5 bar. The Geotrans fit is worst of all in this vicinity, being high by a full bar.

The prescribed description of Problem 5 entailed a value for P_o (the initial system pressure, and the boundary pressure to be maintained along x = 300 meters) which exceeds the saturation pressure for 240°C by 2.5 bars, as discussed above. Unfortunately, these instructions were interpreted differently by the various groups, as illustrated in Table 3. The true value for P_{sat} (240°C) from the ASME Steam Tables is 33.48 bars, so that ideally P_o should be 35.98 bars ($\approx$ 36.0 bars). In the cases of LBL and S-Cubed, who employ exact phase-line fits, no difficulties arose. Both the Stanford and University of Auckland groups used an initial pressure (P_o) of 36.52 bars; this value was chosen so as to maintain the relationship [$P_o = P_{sat} + 2.5$ bars] in spite of the fact that the saturation curve used by the University of Auckland's simulator is about one-half bar high at T = 240°C. Both Intercomp and Geotrans, however, interpreted the problem specifications to mean that P_o should be 36 bars, and made no attempt to correct for deviations in their saturation curve fits from steam table values. In the case of Intercomp, this meant that P_o exceeded P_{sat} by 2.3 bars, or 92 percent of the intended pressure difference. In the Geotrans case, P_o exceeded P_{sat} by only 1.5 bars, or only 60 percent of the intended excess. This error produced substantial deviations between the Geotrans calculations and those of the other groups. Due to the smaller restraining pressure, the two-phase region in the Geotrans results was both larger and more persistant than in the other calculations, as will be seen.*

TOTAL STEAM-IN-PLACE

Figures 3 and 4 show the time-histories of the total mass of steam in the system for Problems 5A and 5B as predicted by each calculation. These calculated results fall into three groups. The LBL and S-Cubed calculations are virtually identical. The Intercomp results indicate a slightly greater steam mass, probably due to the fact that the boundary pressure exceeded saturation pressure by 2.3 bars instead of 2.5. The Stanford University/University of Auckland calculations predict higher steam quantities, particularly for Problem 5A; typically, from 5 to 15 percent higher than LBL and S-Cubed. Stanford and the University of Auckland used the correct restraining pressures; possible reasons for the deviation between LBL/S-Cubed and Stanford/U. Auckland will be discussed later.

---

* Since these calculations were made, Geotrans has corrected their saturation curve fit so that, were they to repeat the calculations, they would obtain correct results.

Finally, as discussed earlier, the Geotrans calculations vastly overpredicted the steam mass (by a factor of as much as 1.6). The differences in results between Problems 5A and 5B arise, of course, from the onset of injection at t = 1 year in the latter case. This causes pressures to rise and boiling to be suppressed.

CALCULATED PRESSURE HISTORIES

Figures 5 and 6 show the calculated pressure histories in the production well-block (i=3, j=3) for the two cases (5A, 5B); Figures 7 and 8 are the corresponding pressure histories in the injection well-block (i=7, j=6). Recall that no injection takes place in Problem 5A. These results are plotted as pressure difference from the initial pressure (P_o) for each calculation. In both cases (5A and 5B), the pressure in the production well-block first drops very rapidly to the saturation pressure; this occurs virtually instantaneously on the time-scale of these plots. Then, the fluid in the well-block begins to boil. Pressures continue to decline, but much more slowly. In Problem 5A, the production well-block remains two-phase until $t \approx 2.8$ years. At this time, sufficient cold water has been drawn into the well-block to cause all the steam to condense. Once single-phase conditions again prevail, the lower resistance to flow permits pressures to recover somewhat, in spite of continued production. In Problem 5B, the pressure increase induced by the onset of injection at t = 1 year causes the production well-block to revert to single-phase conditions shortly thereafter.

The pressure histories calculated by LBL and S-Cubed are essentially indistinguishable. Those computed by Intercomp generally agree with LBL and S-Cubed except at early times (t < 1 year or so). This early disagreement is probably due to the poor temporal resolution of the Intercomp calculation; a four-month time step is too long to accurately resolve the very rapid pressure changes that occur during the first part of the problem. The Geotrans results differ substantially from Intercomp, LBL and S-Cubed for the first several years of history for reasons discussed above, but at late times all four calculations (Geotrans, Intercomp, LBL and S-Cubed) are in reasonably good agreement. The computations of Stanford University and the University of Auckland (both using the latter's simulator), on the other hand, exhibit late time pressure disturbances that are 5 to 10 percent greater than those predicted by the other groups. The reasons for this discrepancy are not known for certain. It is not unlikely, however, that they arise from the constitutive description of the fluid employed, in particular the viscosity. Darcy's law states that, all else being equal, the pressure gradient required to maintain a given fluid mass flow rate will increase in proportion to the fluid's kinematic viscosity. Thus, one would expect that if viscosities were about 5

percent too high, predicted pressure drops would be approximately 5 percent high as well. In this connection, it is worthy of note that the experimental tolerances reported in the ASME Steam Tables for the kinematic viscosities of saturated water and steam in the vicinity of 240°C are typically ± 2 to 3 percent. Furthermore, if the viscosities used by the University of Auckland's simulator were slightly high, the exaggerated pressure drop which would then result would tend to cause more boiling and a greater mass of steam in the system as a whole. This is indeed observed, as was shown in Figures 3 and 4.

RESULTS FOR HEAT TRANSFER

Figures 9 and 10 illustrate the calculated temperature histories for Problems 5A, 5B; Figures 11 and 12 show the evolution with time of the enthalpy of the produced fluid. For early times ($t < 2.8$ years for Problem 5A, < 1 year for Problem 5B), the production well-block is two-phase so that the temperature history is correlated with the pressure history. At late times, the invasion of the production area by colder fluid causes the well-block temperature to decline. This effect is particularly pronounced for Problem 5B which involves the injection of cold (80°C) water in a nearby well. Similar trends may be observed in the discharge enthalpy histories (Figures 11 and 12). The results of all the calculations are in excellent agreement, except that at early times ($t < 3$ years for Problem 5A, < 2 years for 5B) the Geotrans results exhibit lower temperatures and higher discharge enthalpies than the others. Since the Geotrans calculation produced excessive steam, the steam-phase mobility was enhanced so that a greater proportion of high-enthalpy steam entered the production well. The presence of this excessive steam, furthermore, reduced the overall mobility of the water/steam mixture as a whole, causing a greater well-block pressure drop; since, for two-phase flow, pressure and temperature are correlated by the saturation curve P_{sat} (T), the well-block temperatures were correspondingly reduced relative to the other calculations. At late times, however, it is noteworthy that the Geotrans results for both temperature and discharge enthalpy agree with the others.

CONCLUSIONS

The results obtained from four of the five simulators are in excellent agreement for Problem 5. The fifth simulation (that of Geotrans) deviates from the others due only to an unfortunate combination of a misunderstanding concerning the definition of the problem and a somewhat inaccurate fit to the water/steam saturation curve in the vicinity of 240°C; the disagreement does not arise from any fundamental flaw in the Geotrans simulator. As noted earlier, since these calculation were performed, Geotrans has improved their saturation curve fit; there is every reason to believe that a repeat calculation would agree with the other results, particularly in view of the good performance of the Geotrans simulator on the other problems in the DOE Problem Set.

TABLE 1

ROCK PROPERTIES FOR PROBLEM 5

DENSITY OF ROCK GRAIN MATERIAL = 2500 KG/M^3

POROSITY = 0.35

PERMEABILITY = 2.5×10^{-14} M^2 ($\approx$ 25 MILLIDARCIES)

ROCK GRAIN HEAT CAPACITY = 1 JOULE/GRAM-°C

ROCK GRAIN THERMAL CONDUCTIVITY = 1 WATT/M-°C

RELATIVE PERMEABILITY DATA:

$$\left.\begin{aligned} R_L &= 1 \\ R_S &= 0 \end{aligned}\right\} \quad \text{FOR } 0 \leq S \leq 0.1$$

$$\left.\begin{aligned} R_L &= Z^4 \\ R_S &= (1-Z^2)(1-Z)^2 \end{aligned}\right\} \quad \text{FOR } 0.1 \leq S \leq 0.7$$

$$\left.\begin{aligned} R_L &= 0 \\ R_S &= 1 \end{aligned}\right\} \quad \text{FOR } 0.7 \leq S \leq 1$$

S IS STEAM SATURATION

R_L IS RELATIVE PERMEABILITY TO LIQUID WATER

R_S IS RELATIVE PERMEABILITY TO STEAM

$Z = (0.7 - S) / 0.6$

TABLE 2

PROBLEM 5 TEMPORAL RESOLUTION

	CASE "A" (CYCLES/YEAR)		CASE "B" (CYCLES/YEAR)	
	MEAN	MINIMUM	MEAN	MINIMUM
GEOTRANS	8	NR	8	NR
INTERCOMP	3.2	3.0	3.9	3.0
LBL	NR	10	NR	10
S-CUBED	21	20	21	20
STANFORD	225*	183*	205*	183*
U. AUCKLAND	NR	90*	NR	90*

"NR" = NOT REPORTED

* SMALL TIME STEPS REQUIRED FOR COMPUTATIONAL STABILITY

TABLE 3

PROBLEM 5 PRESSURE VALUES

	P_o (Initial and Boundary Pressure)	P_{SAT}(240°C) (Boiling Pressure in Central Region)	$P_o - P_{SAT}$
GEOTRANS	36.00 Bars	34.50 Bars	1.50 Bars
INTERCOMP	35.99 Bars	33.70 Bars	2.29 Bars
LBL	36.00 Bars	33.48 Bars	2.52 Bars
S-CUBED	35.98 Bars	33.48 Bars	2.50 Bars
STANFORD	36.52 Bars	34.02 Bars	2.50 Bars
U. AUCKLAND	36.52 Bars	34.02 Bars	2.50 Bars

Case A: No Injection, Production 50 gram/sec-m.

Case B: Production 50 gram/sec-m. Injection for Time ≥ 1 Year, 30 gram/sec-m, 80°C.

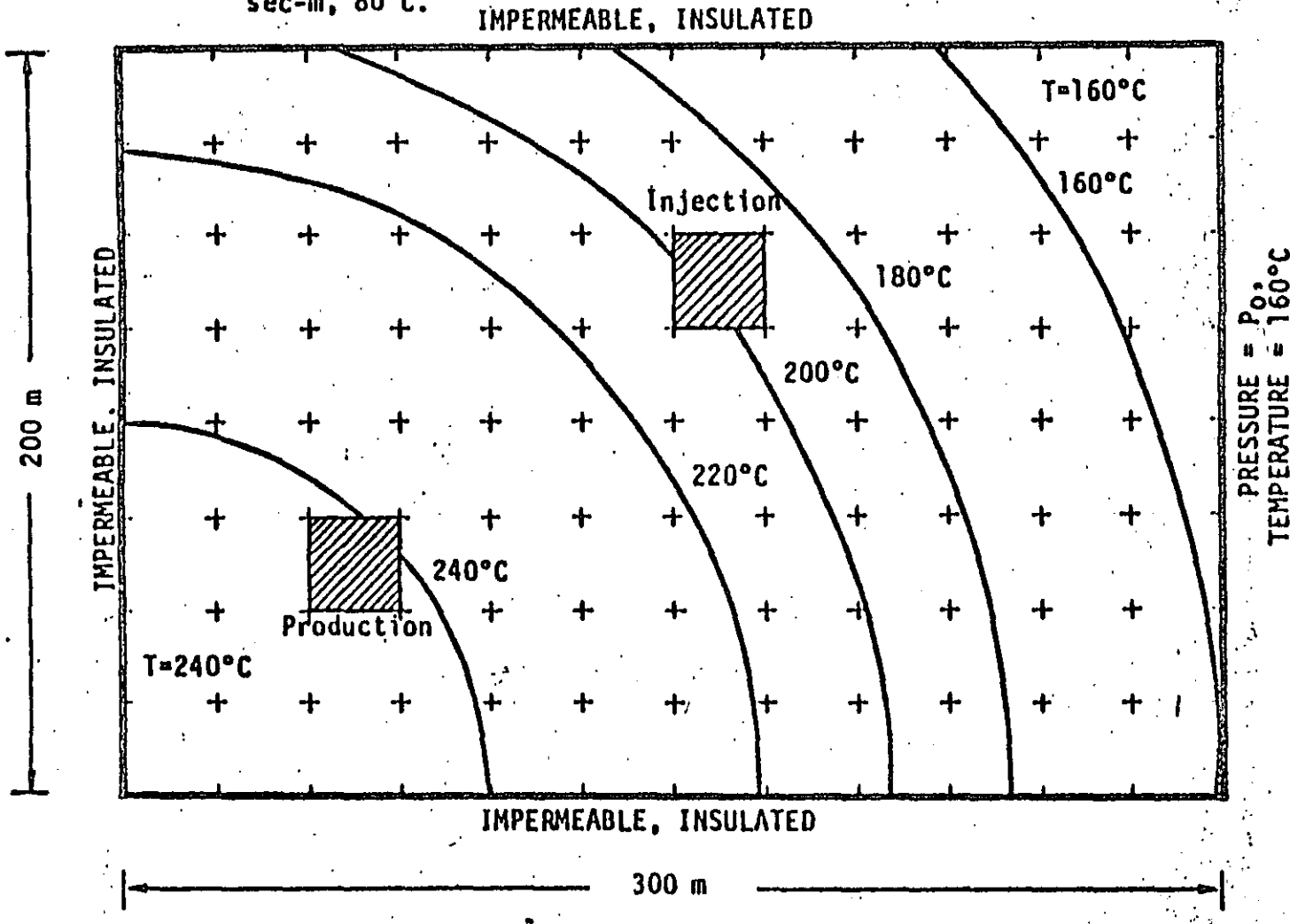

Initial Pressure = Boundary Pressure = $P_o = P_{sat}(240°C) + 2.5$ Bars ≈ 36 Bars

FIGURE 1. PROBLEM 5 GEOMETRY

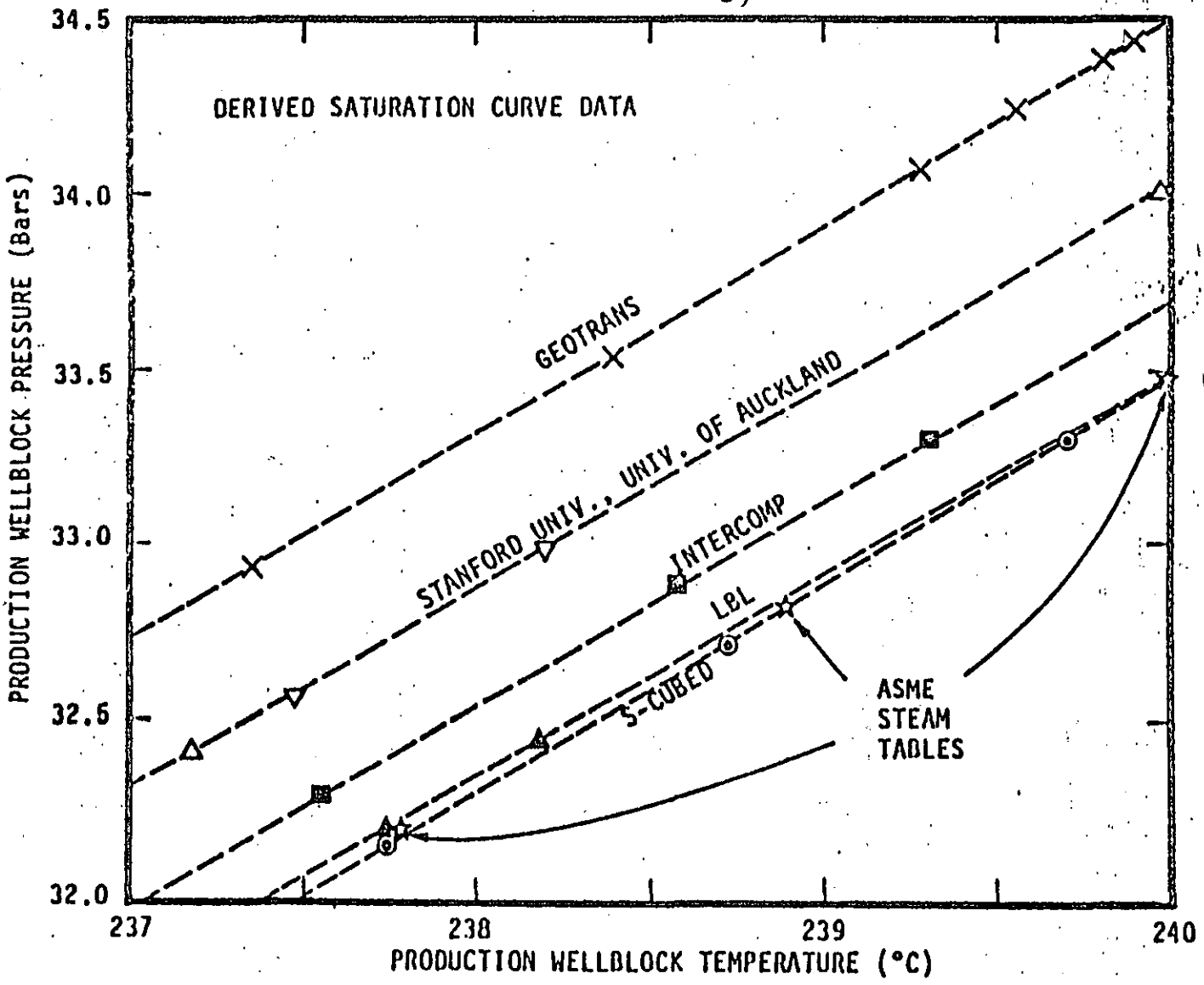

FIGURE 2. EARLY-TIME CORRELATION BETWEEN WELL-BLOCK PRESSURE AND TEMPERATURE

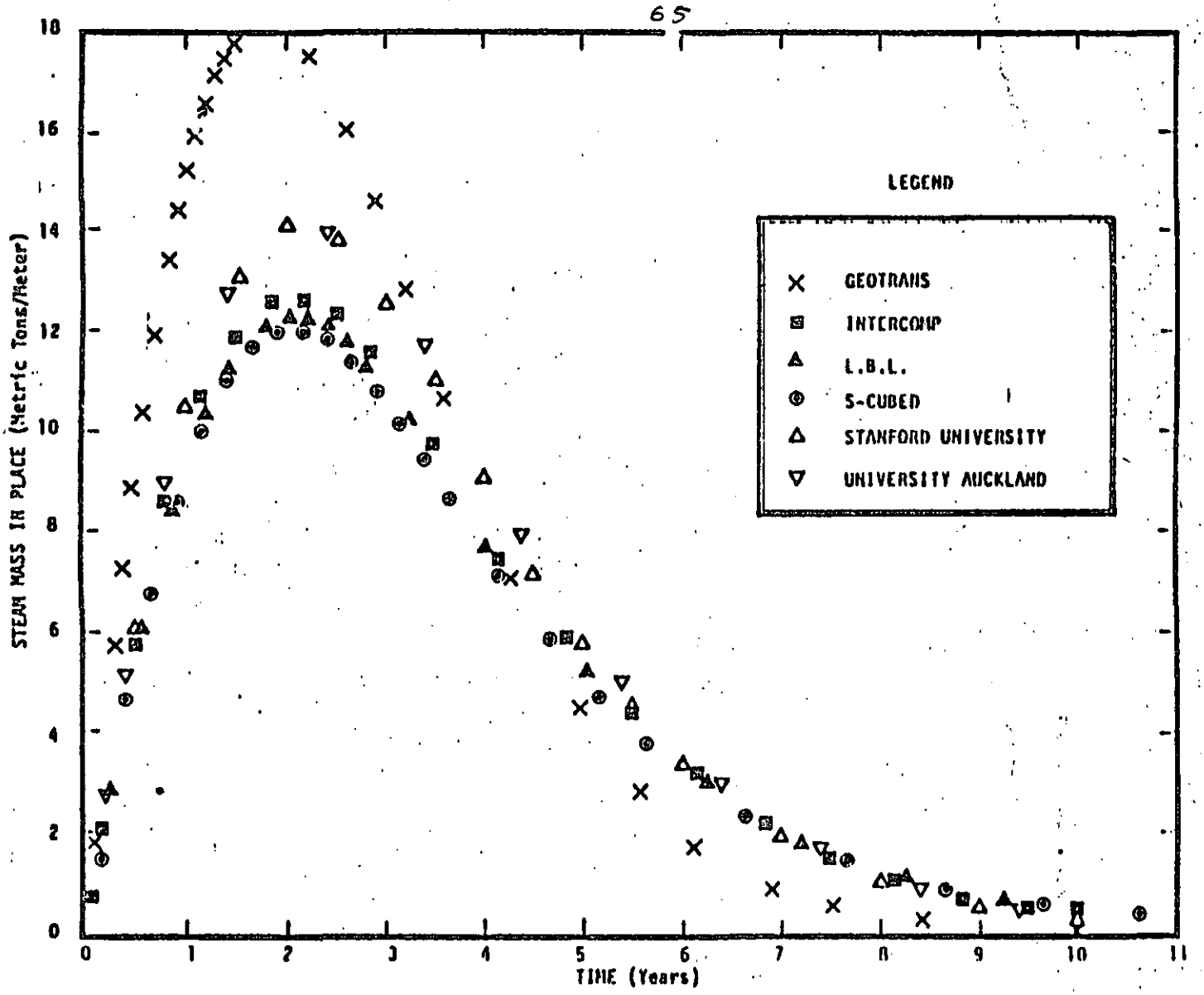

FIGURE 3. HISTORY OF TOTAL STEAM-IN-PLACE PER UNIT THICKNESS -- PROBLEM 5A.

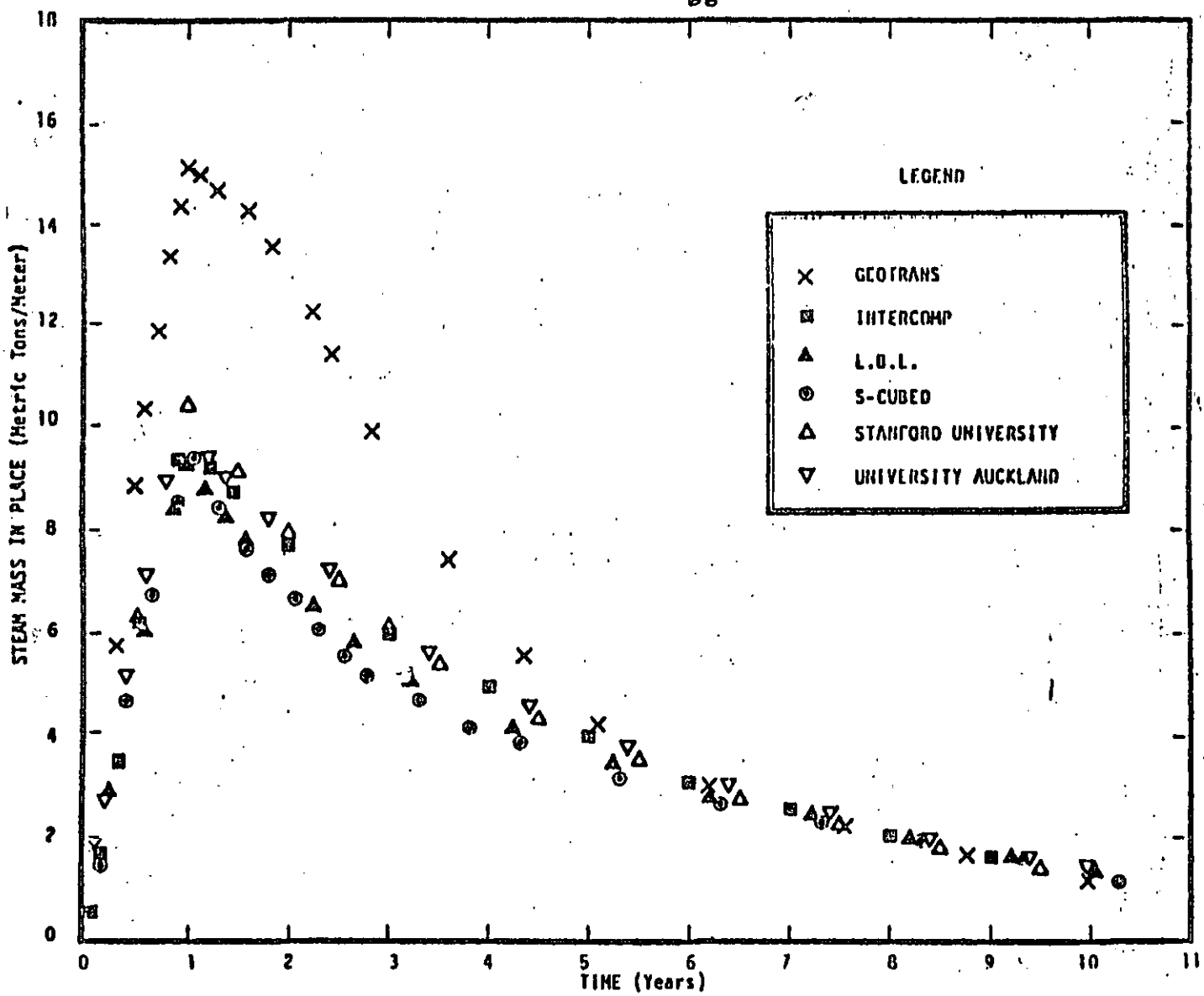

FIGURE 4. HISTORY OF TOTAL STEAM-IN-PLACE PER UNIT THICKNESS -- PROBLEM 5B.

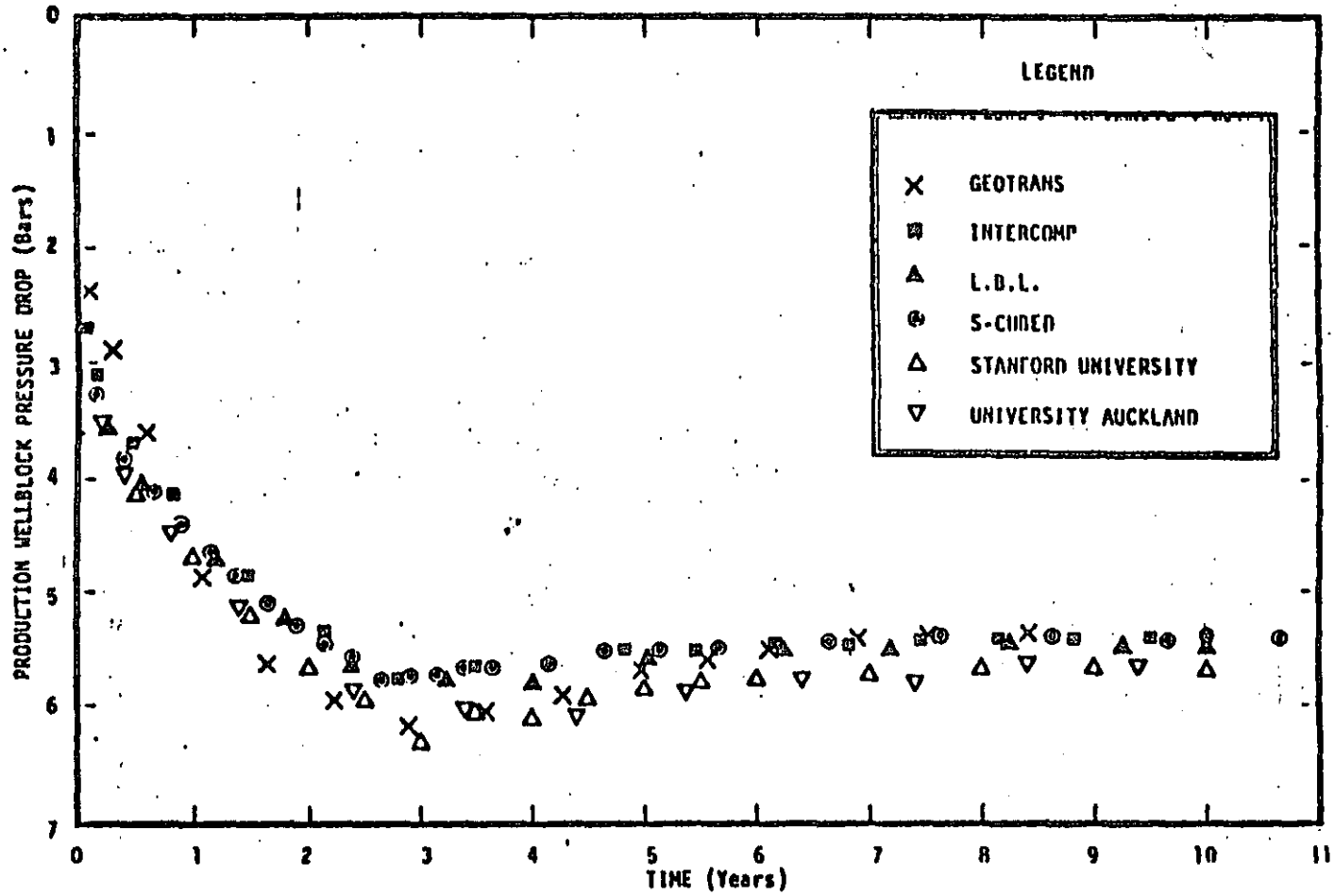

FIGURE 5. PRESSURE HISTORY IN PRODUCTION WELL-BLOCK -- PROBLEM 5A.

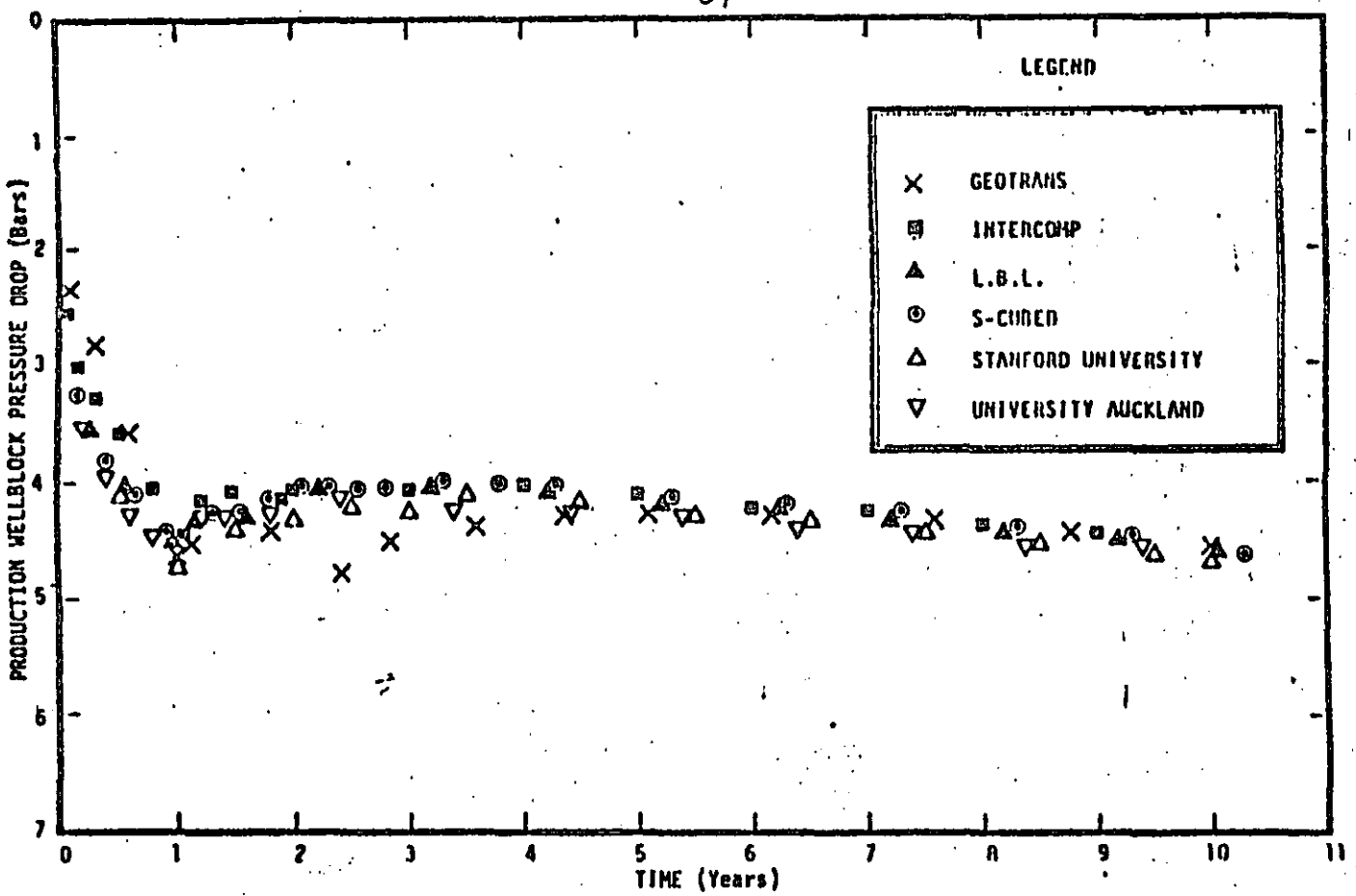

FIGURE 6. PRESSURE HISTORY IN PRODUCTION WELL-BLOCK -- PROBLEM 5B.

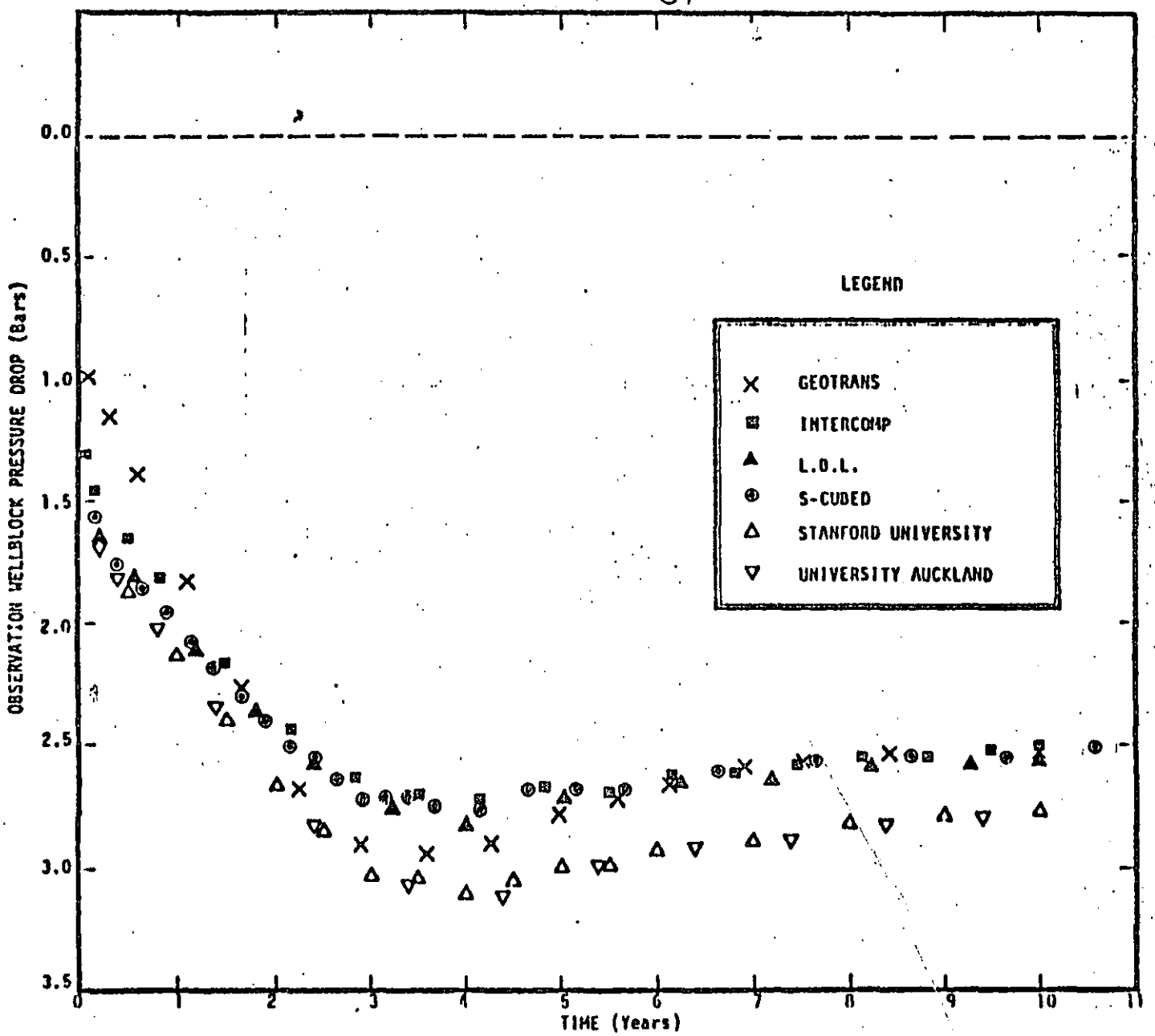

FIGURE 7. PRESSURE HISTORY IN OBSERVATION WELL-BLOCK -- PROBLEM 5A.

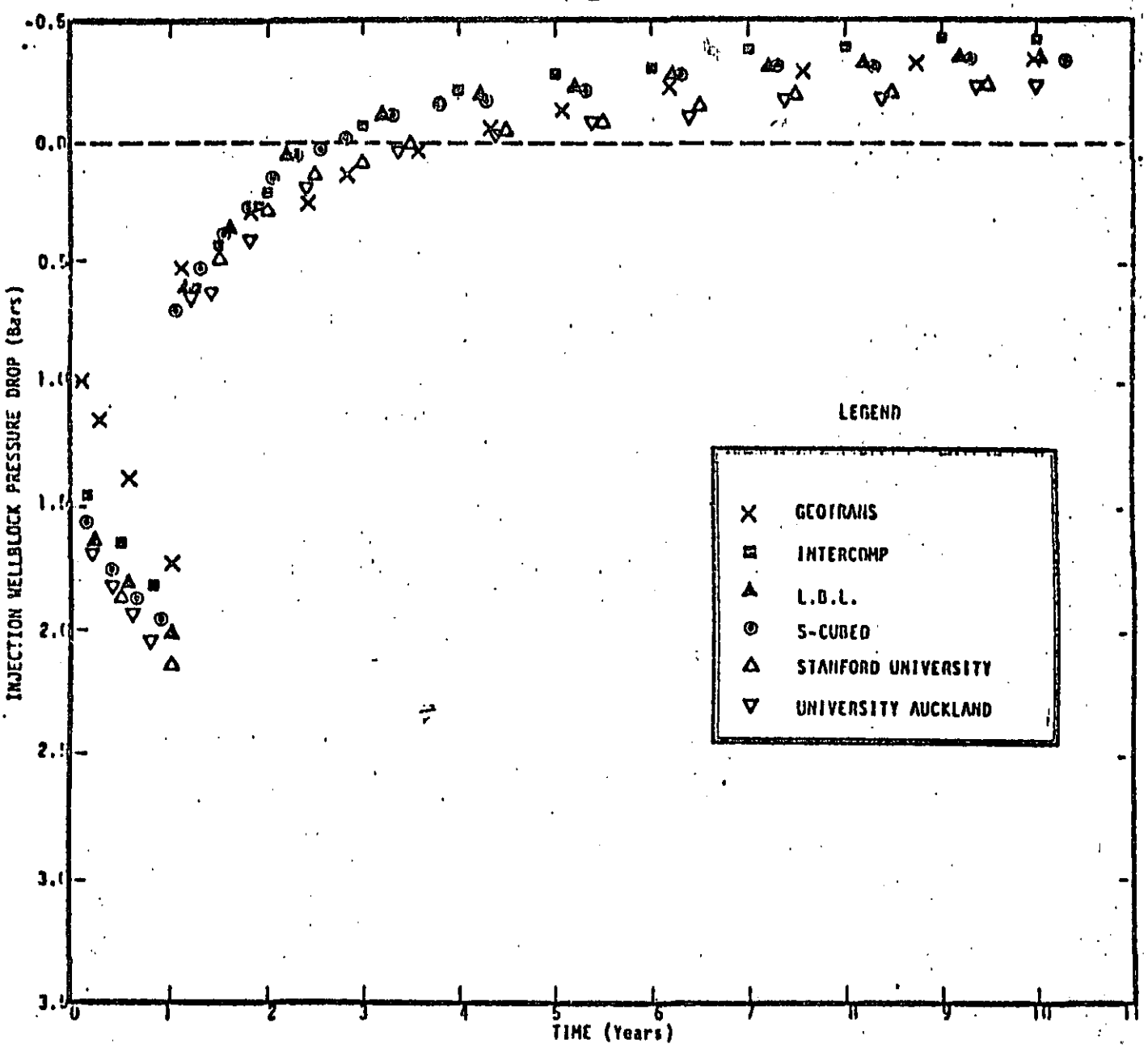

FIGURE 8. PRESSURE HISTORY IN INJECTION WELL-BLOCK -- PROBLEM 5B.

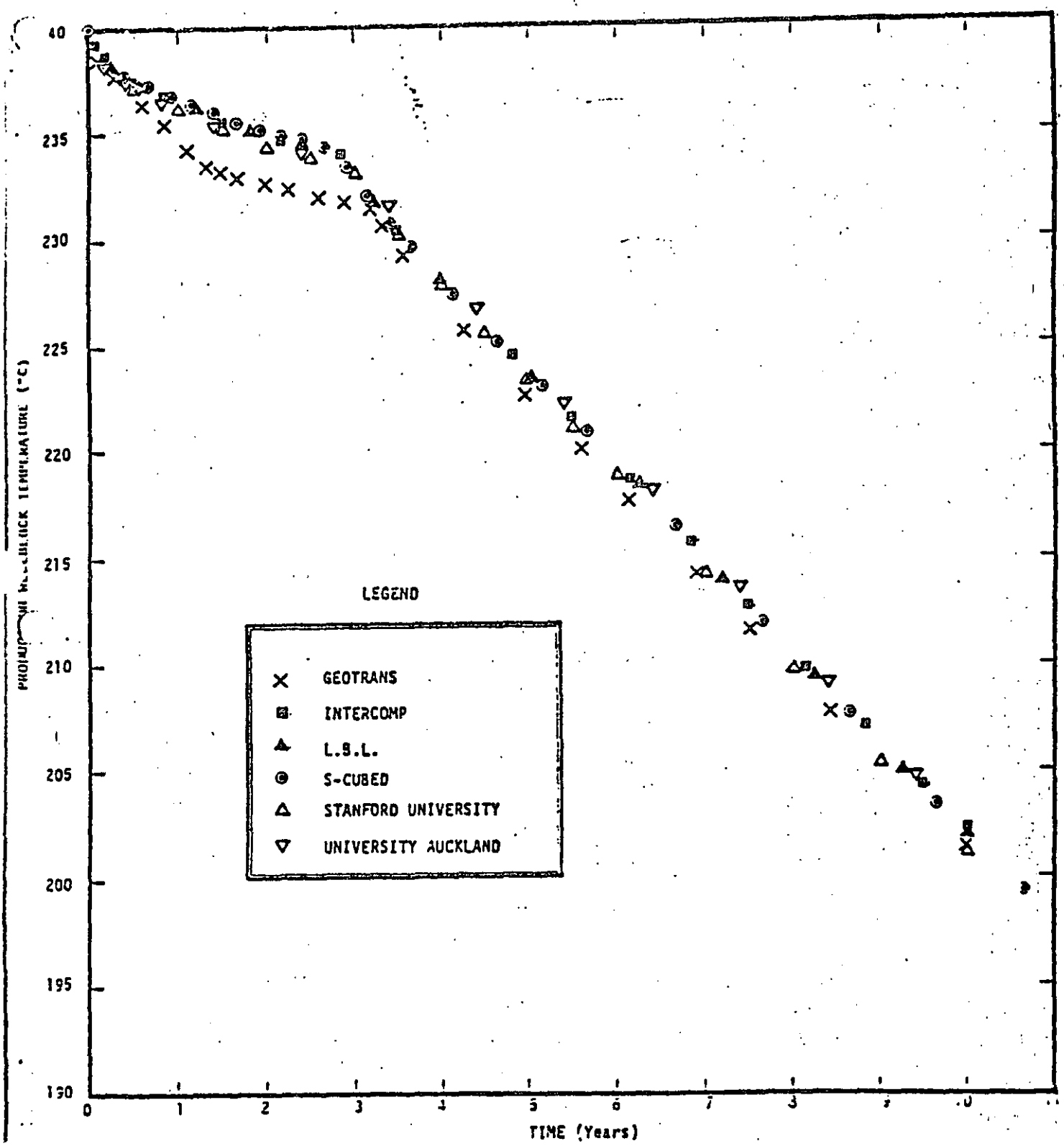

FIGURE 9. PRODUCTION WELL-BLOCK TEMPERATURE HISTORY -- PROBLEM 5A.

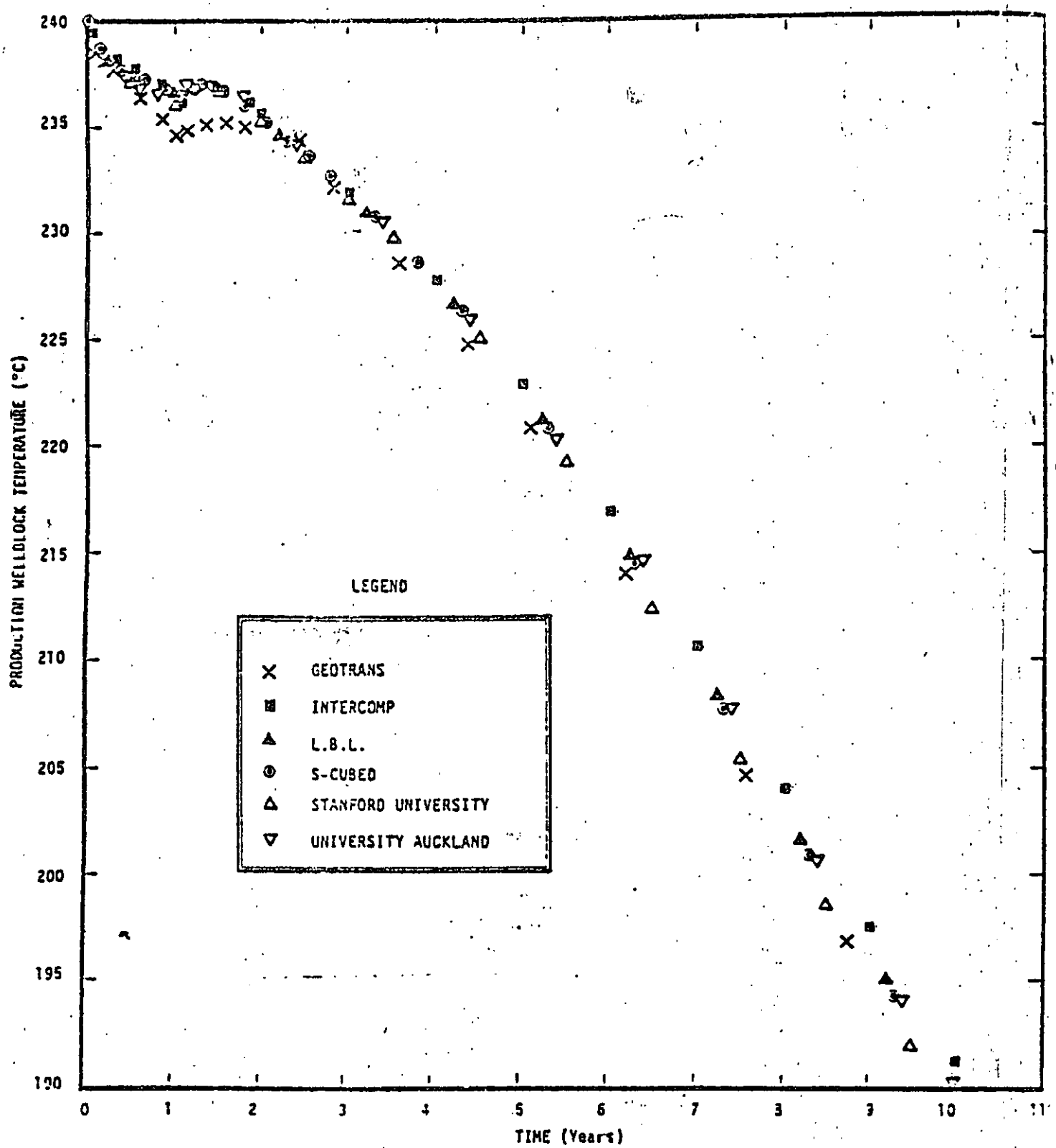

FIGURE 10. PRODUCTION WELL-BLOCK TEMPERATURE HISTORY -- PROBLEM 5B

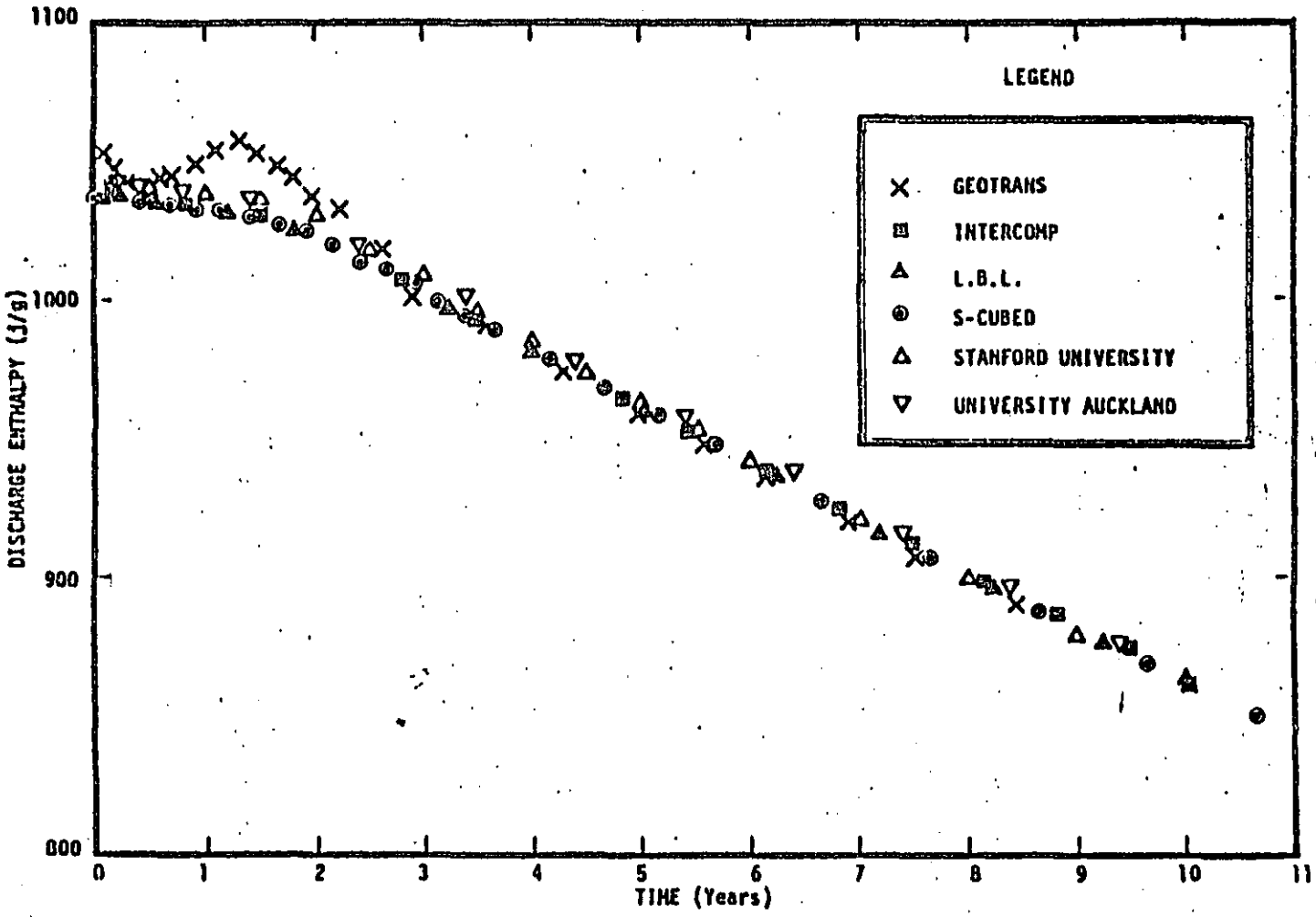

FIGURE 11. PRODUCTION WELL DISCHARGE ENTHALPY HISTORY -- PROBLEM 5A.

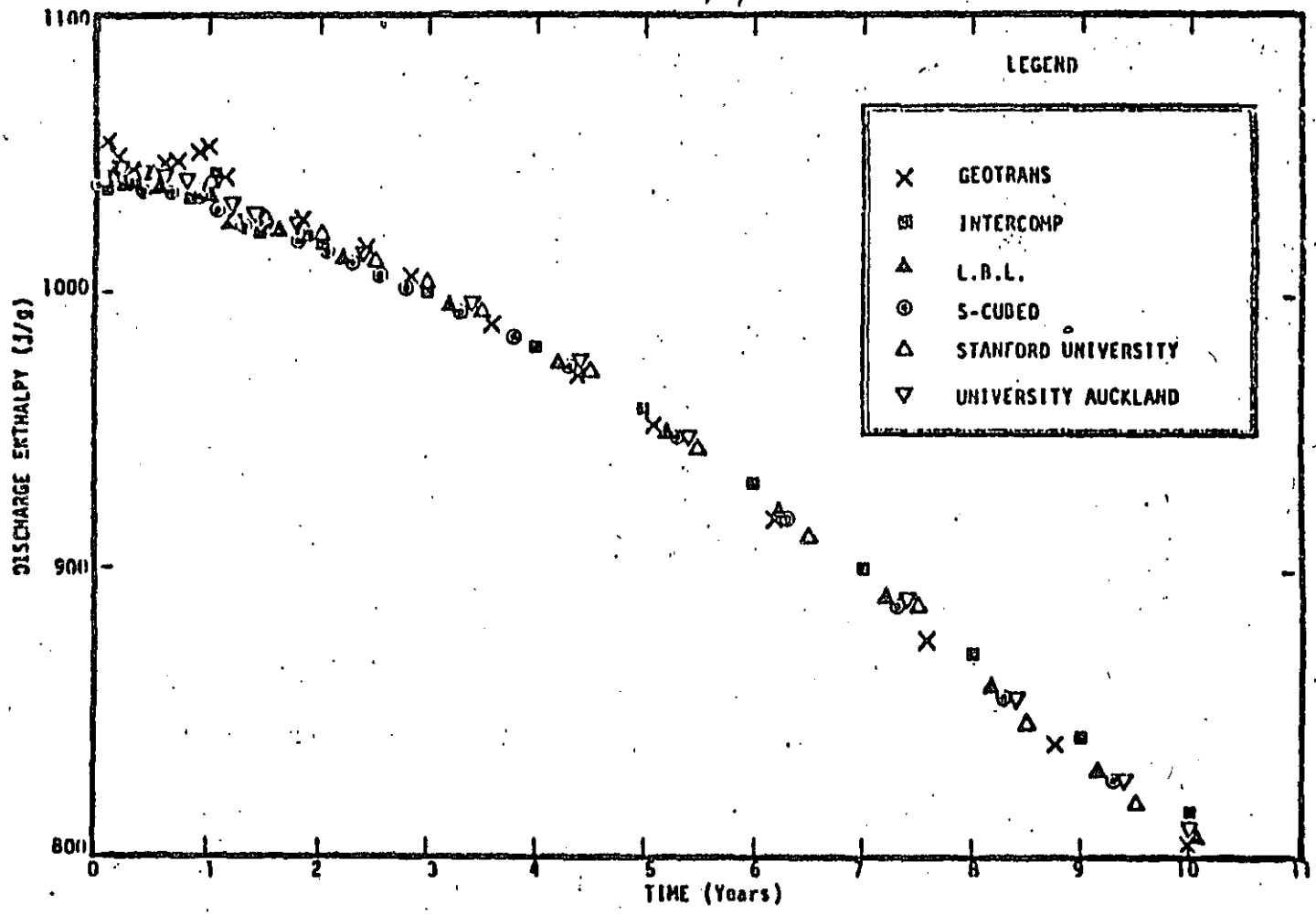

FIGURE 12. PRODUCTION WELL DISCHARGE ENTHALPY HISTORY -- PROBLEM 5B.

DOE-PROJECT ON GEOTHERMAL RESERVOIR ENGINEERING COMPUTER CODE COMPARISON AND VALIDATION

-EVALUATION OF RESULTS FOR PROBLEM 6-

Karsten Pruess
Lawrence Berkeley Laboratory
University of California
Berkeley, California 94720

INTRODUCTION

Problem 6 is a reservoir-wide problem, and the only one in the set which involves three-dimensional flow. The reservoir is of "Wairakei-type," with single-phase liquid at depth, overlain by a two-phase zone with immobile steam, and capped off with a zone of colder single-phase water. Production occurs from a well field with completion intervals below the two-phase zone. Parameters are chosen in such a way that boiling in the well field and two-phase flow commence after a certain period of production.

Although the problem is schematic in nature, it is nonetheless a prototype of field-wide studies which would be undertaken to examine alternative reservoir development plans. Typical questions to be addressed by this type of problem would include: at what depth should the wells be completed? what flowrates can be sustained for what length of time by a well field of given areal extension? what is the evolution of downhole pressures and discharge enthalpies?

Problem 6 is probably the most difficult one in the set for numerical simulators, due to its three-dimensional nature and the occurrence of phase transitions with subsequent two-phase flow, including gravitationally induced steam/water counterflow.

PROBLEM DESCRIPTION

The reservoir is a parallelepiped of 4 x 5 km^2 areal extent and 1.8 km thickness. Figure 1 shows the geometric design of the system, and the zoning to be used in the simulation. Tables 1 through 4 give the complete specifications of all parameters. Formation properties vary somewhat with depth, and there is a large contrast between horizontal and vertical permeability. The lower 2/3 of the reservoir is initially filled with liquid water at 280 °C temperature. This is overlain by a two-phase region, also at 280 °C, which has an immobile steam saturation of 10% by volume. Overlying this is a layer of colder water at T = 160 °C. The entire reservoir is gravitationally equilibrated, so that initially there is no fluid flow. The process to be simulated is production from a specified subregion at depth. Production rates increase with time in such a way that boiling in the wellblock and two-phase flow is initiated. In the process,

temperatures and pressures are kept to their initial values at the upper and lower boundaries, and at the surface at x = 5 km. The other three reservoir faces are closed ("no flow").

GENERAL DESCRIPTION OF RESERVOIR EVOLUTION

The evolution of the reservoir in response to production can be described as follows. As a consequence of production, pressures drop in the wellblock, so that horizontal and vertical flow towards the wellblock is initiated. Downflow from the two-phase zone gives rise to boiling and increasing vapor saturation. As the pressure decline spreads to the margins of the field, water recharge is initiated. One consequence of this is the occurrence of several phase transitions to single-phase conditions in the two-phase layer. The production rates for the first few years are such (small) that pressures in the wellblock stabilize, resulting in an approximately steady flow pattern. The increase in production rate after four years can not be readily sustained for the given permeabilities. Thus, large pressure drops occur in the grid block which represents the well field, as well as in adjacent grid blocks. This causes several phase transitions to two-phase conditions, and subsequent boiling. This is accompanied by a decline in temperatures and pressures, as well as a buildup of vapor saturation. Steam/water counterflow occurs as steam rises from the shallow two-phase layer, whereas water flows downward towards the production well. Conditions again approach a steady flow until the imposed increase in production rate after six years causes a rapid catastrophic decline of pressures in the production region, thus terminating the problem. This is unfortunate, as somewhat smaller production rates and a longer reservoir life would have allowed a more extensive comparison of simulated results.

COMPARISON OF RESULTS

Figures 2-4 show the simulated time evolutions of some of the more sensitive parameters. It is apparent that there is excellent agreement between the results of S^3, Geotrans, and LBL; whereas Intercomp's calculation is somewhat off. A conspicuous feature of Intercomp's results is that pressures below the well block (in layer 1) do not decline at all in the course of production, which gives rise to more water influx into the well block. As a consequence, well block pressures remain higher, particularly after five years, and vapor saturation and discharge enthalpy remain lower. The deviations become larger after the increase of production rate after six years. The nature of the discrepancies suggests some error in the problem definition rather than an error in Intercomp's simulator. It appears that the lower boundary conditions or the permeability below the well block had not been properly specified.

The quality of agreement between the calcuations of S^3, Geotrans, and LBL is quite remarkable, particularly in view of

the significant differences in methodology used in the simulators. S^3 and Geotrans use a finite difference method, whereas LBL's simulator employs an integral finite difference method. The primary dependent variables are, respectively, energy and pressure (S^3), pressure and enthalpy (Geotrans), and energy and density (LBL). Geotrans uses an analytical approximation for thermophysical properties of water substance, whereas S^3 and LBL employ a tabular equation of state.

CONCLUSION

Three of the four simulators used in computing a difficult three-dimensional problem show excellent quantitative agreement. This demonstrates that numerical simulators are capable of producing accurate results for field-wide reservoir depletion problems, involving phase transitions, gravitationally induced steam/water counterflow, and recharge.

Table 1: Rock properties.

	Layer 1	Layer 2	Layer 3	Layer 4	Layer 5
Grain Density (g/cm^3)	2.5	2.5	2.5	2.5	2.5
Porosity	0.2	0.25	0.25	0.25	0.2
x-Permeability (m^2)	100×10^{-15}	200×10^{-15}	200×10^{-15}	200×10^{-15}	100×10^{-15}
y-Permeability (m^2)	100×10^{-15}	200×10^{-15}	200×10^{-15}	200×10^{-15}	100×10^{-15}
z-Permeability (m^2)	2×10^{-15}	50×10^{-15}	50×10^{-15}	50×10^{-15}	2×10^{-15}
Heat Capacity ($J/g-^oC$)	1	1	1	1	1
Rock Therm. Cond.($w/m-^oC$)	1	1	1	1	1
Relative Permeability: Corey equations as in Problem #2, except:					
S_{lr} (liquid residual)	0.3	0.3	0.3	0.3	0.3
S_{gr} (gas residual)	0.1	0.1	0.1	0.1	0.1

Table 2: Initial conditions.

Temperature:

Layers 1-4, 280°C everywhere

Layer 5, 160°C

Pressure:

Layer 4: $P_4^o = P_{sat}\ (280^oC) \approx 64$ Bars

(Steam saturation) $S_s^o = 0.1$ (steam initially immobile)

Layer 5: $P_5^o = P_4^o - (1470\ m^2/s^2) \times (\rho_4^o\text{-liq} + \rho_5^o)$

Layer 3: $P_3^o = P_4^o + (1470\ m^2/s^2) \times (\rho_4^o\text{-liq} + \rho_3^o)$

Layer 2: $P_2^o = P_3^o + (1470\ m^2/s^2) \times (\rho_3^o + \rho_2^o)$

Layer 1: $P_1^o = P_2^o + (1470\ m/s) \times (\rho_2^o + 2\rho_1^o)$

Where ρ_4^o-liq = liquid density in Layer 4

These initial conditions (P^o, ρ^o, S_s^o) are functions of z only. Layers 1, 2, 3 and 5 are initially single-phase liquid; layer 4 is initially 2-phase with an immobile steam phase. The pressure distribution is liquid-hydrostatic throughout at zero time.

Table 3: Boundary conditions.

At z = 1.5 km (top surface), maintain $P_{top} = P_5^o - (1470\ m^2/s^2) \times \rho_5^o$ and T = 100°C.

At z = 0, maintain $P_{bottom} = P_1^o + (2940\ m^2/s^2) \times \rho_1^o$ and T = 280°C.

Along planes at x = 0 and y = 0, impose symmetry conditions.

Treat plane at y = 4 km as impermeable and insulated.

Along plane at x = 5 km, maintain initial distributions of P, T, S_s.

Table 4: Production strategy.

All production is taken from a single corner cell (i=1, j=1, k=2).

$0 \leq t \leq 2$ years,	$Q(t) = 1000$ kg/s
2 years $< t \leq 4$ years,	$Q(t) = 2500$ kg/s
4 years $< t \leq 6$ years,	$Q(t) = 4000$ kg/s
$t > 6$ years,	$Q(t) = 6000$ kg/s

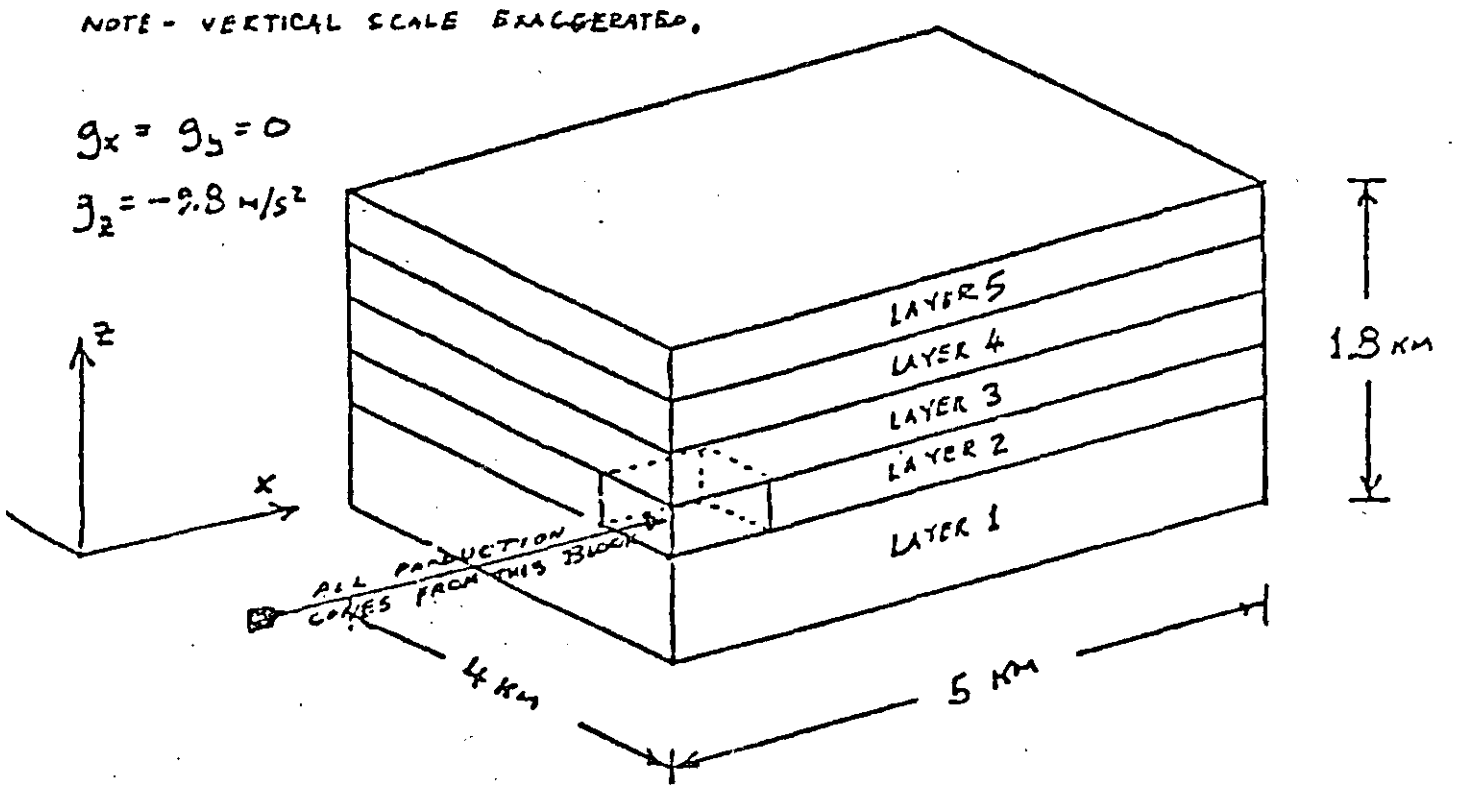

LAYER THICKNESSES:
LAYER 1, 0.6 KM
LAYERS 2-5, 0.3 KM EACH

GRID: 5 x 5 x 5
(Horizontal, uniform, 5 zones each direction)

Figure 1: Geometry of the reservoir and mesh design.

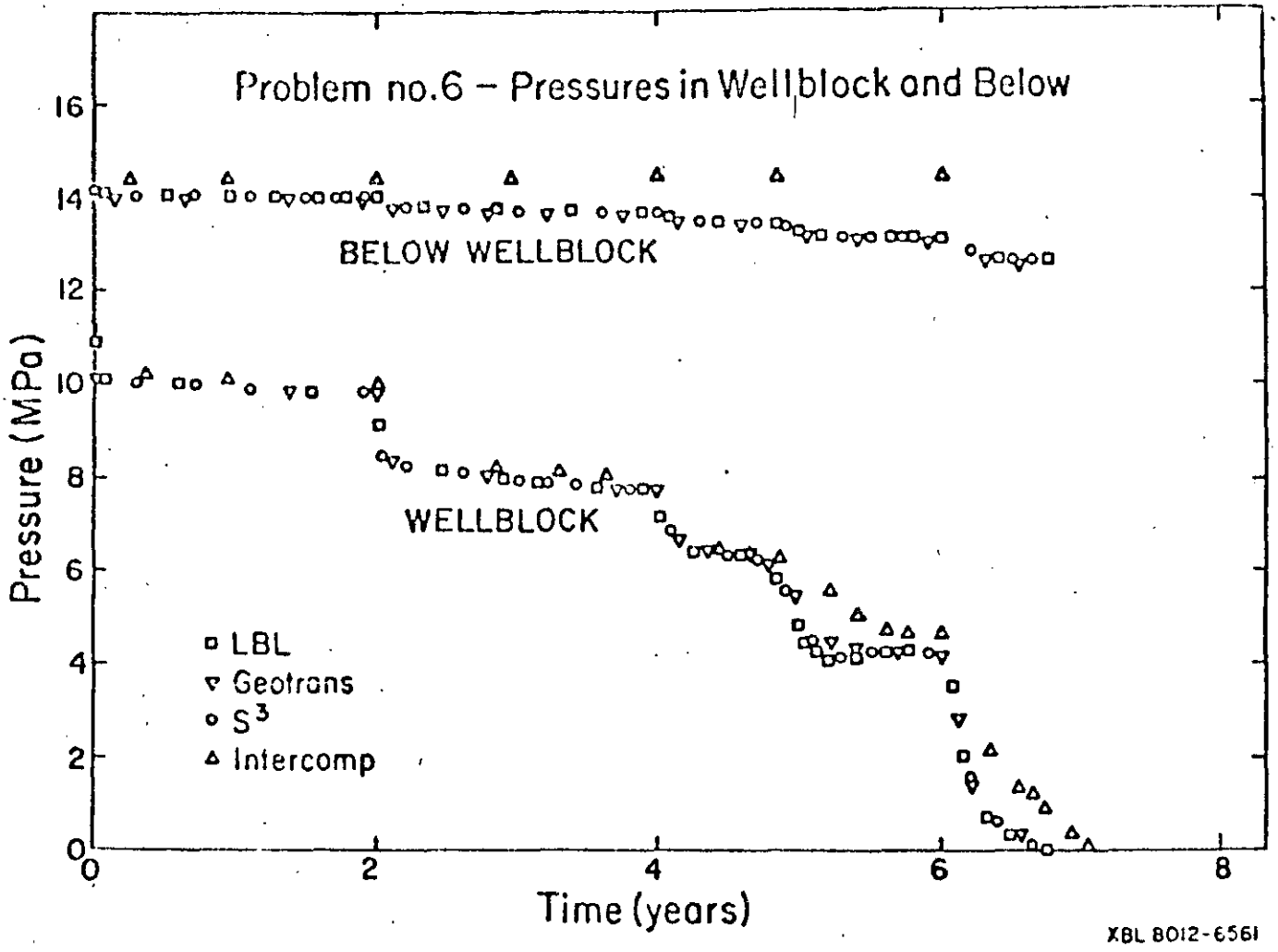

Figure 2: Time dependence of selected pressures.

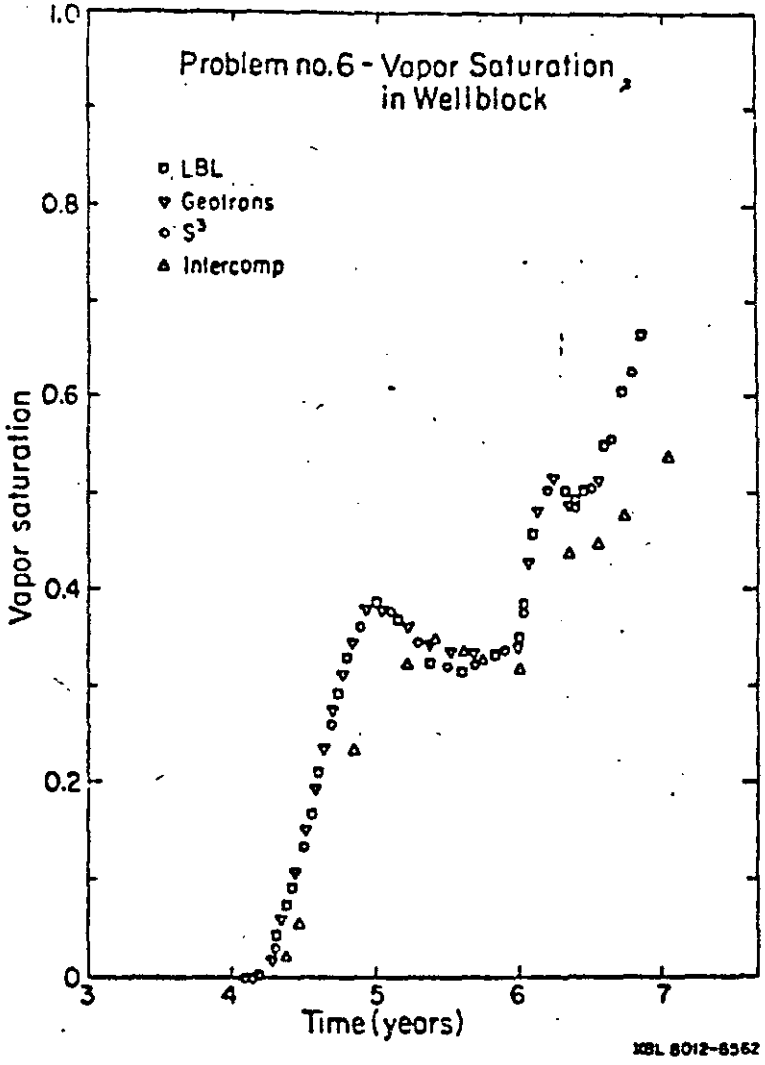

Figure 3: Evolution of vapor saturation in well block.

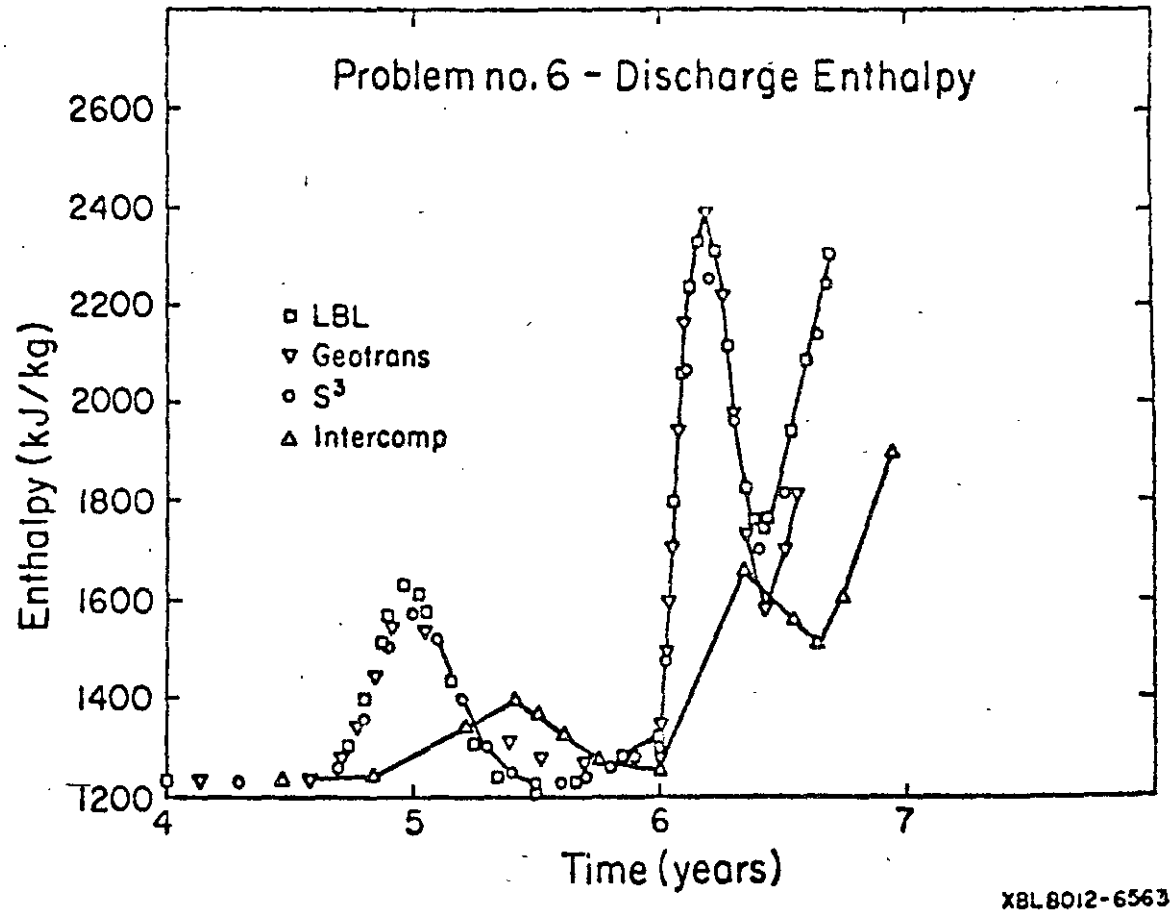

Figure 4: Discharge enthalpy history.

COMMENTS ON SIMULATOR VALIDATION STUDY

by C. W. Morris and D. A. Campbell

Because of the dependence of the geothermal industry on the prediction of the resource performance with little or no production history, the validity of the reservoir engineering estimates, including the reservoir simulation work, is very important. Investors, utilities, government agencies, and other outside parties, therefore, must have confidence that the geothermal simulator can accurately solve the energy and flow equations necessary to describe the physical processes. This is analogous to the use of "black oil" simulators in the petroleum industry.[1] Our experience has shown that many consultants, particularly those who are non-users of geothermal simulators, are reluctant to accept the simulator results. Even when they agree that the model "set-up" is a reasonable representation of a field as known at the time, they commonly limit their endorsement because of uncertainty that the physics of reservoir and well operations are properly replicated.

The studies presented at this workshop clearly indicated that these simulators can solve a wide variety of geothermal problems, using different numerical methods, and arrive at the same results. It must, therefore, be concluded that these computer codes can describe the physical processes as well as we now understand them.

The validity of the geothermal reservoir simulator calculations should not be confused with the accuracy of the reservoir performance predictions since the computer code is only one of many "tools" used by the engineer. A reasonable reservoir model and an accurate description to the reservoir parameters by the engineer are required to achieve good performance predictions. Parametric and sensitivity studies are properly part of any reservoir simulation work. Outside parties must evaluate these phases of reservoir engineering independent of the simulation physics.

Assuming that the reservoir model and input parameters reflect the true reservoir conditions, the reservoir simulation results can be accepted as valid by the outside parties involved in geothermal development. The added advantage of the simulator approach over the consultant's "guess" is that the input is clearly documented for evaluation by others and the results can be modified in a logical manner as experience and knowledge of the resource increases. The complexity of the reservoir simulation effort can also increase with knowledge.

We wish to congratulate the DOE/San Francisco and the contract participants for a job well done. This complex study was accomplished in a timely fashion to support a recognized need of the geothermal industry.

---

1. A. S. Odeh, "Comparison of Solutions to a Three-Dimensional Black-Oil Reservoir Simulation Problem," JPT, January 1981, Vol. 33, No. 1, p.13.

Panelist's Remarks on Intercomparison of Reservoir Models
Sixth Stanford Geothermal Program Workshop
December 17, 1980

by

Evan Hughes and Vasel Roberts
Electric Power Research Institute

The presentations made in this session have shown that simulators are capable of calculating reservoir performance with reasonable agreement among the models. Beyond such confirmation of modeling capability, additional effort in four areas is needed:

- o sensitivity of results to errors in the physical data
- o accurate physical data for use in the models
- o estimates of probabilities and/or levels of confidence associated with production capacity, temperature and pressure profiles, and reservoir life
- o verification of models by comparison with reservoir production data

From our perspective in conducting a geothermal research program for the electric utility industry we have formulated some informal criteria for reservoir simulation models. These constitute a "model of a model," i.e., some expectations of what a reservoir model should do in order to meet the needs of electric utilities engaged in geothermal power development. To develop the model of the model four questions are addressed.

First, what should a reservoir model be to a geothermal utility? In one respect it is no different than any other type of model. It is a device that will allow one to visualize what the product looks like and how it works prior to commitment. While this particular tool is generally used directly by resource companies and reservoir engineering consultants and may be foreign to the utility itself, it can contribute to the utility decision making process if results relevant to risk assessment are presented with clarity. It is expected that the results from reservoir

modeling will make the decision process somewhat easier to the extent that the model is a vehicle for understanding what happens in the reservoir and how this relates to investment risks associated with reliance on the reservoir for the generation of electricity.

Second, how should a reservoir model be packaged, or developed as a product for utility use? It should be understandable by engineers and managers who are not specialists in geothermal or petroleum reservoir engineering. Also, it should be transferable for use on computers and by people other than the particular computing machine and staff that developed the model.

Third, what should the reservoir model do for the utility? Here are some specific capabilities of a useful model. It should be capable of calculating the production of a whole geothermal field over a 30 year life from data based on early tests or production of a well or wells on a limited portion of the field. It should estimate the limits of off-design production conditions that may arise and assign probabilities to different off-design conditions. It should be capable of accepting and using new data that become available as the field is developed and operated. Such data can be used to confirm the model and to improve predictions in two ways: (1) greater confidence and (2) narrower range of probable outcomes.

In addition to the above capabilities, and related to them, a reservoir model should generate the following information for reservoir risk assessments relevant to the decisions on whether and how to build geothermal power plants: curves showing the probabilities associated with the capability of a reservoir to support various levels of

generating capacity; life of a reservoir as a function of generating capacity being supported, indicating the confidence levels of various life versus capacity curves; probability of precipitous decline in production as a function of capacity; identification of detectible changes that would precede or be associated with such a decline; production rate, temperature, pressure and, perhaps chemistry versus time, capacity and well spacing; and, finally, identification and quantification of reservoir risk associated with development of the first power generating unit at a reservoir and with development of subsequent units at the same reservoir.

Fourth, what is the validity of the reservoir model? The model should be verified as to usefulness in performing calculations of interest. The types of results listed above are those of value for power plant commitment decisions, generation expansion plans, and geothermal power plant design considerations. In addition a reservoir model should, of course, be verified by comparison with field experiments and actual operating experience.

The results presented in this workshop suggest that the models agree reasonably well in calculations for the theoretical problems posed. Also, the problems posed are of types that have practical relevance, especially those that involve calculating a production history from parameters whose value could be inferred from measurements made early in the development of a reservoir. What is needed beyond this are calculations that reveal how sensitive the results are to variations in the values of dominant parameters, some probabilities assigned to various possible production histories, good physical data to put into the models, verification of the calculations through comparison to field results, and the development of models that are easy to understand, use and transfer to other users.

SESSION VII

Model Intercomparison Study (Panel)
(Opening Remarks of N. K. Barrett of Corrcon & Black of Pennsylvania, Inc.)

I want to express my thanks to our Stanford University hosts for this opportunity to participate here as a panelist. In order to achieve a realistic perspective of geothermal resource insurance needs, I do welcome this perspective of the current state of the geothermal art.

The INA - C&B Geothermal Resource Insurance Program is a very potent financial tool which has been designed to stimulate private sector financing of geothermal projects. In our opinion, such private funding of geothermal projects will more than offset the expected reduction in government funding alluded to by Mr. Robert Grey in his opening remarks yesterday.

In order to underwrite each geothermal project, the insurance underwriters must obtain a fair assessment of the expected nature and longevity of the resource involved -- then tailor their insurance coverages to protect against the unexpected. Underwriters are leaning heavily upon the expertise of the geothermal engineers of their potential clients for their initial technical perspective of each geothermal project. This is ultimately followed by technical confirmation by a qualified geothermal engineering consultant retained by the underwriters involved.

Such geothermal engineers will be relied upon by the underwriters for decisions concerning the use of numerical code reservoir simulators. It seems likely that in many cases numerical reservoir modeling may be combined with the economic modeling of such projects as an aid in fairly assessing "the realm of the expected".

The INA - C&B Geothermal Resource Insurance Program is designed to insure the long-term availability of the resource at the needed quantity and quality level established for the project during the simulation modeling and sampling period. Insurance is afforded not only against loss arising out of project termination because of resource inadequacy, but also against loss resulting from project capability reduction. Coverages are offered for a noncancellable policy period encompassing the project construction period plus an operational period of up to seven (7) years.

I. DIRECT USE OF GEOTHERMAL RESOURCE
(Electricity Generation Plant)

A. The Expediting Phase (Plant Construction Period):

Coverage for the Expediting Phase will go into effect after completion of the reservoir exploration process and will remain in effect until the commencement of the normal commercial operations. Inception of such insurance coverage occurs only after confirmation of the resource reserve capacity sufficient to operate the proposed geothermal power plant at a specified level of efficiency. In the unlikely event that the proposed project must be scaled down or terminated due to inadequacy of the resource, the policy indemnifies the Insured for the financial loss resulting therefrom.

1. COVERAGE: During Field Development and Facilities Construction Period.

2. INSUREDS: Any persons or entities having a financial interest in the Electricity Generation Project.

3. INDEMNIFICATION in the event of:

a. Project Termination Prior To Project Completion -- payment of the sunk costs of the project as of the date of termination.

b. Project Capability Reduction (inability to achieve the project's target capability -- with subsequent commercial operations at the reduced capability) -- payment of agreed amounts to assure continuation of debt service and payment of the fixed costs.

B. The Operational Phase (Up to Seven Years):

Coverage for the Operational Phase will go into effect at the time of the official commencement of commercial operations. Project termination due to inadequacy of the resource is covered as in the Expediting Phase. Coverage for loss of earnings (business interruption) due to inadequacy or scale-down of the geothermal resource is also available.

1. COVERAGE: During Commercial Operations (Maximum of Seven Years)

2. INSUREDS: Any persons or entities having a financial interest in the geothermal project.

3. INDEMNIFICATION in the event of:

a. Project Termination -- the payment of the unamortized sunk costs of the Insured as of the date of termination.

b. Project Capability Reduction (Inability to continue production at the commencement capability level -- with subsequent continuation of operations at the reduced capability level) -- payment of an agreed amount per day.

NOTE: A self-insured retention of not more than 10% is negotiated for each Geothermal Resource Insurance Program.

II. DIRECT USE OF GEOTHERMAL RESOURCE
(Space Heating, Agriculture, Aquaculture, Greenhouses, Alcohol Production, Food Processing, Health Spas, etc.)

A. THE "RETROFIT" INSURANCE CONCEPT (One Direct-Use Example):

1. INSUREDS: Any persons or entities having a financial interest in the geothermal project.

2. COVERAGE PERIOD -- The Construction Period plus an agreed number of operational years (a maximum of seven operational years).

3. INDEMNIFICATION -- the Insured's Loss resulting from the Geothermal Resource Inadequacy Hazard.

4. "The Insured's Loss" means the total of the following amounts:

(1) The actual cost, including the cost of installation, of an alternatively fueled steam boiler sufficient to produce the degree level and quantity of heat required in the geothermal project specifications.

(2) The actual cost of the alternative fuel required to produce the heat necessary to meet the geothermal project specifications.

B. OTHER INSURANCE CONCEPTS:

This INA - C&B Geothermal Resource Insurance Program can be tailored to meet the particular financial needs of each specific geothermal project.

The aforementioned Geothermal Resource Insurance Programs are being underwritten by INA Underwriters Insurance Company, 1221 Avenue of the Americas, New York, New York 10020. Negotiations and underwriting liaison are being conducted by Corroon & Black of Pennsylvania, Inc. who have been designated by the INA as their sole Managing Agency for this type of insurance.

I repeat that this expediting of private sector financing of geothermal projects will, in our opinion, more than offset the expected curtailment of government funding. Thank you.

SOME GENERAL COMMENTS ON THE DOE CODE COMPARISON PROJECT

J. W. Pritchett
Systems, Science and Software
P. O. Box 1620
La Jolla, CA 92038

The basic purpose of the DOE Code Comparison Project was to attempt to increase the confidence of the financial community in predictions and assessments made by reservoir engineers as regards the performance of geothermal fields. Numerous issues are relevant to this question of confidence, not all of them technical. It should be recognized that this DOE project was directed at only one of these issues: the accuracy and reliability of numerical geothermal reservoir simulation computer programs, or "simulators".

Numerical reservoir simulators are only one of many tools available to an engineer when he attempts to make a prediction. Typically, the engineer proceeds roughly as follows. He starts with a body of measured facts concerning the system in question. These facts might include such things as the results of surface resistivity surveys, gravity anomoly measurements, drilling logs, laboratory tests of core samples, downhole temperature measurements, the results of pressure transient tests in completed wells, downhole static pressure measurements, discharge enthalpy measurements, chemical analyses of reservoir fluids and rock matrix material, and so forth. If the field has already been partially developed, he may have a significant production history at his disposal. All of these data are likely to vary in accuracy, reliability, and relevance.

Based on whatever facts are available to him, he constructs a preliminary conceptual picture, or "model", of the field. Since the actual density of measurements in the field is always very low, considerable guesswork is always involved at this stage. Typical components of this preliminary conceptual "model" will include his best guesses concerning questions such as:

- What kind of a field is it? (Single-phase hot water? Two-phase liquid-dominated? Vapor-dominated?)
- Where are the major permeable zones and how far do they extend?
- Where are the barriers to flow? Is the field a single unified system, or is it really a collection of relatively isolated aquifers?
- What is the subsurface temperature distribution? How large is the anomoly?

- Are there major fractures present which serve as fluid conduits? If so, where are they?

- Where are the major natural recharge paths? What is the source of recharge fluids? Is there significant connection with the shallow groundwater system?

If the conceptual model is simple enough, analytic tools may be adequate (such as "lumped parameter" models, homogeneous radial single-phase aquifer solutions, and the like). For more complex systems, however, the engineer may be forced to employ a numerical simulator. He quantifies his conceptual model, assigning spatial distributions of such quantities as porosity, permeability, fluid pressure, temperature, enthalpy, and the like, and also supplies appropriate boundary conditions to the domain of space under study. He provides all of this information to the computer program (the "simulator"), and observes the computed results.

Almost invariably, the reservoir response computed by the simulator based on the preliminary conceptual model will differ in important ways from the actual observed behavior of the system. Accordingly, the engineer revises the model in such a way as to minimize such discrepancies. This iterative process is likely to be quite lengthy and involve numerous computer runs before a satisfactory match is obtained. At this stage, the engineer is now ready to use the simulator, in connection with his final conceptual model, to make predictions of future performance. Not infrequently, particularly for relatively undeveloped systems, two or more different conceptual models will account adequately for all known historical data, but will result in markedly different future predictions. Under these circumstances, the engineer cannot make a definite prediction. He can, however, by using the simulator, devise a program of experimental measurements capable of discriminating among the various competing models. Clearly, in the absence of experimental facts, numerical reservoir simulation is useless. On the other hand, as more and more data become available, predictions become more precise.

If numerical reservoir simulation is employed as a key element in a prediction of future performance, the question of the accuracy of the simulator itself becomes an issue of legitimate concern. Several large-scale general-purpose simulation programs now exist which are capable of treating geothermal reservoirs. All were developed within the last seven or eight years. The Department of Energy consequently desired to test several such simulators to determine which (if any) are capable of producing accurate results. Originally, it was suggested that these tests be carried out in a manner something like the following. A particular geothermal field would be selected which has a substantial production history. A

partial data set would be assembled, including all available early exploration measurements, early development-phase data, and the first part of the production history. Then, the Department of Energy would provide this partial data set to a number of independent research groups, each with its own numerical simulator. Based upon the partial data set, each group would employ its simulator in an attempt to "predict" the remainder of the history of the field (which is in reality known, but is presumably concealed by DOE). Each simulator would then be judged on the basis of the accuracy of this "prediction".

There are at least two serious shortcomings to this approach. First, the geothermal industry is at present quite small; the number of fields with sufficient history is so limited that completely concealing the later history of such a field would probably prove impossible. Furthermore, "inside" knowledge concerning the "unknown" late-time data is likely to be non-uniformly distributed among the various research groups involved. Accordingly, it would probably prove impossible to devise a test of this type which would be even-handed.

The second shortcoming is even more fundamental; a testing procedure of this type does not really test the numerical simulators themselves as much as it tests the insight, engineering judgement, and good luck of the engineers in the research groups using the simulators. A group with a relatively inaccurate numerical simulator but with a good conceptual "model" of the reservoir will probably make better predictions than a group with a better simulator but a flawed conceptual picture of the system. Stated differently, even if the simulators themselves were in fact identical, the various independent groups would almost certainly produce predictions that differ one from another in varying degrees.

Considerations such as the above led to the approach employed in the DOE Code Comparison Project. To test the various simulators (instead of the engineers), a set of hypothetical problems was selected. These problems were specified completely a priori, so that no engineering judgement whatever is required to define them. The problem set was chosen subject to several constraints. First, it seemed desirable that some of the problems possess known exact analytic solutions (or at least approximate solutions) so that the absolute accuracy of the simulators could be independently assessed (Problems 1 and 2 fall into this category). Unfortunately, many problems of geothermal interest, particularly those involving multi-dimensional multi-phase flow, do not have analytic solutions (if they did, there would be no need for numerical simulators). A wide range of space and time scales was considered, from effects of individual wells (Problems 1-3) to field-wide studies (Problems 4-6) and from short-term pressure transients (Problem 2) to the entire history of a field during depletion (Problems 4, 6). Emphasis was placed on multi-phase flow of water/steam mixtures (Problems 2-6);

the effects of formation heterogeneity were also included (Problems 4, 6, and particularly Problem 3). One-dimensional (Problems 1, 2, 4), two-dimensional (Problems 3, 5) and fully three-dimensional (Problem 6) cases were considered.

On the other hand, all of the problems in the set were computationally small in scope. For uniformity, the spatial zoning was prescribed for all of the problems; for several, the computational time-step was also specified in advance. Grid sizes ranged from 20 zones (Problem 4) to 125 zones (Problem 6). It should be noted that a typical field application of a numerical resevoir simulator usually involves at least several hundred computational zones, and often several thousand are required. Crude zoning was prescribed for two reasons. First, it was desired to maximize both the number of participants in the project and the number of different problems which could be accomodated within the confines of a limited budget. Second, it seemed desirable to emphasize the effects of numerical truncation errors on the computed results.

The results of the project clearly demonstrate that the various simulators involved are indeed adequate. The extent of the agreement among these calculations performed by different groups using independently-developed numerical simulators which employ markedly different mathematical techniques is very reassuring. Such minor discrepancies as do exist are traceable to misunderstandings about problem definition, small variations in the description of water/steam properties such as saturation pressure and viscosity, and such matters as variations in the time-step size chosen by the various groups, rather than to fundamental flaws in the simulators themselves.

Thus, it would seem that the particular concern which motivated this project -- the accuracy of existing numerical geothermal reservoir simulation programs -- has been laid to rest, at least as regards the group of simulators involved. Furthermore, these results may be used as benchmarks by the developers of other programs. Of course, the fundamental issue -- that of the confidence of the financial community in reservoir engineering predictions -- has not been resolved, but an important first step has been taken. It should be noted that the use of numerical reservoir simulation to make practical performance predictions with significant financial relevance is not unique to geothermal development. This same basic approach has been an accepted practice in the petroleum industry for many years. Presumably, the apparent confidence in numerical simulation methods as applied to oil and gas reservoirs arises from a substantial record of successful performance of these techniques in that industry.

Should the Department of Energy decide to pursue the matter further, considerations such as the above suggest that further competitive calculations among various groups would not be

particularly productive. What is lacking in the geothermal area is a significant record of successful predictions for real geothermal systems. This does not mean that those attempts at describing real systems which have been made have been failures; indeed, several quite successful simulations of geothermal field performance have been published in the open literature. The difficulty is simply that there are very few geothermal fields presently in production. Furthermore, in the United States, the developers of such fields as exist typically regard all relevant field data as proprietary information, so that much of the publically-available data on case histories of real geothermal systems comes from foreign projects. Nonetheless, at the present time a substantial body of relevant information is available for several geothermal systems, both within the U.S. and abroad. As time goes on, this body of case-study information will grow.

In order to develop confidence within the financial community in reservoir engineering predictions in general and the application of numerical simulation techniques in particular, it seems that the most productive course would be to encourage the application of these techniques to several real situations for which an adequate data base is available or obtainable. There is no need, however, to employ the competitive approach used in the present Code Comparison Project; indeed, such a diffusion of effort would probably be counterproductive. If a number of research teams were each allowed to concentrate fully upon a particular system, rather than divide their attention in a more cursory fashion over several different systems, more adequate simulation results would undoubtedly occur.

Response to Model Intercomparison Study

by H. Dykstra

The results obtained from the several reservoir simulation models that were used in the study showed very good agreement for the most part. The close agreement indicates that the modellers have done an adequate job in analyzing the physics and in programming the mathematics for computer calculations. This is very encouraging in that it means that one does not have to be as much concerned with the computer model as one does in getting an adequate description of the geothermal reservoir. The latter point forms a basis for determining when a model could be used.

A reservoir simulation model can be thought of as having two purposes. One would be to determine which reservoir and fluid parameters are important in order to obtain an adequate description of a particular reservoir. For example, in a fractured reservoir, the porosity of the rock matrix may be unimportant. A second purpose, and much more important one, is to make a prediction of future performance, such as flow rate, enthalpy, water temperature, and pressure decline. This information is then used in the design of a power plant and in making an economic evaluation of the overall project.

In order to make such a prediction with any degree of confidence it is necessary to have an adequate description of the geothermal reservoir, and this requires a considerable amount of time and effort. Two or three wells will in general not provide sufficient information on which to base a prediction. Five to ten wells may be needed along with well test data and interference test data in order to provide a picture of the reservoir. A computer simulation model can be of help in making an evaluation, or prediction, but it should be kept as simple as possible consistent with the amount of data available.

RAPPORTEUR REPORT ON PANEL RESPONSE TO MODEL INTERCOMPARISON STUDY

G. A. Frye, Division Engineer
Geothermal Resources Division
Aminoil USA, Inc.
Santa Rosa, California

During the panel discussion, several consensus opinions developed. All panelists concurred that the model intercomparison study was a proper and necessary effort for the Department of Energy to support. The results from the problem sets indicate there exists a group of good coders and smart mathematicians. Most results were comparable which satisfied the first part of the original task. Unfortunately, the second part of the original task, code efficiency, was deleted for a reported inability of the model intercomparison advisory committee to agree on criteria for code efficiency.

The models are valid for calculations but do not necessarily yield the right answers. Needs of potential users of geothermal reservoir models require multiple runs. An example would be parameter study to produce an error bound or various sensitivity studies to estimate levels of certainty. The need for multiple runs increases the potential user's concern for model efficiency.

Several technical uncertainties were mentioned. These included the proper means of defining the well bore radius, weighted mean versus upstream weighting of parameters, computed enthalpies as an assessment of model validity, and matching parameters if initial pressure near saturation.

Most panelists concurred that ultimately model results would be a tool for investment decisions, i.e. build a power plant. Models should be a vehicle for understanding the reservoir. If so, then modeling results once understood and accepted as valid, should lead to expedited development of geothermal resources.

RAPPORTEUR'S SUMMARY

by

George F. Pinder
Department of Civil Engineering
Princeton, New Jersey

1.0 INTRODUCTION

On Wednesday, December 17, 1980, a session of the sixth Workshop on Geothermal Reservoir Engineering entitled "Model Intercomparison Study" was held at Tresidder Union at Stanford University. The session was chaired by M. S. Gulati. The program consisted of an introduction by M. W. Molloy, a description of the performance of each of four models on a series of problems, a brief panel presentation and, to close the session, an open discussion. The objectives of the model comparison were stated by M. W. Molloy as

1) to test existing geothermal models on a standard set of problems

2) to compare their output [accuracy]+ and efficiency

The motivation for this project came from the Department of Energy (DOE) congressional mandate and more specifically from a recommendation of the Geothermal Division advisory committee.

2.0 MODEL COMPARISON

Six problems were considered by each of the four groups involved in the project (Intercomp, Geotrans, Stanford University, Systems, Science and Software, Lawrence Berkeley Laboratory and a New Zealand group). Not all problems were attempted by all participating groups. No efforts were made to formally measure the accuracy of the various simulations nor were there any attempts to determine the relative efficiency of the various models. While the discretization parameters (eg. Δx, Δt) were specified in some problems, this was not universally the case. Thus, the comparisons of the resulting simulations were primarily qualitative, rather than quantitative.

At the time of this writing, all of the written reports on the performance of each code on each problem were not available to the rapporteur. Thus, my comments are necessarily rather general and based only on information presented by the author of each test problem (J. Mercer, M. Sorey, A. Moench, M. O'Sullivan, J. Pritchett and K. Pruess).

On the whole, the various codes were able to provide a solution qualitatively similar to the known or anticipated physical behavior. When unexpected results were encountered they were generally attributed to errors in input, interpretation or grid-size selection rather than

+square bracketed comments are rapporteur's interpretation.

- model verification is a two-step procedure

  1) demonstrate that the model is computationally sound
  2) determine its accuracy through a comparison with field information

N. Barrett:

- the limited use of geothermal by utilities is due to the lack of geothermal insurance
- utilities cannot assume risk and must have protection from losses incurred either in the development period or from an inability to provide a contracted level of power availability
- utilities rely on geothermal engineers and geologists to develop, evaluate and confirm technical data
- cutbacks in funding by DOE will be taken up by private industry

J. Pritchett:

- meaningful model results are dependent upon accurate field data input and engineering interpretation
- the objective of this comparison, however, was to demonstrate the veracity of the mathematical apparatus; this was achieved.

H. Dykstra:

- the comparison documented herein demonstrates that the models are mathematically sound
- the principal problem is reservoir definition
- there are three levels of sophistication that have been employed historically in conducting reservoir analysis

  1) guess at answer
  2) employ analytical models
  3) employ relaxation [an early form of numerical analysis used in conjunction with finite difference approximations]

- the basic engineering problem is the number of wells to be put in before making a major financial commitment to a field.

4.0 GENERAL DISCUSSION

While there was spirited discussion from the floor, relatively few distinct topics were considered. The most relevant, from the rapporteurs perspective, follows:

- model efficiency is important because models are becoming more complicated and therefore costly to implement.
- model efficiency is critical to the use of Monte Carlo methods of risk assessment.
- models can and should be used to provide insight into the physical system [the goethermal reservoir]
- a large number of runs are normally required in analyzing a typical field problem
- models can be used to determine the sensitivity of reservoir projections on field parameter accuracy
- there is a lack of consultants who can use the existing computer codes to analyze a field problem
- while some participants felt the models now should be applied to a real field situation, others thought this would only test the ability of the geothermal engineer rather than the simulator

5.0 RAPPORTEUR'S EVALUATION

The stated goals of the project constitute a useful contribution to the geothermal community. Numerical solution of the equations describing geothermal reservoir behavior is difficult and the accuracy of the codes cannot be readily determined. This code comparison demonstrated the general credibility of the models for the selected problems.

The model problems were, for the most part, carefully conceived and the resulting computer solutions conscientiously evaluated. While a qualitative comparison of accuracy was presented at the workshop, a quantitative statement is also needed. This is readily provided for problems with known solutions through one of the generally accepted mathematical norms. It is unfortunate indeed that program efficiency was not documented. The geothermal community would like to know which algorithm leads naturally to a more cost-effective simulator.

The panel presentation was very interesting. It provided an interesting perspective on the role of models in the geothermal community. I feel the addition of an academic panel member would have provided a viewpoint quite different from those presented. The general discussion was lively, relevant and a worthwhile element of the program.

In summary, the code comparison project and the subsequent presentation of the results was well conceived and executed. Extensions beyond this level of effort probably would be of limited benefit. The question of simulator efficiency remains unanswered.

GFP:dh

Code Comparison Project
- Conclusions -

Martin W. Molloy[1] and
Leland L. Mink[2]

U.S. Department of Energy

1. Geothermal Energy Division
   San Francisco Operations Office

2. Office of Geothermal Energy
   Idaho Operations Office

ACCOMPLISHMENTS

The message that the Department of Energy heard at the Stanford Workshop is that the Code Comparison Project was successful. The geothermal industry's need to determine that different reservoir codes yield similar results was satisfied. The "test problem" approach was proper; the Final Reports and the Workshop evaluation were useful.

The models work! Surprisingly consistent results were achieved by seven groups, working independently, with five different models running on six different machines. The sets of output data agree with each other, and with analytical solutions, where available. Minor differences are explained either by use of different steam tables and thermodynamics, or by misunderstandings which resulted in data input errors.

In addition, a set of standard problems for testing other reservoir models is now available to the geothermal industry. The SHAFT '79 code developed by Lawrence Berkeley Laboratory can be obtained as Abstract #893, from the National Energy Software Center, Argonne National Laboratory, 9700 South Cass Ave., Argonne, Illinois 60439.

However, the ability of models to contribute to investment decisions on specific geothermal reservoirs, using field data and skilled engineering teams, has not been demonstrated by the present effort. It is not clear how this might be accomplished to the satisfaction of investors and their consultants; how the needed field data would be obtained; and, how the costs of comparative modeling with several simulators can be met. Whether such an effort needs the participation of the Department of Energy, is uncertain.

UNSATISFIED RECOMMENDATIONS

The original recommendation (in quotes, below) has only been partly satisfied.

"Model comparison and validation" has been "a new initiative in the (DOE) Geothermal Reservoir Engineering Program." Through competitive contracts to industry and cooperative efforts with Lawrence Berkeley Laboratory, U.S. Geological Survey and University of Auckland, N.Z., five "major codes" have been tested on a standard set of problems. "Results" have been compared "with respect to output." The 1980 Stanford Workshop included panel discussion of "the use and limitations of the various codes available."

However, the Code Comparison Project did not "run (the codes) on an actual geothermal system where adequate data exists rather than a hypothetical situation." Nor has an attempt been made to "compare results with respect to... efficiency of the code." John Pritchett observed that it may

not be possible to define fair measures of efficiency for codes run on different machines; only comparisons of numerical accuracy and precision may be possible. Finally, a workshop has not considered "the use and limitations of the various codes available."

The absence of actual field data has limited this evaluation. We have not tested the skills and experience of the team of experts which defines the problem, prepares the input to the computer, analyzes the output, and interprets results in terms of reservoir performance, development, operations and investment decisions.

GEOTHERMAL INDUSTRY VIEWPOINTS

Speaking for the Field Developers, Charles Morris of Republic Geothermal stated that model validation is a major question: Is the simulator actually calculating the physical properties correctly? Morris was relatively satisfied that the simulators provide valid results; but, this exercise does not mean that the answers represent the real world.

Evan Hughes of EPRI, representing the Utilities, suggested that sensitivity studies are needed to define the most important parameters, with verification through operations at actual reservoirs. He underlined the need for geothermal models as tools for making decisions; for understanding the reservoir; for reducing complex problems to a set of variables; for assessing reservoir risk; for predicting field performance over time; and, for improving confidence by accepting new data as it becomes available. It is important that a geothermal reservoir model be understood by non-experts, and be tranferrable to other machines and users.

The Financial Community, through Norman Barrett of Carroon & Black, summarized its heavy reliance on the expertise of geothermal engineers working for potential clients, supplemented by retaining their own consultants to confirm the data. Utilities cannot bear the resource risk of the geothermal power plant's inability to achieve target capability. The private sector is now coming forward with insurance programs to expedite geothermal investment and development.

From the point of view of computer Software Developers, John Pritchett of Systems, Science and Software stated that the Code Comparison results showed that these simulators are solving Darcy's Law and the principles of mass and energy conservation. We have established that it doesn't matter which computer model engineers use. However, much more than a computer program is required to get a meaningful answer for investment decisions. This requires: 1) field data, 2) physical basis for the specific geothermal system, 3) smart engineers to use the computer tool correctly, and 4) regular (yearly) updating. The Code Comparison Project has not addressed these issues. The next step should be to test the engineering groups. Pritchett asked: What is important, in terms of differences in the conceptual models; and, which assumptions (for instance permeability distribution) are critical?

As a Consultant, the focal point of the confidence issue, Herman Dykstra acknowledged that the modeling community has good mathematicians. You can trust the results of the geothermal simulators, provided that you are able to define the reservoir. That is the problem. Most geothermal reservoirs are very difficult to describe. This is compounded by the very limited data available early in the field development phase; and, the limited ability to represent the fractures and blocks that may comprise the reservoir.

RELATED PAPERS

Two other papers in the Proceedings of the 1980 Stanford Workshop bear on the fundamental issue of consultant confidence in reservoir simulators for investment decisions.

P. F. Bixley (1980) from the Wairakei Geothermal Field in New Zealand evaluated simulators from the point of view of development risks, needed information, and actual experience with modeling for investment and operating decisions. Ten years after it was done, one simulation has proven remarkably accurate in predicting steam flows from construction of an 11% increase in system efficiency. But this is only one of many simulations performed.

Kamal Golabi (1980) modeled the overall universe of risks facing an energy development project. Reservoir engineering dominates the reservoir-related uncertainties and contributes to the analysis of adverse environmental impacts and technological uncertainties. Conceptually, the reservoir simulators interact with submodels of groundwater contamination, subsidence, plant design, plant performance, and plant effluents. The reservoir model plays a major role, therefore, in simulating and deciding both reservoir operations and plant design. In turn, these are major factors in the project cost model.

FOR THE FUTURE

1) Field Data

In order to test reservoir models on actual geothermal systems, access to comprehensive field data is required. Because of the proprietary considerations of private development, such access is very limited in the United States, despite extensive drilling and testing of many geothermal reservoirs. Data is needed over an entire reservoir (not just one operator), and over a sustained period of time.

In the United States, only the Geysers field has a lengthy production history. The two joint industry-DOE demonstration projects at Baca, NM and Heber, CA are in early phases of field development, prior to the construction of power production facilities.

Several foreign reservoirs have extensive field data which has formed the basis for modeling studies. These include Lardarello, Italy; Cerro Prieto, Mexico; and Wairakei, New Zealand. The Wairakei data base has recently been compiled and reproduced on computer tape by Systems, Science

and Software (Pritchett, Rice and Garg, 1978) for Lawrence Berkeley Laboratory. Joint research tasks for reservoir code comparison may be needed under Intergovernmental Agreements between the United States and Italy, Mexico and New Zealand.

2) Cost

The total cost of the four contracts for the Code Comparison Project was approximately $100,000. Experts estimate that comprehensive modeling of an actual geothermal reservoir, using a single simulator, could be $250,000. A comparative study, using several codes, would approach $1 million per reservoir.

Costs of this magnitude exceed DOE's priority and anticipated availability of funds.

3) Risk/Uncertainty

There are many sources of risk and related uncertainty facing a geothermal project, such as a power plant. Many of these sources of risk, including the geothermal reservoir, are amenable to reduction of uncertainty by collection and analysis of information (measurement), and by simulation of possible outcomes and their probability of occurrence (modeling).

Except perhaps for Wairakei, geothermal reservoir simulation has yet to be placed in perspective in terms of its contribution to overall confidence in specific investment decisions. Geothermal modelers can aid this process by becoming conversant with risks and models in related disciplines. We need to be able to translate our reservoir engineering conclusions into terms which investors understand.

CONCLUSION

The Department of Energy seeks to accelerate the commercial development of geothermal energy, in accordance with the Geothermal Research, Development and Demonstration Act (Public Law 93-410).

Understanding the geothermal reservoir is a substantial part of project investment decisions. The ability to simulate reservoir behavior with a computer code can contribute to this understanding. Industry is encouraged to evaluate the performance of commercially available simulators on important geothermal reservoir decisions.

The mathematical accuracy of five participating codes has been demonstrated by comparison of results and available analytical solutions. Underlying thermodynamic equations and assumptions have provided similar answers for a standard set of test problems.

The next step is to use field data in evaluating an actual reservoir rather than hypothetical problems. In this way, the engineering teams as well as the computer can participate.

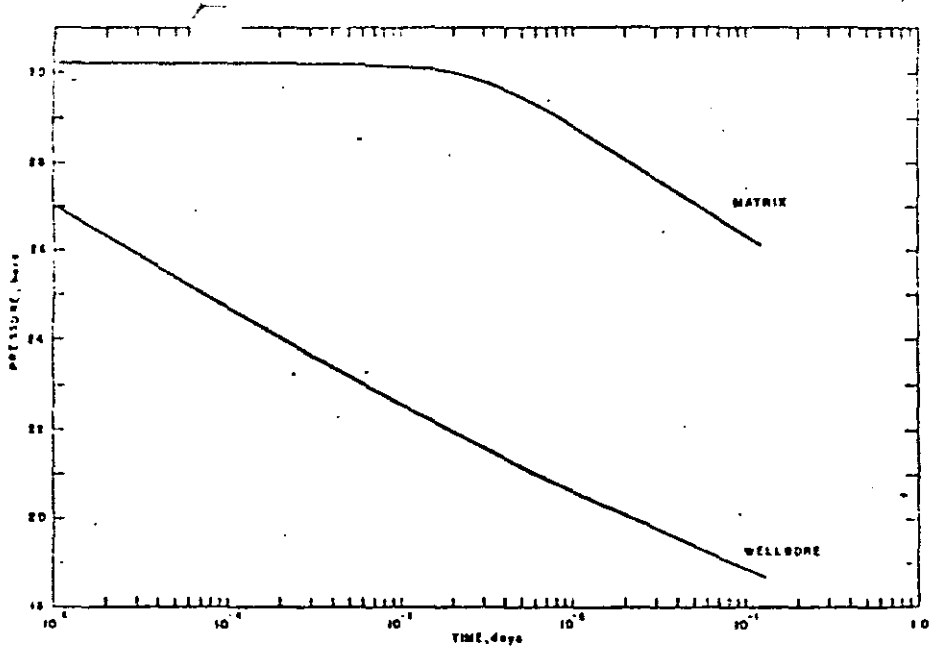

Figure 1 Results of Problem 3B

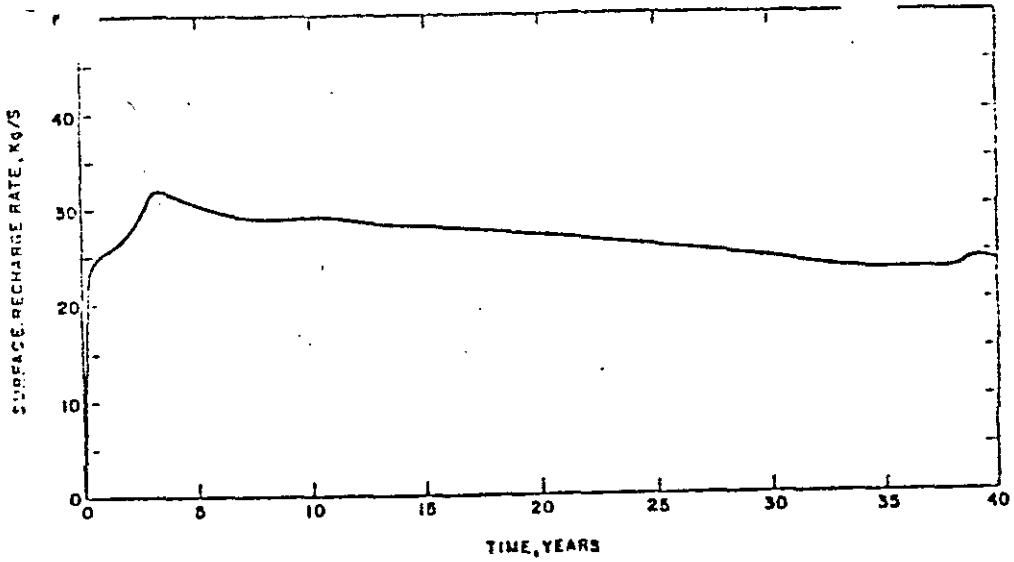

Figure 2 Recharge rate calculated in Problem 4

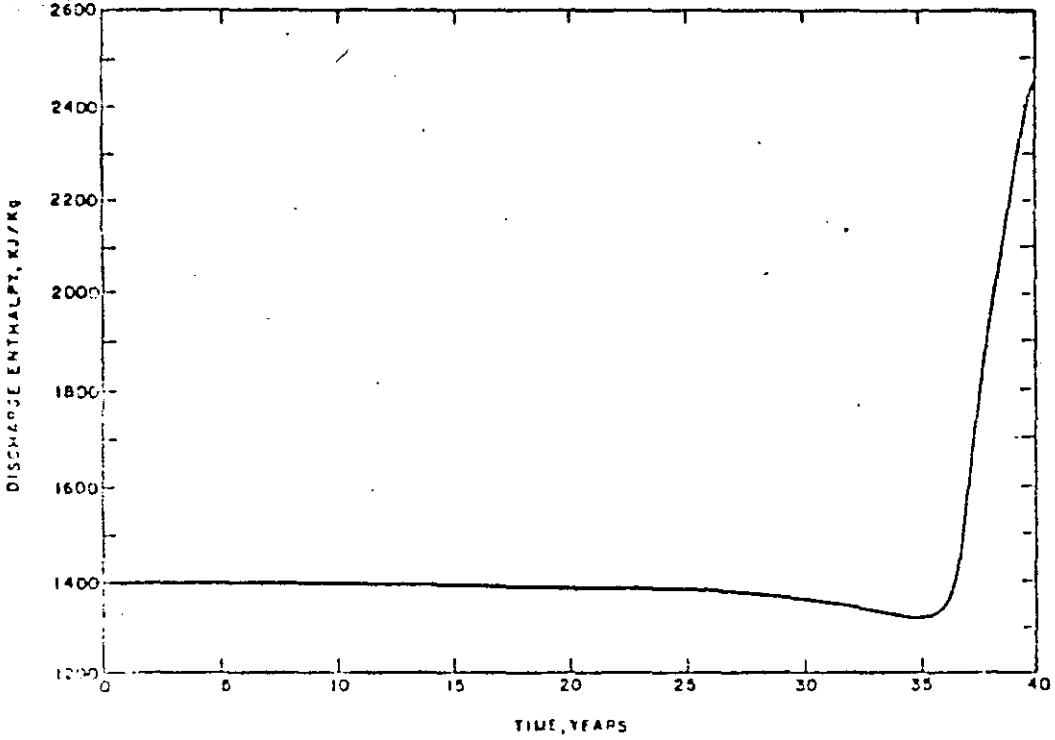

Figure 3 Discharge Enthalpy calculated in Problem 4

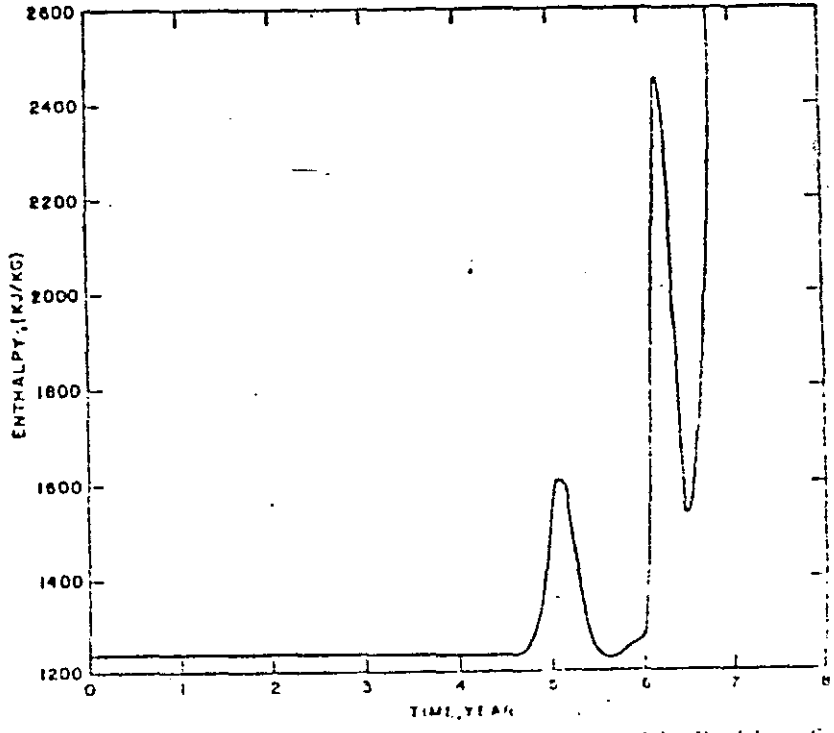

Figure 4 Discharge Enthalpy calculated in Problem 5

CURSO: "INGENIERIA DE YACIMIENTOS GEOTERMICOS "
13 DE MARZO AL 18 DE MAYO 1984

TEMA: "RESERVOIR SIMULATION"

DR. GUILLERMO DOMINGUEZ VARGAS
2-13 DE ABRIL
MATERIAL COMPLEMENTARIO

Distinguished Author Series

Reservoir Simulation: State of the Art

by Keith H. Coats, SPE

Keith H. Coats is chairman of Intercomp Resource Development & Engineering Inc. in Houston. He holds MS and PhD degrees in chemical engineering and an MS degree in mathematics from the U. of Michigan. After teaching chemical engineering at the U. of Michigan from 1959 to 1961, Coats was a senior research engineer and research associate with Esso Production Research Co. during 1961–66 and associate professor of petroleum engineering at the U. of Texas during 1966–70. He was 1969–70 Distinguished Lecturer on reservoir simulation and served on the Nominating Committee during 1977–78.

Introduction

The purpose of this paper is to describe the current level of development in reservoir simulation. This requires some discussion of what a simulation model is and why it is needed or used. Following a brief history of simulation and a general description of a simulation model, two sections describe the reservoir simulator through discussions of recovery mechanisms and model methodology. The second of these sections discusses past and recent developments and summarizes the technology currently used in simulation models. The two descriptive sections are followed by a discussion of why simulation is used (i.e., typical reservoir performance questions addressed by computer simulation), a section with examples pertinent to simulation today, and a summary.

A Brief History

In a broad sense, reservoir simulation has been practiced since the beginning of petroleum engineering in the 1930's. Simulation is simply the use of calculations to predict reservoir performance (to forecast recovery or compare economics of alternative recovery methods). Before 1960, these calculations consisted largely of analytical methods,[1,2] zero-dimensional material balances,[3,4] and one-dimensional (1D) Buckley-Leverett[5,6] calculations.

The term "simulation" became common in the early 1960's, as predictive methods evolved into relatively sophisticated computer programs. These programs represented a major advancement because they allowed solution of large sets of finite-difference equations describing two- and three-dimensional (2- and 3D), transient, multiphase flow in heterogeneous porous media. This advancement was made possible by the rapid evolution of large-scale, high-speed digital computers and development of numerical mathematical methods for solving large systems of finite-difference equations.

During the 1960's, reservoir simulation efforts were devoted largely to two-phase gas/water and three-phase black-oil reservoir problems. Recovery methods simulated essentially were limited to depletion or pressure maintenance. It was possible to develop a single simulation model capable of addressing most reservoir problems encountered. This concept of a single, general model always has appealed to operating companies because it significantly reduces the cost of training and usage, and, potentially, the cost of model development and maintenance.

During the 1970's, the picture changed markedly. The sharp rise in oil prices and governmental trends toward deregulation and partial funding of field pilot projects led to a proliferation of enhanced-recovery processes. This led to simulation of new processes that extended beyond conventional depletion and pressure maintenance to miscible flooding, chemical flooding, CO_2 injection, steam or hot water stimulation/flooding, and in-situ combustion. A relatively comfortable understanding of two-component (gas and oil) hydrocarbon behavior in simple immiscible flow was replaced by a struggle to unravel and characterize the physics of oil displacement under the influence of temperature, chemical agents, and complex multicomponent phase behavior. In addition to simple multiphase flow in porous media, simulators had to reflect chemical adsorption and degradation, emulsifying and interfacial tension (IFT) reduction effects, reaction kinetics, and other thermal effects and complex equilibrium phase behavior.

The proliferation of recovery methods in the 1970's caused a departure from the single-model concept as individual models were developed to represent each of these new recovery schemes. Thus, the emphasis today is on examining and fine tuning the equations and related assumptions pertinent to these techniques.

Research during the 1970's resulted in many significant advances in simulation model formulations and numerical solution methods. These advances allowed simulation of more complex recovery processes and/or reduced computing costs through increased stability of the formulations and efficiency of the numerical solution methods.

Simulation Models—A Brief Description

Odeh[7] gives an excellent description of the conceptual simplicity of a simulation model. He illustrates the subdivision of a reservoir into a 2- or 3D network of grid blocks. He then shows that the simulation model

0149-2136/82/0081-0020$00.25

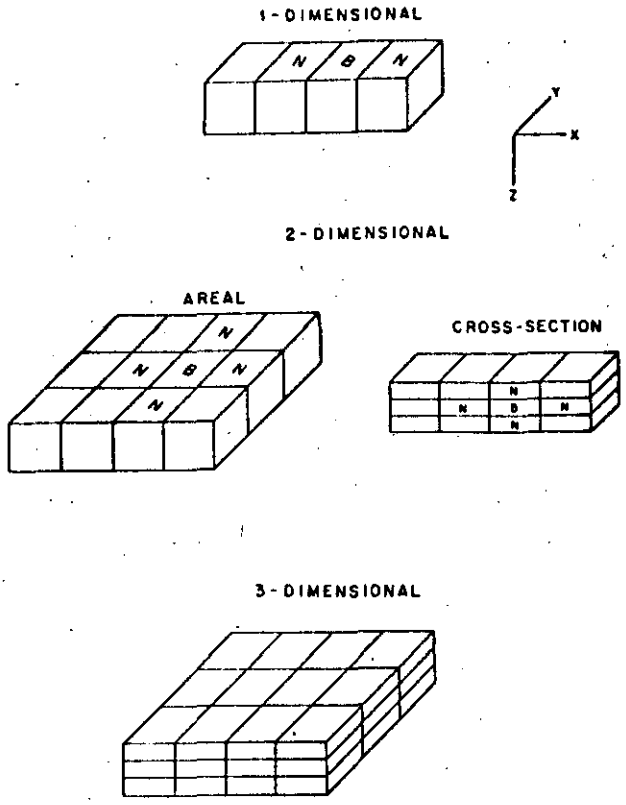

Fig. 1—1-, 2-, and 3D grids.

equations are basically the familiar volumetric material balance equation[3,4] written for each phase for each grid block. The phase flow rates between each grid block and its two, four, or six (in 1-, 2-, or 3D cases, respectively) adjacent blocks are represented by Darcy's law modified by the relative permeability concept. Fig. 1 illustrates 1-, 2-, and 3D grids representing a portion of a reservoir. The block and its two or four neighbors are denoted by B and N in the 1- and 2D grids. One can visualize an interior block of the 3D grid with its six neighbors, two on either side of the block in the x, y, and z directions. In practice, the subsea depths to the top surface of each grid vary with areal position, reflecting reservoir formation dip.

Reservoir properties such as permeability and porosity, and fluid properties such as pressure, temperature, and composition, are assumed uniform throughout a given grid block. However, reservoir and fluid properties vary from one block to another; fluid properties for each grid block also vary with time during the simulation period.

A simulation model is a set of partial-difference equations requiring numerical solution as opposed to a set of partial differential equations amenable to analytical solution. The reasons for this are: (1) reservoir heterogeneity—variable permeability and porosity and irregular geometry; (2) nonlinearity of relative permeability and capillary pressure vs. saturation relationship; and (3) nonlinearity of fluid PVT properties as functions of pressure, composition, and temperature. The models require high-speed digital computers because of the amount of arithmetic associated with the solutions.

A simulation model requires three types of input data. First, reservoir description data include (1) overall geometry, (2) grid size specification, (3) permeability, porosity, and elevation for each grid block, and (4) relative permeability and capillary pressure vs. saturation functions or tables. Geological and petrophysical work involving logs and core analyses is necessary for items 1 and 3. Laboratory tests on core samples yield estimates of relative permeability and capillary pressure relationships. Second, fluid PVT properties, such as formation volume factors, solution gas, and viscosities are obtained by laboratory tests. Finally, well locations, perforated intervals, productivity indices (PI's), and rate schedules must be specified.

Model output or calculated results include spatial fluid pressure and saturation distributions, and producing GOR and WOR and injection/production rate (for wells on injectivity/productivity) for each well at the end of each time step of the computations. Internal manipulation of these results gives average reservoir pressure and instantaneous rates and cumulative injection/production of oil, gas, and water by well and total field vs. time.

Simulation Models and Oil-Recovery Mechanisms

Different types of simulation models are used to describe different oil-recovery mechanisms. The most widely used types are black oil, compositional, thermal, and chemical flood. The four basic recovery mechanisms for recovering oil from reservoirs are: (1) fluid expansion, (2) displacement, (3) gravity drainage, and (4) capillary imbibition. Simple fluid expansion with pressure decline results in oil expulsion from and subsequent flow through the porous matrix. Oil is displaced by gas and injected or naturally encroaching water. Gravity drainage, caused by positive (water/oil and oil/gas) density differences, aids oil recovery by causing upward drainage of oil from below an advancing bottomwater drive and downward drainage from above a declining gas/oil contact. Finally, imbibition, generally normal to the flow direction, can be an important recovery mechanism in lateral waterfloods in heterogeneous sands with large vertical variation of permeability.

To accommodate compositional and the enhanced-recovery processes in this discussion, we add a fifth mechanism, oil *mobilization*. This loosely defined term includes widely different phenomena that create or mobilize recoverable oil. Some of these phenomena are not really distinct from the first four.

The black oil model accounts for the four basic mechanisms in simulation of oil recovery by natural depletion or pressure maintenance (e.g.,

waterflooding). This isothermal model applies to reservoirs containing immiscible water, oil, and gas phases with a simple pressure-dependent solubility of gas in the oil phase. This two-component representation of the hydrocarbon content presumes constant (pressure-independent) oil and gas phase compositions, no volatility of oil in the gas phase, and zero solubility of gas and oil in the water.

The remaining model types discussed here account for some mobilization mechanisms in addition to the four basic recovery mechanisms. Compositional models are used to simulate recovery processes for which the black oil assumption of constant-composition, immiscible gas and oil phases is invalid. Some examples are: (1) depletion of a volatile oil or gas condensate reservoir where phase compositions and properties vary significantly with pressure below bubble- or dewpoint; (2) injection of nonequilibrium gas (dry or enriched) into a black-oil reservoir to mobilize oil by vaporization into the more mobile gas phase or by attainment of outright (single-contact) or dynamic (multiple-contact) miscibility; and (3) injection of CO_2 into an oil reservoir to mobilize oil by Mechanism 2 and by oil viscosity reduction and oil swelling. Holm[8] gives an excellent description of mechanisms active in CO_2 and miscible flooding.

The compositional model describes reservoir hydrocarbon content as an N-component mixture. Gas/oil phase properties and equilibrium (K-values) are calculated from pressure- and composition-dependent correlations or, more recently, from equations of state (EOS).

Thermal simulators are applied to steam injection or in-situ combustion processes in heavy-oil reservoirs where oil is mobilized primarily by (1) reduction of oil viscosity with increased temperature, (2) distillation of intermediate hydrocarbon components from the oil phase to the more mobile gas phase, and (3) cracking of the oil phase [usually above 500°F (260°C)] with subsequent distillation. Thermal models include PVT correlations to describe N-component oil and gas phase properties as functions of pressure, temperature, and composition.

Chemical flood models include polymer, micellar (surfactant), and alkaline (caustic). Polymer waterflooding improves oil recovery by lowering the oil/water mobility ratio by reducing the effective permeability to water and/or by increasing water viscosity. In micellar flooding, surfactants greatly reduce oil/water IFT, thereby solubilizing oil into the micelles and forming an oil bank.[9] The surfactant slug and mobilized oil normally are propelled toward the production well by a graded bank of polymer-thickened water. The mechanisms responsible for improved oil recovery in alkaline flooding are not understood clearly but are thought to include low IFT, wettability alteration, and emulsification.[10] Chemical flooding processes involve complicated fluid/fluid and rock/fluid interactions such as adsorption, ion exchange, viscous shear, and three- (or more) phase flow.

Why Simulation Models Are Used

Reservoir simulation is used to estimate recovery for a given existing producing scheme (forecasting), to evaluate the effects on recovery of altered operating conditions, and to compare economics of different recovery methods. Staggs and Herbeck[11] give an excellent discussion of the uses of simulation with examples. Coats[12] gives a general discussion of simulation use and misuse. McCulloch *et al.*[13] and a number of papers in Ref. 14 describe field applications of simulation models. Harpole and Heam[15] and Killough *et al.*[16] describe recent black-oil models of rather complex reservoirs.

Black-oil models frequently are used to estimate the effect of these parameters on oil recovery: (1) well pattern and spacing, (2) well completion intervals, (3) gas and/or water coning as a function of rate, (4) producing rate, (5) augmenting a natural water drive by water injection and desirability of flank or peripheral as opposed to pattern waterflooding, (6) infill drilling, and (7) gas vs. water vs. gas plus water injection.

Compositional models also are used for most of these purposes but, as stated previously, only in cases where the black-oil two-component, fixed-composition PVT representation is invalid. They are applied in reservoir studies to estimate (1) loss of recovery caused by liquid dropout during depletion of condensate reservoirs and the reduction of this loss by full or partial cycling (reinjection of gas from surface facilities), and (2) effects of pressure level, injected gas composition, and CO_2 or N_2 injection on oil recovery by vaporization or miscibility. Graue and Zana[17] describe application of a compositional model in estimating Rangely field oil recovery by CO_2 injection as a function of injected composition and pressure level.

Results of compositional simulation of a CO_2 project include CO_2 breakthrough time and rate and composition of produced fluids. These are required to design production facilities and CO_2 recycling strategies.[18] Modeling is also useful to optimize pattern size and CO_2/water injection rates to overcome the effects of reservoir heterogeneity.[19]

Thermal models are applied in reservoir studies of in-situ combustion and are used to simulate performance of cyclic steam stimulation and steamflooding. In steam injection, questions addressed by simulation relate to effects of injected steam quality and injection rate, operating pressure level, and inclusion of gas with the injected steam. One question in cyclic stimulation concerns the optimal time periods per cycle for steam injection, soak, and production. The flooding case introduces the issues of well pattern and spacing. A number of steam-injection field studies using models have been published. Herrera and

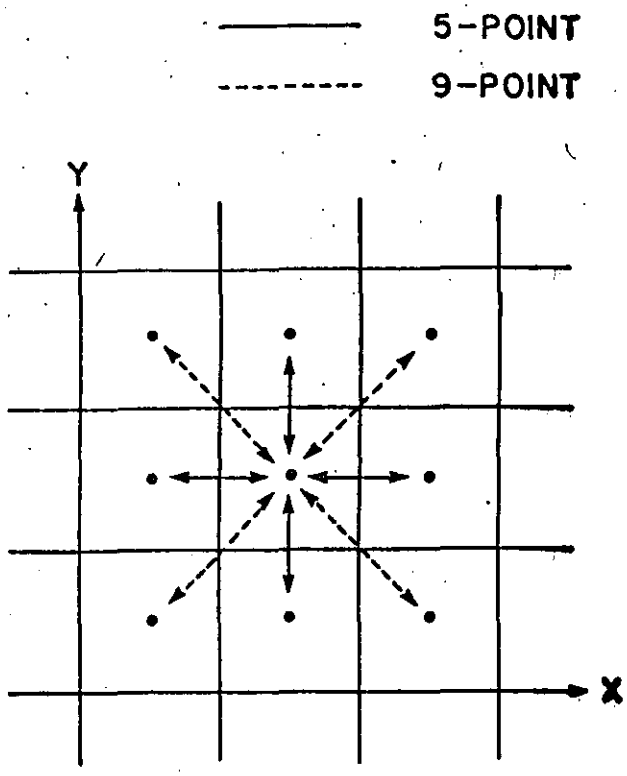

Fig. 2—Five- and nine-point difference schemes.

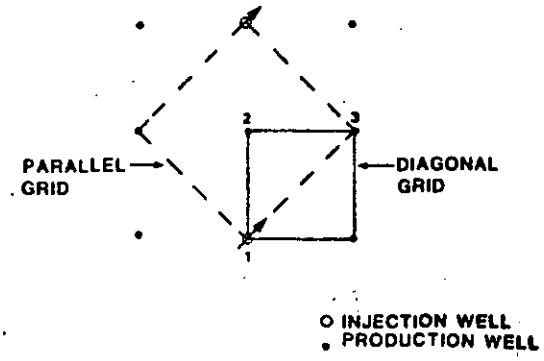

Fig. 3—Nine-spot grids.

Hanzlik[20] compare field data and model results for a cyclic stimulation operation, Williams[21] discusses field performance and model results for stimulation and flooding, and Meldau[22] discusses field and model results related to addition of gas to the injected steam.

Numerical simulation provides a reliable means to predict chemical flood performance in a reservoir environment, because the processes are very complex and many reservoir parameters affect the results. Consequently, chemical flood simulation has been used to construct a screening algorithm for the selection of reservoirs suitable for micellar/polymer flooding[23] and to examine competing EOR strategies—e.g., CO_2 vs. surfactant flooding.[24] For caustic[25] and polymer[26] applications, as well as for the micellar process, chemical flood modeling is useful to discern controlling process mechanisms and to identify laboratory data required for process description.

In recent years, simulation has been used increasingly to estimate and compare recoveries from a given reservoir under alternative enhanced-recovery processes, such as CO_2 injection, thermal methods (steam injection and in-situ combustion), and several types of chemical flooding.

Simulation Models—Methodology

In the interest of brevity and with some oversimplification, the discussion of formulations currently used in simulation models uses a concept of a single, general model. The general model is a set of N partial difference equations written for each grid block comprising the reservoir. Each equation is simply a mathematical statement of conservation of mass of a specified substance or of conservation of energy. Each substance or component may be present in all phases, distributed according to K-values or distribution coefficients obtained from correlations or an equation of state. With allowance for rock adsorption isotherms, chemical reactions, temperature-, pressure-, and composition-dependence of viscosity, relative permeabilities, and capillary pressure, each of the previously described model types is a subset of the single, general model.

Note that *components* (and *energy*), not phases, are the conserved substances requiring equations in the simulation model. Thus, the number of phases is unrelated to the number of model equations.

Until recently, simulation models made use of the common five-point difference scheme for areal (x-y) interblock, Darcy flow terms in each of the conservation equations. Fig. 2 illustrates this flow between a grid block and each of its four neighbors. A strong grid-orientation effect was reported by Todd *et al.*[27] for highly adverse mobility waterfloods and later observed by Coats *et al.*[28] for pattern steamfloods. An areal grid with the usual perpendicular x and y axes may be placed over a five-spot pattern with the x axis either parallel to or at a 45° angle to the line

connecting the injector to a producer (Fig. 3). These parallel and diagonal grids[27] can result in markedly different calculated shapes of the water or steam front and the breakthrough times. This difference was reduced by the nine-point finite difference formulation described by Yanosik and McCracken[29] and is illustrated by the four extra diagonal flow terms in Fig. 2. Their technique is being programmed rapidly into simulators treating steamflooding and miscible CO_2 injection where adverse mobility pattern floods commonly are encountered.

The formulation terms described here apply within the context of either the conventional five- or nine-point finite-difference scheme. The IMPES[28] formulation denotes implicit pressure, explicit saturation. Sheldon *et al.*,[30] Stone *et al.*,[31] and Fagin *et al.*[32] describe the IMPES method for black-oil (three-equation) problems, and Coats[33] gives an obvious extension to the N-equation case. This method is explicit in saturation in that it uses old time-level values of relative permeabilities in the interblock flow terms. Solution of a single pressure equation is followed by an explicit updating of fluid saturations and compositions in each grid block.

MacDonald[34] improved the stability of the IMPES method for the two-phase water/oil case by following the pressure equation solution with solution of a water-saturation equation over the grid using implicit (new-time-level or end-of-time-step) values of relative permeabilities in the interblock flow terms. Spillette *et al.*[35] extended this concept to the three-phase case and called the formulation *sequential*.

The *implicit* formulation makes use of end-of-time-step values of relative permeabilities (and densities, viscosities) in the interblock flow term transmissibilities. This requires simultaneous solution of all N equations. Blair and Weinaug[36] first published this fully implicit formulation. Implementation of implicit or highly implicit formulations in black-oil, geothermal, steamflood, compositional, and combustion models is described in a number of papers.[33,37-44]

The IMPES formulation can become unstable if the volumetric flow through a grid block in a time step exceeds a small fraction of the block PV. The more stable sequential formulation remains stable to much larger ratios of grid block volumetric throughput/PV. The tolerable throughput ratio for the implicit formulation is significantly larger than that of the sequential method.

Arithmetic (or computing cost) per time step and time-step size both increase from IMPES to sequential to implicit formulations. Since the total cost of simulating a given time period is proportional to the product of arithmetic per time step and time-step size, all three formulations are used widely today.

Single-well coning studies generally involve radial grid spacings, resulting in very small grid blocks near the well and large throughput ratios. For these studies, the IMPES formulation is unsuitable, and the implicit formulation is generally the most efficient.

For field-scale, 3D black-oil studies, the overall computing time is frequently less with the sequential than with the IMPES or implicit formulation. The typical black-oil simulator applied today in 1,000- or more grid-block, field-scale studies is an IMPES model with a user-specified option of sequential solution. Smaller black-oil studies and preliminary cross-sectional, coning, and sensitivity studies associated with the large problems are using the implicit formulation more and more frequently.

Thermal models[39,43,45-47] generally involve implicit formulations. The emerging compositional model involves an equation of state, with options of IMPES or implicit formulations. One difficulty here is that the IMPES formulation lacks sufficient stability for some field-scale problems, while the implicit formulation requires too much machine storage capacity (associated with solution of N_c simultaneous equations) to handle problems larger than, say, 2,000 grid blocks. This dilemma is absent for black-oil models because the sequential formulation fills the gap. However, the sequential formulation does not preserve material balances in compositional problems for which adjacent grid block compositions differ greatly.[39]

Meijerink[48] wrote a revised stabilized IMPES formulation that has potential for filling this compositional model gap between IMPES and implicit methods. Meijerink's scheme improves the stability of IMPES, as does the sequential method, without resulting in material balance error in regions of steep composition gradients.

Numerical Dispersion

The term *numerical dispersion* refers to spatial truncation error in finite-difference simulator results. In physical terms, this error generally appears as falsely smeared spatial gradients of water saturation in waterflooding, temperature in steamflooding, solvent in miscible flooding, and chemical agent in chemical flooding. This excessive smearing occurs primarily in the areal (x or y) directions and, if uncontrolled, results in too early calculated breakthrough times of water (heat, solvent, etc.) at production wells.

This numerical dispersion generally increases with increasing areal grid block size (Δx and Δy). Thus, one remedy is use of a finer areal grid. However, a prohibitive increase in required computer time and storage frequently results from use of a grid sufficiently fine to eliminate numerical dispersion.

Kyte and Berry[49] describe control of numerical dispersion in simulation of waterflooding through large areal grid blocks. They use pseudorelative permeability curves obtained from detailed (fine-grid) cross-sectional simulations. Harpole and Hearn[15] used their method in a 3D black-oil study. To date, steamflood simulation generally has been confined to pattern studies for which a sufficient number of grid blocks between unlike wells is used to minimize numerical

TABLE 1—CALCULATED STEAM BREAKTHROUGH TIMES (days) FOR A NINE-SPOT PATTERN

Difference Scheme	Well 2		Well 3	
	Diagonal	Parallel	Diagonal	Parallel
five-point	47.8	204	1,400	117
nine-point	87.7	75.5	900	1,000

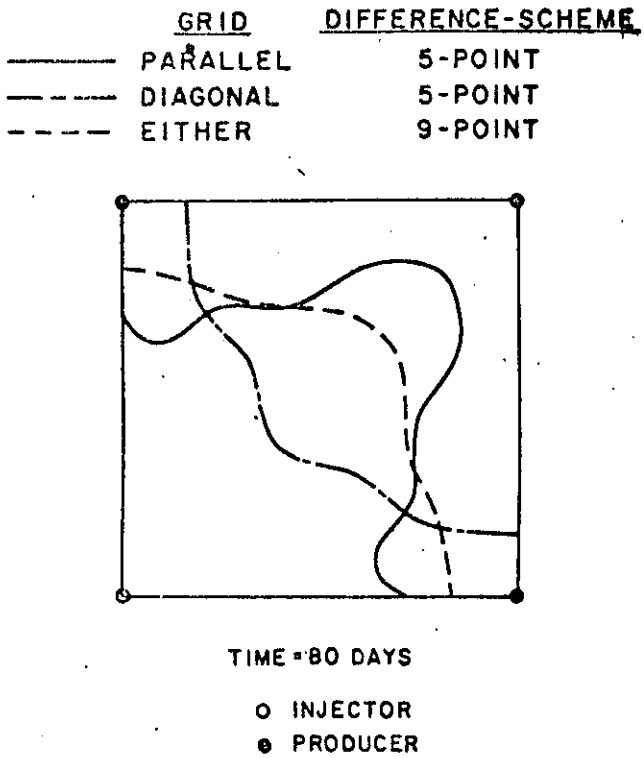

Fig. 4—Calculated shape of steamflood front in a nine-spot pattern.

dispersion effects.

Gas fingering in black-oil reservoirs, and unstable viscous fingering of solvent in adverse-viscosity-ratio miscible floods, can result in simulation results with too little smearing of saturation and concentration gradients. Remedies in these two cases are beyond the scope of this discussion. Killough *et al.*[16] describe alteration of a black-oil formulation to force additional dispersion into the gas saturation profile. Koval[50] and Todd and Longstaff[51] describe methods of forcing additional dispersion to represent viscous fingering in simulation of miscible displacements.

Impact of Hardware Advances on Simulation Practice

The computational speed, storage, and vectorization capabilities of computer hardware have increased sharply in the past few years. As an example, the Cray-1S™ computer provides up to 4,000,000 decimal-words of storage, compared with a typically available 100,000 words on most machines used until 1975. Recently introduced computers offer sharp increases in computational speeds and speed/cost ratios. In addition, vector processing capabilities of Control Data Corp. and Cray computers allow significantly greater efficiency of simulators coded to use this vectorization. Nolen *et al.*[52] found that vectorization of code in the solution technique subroutine of a simulator can reduce solution computing time by factors as large as 40.

This vectorization together with increased machine size and speed contributes strongly to the feasibility of larger reservoir studies. Until recently, most black-oil studies used up to about 3,000 grid blocks. We currently are performing an 11,000-grid-block study; Mrosovsky *et al.*[53] describe a 3D black-oil model study of Prudhoe Bay field using more than 16,000 active grid blocks, and larger studies than this undoubtedly are under way elsewhere.

Examples and Discussion

This section illustrates the grid-orientation effect for a pattern steamflood. Fig. 3 shows a 3-acre (12×10^3-m^2) nine-spot pattern with the diagonal grid and 45°-shifted parallel grid. This pattern has three types of wells—labeled 1 (injector), 2 (near producer), and 3 (far producer).

The isotropic homogeneous formation has permeability of 4,000 md, porosity of 0.36, thickness of 20 ft (6.1 m) and rock-specific heat of 35 Btu/cu ft rock−°F. Oil viscosity is 6,750 cp (6.75 Pa·s) at initial reservoir temperature and 45 cp (0.045 Pa·s) at 500°F (260°C). Initial pressure is 200 psia (1.4 MPa), initial saturations are $S_{wi}=0.19$, $S_{oi}=0.81$, and irreducible water saturation is 0.17.

Specified rate for each injection well is 1,000 B/D (159 m^3/d) of 80% quality steam at 800 psia (5.5 MPa) and 517°F (269°C). All production wells are produced on deliverability against a constant bottomhole pressure (BHP) of 200 psia (1.4 MPa).

The calculated results in Table 1 show the pronounced effect of grid orientation on steam breakthrough times through use of the five-point difference scheme. Obviously, steam should arrive at the near Producer 2 before it reaches the far producer, Well 3. The parallel grid with the five-point scheme actually gives breakthrough at Well 3 at 117 days, *before* breakthrough at Well 2 (204 days).

Table 1 shows that the nine-point difference scheme virtually eliminates the effect of grid orientation for this problem. Fig. 4 shows calculated steam front shapes at 80 days for the two different schemes using parallel and diagonal grids. The difference between the nine-point fronts for the two grids is small and about equal to the error of manual interpolation.

Recent compositional models[42,54] use an EOS as opposed to separate correlations for oil density, gas density, and equilibrium K-values. These papers emphasize that the EOS offers the advantage of

consistency in that phase densities and *K*-values are obtained from a single source. This consistency results in smooth and differentiable convergence of separate phase densities and compositions to identical values as computations approach a critical point. Phase viscosities based on a correlation[55] using EOS densities also converge smoothly to a single value at a critical point.

The EOS's most widely used in reservoir calculations today are Redlich-Kwong[56-58] and Peng-Robinson[59] equations. Martin[60] shows that all cubic EOS's can be obtained from a single, general EOS form. Yarborough[61] describes applications of a modified Redlich-Kwong EOS to reservoir fluids; Katz *et al.*[62] give applications of the Peng-Robinson EOS.

In our compositional work, we have found that nonlinear regression on EOR parameters is necessary. Frequently, prohibitive time requirements result from trial-and-error efforts to match laboratory test data. We generally have found some adjustment of EOS parameters necessary to match laboratory PVT data.

Table 2 compares EOS calculated results with laboratory PVT data reported by Simon *et al.*[63] for mixtures of CO_2 and a SACROC oil sample at 130°F (54°C). Simon *et al.* presented the crude oil sample analysis through C_{13}^+. We performed regressions, using all the data listed, with 14 components (C_1 through C_{13}^+ and CO_2) and with five components after pseudoizing (lumping components) the crude to four components. The calculated results correspond to use of the four pseudocomponents. These results used a modified Redlich-Kwong EOS[57], but very similar results were obtained with the Peng-Robinson EOS. Baker and Luks[64] calculated an equally good saturation pressure match of these data using 39 components, without regression, using a modified Redlich-Kwong EOS.

The predicted values in Table 2 were calculated with no regression using 14 components in the Peng-Robinson EOS. We used binary interaction coefficients given by Katz *et al.*,[62] except that CO_2/hydrocarbon values were 0.10 and the C_1 through C_{13}^+ binary was adjusted to 0.1298 to match the crude bubble-point pressure of 1,660 psia (11.4 MPa). Without the latter adjustment, the Peng-Robinson EOS calculated a bubble-point pressure of 1,469 psia (10.1 MPa). All the predicted saturation pressures are bubble points, while the last three observed and last two pressures, calculated through regression, are dewpoints.

Our compositional simulation of CO_2 injection, using the previously discussed EOS match, indicated completely immiscible displacement at all pressures. The simulations showed pronounced vaporization of light and intermediate oil components into the CO_2, increasing with increasing flood pressure level. Dicharry *et al.*[65] discuss design-stage tests indicating multiple-contact miscibility for CO_2 injection at pressures as low as 1,800 psia (12.4 MPa) for SACROC Unit. Kane[66] reports subsequent work indicating higher pressures necessary for miscibility.

Simulation frequently is employed to study rate sensitivity. We define rate sensitivity as an adverse relationship between ultimate oil recovery and production or reservoir voidage rate. Ref. 67 describes a simulation study of rate sensitivity in different types of reservoirs in Alberta. This study was restricted to pressure-maintained, water/oil displacements and included coning and 2- and 3D calculations in formations ranging from moderate to severe heterogeneity.

The conclusion of that rather lengthy reference is simple and brief: Water/oil displacements are rate-

TABLE 2—SACROC OIL/CO_2 PVT DATA

	Observed[62]	Calculated (after regression)	Predicted
Saturation pressure, psia	1,660*	1,660	1,660
Saturation pressure, psia	1,920	1,870	1,792
Saturation pressure, psia	2,160	2,079	1,947
Saturation pressure, psia	2,420	2,344	2,118
Saturation pressure, psia	2,570*	2,589	2,215
Saturation pressure, psia	3,000	3,000*	2,352
Saturation pressure, psia	3,740	3,724	2,534
Volume ratio	1.0	1.0	1.0
Volume ratio	1.1016	1.1123	1.2385
Volume ratio	1.2791	1.3043	1.4336
Volume ratio	1.5234	1.5562	1.6970
Volume ratio	1.6443	1.6694	1.8270
Volume % liquid	73	73	82
Volume % liquid	59	57	68
Volume % liquid	50	51	62
Volume % liquid	40	39	47
Volume % liquid	7	7	11
Volume % liquid of crude at 610 psia	40	39	—
Crude gas, mol wt	20.3	21.2	20.9
Crude gas, *Z*	0.776	0.781	0.758
ZCO_2 at 2,000 psia	0.38	0.38	—

*Critical point

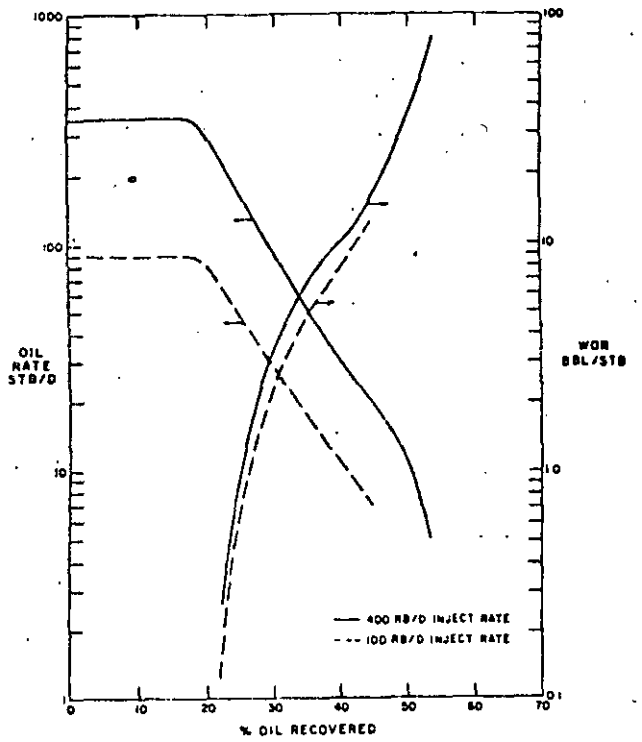

Fig. 5—Belly River B pool, cross section.[67]

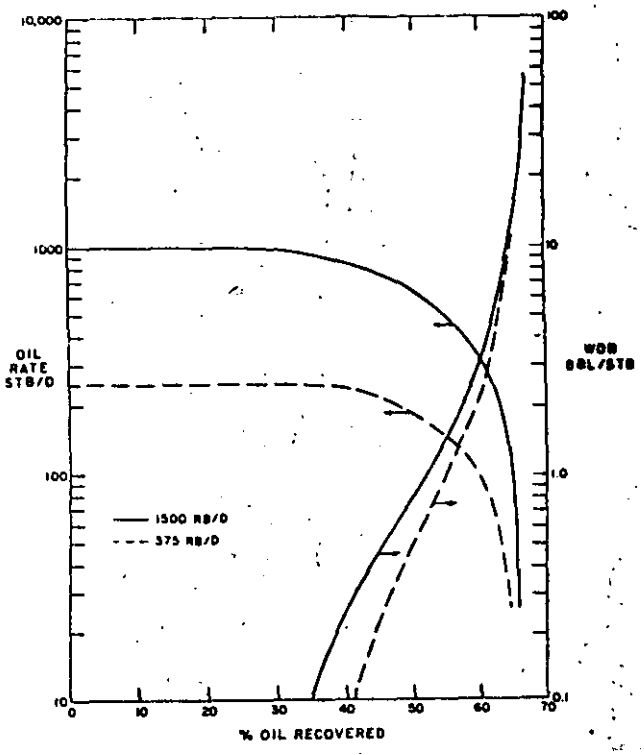

Fig. 6—Sturgeon Lake D-3 pool, Run 1.[67]

sensitive if an economic limit of maximum water cut is used, and are not rate-sensitive if an economic limit of a minimum oil rate is used. Thus, the existence of rate sensitivity in any particular case depends on the relative weights given those two economic limits in the definition of economic limit adopted.

Figs. 5, 6, and 7 illustrate this conclusion. Selecting a fixed oil rate as an economic limit and reading across the figure, we find ultimate oil recovery higher at a higher rate. Selecting a fixed water/oil ratio as the limit and reading across the figure, we find ultimate recovery lower at the higher rate.

Coats *et al.*[68,69] discuss the concept of pseudo capillary pressure curves, which should be used in place of rock or laboratory curves to initialize fluid-saturation distributions correctly. The pseudocurve definition[68] is fairly straightforward if the grid blocks representing the reservoir are viewed as a set of horizontal blocks at staggered depth values representing reservoir structure (dip). The definition becomes more complex as the grid blocks are viewed as inclined in both x and y directions. In practice, the pseudo capillary pressure definition is unimportant if the water/oil and gas/oil transition-zone lengths significantly exceed grid block thickness (horizontal block case) or overall elevation difference (inclined block case).

Where rock and pseudo capillary pressure curves give significantly different initial fluid-saturation distributions, the latter should be used irrespective of arguments about the existence of phase segregation or vertical equilibrium during dynamic reservoir depletion. Strictly speaking, if pseudocurves are not used, the initialized distributions will not reflect horizontal water/oil and gas/oil contacts. In addition, if the reservoir were shut-in, the calculations would not yield (in time) equilibrium distributions corresponding to level contacts. In a sense, the pseudo capillary pressure curves give the background equilibrium condition from which dynamic viscous and gravity forces act in distorting contact shapes (overrides, underrunning).

Several authors, including Jacks *et al.*[70] and Kyte and Berry,[49] discuss the use of pseudo relative permeability curves obtained from comparing detailed cross-sectional results with results using fewer layers.

The Future of Simulation

Within 1 to 2 years, we will be using strongly vectorized black-oil, and perhaps compositional, models on very high-speed, large-capacity machines. The computing cost savings on small studies will be offset by a trend toward larger studies—i.e., use of more grid blocks or reservoir definition.

Research under way now will continue toward the goal of a single, general simulator capable of simulating all or most recovery processes of interest. Ref. 33 is an example of a small step in that direction. Success of this research will depend in part on improved understanding and extension of equations of state to represent the PVT behavior of multicomponent fluid systems in three or more phases over wide ranges of pressure and temperature.

Until this goal is reached, we will witness a

continued development and increasing application of a variety of types of simulation models for different processes.

Conclusions

A reservoir simulation model is a set of partial, finite-difference material balance equations. For each grid block, one equation is written for each component or substance comprising the reservoir fluid description. The model is described here in terms of the various formulations used. Current models generally employ an IMPES formulation with options of increased stability provided by sequential and implicit formulations.

Examples of recent significant advances include (1) a nine-point difference formulation which reduces grid-orientation effects; (2) equation-of-state usage, which promises improvements in compositional simulation and may aid development of a generalized simulator; and (3) increased computer speeds, storage capacities, and vectorization capabilities, which contribute to the feasibility of larger, more detailed field studies.

Current research may lead away from the present proliferation of models of different processes toward a single, generalized model applicable to all or most recovery processes of interest.

Acknowledgment

I appreciate G.W. Paul's provision of information relating to chemical flooding and its simulation.

References

1. Muskat, M.: *The Flow of Homogeneous Fluids Through Porous Media*, J.W. Edwards Inc., Ann Arbor, MI (1946).
2. Muskat, M.: *Physical Properties of Oil Production*, McGraw-Hill Book Co. Inc., New York City (1949).
3. Muskat, M.: "The Production Histories of Producing Gas-Drive Reservoirs," *J. Applied Phys.* (1945) **16**, 147.
4. Katz, D.L.: "Methods of Estimating Oil and Gas Reserves," *Trans.*, AIME (1936) **118**, 18-32.
5. Buckley, S.E. and Leverett, M.C.: "Mechanism of Fluid Displacement in Sands," *Trans.*, AIME (1942) **146**, 107-17.
6. Welge, H.J.: "A Simplified Method for Computing Oil Recoveries by Gas or Water Drive," *Trans.*, AIME (1952) **195**, 91-98.
7. Odeh, A.S.: "Reservoir Simulation—What Is It?" *J. Pet. Tech.* (Nov. 1969) 1383-88.
8. Holm, L.W.: "Status of CO_2 and Hydrocarbon Miscible Oil Recovery Methods," *J. Pet. Tech.* (Jan. 1976) 76-84.
9. Gogarty, W.B.: "Status of Surfactant or Micellar Methods," *J. Pet. Tech.* (Jan. 1976) 93-102.
10. Johnson, C.E. Jr.: "Status of Caustic and Emulsion Floods," *J. Pet. Tech.* (Jan. 1976) 85-92.
11. Staggs, H.M. and Herbeck, E.F.: "Reservoir Simulation Models—An Engineering Overview," *J. Pet. Tech.* (Dec. 1971) 1428-36.
12. Coats, K.H.: "Use and Misuse of Reservoir Simulation Models," *J. Pet. Tech.* (Nov. 1969) 1391-98.
13. McCulloch, R.C., Langton, J.R., and Spivak, A.: "Simulation of High Relief Reservoirs; Rainbow Field, Alberta, Canada," *J. Pet. Tech.* (Nov. 1969) 1399-1408.
14. *Numerical Simulation*, Reprint Series, SPE, Dallas (1973) 11.
15. Harpole, K.J. and Hearn, C.L.: "The Role of Numerical Simulation in Reservoir Management of a West Texas Carbonate Reservoir," paper SPE 10022 presented at the Intl. Petroleum Exhibition and Technical Symposium, Beijing, March 19-22, 1982.
16. Killough, J.E., Pavalas, E.J. Jr., Martin, C., and Doughty, R.K.: "The Prudhoe Bay Field: Simulation of a Complex Reservoir," paper SPE 10023 presented at the Intl. Petroleum Exhibition and Technical Symposium, Beijing, March 19-22, 1982.
17. Graue, D.J. and Zana, E.T.: "Study of a Possible CO_2 Flood in Rangely Field, Colorado," *J. Pet. Tech.* (July 1981) 1312-18.
18. Bloomquist, C.W., Fuller, K.L., and Moranville, M.B.: "Miscible Gas Enhanced Oil Recovery and the Effects of the Windfall Profit Tax," paper SPE 10274 presented at the SPE 56th Annual Technical Conference and Exhibition, San Antonio, Oct. 5-7, 1981.
19. Todd, M.R., Cobb, M., and McCarter, E.D.: "CO_2 Flood Performance Evaluation for the Cornell Unit, Wasson San Andres Field," paper SPE 10292 presented at the SPE 56th Annual Technical Conference and Exhibition, San Antonio, Oct. 5-7, 1981.
20. Herrera, J.Q. and Hanzlik, E.J.: "Steam Stimulation History Match of Multiwell Pattern in the S1-B Zone, Cat Canyon Field," paper SPE 7969 presented at the 1979 California Regional Meeting, Ventura, April 18-20.
21. Williams, R.L.: "Steamflood Pilot Design for a Massive, Steeply Dipping Reservoir," paper SPE 10321 presented at the 56th Annual Technical Conference and Exhibition, San Antonio, Oct. 5-7, 1981.
22. Meldau, R.F., Shipley, R.G., and Coats, K.H.: "Cyclic Gas/Steam Stimulation of Heavy-Oil Wells," *J. Pet. Tech.* (Oct. 1981) 1990-98.
23. "Selection of Reservoirs Amenable to Micellar Flooding," First Annual Report, DOE/BC/00048-20 (Dec. 1980).
24. Fayers, F.J., Hawes, R.I., and Mathews, J.D.: "Some Aspects of Potential Application of Surfactants or CO_2 as EOR Processes in North Sea Reservoirs," *J. Pet. Tech.* (Sept. 1981) 1617-27.
25. deZabala, E.F., Vislocky, E.R., Rubin, E., and Radke, C.J.: "A Chemical Theory for Linear Alkaline Flooding," *Soc. Pet. Eng. J.* (April 1982) 245-58.
26. Patton, J.T., Coats, K.H., and Colegrove, G.T.: "Prediction of Polymer Flood Performance," paper SPE 2546 presented at the SPE 44th Annual Meeting, Denver, Sept. 28-Oct. 1, 1969.
27. Todd, M.R., O'Dell, P.M., and Hirasaki, G.J.: "Methods for Increased Accuracy in Numerical Reservoir Simulators," *Soc. Pet. Eng. J.* (Dec. 1972) 515-30.
28. Coats, K.H., George, W.D., Chu, Chieh, and Marcum, B.E.:

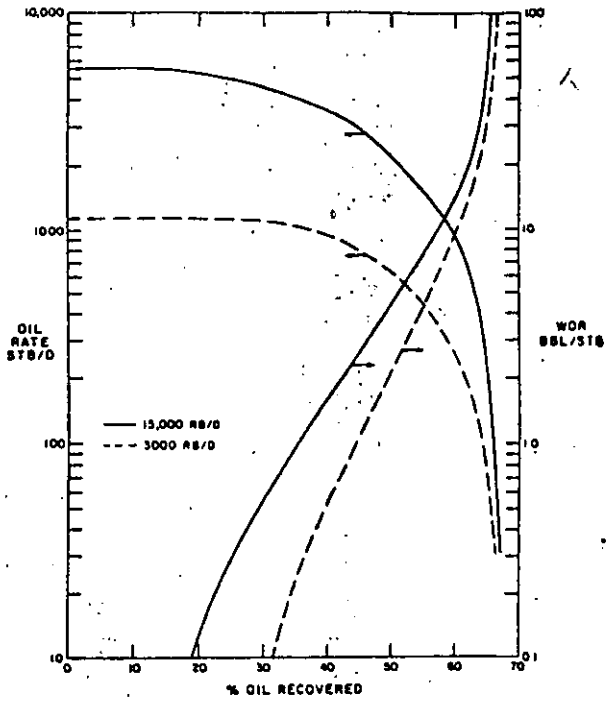

Fig. 7—Simonette D-3 pool, Run 2.[67]

"Three-Dimensional Simulation of Steamflooding," *Soc. Pet. Eng. J.* (Dec. 1974) 573-92.
29. Yanosik, J.L., and McCracken, T.A.: "A Nine-Point, Finite-Difference Reservoir Simulator for Realistic Prediction of Adverse Mobility Ratio Displacements," *Soc. Pet. Eng. J.* (Aug. 1979) 253-62.
30. Sheldon, J.W., Harris, C.D., and Bavly, D.: "A Method for General Reservoir Behavior Simulation on Digital Computers," paper SPE 1521-G presented at the SPE 35th Annual Meeting, Denver, Oct. 2-5, 1960.
31. Stone, H.L. and Garder, A.O. Jr.: "Analysis of Gas-Cap or Dissolved-Gas Drive Reservoirs," *Soc. Pet. Eng. J.* (June 1961) 92-104; *Trans.*, AIME, 222.
32. Fagin, R.G. and Stewart, C.H. Jr.: "A New Approach to the Two-Dimensional Multiphase Reservoir Simulator," *Soc. Pet. Eng. J.* (June 1966) 175-82; *Trans.*, AIME, 237.
33. Coats, K.H.: "Reservoir Simulation: A General Model Formulation and Associated Physical/Numerical Sources of Instability," *Boundary and Interior Layers—Computational and Asymptotic Methods*, J.J.H. Miller (ed.), Boole Press, Dublin (1980) 62-76.
34. MacDonald, R.C. and Coats, K.H.: "Methods for Numerical Simulation of Water and Gas Coning," *Soc. Pet. Eng. J.* (Dec. 1970) 425-36; *Trans.*, AIME, 249.
35. Spillette, A.G., Hillestad, J.G., and Stone, H.L.: "A High-Stability Sequential-Solution Approach to Reservoir Simulation," paper SPE 4542 presented at the SPE 48th Annual Meeting, Las Vegas, Sept. 30-Oct. 3, 1973.
36. Blair, P.M. and Weinaug, C.F.: "Solution of Two-Phase Flow Problems Using Implicit Difference Equations," *Soc. Pet. Eng. J.* (Dec. 1969) 417-24; *Trans.*, AIME, 246.
37. Letkeman, J.P. and Ridings, R.L.: "A Numerical Coning Model," *Soc. Pet. Eng. J.* (Dec. 1970) 418-24; *Trans.*, AIME, 249.
38. Coats, K.H.: "Geothermal Reservoir Modeling," paper SPE 6892 presented at the SPE 52nd Annual Technical Conference and Exhibition, Denver, Oct. 9-12, 1977.
39. Coats, K.H.: "A Highly Implicit Steamflood Model," *Soc. Pet. Eng. J.* (Oct. 1978) 369-83.
40. Bansal, P.P. *et al.*: "A Strongly Coupled, Fully Implicit, Three-Dimensional, Three-Phase Reservoir Simulator," paper SPE 8329 presented at the SPE 54th Annual Technical Conference and Exhibition, Las Vegas, Sept. 23-26, 1979.
41. Patton, J.T. and Coats, K.H.: "A Parametric Study of the CO_2 Huf-n-Puf Process," paper SPE 9228 presented at the 54th Annual Technical Conference and Exhibition, Las Vegas, Sept. 23-26, 1979.
42. Coats, K.H.: "An Equation-of-State Compositional Model," *Soc. Pet. Eng. J.* (Oct. 1980) 363-76.
43. Coats, K.H.: "In-Situ Combustion Model," *Soc. Pet. Eng. J.* (Dec. 1980) 533-53.
44. Trimble, R.H. and McDonald, A.E.: "A Strongly Coupled, Fully Implicit, Three-Dimensional, Three-Phase Well Coning Model," *Soc. Pet. Eng. J.* (Aug. 1981) 454-58.
45. Weinstein, H.G., Wheeler, J.A., and Woods, E.G.: "Numerical Model for Thermal Process," *Soc. Pet. Eng. J.* (Feb. 1977) 65-78.
46. Crookston, H.B., Culham, W.E., and Chen, W.H.: "Numerical Simulation Model for Thermal Recovery Processes," *Soc. Pet. Eng. J.* (Feb. 1979) 37-58; *Trans.*, AIME, 267.
47. Youngren, G.K.: "Development and Application of an In-Situ Combustion Reservoir Simulator," *Soc. Pet. Eng. J.* (Feb. 1980) 39-51.
48. Meijerink, J.A.: "A New Stabilized Method for Use in IMPES Type Numerical Reservoir Simulators," paper SPE 5247 presented at the SPE 49th Annual Meeting, Houston, Oct. 6-9, 1974.
49. Kyte, J.R. and Berry, D.W.: "New Pseudo Functions to Control Numerical Dispersion," *Soc. Pet. Eng. J.* (Aug. 1975) 269-76.
50. Koval, E.J.: "A Method for Predicting the Performance of Unstable Miscible Displacement in Heterogeneous Media," *Soc. Pet. Eng. J.* (June 1963) 145-54; *Trans.*, AIME, 228.
51. Todd, M.R. and Longstaff, W.J.: "The Development, Testing, and Application of a Numerical Simulator for Predicting Miscible Flood Performance," *J. Pet. Tech.* (July 1972) 874-82.
52. Nolen, J.S., Kuba, D.W., and Kasic, M.J. Jr.: "Application of Vector Processors to Solve Finite Difference Equations," *Soc. Pet. Eng. J.* (Aug. 1981) 447-53.
53. Mrosovsky, I., Wong, J.Y., and Lampe, H.W.: "Construction of a Large Field Simulator on a Vector Computer," *J. Pet. Tech.* (Dec. 1980) 2253-64.
54. Fussell, L.T. and Fussell, D.D.: "An Iterative Technique for Compositional Reservoir Models," *Soc. Pet. Eng. J.* (Aug. 1979) 211-20.
55. Lohrenz, J., Bray, B.G., and Clark, C.R.: "Calculating Viscosity of Reservoir Fluids From Their Composition," *J. Pet. Tech.* (Oct. 1964) 1171-76; *Trans.*, AIME, 231.
56. Redlich, O. and Kwong, J.N.S.: "On the Thermodynamics of Solutions. V. An Equation of State. Fugacities of Gaseous Solutions," *Chem. Review* (1949) 44, 233.
57. Zudkevitch, David and Joffe, Joseph: "Correlation and Prediction of Vapor-Liquid Equilibria with the Redlich-Kwong Equation of State," *AIChE J.* (Jan. 1970) 16, 112-19.
58. Soave, G.: *Chem. Eng. Sci.* (1972) 27, 1197.
59. Peng, D.-Y. and Robinson, D.B.: "A New Two-Constant Equation of State," *Ind. Eng. Chem. Fund.* (1976) 15, 59.
60. Martin, J.J.: "Cubic Equations of State—Which?" *Ind. Eng. Chem. Fund.* (May 1979) 18, 81.
61. Yarborough, L.: "Application of a Generalized Equation of State to Petroleum Reservoir Fluids," paper presented at the Symposium on Equations of State in Engineering and Research, 176th ACS Natl. Meeting, Miami Beach, Sept. 10-15, 1978.
62. Katz, D.L. and Firoozabadi, A.: "Predicting Phase Behavior of Condensate/Crude-Oil Systems Using Methane Interaction Coefficients," *J. Pet. Tech.* (Nov. 1978) 1649-55.
63. Simon, R., Rosman, A., and Zana, E.: "Phase-Behavior Properties of CO_2-Reservoir Oil Systems," *Soc. Pet. Eng. J.* (Feb. 1978) 20-26.
64. Baker, L.E. and Luks, K.D.: "Critical Point and Saturation Pressure Calculations for Multicomponent Systems," *Soc. Pet. Eng. J.* (Feb. 1980) 15-24.
65. Dicharry, R.M., Perryman, T.L., and Ronquille, J.D.: "Evaluations and Design of a CO_2 Miscible Flood Project—SACROC Unit, Kelly Snyder Field," *J. Pet. Tech.* (Nov. 1973) 1309-13; *Trans.*, AIME, 255.
66. Kane, A.V.: "Performance Review of a Large-Scale CO_2-WAG Enhanced Recovery Project, SACROC Unit—Kelly Snyder Field," *J. Pet. Tech.* (Feb. 1979) 217-31.
67. "A Study of the Sensitivity of Oil Recovery to Production Rate," Intercomp Ltd., Calgary, attached to and submitted as Schedule I of Shell Canada Ltd.'s submission to the Alberta Energy Resources Conservation Board, Proc. No. 7511 (Feb. 1974).
68. Coats, K.H., Neilsen, R.L., Terhune, M.H., and Weber, A.G.: "Simulation of Three-Dimensional, Two-Phase Flow in Oil and Gas Reservoirs," *Soc. Pet. Eng. J.* (Dec. 1967) 377-88.
69. Coats, K.H., Dempsey, J.R., and Henderson, J.H.: "The Use of Vertical Equilibrium in Two-Dimensional Simulation of Three-Dimensional Reservoir Performance," *Soc. Pet. Eng. J.* (March 1971) 63-71.
70. Jacks, H.H., Smith, O.E., and Mattax, C.C.: "The Modeling of a Three-Dimensional Reservoir With a Two-Dimensional Reservoir Simulator—The Use of Dynamic Pseudo Functions," *Soc. Pet. Eng. J.* (June 1973) 175-85.

SI Metric Conversion Factors

bbl	× 1.589 873	E−01	= m^3/d
psi	× 6.894 757	E−03	= MPa

JPT

Distinguished Author Series articles are general, descriptive presentations that summarize the state of the art in an area of technology by describing recent developments for readers who are not specialists in the topics discussed. Written by individuals recognized as experts in the areas, these articles provide key references to more definitive work and present specific details only to illustrate the technology. Purpose: To inform the general readership of recent advances in various areas of petroleum engineering. The series is a project of the Technical Coverage Committee.

Discussion of Reservoir Simulation: State of the Art

A.K. Khatib,* SPE, Godsey-Earlougher Div.

The following addresses a paper (Aug. 1982 *JPT*, Pages 1633–42) by Keith Coats that is a very good review of the development history and the current status of reservoir simulation. However, the author makes a surprising statement on Page 1636: "Numerical simulation provides a reliable means to predict chemical flood performance in a reservoir environment, because the processes are very complex and many reservoir parameters affect the results."

Numerical simulators have become very useful tools to simulate reservoir performance during primary and secondary recoveries. As for EOR processes, there are now reasonably good simulators for those processes whose mechanisms are fairly well understood—e.g., steamdrive and miscible CO_2 flooding. However, the mechanisms of complex processes, such as in-situ combustion and chemical flooding, are yet to be unraveled, and their governing parameters are therefore ill defined. Simulation attempts of such processes, even on a pilot-field scale, have proved of limited utility. For example, a recent review of published results of surfactant flooding projects that are technically successful showed that recovery was at best 50% of that predicted by simulation.

*Now with Meneven S.A.

0149-2136/83/0061-1927$00.25

Authors' Reply to Discussion of Reservoir Simulation: State of the Art

Keith H. Coats, SPE, Intercomp Resource Development and Engineering Corp.

Regarding chemical flooding, Mr. Khatib is apparently referring to the Bell Creek micellar/polymer pilot simulation as compared to the field results.[1] It is surprising that the simulation came as close as it did to the actual field results because (1) values of remaining oil saturation used to characterize the reservoir for simulation were higher than those existing in the field,[2] (2) there is a permeability barrier between the central injector and one of the producers that was not entirely accounted for in the simulation, (3) the coreflood selected for history matching[3] and used to describe the process for the simulator was optimistic, (4) the interfacial tension, phase viscosity, and phase behavior data used in the simulation were for the most part assumed and were not based on actual laboratory data, and (5) the equivalent weight of the injected sulfonate may have been below design specifications.[2]

Chemical flood simulation of the El Dorado pilot yielded a somewhat better comparison with the results at an observation well, but even here process data were limited.[4]

Although many of the mechanisms operative in chemical flooding are not well understood, a final judgment of currently available simulators cannot be made until adequate laboratory data are available to exploit the mechanisms that are known.

In deference to Mr. Khatib's closing remarks, the paper's statement "Numerical simulation provides a reliable means to predict chemical flood..." might better state "...provides the best available means to..." That is, while the process complexity (or insufficient laboratory data) currently introduces uncertainty in numerical model results, it also widens the gap between reliability of intuitive or rule-of-thumb and model predictions.

Acknowledgment

I thank G.W. Paul for his assistance in writing this Reply.

References

1. "Bell Creek Field Micellar-Polymer Pilot Demonstration," Final Report (June 1976–March 1982) U.S. DOE, DOE/SF/01802-61 (Sept. 1982).
2. "An Evaluation of the Bell Creek Field Micellar-Polymer Pilot," U.S. DOE, DOE/BC/10033-5 (Dec. 1982).
3. Todd, M.R. *et al.*: "Numerical Simulation of Competing Chemical Flood Designs," paper SPE 7077 presented at the 1978 SPE Symposium on Improved Methods for Oil Recovery, Tulsa, April 16–19.
4. "Data Requirements for EOR Surfactant-Polymer Process Simulation and Analysis of El Dorado Pilot Project Simulation, Butler County, Kansas," U.S. DOE, DOE/ET/10145-74 (Jan. 1983).

0149-2136/83/0061-2290$00.25

CURSO: " INGENIERIA DE YACIMIENTOS GEOTERMICOS "
13 DE MARZO al 18 DE MAYO 1984

TEMA: "RESERVOIR SIMULATION: STATE-OF-THE ART"

DR. GUILLERMO DOMIMGUEZ V.
2-13 DE ABRIL
MATERIAL COMPLEMENTARIO

SPE

Society of Petroleum Engineers of AIME

SPE 10020

Reservoir Simulation: State-of-the-Art

by Keith H. Coats,* *INTERCOMP Resource Development and Engineering, Inc.*

*Member SPE-AIME

This paper was presented at the International Petroleum Exhibition and Technical Symposium of the Society of Petroleum Engineers held in Beijing, China, 18-26 March, 1982. The material is subject to correction by the author. Permission to copy is restricted to an abstract of not more than 300 words. Write SPE, 6200 North Central Expressway, Dallas, Texas, 75206 USA. Telex 730989

ABSTRACT

A reservoir simulation model is a set of partial-difference equations expressing conservation of mass of each component present in the reservoir fluid description. This paper describes the current model formulations and equation-solving methods. Emphasis is given to the development in recent years of different models to simulate the recovery mechanisms and phenomena active in a variety of enhanced recovery processes.

Several recent, significant advances are discussed and illustrated, including 1) a nine-point difference scheme, 2) equation-of-state usage and 3) increased machine speed, storage and vectorization capability contributing to larger, more detailed field studies.

Research currently underway, if successful, may lead to development of a single, generalized simulator capable of simulating all or most recovery processes of interest.

INTRODUCTION

The purpose of this paper is a description of the current level of development in reserovir simulation. This requires some discussion of what a simulation model is and why it is needed or used. A simulation model can be described in terms of the nature of its equations, their formulation and methods of solution. This description through "methodology" might be of interest to engineers newly assigned to development or maintenance of simulators.

Simulation models for various recovery processes can be described more simply through relating their features to oil recovery mechanisms pertinent to these processes. This type of description might appeal more to engineers newly assigned in use of simulators.

References and illustrations at end of paper.

This paper gives a brief history of simulation, followed by an equally brief, very general description of a simulation model. This brevity is followed by two sections which, without equations, attempt to describe or characterize the reservoir simulator through methodology and through a discussion of recovery mechanisms. The first of these two sections discusses past and recent developments in arriving at a summary of the technology currently used in simulation models.

The two descriptive sections are followed by a discussion of why simulation is used (i.e. typical reservoir performance questions addressed by computer simulation), a section giving a few examples and miscellaneous points pertinent to simulation today, and, finally, a summary.

A BRIEF HISTORY

In a broad sense, reservoir simulation has been practiced since the beginning of petroleum engineering in the 1930's. Simulation is simply the use of calculations to predict reservoir performance - either forecast recovery or evaluate the economics of alternative recovery methods. Prior to 1960 these calculations largely consisted of analytical methods[2,3], zero-dimensional material balances[4,5] and one-dimensional Buckley-Leverett[6,7] calculations.

The term "simulation" became common in the early 1960's as predictive methods evolved into relatively sophisticated computer programs. These programs represented a major advancement as they allowed solution of large sets of finite-difference equations describing two- and three-dimensional, transient, multiphase flow in heterogeneous porous media. This advancement was made possible by the rapid evolution of large-scale, hi-speed digital computers and development of numerical mathematical methods for solving large systems of finite-difference equations.

During the 1960's, reservoir simulation effort was largely devoted to two phase gas-water and three phase black oil reservoir problems. Recovery methods simulated were essentially limited to depletion or pressure maintenance. Years of research and engineering had resulted in generally accepted fluid flow "laws" reflecting the gravitational, viscous and capillary forces involved in oil displacement and recovery. Thus simulation largely ignored questions related to the physics embodied in the models' equations and was focused more on the models' ability to match reservoir production history.

During the 1960's and early 1970's, it was possible to develop a single simulation model capable of addressing most reservoir problems encountered. This concept of a single, general model has always appealed to operating companies since it significantly reduces the cost of training and usage, and, potentially, the cost of model development and maintenance.

During the 1970's, the picture changed markedly. The sharp rise in oil prices and government trends toward deregulation and partial funding of field pilot projects led to a proliferation of enhanced recovery processes. Consequently, we began to simulate these new processes which extended beyond conventional depletion and pressure maintenance to miscible flooding, chemical flooding, CO_2 injection, steam or hot water stimulation/flooding and in-situ combustion. A relatively comfortable understanding of two-component ("gas" and "oil") hydrocarbon behavior in simple immiscible flow was replaced by a struggle to unravel and characterize the physics of oil displacement under the influence of temperature, chemical agents and complex multi-component phase behavior. In addition to "simple" multiphase flow in porous media, we had to cope with chemical adsorption and degradation, emulsifying and interfacial tension reduction effects, reaction kinetics and other thermal effects and complex equilibrium phase behavior.

The proliferation of recovery methods in the 1970's caused a split from the above-mentioned "single model" concept as individual models were developed to represent each of these new recovery schemes. Thus, a pronounced emphasis exists today in examining and fine tuning the equations and related assumptions pertinent to these techniques.

Research during the 1970's resulted in a number of significant advances in simulation model formulations and numerical methods of solution. These advances extended our ability to simulate more complex recovery processes and/or reduced the models' computing costs through increased stability of the formulations and efficiency of the numerical solution methods.

SIMULATION MODELS - A BRIEF DESCRIPTION

Odeh[1] gives an excellent description of the conceptual simplicity of a simulation model. He illustrates the subdivision of a reservoir into a two- or three-dimensional network of grid blocks. He then shows that the simulation model equations are basically the familiar volumetric material balance equation[4,5] written for each phase for each grid block. The phase flow rates between each grid block and its 2, 4 or 6 (in 1, 2 or 3-dimensional cases, respectively) adjacent blocks are represented by Darcy's law modified by the relative permeability concept.

A simulation model is a set of partial-difference equations requiring numerical solution as opposed to a set of partial differential equations amenable to analytical solution. The reasons for this are:

1. Reservoir heterogeneity - variable permeability, porosity and irregular geometry;
2. Nonlinearity of relative permeability and capillary pressure vs. saturation relationship;
3. Nonlinearity of fluid PVT properties as functions of pressure, composition, and temperature.

The models require hi-speed digital computers simply due to the immense arithmetic associated with the equations' solution.

A simulation model requires three types of input data. First, reservoir description data include 1) overall geometry, 2) grid size specification, 3) permeability, porosity and elevation for each grid block, and 4) relative permeability and capillary pressure vs. saturation functions or tables. Models generally allow specification of different tables to different layers or regions of the reservoir. Geological and petrophysical work using logs and core analyses are necessary for items (1) and (3). Laboratory tests on core samples yield estimates of relative permeability and capillary pressure relationships.

Second, fluid PVT properties, such as formation volume factors, solution gas and viscosities are obtained by laboratory tests. Finally, well locations, perforated intervals, productivity indices and rate schedules must be specified. Additional data or laboratory tests required for thermal, compositional and chemical flood models are discussed briefly below.

Model output or calculated results include spatial fluid pressure and saturation distributions, and producing GOR and WOR and injection/production rate (for wells on injectivity/productivity) for each well at the end of each time step of the computations. Internal manipulation of these results gives average reservoir pressure and instantaneous rates and cumulative injection/production of oil, gas and water by well and total field vs. time.

SIMULATION MODELS - METHODOLOGY

Descriptions of simulation models in the literature generally are given for the development engineer and are confusing to others. Part of this confusion stems from a lengthy list of usually undefined terms assumed to be commonly

understood. With no pretense of eliminating this confusion, I will discuss some of these terms grouped as follows: 1) black oil, compositional, thermal, chemical flood; 2) variational, finite-difference, nine-point, IMPES, sequential, implicit; 3) ADIP, SIP, SOR, direct solution.

The first group refers to model "type", the second to model formulation and the third to solution method or technique. Distinctions of "type" within the first group can be conceptually eliminated by extending Odeh's description. Any simulation model is a set of N partial difference equations written for each grid block comprising the reservoir. Each equation is conceptually trivial in the sense that it is simply a mathematical statement of conservation of mass of a specified substance or of conservation of energy.

The different model types express conservation of mass of different numbers and identities of components and conservation of energy in thermal models. Black oil, compositional and chemical flood models generally simulate isothermal flow and include no energy balance equation.

A black oil model has 3 equations for each grid block expressing mass conservation of the 3 components H_2O, "oil" and "gas". A compositional model consists of N_c equations for each grid block where N_c is the total number of components including (e.g.) H_2O, C_1, C_2, C_3, C_4, C_5, C_6, C_7^+ where C_1 denotes methane, C_2 ethane, etc. A chemical flood model also consists of N_c equations, but the identities of the N_c components are (e.g.) water, oil, surfactant, alcohol (cosurfactant), sodium and calcium ions, and polymer.

The thermal model is similar to the compositional model, with $N_c + 1$ equations expressing conservation of mass of N_c components (e.g.) H_2O, pseudo hydrocarbon components 1, 2, 3, ..., solid component (coke), O_2, N_2, CO_2 and 1 equation for conservation of energy. The pseudo hydrocarbon components typically range from a heavy (nearly) non-volatile component to the lightest (solution gas) component.

One might correctly argue that significant conceptual differences exist in practice among these models due to the PVT treatment accorded the components and fluid phases. For example, a black oil model conventionally assumes zero gas and oil solubility in water, no oil in the gas phase, a pressure-dependent solubility (R_s) of gas in the oil phase and no H_2O in the oil and gas phases. A compositional model, however, treats all components except H_2O as present in both gas and oil phases, obeying an equilibrium dictated by the well known K-values which are normally functions of pressure and composition.

However, even this conceptual difference disappears if we accept as a model definition, a set of N_c (+1) difference equations for each grid block expressing conservation of mass of N_c components (+ energy) with each component present in all phases. This distribution of components among the phases obeys either externally specified K-values/distribution coefficients or an equation-of-state or a combination of the two. With allowance for rock adsorption isotherms, chemical reactions, temperature-, pressure-, and composition-dependence of viscosity, relative permeabilities and capillary pressure, this definition results in each of the above models representing a subset of a single, general model.

I believe we are currently seeing a trend toward this general model and will comment further on it below.

The reader should note from the above discussions that components (and energy), not phases, are the conserved substances requiring equations in a simulation model. Thus, the number of phases is unrelated to the number of model equations.

The second category of terms reflects the type of formulation utilized by the N-equation model. As previously mentioned, each of these equations is a partial-difference equation. The conventional finite-difference scheme most widely used today, utilizes a semi-regular distribution of grid points (grid block centers) throughout the entire areal and vertical expanse of a reservoir. The result of using "enough" grid points or blocks to gain desired definition in regions of high well density or strong reservoir heterogeneity is a large number of grid blocks in inactive or remote regions of the reservoir where we could tolerate much coarser definition. The variational formulation[8] allows fine grid definition where desired and coarse definition elsewhere in a manner not achievable with the conventional finite-difference approach. Theoretically, then, the variational and finite-difference formulations can give equally accurate solutions with considerably fewer grid points (and consequently less computing costs) used in the variational formulation. However, computational problems unique to the latter method have proven difficult to resolve after nearly 20 years of research. While significant progress has been made, the overwhelming majority of simulation activity today utilizes the conventional finite-difference formulation.

A strong grid-orientation effect was reported by Todd et al[9] for highly adverse mobility waterfloods and later observed by Coats et al[10] for pattern steamfloods. An areal grid with the usual perpendicular x - y axes may be placed over (say) a 5-spot pattern with the x-axis either parallel to or at a 45° angle to the line connecting the injector to a producer. These "parallel" and "diagonal" grids[9] can result in markedly different calculated shapes of the water or steam front and breakthrough times. This difference was reduced by the nine-point finite difference formulation described by Yanosik and McCracken[11]. Their technique is rapidly being programmed into simulators treating steamflooding and miscible CO_2 injection where adverse mobility pattern floods are commonly encountered. This nine-point formulation causes large and moderate increases in computing times of currently reported direct and iterative solution techniques, respectively.

The remaining formulation terms described here apply within the context of either the conventional 5-point or 9-point finite-difference scheme. The IMPES formulation denotes implicit pressure, explicit saturation. Sheldon et al[12], Stone et al[13] and Fagin et al[14] describe the IMPES method for black oil (3 equation) problems. Coats[15] gave an obvious extension of IMPES to the N-equation case. Skipping details for brevity, the method eliminates fluid saturation (and component mol fraction and temperature, if present) variables from the N equations for each grid block, resulting in a single, parabolic, partial-difference pressure equation. This pressure equation is solved by an iterative or direct method over all grid blocks and then the saturations (mol fractions, temperature) are explicitly calculated for each grid block using the interblock flow rates given by the calculated pressure solution. This process is then repeated for successive time steps with an updating of relative permeabilities corresponding to the new saturations at the end of each time step.

MacDonald[16] improved the stability of the IMPES method for the two-phase water-oil case by following the pressure equation solution with solution of a water-saturation equation over the grid using implicit (new time level or end-of-time-step) values of relative permeabilities present in the transmissibilities of the interblock flow terms. Spillete et al[17] extended this concept to the 3-phase case and called the method sequential.

The IMPES formulation requires solution of only 1 (pressure) equation over the grid per time step. The sequential method requires solution of 1 pressure equation followed by simultaneous solution of two saturation equations, in the 3-phase case. The arithmetic required to solve N simultaneous equations is proportional to N^3. Therefore, the arithmetic (for solution of the equations) per time step is roughly (on a normalized basis) 1 for IMPES, 2 for 2-phase sequential and 9 ($1 + 2^3$) for 3-phase sequential. If the 3-phase sequential method is approximated to (a) solve a pressure equation, b) solve a single water saturation equation, c) solve a single gas saturation equation, then the arithmetic falls to 3 for the 3-phase case.

In any event, the increased arithmetic per time step of the sequential method, as opposed to the IMPES formulation, is more than offset in many problems by the increased time step size tolerable. That is, overall computing time is frequently less for sequential than IMPES models.

The implicit formulation utilizes end-of-time step values of relative permeabilities (and densities, viscosities) in the interblock flow term transmissibilities. This prevents the IMPES elimination of all variables, except pressure, among the N equations and leaves the task of simultaneously solving N equations at an arithmetic cost (normalized to 1 for IMPES) of N^3. However, the tolerable time step size for the implicit formulation is significantly larger than that of the sequential method. In fact, the implicit formulation is generally referred to as unconditionally stable, meaning that any time step size may be taken with only time truncation error (not stability) as a limit.

Blair and Weinaug[18] first published this fully implicit formulation. Implementation of implicit or highly implicit formulations in black oil, geothermal, steamflood, compositional and combustion models is described in a number of papers[15,19-25].

Each of the model formulations requires solution of 1 and/or some number of simultaneous equations over the grid. The third category of terms listed above refers to different techniques for solving these equations. Alternating Direction Iterative Techniques (ADIP) were published by Peaceman and Rachford[27] and by Douglas and Rachford[28]. The former is restricted to two-dimensions while the latter applies in either two- or three-dimensional cases. The Successive Overrelaxation (SOR) methods are described by Young[29], including point, line and block SOR methods. The iterative Strongly Implicit Procedure (SIP) proposed by Weinstein et al[30] was demonstrated to be superior to ADIP methods in some types of reservoir problems. Price and Coats[31] described a reduced-band-width direct solution (Gaussian elimination) method which utilized a "D4" grid block ordering scheme to reduce conventionally ordered Gaussian computing time by a factor up to 6 for the 3-dimensional case.

New iterative solution techniques currently receiving attention, testing and use are the matrix factorization method (loosely speaking, SIP with introduction of additional diagonals) described by Dupont et al[32] and Letkeman[33] and a conjugate-gradient method published by Watts[34].

It is difficult to concisely describe the currently used simulation model technology. Different models are used for different processes. For a given process or type of reservoir, a large number of company simulators are in use and few are fully published.

A major portion of worldwide simulation activity is devoted to black oil reservoirs. A significant portion of this activity, in turn, is probably represented by very large problems, e.g. Middle East reservoirs. Until recently most black oil studies used up to perhaps 3000 grid blocks. At Intercomp we are currently performing an 11,000 grid block study; Mrosovsky et al[35] describe a 3-dimensional, black oil model study of the Prudhoe Bay Field using over 16,000 active grid blocks and larger studies than this are undoubtedly underway elsewhere.

The "typical" black oil simulator applied today in 1000 or more grid block field-scale studies is an IMPES model with user-specified options of sequential solution and with options of at least two of the mentioned iterative solution techniques. The most widely used iterative techniques are probably block (line, 2-line or slice) SOR and SIP or a version of its matrix factorization extension.

Smaller black oil studies and preliminary cross-sectional, coning and sensitivity studies associated with the large problems are increasingly utilizing the fully implicit black oil model with reduced band width direct or iterative solution.

Thermal models[36-38,21,25] generally utilize fully implicit formulations with direct solution. Iterative methods have had limited success to date due to a "negative transmissibility" problem caused by cold fluids flowing into a steam saturated block causing pressure to fall in response to a net addition of mass[15,21].

The currently emerging compositional model will utilize an equation-of-state in either IMPES or fully implicit formulations with direct and iterative solution technique options. A difficulty faced here is that the IMPES formulation lacks sufficient stability for some field-scale problems while the fully implicit formulation requires too much machine storage capacity (associated with solution of N_c simultaneous equations) to handle problems larger than (say) 2000 grid blocks. This dilemma is not present for black oil models because the sequential formulation fills the gap. However, the sequential formulation does not preserve material balances in compositional problems where adjacent grid block compositions differ greatly[21].

Meijerink[39] published a revised, Stabilized IMPES formulation which has the potential of filling this compositional model gap between IMPES and fully implicit methods. Meijerink's scheme improves the stability of IMPES, as does the sequential method, without resulting in material balance error in regions of steep composition gradients.

The computational speed, storage and vectorization capability of computer hardware have increased sharply in the past few years. As an example, the CRAY-1S computer provides up to 4,000,000 decimal words of storage compared to a "typically" available 100,000 words on most machines used up to 1975. Recently introduced computers offer sharp increases in computational speeds and speed/cost ratios. In addition, vector processing capabilities of CDC and Cray computers allow a significant increase in efficiency of simulators coded to utilize this vectorization. Nolen et al[40] found that vectorization of code in the solution technique subroutine of a simulator can reduce that solution computing time by factors as large as 40.

This vectorization together with increased machine size and speed contribute strongly to the feasibility of the large reservoir studies (10,000 or more grid blocks) now underway and larger ones projected.

The interested reader with a mathematical inclination will find the simulator characterization given by Bansal et al[22] much more concise than that given here.

SIMULATION MODELS AND OIL RECOVERY MECHANISMS

Four basic recovery mechanisms are active in recovering oil from reservoirs: 1) fluid expansion, 2) displacement, 3) gravity drainage and 4) capillary imbibition. Simple fluid expansion accompanying pressure decline results in oil expulsion from and subsequent flow through the porous matrix. Oil is displaced by gas and injected or naturally encroaching water. Gravity drainage, caused by positive (water-oil) and (oil-gas) density differences, aids oil recovery by causing upward drainage of oil from below an advancing bottom water drive and downward drainage from above a declining gas-oil contact. Finally, imbibition, generally normal to the flow direction, can be an important recovery mechanism in lateral water floods in heterogeneous sands with large vertical variation of permeability.

Simulation models in wide use today (black oil, compositional, etc), reflect or account for these four mechanisms. The displacement, gravity drainage and imbibition mechanisms are all represented simply by use of Darcy's law. The simulator interblock flow rate expressions for water, oil and gas phases appropriately use water, oil and gas phase viscosities, pressures and gravity terms, with user-specified saturation-dependent capillary pressure differences between the phase pressures.

To accommodate the new enhanced recovery processes in our discussion, we add a fifth "mechanism" of oil mobilization. This is a loosely defined term in that it includes widely different phenomena which create or mobilize recoverable oil. Some of these phenomena are not really mechanisms distinct from the first four listed.

Today's simulators generally account for the mobilization and other phenomena mentioned below in discussion of the enhanced recovery processes. Some of the phenomena are complex or poorly understood, or under current laboratory study, and are represented in the models by expressions or equations which will undoubtedly be refined and improved in the future.

Thermal processes can mobilize heavy oil by 1) drastically reducing oil viscosity by increasing temperature, 2) distilling intermediate hydrocarbon components from the oil phase to the more mobile gas phase, 3) cracking the oil (usually above 500°F) to create intermediate components which are distilled into the mobile gas phase, 4) emulsifying the oil into water[41], and, to a minor extent, 5) swelling the oil due to temperature rise. In addition, oil relative permeability end-points may be favorably affected by increased temperature so that residual oil saturations may be reduced.

The CO_2 process can mobilize oil by 1) outright (direct contact) or dynamic (multiple-contact) miscibility at flood pressure, 2) stripping or vaporization of a large fraction of the oil into the mobile gas phase (a completely immiscible process), 3) swelling the oil in immiscible regions, leaving less stock tank oil in the residual oil saturation, and 4) reducing oil viscosity in immiscible cases. Holm[42] gives an excellent description of mechanisms active in CO_2 and miscible flooding.

Chemical flood types include polymer waterflooding, micellar (surfactant) flooding, and alkaline (caustic) flooding. Polymer waterflooding improves oil recovery by lowering the oil/water mobility ratio, through either reducing the effective permeability to water and/or increasing water viscosity. In micellar flooding, surfactants in the floodwater greatly reduce aqueous-oil interfacial tension, thereby solubilizing oil into the micelles and forming an oil bank[43]. The surfactant slug and mobilized oil are normally propelled towards the production well by a graded bank of polymer thickened water. The mechanisms responsible for improved oil recovery in alkaline flooding are not clearly understood, but are thought to include low interfacial tension, wettability alteration and emulsification[44]. Chemical flooding processes involve complicated fluid-fluid and rock-fluid interactions, such as adsorption, ion exchange, viscous shear and three (or more) phase flow.

WHY SIMULATION MODELS ARE USED

Reservoir simulation is used to estimate recovery for a given, existing producing scheme (forecasting), to evaluate the effects on recovery of altered operating conditions and to compare recoveries (with economics) of different recovery methods. Some typical questions regarding reservoir performance relate to the effect on recovery of:

1. Well pattern and spacing
2. Well completion intervals
3. Gas and/or water coning as a function of rate
4. Producing rate
5. Augmenting a natural water drive by water injection and desirability of flank or peripheral as opposed to pattern waterflooding
6. Infill drilling
7. Gas vs. water vs. gas + water injection

Staggs and Herbeck[45] give an excellent discussion of the uses of simulation together with a number of actual examples. Coats[46] gives a general discussion of simulation use (and misuse). Both those papers address a second category of questions related not to reservoir performance but to the use and accuracy of the simulation model itself, e.g.:

1. How many grid blocks areally or layers vertically are necessary?
2. When is accuracy of relative permeability data critical?
3. When or to what extent does a good history match ensure reliability of performance predictions?

Among other conclusions, the above papers emphasize, in connection with such questions, that experience and good judgment on the part of the engineer (user) are important in addition to the use of the model itself. In performing "sensitivity" model runs, the engineer often can estimate the dependence of calculated results upon changes in uncertain input data (permeability level/distribution, relative permeability, etc.).

The above two papers and Odeh[1] point out sources of error in simulation results. We continually attempt to reduce these errors through history matching, improved rigor (few and better assumptions) in the models and increased reservoir definition (more grid blocks) allowed by computer hardware advancements and model efficiency improvements.

McCulloch et al[47] and a number of papers in reference 48 describe field applications of simulation models prior to 1973.

Compositional models are applied to volatile oil and gas condensate reservoirs where the fluids cannot be represented by the conventional formation volume factor and solution gas PVT description used for black oils. Unlike black oils, these fluids will generally exhibit significant variation in compositions of reservoir oil and gas phases in response to pressure change and/or injected gas composition. A compositional model is necessary to represent the mass transfer between and volumetric behavior of these phases. Compositional models are applied in studying loss of recovery caused by liquid dropout during depletion of condensate reservoirs and the reduction of this loss by full or partial cycling (reinjection of gas from surface facilities). The simplest indication that an oil is a "volatile oil" as opposed to a black oil is a significant difference in stock tank liquid yield (or formation volume factor value at bubble point) from constant composition and differential laboratory expansions.

In recent years simulation has been used increasingly to estimate and compare recoveries from a given reservoir under alternative enhanced recovery processes, such as CO_2 injection, thermal methods (steam injection and in-situ combustion) and several types of chemical flooding.

Thermal models are used to simulate performance of cyclic steam stimulation and steamflooding. In either case, questions addressed through simulation relate to effects of injected steam quality and injection rate, operating pressure level, and inclusion of gas with the injected steam. A question in cyclic stimulation concerns the optimum time periods per cycle for steam injection, soak and production. The flooding case introduces the questions of well pattern and spacing. A number of steam injection field studies using models have been published. Herrera and Hanzlik[49] compare field data and model results for a cyclic stimulation operation, Williams[50] discusses field performance and model results for stimulation and flooding and Meldau[51] discusses field and model results related to the addition of gas to the injected steam.

The above-mentioned mechanisms of oil recovery by CO_2 injection, swelling, viscosity reduction, immiscible displacement, vaporization,

and miscible displacement can all occur in the same reservoir problem at different times and/or locations. Compositional modeling is necessary to estimate the occurrence and duration of these CO_2 process mechanisms and their effects on oil recovery as a fuhction of reservoir operating parameters. Graue and Zana[52] describe application of a compositional model in estimating Rangely Field oil recovery by CO_2 injection as a function of injected composition and pressure level. Todd et al[53] describe field application of a model to the CO_2 process under (direct contact) miscibility conditions, and compare results for continuous CO_2 vs. alternate CO_2/water injection.

Results of compositional simulation of a CO_2 project include CO_2 breakthrough time and rate and composition of the produced fluids. These are required to design production facilities and CO_2 recycle strategies[54]. Modeling is also useful to optimize pattern size and CO_2/water injection rates in order to overcome the effects of reservoir heterogeneity.

Numerical simulation provides the only reliable means to predict chemical flood performance in a reservoir environment because the processes are so complex and so many reservoir parameters impact the results. Consequently, chemical flood simulation has been utilized to construct a screening algorithm for the selection of reservoirs suitable for micellar-polymer flooding[55] and to examine competing EOR strategies, e.g., CO_2 vs. surfactant flooding[56]. For caustic[57] and polymer[58] application, as well as for the micellar process, chemical flood modeling is useful to discern controlling process mechanisms and to identify laboratory data required for process description.

SOME EXAMPLES AND DISCUSSION

We illustrate here the grid orientation effect for a pattern steamflood. Table 1 shows a 3-acre nine-spot pattern with the diagonal grid and 45°-shifted parallel grid[9]. This pattern has three types of wells labeled 1 (injector), 2 (near producer) and 3 (far producer).

The isotropic homogeneous formation has a permeability of 4000 md, a porosity of .36, a thickness of 20 feet and a rock specific heat of 35 Btu/cu.ft. rock-°F.* Oil viscosity is 6750 cp at initial reservoir temperature and 45 cp at 500°F. Initial pressure is 200 psia, initial saturations are S_{wi} = .19, S_{oi} = .81, and irreducible water saturation is .17.

Specified rate for each injection well is 1000 BPD (barrels per day, cold water equivalent) of 80% quality steam at 800 psia, 517°F. All production wells are produced on deliverability against a constant bottomhole wellbore pressure of 200 psia.

The calculated results listed in Table 1 show a pronounced effect of grid orientation on steam breakthrough times using the 5-point difference scheme.

* A complete set of input data for this problem is available from the author upon request.

We obviously expect that steam should arrive at the near producer 2 before it reaches the far producer 3. The parallel grid with the 5-point scheme actually gave breakthrough at far well 3 at 117 days, before breakthrough at near well 2 (204 days).

Table 1 shows that the 9-point difference scheme virtually eliminates the effect of grid orientation for this problem. Figure 1 shows calculated steam front shapes at 80 days for the two different schemes using parallel and diagonal grids. The difference between the 9-point fronts for the two grids is small and about equal to the error of manual interpolation.

Recent compositional models[59,24] utilize an equation-of-state as opposed to separate correlations for oil density, gas density and equilibrium K-values. These papers emphasize that the equation-of-state (EOS) offers the advantage of consistency in that phase densities and K-values are obtained from a single source. This consistency results in smooth and differentiable convergence of separate phase densities and compositions to identical values as computations approach a critical point. Phase viscosities based on a correlation[60] using EOS densities also smoothly converge to a single value at a critical point.

The equations-of-state most widely used in reservoir calculations today are the Redlich-Kwong[61-63] and Peng-Robinson[64] equations. Martin[65] shows that all cubic equations-of-state can be obtained from a single, general EOS form. Yarborough[66] describes applications of a modified Redlich-Kwong EOS to reservoir fluids; Katz et al[67] gives applications of the Peng-Robinson EOS.

In our compositional work at Intercomp, we have found that nonlinear regression on EOR parameters is necessary. Frequently, prohibitive time requirements result from trial and error efforts to match laboratory test data; and we generally have found some adjustment of EOS parameters is necessary to match laboratory PVT data.

Table 2 compares EOS calculated results with laboratory PVT data reported by Simon et al[68] for mixtures of CO_2 and a SACROC oil sample at 130°F. Simon et al presented the crude oil sample analysis through C_{13}^+. We performed regressions, using all the data listed, with 14 components (C_1-C_{13}^+, CO_2) and with 5 components after pseudoizing (lumping components) the crude to 4 components. The calculated results shown correspond to use of the 4 pseudo components. These results used a modified Redlich-Kwong EOS[62], but very similar results were obtained using the Peng-Robinson EOS. Baker and Luks[69] calculated an equally good saturation pressure match of these data using 39 components, without regression, using a modified Redlich-Kwong EOS.

The "predicted" values listed in Table 2 were calculated with no regression using 14 components in the Peng-Robinson EOS. We used binary interaction coefficients given by Katz et al[57],

except CO_2-hydrocarbon values were .10 and the C_1-C_{13}^+binary was adjusted to .1298 to match the crude bubble point pressure of 1660 psia. Without the latter adjustment, the Peng-Robinson EOS calculated a bubble point presure of 1469 psia. All the predicted saturation pressures are bubble points while the last three observed and last two calculated (with regression) pressures are dew points.

Our compositional simulation of CO_2 injection, using the above discussed EOS match, indicated completely immiscible displacement at all pressures. The simulations showed an effect of pronounced vaporization of light and intermediate oil components into the CO_2, increasing with increasing flood pressure level. Dicharry et al[70] discuss design-stage tests indicating multiple-contact miscibility for CO_2 injection at pressures as low as 1800 psia for the SACROC unit. Kane[71] reports subsequent work indicating higher pressures necessary for miscibility[72].

Simulation is frequently employed to study the question of rate sensitivity. We define "rate sensitivity" as an adverse relationship between ultimate oil recovery and production or reservoir voidage rate. Reference 72 describes a simulation study of rate sensitivity in a number of different types of reservoirs in Alberta, Canada. This study was restricted to pressure-maintained, water-oil displacements and included coning and two- and three-dimensional calculations in formations ranging from moderate to severe heterogeneity.

The conclusion of that rather lengthy reference is very simple and brief:

Water-oil displacements

1. are rate-sensitive if an economic limit of maximum water cut is used
2. are not rate-sensitive if an economic limit of a minimum oil rate is used.

Thus, the existence of rate-sensitivity in any particular case depends upon the relative weights given to those two economic limits in the actual economic limit definition adopted.

Figures 2, 3, and 4, extracted from Reference 72, illustrate the above conclusion. If one selects a fixed oil rate as an economic limit and reads across the figure, he finds ultimate oil recovery higher at a higher rate. If one selects a fixed water-oil ratio as the limit and reads across the figure, he finds ultimate recovery lower at the higher rate.

We discuss here several aspects of simulator initialization, three-phase relative permeability and pseudo relative permeability and capillary pressure. Some of these aspects are not discussed in the literature, but are important in coding and understanding the simulators.

Rock relative permeability and capillary pressure curves as determined by laboratory tests are illustrated in Table 3. The water-oil table represents quantities measured with no free gas in the core. The first water saturation is connate water saturation, S_{wc} = .2. Water-oil capillary pressure P_{cwo} decreases with increasing water saturation. Irreducible water saturation is S_{wir} = .22. Residual oil to water displacement is S_{orw} = .3 and water relative permeability at residual oil is k_{rwro} = .45. Oil relative permeability at connate water, k_{rocw} = .8.

The gas-oil table gives capillary pressure and relative permeabilities measured in a core with connate (immobile) water present. Gas-oil capillary pressure P_{cgo} increases with increasing gas saturation. Residual oil saturation to gas, S_{org} = .1 (.3-.2) and critical gas saturation is S_{gc} = .05. The use of .2 as the first liquid saturation defining gas-oil capillary pressure implies that initial oil saturations should be zero in the gas cap above the top of the gas-oil transition zone. If a residual of .1 were desired in the gas cap, the first saturation entry in the gas-oil table would be .3 rather than .2.

Initialization of fluid pressure and saturation distributions in simulators is performed using capillary-gravitational equilibrium. It is necessary and sufficient to specify values for

1. p_i = initial oil pressure, psia, at Z_i
2. Z_i = reference depth, feet
3. Z_g = depth to initial gas-oil contact
4. Z_w = depth to initial water-oil contact
5. P_{cw} = P_{cwo} at Z_w
6. P_{cg} = P_{cgo} at Z_g

Fluid densities or specific weights will vary somewhat with depth due to pressure variation with depth. For brevity, we will ignore this variation and the additional logic required to treat the case of variable oil bubble point or type with depth. The Z values are subsea depth, measured positively downward.

Thus, the constant fluid densities are calculated as γ_w, γ_o, γ_g (psi/ft.) at pressure p_i. If a gas-oil contact exists, Z_i is normally taken equal to Z_g. Gravitational equilibrium gives the three phase pressures as functions of depth as

$$P_o = p_i + \gamma_o (Z - Z_i) \quad (1a)$$

$$P_w = p_i + \gamma_o (Z_w - Z_i) - P_{cw} + \gamma_w (Z - Z_w) \quad (1b)$$

$$P_g = p_i + \gamma_o (Z_g - Z_i) + P_{cg} + \gamma_g (Z - Z_g) \quad (1c)$$

Using these equations and the definitions $P_{cwo} = P_o - P_w$ and $P_{cgo} = P_g - P_o$, we can then easily calculate P_{cwo} and P_{cgo} as single-valued functions of depth Z.

The pressures at any grid block of depth Z (usually the depth to grid block center) are then obtained from Equation (1). Water and gas saturations are obtained by using the P_{cwo} and P_{cgo} values with interpolation in the water-oil and gas-oil tables. Oil saturation is $1 - S_w - S_g$.

Several "end-point" conditions are encountered in the initialization just described. These end-point conditions are summarized in Table 4. The S_{or} value in Table 4 is $S_{L1} - S_{wc}$, i.e. the difference between the first saturation entries of the gas-oil and water-oil tables. In this case, S_{or} is 0, but if we started the gas-oil table with $S_{L1} = .3$, then S_{or} would be .1.

Case 6 in Table 4 is similar to Case 3 in that the grid block P_{cwo} and P_{cgo} values both lie within their respective tabular ranges. However, in some problems, depending upon a number of factors, Case 3 gives S_w and S_g values which sum to a value exceeding 1.0, giving a negative oil saturation.

In this Case 6 we must simultaneously interpolate in both tables of Table 3, using p_g and p_w from Equations (1) to calculate $P_{cgw} = p_g - p_w$ for the grid block. The simulator code must then find an S_w value between S_{wc} and 1.0, such that $P^*_{cwo}(S_w)$ (from the water-oil table) + P^*_{cgo} from the gas-oil table at $S_g = 1 - S_w - S_{or}$ sum to P_{cgw}. We place an * on the capillary pressure values to denote the fact that they are not the grid block values calculated from differences of pressures from Equations (1). The oil pressure in Case 6 is then either $p_w + P^*_{cwo}$ or $p_g - P^*_{cgo}$, the two values being identical.

It is important that pressures of absent or immobile phases be calculated as indicated in Table 4. The principle used, necessary for correctly determining phase flow potential direction in simulator calculations, is that absent phases must have pressures they would have if an infinitesimal "drop" of the absent phase were added.

Coats et al[73,74] discuss the concept of pseudo capillary pressure curves which should be used in place of rock or laboratory curves to correctly initialize fluid saturation distributions. The pseudo curve definition[73] is fairly straightforward if the grid blocks representing the reservoir are viewed as a set of horizontal blocks at staggered depth values representing reservoir structure (dip). The definition becomes more complex as the grid blocks are viewed as inclined in both x- and y-directions. In practice, the pseudo capillary pressure definition is unimportant if the water-oil and gas-oil transition zone lengths significantly exceed grid block thickness (horizontal block case) or overall elevation difference (inclined block case).

In cases where rock and pseudo capillary pressure curves give significantly different initial fluid saturation distributions, the latter should be used irrespective of arguments regarding the existence of phase segregation or vertical equilibrium during dynamic reservoir depletion. Strictly speaking, if pseudo curves are not used, the initialized distributions will not reflect horizontal water-oil and gas-oil contacts. In addition, if the reservoir were shut in, the calculations would not yield (in time) equilibrium distributions corresponding to level contacts. In a sense, the pseudo capillary pressure curves give the background equilibrium condition from which dynamic viscous and gravity forces act in distorting contact shapes (overrides, underrunning).

Several authors, including Jacks et al[75], discuss the use of pseudo relative permeability curves obtained from comparing detailed cross-sectional results with results using fewer layers.

Water and gas relative permeabilities are treated as single-valued functions of water and gas saturations, respectively. Oil relative permeability generally is treated as a function of both water and gas saturations. Perhaps the most widely used method to represent k_{ro} is that given by Stone[76]. Stone gives

$$k_{ro} = (k_{rw} + k_{row})(k_{rog} + k_{rg}) - k_{rw} - k_{rg} \quad (2)$$

This implies that absolute permeability is defined as effective permeability to oil at connate water saturation and $k_{row} = 1.0$ at $S_w = S_{wc}$. Since 1974 we have used the slight modification

$$k_{ro} = k_{rocw}\left[\left(k_{rw} + \frac{k_{row}}{k_{rocw}}\right)\left(k_{rg} + \frac{k_{rog}}{k_{rocw}}\right) - k_{rw} - k_{rg}\right] \quad (3)$$

If absolute permeability is defined as permeability to oil (or water) at 100% saturation and k_{rocw} were (say) .7, then at $S_w = S_{wc}$, $S_g = 0$, Equation (2) gives $k_{ro} = .49$ while Equation (3) correctly gives $k_{ro} = .7$.

Two constraints in using Equation (3) should be mentioned, since they can affect simulator stability or results in some cases. First, in thermal problems, water saturation can decrease below S_{wc} and even disappear. For $S_w < S_{wc}$, the ratio k_{row}/k_{rocw} in Equation (3) should be retained at a value of 1.0. Inspection shows that if the ratio exceeds 1.0, then k_{ro} will be positive for all values of S_o, even for $S_o = 0$.

Second, Equation (3) can give positive k_{ro} values for mobile water and gas saturations which sum to 1.0, i.e. again, k_{ro} is positive for $S_o = 0$. Premultiplication of Equation (3) by a function $f(S_o)$ which is 1.0 for all but small oil saturations and 0 for $S_o = 0$ aids stability and physical consistency requirements in this case.

THE FUTURE OF SIMULATION

Within one to two years, we will be using strongly vectorized black oil, and perhaps compositional, models on very hi-speed, large capacity machines. In the overall picture, the

computing cost savings on small studies will be offset by a trend toward larger studies, i.e., use of more grid blocks or reservoir definition.

Research underway now will continue toward the goal of a single, general simulator capable of simulating all or most recovery processes of interest. Reference 15 is an example of a small step in that direction. Success of this research will depend in part upon improved understanding and extension of equations-of-state to represent the PVT behavior of multicomponent fluid systems in three or more phases over wide ranges of pressure and temperature.

Until or unless the above goal is reached, we will witness a continued development and increasing application of a variety of types of simulation models for different processes.

SUMMARY

A reservoir simulation model is a set of partial, finite-difference material balance equations. For each grid block one equation is written for each component or substance comprising the reservoir fluid description.

The model is described here in terms of the formulations and equation-solving methods used. Current models generally employ an IMPES formulation with options of increased stability provided by a sequential solution for saturations. Block successive overrelaxation and the strongly implicit procedure or its extension are the most popular iterative methods for solving the model equations. Reduced-band-width direct solution is widely used for moderate or small-size reservoir studies.

Examples of recent significant advances include 1) a nine-point difference formulation which reduces grid-orientation effects, 2) equation-of-state usage which promises improvements in compositional simulation and might aid development of a generalized simulator and 3) increased computer speeds, storage capacities and vectorization capabilities which contribute to the feasibility of larger, more detailed field studies.

Current research may lead away from the present proliferation of models of different processes toward a single, generalized model applicable to all or most recovery processes of interest.

ACKNOWLEDGEMENT

I appreciate Dr. G. W. Paul's provision of information relating to chemical flooding and its simulation.

REFERENCES

1. Odeh, A.S., "Reservoir Simulation - What is it?", J. Pet. Tech. (Nov., 1969), 1383-1388.

2. Muskat, M., The Flow of Homogeneous Fluids Through Porous Media, J. W. Edwards, Inc., Ann Arbor, Michigan, 1946.

3. Muskat, M., Physical Principles of Oil Production, McGraw-Hill Book Company, Inc., New York, 1949.

4. Muskat, M., "The Production Histories of Producing Gas-Drive Reservoirs," J. of Applied Physics, (1945), 16, 147.

5. Katz, D.L., "Methods of Estimating Oil and Gas Reserves", Trans AIME, (1936) 118, 18.

6. Buckley, S.E. and Leverett, M.C., "Mechanism of Fluid Displacement in Sands", Trans, AIME (1942), 146, 107-117.

7. Welge, H.J., "A Simplified Method for Computing Oil Recoveries by Gas or Water Drive", Trans. AIME. (1952) 195, 91.

8. Young, L.C., "A Finite-Element Method for Reservoir Simulation", Soc. Pet. Eng. J. (Feb., 1981), 115-128.

9. Todd, M.R., O'Dell, P.M. and Hirasaki, G.J.: "Methods for Increased Accuracy in Numerical Reservoir Simulators," Soc. Pet. Eng. Jour. (Dec., 1972) 515.

10. Coats, K.H., George, W.D., Chu, Chieh, and Marcum, B.E.: "Three-Dimensional Simulation of Steamflooding," Soc. Pet. Eng. J. (Dec. 1974) 573-592; Trans., AIME (1974) 257.

11. Yanosik, J.L., and T.A. McCracken, "A Nine-Point, Finite-Difference Reservoir Simulator for Realistic Prediction of Adverse Mobility Ratio Displacements", Soc. Pet. Eng. J. (Aug., 1979), 253-262.

12. Sheldon, J.W., Harris, C.D. and Bavly, D.: "A Method for General Reservoir Behavior Simulation on Digital Computers," SPE 1521-G, paper presented at 35th Annual Fall Meeting of SPE, Denver, October 2-5, 1960.

13. Stone, H.L. and Garder, A.O., Jr.: "Analysis of Gas-Cap or Dissolved-Gas Drive Reservoirs," Trans. AIME (1961) 222, 92.

14. Fagin, R.G. and Stewart, C.H. Jr.: "A New Approach to the Two-Dimensional Multiphase Reservoir Simulator," Trans. AIME (1966) 237, 175.

15. Coats, K.H., "Reservoir Simulation: A General Model Formulation and Associated Physical/Numerical Sources of Instability", Boundary and Interior Layers - Computational and Asymptotic Methods ed. by J.J. H. Miller, Boole Press, Dublin, 1980, 62-76.

16. MacDonald, R.C. and Coats, K.H.: "Methods for Numerical Simulation of Water and Gas Coning," Soc. Pet. Eng. J. (Dec. 1970) 425-436; Trans., AIME, Vol. 249.

17. Spillette, A. G., Hillestad, J.G., and Stone, H.L.: "A High-Stability Sequential-Solution Approach to Reservoir Simulation," paper SPE 4542 presented at the SPE-AIME 48th Annual Fall Meeting, Las Vegas, Sept. 30-Oct. 3, 1973.

18. Blair, P.M. and Weinaug, C.F.: "Solution of Two-Phase Flow Problems Using Implicit Difference Equations," Soc. Pet. Eng. J. (Dec. 1969) 417-424; Trans., AIME, Vol. 246.

19. Letkeman, J.P. and Ridings, R.L.: "A Numerical Coning Model," Soc. Pet. Eng. J. (Dec. 1970) 418-424; Trans, AIME, 249.

20. Coats, K.H., "Geothermal Reservoir Modelling", SPE Paper 6892 presented at the 52nd Annual Fall Technical Conference of the Society of Petroleum Engineers of AIME, Denver, Colorado, Oct. 9-12, 1977.

21. Coats, K.H.: "A Highly Implicit Steamflood Model," Soc. Pet. Eng. J. (Oct. 1978) 369-383.

22. Bansal, P.P., Harper, J.L., McDonald, A.E., Moreland, E.E., and Odeh, A.S. and R.H. Trimble, "A Strongly Coupled, Fully Implicit, Three Dimensional, Three Phase Reservoir Simulator", SPE Paper 8329 presented at the 54th Annual Fall Technical Conference of the Society of Petroleum Engineers of AIME, Las Vegas, Nevada, Sept. 23-26, 1979.

23. Patton, J.T. and K.H. Coats, "A Parametric Study of the CO_2 HUf-n-Puf Process", SPE Paper 9228 presented at the 54th Annual Fall Technical Conference of the Society of Petroleum Engineers of AIME, Las Vegas, Nevada, Sept. 23-26, 1979.

24. Coats, K.H., "An Equation-of-State Compositional Model", Soc. Pet. Eng. J., (Oct., 1980), 363-376.

25. Coats, K.H., "In-Situ Combustion Model", Soc. Pet. Eng. J., (Dec. 1980), 533-553.

26. Trimble, R.H. and McDonald, A.E.: "Strongly Coupled, Implicit Well Coning Model," Soc. Pet. Eng. J., (Aug. 1981), 454-458.

27. Peaceman, D.W. and Rachford, H.H. Jr.: "The Numerical Solution of Parabolic and Elliptic Differential Equations", J. Soc. Indust. Appl. Math., vol. 3, pp. 28-41, 1955.

28. J. Douglas, Jr. and H. H. Rachford,Jr., "On the Numerical Solution of Heat Conduction Problems in Two and Three Space Variable", Trans. Amer. Math. Soc., vol. 82, pp. 421-439, 1956.

29. Young, D., "The Numerical Solution of Elliptic and Parabolic Partial Differential Equations", Survey of Numerical Analysis, ed. by John Todd, McGraw-Hill Book Co., Inc., New York, 1962, pp. 380-438.

30. Weinstein, H.G., Stone, H.L. and T.V. Kwan, "Interactive Procedure for Solution of Systems of Parabolic and Elliptic Equations in Three Dimensions", I & EC Fundamentals, Vol. 8, No. 2, May 1969, 281-287.

31. Price, H.S. and Coats, K.H.: "Direct Methods in Reservoir Simulation," Soc. Pet. Eng. J. (June 1974) 295-308; Trans. AIME, 257.

32. Dupont, T., Kendal, R.P. and H.H. Rachford, "An Approximate Factorization Procedure for Solving Self-Adjoint Elliptic Difference Equations," J. Numer. Anal., SIAM (1968) Vol. 5, No. 3, 559-573.

33. Letkman, J.P., "Semi-Direct Iterative Methods in Numerical Reservoir Simulation" SPE 5730, 4th Numerical Simulation Symposium, L.A., Calif. 1976.

34. Watts, J.W., "A Conjugate Gradient-Truncated Direct Method for the Iterative Solution of the Reservoir Simulation Pressure Equation", Soc. Pet. Eng. J., (June, 1981), 345-353.

35. Mrosovsky, I., Wong, J.Y. and H.W. Lampe, "Construction of a Large Field Simulator on a Vector Computer", J. Pet. Tech., (Dec. 1980), 2253-2264.

36. Weinstein, H.G., Wheeler, J.A. and E.G. Woods, "Numerical Model for Thermal Process", Soc. Pet. Eng. J., (Feb., 1977) 65-78.

37. Crookston, H.B., Culham, W.E., and Chen, W.H.: "Numerical Simulation Model for Thermal Recovery Processes," Soc. Pet. Eng. J. (Feb. 1979) 37-58; Trans., AIME, 267.

38. Youngren, G.K.: "Development and Application of an In-Situ Combustion Reservoir Simulator," Soc. Pet. Eng. J. (Feb. 1980) 39-51.

39. Meijerink, J.A., "A New Stabilized Method for Use in IMPES type Numerical Reservoir Simulators", SPE 5247, 49th Annual Fall Meeting of SPE, Houston, Tx. Oct. 6-9, 1974.

40. Nolen, J.S., Kuba, D.W., and M.J. Kasic, Jr., "Application of Vector Processors to Solve Finite Difference Equations", Soc. Pet. Eng. J., (Aug., 1981), 447-453.

41. Garthhoffner, E.H., "The Role of Oil-in-Water Emulsions in Thermal Oil Recovery Processes", SPE Paper 7952 presented at the 1979 California Regional Meeting of the Society of Petroleum Engineers of AIME, Ventura, California, April 18-20, 1979.

42. Holm, L.W., "Status of CO_2 and Hydrocarbon Miscible Oil Recovery Methods", J. Pet. Tech., (Jan. 1976) 76-84.

43. Gogarty, W.B.: "Status of Surfactant or Micellar Methods," J. Pet. Tech. (January, 1976), 93-102.

44. Johnson, C.E. Jr.: "Status of Caustic and Emulsion Floods," J. Pet. Tech. (January, 1976), 85-92.

45. Stagge, H.M. and E.F. Herbeck, "Reservior Simulation Models - An Engineering Overview", J. Pet. Tech., (Dec., 1971), 1428-1436.

46. Coats, K.H., "Use and Misuse of Reservoir Simulation Models", J. Pet. Tech. (Nov. 1969), 1391-1398.

47. McCulloch, R.C., Langton, J.R. and A. Spivak, "Simulation of High Relief Reservoirs; Rainbow Field, Alberta, Canada", J. Pet. Tech. (Nov. 1969), 1399-1408.

48. Numerical Simulation, SPE Reprint Series No. 11, Committee Chairman R. A. Morse, Society of Petroleum Engineers, Dallas, Texas, 1973.

49. Herrera, J.Q. and E.J. Hanzlik, "Steam Stimulation History Match of Multi-Well Pattern in the S1-B Zone, Cat Canyon Field", SPE Paper 7969 presented at the 1979 California Regional SPE Meeting, Ventura, California, April 18-20, 1979.

50. Williams, R.L. "Steamflood Pilot Design for a Massive, Steeply Dipping Reservoir", SPE Paper 10321 presented at the 56th Annual Fall Technical Conference of SPE in San Antonio, Texas, October 5-7, 1981.

51. Meldau, R.F., "Gas-Steam Injection in Heavy Oil Wells", SPE Paper 8911 presented at the 50th Annual California Regional Meeting of SPE, Los Angeles, Calif., April 9-11, 1980.

52. Graue, D.J. and Zana, E.T.: "Study of a Possible CO_2 Flood in Rangely Field", J. Pet. Tech. (July, 1981), 1312-1318.

53. Todd, M.R., Cobb, M. and E.D. McCarter, "CO_2 Flood Performance Evaluation for the Cornell Unit, Wasson San Andres Field", SPE Paper 10292 presented at the 56th Annual Fall Technical Conference of SPE, San Antonio, Texas, October 5-7, 1981.

54. Bloomquist, C.W., Fuller, K.L. and Moranville, M.B.: "Miscible Gas Enhanced Oil Recovery and The Effects of the Windfall Profit Tax", SPE 10274, presented at 56th Annual Fall SPE Meeting, San Antonio, Texas, October 5-7, 1981.

55. "Selection of Reservoir's Amenable to Micellar Flooding", First Annual Report, DOE/BC/00048-20, December, 1980.

56. Fayers, F.J., Hawes, R.I., and Mathews, J.D.: "Some Aspects of Potential Application of Surfactants or CO_2 as EOR Processes in North Sea Reservoirs", J. Pet. Tech. (September, 1981), 1617-1627.

57. deZabala, E.F., Vislocky, E.R., and Radke, C.J.: "A Chemical Theory for Linear Alkaline Flooding," SPE 8997, presented at the SPE Fifth International Symposium on Oilfield and Geothermal Chemistry, Stanford, California, May 28-30, 1980.

58. Patton, J.T., Coats, K.H., and Colegrove, G.T.: "Predition of Polymer Flood Performance.": SPE 2546, presented at the 44th Annual Fall SPE Meeting, Denver, Colorado, September 28-October 1, 1969.

59. Fussell, L.T. and Fussell, D.D.: "An Iterative Technique for Compositional Reservoir Models," Soc. Pet. Eng. J. (Aug. 1979) 211-220.

60. Lohrenz, J., Bray, B.G., and Clark, C.R.: "Calculating Viscosity of Reservoir Fluids From Their Composition," J. Pet. Tech. (Oct. 1964) 1171-1176; Trans., AIME, 231.

61. Redlich O.; Kwong, J.N.S. "On the Thermodynamics of Solutions. V. An Equation of State. Fugacities of Gaseous Solutions," Chem. Review. 1949, 44, 233.

62. Zudkevitch, David and Joffe, Joseph: "Correlation and Prediction of Vapor-Liquid Equilibria with the Redlich-Kwong Equation of State," AIChE J. (Jan. 1970) 16, No. 1, 112-119.

63. Soave, G. Chem. Eng. Sci. 1972, 27. 1197.

64. Peng, D.-Y.; Robinson, D.B. "A New Two-Constant Equation of State," Ind. Eng. Chem. Fundam. 1976, 15, 59.

65. Martin, J.J., "Cubic Equations of State-Which?", I & E C Fundamentals, Vol. 18, p. 81, May 1979.

66. Yarborough, L.: "Application of a Generalized Equation of State to Petroleum Reservoir Fluids," paper presented at the Symposium of Equations of State in Engineering and Research, 176th ACS National Meeting, Miami Beach, FL, Sept. 10-15, 1978.

67. Katz, D.L. and A Firoozabadi, "Predicting Phase Behavior of Condensate/Crude-Oil Systems Using Methane Interaction Coefficients", J. Pet. Tech (Nov. 1978), 1649-1655.

68. Simon, R., Rosman, A., and Zana, E.: "Phase-Behavior Properties of CO_2-Reservoir Oil Systems," Soc. Pet. Eng. J. (Feb. 1978) 20-26.

69. Baker, L.E. and K.D. Luks, "Critical Point and Saturation Pressure Calculations for Multicomponent Systems", Soc. Pet. Eng. J., (Feb., 1980), 15-24.

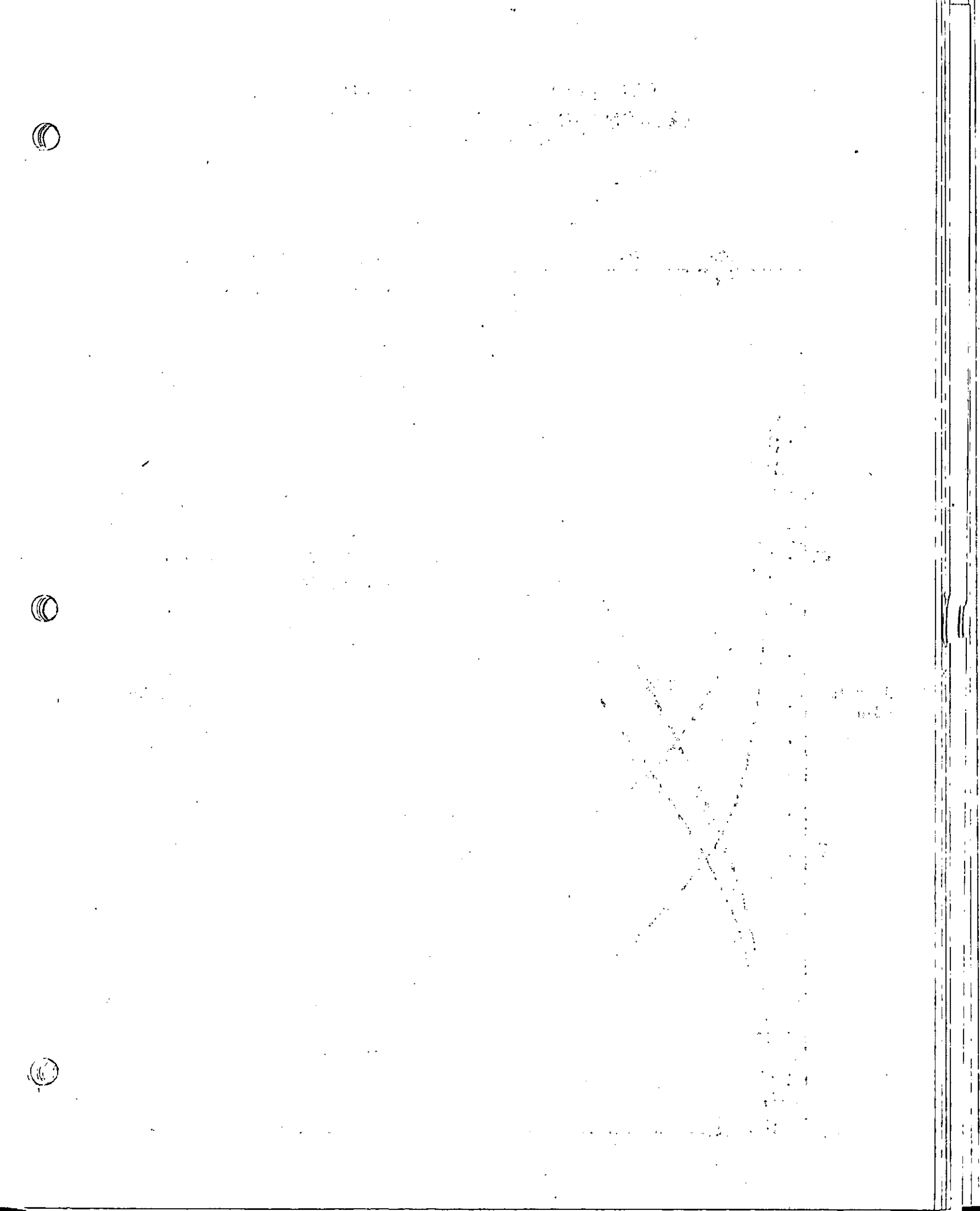

CURSO: "INGENIERIA DE YACIMIENTOS GEOTERMICOS "
13 DE MARZO AL 18 DE MAYO 1984

TEMA: "RESERVOIR MODELING"

DR. GUILLERMO DOMINGUEZ VARGAS
13 ABRIL 1984
MATERIAL COMPLEMENTARIO

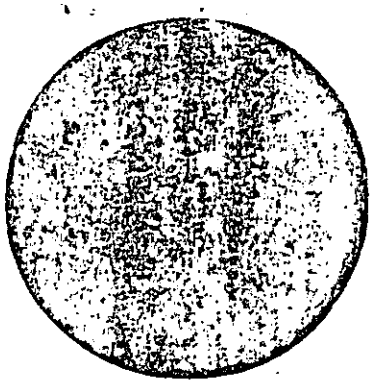
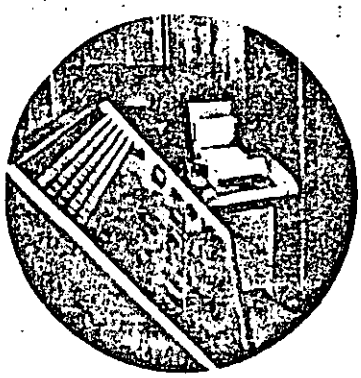
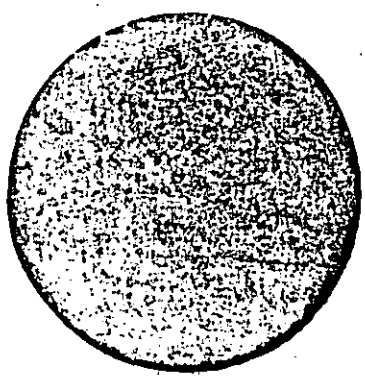
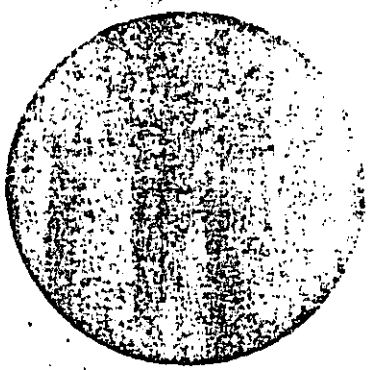

RESERVOIR MODELING

by Dr. H. K. van Poollen
H. C. Bixel
J. R. Jargon

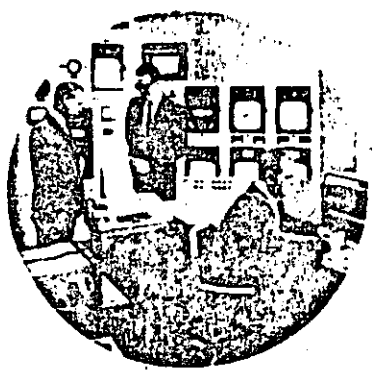
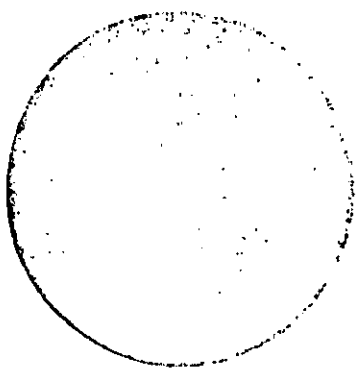

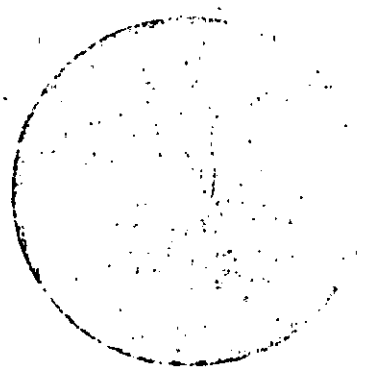
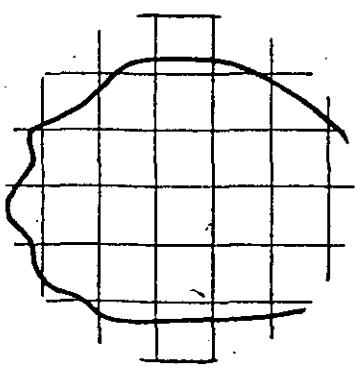


ABOUT THE AUTHORS

van Poollen

Bixel

Jargon

H. K. van Poollen is an adjunct professor at the Colorado School of Mines, Golden, Colo. Until July 1969, he was employed by Marathon Oil Co. as a Research Associate engaged in reservoir modeling. He holds a bachelors degree from the University of Delft, Holland, and master and doctors degrees from the Colorado School of Mines. During 1967-68 he was a distinguished lecturer for the SPE of AIME. He heads the newly formed consulting firm of H. K. van Poollen & Associates. He is a frequent contributor to The Oil and Gas Journal.

H. C. Bixel is an advanced engineer at the Marathon Oil Co. Research Center at Littleton, Colo. Before joining Marathon he was employed by the General Electric Co. at its Hanford Atomic Products plant. He received his BS degree in chemical engineering from the University of Colorado and his MS degree in chemical engineering from the University of Denver. He has worked on several enhanced recovery methods and has spent considerable time on transient pressure response of oil and gas wells. At present he is involved in the development of mathematical flow simulation for large digital computers.

J. R. Jargon is an engineer with Marathon Oil Co. at the Research Center in Littleton, Colo. He received his BS degree in chemical engineering from the University of Illinois in 1963 and his MS degree in chemical engineering from the University of Denver in 1967. He joined Marathon in 1963 and is presently working in the area of reservoir modeling. He has coauthored articles appearing in the Journal.

CONTENTS

Reservoir

NUMERICAL reservoir modeling is a new tool for studying reservoirs.

The various reservoir engineering functions may be explained by the diagram in Fig. 1. The objective of reservoir engineering is to estimate the recoverable reserves and to predict the rate of recovery.

To estimate recoverable reserves, one first has to estimate the total reserves, which may be accomplished by the use of geological information, core analyses, electric logs, etc. On the other hand, the reserve may be estimated by studying the pressure and volume behavior of the reservoir using various mathematical techniques which are indicated in the diagram by black box. Similiary, these techniques will help determine the mechanism to differentiate between depletion drive, gas-cap drive, water drive, etc.

By knowing the type of mechanism, one can arrive at the recovery factor applicable to the field. Applying this recovery factor to the estimated reserves renders the estimated recoverable reserves.

To predict the rate of recovery, one may make use of well tests or one may make use again of the black box to extrapolate future behavior of the field under various operating conditions.

Black box. The objective is to find a simulator that matches past performance. In turn, this simulator may be used to predict future performance.

Various simulation techniques have been available to the industry for many years. They differ in degree of sophistication and are used for different applications. Fig. 2 lists the number of possible techniques that have been used with various degrees of success.

Decline curves are plots of rate of withdrawal vs. time or cumulative withdrawal of a variety of coordinate scales. Usually a straight line is drawn through these observations and extrapolated to give ultimate recovery and

modeling: What it is, what it does

rates of recovery.

Decline curves only use rates of withdrawal and pay relatively little attention to reservoir or flowing pressures. A change in the mode of operation of the field could change the slope of the decline curve; hence, this is one of the weaknesses of this technique.

In material-balance studies, the pressure-volume behavior of the entire field is studied assuming an infinite permeability for the reservoir. By assuming an initial oil-in-place from volumetric calculations, the pressure is allowed to decline following fluid withdrawal.

This decline is matched against the observed pressure behavior and, if necessary, the original oil-in-place figure is modified until a match is obtained. In the presence of a water drive, additional variables are included by allowing water influx into the field. Water influx is governed by mathematical relationships known as response functions.

Another attempt to calculate the water influx into the reservoir during material-balance calculations has been by RC networks; the R standing for resistance and C standing for capacitance. This RC network simulates the flow of fluids through the aquifer under transient conditions; by changing values for both R and C, eventually a match between observed and calculated reservoir performance may be obtained.

Similarly, analog computers have been used to simulate the transient aquifer behavior.

For the purpose of displacement studies, various models and techniques have been used. They include mathematical front tracking. When employing unit mobility ratios, electrolitic models have been used. Similarly, Hele-Shaw models have been used to study displacement in the laboratory. The Buckley-Leverett relationships allow for varying mobility ratios due to saturation changes and relative permeability effects. Shortcuts have been offered for more complicated systems using the Higgins-Leighton models.

A newcomer in the field of modeling is numerical reservoir modeling—the subject of this series of articles.

What it is. In numerical reservoir modeling one first writes the fundamental fluid-flow equations in partial differential form for each of the phases present. These partial differential equations are obtained by writing the conventional equations such as the continuity equation, equation of flow, and the equation of state. These three are then combined into a single partial differential equation.

The continuity equation expresses the conservation of mass. For most fluid flow through porous media situation, the equation of flow is Darcy's law. For very high rates of flow and gas flow, modified Darcy law equations, including turbulence terms, can be used. The equation of state consists of a description of the pressure-volume or pressure-density relationship of the various fluids present. Next, the partial differential equation, possibly following combination, is written in finite differences form, both in space and time.

A finite differences grid is laid over the field as shown in Fig. 3. Each grid point or node is assigned a value for permeability, thickness, porosity, fluid content, elevation, and pressure.

Fig. 1

Reservoir engineering functions

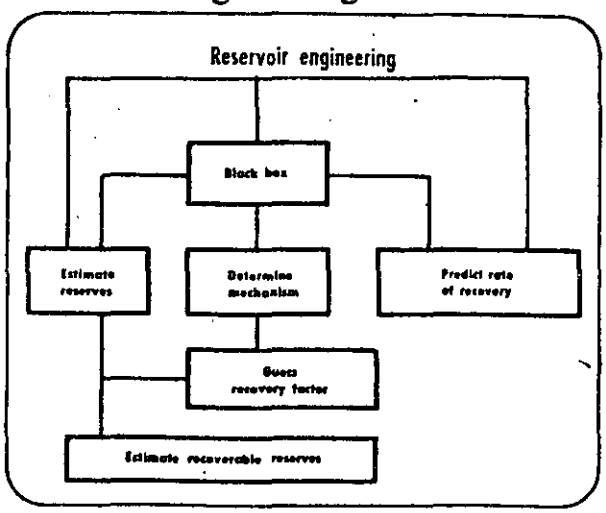

Fig. 2

What's in the black box

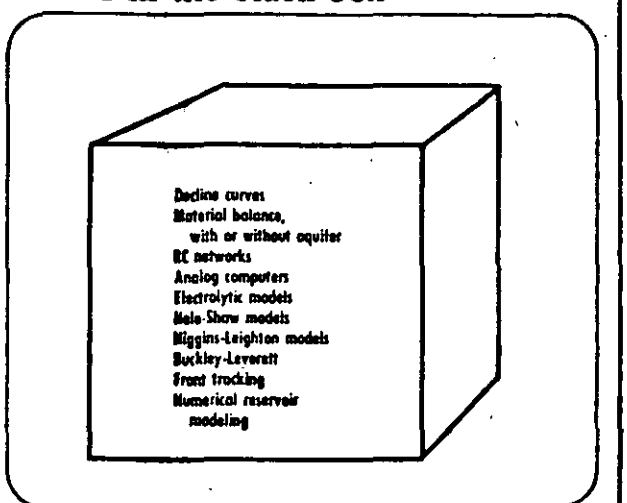

Fig. 3

Field's finite grid system

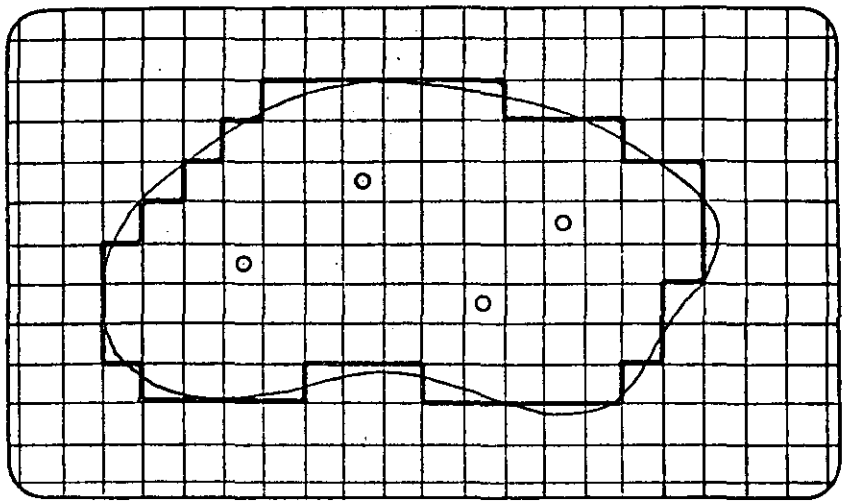

The fluids are assigned values for viscosity, formation volume factor, solution gas/oil ratio, and density. The rock is assigned a value of compressibility.

Rates for one of the produced fluid phases are assigned to the well. Then, for a finite time difference (time step), new pressures and rates for all producing phases are calculated. The rates for the wells are calculated from the saturations existing at each point in the grid system. This process is repeated for a number of time steps, and in this manner both rate and pressure histories are calculated for each well in the system.

INPUT DATA

For each node in the grid system, a value for each of the following is required:

- Permeability
- Porosity
- Thickness
- Elevation
- Grid dimensions
- Initial saturation for each phase
- Initial pressure
- Rock compressibility

Fluid characteristics are assigned by the following relationships:

- Oil formation volume factor vs. pressure
- Water formation volume factor vs. pressure
- Gas formation volume factor vs. pressure
- Oil viscosity vs. pressure
- Water viscosity vs. pressure
- Gas viscosity vs. pressure
- Solution gas/oil ratio vs. pressure
- Solution gas/water ratio vs. pressure
- Liquid/gas ratio vs. pressure
- Oil density
- Water density
- Gas density

The interaction of forces between rock and fluids is given by the following saturation dependent functions:

- Relative permeability for each phase
- Capillary pressure between oil and water
- Capillary pressure between gas and oil

Additional data may come from wells and include:

- Producing interval
- Oil-production rate vs. time
- Water-production rate vs. time
- Gas-production rate vs. time
- Observed pressures vs. time

Practical applications. Probably the best known application of numerical reservoir modeling is that of matching and prediction of oil-field behavior. In matching, one uses the best data available for all items listed in the previous paragraph. Then the wells are allowed to produce at the observed rate for one of the phases.

Next, pressure behavior for all wells and the production rate of the remaining phases are calculated. Calculated plots are compared with observed pressures and rates.

Comparison between these two will indicate the accuracy of the initial estimate of input data. It may be necessary to modify some of the input data until all observed and calculated data compare sufficiently favorably.

No hard and fast rules exist to indicate when a match is obtained. The number of runs before a satisfactory match depends on the complexity and length of history. In this manner, a rather sophisticated black box has been obtained, and it can be used to predict the future behavior of the field.

In prediction, one may set the production rates for all wells or for the entire field, or one may set a production rate to be maintained until the reservoir pressure falls below a certain point, whereafter water injection should take place somewhere else. Then, with these hypothetical rate schedules, performance of the field is studied.

In this manner, various exploitation schemes may be evaluated, economics may be applied to the results, and the optimum exploitation scheme may be selected.

A word of caution appears warranted. The black box was derived with a certain kind of history, for example, depletion at moderate rates. One should not expect any degree of accuracy if suddenly the mechanism is changed to that of water injection without any history to predict the behavior of that water injection. Similarly, if suddenly the field is produced at very high rates causing pressure to drop below the bubble point, when, during the match, the pressures were always above the bubble point, the predicted results should be viewed with caution. A general rule of thumb may be that one should not predict more than twice the period used for matching under similar modes of operation.

Although reservoir modeling was developed to study overall field performance and to predict that performance following matching, it has many other applications. Typical sections of fields can be analyzed, and by assigning the best known values to the section, its mechanism can be studied. Then, some of the parameters can be changed to learn what effect they may have on the overall mechanism. In turn, we may find what parameter needs most study to better understand the performance of the field.

Reservoir models may be used to study well problems such as pressure buildup and drawdown behavior, gas/oil ratio behavior, and water/oil ratio histories. It has application in studying the coning and fingering of water and gas into oil-producing wells.

Laboratory studies may include core floods and imbibition studies. Where the numerical fluid-flow simulators essentially solve the fundamental flow equations, they should find considerable application in the evaluation of laboratory studies.

Single-phase fluid-flow equations

IN STUDYING flow of any kind—heat flow, fluid flow, electrical flow—the mathematics are obtained by applying a conservation principle. A conservation principle simply states that some physical quantity is neither created nor destroyed.

Continuity equation. The continuity is the mathematical expression of the law of conservation of mass. It can be developed by considering the mass flow of fluid through a cubical element of space having dimensions Δx, Δy, Δz with its edges parallel to the x, y, z axes, Fig. 1. For this cube, one may write a mass balance in the form

$$(\text{mass in} - \text{mass out}) + \text{mass generation} = \text{mass accumulation} \quad (1)$$

At the x face of the cube, the fluid velocity and density are v_x and ρ_x respectively. At the $x + \Delta x$ face of the cube, the velocity and density are $V_{x+\Delta x}$ and $\rho_{x+\Delta x}$.

The fluid velocity and density at the y and z faces can be similarly defined as v_y, v_z, ρ_y, ρ_z, and at the $y + \Delta y$ and $z + \Delta z$ faces, the velocities and densities are $v_{y+\Delta y}$, $v_{z+\Delta z}$, $\rho_{y+\Delta y}$, and $\rho_{z+\Delta z}$.

Furthermore, let the amount of mass released be W expressed in mass per unit time per unit volume.

Figs. 1, 2, 3

Development of continuity equation

Fig. 1

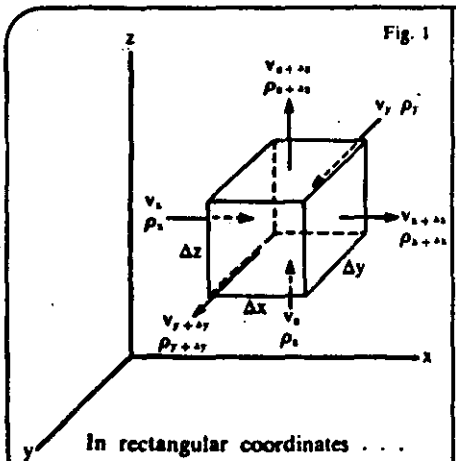

In rectangular coordinates . . .

Fig. 2

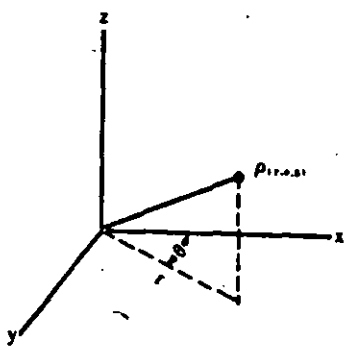

in cylindrical coordinates, and . . .

Fig. 3

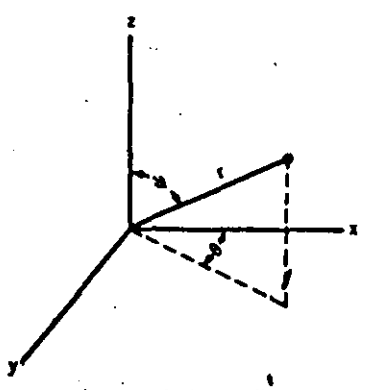

in spherical coordinates.

With these definitions, the conservation of mass can be stated from Equation 1. The amount of mass entering the element during a time interval, Δt, is

$$\rho_x v_x \Delta y \Delta z \Delta t + \rho_y v_y \Delta x \Delta z \Delta t + \rho_z v_z \Delta x \Delta y \Delta t.$$

The amount of mass leaving the element during this time is

$$\rho_{x+\Delta x} v_{x+\Delta x} \Delta y \Delta z \Delta t + \rho_{y+\Delta y} v_{y+\Delta y} \Delta x \Delta z \Delta t + \rho_{z+\Delta z} v_{z+\Delta z} \Delta x \Delta y \Delta t.$$

Also, during this time an amount of mass

$$W(x, y, z, t) \Delta x \Delta y \Delta z \Delta t$$

is released from the element.

The amount of excess of inflow over outflow and the release of mass from the element, accumulation of mass, is

$$(\phi_{x,y,z,t+\Delta t} \rho_{x,y,z,t+\Delta t} - \phi_{x,y,z,t} \rho_{x,y,z,t}) \Delta x \Delta y \Delta z \Delta t$$

where ϕ is the porosity.

Substituting these expressions into Equation 1, dividing through by $\Delta x \Delta y \Delta z \Delta t$, and taking the limits as Δx, Δy, Δz, and Δt are allowed to each approach zero gives

$$\frac{\partial}{\partial x}(\rho v_x) + \frac{\partial}{\partial y}(\rho v_y) + \frac{\partial}{\partial z}(\rho v_z) - W_{(x,y,z,t)} = -\frac{\partial}{\partial t}(\phi\rho) \qquad (2)$$

This is the equation of continuity in rectangular coordinates including a generation term.

It can also be derived in cylindrical and spherical coordinates. In these cases it would have the form[1]:

Cylindrical coordinates (r, θ, z)

$$\frac{1}{r}\frac{\partial}{\partial r}(\rho r v_r) + \frac{1}{r}\frac{\partial}{\partial \theta}(\rho v_\theta) + \frac{\partial}{\partial z}(\rho v_z) = -\frac{\partial}{\partial t}(\phi\rho)$$

Spherical coordinates (r, θ, ψ)

$$\frac{1}{r^2}\frac{\partial}{\partial r}(\rho r^2 v_r) + \frac{1}{r \sin\theta}\frac{\partial}{\partial \theta}(\rho v_\theta \sin\theta) + \frac{1}{r \sin\theta}\frac{\partial}{\partial \psi}(\rho v_\psi) = -\frac{\partial}{\partial t}(\phi\rho)$$

where θ and ψ are angular dimensions as shown in Figs. 2 and 3. The generation term is not included in these equations.

Equation 2 can be used to formulate differential equations which describe fluid movement within a porous body. To do this it is necessary to have a law of flow which can be used to evaluate the velocity terms in Equation 2 and an equation of state which describes the dependence of fluid density on pressure.

Darcy's law can be used to define the velocities as

$$v_x = -k/\mu \frac{d\Phi}{dx}$$

$$v_y = -k/\mu \frac{d\Phi}{dy}$$

and $$v_z = -k/\mu \frac{d\Phi}{dz}$$

where k is the permeability which may be different in three coordinate directions

μ is the fluid viscosity
Φ is the flow potential.

The flow potential may be expressed as

$$\Phi = p + \rho g h$$

where g is the acceleration due to gravity

p is the pressure
h is a vertical distance
ρ is the fluid density.

Since the x-y plane is horizontal, the only potential which will contain the gravitational term will be the one in the z direction. Therefore, the velocities may be defined as

$$v_x = -k/\mu \frac{dp}{dx}$$

$$v_y = -k/\mu \frac{dp}{dy}$$

$$v_z = -k/\mu \left(\frac{dp}{dz} + \rho g\right)$$

Substituting these expressions for velocity into Equation 2 gives

$$\frac{\partial}{\partial x}\left(\frac{\rho k}{\mu}\frac{\partial p}{\partial x}\right) + \frac{\partial}{\partial y}\left(\frac{\rho k}{\mu}\frac{\partial p}{\partial y}\right) + \frac{\partial}{\partial z}\left[\frac{\rho k}{\mu}\left(\frac{\partial p}{\partial z} + \rho g\right)\right] = \frac{\partial}{\partial t}(\phi\rho) \qquad (3)$$

This equation has two dependent variables, pressure and density. It is necessary to eliminate one of the variables to obtain a solution to the equation.

To do this we must have a relationship between density and pressure. Such a relationship is provided by an equation of state. The equation of state which is chosen will depend upon the type of fluid under consideration.

As a result, the differential equation resulting from the substitution of the equation of state into Equation 3 will have a different form depending upon the type of fluid flowing.

Here are some of the forms that may be derived:

Incompressible flow. The volume of an element of fluid is not a function of pressure for incompressible flow. Therefore, the fluid density does not change with position or time and Equation 3 can be written as

$$\frac{\partial}{\partial x}(k/\mu\, \partial p/\partial x) + \frac{\partial}{\partial y}(k/\mu\, \partial p/\partial y) + \frac{\partial}{\partial z}[k/\mu(\partial p/\partial z + \rho g)] = 0$$

where the porosity, ϕ, is assumed constant and the region contains no sources or sinks, $W_{(x,y,z,t)} = 0$. If the permeability and viscosity are assumed constant and since ρ and g are both constant, the equation reduces to La-Place's equation

$$\frac{\partial^2 p}{\partial x^2} + \frac{\partial^2 p}{\partial y^2} + \frac{\partial^2 p}{\partial z^2} = 0$$

Slightly compressible fluid. A slightly compressible liquid can be defined as one whose volume change with pressure is small. The compressibility, c, is defined for isothermal conditions by

$$c = -\frac{1}{V}\frac{dV}{dp}$$

where V denotes fluid volume. Since the mass of fluid does not change when the fluid is compressed, c can be expressed as

$$c = \frac{1}{\rho}\frac{d\rho}{dp}.$$

Assuming c to be independent of p, integration gives:

$$\rho = \rho_o e^{cp} \qquad (4)$$

where ρ_o is the fluid density at zero pressure. Taking the partial derivative of Equation 4 with distance, l, gives:

$$\frac{\partial \rho}{\partial l} = \rho_o c e^{cp}\frac{\partial p}{\partial l} = \rho c \frac{\partial p}{\partial l}$$

Solving for $\partial p/\partial l$ and substituting into Equation 3 gives

$$\frac{\partial}{\partial x}(k/\mu c\, \partial\rho/\partial x) + \frac{\partial}{\partial y}\left(\frac{k}{\mu c}\partial\rho/\partial y\right)$$

$$+ \frac{\partial}{\partial z}\left[\frac{k}{\mu c}(\partial\rho/\partial z + \rho g)\right] = \frac{\partial \phi\rho}{\partial t} \qquad (5)$$

Again we have chosen a region free of sources or sinks, $W_{(x,y,z,t)} = 0$.

Gravitational effects are negligible when considering single-phase flow. This assumption reduces Equation 5 to:

$$\frac{\partial}{\partial x}(k/\mu c \frac{\partial \rho}{\partial x}) + \frac{\partial \rho}{\partial y}(k/\mu c \frac{\partial \rho}{\partial y}) +$$

$$\frac{\partial}{\partial z}(k/\mu c \frac{\partial \rho}{\partial z}) = \frac{\partial \phi \rho}{\partial t} \qquad (6)$$

This equation has only one dependent variable, fluid density. However, it is more natural to have pressure as the dependent variable rather than fluid density.

Equation 4 may be represented by a series expansion as

$$\rho = \rho_o (1 + cp + \frac{(cp)^2}{2!} + \frac{(cp)^3}{3!} +$$

$$\ldots + \frac{(cp)^n}{n!})$$

Since the fluid compressibility is considered to be small, the first two terms of this expression give a good approximation to the fluid density at a given pressure or:

$$\rho = \rho_o (1 + cp)$$

Substituting this equation into Equation 6 gives

$$\frac{\partial}{\partial x}(k/\mu \frac{\partial p}{\partial x}) + \frac{\partial}{\partial y}(k/\mu \frac{\partial p}{\partial y}) +$$

$$\frac{\partial}{\partial z}(k/\mu \frac{\partial p}{\partial z}) = c\frac{\partial \phi p}{\partial t} \qquad (7)$$

If permeability, porosity, and viscosity are assumed constant, Equation 7 can be written as

$$\frac{\partial^2 p}{\partial x^2} + \frac{\partial^2 p}{\partial y^2} + \frac{\partial^2 p}{\partial z^2} = \frac{\phi c \mu}{k}\frac{\partial p}{\partial t} \qquad (8)$$

This equation has the same form as the Fourier equation of heat conduction.

Gas flow. The density of an ideal gas can be expressed as

$$\rho = \frac{M}{RT} p$$

where M is the molecular weight
R is the gas constant
T is the absolute temperature.

Substituting into Equation 3, neglecting the source term and assuming gravitation effects may be neglected, gives

$$\frac{\partial}{\partial x}(k/\mu \frac{\partial p^2}{\partial x}) + \frac{\partial}{\partial y}(k/\mu \frac{\partial p^2}{\partial y}) +$$

$$\frac{\partial}{\partial z}(k/\mu \frac{\partial p^2}{\partial z}) = \frac{1}{p}\frac{\partial \phi p^2}{\partial t}$$

If it is assumed that permeability, viscosity, and porosity are constant, this equation may be written as

$$\frac{\partial^2 p^2}{\partial x^2} + \frac{\partial^2 p^2}{\partial y^2} + \frac{\partial^2 p^2}{\partial z^2} = \frac{\phi \mu}{kp}\frac{\partial p^2}{\partial t} \qquad (9)$$

This equation is similar to Equation 8, although it is nonlinear due to the 1/p term on the right-hand side of the equation.

The density of a real gas may be expressed as

$$\rho = \frac{M}{RT}\frac{p}{Z}$$

where Z is the gas compressibility factor and is a function of pressure and temperature. Making this substitution into Equation 4 and assuming constant permeability, viscosity, and porosity, gives

$$\frac{\partial}{\partial x}\left(\frac{p}{Z}\frac{\partial p}{\partial x}\right) + \frac{\partial}{\partial y}\left(\frac{p}{Z}\frac{\partial p}{\partial y}\right) +$$

$$\frac{\partial}{\partial z}\left(\frac{p}{Z}\frac{\partial p}{\partial z}\right) = \frac{\phi \mu}{k}\frac{\partial (p/Z)}{\partial t}$$

This equation is also nonlinear; however, it will reduce to Equation 9 if Z is constant.

References

1. Bird, R. B., Stewart, W. E., and Lightfoot, E. N., Transport Phenomena, John Wiley & Sons, Inc., 1965.

Finite differences

ONLY A small number of the partial-differential equations which are generated by engineering problems can be solved by analytical means. More often than not, an analytical solution is beyond the power of present analytical methods.

When such a situation arises, the problem may generally be solved by finite-difference methods. Even in some cases where analytical solutions are available, the evaluation of infinite series or integrals may be more time consuming and complicated than the finite-difference solution of the partial-differential equation.

Finite-difference techniques can be used to solve extremely complicated problems. In the complex problems in reservoir fluid flow, the solution must be carried out on high-speed computers.

Errors involved. Two types of error are involved in solving partial-differential equations by the method of finite differences.

For square boundaries, the error will be mostly roundoff error. But an iterative type of solution can be carried to enough significant digits to keep this error small.

The second type is the truncation error resulting from replacing the partial-differential equation with the difference approximation.

Decreasing the spatial and time-increment size will usually decrease this error. Also, a higher order approximation to the partial derivatives can be used to decrease the truncation error.

For the situation where the boundary is curved and not square or rectangular, the mesh points will generally not coincide with the boundary. Errors will then arise in approximating the values of a function at the boundary.[1]

This situation seldom arises in reservoir modeling because the location of the boundaries of a reservoir are not known accurately enough to warrant approximating a curved boundary.

Approximating partial derivatives. The finite-difference approximation to a partial derivative can be arrived at by using a Taylor series expansion of a function around a point $x + h$ as follows:[1,2]

$$f(x+h) = f(x) + h\frac{\partial f}{\partial x} + \frac{h^2}{2!}\frac{\partial^2 f}{\partial x^2} \ldots \quad (1)$$

where h is the increment size.

We can now solve for the first derivative, $\frac{\partial f}{\partial x}$.

$$\frac{\partial f}{\partial x} = \frac{f(x+h) - f(x)}{h} - \frac{h}{2!}\frac{\partial^2 f}{\partial x^2} - \ldots \quad (2)$$

The term $\left(-\frac{h}{2!}\frac{\partial^2 f}{\partial x^2} - \ldots\right)$ is to be neglected and thus is the truncation error associated with this approximation. The error is then of the order of h.

The numerator of this finite-difference approximation is called a forward difference. Likewise, there are backward differences and central differences. These three differences can be defined by the use of operators as follows.

$$\Delta f(x) = f(x+h) - f(x) \quad \text{(forward difference)} \quad (3)$$

$$\nabla f(x) = f(x) - f(x-h) \quad \text{(backward difference)} \quad (4)$$

$$\delta f(x) = f\left(x+\frac{h}{2}\right) - f\left(x-\frac{h}{2}\right) \quad \text{(central difference)} \quad (5)$$

These difference operators are included for the sake of definition of these terms. Other difference operators are used in mathematical texts, but will not be defined here.

Getting back to finite-difference approximation of partial derivatives, more accurate approximations for the first derivative can be obtained by subtracting two Taylor's series.

$$f(x+h) = f(x) + h\frac{\partial f}{\partial x} + \frac{h^2}{2!}\frac{\partial^2 f}{\partial x^2} + \frac{h^3}{3!}\frac{\partial^3 f}{\partial x^3} + \ldots \quad (6)$$

$$f(x-h) = f(x) - h\frac{\partial f}{\partial x} + \frac{h^2}{2!}\frac{\partial^2 f}{\partial x^2} - \frac{h^3}{3!}\frac{\partial^3 f}{\partial x^3} + \ldots \quad (7)$$

Subtracting Equation 7 from Equation 6 gives

$$f(x+h) - f(x-h) = 2h\frac{\partial f}{\partial x} + \frac{2h^3}{3!}\frac{\partial^3 f}{\partial x^3} + \ldots \quad (8)$$

or

$$\frac{\partial f}{\partial x} = \frac{f(x+h) - f(x-h)}{2h} - \frac{h^2}{3!}\frac{\partial^3 f}{\partial x^3} + \ldots \quad (9)$$

The truncation error associated with this expression is of the order of h^2. Thus, for small h, the expansion shown in Equation 9 is more accurate than the expansion shown in Equation 2.

The second derivative can be obtained in the same way. Adding Equations 6 and 7 with the fourth derivative included in the expansion gives

$$f(x+h) + f(x-h) = 2f(x) + h^2 \frac{\partial^2 f}{\partial x^2} + \frac{2h^4}{4!} \frac{\partial^4 f}{\partial x^4} \ldots \quad (10)$$

or

$$\frac{\partial^2 f}{\partial x^2} = \frac{f(x+h) - 2f(x) + f(x-h)}{h^2} - \frac{2h^2}{4!} \frac{\partial^4 f}{\partial x^4} \quad (11)$$

The truncation error associated with this expansion is of the order of h^2.

All of these expansions are valid for a constant increment size h. For unequal increments, as shown in the drawing, the expansion proceeds as follows:

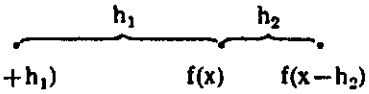

To obtain the second derivative using these three points, first assume that the second derivative will have the following form.

$$\frac{\partial^2 f}{\partial x^2} = A\, f(x+h_1) + B\, f(x) + C\, f(x-h_2) \quad (12)$$

where A, B, and C are constants. Now expand the functions $f(x+h_1)$ and $f(x-h_2)$ in a Taylor series.

$$f(x+h_1) = f(x) + h_1 \frac{\partial f}{\partial x} + \frac{h_1^2}{2!} \frac{\partial^2 f}{\partial x^2} + \ldots \quad (13)$$

$$f(x-h_2) = f(x) - h_2 \frac{\partial f}{\partial x} + \frac{h_2^2}{2!} \frac{\partial^2 f}{\partial x^2} + \ldots \quad (14)$$

Substituting Equations 13 and 14 into Equation 12 gives

$$\frac{\partial f^2}{\partial x^2} = (A+B+C) f(x) + (Ah_1 - Ch_2) \frac{\partial f}{\partial x} + \left(A \frac{h_1^2}{2!} + C \frac{h_2^2}{2!}\right) \frac{\partial^2 f}{\partial x^2} \quad (15)$$

A, B, and C can be determined by setting the coefficients which multiply like terms equal to zero.

$$A + B + C = 0$$
$$Ah_1 - Ch_2 = 0$$
$$Ah_1^2 + Ch_2^2 = 2$$

16/I/75

Solving these three equations for A, B, and C and substituting back into Equation 12 gives the following expansion for the second derivative over nonequal space increments.

$$\frac{\partial^2 f}{\partial x^2} = \frac{2\, f(x+h_1)}{h_1^2 + h_2 h_1} - \frac{2\, f(x)}{h_1 h_2} + \frac{2\, f(x-h_2)}{h_2 h_1 + h_2^2} \quad (16)$$

Mixed derivatives such as $\frac{\partial^2 f}{\partial x \partial t}$ can be approximated by expanding a Taylor series about f(x+h, t+k). This expansion is[2]

$$f(x+h, t+k) = f(x,t) + h \frac{\partial f}{\partial x} + k \frac{\partial f}{\partial t} + \frac{1}{2}\left(h^2 \frac{\partial^2 f}{\partial x^2} + 2hk \frac{\partial^2 f}{\partial x \partial t} + k^2 \frac{\partial^2 f}{\partial t^2}\right) + \ldots \quad (17)$$

If the terms $\frac{\partial f}{\partial x}$, $\frac{\partial f}{\partial t}$, $\frac{\partial^2 f}{\partial x^2}$, $\frac{\partial^2 f}{\partial t^2}$ are replaced by their finite-difference approximations, the following approximation can be obtained for the mixed derivative.

$$\frac{\partial^2 f}{\partial x \partial t} = [2f(x+h, t+k) - 3f(x+h, t) - 3f(x, t+k) + 2f(x, t) - f(x-h, t) - f(x, t-k)]/2hk \quad (18)$$

The diffusivity equation. The diffusivity equation can be used to describe the single-phase flow of slightly compressible fluids through a homogeneous porous medium. This equation, along with the appropriate boundary conditions, has been used to describe the transient behavior of production and injection wells. This equation is

$$\frac{\partial^2 p}{\partial x^2} = \frac{\phi \mu c}{k} \frac{\partial p}{\partial t} \quad (19)$$

Using Equations 2 and 11 and using subscripts in place of x, x+h, etc., Equation 19 becomes

$$\frac{p_{i+1,n} - 2p_{i,n} + p_{i-1,n}}{\Delta x^2} = \frac{\phi \mu c}{k} \frac{(p_{i,n+1} - p_{i,n})}{\Delta t} \quad (20)$$

where i refers to the space index and n refers to the time index.

It should be noted that the boundary conditions must be included before this equation can be solved.

This equation is called an explicit finite-difference equation. The pressure at point i,n+1 can be solved for explicitly in terms of all known values at time step n.

This explicit equation has severe stability limitations and is seldom used in practice. The pressure difference in time is a forward difference with truncation error of the order of Δt.

The pressure difference in space is a central difference applied twice with truncation error of the order of Δx^2.

If a backward pressure difference in time had been taken, the resulting equation would have been implicit. That is, a number of simultaneous equations corresponding to the number of space increments would have to be solved at each time level.

One may wonder why a more accurate approximation for the time derivative has not been used. If Equation 9 had been used to approximate the time derivative, the truncation error in time would be of the same order as that in space. This difference approximation for the parabolic equation (the diffusivity equation) always leads to unstable solutions.

References

1. Lapidus, L., "Digital computation for chemical engineers," Chap. 4, McGraw-Hill Book Co. Inc., New York, 1964.
2. Mickley, H. W., Sherwood, T. K., and Reed, C. E., "Applied mathematics in chemical engineering," pp. 351-352, 2nd edition, McGraw-Hill Book Co. Inc., New York, 1957.

Explicit finite-difference technique

MANY of the finite-difference techniques applied to fluid flow partial differential equations result in equations similar to those for heat flow, flow of electricity, and others.

This chapter shows examples of the more important explicit finite difference solution techniques. Some of these are especially applicable for single-phase flow problems or multiphase flow problems with relatively constant flow coefficients.

The reader should keep in mind that this section is written to acquaint the nonmathematician with these techniques.

The equations are not written in the more appropriate residual form, nor does the text give any indication of the relative merits of the methods.

Fig. 1

Typical block

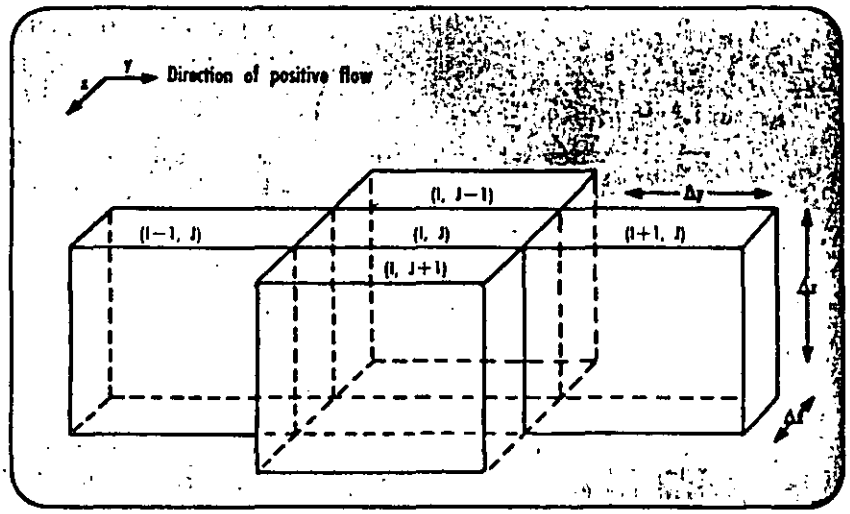

Fig. 2

Basic explicit

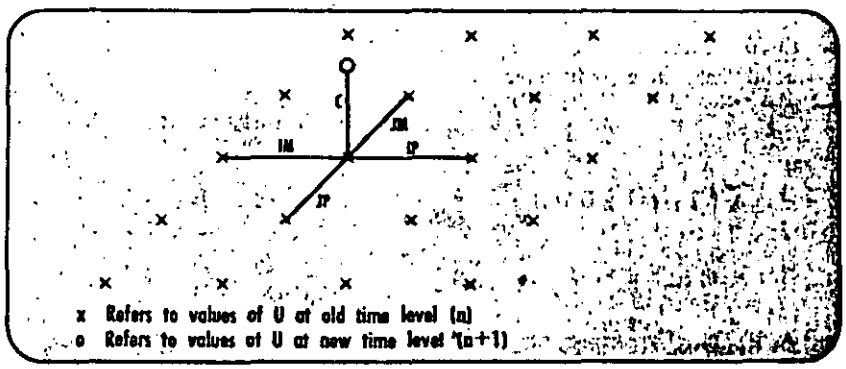

General form of equations

The diffusivity equation with nonconstant coefficients for two dimensions can be written as

$$\frac{\partial}{\partial x}\left(Kx\frac{\partial U}{\partial x}\right)+\frac{\partial}{\partial y}\left(Ky\frac{\partial U}{\partial y}\right)-Q=C\frac{\partial U}{\partial t} \qquad (1)$$

This equation can now be expanded in finite differences to yield

$$\frac{1}{\Delta x_J}\left(Kx_{I,J+1/2}\frac{(U_{I,J+1}-U_{I,J})}{\Delta x_{J+1/2}}-Kx_{I,J-1/2}\frac{(U_{I,J}-U_{I,J-1})}{\Delta x_{J-1/2}}\right)$$

$$+\frac{1}{\Delta y_I}\left(Ky_{I+1/2,J}\frac{(U_{I+1,J}-U_{I,J})}{\Delta y_{I+1/2}}-Ky_{I-1/2,J}\frac{(U_{I,J}-U_{I-1,J})}{\Delta y_{I-1/2}}\right)$$

$$-Q_{I,J}=C_{I,J}\frac{(U_{I,J,n+1}-U_{I,J,n})}{\Delta t} \qquad (2)$$

Fig. 1 shows a diagram of a typical block in this system. The subscript n on the right-hand side of Equation 2 refers to the time-step level. This subscript has temporarily been omitted from the left-hand side of the equation, but will be added when the specific explicit techniques are discussed.

Note that if the coefficients are constant and the grid spacing is constant this equation will reduce to the same equation shown in the previous installment with the exception that the present finite-difference equation is in two dimensions.

Simplifying the nomenclature in Equation 2 further, we obtain

$$JP \cdot U_{I,J+1} + IP \cdot U_{I+1,J} - (JP+IP+JM+IM)\, U_{I,J} + JM \cdot U_{I,J-1} + IM \cdot U_{I-1,J} - Q_{I,J} = \frac{C_{I,J}}{\Delta t}(U_{I,J,n+1} - U_{I,J,n}) \qquad (3)$$

Where:

U is the temperature or potential;

IM, JM, IP, JP are coefficients including resistance, thickness, length, fluid viscosity;

Q is rate of withdrawal of heat, electricity, or fluids;

C is a coefficient which includes compressibility, heat capacity, or capacitance; and

Δt is the time step from one solution of U to the next.

In Equation 4 the expression $\left(\frac{k\,\Delta Z\,\Delta y}{\mu\,\Delta x}\right)_{I+1/2,J}$ corresponds to IP in Equation 3; the expression $(\phi\,\Delta x\,\Delta y\,\Delta ZC)_{I,J}$ corresponds to C in Equation 2, and we use p instead of U.

Let us assume that the coefficients IP, IM, JP, JM, Q, and C in Equation 3 are constant. In Equation 4 this would mean that the viscosity, porosity, compressibility, and permeability are constant at any point in the system.

Equation 3 does not indicate whether the values of U on the left-hand side are for time t (nth time step) or for time $t+\Delta t$ ($n+1$st time step). By assigning the time level to the U's on the left-hand side, we can arrive at different forms of solution. In general we recognize

1. Explicit techniques
2. Implicit techniques
3. Iterative techniques which are merely a special form of implicit techniques.

For single-phase flow through porous media, Equation 3 becomes

$$(p_{I+1,J} - p_{I,J})\left(\frac{k\,\Delta Z\,\Delta y}{\mu\,\Delta x}\right)_{I+1/2,J} + (p_{I,J+1} - p_{I,J})\left(\frac{k\,\Delta Z\,\Delta x}{\mu\,\Delta y}\right)_{I,J+1/2} - (p_{I,J} - p_{I-1,J})\left(\frac{k\,\Delta Z\,\Delta y}{\mu\,\Delta x}\right)_{I-1/2,J} - (p_{I,J} - p_{I,J-1})\left(\frac{k\,\Delta Z\,\Delta x}{\mu\,\Delta y}\right)_{I,J-1/2} - Q_{I,J} = (p_{I,J,n+1} - p_{I,J,n})\frac{(\Phi\,\Delta X\,\Delta y\,\Delta Z\,C)_{I,J}}{\Delta t} \qquad (4)$$

The subscript $I+1/2$ refers to the average values of its related expression between I and $I+1$, etc. In Equation 4

p is pressure
k is permeability
μ is viscosity
ϕ is porosity, and
c is compressibility

Explicit methods

Basic explicit technique. In the explicit solution technique the values of U on the left-hand side are those from the previous time step (n); the right-hand side uses both a value from the previous time step (n) and the new time step ($n+1$).

Ignoring the withdrawal term $Q_{I,J}$ the explicit solution technique may be shown graphically in Fig. 2. It can readily be seen that for each node an equation with only one new time level value for U can be written.

For the explicit solution, the equation for node (I,J) becomes

$$(U_{I,J,n} - U_{I+1,J,n})\,IP + (U_{I,J,n} - U_{I,J+1,n})\,JP - (U_{I-1,J,n} - U_{I,J,n})\,IM - (U_{I,J-1,n} - U_{I,J,n})\,JM + Q_{I,J} = (U_{I,J,n} - U_{I,J,n+1})\frac{C}{\Delta t} \qquad (5)$$

Rearranging to solve for $U_{I,J,n+1}$ gives

$$U_{I,J,n+1} = -\frac{\Delta t}{C}[-U_{I-1,J,n}\,IM - U_{I,J-1,n}\,JM + U_{I,J,n}((IM + IP + JM + JP) - \frac{C}{\Delta t}) - U_{I,J+1,n}\,JP - U_{I+1,J,n}\,IP + Q_{I,J}] \qquad (6)$$

At each point, the values of U_{n+1} are calculated explicitly. The calculation at each point in the system depends only on values of U_n, so that the calculations can be arranged in any order of sequence.

Alternating direction explicit. The alternating direction explicit method[2] (ADE) also involves solving an equation with only one unknown at each point in the system. This method is directionally biased and makes use of values at time step $n+1$ that have already been calculated.

Fig. 3 shows graphically how each equation may be written for each point. It exhibits the configuration when sweeping in the +I and +J direction.

Fig. 4 shows a series of consecutive calculations in the +I and +J direction. When calculating the new value for U at (1,1) only the one value of U in the new time step appears due to the boundary condition (no flow boundaries are assumed for this example).

When calculating $U_{2,1}$ the previously calculated value for $U_{1,1}$ is used. This procedure is followed until all new values for U in the first row have been calculated. Then the values in

Fig. 3

Alternating direction

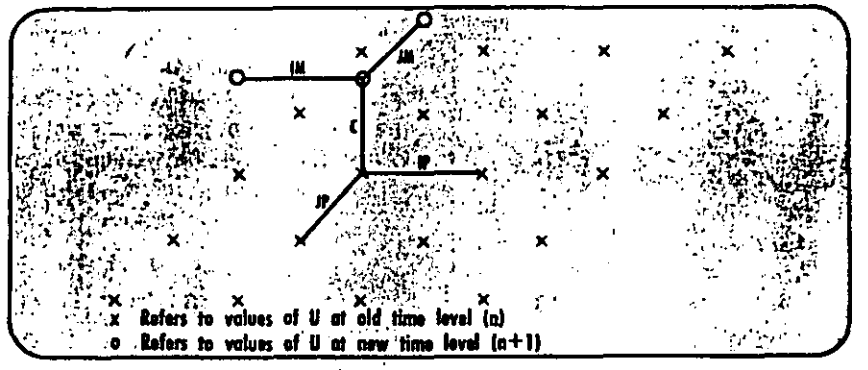

Fig. 4

Order of calculations

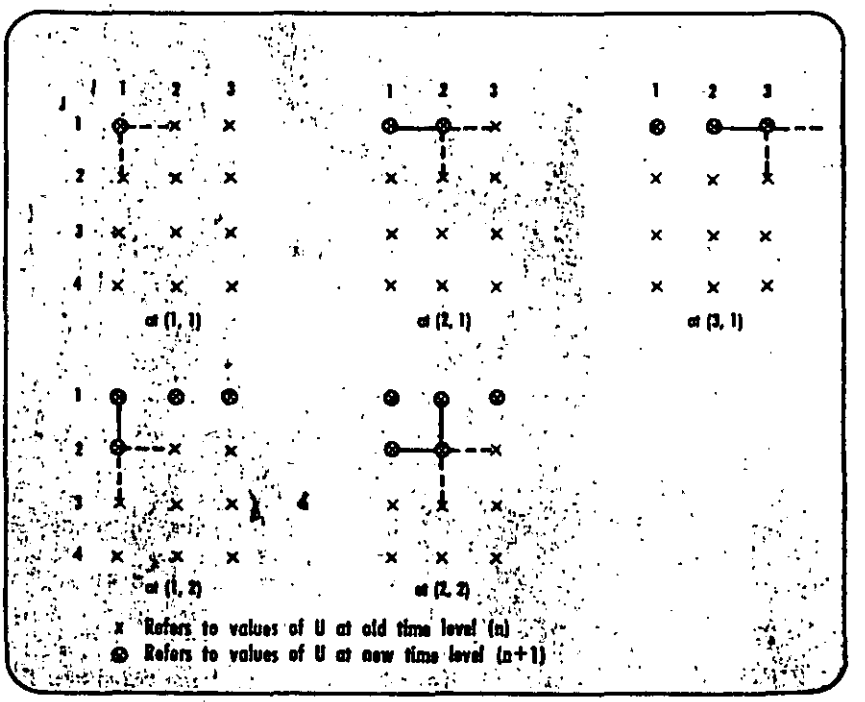

the second row are determined as shown in Fig. 4.

When at 2,2 it can be seen that the previously calculated values for the new time step for $U_{2,1}$ and $U_{1,2}$ are used along with the values for the old time step for $U_{3,2}$ and $U_{2,3}$.

Following a sweep in the +I and +J direction, it may be followed by sweeps in the −I, −J direction, the −I, +J direction and the +I, −J direction. Hence, the name alternating direction.

When calculating points in increasing I and J, this method has the form

$$(U_{I,J,n} - U_{I+1,J,n})\,IP + U_{I,J,n} - U_{I,J+1,n})\,JP - (U_{I-1,J,n+1} - U_{I,J,n+1})\,IM - (U_{I,J-1,n+1} - U_{I,J,n+1})\,JM + Q_{I,J} = (U_{I,J,n} - U_{I,J,n+1})\,\frac{C}{\Delta t} \quad (7)$$

Following rearrangement, the equation for the +I, +J direction sweep becomes

$$U_{I,J,n+1}\,(IM + JM + \frac{C}{\Delta t}) = -U_{I+1,J,n}\,IP - U_{I,J+1,n}\,JP + U_{I,J,n}\,(IP + JP + \frac{C}{\Delta t}) - U_{I-1,J,n+1}\,IM - U_{I,J-1,n+1}\,JM - Q_{I,J} \quad (8)$$

Three more forms are possible for sweep in other directions. Sweeping in the −I, −J direction

$$(U_{I,J,n+1} - U_{I+1,J,n+1})\,IP + (U_{I,J,n+1} - U_{I,J+1,n+1})\,JP - (U_{I-1,J,n} - U_{I,J,n})\,IM - U_{I,J-1,n} - U_{I,Jn})\,JM + Q_{I,J} = (U_{I,J,n} - U_{I,J,n+1})\,\frac{C}{\Delta t} \quad (9)$$

Rearranging terms

$$U_{I,J,n+1}\,(IP + JP + \frac{C}{\Delta t}) = -U_{I+1,J,n+1}\,IP - U_{I,J+1,n+1}\,JP + U_{I,J,n}\,(IM + JM + \frac{C}{\Delta t}) - U_{I-1,J,n}\,IM - U_{I,J-1,n}\,JM - Q_{I,J} \quad (10)$$

Sweeping in the −I, +J direction

$$(U_{I,J,n+J} - U_{I+1,J,n+1})\,IP + (U_{I,J,n} - U_{I,J+1,n})\,JP - (U_{I-1,J,n} - U_{I,J,n})\,IM - (U_{I,J-1,n+1} - U_{I,J,n+1})\,JM + Q_{I,J} = (U_{I,J,n} - U_{I,J,n+1})\,\frac{C}{\Delta t} \quad (11)$$

Rearranging terms

$$U_{I,J,n+1}\,(IP + JM + \frac{C}{\Delta t}) = -U_{I+1,J,n+1}\,IP - U_{I,J+1,n}\,JP + U_{I,J,n}\,(JP + IM + \frac{C}{\Delta t}) - U_{I-1,J,n}\,IM - U_{I,J-1,n+1}\,JM - Q_{I,J} \quad (12)$$

Sweeping in the +I, −J direction

$$(U_{I,J,n} - U_{I+1,J,n})\,IP + (U_{I,J,n+1} - U_{I,J+1,n+1})\,JP - (U_{I-1,J,n+1} - U_{I,J,n+1})\,IM - (U_{I,J-1,n} - U_{I,J,n})\,JM$$

$$+Q_{I,J} = (U_{I,J,n} - U_{I,J,n+1}) \frac{C}{\Delta t} \quad (13)$$

Rearranging terms

$$U_{I,J,n+1}\left(JP+IM+\frac{C}{\Delta t}\right) = -U_{I+1,J,n}$$

$$IP - U_{I,J+1,n+1}\,JP + U_{I,J,n}\left(IP+JM+\frac{C}{\Delta t}\right) - U_{I-1,J,n+1}\,IM - U_{I,J-1,n}$$

$$JM - Q_{I,J} \quad (14)$$

The order of calculation in the alternating direction explicit method is important because the calculation for each node depends on the previous calculation from its neighbors on the back side.

Dufort-Frankel method. This explicit procedure is directionally biased and requires the values at time step $n-1$. To get started, one makes the first time step calculation with some other method. Thereafter the equation for each node has the form

$$(U_{I,J,n-1} - U_{I+1,J,n})\,IP + (U_{I,J,n-1} - U_{I,J+1,n})\,JP - (U_{I-1,J,n} - U_{I,J,n+1})\,IM - (U_{I,J-1,n} - U_{I,J,n+1})\,JM + Q_{I,J} = (U_{I,J,n-1} - U_{I,J,n+1})\frac{C}{t_{n+1} - t_{n-1}} \quad (15)$$

Following rearrangement, to solve explicity

$$U_{I,J,n+1}\left(IM + JM + \frac{C}{t_{n+1} - t_{n-1}}\right) = U_{I+1,J,n}\,IP + U_{I,J+1,n}\,JP - U_{I,J,n-1}\left(IP + JP - \frac{C}{t_{n+1} - t_{n-1}}\right) + U_{I-1,J,n}\,IM + U_{I,J-1,n}\,JM - Q_{I,J} \quad (16)$$

Three other combinations are again possible by sweeping the grid in different directions.

Exponential approximation. The last explicit method to be discussed is the exponential method.[8] Like the alternating direction explicit method, it depends on values calculated at neighbors during sweeps.

The general equation is next written as

$$U_{I,J}\,IP - U_{I+1,J,n}\,IP + U_{I,J}\,JP - U_{I,J+1,n}\,JP - U_{I-1,J,n+1}\,IM + U_{I,J}\,IM - U_{I,J-1,n+1}\,JM + U_{I,J}\,JM + Q_{I,J} = (U_{I,J,n} - U_{I,J,n+1})\frac{C}{\Delta t} = -C\frac{du}{dt} \quad (17)$$

or $$-\frac{C}{dt} = \text{(left-hand side)}/(dU)$$

or $$-\frac{dt}{C} = (dU)/\text{(left-hand side)}$$

or $$-\int_{t(n)}^{t(n+1)} \frac{dt}{C} (IP+JP+IM+JM) = \int_{t(n)}^{t(n+1)} \frac{(dU)\,(IP+JP+IM+JM)}{\theta}$$

where: $\theta = U_{I,J}(IP+JP+IM+JM) - (U_{I+1,J,n}IP + U_{I,J+1,n}JP + U_{I-1,J,n+1}IM + U_{I,J-1,n+1}JM)$

For convenience, call

$$IP+JP+IM+JM=S$$

and

$$U_{I+1,J,n}IP + U_{I,J+1,n}JP + U_{I-1,J,n+1}IM + U_{I,J-1,n+1}JM = K$$

Fig. 5

Example problem

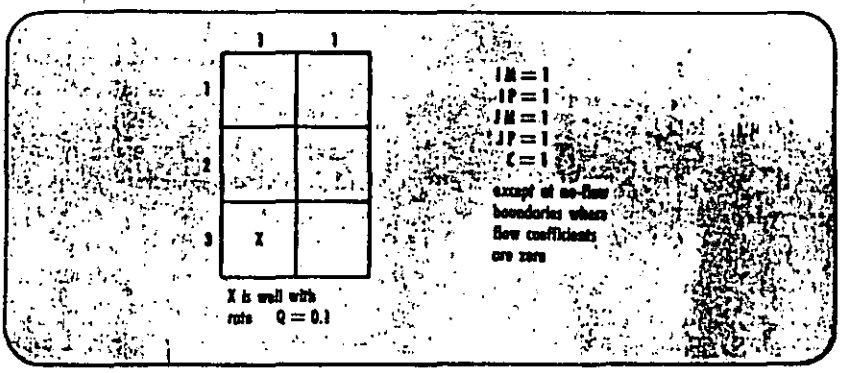

Values for U at different times for different explicit methods

Table 1

	Explicit		Alternating direction explicit		Dufort-Frankel		Exponential	
t	1.0000	1.0000	1.0000	1.0000	1.0000	1.0000	1.0000	1.0000
0	1.0000	1.0000	1.0000	1.0000	1.0000	1.0000	1.0000	1.0000
	1.0000	1.0000	1.0000	1.0000	1.0000	1.0000	1.0000	1.0000
	1.0000	1.0000	0.9999	0.9999	0.9999	0.9999	0.9998	0.9999
0.1	1.0000	1.0000	0.9990	0.9998	0.9990	0.9998	0.9982	0.9996
	0.9900	1.0000	0.9900	0.9990	0.9900	0.9990	0.9847	0.9981
	1.0000	1.0000	0.9997	0.9999	0.9998	0.9999	0.9995	0.9998
0.2	0.9990	1.0000	0.9976	0.9994	0.9984	0.9997	0.9968	0.9991
	0.9820	0.9990	0.9818	0.9975	0.9825	0.9982	0.9787	0.9966
0.3	0.9999	1.0000	0.9993	0.9997	0.9996	0.9999	0.9992	0.9996
	0.9975	0.9998	0.9959	0.9989	0.9968	0.9994	0.9953	0.9985
	0.9754	0.9974	0.9749	0.9957	0.9759	0.9965	0.9734	0.9949
0.4	0.9996	0.9999	0.9989	0.9995	0.9993	0.9998	0.9988	0.9994
	0.9957	0.9993	0.9941	0.9981	0.9953	0.9988	0.9937	0.9978
	0.9698	0.9954	0.9691	0.9935	0.9704	0.9947	0.9688	0.9931
1.0	0.9959	0.9979	0.9942	0.9963	0.9955	0.9974	0.9955	0.9971
	0.9846	0.9928	0.9826	0.9907	0.9844	0.9923	0.9854	0.9924
	0.9471	0.9815	0.9455	0.9794	0.9474	0.9813	0.9511	0.9829

Then

$$-\int_{t(n)}^{t(n+1)} \frac{Sdt}{C} = \int_{t(n)}^{t(n+1)} \frac{SdU}{SU-K}$$

or, following integration,

$$-\frac{S}{C}(t_{n+1}-t_n) = \ln \frac{SU_{n+1}-K}{SU_n-K}$$

or

$$SU_{n+1}-K=(SU_n-K)e^{-S\Delta t/C}$$

or

$$U_{n+1}=\frac{(SU_n-K)e^{-S\Delta t/C}+K}{S}$$

or

$$U_{n+1}=U_n e^{-(IM+IP+JM+JP)\Delta t/C}+$$

$$\frac{1-e^{-(IM+IP+JM+JP)\Delta t/C}}{(IM+IP+JM+JP)}\times$$

$$(U_{I+1,J,n}IP+U_{I,J+1,n}JP+$$

$$U_{I-1,J,n+1}IM+U_{I,J-1,n+1}JM) \quad (18)$$

which is the form when sweeping in the +I and +J directions. Three different forms are again possible.

Stability of explicit methods. One of the most critical problems in the generation of numerical solutions is that of stability. If a numerical computing scheme is stable one is assured that the errors committed at one time level will not appear in a later time level amplified in magnitude.

Analytical tests for stability that are valid for a wide variety of problems that arise in practice are not available.

However, tests have been developed which apply to the finite-difference methods used to solve linear partial differential equations with constant coefficients. Thus we cannot look at the stability of Equation 1, but must refer to Equation 20 in the previous article[1] in this series. This equation is

$$\frac{p_{I+1}-2p_I+p_{I-1}}{\Delta x^2} = \frac{\phi\mu c}{k}\frac{(p_{I,n+1}-p_{I,n})}{\Delta t} \quad (19)$$

For the explicit method, the pressures on the left-hand side of Equation 19 are taken at time step n. It can be shown that the condition

$$\frac{k\Delta t}{\phi\mu c\Delta x^2} \leq \frac{1}{2}$$

must be met for stability.

The other three explicit methods have been shown to be unconditionally stable for any $\Delta t > 0$ for this problem[3]. Thus the basic explicit method is seldom used due to this severe limitation for stability.

From these results, the conjecture might be made that the same criterion applies to the same type of problem containing nonconstant coefficients.

Example Problem. Fig. 5 shows the grid system for an example problem which was used to solve Equation 3 using each of the explicit techniques which have been discussed. The following boundary conditions have been used:

$$U_{(x,y,0)}=1 \text{ for } t=0$$

$$\frac{\partial U}{\partial x}=0 \text{ and } \frac{\partial U}{\partial y}=0$$

at the boundaries

$$Q_{3,1}=0.1 \text{ for all } t$$

(this could be a production well located at this position producing at a constant rate)

The coefficients of U in Equation 3 are taken to be constant and equal to 1 (i.e., IM = JM = JP = JM = C = 1). Table 1 shows the value of U that is calculated at various time levels using each explicit method.

References

1. Van Poollen, H. K., Bixel, H. C., and Jargon, J. R., "Reservoir modeling-3: Finite differences," The Oil and Gas Journal, Sept. 15, 1969, p. 120.
2. Saul'ev, V. K., "Numerical integration of parabolic equations," Dokl. Akad. Nank, SSSR(NS), 117, p. 36, 1957.
3. Larkin, B. K., "Some finite difference methods for problems in transient heat flow," AIChE preprint 16, presented at the 7th National Heat Transfer Conference AIChE-ASME held in Cleveland, Ohio, Aug. 1964.

Implicit finite difference approximation

A PREVIOUS chapter of this manual[1] showed a number of examples of explicit finite difference solutions to the diffusivity equation. This chapter will discuss some of the more popular implicit finite difference solutions to this equation.

Again the reader is reminded that this manual is written to acquaint the nonmathematician with these techniques.

Implicit finite difference equations. The diffusivity equation for two dimensions can be written as

$$\frac{\partial}{\partial x}\left(Kx\frac{\partial U}{\partial x}\right)+\frac{\partial}{\partial y}\left(Ky\frac{\partial U}{\partial y}\right)-Q=C\frac{\partial U}{\partial t} \quad (1)$$

This equation can be expanded where Kx and Ky are variable in space.

$$\frac{1}{\Delta x_J}\left(Kx_{I,J+1/2}\frac{(U_{I,J+1}-U_{I,J})}{\Delta x_{J+1/2}}-Kx_{I,J-1/2}\frac{(U_{I,J}-U_{I,J-1})}{\Delta x_{J-1/2}}\right)+\frac{1}{\Delta y_I}\left(Ky_{I+1/2,J}\frac{(U_{I+1,J}-U_{I,J})}{\Delta y_{I+1/2}}-Ky_{I-1/2,J}\frac{(U_{I,J}-U_{I-1,J})}{\Delta y_{I-1/2}}\right)-Q_{I,J}=C_{I,J}\frac{(U_{I,J,n+1}-U_{I,J,n})}{\Delta t} \quad (2)$$

Simplifying Equation 2 further gives

$$JP\cdot U_{I,J+1}+IP\cdot U_{I+1,J}-(JP+IP+JM+IM)\,U_{I,J}+JM\cdot U_{I,J-1}+IM\cdot U_{I-1,J}-Q_{I,J}=\frac{C_{I,J}}{\Delta t}(U_{I,J,n+1}-U_{I,J,n}) \quad (3)$$

Where: IM, JM, IP, JP are coefficients which contain the terms shown in Equation 2;

Q is the rate of withdrawal;

C is a coefficient which may include compressibility, heat capacity, or capacitance:

Δt is the time step from one solution of U to the next.

In an implicit solution technique, the values of U on the left-hand side of Equation 3 are taken to be those at the new time level, n+1. In this case Equation 3 will be

$$(U_{I,J,n+1}-U_{I+1,J,n+1})\,IP+(U_{I,J,n+1}-U_{I,J+1,n+1})\,JP-(U_{I-1,J,n+1}-U_{I,J,n+1})\,IM-(U_{I,J-1,n+1}-U_{I,J,n+1})JM+Q_{I,J}=(U_{I,J,n}-U_{I,J,n+1})\frac{C_{I,J}}{\Delta t}$$

Fig. 1

Two-dimensional system and resulting equations

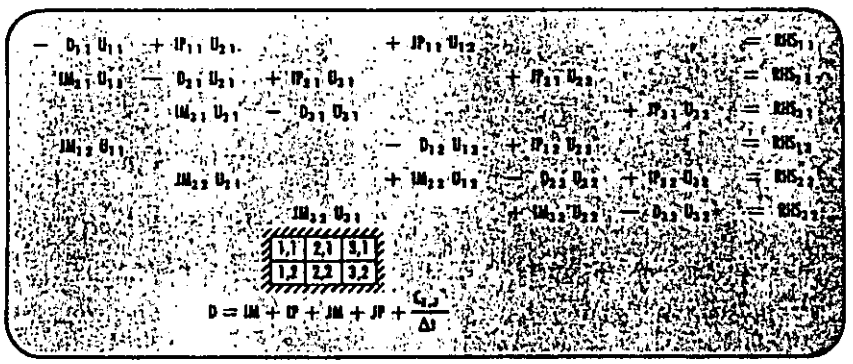

Fig. 2

Fig. 1 equations in matrix form

Fig. 3

Two implicit schemes

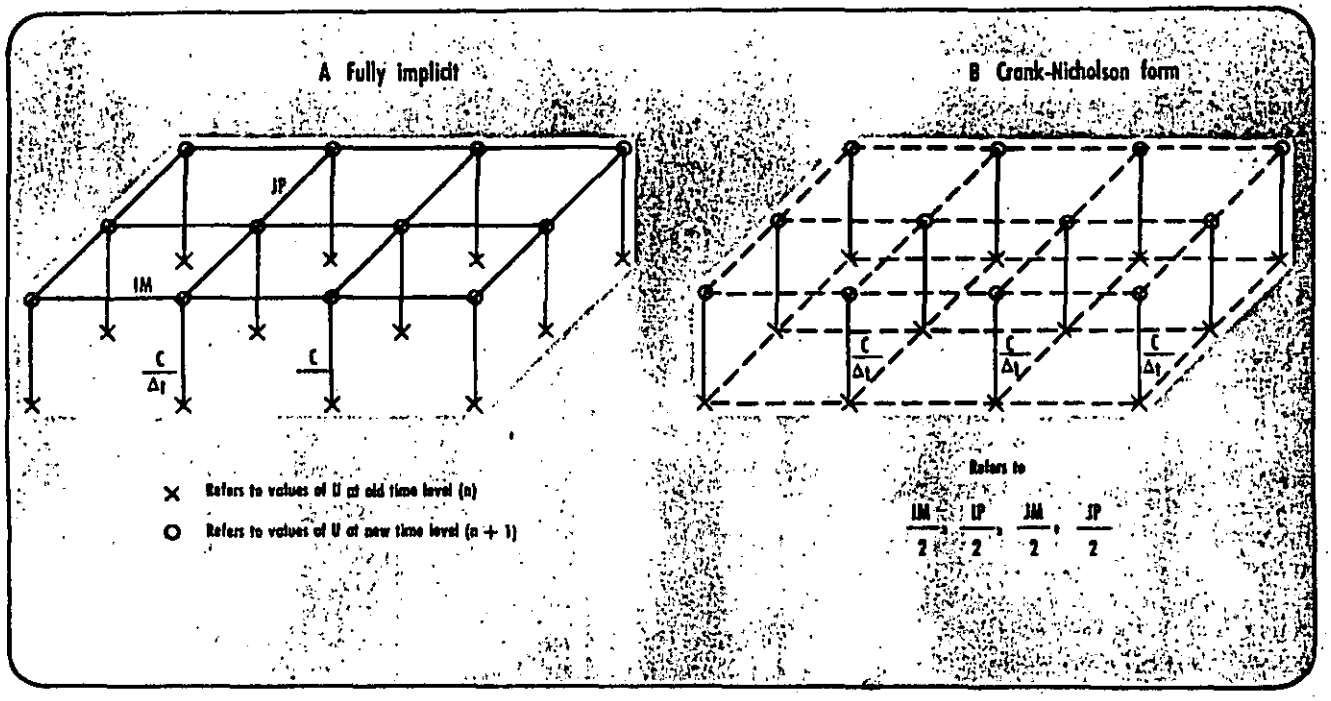

Or upon rearranging

$$
\begin{aligned}
&- U_{I-1,J,n+1}\,IM \\
&- U_{I,J-1,n+1}\,JM \\
&+ U_{I,J,n+1}\left[(IM + IP + JM + JP) + \frac{C}{\Delta t}\right] \\
&- U_{I+1,J,n+1}\,IP \\
&- U_{I,J+1,n+1}\,JP \\
&= U_{I,J,n}\frac{C_{I,J}}{\Delta t} - Q_{I,J} \\
&= RHS_{I,J}\ \text{(right hand side)}
\end{aligned}
$$

This equation can be written for each of N nodes in the system and when combined with boundary conditions will result in a system of N equations in N unknown values of U. Each equation will contain no more than three unknowns in a one-dimensional system; no more than five unknowns in a two-dimensional system, or no more than seven unknowns in a three-dimensional system.

This is shown in Fig. 1 for a two-dimensional, six-node system which has a no-flow boundary condition imposed completely around the perimeter. These same equations are shown in matrix form in Fig. 2.

Crank-Nicholson. The Crank-Nicholson difference form uses both old and new values of U in evaluating the space derivatives of Equation 1, or

$$
\begin{aligned}
&(U_{I,J,n} - U_{I+1,J,n})\frac{IP}{2} \\
&+ (U_{I,J,n+1} - U_{I+1,J,n+1})\frac{IP}{2} \\
&+ (U_{I,J,n} - U_{I,J+1,n})\frac{JP}{2} \\
&+ (U_{I,J,n+1} - U_{I,J+1,n+1})\frac{JP}{2} \\
&- (U_{I-1,J,n} - U_{I,J,n})\frac{IM}{2} \\
&- (U_{I-1,J,n+1} - U_{I,J,n+1})\frac{IM}{2} \\
&- (U_{I,J-1,n} - U_{I,J,n})\frac{JM}{2} \\
&- (U_{I,J-1,n+1} - U_{I,J,n+1})\frac{JM}{2} \\
&+ Q_{I,J} \\
&= (U_{I,J,n} - U_{I,J,n+1})\frac{C_{I,J}}{\Delta t}
\end{aligned}
$$

and, following rearrangement,

$$
\begin{aligned}
&- U_{I+1,J,n+1}\frac{IP}{2} \\
&- U_{I,J+1,n+1}\frac{JP}{2} \\
&+ U_{I,J,n+1}\left(\frac{IP + JP + IM + JM}{2} + \frac{C_{I,J}}{\Delta t}\right) \\
&- U_{I+1,J,n+1}\frac{IM}{2} - U_{I,J-1,n+1}\frac{JM}{2} \\
&= - U_{I+1,J,n}\frac{IP}{2} - U_{I,J+1,n}\frac{JP}{2} \\
&+ U_{I,J,n}\left(\frac{IP + JP + IM + JM}{2} + \frac{C_{I,J}}{\Delta t}\right) - U_{I-1,J,n}\frac{IM}{2} \\
&- U_{I,J-1,n}\frac{JM}{2} - Q_{I,J} = RHS_{I,J}
\end{aligned}
$$

Fig. 4

Calculations for ADIP

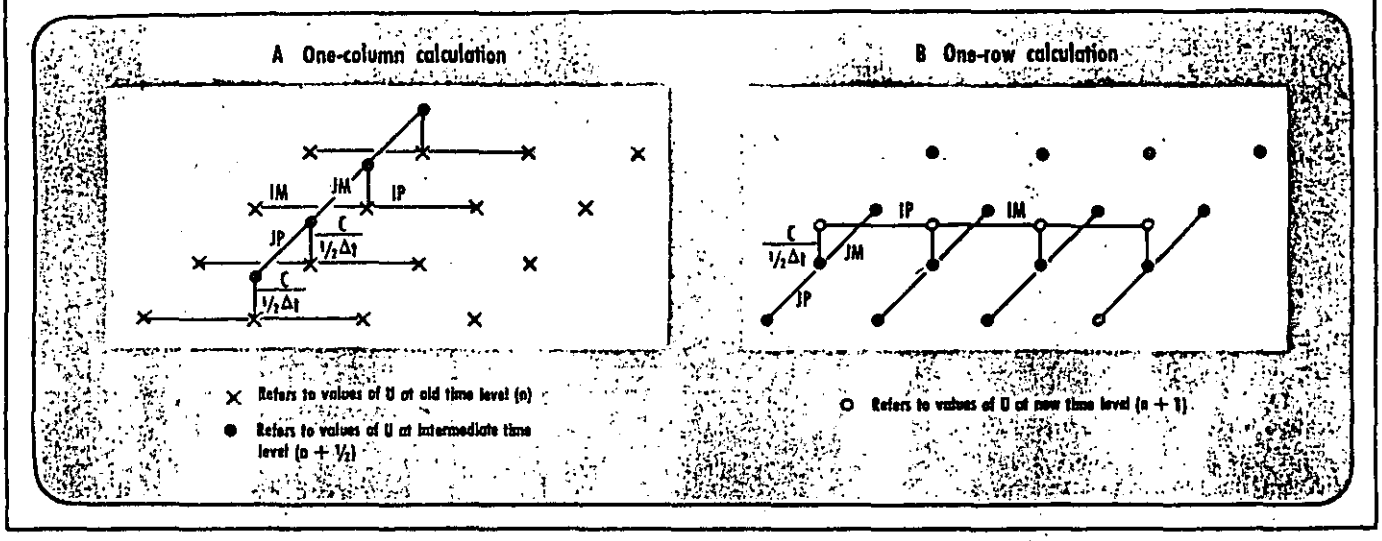

Again a system of N equations with N unknowns is developed. The only difference lies in the coefficients and the right-hand side of each equation.

Fig. 3 graphically shows the two implicit schemes.

Under either differencing scheme it is necessary to have a method for solving the N unknown values of U to move from one time level to the next.

Gauss elimination. Gauss elimination is a direct method of solving systems of linear equations. Basically it consists of eliminating unknowns from the equations until the system is reduced to one equation and one unknown. This equation is solved for the remaining unknown after which the other unknowns are evaluated by back substitution. For example, $U_{1,1}$, can be eliminated from the first two equations of Fig. 1 by dividing the first equation through by $-D_{1,1}$ and solving the resulting equation for $U_{1,1}$. $U_{1,1}$ can then be eliminated from the second equation by substituting from the first equation.

The remaining equations can be reduced in a like manner until there is only one equation and one unknown.

The system can then be solved by back substitution.

Here's an example. Given

$$\begin{aligned} 2x + y &= 4 \\ 3y - z &= 3 \\ x + z &= 4 \end{aligned}$$

Solve for x, y and z.

Solution: The last equation may be written as

$$z = 4 - x$$

Substituting z into the second equation gives

$$3y - 4 + x = 3$$

or

$$x = 7 - 3y$$

Substitution of x into the first equation gives

$$14 - 6x + y = 4$$

or

$$y = 2$$

Substitution of y into the first equation gives

$$2x + 2 = 4$$

or

$$x = 1$$

And from the last equation we find $z = 3$

Alternating direction implicit procedure.[3] A presumed approximation to the implicit solution is the alternating direction implicit procedure (ADIP). For one-half time step we calculate implicitly by columns and thereafter for another one-half timestep by rows.

Calculating by columns gives

$$\begin{aligned} &(U_{I,J,n} - U_{I+1,J,n})\,IP \\ &+ (U_{I,J,n+1/2} - U_{I,J+1,n+1/2})\,JP \\ &- (U_{I-1,J,n} - U_{I,J,n})\,IM \\ &- (U_{I,J-1,n+1/2} - U_{I,J,n+1/2})\,JM \\ &\quad + Q_{I,J} \\ &= (U_{I,J,n} - U_{I,J,n+1/2})\frac{2C_{I,J}}{\Delta t} \end{aligned}$$

Following rearrangement, we get

$$\begin{aligned} &- U_{I,J+1,n+1/2}\,JP \\ &+ U_{I,J,n+1/2}\left(JP + JM + \frac{2C_{I,J}}{\Delta t}\right) \\ &- U_{I,J-1,n+1/2}\,JM \\ &= - U_{I+1,J,n}\,IP \\ &+ U_{I,J,n}\left(IP + IM + \frac{2C_{I,J}}{\Delta t}\right) \\ &- U_{I-1,J,n}\,IM - Q_{I,J} \end{aligned}$$

Calculating by rows gives

$$\begin{aligned} &(U_{I,J,n+1} - U_{I+1,J,n+1})\,IP \\ &+ (U_{I,J,n+1/2} - U_{I,J+1,n+1/2})\,JP \\ &- (U_{I-1,J,n+1} - U_{I,J,n+1})\,IM \\ &- (U_{I,J-1,n+1/2} - U_{I,J,n+1/2})\,JM \\ &\quad + Q_{I,J} \\ &= (U_{I,J,n+1/2} - U_{I,J,n+1})\frac{2C_{I,J}}{\Delta t} \end{aligned}$$

and, following rearrangement,

$$\begin{aligned} &- U_{I+1,J,n+1}\,IP \\ &+ U_{I,J,n+1/2}\left(JP + JM + \frac{2C_{I,J}}{\Delta t}\right) \\ &- U_{I-1,J,n+1}\,IM \\ &= - U_{I,J,n+1/2}\,JP \\ &+ U_{I,J,n+1/2}\left(JP + JM + \frac{2C_{I,J}}{\Delta t}\right) \\ &- U_{I,J-1,n+1/2}\,JM - Q_{I,J} \end{aligned}$$

While calculating in a column-by-column fashion, we will have one equation with three unknowns for each node. For each column or each row, Gauss elimination is used to solve the new values. After one column is finished, we move on to the next.

No special order is required in these calculations where values used from the neighboring column are at the old time level. After all columns have been treated, the procedure is repeated by rows using the column-wise calculated values as old values.

Fig. 4 is a graphical illustration of the method. This method is only an approximation to the exact solution. Values obtained at intermediate time levels should not be considered solutions.

The method is sometimes referred to as single-sweep ADIP to differentiate it from iterative ADIP, which is discussed later.

Iterative methods. The Gauss elimination is one technique for solving matrices of the type shown in Fig. 2. It results in the direct evaluation of the unknown values of U. The procedure is applied only once in obtaining a solution. An iterative scheme makes use of an initial guess at the solution and continues to improve on this until some convergence criteria are met. The iterative methods are usually faster although there may be some loss in accuracy.

Jacobi Relaxation (Simultaneous Displacements). For each node we have the equation

$$
\begin{aligned}
&(U_{I,J,n+1} - U_{I+1,J,n'})\,IP \\
&+ (U_{I,J,n+1} - U_{I,J+1,n'})\,JP \\
&- (U_{I,J-1,n'} - U_{I,J,n+1})\,JM \\
&- (U_{I-1,J,n'} - U_{I,J,n+1})\,IM + Q_{I,J} \\
&= (U_{I,J,n} - U_{I,J,n+1})\frac{C_{I,J}}{\Delta t}
\end{aligned}
$$

In this method we solve for the value of $U_{I,J,n+1}$ explicitly, or $U_{I,J,n+1} =$

$$
\begin{aligned}
&\{ U_{I-1,J,n'}\,IM \\
&+ U_{I,J-1,n'}\,JM \\
&+ U_{I,J,n}\frac{C_{I,J}}{\Delta t} \\
&+ U_{I,J+1,n'}\,JP \\
&+ U_{I+1,J,n'}\,IP - Q_{I,J}\}/ \\
&\left\{\frac{C_{I,J}}{\Delta t} + IM + JM + IP + JP\right\}
\end{aligned}
$$

During the first iteration $U_{I,J,n'} = U_{I,J,n}$. For all nodes, the value $U_{I,J,n+1}$ is calculated. All values for $U_{I,J,n+1}$ are compared with those for $U_{I,J,n'}$. If the difference between any set is larger than the present value of the allowable error, ϵ, all values of $U_{I,J,n'}$ are replaced by $U_{I,J,n+1}$ and the calculation is repeated.

If $|U_{I,J,n+1} - U_{I,J,n'}| < \epsilon$ for all nodes, the latest values for $U_{I,J,n+1}$ are accepted as correct.

In this method all values have to be calculated prior to replacement, hence the name "Simultaneous Displacements." Fig. 5 shows the method for one dimension in graphical form.

GAUSS-SEIDEL. (Successive Displacement). For each node, we have the equation

$$
\begin{aligned}
&(U_{I,J,n+1} - U_{I+1,J,n'})\,IP \\
&+ (U_{I,J,n+1} - U_{I,J+1,n'})\,JP \\
&- (U_{I-1,J,n+1} - U_{I,J,n+1})\,IM \\
&- (U_{I,J-1,n+1} - U_{I,J,n+1})\,JM \\
&\quad + Q_{I,J} \\
&= (U_{I,J,n} - U_{I,J,n+1})\frac{C_{I,J}}{\Delta t}
\end{aligned}
$$

Following rearrangement, it reads

$$
\begin{aligned}
&U_{I,J,n+1} = \\
&\{ U_{I+1,J,n'}\,IP \\
&+ U_{I,J+1,n'}\,JP \\
&+ U_{I,J,n}\frac{C_{I,J}}{\Delta t} \\
&+ U_{I-1,J,n+1}\,IM \\
&+ U_{I,J-1,n+1}\,JM - Q_{I,J}\}/ \\
&\left\{IP + IM + JP + JM + \frac{C_{I,J}}{\Delta t}\right\}
\end{aligned}
$$

This is the form when sweeping in the +I and +J directions. One solves explicitly for $U_{I,J,n+1}$ compares it with the previously calculated $U_{I,J,n'}$ and replaces $U_{I,J,n+1}$ by the just calculated $U_{I,J,n'}$. If the largest observed difference between $U_{I,J,n+1}$ and $U_{I,J,n'}$ is less than ϵ, the last values are accepted; otherwise, a new sweep has to be made. For the first iteration $U_{I,J,n'} = U_{I,J,n}$.

Fig. 6 shows the method for one dimension in graphical form.

Point-by-point successive over-relaxation. The Gauss-Seidel method has been modified by boosting the correction during each iteration as follows $U_{I,J,n+1}$ becomes

$$\frac{U_{I,J,n+1} - (\omega - 1)\,U_{I,J,n'}}{\omega}$$

or

$$
\begin{aligned}
&U_{I,J,n+1} = \\
&\omega\,[\,U_{I+1,J,n'}\,IP \\
&+ U_{I,J+1,n'}\,JP \\
&+ U_{I,J,n}\frac{C_{I,J}}{\Delta t} \\
&+ U_{I-1,J,n+1}\,IM \\
&+ U_{I,J-1,n+1}\,JM - Q_{I,J}]/ \\
&\qquad \left[IP + JP + IM + JM + \frac{C_{I,J}}{\Delta t}\right] \\
&+ (\omega - 1)\,U_{I,J,n'}
\end{aligned}
$$

The value of the iteration parameter, ω, is between 1 and 2. When $\omega = 1$, the equation is the same as Gauss-Seidel. When applied to the LaPlace equation (or when $C = 0$), the above equation is referred to as the Liebmann method.

Various techniques have been proposed to find the optimum value for ω.[2]

Line SOR.[2] In Line SOR, equations are solved row by row, rather than

Fig. 5

Jacobi Relaxation method

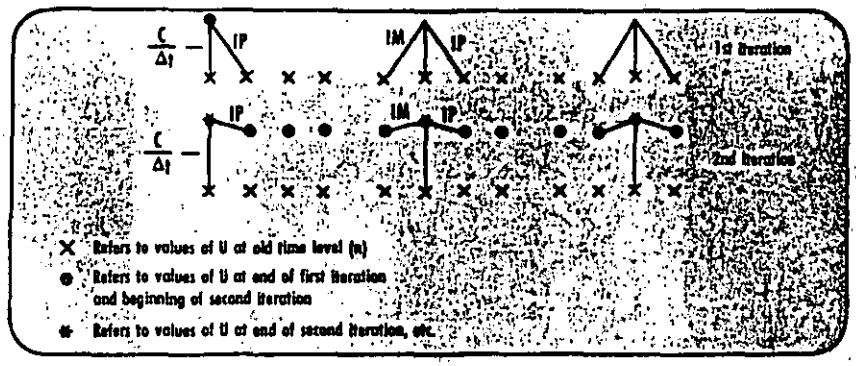

Fig. 6

Gauss-Seidel relaxation method

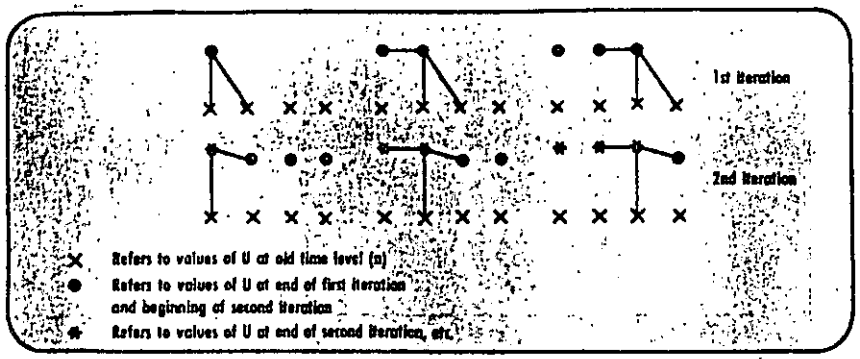

point by point. Also, we write for U_{n+1}, on the row under consideration,

$$\frac{U_{n+1} - (\omega - 1)\, U_n}{\omega} \text{ or}$$

$$U_{I-1,J,n+1}\, IM$$
$$- U_{I,J,n+1} \left(IM + JM + IP + JP + \frac{C_{I,J}}{\Delta t}\right)$$
$$+ U_{I+1,J,n+1}\, IP =$$
$$\omega \left[Q_{I,J} - U_{I,J-1,n+1}\, JM - U_{I,J+1,n}\, JP - \frac{C_{I,J}}{\Delta t} U_{I,J,n}\right]$$
$$+ (\omega - 1) \left[\left(IM + IP + JM + JP + \frac{C_{I,J}}{\Delta t}\right) U_{I,J,n} - U_{I-1,J,n}\, IM - U_{I+1,J,n}\, IP\right]$$

This equation is solved implicitly for each row and sweeps down the column in row-by-row fashion.

Iterative ADIP.[2,4] Iterative ADIP is a modification of the regular ADIP and has the appearance as follows for calculations by columns.

$$- U_{I,J+1,n+1/2}\, JP$$
$$+ U_{I,J,n+1/2} \left(JP + JM + \frac{2C_{I,J}}{\Delta t} + \gamma_m\right)$$
$$- U_{I,J-1,n+1/2}\, JM =$$
$$- U_{I+1,J,n}\, IP$$
$$+ U_{I,J,n} \left(IP + IM - \gamma_m + \frac{2C_{I,J}}{\Delta t}\right)$$
$$+ U_{I,J,n}$$

Table 1

Values of U at various time levels using implicit schemes

t	Implicit		Crank-Nicholson		ADIP		Successive over relaxation	
0.0	1.0000	1.0000	1.0000	1.0000	1.0000	1.0000	1.0000	1.0000
	1.0000	1.0000	1.0000	1.0000	1.0000	1.0000	1.0000	1.0000
	1.0000	1.0000	1.0000	1.0000	1.0000	1.0000	1.0000	1.0000
0.1	0.9999	1.0000	0.9999	0.9999	0.9999	0.9999	0.9999	0.9999
	0.9993	0.9998	0.9996	0.9999	0.9995	0.9999	0.9993	0.9999
	0.9915	0.9992	0.9908	0.9995	0.9908	0.9995	0.9915	0.9992
0.2	0.9998	0.9999	0.9999	0.9999	0.9998	0.9999	0.9998	0.9999
	0.9982	0.9996	0.9985	0.9998	0.9985	0.9998	0.9982	0.9996
	0.9843	0.9980	0.9832	0.9984	0.9932	0.9984	0.9843	0.9980
0.3	0.9995	0.9998	0.9997	0.9999	0.9997	0.9999	0.9995	0.9998
	0.9968	0.9991	0.9971	0.9994	0.9971	0.9994	0.9968	0.9992
	0.9780	0.9964	0.9768	0.9969	0.9768	0.9968	0.9780	0.9964
0.4	0.9992	0.9996	0.9994	0.9998	0.9994	0.9998	0.9991	0.9996
	0.9953	0.9985	0.9955	0.9989	0.9955	0.9989	0.9953	0.9986
	0.9725	0.9946	0.9712	0.9950	0.9712	0.9950	0.9724	0.9946
1.0	0.9952	0.9970	0.9955	0.9974	0.9955	0.9974	0.9952	0.9970
	0.9847	0.9921	0.9847	0.9925	0.9847	0.9925	0.9847	0.9921
	0.9490	0.9817	0.9480	0.9816	0.9480	0.9816	0.9491	0.9818

$$- U_{I-1,J,n}\, IM - Q_{I,J}$$

and for calculation by rows

$$- U_{I+1,J,n+1}\, IP$$
$$+ U_{I,J,n+1} \left(IP + IM + \frac{2C_{I,J}}{\Delta t} + \gamma_m\right)$$
$$- U_{I-1,J,n+1}\, JP =$$
$$- U_{I,J+1,n+1/2}\, JP$$
$$+ U_{I,J,n+1/2} \left(JP + JM + \frac{2C_{I,J}}{\Delta t} - \gamma_m\right)$$
$$- U_{I,J-1,n+1/2}\, JM - Q_{I,J}$$

As in regular ADIP, we calculate the column-by-column equations and thereafter the row-by-row equations. We then compare the values at n+1 iterations with those at n'. If the difference is small enough, the n+1st values are accepted; otherwise, the calculation is repeated. Usually a different value is chosen for the γ_m for the next iteration.

Residual form. All previous examples of numerical techniques were given where a new value for U is calculated with a known value for U at the previous time level. Some real advantages can be obtained by solving for the difference between the old and new values or by solving for

$$\epsilon = U_{n+1} - U_n$$

In this text, these matters will not be discussed. Those interested in constructing numerical models should realize that solving for residuals is far superior to solving directly for new values.

Example problem. Fig. 5 of the previous installment[1] shows conditions for a simple 2 by 3 grid. Table 1 of that installment shows the value of U at various time levels using different explicit methods. Table 1 of the present installment shows similar information for various implicit schemes.

References

1. Van Poollen, H. K., Bixel, H. C., and Jargon, J. R., "Reservoir Modeling—4: Explicit finite difference approximations," The Oil and Gas Journal, Nov. 3, 1969.
2. Breitenbach, E. A., Thurnau, D. H., and van Poollen, H. K., "Solution of the immiscible fluid flow simulation equations," Society of Petroleum Engineers Journal, June 1969, Vol. 9, No. 2, p. 155.
3. Peaceman, D. W., and Rachford, H. H. Jr., "The numerical solution of parabolic and elliptical difference equations," J. Soc. Indust. Appl. Math., 1955, Vol. 3, 28.
4. Douglas, Jim, Peaceman, D. W., Rachford, H. H., Jr., "A Method for calculating multidimensional immiscible displacement," Petroleum Transactions, AIME, Vol. 216, 1959, p. 297.

General form of finite

MANY of the finite difference approximations shown in the past two chapters[1,2] in this manual can be obtained from a more general formulation of these equations. Some of these finite difference approximations are special cases of the more general equation[3]

$$\theta\,[JP{\cdot}U_{I,J+1,n+1} + IP{\cdot}U_{I+1,J,n+1} - (JP+IP+JM+IM)\,U_{I,J,n+1} + JM{\cdot}U_{I,J-1,n+1} + IM{\cdot}U_{I-1,J,n+1}] + (1-\theta)\,[JP{\cdot}U_{I,J+1,n} + IP{\cdot}U_{I+1,J,n} - (JP+IP+JM+IM)\,U_{I,J,n} + JM{\cdot}U_{I,J-1,n} + IM{\cdot}U_{I-1,J,n}] - Q_{I,J} = C_{I,J}/2\Delta t\,[(1+2Y)\,U_{I,J,n+1} - 4YU_{I,J,n} - (1-2Y)\,U_{I,J,n-1}] \quad (1)$$

where θ and Y are constants and may have values from zero to one.

Again, U is the temperature or potential;

IM, JM, IP, JP are coefficients including resistance, thickness, length, fluid viscosity;

Q is rate of withdrawal of heat, electricity, or fluids;

C is a coefficient which includes compressibility, heat capacity, or capacitance;

Δt is the time step from one solution of U to the next.

The formulation of Equation 1 requires that the time step Δt remain constant if Y is chosen such that the terms $U_{I,J,n+1}$ and $U_{I,J,n-1}$ appear simultaneously on the right side of this equation. Reference 3 gives the more general case for unequal time-step size.

The standard explicit finite difference approximation can be obtained by letting $\theta = 0$ and $Y = \frac{1}{2}$. This gives

$$JP{\cdot}U_{I,J+1,n} + IP{\cdot}U_{I+1,J,n} - (JP+IP+JM+IM)\,U_{I,J,n} + JM{\cdot}U_{I,J-1,n} + IM{\cdot}U_{I-1,J,n} - Q_{I,J} = C_{I,J}/\Delta t\,(U_{I,J,n+1} - U_{I,J,n}) \quad (2)$$

The standard implicit finite difference approximation can be obtained by letting $\theta = 1$ and $Y = \frac{1}{2}$. This gives

$$JP{\cdot}U_{I,J+1,n+1} + IP{\cdot}U_{I+1,J,n+1} - (JP+IP+JM+IM)\,U_{I,J,n+1} + JM{\cdot}U_{I,J-1,n+1} + IM{\cdot}U_{I-1,J,n+1} - Q_{I,J} = C_{I,J}/\Delta t\,(U_{I,J,n+1} - U_{I,J,n}) \quad (3)$$

The Crank-Nicholson finite difference approximation can be obtained by letting $\theta = \frac{1}{2}$ and $Y = \frac{1}{2}$. This gives

$$\tfrac{1}{2}\,[JP{\cdot}(U_{I,J+1,n+1} + U_{I,J+1,n}) + IP{\cdot}(U_{I+1,J,n+1} + U_{I+1,J,n}) - (JP+IP+JM+IM)\,(U_{I,J,n+1} + U_{I,J,n}) + JM{\cdot}(U_{I,J-1,n+1} + U_{I,J-1,n}) + IM{\cdot}(U_{I-1,J,n+1} + U_{I-1,J,n})] - Q_{I,J} = C_{I,J}/\Delta t\,(U_{I,J,n+1} - U_{I,J,n}) \quad (4)$$

difference approximations

If $\theta = 1$ and $Y = 1$, the approximation used by West, Garvin, and Sheldon[4] is obtained, or

$$JP \cdot U_{I,J+1,n+1} + IP \cdot U_{I+1,J,n+1} - (JP+IP+JM+IM) \cdot U_{I,J,n+1} + JM \cdot U_{I,J-1,n+1} + IM \cdot U_{I-1,J,n+1} - Q_{I,J} = C_{I,J}/2\Delta t \, [3 \cdot U_{I,J,n+1} - 4 \cdot U_{I,J,n} + U_{I,J,n-1}] \quad (5)$$

This equation gives a higher order accuracy in the time derivative than any of the other approximations shown, but requires more storage as values for U at time level n-1 must be available.

One further approximation can be obtained by letting $\theta = 0$ and $Y = 0$, or

$$JP \cdot U_{I,J+1,n} + IP \cdot U_{I+1,J,n} - (JP+IP+JM+IM) \cdot U_{I,J,n} + JM \cdot U_{I,J-1,n} + IM \cdot U_{I-1,J,n} - Q_{I,J} = C_{I,J}/2\Delta t \, (U_{I,J,n+1} - U_{I,J,n-1}) \quad (6)$$

This equation also gives a higher order accuracy in the time derivative and requires additional storage for the values of U at time step n−1. However, this approximation should not be used as it has been shown to be unstable.

Stability requirements. Stability analyses have been performed for these finite difference approximations when the coefficients are constant. For the special case of $Y = ½$ and for one-dimensional, single-phase flow of a slightly compressible fluid through porous media, the following restrictions must be met for stability[6].

$$2k\,\Delta t/\phi\mu c\Delta x^2 \gtrless 1/(1-2\theta) \text{ if } 0 \gtrless \theta < ½$$

$$\text{No restriction if } ½ \gtrless \theta \gtrless 1 \quad (7)$$

Conditional stability occurs for $\theta < 0$ and unconditional stability for $\theta > 1$, however, these values of θ are generally not of interest.

Again for $Y = ½$ and two-dimensional flow of a slightly compressible fluid through porous media the stability requirements are

$$\frac{k_x\,\Delta t}{\phi\mu c\Delta x^2} + \frac{k_y\,\Delta t}{\phi\mu c\Delta y^2} \gtrless \frac{1}{2-4\theta} \text{ if } 0 \gtrless \theta < ½ \quad (8)$$

$$\text{No restriction if } ½ \gtrless \theta \gtrless 1$$

Finite difference Equations 2, 3, and 4 fit into this category. Thus the explicit formulation must meet the restriction of Equation 8, and the standard implicit method and Crank-Nicholson method suffer from no requirements for stability. It has also been shown that Equation 5 has no restriction for stability and that Equation 6 is always unstable.

References

1. van Poollen, H. K., Bixel, H. C., and Jargon, J. R., "Reservoir Modeling—4: Explicit finite difference approximations," The Oil and Gas Journal, Nov. 3, 1969, p. 81.
2. van Poollen, H. K., Bixel, H. C., and Jargon, J. R., "Reservoir Modeling—5: Implicit finite difference approximations, The Oil and Gas Journal, Jan. 5, 1969, p. 88.
3. Ridings, R. L., Dalton, R. L., Greene, H. W., Kyte, J. R., and Naumann, V. O., "Experimental and calculated behavior of dissolved-gas-drive systems," Soc. Pet. Eng. Journal, March 1963, p. 41.
4. West, W. J., Garvin, W. W., and Sheldon, J. W., "Solution of the equations of unsteady state two-phase flow in oil reservoirs," Trans. AIME, Vol. 201, p. 217, 1954.
5. Richtmyer, R. D., "Difference methods for initial-value problems," first edition, Interscience Publishers, Inc., New York, 1957.

Single-phase reservoir models

ONE, TWO, and three-dimensional single-phase flow equations for slightly compressible fluids offer considerable promise for studying various aspects of reservoir fluid flow. Many types of phenomena can be simulated with such a model.

These models can be used to study single well problems (simulating pressure buildup and drawdown behavior with cylindrical or cartesian coordinate systems); calculate stream lines in heterogeneous reservoirs and reservoirs with odd well patterns; obtain flood-out patterns for unit mobility ratios; and history-match black oil reservoirs where little saturation changes have occurred.

The three-dimensional flow equation for a slightly compressible fluid, neglecting gravity and assuming that the pressure gradients in the x, y and z directions are small reads:[1]

$$\frac{\partial}{\partial x}\left(\frac{k_x}{\mu}\frac{\partial p}{\partial x}\right)+\frac{\partial}{\partial y}\left(\frac{k_y}{\mu}\frac{\partial p}{\partial y}\right)+\frac{\partial}{\partial z}\left(\frac{k_z}{\mu}\frac{\partial p}{\partial z}\right)=\phi c\frac{\partial p}{\partial t} \qquad (1)$$

where

p = pressure of the fluid
ρ = density
k_x = x direction permeability
k_y = y direction permeability
k_z = z direction permeability
μ = viscosity
ϕ = porosity
x,y,z = distances and
t = time.

In one-dimensional flow only one of the terms on the left remains and the other two are zero. And for two-dimensional flow only two terms remain.

The equation for two-dimensional flow for constant thickness, permeability and viscosity becomes

$$\frac{\partial^2 p}{\partial x^2}+\frac{\partial^2 p}{\partial y^2}=\frac{\phi\mu c}{k}\frac{\partial p}{\partial t} \qquad (2)$$

in cartesian coordinates and

$$\frac{1}{r}\frac{\partial}{\partial r}\left(r\frac{\partial p}{\partial r}\right)=\frac{\phi\mu c}{k}\frac{\partial p}{\partial t} \qquad (3)$$

in one-dimensional radial coordinates.

This equation for the radial flow of a fluid of small and constant compressibility is one of the most often used in petroleum engineering. It forms the basis for most of the transient pressure analysis techniques used today. Analytical solutions to this equation have been obtained for a well located in an infinite media,[2] for a well located at the center of a closed circular reservoir,[3] for a well located at the center of a circular reservoir having a constant pressure at its outer boundary,[3] for a well located at the center of a radial discontinuity,[4,5] and for a well located near a linear discontinuity,[6] to name a few examples only.

However, many of these analytical solutions contain complicated mathematical terms which necessitate the use of a digital computer for their evaluation. In these cases one might prefer the use of finite-difference techniques over analytical techniques.

To incorporate varying formation thickness, the two-dimensional flow equation may be rewritten as

$$\frac{\partial}{\partial x}\left(\frac{k_x h}{\mu}\frac{\partial p}{\partial x}\right)+\frac{\partial}{\partial y}\left(\frac{k_y h}{\mu}\frac{\partial p}{\partial y}\right)=\phi ch\frac{\partial p}{\partial t} \qquad (4)$$

Fig. 1

The finite-differences grid

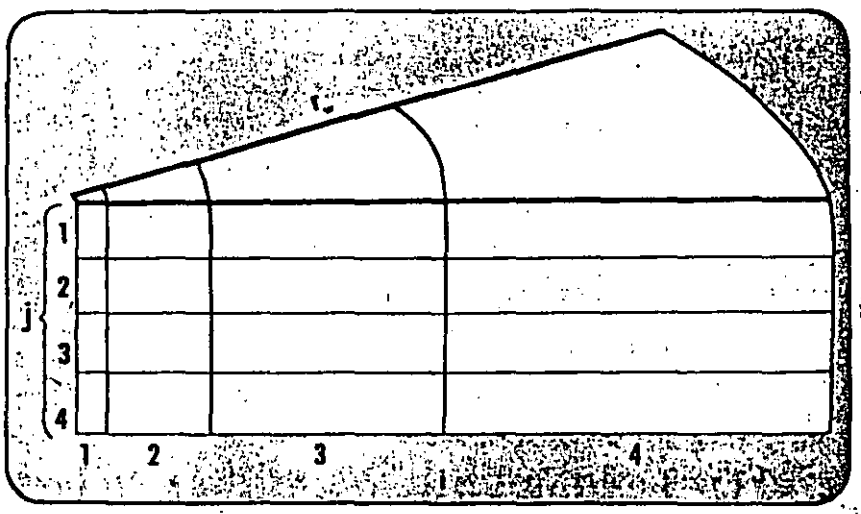

To solve this equation when k_x, k_y, μ, or h is not constant, one must resort to finite-difference methods. This equation can be written in finite-difference form as:

$$\frac{1}{\Delta x_j}\left[\left(\frac{k_x h}{\mu}\right)_{i,j+1/2}\frac{(p_{i,j+1}-p_{i,j})}{\Delta x_{j+1/2}}-\left(\frac{k_x h}{\mu}\right)_{i,j-1/2}\frac{(p_{i,j}-p_{i,j-1})}{\Delta x_{j-1/2}}\right]+$$

$$\frac{1}{\Delta y_i}\left[\left(\frac{k_y h}{\mu}\right)_{i+1/2,j}\frac{(p_{i+1,j}-p_{i,j})}{\Delta y_{i+1/2}}-\left(\frac{k_y h}{\mu}\right)_{i-1/2,j}\frac{(p_{i,j}-p_{i-1,j})}{\Delta y_{i-1/2}}\right]-$$

$$q_{i,j}=(\phi ch)_{i,j}\frac{(p_{i,j,n+1}-p_{i,j,n})}{\Delta t} \quad (5)$$

The pressures on the left-hand side of Equation 5 may be taken at time level n+1 so that an implicit finite-difference scheme is used, and q is a source or sink term that represents a production or injection well.

A more accurate solution method would consist of solving for changes in pressure rather than actual pressures. Let $\epsilon = p_{n+1} - p_n$. Solve for p_{n+1} and substitute into Equation 5.

Result is in an equation containing p_n and ϵ with ϵ being the unknown variable.

A system of N simultaneous equations will be formed by writing Equation 5 about each node in the system and including the appropriate boundary conditions.

This system of equations may then be solved by several methods some of which are Gaussian elimination, alternating direction implicit, or successive over relaxation.[7]

The flow equations can also be written in a cylindrical-coordinate system—especially useful when studying single well problems. This gives the equation shown at the top of the next column.

$$\frac{1}{r}\frac{\partial}{\partial r}\left(r\frac{k_r}{\mu}\frac{\partial p}{\partial r}\right)+\frac{\partial}{\partial z}\left(\frac{k_z}{\mu}\frac{\partial p}{\partial z}\right)=\phi c\frac{\partial p}{\partial t} \quad (6)$$

This equation assumes angular symmetry about the well.

Equation 6 can be written in finite-difference form as it stands; however, the analytical solutions show that the pressure tends to vary exponentially with the distance from the well bore.

This indicates that in setting up the finite-difference grid the best results would be obtained using small increments of r around the well and letting the increment size increase logarithmically with the distance from the well. Doing this directly in terms of the radius, r, adds an unnecessary complication to the calculation. The same effect can be accomplished by making a logarithmic transformation to the space dimension, r.

Let

$$u = \ln (r/r_w)$$

or

$$e^u = \frac{r}{r_w}$$

then

$$\frac{\partial p}{\partial r}=\frac{\partial p}{\partial u}\frac{\partial u}{\partial r}=\frac{\partial p}{\partial u}\frac{1}{e^u r_w}=\frac{1}{r}\frac{\partial p}{\partial u} \quad (7)$$

making this substitution

$$\frac{\partial}{\partial u}\left(\frac{k_r}{\mu}\frac{\partial p}{\partial u}\right)+e^{2u}r_w^2\frac{\partial}{\partial z}\left(\frac{k_z}{\mu}\frac{\partial p}{\partial z}\right)=e^{2u}r_w^2\,\phi c\frac{\partial p}{\partial t} \quad (8)$$

This equation can be expanded in finite-difference form. Fig. 1 shows a graphical layout of the finite-difference grid.

In finite-differences form, Equation 8 becomes

$$\frac{1}{\Delta u_j}\left[\left(\frac{k_r}{\mu}\right)_{i+1/2,j}\frac{(p_{i+1,j}-p_{i,j})}{\Delta u_{i+1/2}}-\left(\frac{k_r}{\mu}\right)_{i-1/2,j}\frac{(p_{i,j}-p_{i-1,j})}{\Delta u_{i-1/2}}\right]+$$

$$\frac{1}{\Delta z_j}(e^{2iu}r_w^2)\left[\left(\frac{k_z}{\mu}\right)_{i,j+1/2}\frac{(p_{i,j+1}-p_{i,j})}{\Delta z_{j+1/2}}-\left(\frac{k_z}{\mu}\right)_{i,j-1/2}\frac{(p_{i,j}-p_{i,j-1})}{\Delta z_{j-1/2}}\right]-q_{i,j}=$$

$$e^{2iu}r_w^2(\phi c)_{i,j}\frac{(p_{i,j,n+1}-p_{i,j,n})}{\Delta t} \quad (9)$$

The logarithmic transformation allows for a logarithmic variation in increment size in the radial direction if Δu is chosen as constant. That is, the increments are small around the well bore where the changes in the pressure surface are the greatest and they are large at large distances from the well where the pressure changes are small.

Boundary conditions. Boundary conditions and an initial condition are needed to solve the finite-difference equations. An initial condition generally applied is that the pressure distribution at time equal to zero is specified. The boundary conditions most often used are either no flow or constant pressure at the boundaries.

The rate q may be treated as a source term or as a boundary condition. If treated as a boundary condition in radial coordinates it reads

$$q = -2\pi r_w h\frac{k}{\mu}\frac{dp}{dr}$$

In equation form the initial conditions read

$$\text{when } t = 0 \qquad p = p_{orig},$$

where p_{orig} is a specified pressure and could be different for different points.

For a no-flow boundary between nodes I and I-1, the boundary condition reads

$$\frac{p_I - p_{I-1}}{\Delta x} = 0$$

A constant pressure boundary condition between nodes I and I-1 is given by

$$p_I = \text{constant}.$$

Example. A major application of the two-dimensional single-phase flow system is front tracking.[11] In front tracking we follow the path a droplet of fluid follows when traveling from injection to production well. In the single-phase application the mobility ratio is assumed equal to one.

First we establish the potential distribution throughout the field. This is accomplished by solving the Equation 4 with the right-hand side equal to zero. Finite differences are applied according to a two-dimensional grid laid over a field as shown in Fig. 2. Each node will be assigned a value for

h, formation thickness

ϕ, porosity

k_x, permeability in the x direction

k_y, permeability in the y direction

Δx, Δy, grid dimensions.

Production and injection rates are established for each node representing a well. Where steady state applies, the total injection minus production for the field should be zero.

After the potential distribution has been established, we follow the advance of a point located on the interface between the displacing and displaced phases. We start the tracking procedure by assigning initial positions around the injection wells. Fig. 3 shows the location of a well in a grid and the initial position of the front. Usually anywhere from 40 to 100 points are used. Each of these points is assigned an x and y coordinate.

For each grid point, velocity in both the x and y directions is calculated as follows:

$$v_{x,i,j} = (p_{i+1/2,j} - p_{i-1/2,j})\left(\frac{k_x}{\Delta x \phi S_m}\right)_{i,j} \frac{1}{\mu}$$

$$v_{y,i,j} = (p_{i,j+1/2} - p_{i,j-1/2})\left(\frac{k_y}{\Delta y \phi S_m}\right)_{i,j} \frac{1}{\mu}$$

where S_m is the mobile fluid saturation which is equal to one minus residual water saturation minus residual oil saturation.

Next, for each tracking point, the x and y velocities are determined by (bilinear) interpolation between velocities at the (four) surrounding nodes. Next, tracking-point locations are obtained from

$$x_{n+1} = x_n + v_{x,n}\,\Delta t$$

$$y_{n+1} = y_n + v_{y,n}\,\Delta t$$

Fig. 4 shows the flood front at various time increments in a field having three injection and four producing wells.

Fig. 2

Reservoir grid

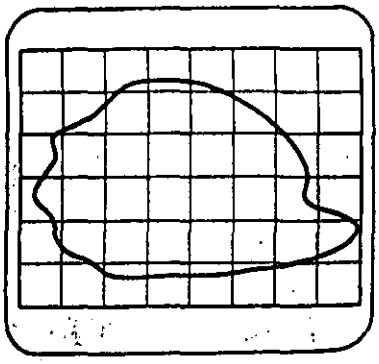

Fig. 3

Well and flood front

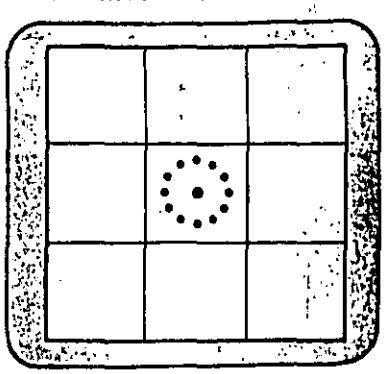

Fig. 4

Flood fronts at various times

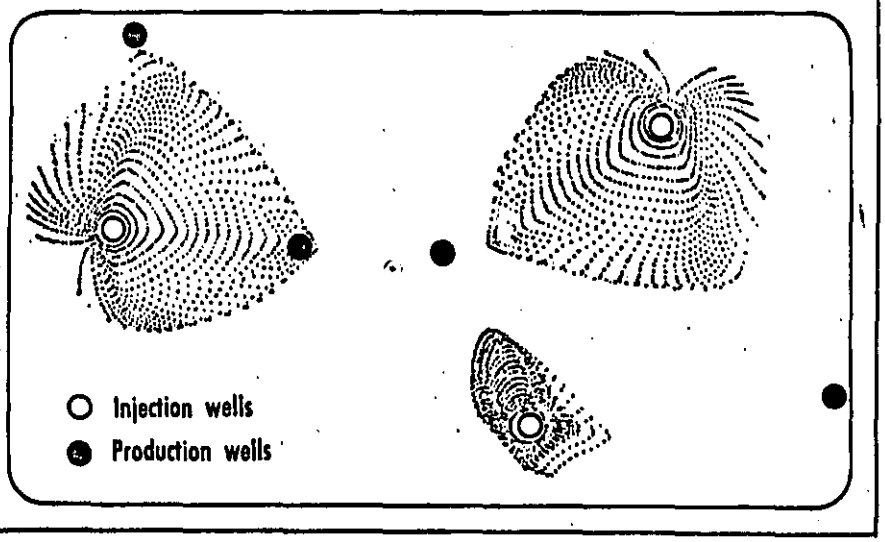

Use of radial form. In the evaluation of transient tests in wells containing radial and vertical permeability variations the reservoir and well system may be represented by the radial form of the flow equations. In this manner it is possible to calculate typical drawdown curves for radial discontinuities.[8] Or by changing the permeability and porosity values for various finite-difference blocks one can eventually obtain a match between calculated and observed values on tests.[10] These techniques have also been applied to studies where fluid viscosities are functions of flow rates through porous media.[9]

References

1. van Poollen, H. K., Bixel, H. C., and Jargon, J. R., "Single-phase fluid-flow equation," OGJ, Aug. 18, 1969, p. 94.

2. Polubarinova-Kochina, P. Ya., "Theory of ground-water movement," translated from the Russian by J. M. R. DeWeist, Princeton University Press, Princeton, N.J., (1962) 549.

3. van Everdingen, A. F., and Hurst, W., "The application of the Laplace transformation to flow problems in reservoirs," Trans. AIME, 1949, 186, 305-324.

4. Hurst, William, "Interference between oil fields," Trans. AIME, 1960, 219, 175.

5. Larkin, Bert K., "Solution to the diffusion equation for a region bounded by a circular discontinuity," Society of Petroleum Engineers Journal, 1963, 113.

6. Bixel, H. C., Larkin, B. K., and van Poollen, H. K., "Effect of linear discontinuities on pressure build-up and drawdown behavior," JPT, Aug. 1963, 885-895.

7. van Poollen, H. K., Bixel, H. C., and Jargon, J. R., "Reservoir modeling—5: Implicit finite difference approximations," OGJ, Jan. 5, 1970.

8. Bixel, H. C., and van Poollen, H. K., "Pressure drawdown and buildup in the presence of radial discontinuities," SPEJ, Sept. 1967, 301.

9. Jargon, J. R., and van Poollen, H. K., "Steady-state and unsteady-state flow of non-Newtonian fluids through porous media," Society of Petroleum Engineers Journal, Mar. 1969, 89-98.

10. Brill, J. P., Bourgoyne, A. T., and Dixon, T. N., "Numerical simulation of drill-stem tests as an interpretation technique," JPT, Nov. 1969, p. 1413.

11. McCarty, D. G., and Barfield, E. C., "The use of high-speed computers for predicting flood-out patterns," Petroleum Transactions AIME, Vol. 213, 1958, p. 139.

Single-phase gas flow

UNSTEADY-STATE gas flow through reservoirs gives rise to nonlinear partial differential equations which cannot be solved by analytical methods.

The need for treating the nonlinear terms in a rigorous manner rather than making simplifying assumptions means we must solve the gas-flow equations by finite-difference methods.

One of the first papers published on the numerical solutions of gas flow appeared in 1952.[1] Since that time many papers have been published covering nearly every possible phase of gas-reservoir production. These include everything from the planning and operation of multiwell reservoirs and gas-storage reservoirs to the study of single-well problems. The single-well problems studied include pressure buildup and drawdown behavior and the effects of darcy vs. non-darcy flow.

Development of equations. Several approaches are available for single-phase gas-flow through porous media. One is to formulate the gas-flow equation in terms of gas pressure. This may be done for either an ideal gas or a real gas. Darcy flow is assumed to be valid.

Ideal gas. The equation for ideal gas flow is[2]

$$\frac{\partial}{\partial x}\left(\frac{k}{\mu}\frac{\partial p^2}{\partial x}\right)+\frac{\partial}{\partial y}\left(\frac{k}{\mu}\frac{\partial p^2}{\partial y}\right)=2\phi\frac{\partial p}{\partial t} \quad (1)$$

where the porosity, ϕ, is taken to be independent of pressure.

Expanding in finite differences

$$\frac{1}{\Delta x_j}\left[\left(\frac{k}{\mu}\right)_{i,j+1/2}\frac{p^2_{i,j+1}-p^2_{i,j}}{\Delta x_{j+1/2}}-\left(\frac{k}{\mu}\right)_{i,j-1/2}\frac{p^2_{i,j}-p^2_{i,j-1}}{\Delta x_{j-1/2}}\right]$$

$$+\frac{1}{\Delta y_i}\left[\left(\frac{k}{\mu}\right)_{i+1/2,j}\frac{p^2_{i+1,j}-p^2_{i,j}}{\Delta y_{i+1/2}}-\left(\frac{k}{\mu}\right)_{i-1/2,j}\frac{p^2_{i,j}-p^2_{i-1,j}}{\Delta y_{i-1/2}}\right]$$

$$=2\phi_{i,j}\frac{p_{i,j,n+1}-p_{i,j,n}}{\Delta t} \quad (2)$$

The implicit approximation is assumed so that the pressures appearing on the left-hand side of Equation 2 are taken at time step n+1. This equation is nonlinear in pressure.

To obtain a solution, the p^2 term must be linearized. The nonlinear terms are all present as differences of the form

$$p^2_m-p^2_{m-1}$$

Bruce, Peaceman, Rachford and Rice[1] tried three methods of factoring this term. They are as follows.

$$\begin{aligned}p^2_m-p^2_{m-1}&=p^*_m\,p_m-p^*_{m-1}\,p_{m-1}\\ p^2_m-p^2_{m-1}&=(p^*_m+p^*_{m-1})(p_m-p_{m-1})\\ p^2_m-p^2_{m-1}&=(p^*_m-p^*_{m-1})(p_m+p_{m-1})\end{aligned} \quad (3)$$

Equation 2 becomes linear when one of the above expansions is substituted for the pressure-squared differences.

Here an iterative-type solution is required and the p^* term is the pressure at the last iterate level. The first method of factoring may diverge or converge slowly; the second method generally converges rapidly; and the third method diverges rapidly.

Another method by which Equation 2 could be

linearized is to expand p^2 in a Taylor's series. Then

$$p^2 = (p^*)^2 + (p-p^*)\,2p^*$$

$$\text{or } p^2 = -(p^*)^2 + 2p^*p \qquad (4)$$

where p^* again refers to the pressure at the last iterate level.

Real gas

The equation for flow of a real gas can be written as

$$\frac{\partial}{\partial x}\left(\frac{k}{\mu Z}\frac{\partial p^2}{\partial x}\right) + \frac{\partial}{\partial y}\left(\frac{k}{\mu Z}\frac{\partial p^2}{\partial y}\right) = 2\phi\frac{\partial(p/Z)}{\partial t} \qquad (5)$$

The left-hand side of this equation can be expanded in finite-difference form as previously shown with the exception that we now have the coefficient $(k/\mu Z)$ appearing instead of (k/μ), where Z is the gas deviation factor.

Now, the right-hand side of Equation 5 is somewhat different, as the derivative of (p/Z) with respect to time is present. This term can be expanded as follows

$$\frac{\partial(p/Z)}{\partial t} = \frac{1}{Z}\frac{\partial p}{\partial t} + p\frac{\partial(1/Z)}{\partial t}$$

or in finite-difference form

$$\frac{\partial(p/Z)}{\partial t} = \frac{1}{Z_{n+1}}\frac{(p_{n+1}-p_n)}{\Delta t} + p_n\frac{[(1/Z)_{n+1}-(1/Z)_n]}{\Delta t} \qquad (6)$$

Since we are solving for p_{n+1}, we cannot know what the value of Z_{n+1} is. But since an iterative type of solution is being used, the Z_{n+1} can be taken as Z^*, the gas deviation factor at the latest iterate level. Then Z^* will be almost exactly equal to Z_{n+1} when the solution converges.

Real gas potential. Another approach to solve gas-flow problems has been to formulate the equations in terms of a real gas potential or pseudopressure.[3] The use of this pseudopressure simplifies Equation 5 by removing the non-linear pressure-squared term. Rewrite Equation 5 as

$$\frac{\partial}{\partial x}\left(\frac{k\,p}{\mu Z}\frac{\partial p}{\partial x}\right) + \frac{\partial}{\partial y}\left(\frac{k\,p}{\mu Z}\frac{\partial p}{\partial y}\right) = \phi\frac{\partial(p/Z)}{\partial t} \qquad (7)$$

and define the pseudopressure as

$$m(p) = 2\int_{p_m}^{p}(p/\mu Z)\,dp \qquad (8)$$

Then

$$\frac{\partial m}{\partial x} = \frac{\partial m}{\partial p}\frac{\partial p}{\partial x} = \frac{2p}{\mu Z}\frac{\partial p}{\partial x}$$

and

$$\frac{\partial m}{\partial t} = \frac{\partial m}{\partial p}\frac{\partial p}{\partial t} = \frac{2p}{\mu Z}\frac{\partial p}{\partial t} \qquad (9)$$

Now the right-hand side of Equation 7 can be written as

$$\phi\frac{\partial(p/Z)}{\partial t} = \phi\left(\frac{1}{Z}\frac{\partial p}{\partial t} + p\frac{\partial(1/Z)}{\partial t}\right)$$

$$= \phi\left(\frac{1}{Z} + p\frac{\partial(1/Z)}{\partial p}\right)\frac{\partial p}{\partial t}$$

$$= \phi\frac{p}{Z}\left(\frac{1}{p} - \frac{1}{Z}\frac{\partial Z}{\partial p}\right)\frac{\partial p}{\partial t} \qquad (10)$$

Substituting Equations 9 and 10 into Equation 7 and using the definition of the isothermal gas compressibility, $c_g = \frac{1}{p} - \frac{1}{Z}\frac{\partial Z}{\partial p}$, we obtain

$$\frac{\partial}{\partial x}\left(k\frac{\partial m}{\partial x}\right) + \frac{\partial}{\partial y}\left(k\frac{\partial m}{\partial y}\right) = \phi\mu c_g\frac{\partial m}{\partial t} \qquad (11)$$

This equation can now be expanded in finite-difference form as

$$\frac{1}{\Delta x_i}\left[k_{i,j+1/2}\frac{m_{i,j+1}-m_{i,j}}{\Delta x_{j+1/2}} - k_{i,j-1/2}\frac{m_{i,j}-m_{i,j-1}}{\Delta x_{j-1/2}}\right]_{n+1}$$

$$+\frac{1}{\Delta y_i}\left[k_{i+1/2,j}\frac{m_{i+1,j}-m_{i,j}}{\Delta y_{i+1/2}} - k_{i-1/2,j}\frac{m_{i,j}-m_{i-1,j}}{\Delta y_{i-1/2}}\right]_{n+1}$$

$$= (\phi\mu c_g)_{i,j,n+1}\frac{(m_{i,j,n+1}-m_{i,j,n})}{\Delta t}$$

An iterative-type solution is still required if the pressure dependent coefficients μ and c_g are to be updated to the new time level. In addition, tables must be available so that pressure can be obtained from the pseudopressure, m. Al-Hussainy, Ramey, and Crawford[3] present tabulations of the real gas pseudopressure integrals vs. pseudoreduced pressure so that the actual pressures can be obtained.

References

1. G. H. Bruce, D. W. Peaceman, H. H. Rachford, Jr., and J. D. Rice, "Calculations of unsteady-state gas flow through porous media," Trans. AIME, 198, 1963, p. 79.
2. H. K. van Poollen, H. C. Bixel, and J. R. Jargon, "Reservoir modeling—2: Single-phase fluid-flow equations," OGJ, Aug. 18, 1969, p. 94.
3. R. Al-Hussainy, H. J. Ramey, Jr., and P. B. Crawford, "The flow of real gases through porous media," JPT, May 1966, p. 624.

Here are fundamental equations for multiphase fluid flow

THE fundamental flow equations and their solutions constitute the heart of a fluid-flow simulation. A fundamental flow equation can be derived for each phase by combining the law of conservation of mass, the law of flow, and an equation of state which describes the pressure-volume-temperature behavior of the fluid.

Conservation of mass. The conservation of mass simply states that for a reservoir element (rate of mass flow out) = (rate of mass flow in) + (rate of mass production) = rate of mass depletion.

In other words, the material balance states that no mass can be gained or lost from the system. In differential equation form it reads

$$\frac{\partial}{\partial x}\left(\frac{v_{ix}}{B_i}\right) + \frac{\partial}{\partial y}\left(\frac{v_{iy}}{B_i}\right) + \frac{\partial}{\partial z}\left(\frac{v_{iz}}{B_i}\right) + Q_i = -\frac{\partial}{\partial t}\left(\frac{\phi s_i}{B_i}\right) \qquad (1)$$

where

v_i is the velocity of phase i

B_i is the formation volume factor of phase i

Q_i is the production rate per unit volume of phase i

ϕ is porosity

s_i is the saturation of phase i

t is time and

x, y, z are distances.

This equation is a slightly modified continuity equation[1] in that the units of mass are stock-tank barrels or standard cubic feet.

Although the procedure is not completely rigorous, Equation 1 can be written in another form by multiplying through the volume $\Delta z\,\Delta y\,\Delta z$. Then:

$$\frac{\partial}{\partial x}\left(\frac{q_{ixR}}{B_i}\right)\Delta x + \frac{\partial}{\partial y}\left(\frac{q_{iyR}}{B_i}\right)\Delta y + \frac{\partial}{\partial z}\left(\frac{q_{izR}}{B_i}\right)\Delta z + Q_i = -V_b\frac{\partial}{\partial t}\left(\frac{\phi s_i}{B_i}\right) \qquad (2)$$

where

q_{ixR} refers to the volumetric flow rate of phase i at reservoir condition

V_b is the bulk volume of rock in which flow takes place and

Q_i is the production rate.

Equation of flow. It may be assumed that miscible Darcy flow prevails. In equation form

$$q_{ix} = -\frac{A\,k\,k_{ri}}{\mu_i}\frac{\partial \Phi_i}{\partial x} \qquad (3)$$

where

k is the absolute permeability

k_{ri} is the relative permeability of phase i

μ is the viscosity of phase i

Φ is the potential of phase i

A is the cross-sectional area.

Equation of state. The equations of state describe the pressure-temperature-volume relationship. It may be assumed that flow is isothermal. Furthermore, it may be assumed that stock-tank densities of components remain constant. The pressure-volume relationships are the usual formation volume factor and solution-gas pressure relationships.

The following equations for oil, water, and gas can be derived.[2]

Oil:

$$\frac{\partial}{\partial x}\left(\frac{q_{oR}}{B_o}\right)\delta x + \frac{\partial}{\partial y}\left(\frac{q_{oR}}{B_o}\right)\delta y + \frac{\partial}{\partial z}\left(\frac{q_{oR}}{B_o}\right)\delta z + Q_o = -\frac{V_b \partial}{\partial t}\left(\frac{\phi S_o}{B_o}\right) \quad (4)$$

Water:

$$\frac{\partial}{\partial x}\left(\frac{q_{wR}}{B_w}\right)\delta x + \frac{\partial}{\partial y}\left(\frac{q_{wR}}{B_w}\right)\delta y + \frac{\partial}{\partial z}\left(\frac{q_{wR}}{B_w}\right)\delta z + Q_w = -\frac{V_b \partial}{\partial t}\left(\frac{\phi S_w}{B_w}\right) \quad (5)$$

Gas:

$$\frac{\partial}{\partial x}\left(\frac{q_{gR}}{B_g} + \frac{q_{oR}R_s}{B_o} + \frac{q_{wR}R_{sw}}{B_w}\right)\delta x + \frac{\partial}{\partial y}\left(\frac{q_{gR}}{B_g} + \frac{q_{oR}R_s}{B_o} + \frac{q_{wR}R_{sw}}{B_w}\right)\delta y + \frac{\partial}{\partial z}\left(\frac{q_{gR}}{B_g} + \frac{q_{oR}R_s}{B_o} + \frac{q_{wR}R_{sw}}{B_w}\right)\delta z + Q_g = -V_b \frac{\partial}{\partial t}\left(\phi\left[\frac{S_g}{B_g} + \frac{S_o R_s}{B_o} + \frac{S_w R_{sw}}{B_w}\right]\right) \quad (6)$$

where

R is the solution gas ratio.

All other terms were previously defined.

The fundamental flow equations are organized such that the first three terms describe flow in the x, y, and z direction; the fourth term is the production or injection term; and the right-hand side of the equation contains the compressibility and saturation terms.

The following auxiliary equations may be used to link these equations together and to allow expansion of terms.

Rock compressibility: The rock compressibility may be incorporated by stating that

$$\phi = \phi_{original}\,[1 + C_f\,(P - P_{original})] \quad (7)$$

where

ϕ is the porosity at pressure P (we shall use oil pressure)

$\phi_{original}$ is the porosity at the original pressure and

C_f is the rock (pore) compressibility.

Saturation:

$$S_o + S_w + S_g = 1 \quad (8)$$

Capillary Pressure:

$$p_g = p_o + p_{cgo}$$

$$p_w = p_o - p_{cow} \quad (9)$$

Darcy's Law:

$$q_{oR(x)} = -\frac{Akk_{ro}}{\mu_o}\frac{dp_o}{dx} + \rho_o\frac{dz}{dx}$$

$$q_{wR(x)} = -\frac{Akk_{rw}}{\mu_w}\frac{dp_w}{dx} + \rho_w\frac{dz}{dx}$$

$$q_{gR(x)} = -\frac{Akk_{rg}}{\mu_g}\frac{dp_g}{dx} + \rho_g\frac{dz}{dx} \quad (10)$$

Equations 7, 8, 9, and 10 can be substituted into Equations 4, 5, and 6 in various ways so that the unknowns are oil pressure, water pressure, gas pressure, etc., depending on the manner in which one desires to solve these equations. Of course, these equations must then be expanded in finite-difference form and a numerical method must be chosen by which to solve this system of equations.

These equations are nonlinear. The relative permeabilities and capillary pressures are func-

Fig. 1

Gross flow diagram

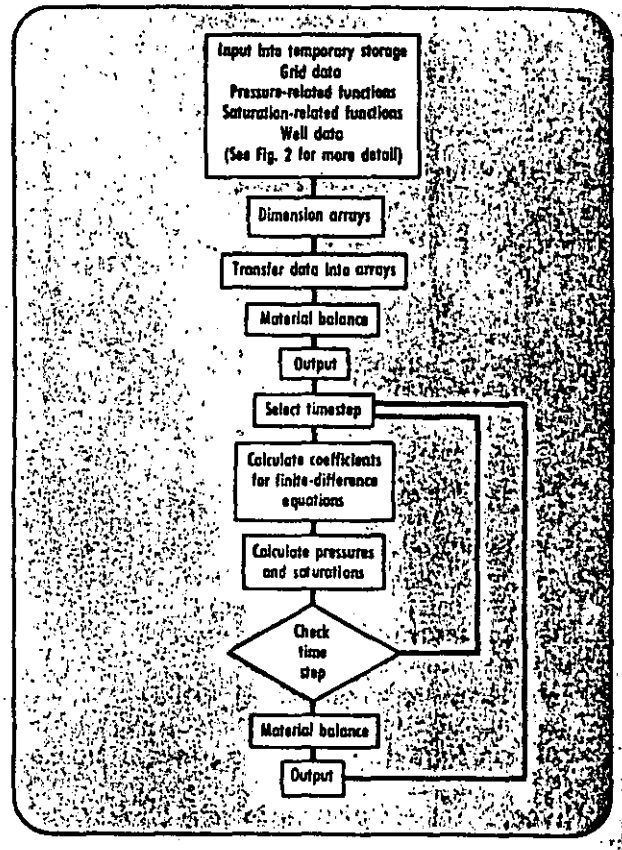

Fig. 2

Input into temporary storage

Grid data:
- Permeability, k
- Porosity, ϕ
- Thickness, h
- Elevation, z
- Dimensions, Δx, Δy, Δz
- Initial saturations, s_{wi}, s_{oi}, s_{gi}
- Initial pressure, P_{si}
- Rock compressibility, c_r

Pressure-related functions:
- Formation volume factors, B_o, B_w, B_g
- Fluid viscosities, μ_o, μ_w, μ_g
- Solution gas-liquid ratios, R_s, R_{sw}
- Fluid densities, ρ_o, ρ_w, ρ_g

Saturation-related functions:
- Relative permeabilities, k_{ro}, k_{rw}, k_{rg}
- Capillary pressures, P_{cow}, P_{cog}

Well data:
- Producing interval, Δh
- Production, injection rates, q_o, q_w, q_g
- Observed pressures, P

Fig. 3

Checks on time-step size

Time-step size control

Criteria:
- Saturation change
- Pressure change
- Saturation and pressure change
- Change in coefficient
- Rate change
- Material-balance error

tions of saturation and the formation volume factors, solution gas ratios, reservoir densities, and fluid viscosities are functions of pressure. Consequently, coefficients can be stated to be both pressure and saturation dependent.

Flow diagrams. In the following paragraphs some possible flow diagrams are given for the construction of a straightforward reservoir fluid-flow simulator.

First, all data are read into the model, Fig. 1. A more detailed description of the input data is given in Fig. 2 and Reference 3. Next, a material-balance calculation is performed which merely gives an account of fluids present.

A timestep size is selected, and the coefficients for the finite differences equations are then calculated.

So far, we have not discussed the exact form of the simultaneous set of multiphase flow equations. However, for the moment let it suffice to say that one can have a set of equations such that pressure and saturation can be solved simultaneously, or a set of equations permitting the calculation of pressures first and the saturations second. In either case, one has to calculate pressure and saturation-dependent coefficients. One may assume the coefficients to remain sufficiently constant during a timestep, use "implicit" coefficients by an extrapolation routine or iterate on the coefficients.

At the end of the timestep, it then becomes necessary to check if the timestep size was too large according to some predetermined criteria for maximum allowable changes.

If these criteria were not met the timestep size needs to be reduced and the calculation repeated. Otherwise, a new timestep may be selected and the series of calculations may be continued.

Fig. 3 shows more detail on the timestep check.

Criteria for time checks vary in different models. Sometimes it is considered that the saturation-dependent functions affect the coefficients to the greatest extent. This is true if pressure changes are moderate. Then a saturation change will suffice as a timestep check. However, in single-phase flow problems the pressure-dependent functions can be used to control the timestep size. In other problems both pressure and saturation-dependent functions affect the coefficients.

Maybe a more accurate check is the change in coefficients between start and end of a timestep. If changes are too large, the coefficients may be "updated" while repeating the timestep until coefficients, pressure solutions, and saturation solutions have converged.

The change in rate controls the timestep size. For example, a 100-day timestep satisfies all coefficient requirements. However, if the wells experience drastic monthly production changes, the timestep is limited by the production changes.

At the end of each timestep one should perform a check on the material balance. If losses or gains exceed a preset criteria, something may be in error, possibly an excessive timestep.

Another check is to calculate residuals to check the validity of the calculations.

This discussion gives some of the basic information needed to construct a reservoir fluid-flow simulator. The flow diagram presented is only one of many which could be used. The actual flow diagram used will depend on the formulation of the equation, the method of solution, and to some extent on the type of computer used. The equations are not shown in the final finite-difference form due to the length of such a presentation.

References

1. van Poollen, H. K., Bixel, H. C., and Jargon, J. R., "Reservoir Modeling—2: Single-phase fluid-flow equations," OGJ, Aug. 18, 1969.
2. Breitenbach, E. A., Thurnau, P. H., and van Poollen, H. K., "Inmiscible fluid flow simulator," SPE preprint 2019, presented at symposium on numerical simulation, Dallas, Tex., Apr. 1968.
3. van Poollen, H. K., Bixel, H. C., and Jargon, J. R., "Reservoir Modeling—1: What it is, what it does," OGJ, July 28, 1969, p. 158.

Applications of multiphase immiscible fluid flow simulator

THE previous chapter of this manual[1] presented equations which describe the movement of oil, gas, and water in a porous media. That chapter also gave a flow diagram which can be used in the construction of a computer program to solve the flow equation. Applications of such a fluid-flow simulation program will now be given.

Reservoir modeling. Perhaps the greatest use that has been made of fluid-flow simulators has been in modeling the entire flow systems associated with an oil or gas reservoir.

Once a model of such a system has been established, it can be used to investigate various modes of production and select the most profitable

Table 1

Intermediate or final output of reservoir model

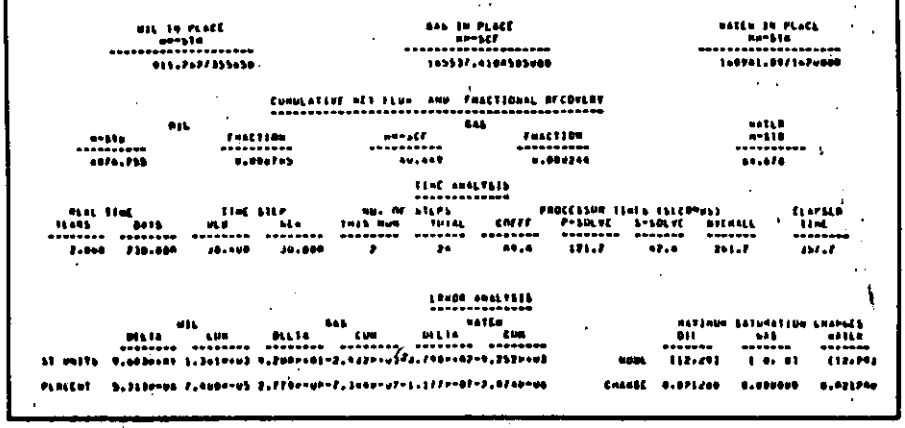

Figs. 1-4

Grid types

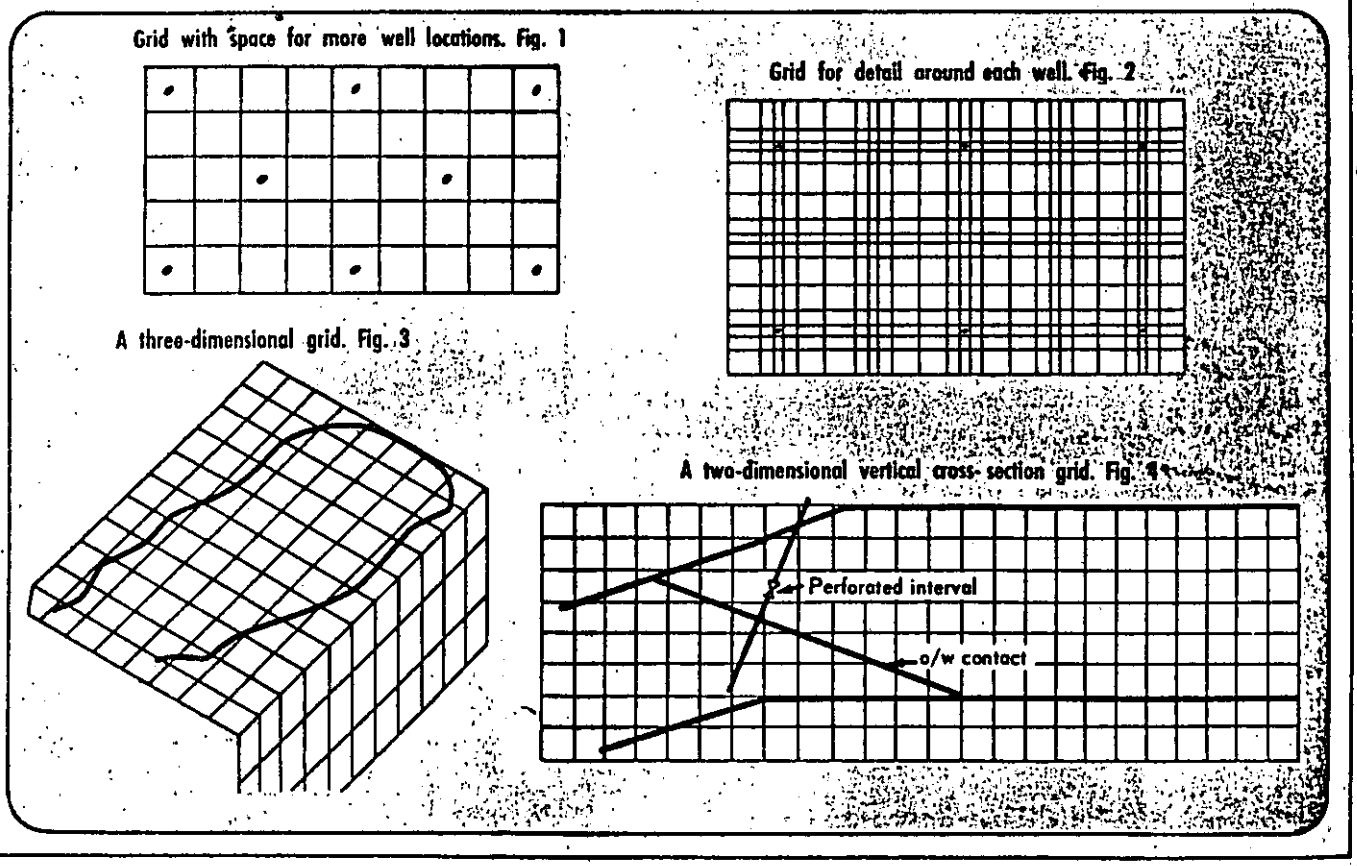

operating procedure for a particular reservoir.

The reservoir model itself consists of a set of data that describes the geometry of the flow system, its rock properties, the distribution of the fluids, and their PVT properties. A list of the necessary data is given in Reference 1.

After it has been determined that the necessary data are available, a finite-difference grid network is selected for the reservoir. The objectives of the study should be considered in selecting the grid.

For example, the grid shown in Fig. 1 could be used to study individual well performance and saturation distribution in fairly good detail. This grid provides for several empty grid blocks between well blocks.

This allows one to obtain some detail in the pressure and saturation distribution between injection and production wells. It also provides room to establish additional well locations that may be necessary in determining the optimum scheme for exploiting the reservoir.

Additional detail around the well can be obtained by selecting a grid such as that shown in Fig. 2. A grid such as this might be considered if it is desirable to know what will happen in an oil reservoir when the pressure goes below the bubble point in the area around a well.

However, one should keep in mind that the number of cells in a finite-grid system determines the number of equations to be solved in each time step; and the cost of a run is heavily dependent upon the number of equations solved per time step.

The gross behavior of a reservoir can be studied by selecting a coarse grid. In this case, several wells may be included in one well block. For example, this type of grid could be used in a field with an edgewater drive to study the pressure and production behavior of the field under various modes of operation; or it might be used to estimate flow across lease lines.

In selecting the grid, it will be necessary to decide if the question to be answered requires the use of a three-dimensional model; or if a pseudo third dimension[2,3] can be used in a two-dimensional model.

An example of a three-dimensional grid is shown in Fig. 3. This type of grid is a definite possibility in conducting a study where significant movement of fluids in the vertical direction is expected. An example of such a study would be to determine the degree of gas override in a project using gas injection for pressure maintenance.

However, a less-expensive solution to this problem could be obtained by using a two-dimensional vertical cross section. A grid for this type of study is shown in Fig. 4.

Another approach to this problem could be an initial feasibility run using a one-dimensional grid, then additional runs in two and three dimensions if refinement of the answer is believed necessary.

Fig. 5

Pressure vs. time plots

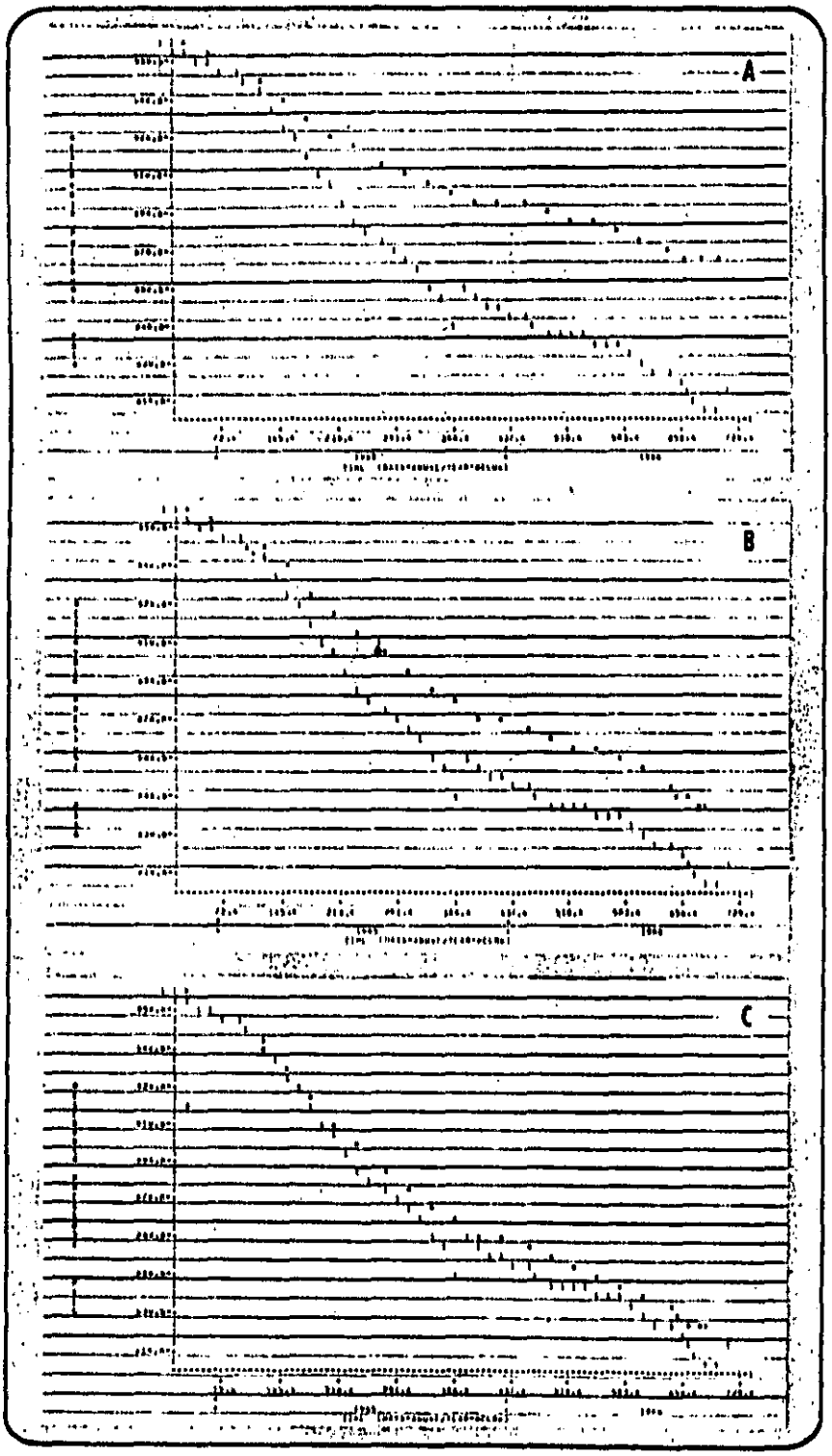

Well report, history-matching

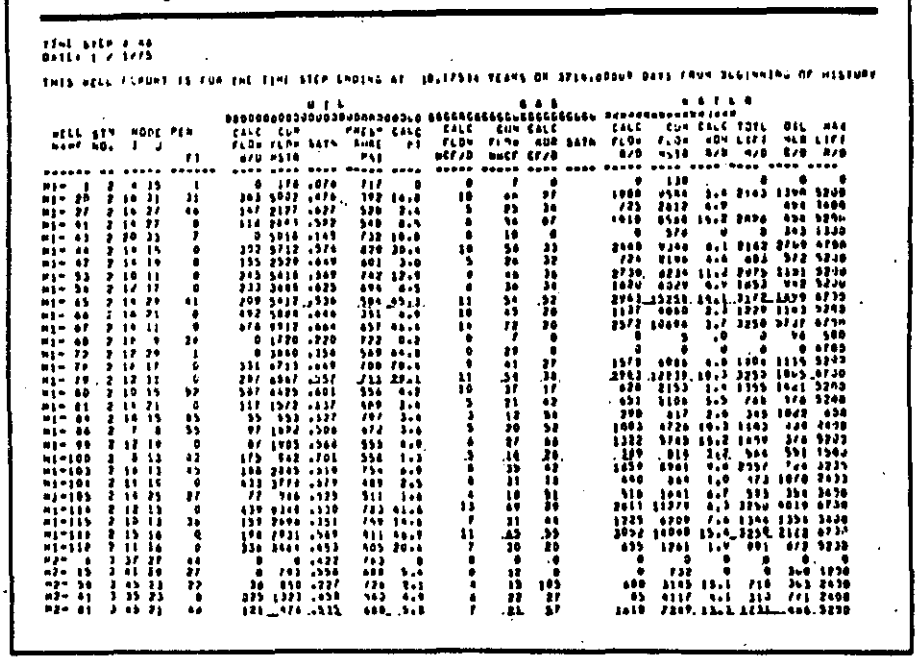

Fig. 6

Pressure performance of Well A.

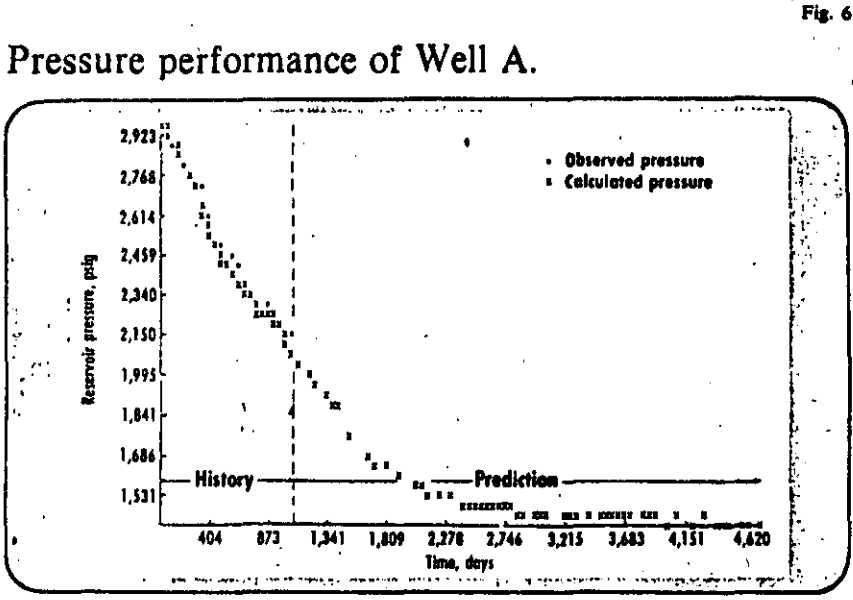

Fig. 7

Field performance under depletion and waterflooding

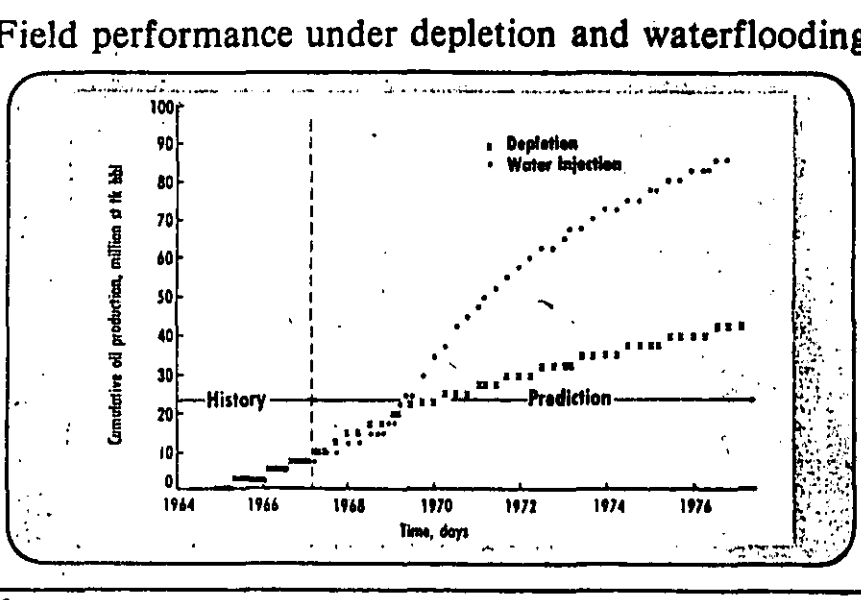

The importance of this example is not the actual grid selection, but to show that several selections are possible and that these selections are problem dependent.

History matching. Once the grid has been selected and the data have been digitized, a run is made to determine if the model is capable of computing the past behavior of the reservoir.

If it is not, the data are adjusted and additional runs are made until a satisfactory match between computed and observed values are obtained. This procedure is called "history matching" and is necessary to obtain a good mathematical representation of the reservoir.

History matching usually consists of supplying each well in the simulator with the actual oil production or injection rate experienced by its counterpart in the real world and comparing the values of pressure, gas/oil ratio and water/oil ratio calculated by the simulator with those observed during the production history of the well.

The calculated pressure for a well is the pressure at the node in which the well is located. This pressure will not be the same as the pressure measured from a pressure-buildup test taken on a well that is normally flowing. Therefore, it is necessary to calculate a pressure from the buildup curve which is compatible with the pressure calculated for the well node.

Such a pressure has been referred to as a dynamic pressure.[2] The dynamic pressure can be read from the buildup curve at a shut-in time which is calculated from the equation:

$$\theta = \frac{\phi \mu c r_b^2}{15.822 \times 10^{-4} k}$$

where

θ = the required shut-in time (hr)
ϕ = fractional porosity
μ = viscosity (cp)
c = total compressibility (psi^{-1})
k = permeability (md)
r_b = equivalent block radius (ft)

This equation is derived in Reference 2 where it is pointed out that the equation assumes the area is of uniform thickness, is in single-phase flow, and that the porosity, compressibility, and

permeability are constant. These assumptions hold true when considering only the well node. The possible exception is the assumption of single-phase flow.

The observed pressures can then be used as input to an auxiliary program which plots both the observed and calculated pressures vs. time for comparison purposes. Figs. 5a, b, and c are a series of pressure-vs.-time plots obtained for a well during a history-matching study.

These figures show both the observed pressures, 1, and the calculated pressures, x, and represent results from three different matching runs. In each of the runs, reservoir parameters had been adjusted before making the run. Fig. 5c was considered to be a good match on pressure.

Similar plots of water/oil ratio and gas/oil ratios vs. time are made for calculated and observed values of these parameters.

The set of data which produces a satisfactory history match constitutes the reservoir model. This model can then be used to predict the behavior of the reservoir under various types of operations.

Use of the model in prediction. Rules for establishing well rates during the prediction phase have to be set down. The rules usually specify how the production or injection rate for each well is to be calculated, i.e. from the PI, maximum efficient rate, pump capacity, etc., and can be as simple or complicated as deemed necessary.

This rate generator is an integral part of the simulation program. A new rate generator may have to be programmed into the simulator if the rules for a particular study are not covered by the general subroutine presently in the computer program.

The work from this point on consists of selecting well sites for proposed injection or production wells, establishing these wells in the model, and analyzing the results of the run. Figs. 6 and 7 are examples of the results that might be expected from this type of study.

Other applications. Fluid-flow simulation programs are capable of many applications other than modeling reservoirs and their behavior. The programs solve the flow equations for oil, gas, and water in up to three dimensions and apply to most problems involving any or all of these phases and dimensions.

Some problems may take a special-purpose simulation program for their solution. Water and gas coning is such a problem. Nevertheless, a multitude of applications exist for which such a special-purpose program is not needed. Some examples of those applications are:

Fig. 8

Grid for segment of a reservoir

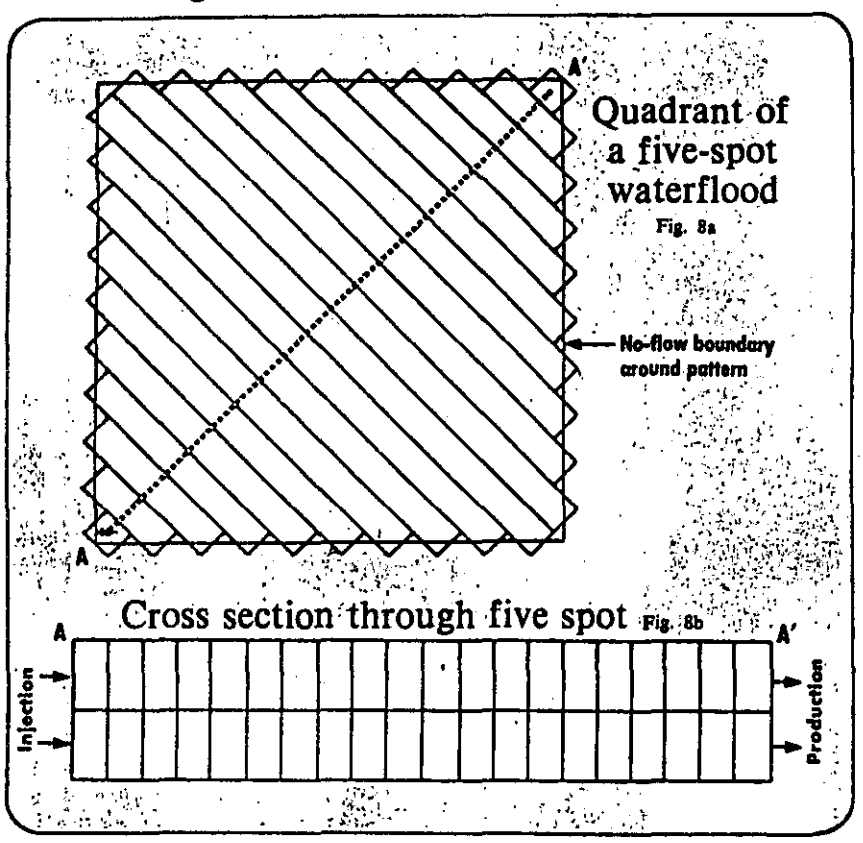

Figs. 9-10

Array of oil saturations

```
 TIME STEP #   1

    *     1     2     3     4     5     6     7     8     9    10    11    12    13    14    15    16    17    18    19
    1 0.622 0.650 0.650 0.650 0.650 0.650 0.650 0.650 0.650 0.650 0.650 0.650 0.650 0.650 0.650 0.650 0.650 0.650 0.650
    2 0.537 0.650 0.650 0.650 0.650 0.650 0.650 0.650 0.650 0.650 0.650 0.650 0.650 0.650 0.650 0.650 0.650 0.650 0.650

    *    20
    1 0.650
    2 0.650

 TIME STEP #  55

    *     1     2     3     4     5     6     7     8     9    10    11    12    13    14    15    16    17    18    19
    1 0.222 0.310 0.381 0.448 0.510 0.619 0.650 0.650 0.650 0.650 0.650 0.650 0.650 0.650 0.650 0.650 0.650 0.650 0.650
    2 0.157 0.180 0.198 0.202 0.213 0.230 0.243 0.281 0.310 0.343 0.373 0.400 0.421 0.437 0.447 0.452 0.459 0.471 0.495

    *    20
    1 0.650
    2 0.634
```

1. Evaluation of flooded patterns
2. Gravity drainage
3. Bottomwater and edgewater drive
4. Modeling small-scale laboratory flow experiments
5. Gravity drainage

These are only a few of the problems that can be studied using small models. The model will usually be a small segment of the reservoir or a simple cross section of a representative portion of the reservoir.

Approximate data can usually be used in these studies. Several runs can be made varying the data within certain bounds since the models are small and inexpensive to run. From this type of study, it is possible to learn what might be expected from waterflooding a field, for example.

An example grid for such is shown in Fig. 8. It was desired to learn to what extent cross flow would be a factor in waterflooding a reservoir which had two zones of highly different permeabilities.

The permeability of the bottom layer was approximately 10 times greater than that of the top layer, and it was assumed that the zones were in complete vertical communication. A two-dimensional vertical cross section of a quadrant of a repeated five-spot was modeled.

Fig. 9 is a printout of the saturation distribution between the left-side injection well and the right-hand-side production well at the end of 5 days of injection.

Fig. 10 shows the saturation distribution at water breakthrough into the production well and shows the rapid movement of the water through the lower, more permeable zone.

Since this model was small and ran rapidly on the computer, it would be possible to make several runs varying the amount of vertical communications, the injection rate, the production rate, etc.

A good deal of insight into the mechanisms that are controlling a reservoir behavior can be gained from this type of study.

Simulation program output. Considerable amount of thought should be given to designing the output routine of the fluid-flow simulation program. This type of program generates a great deal of data that is valuable to both the field engineer and the research scientist.

For example, the field engineer is interested in determining the oil, gas, and water in place, the cumulative production of each phase, and the fractional recovery to date.

The research scientist, on the other hand, is interested in output that will let him determine how the program is functioning on a particular problem. His interest would be in learning how much computer time is consumed in completing a time step, the material-balance error during the last time step, and where the maximum saturation change occurred since this is controlling the size of the time step. An example of such an output format is given in Table 1.

Table 3

Well report, prediction

TIME STEP # 48
DATE: 1 / 1/75

THIS WELL REPORT IS FOR THE TIME STEP ENDING AT 10.37536 YEARS OR 3719.00000 DAYS FROM BEGINNING OF HISTORY

WELL NAME	STN NO.	NODE I	NODE J	PEN FT	OIL CALC FLOW B/D	OIL CUM FLOW MSTB	OIL SATN	PRESS AVRG PSI	PRESS CALC PI	GAS CALC FLOW MCF/D	GAS CUM FLOW MMCF	GAS CALC CUM CF/B	GAS SATN	WATER CALC FLOW B/D	WATER CUM FLOW MSTB	WATER CALC WCN B/D	WATER TOTL LIFT H/D	OIL WLR B/D	OIL WAC LIFT B/D
W1= 1	2	4	15	1	0	170	.076	717	0	0	7	0		0	130		0	0	0
W1= 20	2	14	31	31	363	5032	.476	192	10.6	10	66	27		1980	9566	5.5	2163	1349	5230
W1= 27	2	16	27	46	147	2127	.427	526	2.4	5	25	34		725	2812	4.9		498	1480
W1= 41	2	16	27	0	110	2843	.522	540	6.5	8	74	67		1910	8568	16.2	2494	434	5294
W1= 43	2	20	33	7	0	5018	.149	732	10.8	0	10	0		0	574	0	0	343	1330
W1= 44	2	14	15	0	302	5712	.574	820	30.4	10	56	33		2460	9366	8.1	2162	2769	6750
W1= 47	2	16	19	0	155	2529	.469	601	3.0	5	26	32		724	2196	4.6	885	572	5240
W1= 53	2	10	11	0	245	5819	.569	742	12.9	9	46	36		2730	8234	11.2	2475	1191	5210
W1= 56	2	12	17	0	233	3683	.425	694	6.5	8	34	34		1670	6529	4.9	1453	992	5200
W1= 65	2	14	29	41	299	5412	.538	504	9.53	11	54	32		2983	13258	15.1	3172	1699	6733
W1= 66	2	16	21	0	182	3868	.496	181	6.9	10	65	20		1137	4880	2.1	1228	1383	5263
W1= 67	2	18	11	0	676	9912	.664	657	80.6	14	72	20		2572	10696	3.7	3250	5727	6734
W1= 68	2	18	9	26	0	1720	.220	722	0.2	0	7	0		0	0	0	0	98	500
W1= 72	2	17	29	1	0	3449	.356	569	80.6	0	29	0		0	0	0	0	0	6703
W1= 77	2	14	17	0	331	4713	.449	700	70.4	9	61	27		1573	6036	4.4	1804	1185	5203
W1= 79	2	12	11	0	287	4847	.357	711	27.1	11	54	38		2393	12037	10.3	3252	1045	6730
W1= 80	2	10	15	52	587	4425	.401	554	4.2	10	37	17		628	2153	1.4	1355	1461	5263
W1= 81	2	14	21	0	117	1572	.437	489	3.4	5	21	42		651	2106	5.5	766	378	5240
W1= 84	2	18	15	45	55	553	.327	787	1.4	3	12	54		290	617	2.4	345	1042	630
W1= 86	2	7	8	55	97	1672	.506	672	3.6	5	20	52		1003	4726	10.3	1103	439	6030
W1= 98	2	12	19	0	87	1905	.566	553	6.9	6	37	68		1322	5765	15.2	1659	378	5203
W1=100	2	8	13	42	175	562	.701	558	1.3	3	14	24		189	818	2.2	566	538	1964
W1=103	2	16	13	45	168	2845	.519	754	6.9	8	35	42		1659	6981	9.6	2757	748	5235
W1=104	2	19	15	0	633	3777	.679	669	2.5	8	31	19		640	864	1.0	473	1078	2433
W1=105	2	14	25	27	77	746	.525	911	1.4	4	18	51		518	1641	0.7	583	356	2630
W1=114	2	12	13	0	439	8348	.530	783	4.6	13	69	29		2611	11279	6.3	3250	4019	6730
W1=115	2	10	13	36	159	2696	.351	759	14.4	7	31	44		1225	6209	7.6	1346	1356	3430
W1=116	2	15	16	0	198	7931	.569	611	46.9	11	63	55		3052	16000	15.4	3250	2162	6733
W1=118	2	11	16	0	336	3684	.453	605	20.6	7	30	20		655	1761	1.9	991	672	5233
W2= 6	3	37	27	44	0	0	.422	763	0	0	0	0		0	0	0	0	0	0
W2= 15	3	41	29	27	0	193	.558	680	5.4	0	12	0		0	732	0	0	340	1250
W2= 58	3	45	23	22	36	858	.227	726	3.1	4	15	105		680	3145	19.1	718	343	2430
W2= 81	3	35	23	0	225	1323	.458	563	6.9	6	22	27		85	4117	0.1	313	771	2400
W2= 84	3	45	21	46	121	976	.535	690	5.5	7	21	57		1410	7269	11.1	1231	486	5250

Fig. 11

Saturation shadowgraph

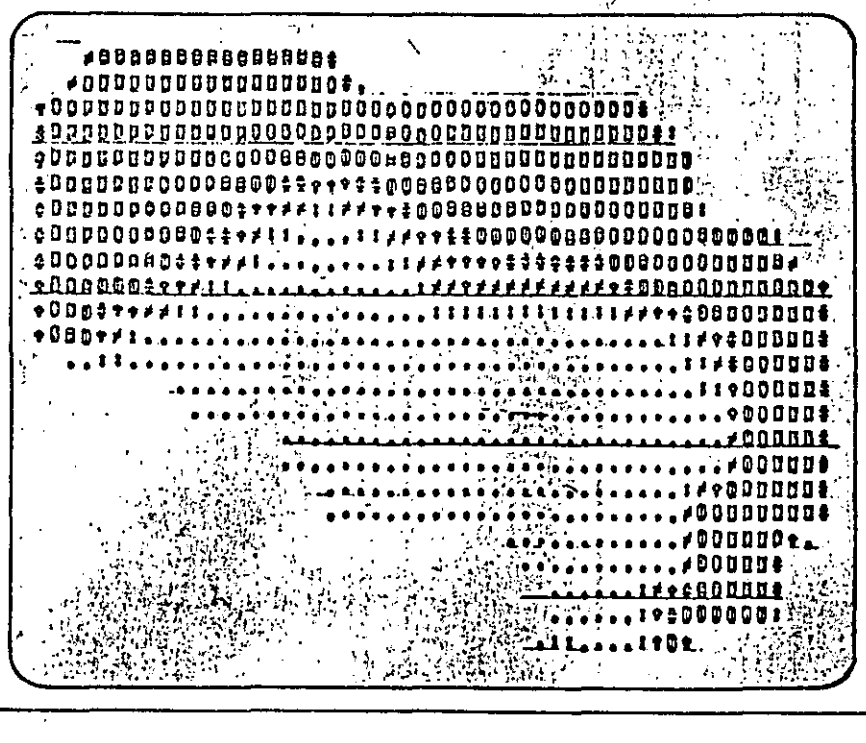

Table 2 is an example of a well report used during matching. The station number refers to the lease in which the well is located for oil-accounting purposes; and the grid cell (I,J) is the location of the well in the computing grid.

Penetration (PEN) represents the perforated interval. Under the major heading "oil" are the observed and calculated flow rates and the cumulative oil production. Both calculated and observed values are shown.

The saturation in the cell where the well is located is given along with the average oil pressure in that cell, corrected to datum, as indicated at the bottom of the table.

The calculated productivity index follows.

Similar well data are shown under the major headings for "gas" and "water."

The last column on this table shows the maximum lift, which is an indication of the pump size required.

Table 3 is similar to Table 2 except it shows a typical well report used during prediction. Only calculated values can be shown. The last three columns are worth special mention. The total life shows the total amount of oil plus water produced, where the "maxlift" is the maximum oil plus water that can be produced. The oil MER is the maximum oil rate the well can make, independent of lift restrictions.

Fig. 11 shows shadowgraph output of saturation. All other data may be shown in this form.

Fig. 12 shows a single well crossplot of observed and calculated pressures, and producing oil rates as functions of time.

Similar plots can be made for a field on a lease-by-lease basis. Fig. 13 is an example of cumulative oil production by layers and by field in a two-layer, three-dimensional study.

Fig. 12

Individual well plots

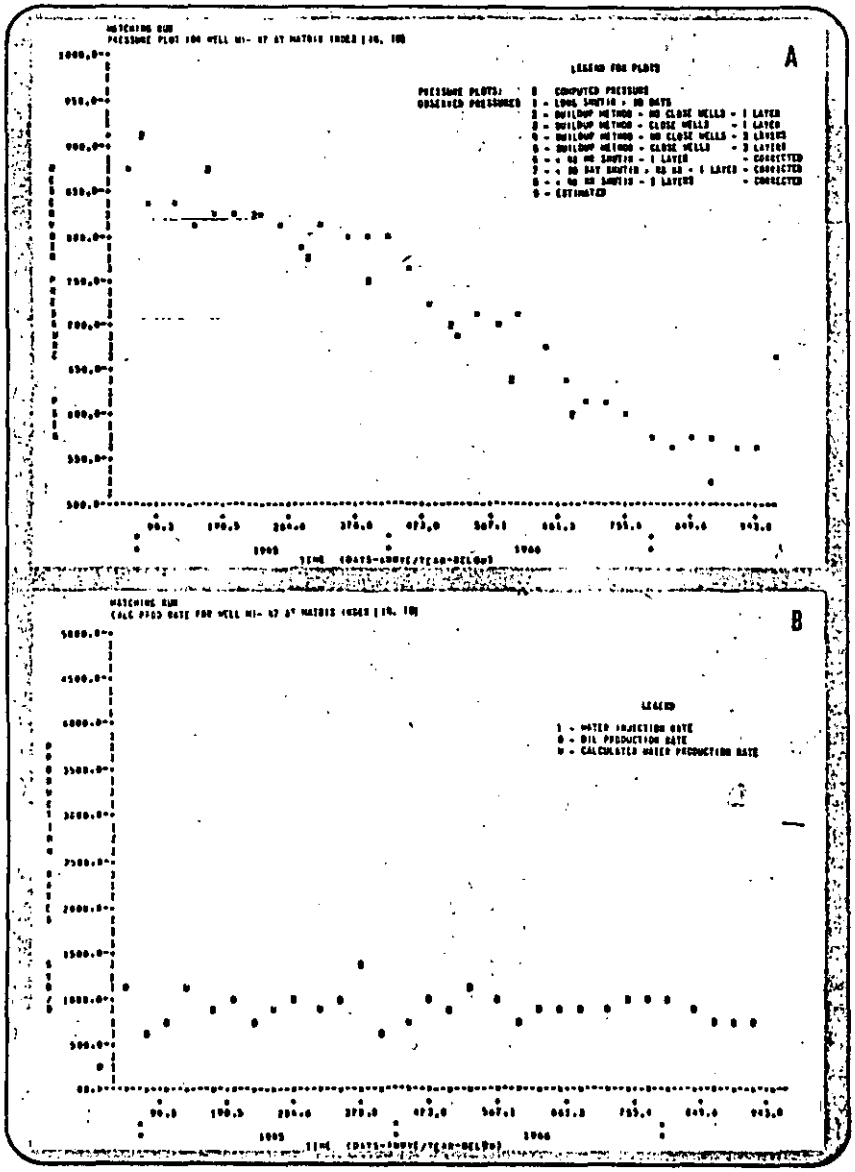

Fig. 13

Total field plot

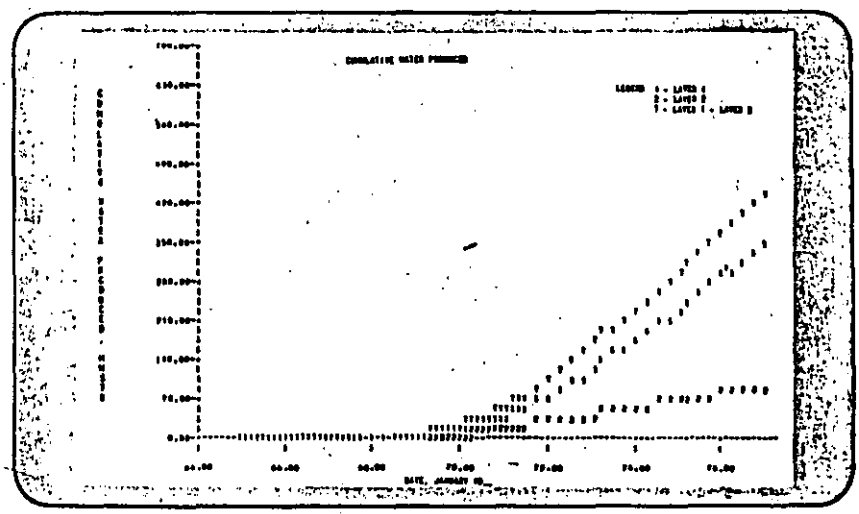

References

1. van Poollen, H. K., Bixel, H. C., and Jargon, J. R., "Reservoir Modeling—9: Multiphase immiscible fluid flow simulation," The Oil and Gas Journal, May 11, 1970, p. 72.

2. Breitenbach, E. A., Thurnau, D. H., and van Poollen, H. K., "Treatment of individual wells and grids in reservoir modeling," (Tech. Paper) SPEJ, Dec. 1968, p. 341.

3. Coats, K. H., Nielson, R. L., Terhune, M. H., and Weber, A. G., "Simulation of three dimensional, two-phase flow in oil and gas reservoirs," Soc. Pet. Eng. J., Dec. 1967, pp. 377-388.

Comparison of multiphase models

MANY different types of reservoir simulators can be constructed to study fluid-flow phenomena.

Three-phase, three-dimensional simulators are frequently constructed as the general-purpose reservoir problem solver.

This type of model can be used for making the large reservoir studies, cross-section studies, pilot waterflood studies—just about all problems where multiphase flow occurs, except for the cases where individual well problems must be studied.

Individual well-problem models, such as water or gas coning, try to simulate multiphase flow in the immediate vicinity of the well bore.

This requires very small grid sizes around the well bore, and, as a result, special techniques must be used to keep instabilities from developing in the calculations. Thus, special purpose models are constructed to study problems of this type.

The purpose of this article is to present a comparison of some of the types of three-phase reservoir simulators available and the problems encountered with certain of these models.

Three-phase simulators are generally classified in two categories: (1) The implicit pressure-explicit saturation method of solution, and (2) The simultaneous method of solution.

The simultaneous solution method can be broken into numerous categories, depending on which variables one wishes to find. The variables generally chosen are the pressure of the three phases, but one could also choose one or more saturations as the unknown variable.

In one dimension, the equations to be solved[1] are:

For oil:

$$\frac{\partial}{\partial x}\left[\frac{A_x k k_{ro}}{\mu_o B_o}\left(\frac{\partial p_o}{\partial x}+\rho_o\frac{\partial z}{\partial x}\right)\right]\delta x - Q_o = V_b\frac{\partial}{\partial t}\left(\frac{\phi S_o}{B_o}\right) \quad (1)$$

For water:

$$\frac{\partial}{\partial x}\left[\frac{A_x k k_{rw}}{\mu_w B_w}\left(\frac{\partial p_w}{\partial x}+\rho_w\frac{\partial z}{\partial x}\right)\right]\delta x - Q_w = V_b\frac{\partial}{\partial t}\left(\frac{\phi S_w}{B_w}\right) \quad (2)$$

For gas:

$$\frac{\partial}{\partial x}\left[\frac{A_x k k_{rg}}{\mu_g B_g}\left(\frac{\partial p_g}{\partial x}+\rho_g\frac{\partial z}{\partial x}\right)+\frac{A_x k k_{ro}}{\mu_o B_o}R_s\left(\frac{\partial p_o}{\partial x}+\rho_o\frac{\partial z}{\partial x}\right)+\frac{A_x k k_{rw}}{\mu_w B_w}R_{sw}\left(\frac{\partial p_w}{\partial x}+\rho_w\frac{\partial z}{\partial x}\right)\right]\delta x - Q_g - Q_o R_s - Q_w R_{sw}$$

$$= V_b\frac{\partial}{\partial t}\left[\phi\left(\frac{S_g}{B_g}+\frac{R_s S_o}{B_o}+\frac{R_{sw}S_w}{B_w}\right)\right] \quad (3)$$

Now, some means must be devised by which these three equations can be solved. First, expand the right-hand side of Equations 1, 2, and 3 as follows:

$$V_b\frac{\partial}{\partial t}\left(\frac{\phi S_o}{B_o}\right) = V_b\left[\left(\frac{\phi}{B_o}\right)_{n+1}\frac{\partial S_o}{\partial t}+S_{o,n}\frac{\partial(\phi/B_o)}{\partial t}\right] \quad (4a)$$

$$V_b\frac{\partial}{\partial t}\left(\frac{\phi S_w}{B_w}\right) = V_b\left[\left(\frac{\phi}{B_w}\right)_{n+1}\frac{\partial S_w}{\partial t}+S_{w,n}\frac{\partial(\phi/B_w)}{\partial t}\right] \quad (4b)$$

$$V_b\frac{\partial}{\partial t}\left(\phi\left[\frac{S_g}{B_g}+\frac{R_s S_o}{B_o}+\frac{R_{sw}S_w}{B_w}\right]\right) = V_b\left[\left(\frac{\phi}{B_g}\right)_{n+1}\frac{\partial S_g}{\partial t}+S_{g,n}\frac{\partial(\phi/B_g)}{\partial t}+\left(\frac{\phi R_s}{B_o}\right)_{n+1}\frac{\partial S_o}{\partial t}+S_{o,n}\frac{\partial(\phi R_s/B_o)}{\partial t}+\left(\frac{\phi R_{sw}}{B_w}\right)_{n+1}\frac{\partial S_w}{\partial t}+S_{w,n}\frac{\partial(\phi R_{sw}/B_w)}{\partial t}\right] \quad (4c)$$

In these forms, n+1 and n refer to the new and old time levels respectively. This is required for a consistent expansion. Combining Equations 4a, 4b, and 4c with Equations 1, 2, and 3 rearranging terms slightly, we obtain:

For oil:

$$\frac{\partial}{\partial x}\left[TR_o\left(\frac{\partial p_o}{\partial x}+\rho_o\frac{\partial z}{\partial x}\right)\right]\delta x - Q_o - V_b S_{o,n}\frac{\partial(\phi/B_o)}{\partial t}$$

$$= V_b\left(\frac{\phi}{B_o}\right)_{n+1}\frac{\partial S_o}{\partial t} \qquad (5)$$

For water:

$$\frac{\partial}{\partial x}\left[TR_w\left(\frac{\partial p_w}{\partial x}+\rho_w\frac{\partial z}{\partial x}\right)\right]\delta x - Q_w - V_b S_{w,n}\frac{\partial(\phi/B_w)}{\partial t}$$

$$= V_b\left(\frac{\phi}{B_w}\right)_{n+1}\frac{\partial S_w}{\partial t} \qquad (6)$$

For gas:

$$\frac{\partial}{\partial x}\left[TR_g\left(\frac{\partial p_g}{\partial x}+\rho_g\frac{\partial z}{\partial x}\right)+TR_oR_s\left(\frac{\partial p_o}{\partial x}+\rho_o\frac{\partial z}{\partial x}\right)\right.$$

$$\left.+\,TR_w\,R_{sw}\left(\frac{\partial p_w}{\partial x}+\rho_w\frac{\partial z}{\partial x}\right)\right]\delta x - Q_g - Q_oR_s - Q_wR_{sw}$$

$$- V_b\left[S_{g,n}\frac{\partial(\phi/B_g)}{\partial t}+S_{o,n}\frac{\partial(\phi R_s/B_o)}{\partial t}+S_{w,n}\frac{\partial(\phi R_{sw}/B_w)}{\partial t}\right]$$

$$= V_b\left[\left(\frac{\phi}{B_g}\right)_{n+1}\frac{\partial S_g}{\partial t}+\left(\frac{\phi R_s}{B_o}\right)_{n+1}\frac{\partial S_o}{\partial t}+\left(\frac{\phi R_{sw}}{B_w}\right)_{n+1}\frac{\partial S_w}{\partial t}\right] \qquad (7)$$

where TR is the transmissibility term for oil, water or gas.

Implicit pressures, explicit saturation. Equations 5, 6, and 7 are arranged so that the left-hand side of each equation contains pressures or variables which are functions of pressure, except for the relative permeability and the saturation values which we will take at time step n.

All variables at time step n are known so that values for relative permeability and saturations are available.

The right-hand side of Equations 5, 6, and 7 contains the change of saturation with respect to time. These three equations can be combined to form one equation which contains oil, water, and gas pressures as the unknown variables. To obtain this equation, one must make use of the relationship:

$$S_o + S_w + S_g = 1$$

or

$$\frac{\partial S_o}{\partial t}+\frac{\partial S_w}{\partial t}+\frac{\partial S_g}{\partial t}=0 \qquad (8)$$

First, solve for $\frac{\partial S_g}{\partial t}$ in Equation 8 and substitute this expression into Equation 7. The right-hand side of Equation 7 now contains $\frac{\partial S_w}{\partial t}$ and $\frac{\partial S_o}{\partial t}$.

Solve for $\frac{\partial S_o}{\partial t}$ in Equation 5 and $\frac{\partial S_w}{\partial t}$ in Equation 6 and substitute into Equation 7.

If we now define the left-hand side of Equation 5 as $(LHS)_{oil}$, the left-hand side of Equation 6 as LHS_{water}, and the left-hand side of Equation 7 as $(LHS)_{gas}$, we finally obtain:

$$(LHS)_{gas} = -\left[\left(\frac{B_o}{B_g}-R_s\right)_{n+1}(LHS)_{oil}\right.$$

$$\left.+\left(\frac{B_w}{B_g}-R_{sw}\right)_{n+1}(LHS)_{water}\right] \qquad (9)$$

Equation 9 still contains derivatives of the reciprocal of the formation volume factor, porosity, and solution gas ratio with respect to time.

Since these variables are functions of pressure, these derivatives may be taken with respect to pressure; and then take the derivative of pressure with respect to time.

As an example, let us look at the following term and expand it so that pressure becomes the dependent variable.

$$\frac{\partial(\phi/B_o)}{\partial t}=\phi_{n+1}\frac{\partial(1/B_o)}{\partial t}+\frac{1}{B_{o,n}}\frac{\partial\phi}{\partial t}$$

$$=\phi_{n+1}\frac{\partial(1/B_o)}{\partial p_o}\frac{\partial p_o}{\partial t}+\frac{1}{B_{o,n}}\frac{\partial\phi}{\partial t} \qquad (10)$$

The term $\frac{\partial(1/B_o)}{\partial p_o}$ can be evaluated from a table of B_o or $\frac{1}{B_o}$ vs. p in the vicinity of the new pressure; and the porosity, ϕ, has been defined as pressure dependent by the equation:

$$\phi = \phi_{orig}\,[\,1 + C_f\,(p_o - p_{o,orig})] \qquad (11)$$

Other terms of this type appearing in Equation 9 can be expanded in the same manner as shown in Equation 10.

Equation 9 now contains oil, water, and gas pressures as unknown quantities, along with coefficients of the type

$$\left(\frac{B_o}{B_g} - R_s\right)_{n+1} \text{ and } \phi_{n+1}.$$

Three alternatives exist for treating these unknown coefficients.

1. They may be taken at time step n instead of n+1. This may work if the pressure changes during any time step are small; however, the material balance error can become excessive for large pressure changes.

2. If an iterative solution technique is used, such as alternating direction iterative or successive over relaxation, these quantities may be updated to the latest pressure level between iterations.

3. The complete solution process may be repeated until these quantities do not change in value. This means is generally too costly for frequent use.

We still have only one equation, Equation 9, and three unknown pressures. This may be reduced to one unknown pressure by introducing capillary pressure for water and gas pressure[1] and taking the capillary pressure derivatives with time and space at the old time level and hope that these values at the old time level are close to what the new values would be. This leaves one equation and one unknown, the oil pressure.

Equation 9, with these modifications, still needs to be expanded in finite-difference form. This can be accomplished by referring to the previous articles in this series.[2,3,4] This expansion will give I × J × L equations to be solved simultaneously for a three-dimensional problem, where I is the number of nodes in the y direction, J is the number of nodes in the x direction, and L is the number of layers in the z direction. Also, a numerical method such as ADIP, SOR, Gauss Elimination, SIP, etc. must be chosen to solve these equations.

The new saturation values are obtained by expanding Equations 5, 6, and 7 in finite-difference form and solving explicitly for new saturation values at each grid point in the model. The only unknown in each equation will be the saturation, S_o, S_w, or S_g at time level n+1.

The saturations may also be obtained by solving two of the equations for the new values of saturation, and then calculate the third saturation value from Equation 8.

Simultaneous solution. Equations 5, 6, and 7 each contain some combination of oil, water, and gas pressures and oil, water, and gas saturations if terms of the type

$\frac{\partial(\phi/B)}{\partial t}$ are made pressure dependent, and terms of the type $(\phi/B)_{n+1}$ are treated as previously discussed.

Now, the derivatives of saturation with respect to time may be changed to derivatives of saturation with respect to capillary pressure times the derivative of capillary pressure with respect to time. For example:

$$\frac{\partial S_o}{\partial t} = \frac{\partial S_o}{\partial p_{cow}} \frac{\partial p_{cow}}{\partial t}$$

where:

$$p_{cow} = p_o - p_w$$

then:

$$\frac{\partial S_o}{\partial t} = \frac{\partial S_o}{\partial p_{cow}}\left(\frac{\partial p_o}{\partial t} - \frac{\partial p_w}{\partial t}\right) \qquad (12)$$

The derivative $\frac{\partial S_o}{\partial p_{cow}}$ can be taken at the old time step or extrapolated to the new time step. Equations 5, 6, and 7 will now contain the three unknowns, oil, water, and gas pressures, with the result that three times as many equations must be solved as in the previous case.

New saturation values are obtained from the capillary pressure-saturation curves. The one drawback with this type of model is that it cannot be run with capillary pressure set completely equal to zero.

The simultaneous solution technique can also be modified so that one pressure and two saturations appear as the unknown variables. Use of these variables will allow capillary pressure to be set to zero.

The simultaneous solution method has an advantage over the implicit pressure—explicit saturation method when capillary pressure is used. Capillary pressure is essentially treated implicitly in the simultaneous solution method and explicitly in the other.

The implicit treatment should allow a larger time step size to be taken and should give smoother changes in the pressure and saturation surfaces.

Special purpose models

Simulation of multiphase flow in the immediate vicinity of the well bore is difficult due to instabilities that develop during the calculation process. Water and gas-coning problems encounter these computational difficulties because the nodes near the well bore are very small.

For a normal-size time step, the fluid throughput in one of the small nodes may be in the range of 10,000 times the pore volume of that node. In a model where the relative permeabilities and rates are taken at the old time level (explicit), the proportions in which the fluids flow is always somewhat out of date, and abnormally large saturation changes can occur. This, in turn, causes large oscillations in the produced water/oil or gas/oil ratio.

The end result is that very small time steps must be taken, and the model becomes very expensive to run.

Special techniques have been devised to cure these problems.[5,6] These techniques require that the mobilities of the fluids in the vicinity of the well bore be taken implicitly (at the new time level) and that the production rate also be taken implicitly.

Water and gas-coning models can use the same equations as already developed for multiphase flow, except that the coordinate system used is generally cylindrical rather than the X, Y, Z coordinate system.

Also, the radial node size is allowed to vary logarithmically to give good definition of fluid distributions around the well bore where we are more interested in detail.

Many coning models are treated as incompressible since this simplifies the mathematics without simplifying the

actual flow phenomena that we desire to model.

The implicit rate calculation can be treated by first specifying that the total production rate, Q_T, is known. For oil and water flow, the following two equations can be used to distribute the flow.

$$Q_w = Q_T \frac{\frac{k_{ro}}{\mu_o}}{\left(\frac{k_{ro}}{\mu_o} + \frac{k_{rw}}{\mu_w}\right)} \qquad (13a)$$

and

$$Q_o = Q_T \frac{\frac{k_{rw}}{\mu_w}}{\left(\frac{k_{ro}}{\mu_o} + \frac{k_{rw}}{\mu_w}\right)} \qquad (13b)$$

The production rate of the water phase at the new time level n+1 is:

$$Q_{w,n+1} = Q_{w,n} + dQ_w$$

where dQ_w is the change in rate during that time step.

If we assume that the total mobility will remain relatively constant during one time step, then:

$$dQ_w = \left(\frac{Q_T}{(k_{ro}/\mu_o)+(k_{rw}/\mu_w)}\right) \frac{1}{\mu_w} \frac{d(k_{rw})}{dS_w} \Delta_t S_w \qquad (14)$$

where

$$\frac{d(k_{rw})}{dS_w} = \frac{k_{rw,n+1} - k_{rw,n}}{S_{w,n+1} - S_{w,n}}$$

and $\Delta_t S_w$ is the time derivative of the water saturation. Then, if $Q_{w,n+1}$ is substituted into Equation 6 for Q_w, the dQ_w term can be transposed to the right-hand side of the equation with the result that one additional term will be multiplying the time derivative of water saturation.

Implicit relative permeabilities can be obtained in the same manner:

$$k_{rw,n+1} = k_{rw,n} + \frac{d(k_{rw})}{dS_w} \Delta_t S_w \qquad (15)$$

Again, substituting this expression into Equation 6, the following additional term is obtained.

$$\frac{A_x k}{\mu_w B_w} \frac{d(k_{rw})}{dS_w} \Delta_t S_w \left(\frac{\partial p_w}{\partial x} + \rho_w \frac{\partial z}{\partial x}\right)$$

This term is nonlinear if the pressure derivative is taken implicitly.[5] This gives the product $(S_{w,n+1} - S_{w,n})(p_{w(i+1,n+1)} - p_{w(i,n+1)})$.

However, if the pressure derivative is taken at the old time level, this additional term can be taken to the right-hand side of Equation 6, in the same manner as the change in rate term.

References

1. van Poollen, H. K., Bixel, H. C., and Jargon, J. R., "Reservoir Modeling—9: Multiphase fluid flow," OGJ, May 11, 1970, p. 72.
2. van Poollen, H. K., Bixel, H. C., and Jargon, J. R., "Reservoir Modeling—3: Finite differences," OGJ, Sept. 15, 1969, p. 120.
3. van Poollen, H. K., Bixel, H. C., and Jargon, J. R., "Reservoir Modeling—7: Single phase reservoir models," OGJ, Mar. 2, 1970, p. 77.
4. van Poollen, H. K., Bixel, H. C., and Jargon, J. R., "Reservoir Modeling—8: Single phase gas flow," OGJ, Mar. 30, 1970, p. 106.
5. Letkeman, J. P., and Ridings, R. L., "A numerical coning model," SPE paper no. 2812, presented at Second Symposium on Numerical Simulation, Feb. 5-6, 1970.
6. MacDonald, R. C., and Coats, K. H., "Methods for numerical simulation of water and gas coning," SPE paper no. 2796, presented at Second Symposium on Numerical Simulation, Feb. 5-6, 1970.

Individual well pressures in reservoir modeling

IN AN earlier chapter,[1] we referred to considerations for grid size in reservoir modeling. But now let's turn our attention to what calculated pressure corresponds to the observed pressure in the field.

In the model, a pressure is calculated for a block or grid rather than for the well. In the field, we measure static pressures, buildup pressures, and pressures at observation wells. Depending on the grid size, well spacing, and reservoir characteristics, we have to modify either the measured or calculated pressures to conform to one another.

It has been found easier to modify the field measurements rather than to make a correction to the calculated model pressures.

Fig. 1

At least one empty block separates well blocks

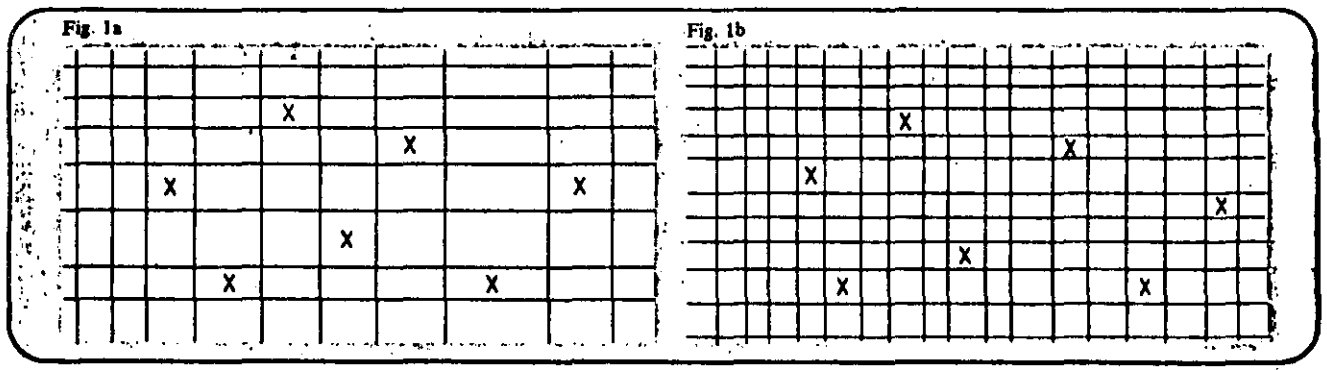

Fig. 2

Other possibilities

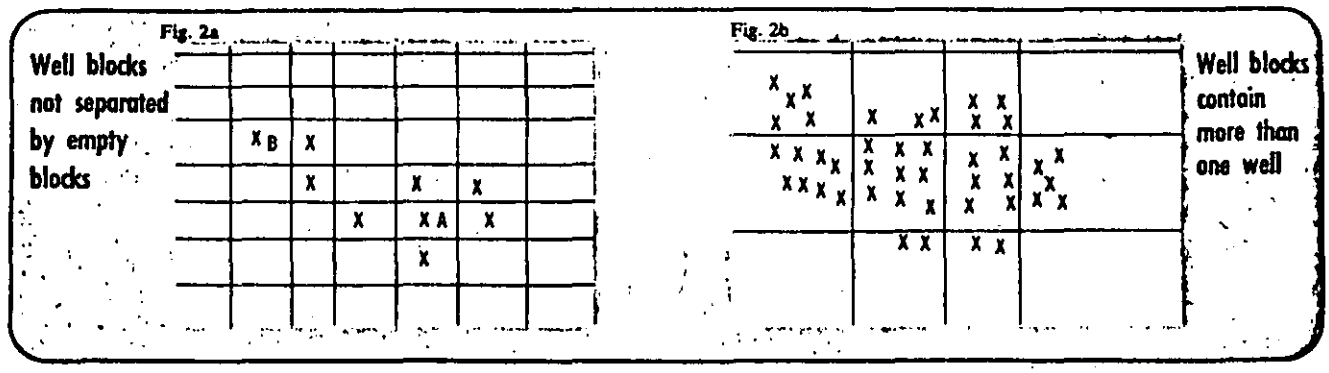

Field pressures. In the field, we may observe the flowing pressure of a well, the buildup pressure, the static pressure after a predetermined shut-in period, or we may have a well which was shut in for a long time as an observation well.

The flowing pressure of a well is affected by wellbore conditions such as wellbore damage, turbulence, stimulation, partial penetration and actual wellbore size, to name a few. It is impractical to simulate these conditions in a reservoir model. Consequently, these values are of little use in the matching of calculated and observed pressure histories.

The pressures at observation wells are probably the best values to use in history matching. Without production from a well, the pressure profile in the vicinity of the well is relatively flat, and the observed pressure is probably quite representative of the area the size of a grid dimension in an actual model. Of course, it is assumed that the observation well is the only well in a reservoir model block.

Static and build-up pressures will be reviewed next. However, it is first necessary to evaluate the grid that is used in the study.

It could be that no more than one well exists in a block with at least one empty block between wells as shown in Fig. 1. In Fig. 1a, that criteria is barely met. Fig. 1b shows a grid with a larger number of empty grids between wells.

Excellent calculations can be made using pressure build-up data or static pressures and a knowledge of reservoir properties as will be shown later.

Sometimes, grids containing wells are adjacent to one another, Fig. 2a; or even more than one well exists in one block as shown in Fig. 2b.

The situation depicted in Fig. 2b requires that one calculates the average reservoir pressure for the volume represented by the model block. Various techniques have been described in the litrature,[2] but all suffer from the same shortcoming—lack of true knowledge of the drainage radius and shape.

These problems are well known to the engineer who needs to perform material-balance studies on a field-wide basis. In essence, a study with a coarse grid, as shown in Fig. 2b, is no more than a series of connected material balances. (Nevertheless, these studies have considerable use.)

The grid density in Fig. 2a is between that of Fig. 1a and Fig. 2b. The radius of drainage for well A is defined where the well is surrounded by other producing wells. Most reservoir modelers will calculate the static reservoir pressure for well A and attempt to match it mathematically.

Fig. 3

Hypothetical drainage shapes

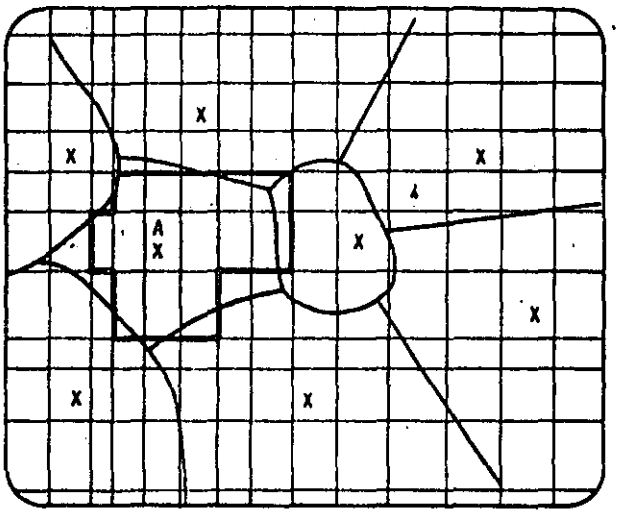

Fig. 4

Approximations for average pressure

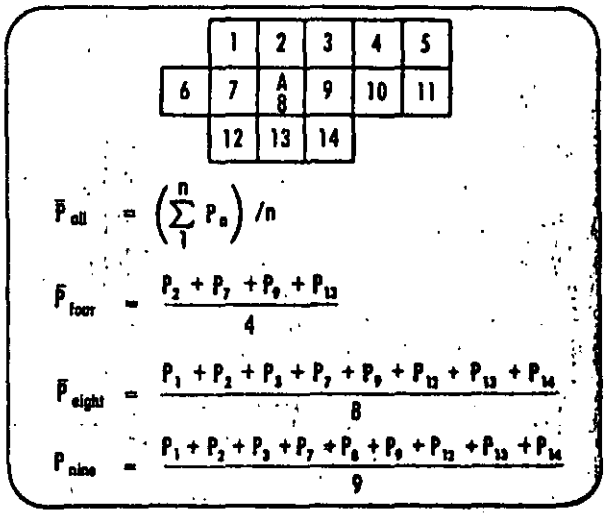

Fig. 5

Dynamic pressure from buildup curve

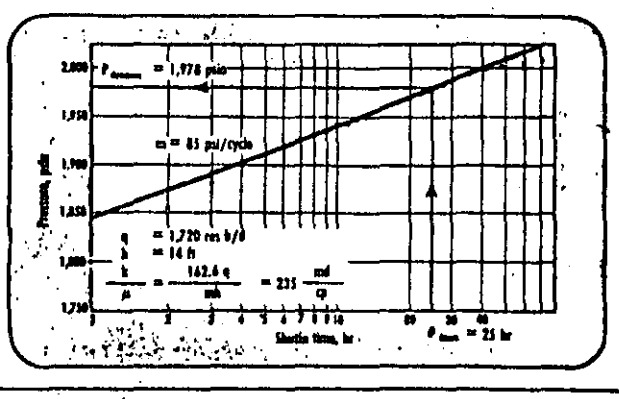

Fig. 6

Dynamic pressure from static pressure

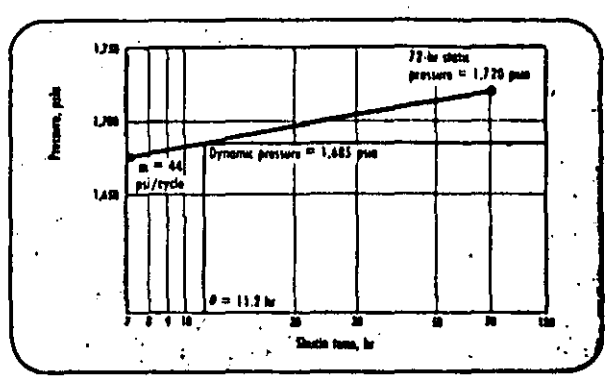

Well B, being at the edge of the reservoir, near an oil-water contact, or near gas-oil contact has an undefined drainage radius.

The calculated pressure in the block will be less than static and the following paragraphs may show how to handle that situation.

Drainage radius and volume of influence. In this discussion, we will assume that all wells in the fields will have produced long enough that a semisteady state exists. Then, the radius of drainage or the volume of pressure influence is stable. Let us, for the sake of explanation, say that the stable drainage pattern for a set of wells is as indicated in Fig. 3.

Also shown are the grid lines of the reservoir model. We further assume that a static pressure can be measured or calculated from the pressure build-up curve. That static reservoir pressure corresponds with the average reservoir pressunre within the drainage boundaries of the well.

For example, for well A, the field drainage boundaries are shown in the hatched area. In the finite-differences reservoir model, this might be represented by the solid lines showing the grid boundaries. One possibility would be to calcuate volumetrically averaged pressure of all calculated grid pressures and to compare this with the observed or extrapolated field pressures.

The drainage pattern changes with rate changes for wells. Therefore, it would be necessary to determine new drainage shapes, both in the model and the real world, every time rates are modified. It becomes readily apparent that such calculation would be too cumbersome and time-consuming.

Therefore, some modelers prefer to use the average pressure of the four surrounding nodes as an approximation of the calculated model pressure. Some prefer the eight surrounding nodes, and others use nine nodes as shown in Fig. 4.

The experienced pressure analyst is aware of the difficulties of static-pressure extrapolation, especially in tight reservoirs. What if the drainage boundary cannot be defined, for example, for a well surrounded by producers on one side and a gas-oil contact on the other? Therefore, a method was devised to eliminate boundary effects.[3]

Dynamic pressures. The method referred to was developed for extreme boundary conditions such as pressure maintenance and a bonded reservoir.[3] It can be shown to hold for a well in an infinite reservoir.

The dynamic pressure is defined as the average in a reservoir area equivalent to the reservoir model block. This dynamic pressure would preferably be obtained from a pressure build-up curve. It is equal to the build-up pressure after a shut-in time equal to:

$$\Theta = \frac{\phi \mu c r_b^2}{15.822 \times 10^{-4} k} \qquad (1)$$

where Θ is the shut-in time, hr
ϕ is the porosity as a fraction
c is the total compressibility, psi^{-1}
r_b is the equivalent block radius, ft
k is the permeability, md

Fig. 5 is the build-up curve of a well in a grid block with node dimensions equal to 2,720 and 3,150 ft on either side. The block is completely surrounded by empty nodes—nodes not containing producing wells. Furthermore, the porosity is 21.5%, and the total compressibility of the rock and fluid system is 15.9 by 10^{-6} psi^{-1}.

From the build-up curve, a total mobility (k/μ) is calculated to be 235 md/cp. The equivalent block radius, r_b, is calculated from:

$$r_b = \sqrt{\frac{2{,}720 \times 3{,}150}{\pi}} = 1{,}651.86 \text{ ft}$$

Next, the time at which the dynamic pressure is read from the build-up curve is calculated as:

$$\Theta = \frac{(0.215)\,(15.9 \times 10^{-6})\,(1{,}651.86)^2}{(15.822 \times 10^{-4})\,(235)} \cong 25 \text{ hr}$$

From Fig. 5, we read that the dynamic pressure is 1,978 psi. This, then, is the pressure we hope to calculate in the block where the well is located.

Sometimes, only a static pressure is available. Let us assume that a static pressure of 1,720 psi was measured at a well after 72 hr of shut in. Assume that the transmissibility of the well is 5,000 md ft/cp, that

$h = 12$ ft
$q = 1{,}350$ res bbl/day
$\phi = 22.5\%$
$c_{total} = 14.8 \times 10^{-6}$

and the equivalent block radius, r_b, is 1,490 ft.
We then calculate that:

$$\Theta = \frac{(0.225)\,(14.8 \times 10^{-6})\,(1{,}490)^2\,(12)}{(15.822 \times 10^{-4})\,(5{,}000)} = 11.2 \text{ hr}$$

Next, we have to reconstruct the pressure at 11.2 hr. Assuming that the straight line slope is valid between 11.2 and 72 hr, we can construct Fig. 6.

$$m = \frac{162.6\,q}{kh/\mu} = \frac{(162.6)\,(1{,}350)}{5{,}000} \cong 44 \text{ psi/cycle}$$

And at $\Theta_{block} = 11.2$ hr we read the block pressure at 1,685 psi.

Limitations. The method described by Equation 1 requires that (a) the well has been flowing at a fairly constant rate for a period of time equal to at least:

$$t_{stab} = \frac{\phi \mu c r_b^2}{50\,k}$$

with t_{stab} in days, and (b) r_b is more than one-half of the well spacing.

References

1. van Poollen, H. K., Bixel, H. C., Jargon, J. R., "Applications of Multiphase Immiscible Fluid Flow Simulator," The Oil and Gas Journal, June 29, 1970.
2. Matthews, C. S., and Russell, D. G., "Pressure Buildup and Flow Tests in Wells," SPE Monograph, Vol. 1, p. 35.
3. van Poollen, H. K., Breitenbach, E. A., Thurneau, D. H., "Treatment of Individual Wells and Grids in Reservoir Modeling," SPE Journal, Dec. 1968, p. 341.

A review—and a look ahead

THIS manual has dealt with one aspect of reservoir engineering — the development and applications of reservoir simulators as a tool to aid the engineer in predicting the rate of recovery of hydrocarbon deposits.

Use of these reservoir models allows the engineer to investigate various operating schemes and to select the economic optimum from the cases which were run.

Discussions have been presented on various models which include one-dimensional, single-phase models, to the more complicated three-dimensional, three-phase models. The development of the three-phase models has assumed that the composition of the stock-tank fluids does not change with reservoir pressure.

This assumption is good for black-oil systems which constitute a high percentage of the reservoirs studied. Volatile oil and condensate systems normally cannot be handled by this type of model.

Simulation of flow with compositional change was not considered in this series; however, reservoir-simulation programs which handle this type of problem have been developed.

Other simulators which were not considered in this manual are those which model thermal-recovery and miscible-displacement processes. Simulators of this type are in various stages of development; however, they are normally needed for a percentage of problems studied by the reservoir engineer.

What can we do with modeling? Reservoir-simulation programs have allowed us to reach the point in reservoir engineering where we can produce answers that could not be arrived at intuitively. Following is a partial list of problems which can be solved using models which were discussed in this series.

1. Determination of oil-field performance under depletion or various fluid-injection operations.
2. Calculation of the effect of well spacing on recovery.
3. A look at various flooding patterns.
4. Determination of the effect of producing rate on recovery.
5. Calculation of critical rates for water and gas coning.
6. Estimation of lease-line drainage.
7. Calculation of gas field deliverability.
8. An estimate of the effect of nuclear stimulation on wells producing from tight gas reservoirs.
9. Insight into the physical description of the oil reservoir by matching past performance.
10. Modeling of small-scale laboratory experiments.
11. Use of models as research and educational tools to study various mechanisms and to generate correlations for specific types of reservoirs.

What type model to use? At the start of any reservoir-engineering study, the objectives should be set forth so that a decision can be made as to which of the engineering tools available should be used to meet objectives.

If a simple material balance is sufficient, then why use a large reservoir simulator? However, if a material-balance computer program is not available, the same results can be obtained by setting up a one-node model on the reservoir simulator and, incidentlly, at a very small cost.

Models of all degree of sophistication are available—from the material balance to the three-dimensional, three-phase simulator, to the multicomponent model which can account for the flow and interphase transport of up to as many as 10 components.

Good engineering judgment should be used to determine the complexity of the model needed to solve the problem at hand. Some of the three-dimensional, three-phase simulators are constructed so any combination may be handled, down to the one-dimensional, single-phase problem.

Also, various options can be turned on or off, such as gravity effects or capillary pressure. If gravity and capillary pressure are thought to be necessary, computer runs with and without these options can be made to show their effect. If not needed, then a considerable savings in computer costs can be made by turning these options off.

If sweep efficiencies are desired for a particular waterflood pattern, a front-tracker type of simulator might be used. However, a front-tracker model can give misleading results if mobility ratios are not close to unity or if gravity effects are important.

Types of errors involved? In general, four types of errors are involved in using a reservoir simulator. They are those associated with the computer, the program, grid or time-step size, and reservoir data.

1. Errors associated with the computer.

These errors are roundoff errors and are directly connected to the word length of the computer. There is very little to worry about with most present-day computers as many carry 11 or 12 significant figures. Also, double precision is available and can be used in machines having shorter word lengths.

2. Errors associated with the programming.

These errors exist because certain assumptions must be made to solve the equations. Finite differences are used to approximate the partial derivatives. These errors will vary in magnitude, depending on what order of accuracy is desired. Also, consistency of expansion of partial derivatives will greatly affect the accuracy obtained. Inconsistent expansion will be evident by a larger material-balance error.

3. Errors caused by using too large a grid size or time-step size.

These errors are called truncation errors. They may be investigated by changing the grid size and the time-step size. This type of error will often depend a great deal on the type of problem being studied.

4. Error caused by inaccurate reservoir data.

The magnitude of this error is difficult to determine since a true description of the reservoir is never really known. Simulation efforts can pay off in studies with good input data. Studies made on a field developed 30 years ago (when data were scarce) will often produce disappointing results.

Time spent in analyzing the basic

input data is well spent. A thorough analysis of the basic input data might answer some of the questions the reservoir simulation study is supposed to answer. These data will include core analysis, log analysis, well-pressure tests and geological studies.

Frequently, error in some portions of the data can be tolerated while a small amount of error in other data will cause the calculated answers to vary a great deal. A sensitivity study should be made to determine which portions of the data cause the widest variations in calculated results.

If reasonable variations in some of the basic reservoir parameters cause wide variation in computed results, then the variables which cause these variations should be examined in more detail. It might be that the answer to a problem is actually given by some of the assumed data.

If past performance of the reservoir is available, then a history match will often help pinpoint many of the unknown parameters. In general, the longer the matched period, the more reliable the predicted performance will be.

What makes a model useful? As indicated earlier, some models are constructed to solve a number of problems. The term "universal" is used to differentiate them from a "specific-purpose" model.

The advantage of a universal model over a specific-purpose model is that certain features such as input and output, function tables, and certain parts of coefficient generators need not be repeated.

Some of the disadvantages are large computer storage. Also, the cost of a universal program may be excessive if only a simple application is required.

Let us next look at the various special features a program may offer and discuss their pros and cons. This discussion may aid the prospective buyer of a program.

Input facilities may differ greatly. In an earlier article, we discussed the parameters which need to be fed to the program. For example, for each grid point one needs to supply values for porosity, thickness, permeability, and elevation to name a few. While matching one needs to change these numbers between runs. A good program allows one to do this with ease without a chance of overriding or modifying values in other grids.

Also, the input should be as self-checking as possible. Some programs somewhat modify the numbers from input cards when they are placed in arrays and as they are used in actual calculations. Therefore, one wants to see a complete display of all input parameters as they are actually used in the program.

The same reasoning applies to the impirical functions such as relative permeabilities and P-V-T relationships. These are read in as polynomials or as tables.

Another self-checking feature of a reservoir-modeling program is to check that capillary-pressure curves and relative - permeability curves (residual or irreducible saturations) are compatible.

Output should be flexible. Although one calculates new values for pressure and saturations at each time step, a complete printout of all of these values is not required.

One should be able to call for a variety of output formats at predetermined intervals. For example, a complete pressure and saturation output for all grid points may only be desirable following 1 year of actual time, however, individual well behavior may be wanted each month.

Frequently, the user does not know beforehand how much output he wants until a run is completed. Therefore, a desirable feature would be that all possible output be placed on tapes for future reference. These tapes may subsequently be used to generate any type of printed output.

Numerical methods differ in speed and accuracy. One should check on the ease by which different numerical methods may be used in the program or new ones inserted.

When iterative schemes are used, the user should know the error tolerances. The best way would be to calculate the residuals. Also, a careful check on material balance should be made and this number should be printed as a run is performed.

Coefficients change with pressures and saturations. It would be advantageous to know what part of the model experiences the greatest change.

One should see how the pressure and saturations are calculated; i.e., simultaneously or in sequence.

Individual wells are treated in different manners. Some programs calculate water and gas rates from given oil rates and empirical functions. Others calculate total well withdrawal with water-oil and gas-oil ratios from the empirical functions. During prediction rates are sometimes assigned or calculated from pressures and productivity index. In the latter case, the possibility of calculating the rates implicity has advantages.

Some programs have the capability of using capillary pressures; others do not. However, capillary pressure is not always used even if the capability exists.

A problem encountered in some of the less-sophisticated models is the treatment of passing through the bubblepoint. If, for example, the pressure is decreased and excessive gas produced, the bubblepoint of the reservoir fluid is changing. If one does not account for this, gas may be "generated" when pressures are increased, resulting in strange pressure behavior and material-balance errors.

The speed of various models differs greatly and depends on the degree of program sophistication.

In general, one can see that although the basic equations for all models are essentially the same, programs and models differ widely.

What Now? The development of the high-speed computer has made it possible to better engineer the development of a hydrocarbon-bearing reservoir. This is because the computer has allowed us to carry out the large number of computations that are necessary for a detailed analysis of the reservoir. We can also determine the restraints that such factors as tubing size, lifting capacity, and separator facilities may be applying to the full economic development of the reservoir.

Computer hardware is getting better, more accurate, and less expensive. These improvements in the hardware will allow the engineer to perform studies that are uneconomical today because of the amount of computer time necessary to solve the problem.

The improved speed of computers will allow the more effective use of simulation programs that have been developed and proved on the smaller machines.

However, problems that are now being investigated, such as miscible flooding, thermal production and polymer flooding, will require better mathematics and better understanding of the displacement mechanism.

In short, more research is justified to fully exploit the computer's usefulness.

CURSO: " INGENIERIA DE YACIMIENTOS GEOTERMICOS "
13 DE MARZO AL 18 DE MAYO 1984

TEMA: "USE AND MISUSE OF RESERBOIT SIMULATION"

DR. GUILLERMO DOMINGUEZ V.
2-13 DE ABRIL
MATERIAL COMPLEMENTARIO

Use and Misuse of Reservoir Simulation Models

K. H. Coats, SPE-AIME, The U. of Texas at Austin

Introduction

Webster defines "simulate" as "to assume the appearance of without the reality". Simulation of petroleum reservoir performance refers to the construction and operation of a model whose behavior assumes the appearance of actual reservoir behavior. The model itself is either physical (for example, a laboratory sandpack) or mathematical. A mathematical model is simply a set of equations that, subject to certain assumptions, describes the physical processes active in the reservoir. Although the model itself obviously lacks the reality of the oil or gas field, the behavior of a valid model simulates (assumes the appearance of) that of the field.

The purpose of simulation is to estimate field performance (e.g., oil recovery) under a variety of producing schemes. Whereas the field can be produced only once — and at considerable expense — a model can be produced or "run" many times at low expense over a short period of time. Observation of model performance under different producing conditions, then, aids in selecting an optimum set of producing conditions for the reservoir. More specifically, with reservoir simulation the following are possible.

1. We can determine the performance of an oil field under water injection or gas injection, or under natural depletion.
2. We can judge the advisability of flank waterflooding as opposed to pattern waterflooding.
3. We can determine the effects of well location and spacing.
4. We can estimate the effect of producing rate on recovery.
5. We can calculate the total gas field deliverability for a given number of wells at certain specified locations.
6. We can estimate the lease-line drainage in heterogeneous oil or gas fields.

The tools of reservoir simulation range from the intuition and judgment of the engineer to complex mathematical models requiring use of digital computers. The question is not whether to simulate but rather which tool or method to use. There is no general answer to the question as to when the computerized mathematical model should be employed. After some preliminary discussion of the nature of mathematical models and sources of error, some valid and invalid model applications will be illustrated here with specific examples. It should be noted that this discussion is restricted to models for multidimensional, single or multiphase flow in reservoirs. These models apply to dry gas reservoirs and to oil reservoirs undergoing natural depletion or pressure maintenance (such as natural water drive, waterflood or gas injection).

The Mathematical Model

In 1959 Douglas, Peaceman and Rachford[1] proposed the "Leap-Frog" and "Simultaneous Solution" methods for solving two-dimensional, two-phase flow problems. In 1960, Stone[2] and Sheldon[3] described an "Implicit Pressure-Explicit Saturation" method. Since

In reservoir simulation, the question is not whether, but how and how much. The complexity of the questions being asked, and the amount and reliability of the data available, must determine the sophistication of the system to be used.

JPT November 1969

that time, computer simulation of two-dimensional, two-phase flow has become increasingly efficient as larger, higher-speed computers have evolved with attendant reduced computing costs. Peaceman and Rachford performed a three-dimensional calculation of two-phase flow in a five-spot by the Leap-Frog method[4] in 1962. Three-dimensional, two-phase simulators have been developed and applied, using the simultaneous method, since early 1963.[4] Recent articles describe simulators for three-dimensional, three-phase incompressible[5] and compressible[6] flow.

The mathematical reservoir simulator consists basically of sets of partial differential equations that express conservation of mass and/or energy. In addition, the model entails various phenomenological "laws" describing the rate processes active in the reservoir. Example laws are those of Darcy (fluid flow), Fourier (heat conduction), and Fick (solute transport by diffusion or dispersion). Finally, various assumptions may be invoked, such as those of one- or two-dimensional flow and single- or two-phase flow, negligible dispersion or gravity or capillary effects.

The model equations are generally nonlinear and require numerical solution. A computer program is written to utilize some numerical technique in solving the equations. Required program input data include fluid PVT data — formation volume factors and solution gas (R_s, Mcf/STB) as functions of pressure — rock relative permeability and capillary pressure curves, and reservoir description data. This last category usually constitutes the bulk of the input data and is the most difficult to determine accurately.

Computed results generally consist of pressures and fluid saturations at each of several hundred grid points throughout the reservoir. In problems involving heat or solute flow the model will also entail calculation of temperature or concentration at each grid point. These spatial distributions of pressure, etc., are determined at each of a sequence of time levels covering the producing period of interest.

Sources of Error in Computed Results

There are several potential sources of error in computed results.

1. The model itself is usually approximate since it involves certain assumptions that are only partly valid.
2. Replacement of the model differential equations by difference equations introduces truncation error; that is, the exact solution of the difference equations differs somewhat from the solution to the original differential equations.
3. The exact solution of the difference equations is not obtained due to round-off error incurred by the finite word length of the computer.
4. Perhaps most important, reservoir description data (for example, permeability, porosity distributions) seldom are accurately known.

The level of truncation error in computed results may be estimated by repeating runs or portions of runs with smaller space or time increments. Significant sensitivity of computed results to changes in these increment sizes indicates a significant level of truncation error and the corresponding need for smaller spatial or time steps. Compared with errors from other sources, round-off errors generally are negligible.

Error caused by faulty reservoir description data is difficult to determine since the true reservoir description is virtually never known. A combination of core analyses, well pressure tests and geological studies often gives valid insight into the nature of permeability and porosity distributions and reservoir geometry. The best method of obtaining a valid reservoir description is to determine in some manner the particular description that results in best agreement between calculated and observed field performance over a period of available reservoir history.

In many cases, the engineer is less concerned with the absolute accuracy of his reservoir description data and results than he is with the sensitivity of calculated results to variations in those data. The reason for this is that most questions regarding reservoir performance involve comparison of performances under alternative exploitation schemes. Sensitivity to errors in reservoir description data can be determined by performing several runs with variations in those data covering a reasonable range of uncertainty. For example, assume that a computerized mathematical model using a certain reservoir description yields oil recoveries of 57 percent under a flank waterflood and 32 percent under natural depletion. If additional runs, with reservoir descriptions varied over a considerable range of uncertainty, yield small variations (say about 3 percent) in these recoveries, then the estimated recoveries might be accepted as meaningful. In addition, the reservoir description would be considered as "adequate". If, however, reasonable variations (with regard to range of uncertainty) in reservoir description result in large variations (say about 20 percent) in computed recoveries, then attention should be given to obtaining a more accurate reservoir description. Even if calculated recoveries show considerable sensitivity to variations in reservoir description, some meaning might be attached to an essentially invariant difference between computed recoveries by waterflood and computed recoveries by natural depletion.

This discussion of sensitivity of computed results to errors in description data applies equally to sensitivity to errors or uncertainty in any other model input data. Too often we tend to demand accurate determination of all types of input data before we accept the computed results as meaningful or reliable. Actually, interest in accuracy of input data should be proportional to the sensitivity of computed results to variations in those data. If, for example, wide variations in the gas relative permeability curve result in virtually no change in computed oil recovery, then the accuracy of this curve warrants little attention.

The simulation model itself can be useful in allocating effort and expense in the determination of reservoir fluid and rock data. Computer runs may be performed at an early stage of the reservoir study to estimate sensitivity of calculated reservoir performance to variations in the assorted necessary input data. Obviously, effort should be concentrated on obtaining those data that have the greatest effect on calculated performance. For example, in cases where the gravity

drainage mechanism dominates oil recovery, the relative permeability curve to oil at low and middle-range oil saturations has a pronounced effect on calculated oil recovery. Gas viscosity and relative permeability and capillary pressure may play virtually no role whatever, and effort expended in determining them is largely wasted.

Educational Value of Simulation Models

Simulation model results frequently have considerable educational value, quite apart from their aid in reaching decisions regarding reservoir operation. The complex interactions of gravity, viscous, and capillary forces in heterogeneous reservoirs often result in seemingly anomalous, or at least unexpected, calculated flow patterns. Verification of the validity of such patterns requires considerable insight into the physics of the situation. Such verification can often be attained by recourse to simpler models. For example, calculated water saturation profiles for a one-dimensional vertical water drive in a heterogeneous pinnacle reef reservoir exhibit pronounced oscillation with vertical distance. These calculated oscillations persist virtually unchanged, despite considerable reduction of spatial and time increments; i.e., they are not caused by truncation error. The oscillations are caused by the dependence of frontal water saturation upon both gravity and viscous forces. The ratio of these forces varies markedly with the permeability of successive layers upward through the reservoir. The simpler Buckley-Leverett model, extended to heterogeneous one-dimensional systems, shows the same oscillations. In high permeability layers, gravity forces dominate viscous forces and a high frontal water saturation develops. However, as this front passes upwards into a low permeability block, viscous forces are dominant and give a low frontal saturation. Upon leaving the tight layer and again entering a loose one, the frontal saturation again jumps to a high value, resulting in an oscillatory water saturation profile at any given time.

Another example of the educational value of simulation models is their application to the question of lease-line drainage. Consider a heterogeneous gas reservoir or undersaturated oil reservoir with given (estimated) kh and ϕh maps. The reservoir consists of a number of leases with various numbers of producing wells in each lease. The problem is that of estimating net drainage rate into or out of each lease for given well producing rates under a semisteady state reservoir depletion. As discussed below, simple examination of the simulator equations allows isolation of that portion of field data that determines these net drainage rates. In fact, under certain conditions, the rates can be quickly determined, quantitatively, without any numerical solution of the simulator equations. In cases like this, the simulator, either by simple examination or by a limited number of computer runs, allows more intelligent formulation of general rules for field operation.

Some Applications of Numerical Reservoir Models

Here we will briefly describe some valid applications of computerized reservoir models. Features responsible for this validity are pointed out. Henderson, Dempsey, and Tyler[7] described a computer simulation of two-dimensional, transient gas flow in a dry gas storage reservoir. The practical problem was that of meeting a required (contractual) deliverability schedule over a 110-day withdrawal period. The peak required delivery rates occurred at the end of the period, when gas in place and hence reservoir pressure and field deliverability were at their lowest levels. The reservoir had 41 wells currently drilled and the problem was to select the number and locations of additional wells to be drilled before the next withdrawal season. The incentive to minimize the number of additional wells was strong, since each well cost about $125,000. On the other hand, the incentive to have enough wells was also strong since the contract specified a penalty of $10 to $100 for each Mcf of contractual gas not delivered.

The numerical model employed simulated two-dimensional (areal) unsteady-state gas flow in a closed heterogeneous reservoir of arbitrary geometry with an arbitrary number of wells arbitrarily located. Model results included pressure distributions in the field at various times covering the 110-day period, and field deliverability (Mcf/D) by well and for the total field at each of these times. Input data specified a gathering system or flowing wellbore pressure. The model was run a number of times for different proposed numbers and locations of additional wells and under different strategies regarding the order in which various wells were brought "on stream". Results indicated that field deliverability depended strongly upon the locations of additional wells and upon the order in which they were turned on during the 110-day period. A somewhat simplified statement of study results is that additional wells should be drilled preferentially in the tighter (lower kh) areas of the reservoir. Further, these tighter wells should be turned on early in the withdrawal period, saving the wells in the high kh portions of the reservoir for the peak withdrawal period.

The well locations and operating strategy recommended on the basis of those model results were largely adopted by the operating company. Recent performance of the reservoir is comparing reasonably well with that predicted by the model.

The practical benefit derived from this application was the elimination of a considerable number of expensive wells that would otherwise have been drilled. That is, the proper locations of additional wells relative to field heterogeneity and an "optimum" operating strategy allowed satisfaction of field deliverability requirements with considerably fewer additional wells.

Features contributing to the benefit of this application are: (1) the clearcut incentive to reduce additional well cost, and (2) the extensive field performance data available over several withdrawal seasons. The critical data in this case (from a standpoint of sensitivity of model results) were the reservoir kh distribution and individual well backpressure curves. These data were fairly well known from the performance data for the existing 41 wells.

Rainbow Field, Alberta

Applications of computerized multidimensional simulators are frequently subject to justification as well as to criticism. The recent pinnacle reef discoveries in the Rainbow field of Alberta offer such an example. For this field the immediate problem is to estimate oil recovery under natural depletion as opposed to various pressure maintenance schemes. The effect of producing rate on recovery is a subsidiary question. The zero-dimensional material balance calculation can be easily modified by including the capillary-gravitational equilibrium concept to yield one-dimensional (vertical) results. That is, an average field oil saturation of 70 percent need not be viewed as a uniform 70 percent saturation from the top to bottom of the reef. Rather the 70 percent can be considered the average corresponding to a nearly segregated fluid column. However, by virtue of this equilibrium assumption, the material balance calculation fixes ultimate recovery at essentially $1 - S_{or}$, where S_{or} is the residual oil saturation at which relative permeability to oil is zero. Equivalently stated, the material balance calculation assumes gravity drainage of oil from behind the declining gas-oil contact to be complete and instantaneous.

This complete recovery predicted by a material balance calculation might be reasonable if reservoir permeability were sufficiently high throughout the reservoir. However, core analyses from wells in most of these fields indicate rather severe heterogeneity with layers of considerable thickness (several feet) having vertical permeabilities of only 1 to 10 md. Fig. 1 shows a permeability distribution through reservoir thickness, typical of these reef reservoirs. One-dimensional (vertical), transient two- and three-phase flow models indicated that gravity drainage was a serious problem in that oil saturations appreciably above residual persisted in tight layers well above the declining, primary gas-oil contact. Fig. 2 shows computed oil saturation vs depth for one of the reef reservoirs after 15 years of natural depletion. This distribution indicates the inadequacy of the complete gravity drainage assumption inherent in the conventional material balance calculation. In this case the conventional material balance calculation is totally incapable of yielding meaningful estimates of oil recovery.

Use of the computerized numerical model in these reef studies can be criticized since the answers obtained are considerably dependent upon the reservoir description (essentially vertical permeability) employed. And in many pools, permeability data are available from only a single well. This scarcity of information about rather critical data required by the model spurred an intensive geological study. The geological work utilized data from many pools in a single area in an attempt to gain a more reliable reservoir description than that of a simple extrapolation over entire pool cross-sectional area from the well core data. The geological work and numerical model studies are discussed in the literature.[8,9]

One justification for application of numerical modeling to these reef reservoirs is simply the fact that it is not possible to estimate recoveries and effects of rate on recovery using conventional material balance calculations. Uncertainties in critical reservoir description data are partly offset by geological study and will be reduced further as performance history becomes available for matching purposes.

Field "X" — Crestal Gas Injection

The question often arises as to when it is necessary to

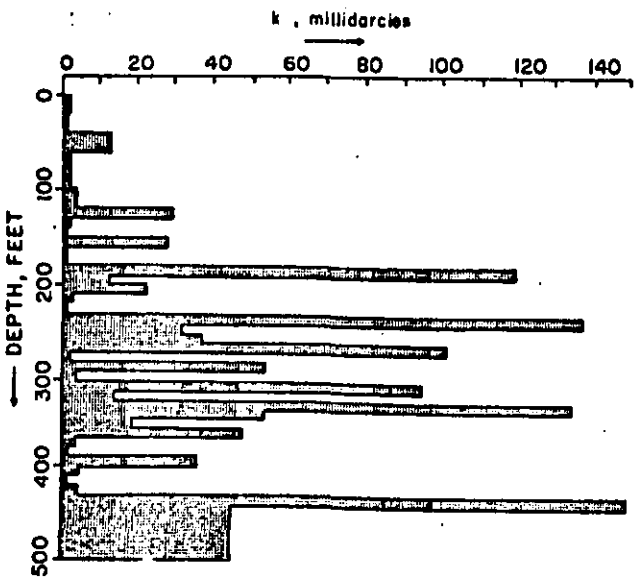

Fig. 1—Reef reservoir description.

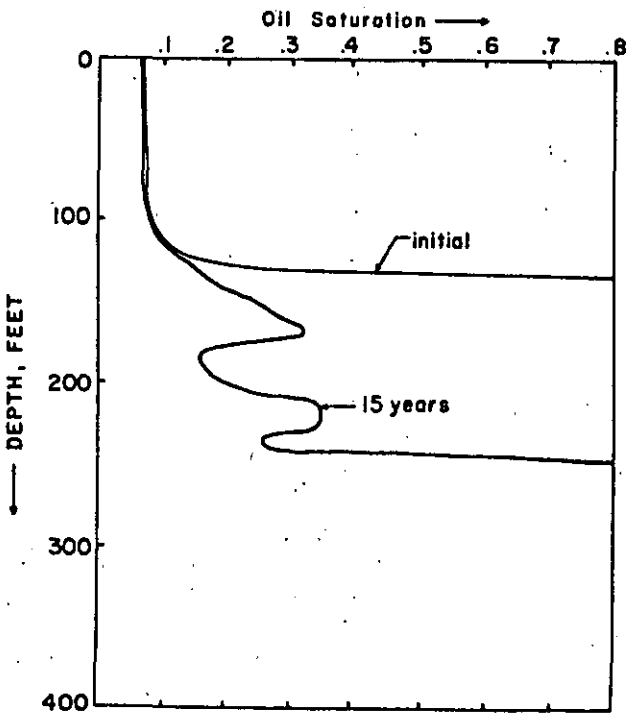

Fig. 2—Reef reservoir prediction.

simulate in three dimensions as opposed to two or even one dimension. Inclusion of flow in the third (nearly vertical) direction is often recommended only if reservoir thickness is "large" in relation to areal extent or if pronounced heterogeneity exists in the vertical direction (if, for example, there is high stratification). The recommendation may be helpful in some cases, but certainly is not binding. The following example of a three-dimensional problem is a somewhat generalized and simplified version of an actual field study. The problem was to estimate oil recovery by crestal gas injection in a steeply dipping reservoir. The reservoir sand was only 40 ft thick and was clean and unusually isotropic (see Fig. 3). Permeability was low at the southern boundary and increased uniformly toward the northern boundary.

Neither gas injection nor oil production wells were equally spaced or symmetrically located. The areal heterogeneity, along with nonuniform well spacing, dictated simulation of flow at least in the two areal (x-y) directions. In spite of the small sand thickness and homogeneity in the vertical direction, simulation of flow in that direction was also required. The reason was the low relative permeability to oil in the low and middle oil saturation range (an example, again, of the gravity drainage problem). The injected gas overrode and bypassed the oil, leaving appreciable amounts of oil behind the gas front. This oil slowly drained downdip and normal to the bedding planes. This vertical gravity drainage of oil was an important mechanism in the recovery and could not be accounted for in an areal, two-dimensional (x-y) calculation.

Field "Y" — Lease-Line Drainage

The question of lease-line drainage leads to an interesting application of the numerical reservoir simulator. Consider the heterogeneous oil or gas field shown in Fig. 4. A two-dimensional grid is superimposed for computing purposes. Estimated values of kh and ϕh are given for each block, along with the locations of producing wells and a lease line. We assume a single-phase, semisteady-state flow regime and a closed reservoir, i.e., a negligible water drive. The semisteady-state assumption implies that at any given time, the rate of pressure decline ($\partial p/\partial t$) is about the same at all spatial points in the field. The first question is: What is the net drainage or flow rate across the lease line for given producing rates of all wells? Examination and elementary manipulation on the finite difference form of the equation describing the two-dimensional flow shows that the answer is entirely independent of the kh distribution or level and of the well locations or individual rates. The answer depends only upon the total producing rates and pore volumes of each lease. In fact, the drainage rate from Lease I to Lease II is simply

$$q_{I \to II} = q_{II} - \frac{V_{pII}}{V_p} q \quad . \quad . \quad . \quad . \quad . \quad . \quad . \quad . \quad (1)$$

where

q = total field producing rate,
q_{II} = total Lease II producing rate
V_p = total field pore volume, and
V_{pII} = total Lease II pore volume.

Thus drainage is zero if each lease produces in proportion to its pore volume. This same result can be obtained by using Green's theorem in conjunction with the differential equation describing flow in a two-dimensional heterogeneous reservoir. Actually, the result can be obtained by simple reasoning, utilizing the definition of semisteady state, which implies

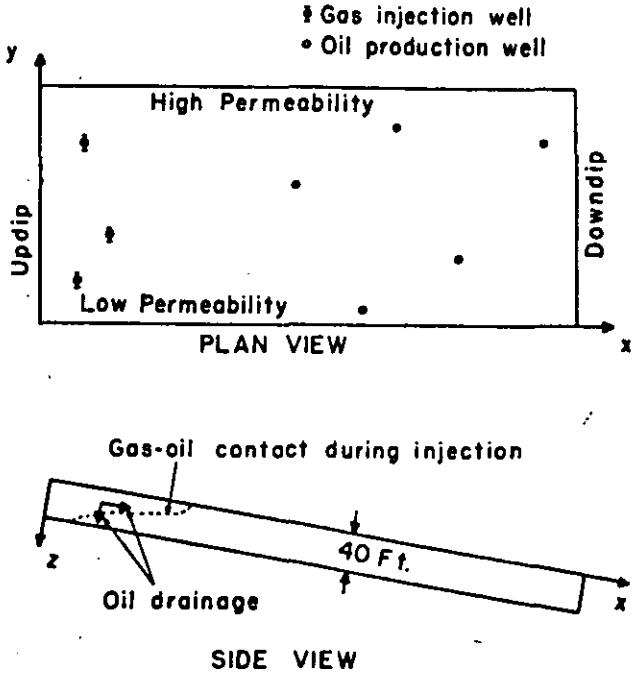

Fig. 3—A three-dimensional flow problem.

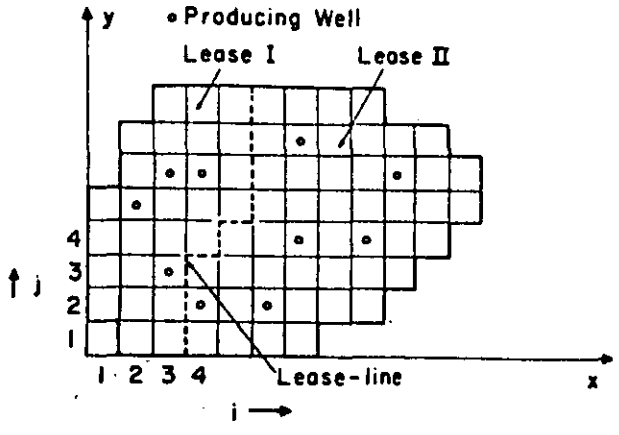

Fig. 4—Oil or gas field with two leases.

a uniform depletion rate per unit pore space over the entire field.

Whereas Eq. 1 appears trivial or immediately obvious, a somewhat more difficult answer to obtain is the net drainage rate for a given backpressure p_w where all well production rates are given by

$$q_{ij} = \alpha\,(kh)_{ij}\,(p_{ij} - p_w) \quad , \quad . \quad . \quad . \quad . \quad . \quad (2)$$

where

q_{ij} = producing rate of well located in Grid Block i, j
α = constant
$(kh)_{ij}$ = kh of Block i, j
p_{ij} = average pressure in Block i, j

Again, the answer is independent of the kh distribution, but is dependent upon the individual $(kh)_{ij}$ values where wells are located. A simple answer cannot be given for this case. However, computer solution of the two-dimensional, single-phase, semisteady-state flow equation gives the answer in less than 1 second of computing time on a high-speed digital computer.

Misuse of Reservoir Models

A kind of "overkill" is the most frequent misuse of reservoir models. Just a few years ago we made decisions regarding reservoir performance using only the tools of judgment and the conventional (zero-dimensional) material balance, or perhaps a one-dimensional Buckley-Leverett analysis. Now, almost overnight it seems, questions regarding reservoir performance can only be answered by performing two- or three-dimensional simulations of two- or three-phase flow, in several thousand blocks. Recently we have been told that even the three-phase (water, "oil", "gas") system is insufficient and should be replaced in many cases by a multicomponent calculation accounting for flow and interphase transfer of 10 or more hydrocarbon components.[10-12] This introduction of multicomponent phase behavior can result in computing times about 100 times greater than those required for the basic three-phase flow calculation.

Too often we automatically apply to a problem the most sophisticated and complex calculation tool available. Typically, grid sizes are used that are smaller than justified by available information concerning reservoir properties. Often the reasons given for fine grid structure have little basis in fact. In short, the overkill referred to here is the application of models accounting for m-phase flow using n grid blocks where questions could be equally well answered using a model describing m-1 or even m-2 phase flow in a grid of $n/2$ or $n/3$ blocks.

This is not meant to imply that there is no need for small-grid-element, three-dimensional simulations, or for multiphase flow calculation accounting for multicomponent mass transfer. There have been well founded three-dimensional studies and ill-conceived one-dimensional simulations and more than one problem has been faced in which a multiphase, multicomponent phase behavior calculation would have been welcome. However, the use of engineering judgment in many cases would dictate the use of a less complex model. Equally valid answers would be obtained at appreciably lower man and machine cost and in a shorter time.

A general rule that should be, but seldom is, followed is "select the *least* complicated model and grossest reservoir description that will allow the desired estimation of reservoir performance". Following is a case in point. A recently discovered oil reservoir with no initial gas cap and negligible water drive has been produced under natural depletion. Pressure has fallen below bubble point. A company is considering drilling one or several additional wells along a lease line to offset drainage believed to be occurring. The problem is to estimate the extent of drainage under current conditions and to estimate the effect of one or more additional wells. Little information is available regarding reservoir heterogeneity normal to the bedding planes. The use of a two- or three-dimensional, two-phase (gas-oil) flow model has been proposed. It appears that a two-dimensional areal (x-y), single-phase flow calculation should be employed in this case, first, because a single-phase flow study is considerably easier to conduct and requires much less computer time than a two-phase flow study, and second, because the extent of depletion below the bubble point has been such that probably only a few percent free gas saturation exists in the reservoir. This free gas, even if above critical saturation (i.e., mobile), should play a negligible role in the direction or rate of oil drainage across the lease line. Strictly speaking, the problem involves two-phase flow. But considering the question being asked, a single-phase flow calculation would undoubtedly be sufficient.

The necessity for a fine grid is sometimes argued on the grounds that accuracy is lost by placing wells in adjacent grid blocks. That is, the grid must be sufficiently fine that at least one "empty" grid block separates blocks containing wells. This is not necessarily true; in fact, in some cases more than one well can be placed in a single block. As an illustration (taken from Ref. 13), Fig. 5 shows two producing wells in a square, closed reservoir, 18,000 ft on a side. Two single-phase, semisteady-state calculations were performed using 9×9 and 3×3 grids. In the former case, two blocks separated those containing the wells, whereas in the latter case, the wells were in adjacent blocks. A common flowing well pressure was specified for both wells. Total field producing rate was specified as 5,000 Mcf/D, and the two-dimensional calculations determined (1) pressure distribution, (2) each well's contribution to the total rate, and (3) the gas in place (or average field pressure level) necessary to meet the required total field rate. The results are summarized in Table 1. The loss in accuracy due to the use of 9 as opposed to 81 grid blocks is clearly negligible.

Often a considerable amount of computing time can be saved in a study if the minimum required definition is determined at the outset. This involves repeated runs using fewer blocks until resolution is lost concerning the facets of field performance being estimated.

Reservoir models are also misapplied when there is gross uncertainty regarding input data that critical-

TABLE 1—EFFECT OF GRID SIZE ON CALCULATED WELL DELIVERABILITY

Grid Size	Deliverability (Mcf/D) Well 1	Well 2	Gas In Place (Mcf)
9×9	3732.8	1258.1	68,869,784
3×3	3723.1	1274.8	68,897,904

ly affect computed results. Let us take as an example a recent study of oil recovery by gas injection in a dipping cross-section (two-dimensional vertical slice). Initially, relative permeability and other reservoir data were rather crudely estimated and a considerable number of runs were performed to investigate the effect of injection rate on recovery. Subsequent sensitivity studies showed these early computed results to be largely meaningless for the following reason. The answers obtained were entirely dependent upon the oil relative permeability curve employed. And variations of it well within the range of uncertainty gave significantly different estimates of oil recovery. The computed recovery was almost totally insensitive to gas relative permeability and capillary pressure curves and to reservoir porosity. Also, reservoir permeability had an insignificant effect within a reasonable range of uncertainty. Having isolated the particular data of importance (oil relative permeability curve) we performed considerable laboratory work to determine it. Subsequent computer runs were then believed to yield reliable estimates of oil recovery and the quantitative effect of rate on recovery. This overriding importance of the oil relative permeability curve is typical, of course, in problems where oil recovery is dominated by the gravity drainage process.

Erroneous use of reservoir models occasionally occurs in two-dimensional areal studies. The error involves inadequate representation of fluid saturation distributions through the thickness of the reservoir. An areal calculation, as opposed to a three-dimensional calculation is justified in the two limiting cases when (1) fluids are completely segregated (i.e., gravitational-capillary equilibrium exists) throughout the thickness, and (2) no segregation exists (i.e., fluid saturations are uniform throughout the thickness). In the latter case, laboratory-derived rock relative permeability, as well as capillary pressure curves, should be used in the areal calculation. In the former case, pseudo relative permeability curves and capillary pressure curves, reflecting the state of segregation, should be employed.[4] In most cases, the assumption of segregation is more nearly correct than the assumption of uniform saturations, but in many cases neither assumption is valid. If neither assumption is valid, then (1) a three-dimensional calculation should be performed, or (2) totally empirical pseudo curves for areal calculations should be determined. These curves, when used in one-dimensional areal calculations, should result in agreement with two-dimensional cross-sectional calculations using laboratory curves.

Fig. 6 illustrates the error in computed results, caused by the use of laboratory relative permeability and capillary pressure curves in an areal study where the assumption of segregation is nearly correct. This figure shows depth-averaged gas saturation vs distance along a dipping (3°) cross-section. The gas was injected at the crest into the initially oil-saturated formation. The vertical slice is 800 ft long and 25 ft thick. A two-dimensional cross-sectional (x-z) calculation was performed using laboratory relative permeability and capillary pressure curves. The calculated gas saturations were then depth-averaged and plotted as the solid line in Fig. 6. This is the "correct" answer. The triangular points correspond to a one-dimensional calculation that utilized laboratory relative permeability and capillary pressure curves. These curves correspond to the assumption that fluid saturation is uniform throughout the thickness. The circular points correspond to a one-dimensional areal calculation that used pseudo curves reflecting the assumption of gravitational-capillary equilibrium (i.e., segregation) throughout the thickness. The use of these pseudo curves in the areal calculation gives a far more accurate result than does the use of the laboratory curves.

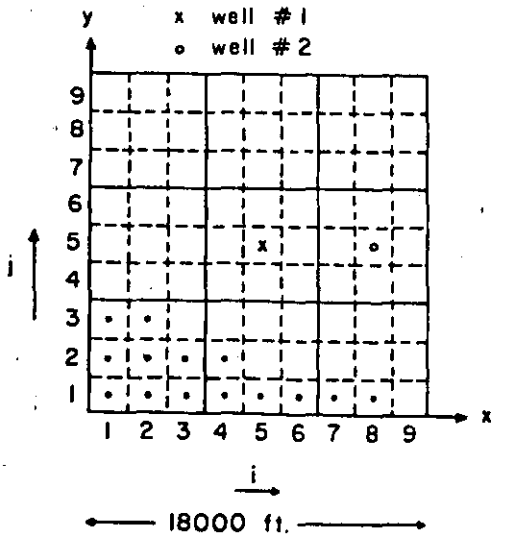

Fig. 5—9 × 9 and 3 × 3 grids.

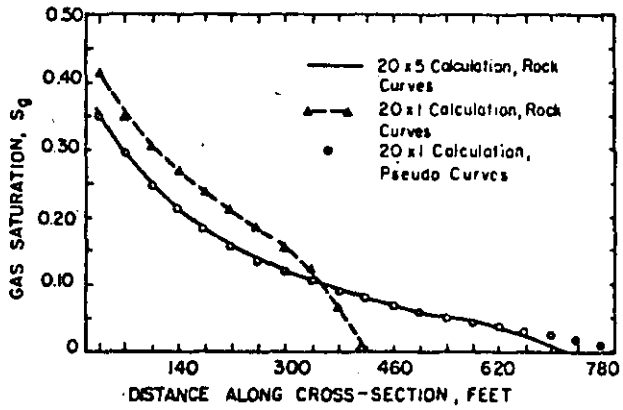

Fig. 6—Comparison of saturation profiles at Time = 360 days for 800-ft × 25-ft cross-section under gas injection.

Conclusions

Error in numerical simulation of reservoir performance results from truncation error and from inaccuracies in reservoir description or other input data. The presence of appreciable truncation error can generally be determined by noting the sensitivity of calculated performance to changes in spatial and time increment sizes. Adequate accuracy of input data is indicated by insignificant variations in computed reservoir performance caused by variations in the input data over the ranges of uncertainty. The mathematical model can be used in many cases to determine which particular input data should be determined accurately.

The complex interactions of capillary, gravitational and viscous forces reflected in the calculated reservoir performance often result in flow patterns or performance characteristics that are of considerable educational value.

Valid application of reservoir simulation models generally possess the following three features: (1) a well posed question of economic importance (such as "Should oil be recovered under natural depletion as opposed to water injection?", "What are the best locations for additional wells to maximize incremental field deliverability per dollar of additional investment?"), (2) adequate accuracy of reservoir description and other required input data, and (3) strong dependence of the answer to the question upon non-equilibrium, generally time-dependent, spatial distributions of pressure and fluid saturations. This dependence renders meaningless the conventional material balance calculations.

A frequent misuse of reservoir models is the application of one that is more complex or sophisticated than the problem warrants, which can greatly increase the required man and machine time. In general, we shou!d apply the least sophisticated model and largest grid size that will yield an adequate estimate of field performance. Application of models in cases where critical input data are poorly known constitutes another misuse. Finally, care should be exercised in respect to the relative permeability and capillary pressure curves employed when using a two-dimensional areal (x-y) calculation to simulate three-dimensional flow in reservoirs.

References

1. Douglas, J., Jr., Peaceman, D. W. and Rachford, H. H., Jr.: "A Method for Calculating Multi-Dimensional Immiscible Displacement", *Trans.*, AIME (1959) 216, 297-308.
2. Stone, H. L. and Garder, A. O., Jr.: "Analysis of Gas-Cap or Dissolved-Gas Drive Reservoirs", *Soc. Pet. Eng. J.* (June, 1961) 92-104.
3. Sheldon, J. W., Harris, C. D. and Bavly, D.: "A Method for General Reservoir Behavior Simulation on Digital Computers", paper 1521-G presented at SPE 35th Annual Fall Meeting, Denver, Colo., Oct. 2-5, 1960.
4. Coats, K. H., Nielsen, R. L., Terhune, M. H. and Weber, A. G.: "Simulation of Three-Dimensional, Two-Phase Flow in Oil and Gas Reservoirs", *Soc. Pet. Eng. J.* (Dec., 1967) 377-388.
5. Coats, K. H.: "An Analysis for Simulating Reservoir Performance Under Pressure Maintenance by Gas and/or Water Injection", *Soc. Pet. Eng. J.* (Dec., 1968) 331-340.
6. Coats, K. H.: "A Mathematical Model for Simulating Three-Dimensional Three-Phase Fluid Flow in Reservoirs", The U. of Texas, Austin (Nov., 1968).
7. Henderson, J. H., Dempsey, J. R. and Tyler, J. C.: "Use of Numerical Reservoir Models to Develop and Operate Gas Storage Reservoirs", *J. Pet. Tech.* (Nov., 1968) 1239-1246.
8. Coats, K. H.: "A Treatment of the Gas Percolation Problem in Simulation of Three-Dimensional, Three-Phase Flow in Reservoirs", *Soc. Pet. Eng. J.* (Dec., 1968) 413-419.
9. McCulloch, R. C., Langton, J. R. and Spivak, A.: "Simulation of High Relief Reservoirs, Rainbow Field, Alberta, Canada", *J. Pet. Tech.* (Nov., 1969) 1399-1408.
10. Roebuck, I. F., Henderson, G. E., Douglas, J., Jr., and Ford, T. W.: "The Compositional Reservoir Stimulator: Case I—The Linear Model", *Soc. Pet. Eng. J.* (March, 1969) 115-130.
11. Roebuck, I. F., Henderson, G. E., Douglas, J., Jr., and Ford, T. W.: "The Compositional Reservoir Simulator: Case IV — The Two-Dimensional Model", paper SPE 2235 presented at SPE 43rd Annual Fall Meeting, Houston, Tex., Sept. 29-Oct. 2, 1968.
12. Gondouin, M., Canevet, G. and Knizzeff, V.: "A Compositional Three-Phase, Three-Dimensional Reservoir Model", paper SPE 2236 presented at SPE 43rd Annual Fall Meeting, Houston, Tex., Sept. 29-Oct. 2, 1968.
13. Coats, K. H.: "An Approach to Locating New Wells in Heterogeneous, Gas Producing Fields", *J. Pet. Tech.* (May, 1969) 549-588. **JPT**

Manuscript received in Society of Petroleum Engineers office Feb. 6, 1969. Paper (SPE 2367) was presented at SPE Gas Technology and Peripheral Waterflooding Symposium held in Liberal, Kans., Nov. 14-15, 1968.

CURSO: "INGENIERIA DE YACIMIENTOS GEOTERMICOS "
13 DE MARZO AL 18 DE MAYO 1984

TEMA: "RESERVOIR SIMULATION ...QHAT IS IT "

DR. GUILLERMO DOMINGUEZ VARGAS

2-13 DE ABRIL
MATERIAL COMPLEMENTARIO

RESERVOIR SIMULATION ...What is it?

A. S. Odeh, SPE-AIME, Mobil Research & Development Corp.

Introduction

Reservoir simulation is based on well known reservoir engineering equations and techniques — the same equations and techniques the reservoir engineer has been using for years.

In general, simulation refers to the representation of some process by either a theoretical or a physical model. Here, we limit ourselves to the simulation of petroleum reservoirs. Our concern is the development and use of models that describe the reservoir performance under various operating conditions.

Reservoir simulation itself is not really new. Engineers have long used mathematical models in performing reservoir engineering calculations. Before the development of modern digital computers, however, the models were relatively simple. For example, when calculating the oil in place volumetrically, the engineer simulated the reservoir by a simple model in which average values for the porosity, saturation, and thickness were used.

Although simulation in the petroleum industry is not new, the new aspects are that more detailed reservoir features, and thus more accurate simulations, have become practical because of the capability afforded by the computers now available. The more detailed description, however, requires complex mathematical expressions that are difficult to understand, and this difficulty has caused some engineers to shy away from using simulators, and others to misuse them.

We in the petroleum industry are in the reservoir simulation revolution. As time goes on, simulators will be used more and more, so a basic understanding of reservoir modeling is essential. The engineer, especially, must become competent in setting up simulation problems, in deciding on appropriate input data, and in evaluating the results.

Basic Analysis

If a reservoir is fairly homogeneous, average values of the reservoir properties, such as porosity, are adequate to describe it. The average pressure, time, and production behavior of such a reservoir under a solution gas drive, for example, are normally calculated by the familiar methods[1] of Tarner, Muskat, or Tracy. All of these methods use the material balance equation normally referred to as the MBE. A simple expression for the oil MBE is the following:

(cumulative net withdrawal in STB) = (original oil in place in STB) − (oil remaining in place in STB).

The cumulative net withdrawal is the difference between the oil that leaves the reservoir and the oil that enters it. In this basic analysis, there is no oil entering the reservoir since the boundaries are considered impermeable to flow. Thus, the MBE reduces to its simplest form. Such a reservoir model is called the tank model (Fig. 1). It is zero dimensional because rock, fluid properties, and pressure values do not vary from point to point. Instead, they are calculated as average values for the whole reservoir. ***This tank model is the basic building block of reservoir simulators.***

Now let us consider a reservoir represented by a sandbar. Let the two halves of the sandbar vary in lithology. The sandbar as a whole cannot be represented by average properties, but each half can. Thus, the sandbar consists of two tank units, or cells, as they are normally called. The MBE describes the fluid behavior in each cell as in the previous tank model. However, the net withdrawal term of the MBE is more complicated because there can be migration of fluid from one cell to another, depending on the aver-

JPT November 1969

age pressure values of the two cells. This fluid transfer between the two cells is calculated by Darcy's law. The MBE, together with Darcy's law, describes the behavior of each cell. This model is not a zero-dimensional reservoir simulator since reservoir parameters may vary between the two cells. Instead it is a one-dimensional model, because it consists of more than one cell in one direction and of only one cell in the other two directions (Fig. 2).

This analysis can be extended to reservoirs where properties as well as pressure values vary in two dimensions, and to others where the variation occurs in three dimensions. The simulators representing these reservoirs are called, respectively, two-dimensional and three-dimensional simulators, as illustrated in Figs. 3 and 4. Thus, a two-dimensional reservoir simulator consists of more than one cell in two dimensions and of one cell in the third dimension. And a three-dimensional simulator consists of more than one cell in all of the three dimensions.

Regardless of the number of dimensions used, the MBE is the basic equation describing the fluid behavior within a cell; and Darcy's law describes the interaction between the cells. In one-, two-, and three-dimensional models each cell, except the boundary cell, interacts respectively with 2, 4, and 6 cells. Since a simulator can consist of hundreds of cells, keeping account of the MBE for each cell is a formidable bookkeeping operation ideally suited to digital computation. But we emphasize once again that the principles and equations used in reservoir simulation are not new. They only appear so because of the complexity of the bookkeeping.

Types of Reservoir Simulators

There are several types of reservoir simulators. Choice of the proper simulator to represent a particular reservoir requires an understanding of the reservoir and a *careful examination of the data available*. A model that fits Reservoir A may not be appropriate for Reservoir B, in spite of apparent similarities between Reservoirs A and B. A reservoir model is useful only when it fits the field case.

One basis for classifying models, as discussed earlier, is the number of dimensions. The two-dimensional model is the most commonly used. There are several two-dimensional geometries, the most popular of which is the horizontal (x-y) geometry; but the vertical (x-z) and the radial (r-z) geometries are also used quite often.

Simulators can be classified also according to the type of reservoir or process they are intended to simulate. There are, for example, gas, black oil, gas condensate, and miscible displacement reservoir simulators. Moreover, there are one-, two- and three-phase reservoir models. Furthermore, any of these simulators may or may not account for gravitational or capillary forces. It is not enough to choose the proper simulator with respect to dimensionality; the simulator must represent the type of hydrocarbon and the fluid phases present.

Simulation Steps

Preparation of Data

After the type of model to use in a study has been selected, the next step is to divide the reservoir into a number of cells, as illustrated in Figs. 2 through 4. This is accomplished by laying out a grid system for the reservoir. In a two-dimensional study, the grid is established by drawing lines on a map of the reservoir. All grid lines must extend across the reservoir. Each cell is identified by its x, y, z coordinates. Then the flow conditions around the perimeter of the reservoir are established. Normally the reservoir boundary is considered sealed, but influx or efflux at an assigned pressure or rate may also be specified.

The next step is to assign the following for each cell: rock properties, geometry, initial fluid distribution, and fluid properties. The rock properties consist of specific permeability, porosity, relative permeability and sometimes capillary pressure. The cell geometry includes the depth, thickness and locations of wells. Usually the wells are assumed to be located at the centers of the cells in which they fall. The initial fluid distribution consists of the oil, water and gas saturations at the beginning of simulation. Also, the average pressure of the cell at that time is assigned or calculated from known data. Fluid properties are specified by the usual PVT data. In addition, for each well it is necessary to provide a production schedule and a productivity index or a skin value (i.e., damage or improvement).

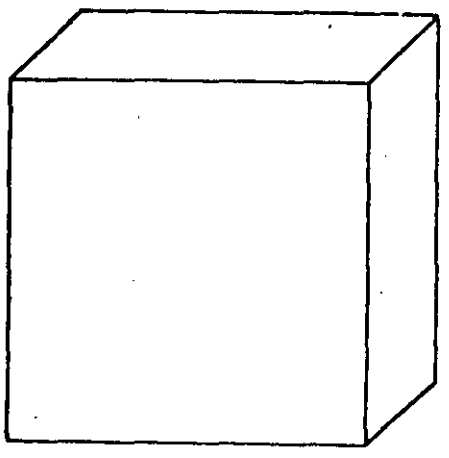

Fig. 1—Tank model.

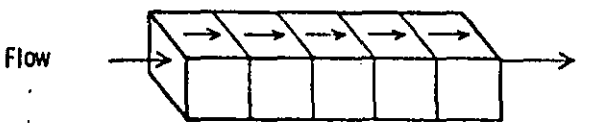

Fig. 2—One-dimensional simulator.

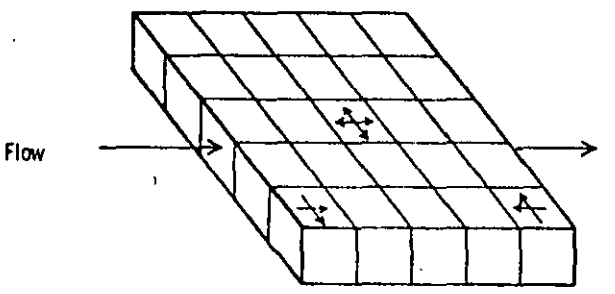

Fig. 3—Two-dimensional simulator.

The engineer should scrutinize carefully these basic data for consistency and accuracy. For example, if pressure buildup data are available on a well, the permeability-thickness product of the cell where the well is located and the flow rate assigned to the well, should be compatible with the buildup data. The time spent in examining the basic data is well spent, for it can lead to fewer simulation runs. Moreover one must always remember that *the answer is only as good as the input data.*

History Matching and Performance Prediction

The main purpose of reservoir simulation is to predict the rate of hydrocarbon recovery for different methods of field operation. If adequate field data exist, reasonably accurate performance predictions can be made. If data are incomplete or suspect, simulators may be used only to compare semi-quantitatively the results of different ways of operating the reservoir. In either case, the accuracy of the simulator can be improved by history matching.

The first step in a history match is to calculate reservoir performance using the best data available. The results are compared with the field recorded histories of the wells. If the agreement is not satisfactory, such data as permeability, relative permeability, and porosity are varied from one computer run to another until a match is achieved. The simulator is then used to predict performance for alternative plans of operating the reservoir.

The behavior of the reservoir is influenced by many factors — permeability, porosity, thickness, saturation distributions, relative permeability, etc. — that are never known precisely all over the reservoir. What the engineer arrives at is only a *combination* of these variables, which results in a match. This combination is not unique, so it may not represent precisely the condition of the reservoir. When the simulator, after a match, is used to predict, it is not certain that the physical picture of the reservoir described in the simulator will give predictions sufficiently close to the actual reservoir performance. In general, the longer the matched history period, the more reliable the predicted performance will be. It behooves the engineer to monitor periodically the predicted vs the actual performance and to update his physical picture of the reservoir.

Mathematical Considerations

Derivation of Equations

For the engineer to adequately understand reservoir simulation, he should be acquainted with the equations used. These are basically material balances about cells for each phase, and Darcy's law, which describes the interactions between cells. For illustration, we derive here the fundamental equations for a black oil system and explain their physical significance.

For the sake of simplicity, consider a cell in a one-dimensional reservoir simulator, as shown in Fig. 5. The same analysis is applicable to a cell in two- and three-dimensional models. (An expression for the oil material balance of the cell was given earlier.)

(Oil volume entering the cell during a time increment Δt, in STB) minus (oil volume leaving the cell during the same time increment, in STB) equals (the change in oil volume in the cell, in STB).

Volume of oil entering the cell during Δt, in STB, equals $Q_{in}\Delta t$.

Volume of oil leaving the cell during Δt, in STB, equals $(Q_{out} + q_o)\Delta t$.

Change in volume of oil in the cell during Δt, in STB, equals

$$\Delta x \Delta y h \left[\left(\frac{\phi s_o}{B_o}\right)^{n+1} - \left(\frac{\phi s_o}{B_o}\right)^{n}\right],$$

where Q_{in} is the average flow rate of oil into the cell during Δt in STB/unit time, Q_{out} is the average flow rate of oil leaving the cell to its neighbors during Δt in STB/unit time, and q_o is the oil production rate from the cell, if it contains a well, in STB/unit time; $\frac{\Delta x \Delta y h \phi s_o}{B_o}$ represents the volume of oil in the cell at any time, $n+1$ refers to the end of the time step, and n to the beginning.

Substitution in the oil MBE, after dividing through by Δt, gives

$$Q_{in} - Q_{out} - q_o = \frac{\Delta x \Delta y h}{\Delta t}\left[\left(\frac{\phi s_o}{B_o}\right)^{n+1} - \left(\frac{\phi s_o}{B_o}\right)^{n}\right] \quad \ldots\ldots\ldots\ldots\ldots\ldots (1)$$

However, by Darcy's law, assuming the flow to be

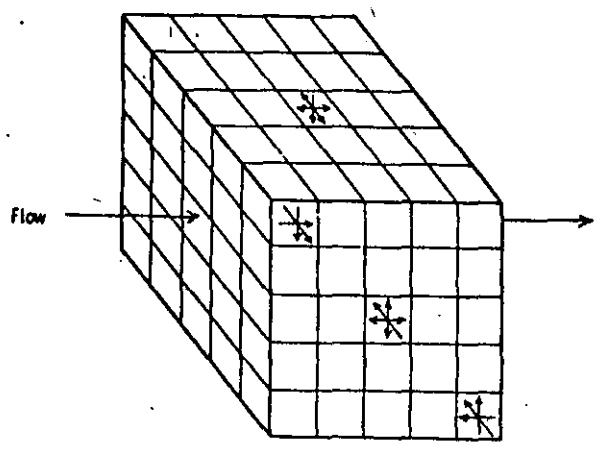

Fig. 4—Three-dimensional simulator.

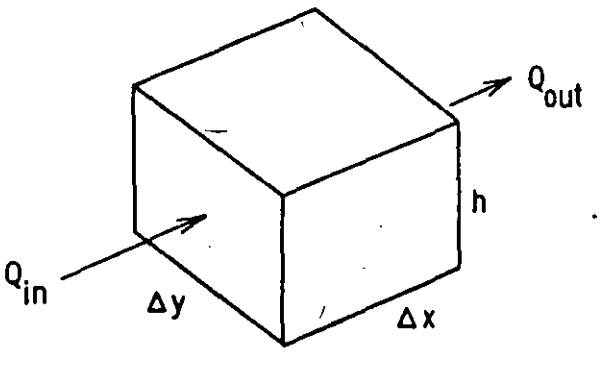

Fig. 5—Cell in a one-dimensional simulator.

from left to right as shown in Fig. 5,

$$Q_{in} = \frac{\Delta y h k_o}{\mu_o B_o}\left(\frac{\Phi_{oi-1}^{n+1} - \Phi_{oi}^{n+1}}{\Delta x}\right) , \quad . \quad . \quad . \quad (2)$$

and

$$Q_{out} = \frac{\Delta y h k_o}{\mu_o B_o}\left(\frac{\Phi_{oi}^{n+1} - \Phi_{oi+1}^{n+1}}{\Delta x}\right) , \quad . \quad . \quad . \quad (2)$$

where Δyh is the cross-sectional area of the cell, Δx is the length of the cell, Φ_o is the flow potential in the oil phase, i refers to the cell of interest, $i-1$ refers to the left-hand neighbor, and $i+1$ refers to the right-hand neighbor. The flow potential Φ_o equals pressure plus capillary pressure plus gravitational potential, and its use at the $(n+1)$-time level is explained later. Substituting Eq. 2 in Eq. 1 and dividing through by $\Delta y \Delta x$ gives

$$\frac{1}{\Delta x}\left[\frac{hk_o}{\mu_o B_o}\left(\frac{\Phi_{oi-1}^{n+1} - \Phi_{oi}^{n+1}}{\Delta x}\right) - \frac{hk_o}{\mu_o B_o}\left(\frac{\Phi_{oi}^{n+1} - \Phi_{oi+1}^{n+1}}{\Delta x}\right)\right] - \frac{q_o}{\Delta x \Delta y} = \frac{1}{\Delta t}\left[\left(\frac{h\phi s_o}{B_o}\right)^{n+1} - \left(\frac{h\phi s_o}{B_o}\right)^{n}\right] \quad . \quad . \quad (3)$$

Eq. 3 is rearranged to give

$$\frac{1}{\Delta x}\left[\lambda_{oi+\frac{1}{2}}\left(\frac{\Phi_{oi+1}^{n+1} - \Phi_{oi}^{n+1}}{\Delta x}\right) - \lambda_{oi-\frac{1}{2}}\left(\frac{\Phi_{oi}^{n+1} - \Phi_{oi-1}^{n+1}}{\Delta x}\right)\right] - \frac{q_o}{\Delta x \Delta y} = \frac{1}{\Delta t}\left[\left(\frac{h\phi s_o}{B_o}\right)^{n+1} - \left(\frac{h\phi s_o}{B_o}\right)^{n}\right] \quad , \quad . \quad (4)$$

where $\lambda = \frac{hk}{\mu B}$, and the subscripts $i+\frac{1}{2}$ and $i-\frac{1}{2}$ indicate that the quantity is evaluated as an average for the $(i+1, i)$ and $(i, i-1)$ cells, respectively. Different investigators use different averaging techniques. The upstream value for λ is the most commonly used.

Eq. 4 is the oil mass balance equation in one dimension, in difference form, which is used in the simulation calculations. In two and three dimensions, y- and z-direction terms identical with the x-direction term are added.

Eq. 4 may be written in differential form as

$$\frac{\partial}{\partial x}\left(\lambda_o \frac{\partial \Phi_o}{\partial x}\right) - \frac{q_o}{\Delta x \Delta y} = \frac{\partial}{\partial t}\left(\frac{\phi h s_o}{B_o}\right) . \quad . \quad (4a)$$

and in vector notation as

$$\nabla \cdot (\lambda_o \nabla \Phi_o) - \frac{q_o}{\Delta x \Delta y} = \frac{\partial}{\partial t}\left(\frac{\phi h s_o}{B_o}\right) . \quad . \quad (4b)$$

These three forms of the MBE are used interchangeably in the literature. Because of its compactness, Eq. 4b is the most commonly used.

In deriving Eq. 4 we used the value of Φ_o at the $(n+1)$-time level, i.e., at the end of the time step. This differencing technique is called the implicit[2] or *backward* difference method and is the most commonly used. The Crank-Nicholson method[2] uses an *average* value for Φ_o—i.e., at the $(n+\frac{1}{2})$-time level—while the *forward* difference method[2] uses Φ_o at the beginning of the time step — i.e., at the n-time level. The implicit method is the most stable of the three. The time at which $hk_o/B_o\mu_o$ is evaluated was left unspecified. Most authors use the n-time level, but some use the $(n+1)$-time level. This will be discussed later.

Similar derivations can be made for the water and gas. The water and gas equations in vector notation form are, respectively,

$$\nabla \cdot (\lambda_w \nabla \Phi_w) - \frac{q_w}{\Delta x \Delta y} = \frac{\partial}{\partial t}\left(\phi h \frac{s_w}{B_w}\right), \quad . \quad (5)$$

and

$$\nabla \cdot (\lambda_g \nabla \Phi_g) + \nabla \cdot (R_{so}\lambda_o \nabla \Phi_o) + \nabla \cdot (R_{sw}\lambda_w \nabla \Phi_w) - \frac{q_g}{\Delta x \Delta y} = \frac{\partial}{\partial t}\left[\phi h\left(\frac{s_g}{B_g} + R_{so}\frac{s_o}{B_o} + R_{sw}\frac{s_w}{B_w}\right)\right] , \quad (6)$$

where in Eq. 6 the gas dissolved in the oil and water is accounted for.

Eqs. 4b, 5, and 6 are the MB equations for three-phase immiscible flow in a black oil system, and were derived by Muskat.[3] Written in difference form, these are virtually the only equations used in the most common type of simulation, that of a black oil reservoir.

Method of Solution

Eq. 4 and its comparable forms for the water and gas give the relationships, for each cell, among pressure; and oil, water, and gas saturations; and time. If there are m cells, then we have m equations for each phase, giving a total of $3m$ equations. The solution of these equations is the major chore of reservoir simulation.

Two methods of solution are generally used; these are the implicit-implicit[4,5] and the implicit-explicit.[6] They are similar in one respect. Given a value for the saturations and pressure at each cell at the beginning of a time step, new saturations and pressure values are found at the end of the time step. These values in turn represent the starting point for the next time step. This step-wise process is continued until the desired amount of time elapses.

The implicit-implicit[4,5] method solves Eqs. 4 and the difference forms of Eqs. 5 and 6 directly. The solution usually involves an iterative procedure. Capillary pressure occasionally causes instability problems.* The implicit-implicit method overcomes the problem by expressing saturation as a function of capillary pressure. To start the calculations, values of saturations are assumed, and the pressures in the oil, water, and gas phases are calculated. These calculated pressures result in new capillary pressures, which are used to calculate saturations. These are compared with the assumed values, and if necessary the calculations are repeated.

Using the fact that the oil, water, and gas saturations add up to one, we can manipulate the three MB

*For definition, refer to the section on Computational Consideration.

equations in such a way as to result in a pressure equation. The pressure equation in symbolic form and vector notation is

$$\nabla \cdot \lambda_T \nabla p - q_T = c_T \frac{\partial p}{\partial t} \quad , \quad . \quad . \quad . \quad . \quad (7)$$

where λ_T is the total effective mobility of the three phases, q_T is the total production, and c_T is the total effective compressibility. (Capillary and gravity forces have been neglected.) In the implicit-explicit[6] method, at any given time, the pressure equation (Eq. 7) is solved first, giving the pressure distribution at each cell. Then the saturations are determined from the solution of the three MB equations.

To illustrate the method of solving Eq. 7 we write it in difference form in one dimension. We also assume that $\lambda_T = c_T = 1$, and that $q_T = 0$. The implicit difference formulation[2] is

$$\frac{p_{i+1}^{n+1} - 2p_i^{n+1} + p_{i-1}^{n+1}}{\Delta x^2} = \frac{p_i^{n+1} - p_i^n}{\Delta t} \quad , \quad (8)$$

where i, $i-1$, and $i+1$ refer to the cell of interest and its two neighbors, and n refers to the time level. Eq. 8 gives p_i^{n+1}, the pressure to be determined, as a function of two unknowns p_{i-1}^{n+1} and p_{i+1}^{n+1}. Thus, we cannot solve for p_i^{n+1} with this equation alone. For this reason we call this an implicit equation in pressure. However, similar equations can be written for all cells, resulting in m equations with m unknowns.

Several methods have been devised to solve the m pressure equations. The simplest are the relaxation techniques.[2] The pressures at $i-1$ and $i+1$ are assumed, and the pressure p_i^{n+1} is calculated. This trial-and-error process is repeated at each point in turn until a sufficiently accurate solution to the m equations is found. Given this pressure solution, we then solve explicitly for the saturations, using the three MB equations.

The coefficients λ_T and c_T contain effective permeabilities, viscosities, and formation volume factors, so they are functions of saturation and pressure. Until now we have ignored this fact. However, if we want to account for this dependency, which is sometimes necessary due to instability, then an iterative method is used. The method is summarized by the following steps, which are symbolically correct. In actuality the calculations are more involved.[7]

1. Begin with known pressure and saturation distribution at time n and, using the pressure equation, and the values for λ_T and c_T calculated from the saturation distribution and the pressure values at time n, solve for pressures at time $n+1$.
2. Solve for the saturation distribution at time $n+1$ using the three MB equations.
3. Using the new saturations and the pressures calculated in Step 1, recalculate λ_T and c_T values.
4. Repeat Steps 1 through 3 until the convergence criterion is achieved. In repeating Step 1, the values of λ_T and c_T of Step 3 are used.
5. Proceed with the next time step.

Methods that cycle between pressure and saturation equations are called fully implicit or iterative,[7] whereas those that do not, and in which essentially only Steps 1 and 2 and then 5 are executed, are called mixed.[7] Mixed methods are extensively used because they require less computer time.

One criterion for determining the compatibility of the pressure and saturation values is the material balance error. One form of the material balance is the summation of the stock tank oil at the beginning and at the end of the time step. The difference between the values should be equal to the total production during the time step. The incremental error is calculated by the following equation.

$$\text{incremental MBE error} = \frac{\sum_1^m \left[V\phi \left(\frac{S_o}{B_o} \right) \right]_j^n - \sum_1^m \left[V\phi \left(\frac{S_o}{B_o} \right) \right]_j^{n+1}}{q_o \Delta t} - 1,$$

where V is the volume of the cell and the summation is taken over the m cells.

Some authors use cumulative MBE error, which is given by the following equation.

$$\text{cumulative MBE error} = \frac{\text{initial oil in place} - \sum_1^m \left[V\phi \left(\frac{S_o}{B_o} \right) \right]_j^{n+1}}{\text{cumulative total production}} - 1.$$

A low value for MBE error is a necessary but not a sufficient criterion for a correct solution. In essence, low error indicates that the total oil in the reservoir at time $n+1$ is correct, but it does not guarantee that the oil is distributed properly.

Computational Considerations

Computing Time

For a given computer, the time required for a particular reservoir simulation depends primarily upon (1) the number of cells, and (2) the number of time steps.

The computing time required for a time step is proportional to the number of mesh points. Doubling the number of mesh points approximately doubles the computer time per time step.

The number of time steps required to simulate an assigned number of years depends on the allowed length of the time step Δt. The maximum value Δt may take is a function of the volume and shape of the cell. In a two-dimensional horizontal model, for example, the cell volume is $\Delta x \Delta y$ times thickness, and the shape is given by the ratio of $\Delta x/\Delta y$, where Δx and Δy are the horizontal dimensions of the cell. The allowed time step decreases as Δx and Δy decrease, and as $\left| \frac{\Delta x}{\Delta y} - 1 \right|$ increases. For example, the allowed Δt in a simulation study in which $\Delta x = \Delta y = 300$ ft will be about four times the Δt if $\Delta x = \Delta y = 150$ ft.

Instability

Numerical techniques do not yield exact solutions. There is an error associated with the answers. This error sometimes grows very rapidly, causing the solu-

tion to "blow up"; in other words, the solutions become physically unrealistic. The most common cause of this instability is excessively large changes in saturations and pressures during the time step. Usually this may be remedied by reducing the size of the time step.

Numerical Dispersion

This is an inherent property of digital simulation. It is due to the representation of the reservoir by cells in which properties are averaged. When a saturation front enters the cell, it is spread out over the cell to arrive at average saturation values. Numerical dispersion can be minimized by decreasing the dimensions of the cells. However, this leads to increased computer time.

Validity of Solution

Once a simulation run has been made, the question arises: "How good is the solution?" Small MBE error indicates that the total fluid volumes are correct, but does not guarantee that the fluid distribution is valid. If the resulting fluid distribution is questionable, a systematic analysis is needed. Variables that influence the saturation distribution are the time step size Δt, and the cell dimensions Δx and Δy. For a correct mathematical analysis, the sensitivity of the results to Δx, Δy, and Δt should be examined. A change in Δx, Δy values may require a major revision of the data, which is not practical. A common practice is to study only the effect of the time-step size. This is done by rerunning the simulation with reduced time steps and comparing the results. The time step is reduced until further reduction does not change the results significantly, thus indicating that the best solution has been obtained for the chosen sizes of the cells.

Acknowledgments

I should like to thank G. L. Smith, J. W. Watts and J. E. Walraven for helpful comments, and Mobil Research & Development Corp. for permission to publish this paper.

References

1. Craft, B. C. and Hawkins, M. F., Jr.: *Applied Petroleum Reservoir Engineering*, Prentice-Hall Inc., Englewood Cliffs, N. J. (1959).
2. Smith, G. D.: *Numerical Solution of Partial Differential Equations*, Oxford U. Press, Inc., New York (1965).
3. Muskat, M.: *Physical Principles of Oil Production*, McGraw-Hill Book Co., Inc., New York (1949).
4. Douglas, Jim, Jr., Peacemen, D. W. and Rachford, H. H., Jr.: "A Method for Calculating Multi-Dimensional Immiscible Displacement", *Trans.*, AIME (1959) **216**, 297-308.
5. Coats, K. H., Nielsen, R. L., Terhune, M. H. and Weber, A. G.: "Simulation of Three-Dimensional, Two-Phase Flow in Oil and Gas Reservoirs", *Soc. Pet. Eng. J.* (Dec., 1967) 377-388.
6. Fagin, R. G. and Stewart, C. H., Jr.: "A New Approach to the Two-Dimensional Multiphase Reservoir Simulator", *Soc. Pet. Eng. J.* (June, 1966) 175-182.
7. Blair, P. M. and Weinaug, C. F.: "Solution of Two-Phase Flow Problems Using Implicit Difference Equations", paper SPE 2185 presented at SPE 43rd Annual Fall Meeting, Houston, Tex., Sept. 29-Oct. 2, 1968. **JPT**

CURSO DENOMINADO " INGENIERIA DE YACIMIENTOS GEOTERMICOS "

CEREMONIA DE CLAUSURA

ORGANIZACION LATINOAMERICANA DE ENERGIA (OLADE)

COMISION FEDERAL DE ELECTRICIDAD (C. F. E.)

INSTITUTO DE INVESTIGACIONES ELECTRICAS (I.I.E.)

FACULTAD DE INGENIERIA, UNIVERSIDAD NACIONAL AUTONOMA DE MEXICO
DIVISION DE EDUCACION CONTINUA (DECFIUNAM)

I N D I C E

CURSO: "INGENIERIA DE YACIMIENTOS GEOTERMICOS"

CEREMONIA DE CLAUSURA

P R O G R A M A

HORARIO	EVENTO	PARTICIPANTES	LUGAR
15.00 h.	MESA REDONDA (COMIDA)	PROFESORES, ALUMNOS Y ORGANIZADORES	COMEDOR DEL PALACIO DE MINERIA
17.00 h.	CEREMONIA DE CLAUSURA	PROFESORES, ALUMNOS Y ORGANIZADORES	SALON DE LAS SIBILAS

18 DE MAYO DE 1984
PALACIO DE MINERIA
MEXICO, D.F.

MINUTA DE LA "MESA REDONDA" CELEBRADA EL DIA 6 DE ABRIL DE 1984.

MINUTA DE LA "MESA REDONDA" CELEBRADA EL DIA 6 DE ABRIL DE 1984 A LAS 14.00 HORAS EN LAS INSTALACIONES DE LA DIVISION DE EDUCACION CONTINUA DE LA FACULTAD DE INGENIERIA (DECFI) UNAM. UBICADAS EN EL PALACIO DE MINERIA CALLE DE TACUBA No. 5 MEXICO 06000, D.F.

EN LA MESA REDONDA SE TUVO LA PRESENCIA DEL DOCTOR EDUARDO IGLESIAS RODRIGUEZ, COORDINADOR DEL CURSO, DE LOS DOCTORES GUILLERMO DOMINGUEZ VARGAS, FERNANDO SAMANIEGO VERDUZCO, CESAR SUAREZ, PROFESORES DEL CURSO, EL M. EN I. GABRIEL MORENO PECERO, JEFE DE LA DECFI, EL ING. LUIS MORALES FLORES JEFE DEL DPTO. DE CURSOS INSTITUCIONALES DE LA DECFI Y DE 14 ALUMNOS DEL CURSO.

EL M. EN I. GABRIEL MORENO PECERO DIO A TODOS LOS ASISTENTES A LA REUNION, LA BIENVENIDA Y EXPLICO ALGUNOS ANTECEDENTES REFERENTES AL PALACIO DE MINERIA Y A LA DECFI, Y SE PUSO A CONSIDERACION DE LOS ASISTENTES EL ORDEN DEL DIA DE LA REUNION.

O R D E N D E L D I A

1. OBJETIVO DE LA REUNION
2. COMENTARIOS POR PARTE DE LOS ALUMNOS EN EL CURSO
3. COMENTARIOS POR PARTE DE LOS PROFESORES EN EL CURSO
4. ASUNTOS VARIOS

No habiendo objeción por parte de los asistentes respecto al orden del día, se procedió a iniciar la mesa redonda.

PRINCIPALES COMENTARIOS EXPRESADOS EN LA REUNION, POR LOS ALUMNOS.

1. El contenido académico del curso ha resultado, según los alumnos, de óptima calidad.
2. El tiempo en el cual se han distribuido los temas del curso ha sido corto.
3. Se mencionó que el curso había sido organizado para proporcionar los conocimientos básicos, las orientaciones y principales puntos a seguir en diversos aspectos de Yacimientos Geotérmicos y de manera que cada alumno estuviese capacitado para profundizar en todos los temas

según lo requiera su actividad profesional.

4. Se mencionó, por parte de los alumnos, la conveniencia de considerar dos semanas antes del inicio del curso, exclusivamente para impartir unos "cursos introductorios" de matemáticas, mecánica de fluídos y termodinámica, lo que proporcionaría una mejor fluidez académicamente al curso, o bien que se comentara ampliamente en la difusión del curso, de la necesidad de contar con esos conocimientos.
5. Se comentó sobre la conveniencia de que con toda anticipación al inicio del curso, se seleccionen los participantes a fin de que pudieran, por ejemplo, contar -- previo al curso con el material didáctico.
6. Se solicitó que también se recomendase a los futuros asistentes el hacer lecturas de bibliografía seleccionada por los profesores.
7. Las conferencias que se tratarán en la segunda parte del curso son:
   - 7.1. Geología del Campo Geotérmico de "Los Azufres", por el ingeniero Antonio Rosso.
   - 7.2. Geofísica para la exploración geotérmica por
   - 7.3. Geoquímica en la exploración geotérmica por el doctor David Nieva.
   - 7.4. Curvas características de producción y su interpretación por el doctor Eduardo Iglesias R.
   - 7.5. Perforación de pozos geotérmicos por el ingeniero Bernardo Domínguez Aguirre.
   - 7.6. Registros de producción por el ingeniero Francisco Bermejo.
8. Finalmente se realizaron algunos comentarios respecto al período de prácticas, semana mayor, visas, hospedaje y transportación.

A t e n t a m e n t e .

Ing. Luis Morales Flores
Jefe del Dpto. de Cursos Institucionales.

'jdv

LISTA DE ASISTENTES AL CURSO DENOMINADO
"INGENIERIA DE YACIMIENTOS GEOTERMICOS". 1984

ASISTENTES AL CURSO "INGENIERIA DE YACIMIENTOS GEOTERMICOS"

N O M B R E	P R O C E D E N C I A
1.- ACOSTA SILVA JAIME	MEXICO
2.- ASCH ROGER OSCAR	COSTA RICA
3.- ASCENCIO CENDEJAS FERNANDO	MEXICO
4.- ALVARADO SANCHEZ GUILLERMO	ECUADOR
5.- CAMPOS VILLAFUERTE TOMAS ANTONIO	EL SALVADOR
6.- ESCOBAR CORDOVA DAVID	EL SALVADOR
7.- GONZALEZ RENE	BOLIVIA
8.- GALVAN GARCIA EDUARDO	MEXICO
9.- IRVING RAMDEEN DEREK	PANAMA
10.- JASSO PEÑA CARLOS ARMANDO	MEXICO
11.- LOPEZ DAVILA ERASMO	MEXICO
12.- PALMA AMALA JULIO CESAR	GUATEMALA
13.- PIMENTEL SANTANA VICTOR	REPUBLICA DOMINICANA
14.- QUINTERO BARRERA ANGEL M.	COLOMBIA
15.- RECARTE ORLANDO	HONDURAS
16.- RAMIREZ SABAG JETZABETH	MEXICO
17.- ROSAS ELGUERA JOSE	MEXICO
18.- SANCHEZ UPTON PEDRO	MEXICO
19.- TORRES MERIZALDE MARCO P.	ECUADOR
20.- VERASTEGUI TOCRE DARIO	PERU

PAIS	REPRESENTANTE	No
BOLIVIA	GONZALEZ RENE	1
COLOMBIA	QUINTERO BARRERA ANGEL M.	1
COSTA RICA	ASCH ROGER OSCAR	1
ECUADOR	ALVARADO SANCHEZ GUILLERMO TORRES MERISALDE MARCO P.	2
EL SALVADOR	CAMPOS VILLAFUERTE TOMAS A. ESCOBAR CORDOVA DAVID	2
GUATEMALA	PALMA AMALA JULIO CESAR	1
HONDURAS	RECARTE ORLANDO	1
MEXICO	ACOSTA SILVA JAIME ASCENCIO CENDEJAS FERNANDO GALVAN GARCIA EDUARDO JASSO PEÑA CARLOS ARMANDO LOPEZ DAVILA ERASMO RAMIREZ SABAG JETZABETH ROSAS ELGUERA JOSE SANCHEZ UPTON PEDRO	8
PANAMA	IRVING RAMDEEN DEREK	1
PERU	VERASTEGUI TOCRE DARIO	1
REPUBLICA DOMINICANA	PIMENTEL SANTANA VICTOR	1

FORMATO DE EVALUACION DEL CURSO

EVALUACION DEL PERSONAL DOCENTE

CURSO:

FECHA:

CONFERENCISTA	DOMINIO DEL TEMA	EFICIENCIA EN EL USO DE AYUDAS AUDIOVISUALES	MANTENIMIENTO DEL INTERES. (COMUNICACION CON LOS ASISTENTES, AMENIDAD, FACILIDAD DE EXPRESION).	PUNTUALIDAD	
1.					
3.					
4.					
5					
6.					
7.					
8.					

ESCALA DE EVALUACION: 1 a 10

EVALUACION DE LA ENSEÑANZA

SU EVALUACION SINCERA NOS AYUDARA A MEJORAR LOS PROGRAMAS POSTERIORES QUE DISEÑAREMOS PARA USTED.

TEMA	ORGANIZACION Y DESARROLLO DEL TEMA	GRADO DE PROFUNDIDAD LOGRADO EN EL TEMA	GRADO DE ACTUALIZACION LOGRADO EN EL TEMA	UTILIDAD PRACTICA DEL TEMA	

ESCALA DE EVALUACION: 1 a 10

EVALUACION DEL CURSO

③

	CONCEPTO	EVALUACION
1.	APLICACION INMEDIATA DE LOS CONCEPTOS EXPUESTOS	
2.	CLARIDAD CON QUE SE EXPUSIERON LOS TEMAS	
3.	GRADO DE ACTUALIZACION LOGRADO CON EL CURSO	
4.	CUMPLIMIENTO DE LOS OBJETIVOS DEL CURSO	
5.	CONTINUIDAD EN LOS TEMAS DEL CURSO	
6.	CALIDAD DE LAS NOTAS DEL CURSO	
7.	GRADO DE MOTIVACION LOGRADO CON EL CURSO	

ESCALA DE EVALUACION DE 1 A 10

1. ¿Qué le pareció el ambiente en la División de Educación Continua?

MUY AGRADABLE	AGRADABLE	DESAGRADABLE

2. Medio de comunicación por el que se enteró del curso:

PERIODICO EXCELSIOR ANUNCIO TITULADO DI VISION DE EDUCACIÓN CONTINUA	PERIODICO NOVEDADES ANUNCIO TITULADO DI VISION DE EDUCACIÓN CONTINUA	FOLLETO DEL CURSO

CARTEL MENSUAL	RADIO UNIVERSIDAD	COMUNICACION CARTA, TELEFONO, VERBAL, ETC.

REVISTAS TECNICAS	FOLLETO ANUAL	CARTELERA UNAM "LOS UNIVERSITARIOS HOY"	GACETA UNAM

3. Medio de transporte utilizado para venir al Palacio de Minería:

AUTOMOVIL PARTICULAR	METRO	OTRO MEDIO

4. ¿Qué cambios haría usted en el programa para tratar de perfeccionar el curso?

_____

_____

_____

5. ¿Recomendaría el curso a otras personas?

SI	NO

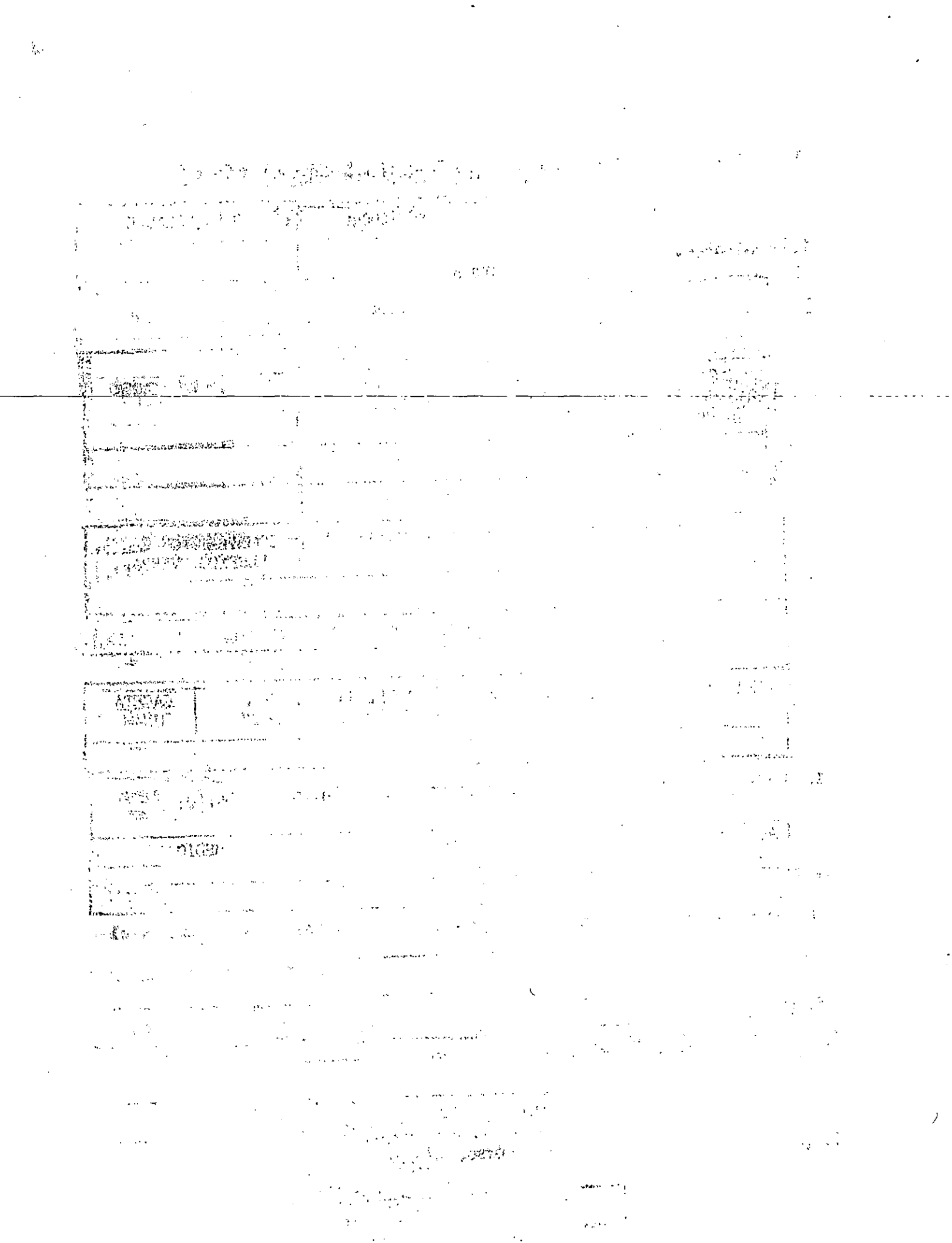

6. ¿Qué cursos le gustaría que ofreciera la División de Educación Continua?

7. La coordinación académica fue:

EXCELENTE	BUENA	REGULAR	MALA

8. Si está interesado en tomar algún curso intensivo ¿Cuál es el horario más conveniente para usted?

LUNES A VIERNES DE 9 A 13 H. Y DE 14 A 18 H. (CON COMIDAS)	LUNES A VIERNES DE 17 A 21 H.	LUNES, MIERCOLES Y VIERNES DE 18 A 21 H.	MARTES Y JUEVES DE 18 A 21 H.

VIERNES DE 17 A 21 H. SABADOS DE 9 A 14 H.	VIERNES DE 17 A 21 H. SABADOS DE 9 A 13 Y DE 14 a 18 H.	O T R O

9. ¿Qué servicios adicionales desearía que tuviese la División de Educación Continua, para los asistentes?

10. Otras sugerencias:

ENCUESTA DENOMINADA DE SEGUIMIENTO, LA CUAL, ES MUY CONVENIENTE SEA CONTESTADA POR LOS ALUMNOS ASISTENTES CADA SEIS MESES A PARTIR DE ESTA FECHA 17 DE MAYO DE 1984.

EL OBJETO DE LA PRESENTE ENCUESTA ES DE OBTENER UNA MAYOR INFORMACION DE LA EFECTIVIDAD Y EFICACIA DEL CURSO UNA VEZ TERMINADO ESTE

EL DOMICILIO DONDE DEBE SER ENVIADA LA ENCUESTA ES: CALLE TACUBA 5 COL. CENTRO MEXICO, 06000 D.F.

A continuación encontrará enunciados los temas que estudió en el curso: "INGENIERIA DE YACIMIENTOS GEOTERMICOS", por favor léalos cuidadosamente y conteste luego las preguntas que siguen.

T E M A S

1. CONCEPTOS BASICOS Y CLASIFICACION DE YACIMIENTOS GEOTERMICOS.
2. FLUJO DE FLUIDOS Y CALOR EN YACIMIENTOS.
3. PRUEBAS DE PRESION.
4. SIMULACION NUMERICA DE YACIMIENTOS GEOTERMICOS.
5. FLUJO DE FLUIDOS Y CALOR EN POZOS GEOTERMICOS
6. ASPECTOS PRACTICOS DE LA SIMULACION NUMERICA DE YACIMIENTOS.
7. ASPECTOS PRACTICOS DE LA SIMULACION NUMERICA DE FLUJOS EN POZOS GEOTERMICOS.
8. MEDICION DE PROPIEDADES FISICAS DE ROCAS.
9. ASPECTOS PRACTICOS DE LA PRODUCCION.
10. CONFERENCIAS.

1) ¿Qué temas le resultaron de mayor interés?

¿Por qué?

2) ¿Qué temas le resultaron de menor interés?

¿Por qué?

3) ¿Qué temas piensa que debería desarrollarse con más tiempo?

¿Por qué?

4) ¿En qué temas se combinaron la teoría y la práctica en forma adecuada?

5) ¿En qué temas no se combinaron la teoría y la práctica en forma adecuada?

6) ¿Cuáles son las funciones que Ud. desempeña en su trabajo, que estén directamente relacionadas con los temas del curso?

7) ¿Qué temas del curso pudo aplicar inmediatamente a sus funciones laborales?

8) ¿Qué temas agregaría al curso, que ayuden a resolver problemas que surjan en sus funciones actuales?

LMF'jdv

DIRECTORIO DE PROFESORES DEL CURSO: "INGENIERIA DE YACIMIENTOS GEOTERMICOS"

DR. HEBER CINCO LEY
(COORDINADOR)
SUBJEFE DEL AREA DE INGENIERIA
DE RECURSOS DEL SUBSUELO
DIVISION DE ESTUDIOS DE
POSGRADO, F.I.
U.N.A.M.
TEL. 550-87-12

DR. EDUARDO IGLESIAS RODRIGUEZ
JEFE DE INGENIERIA DE RESERVORIOS
GEOTERMICOS
INSTITUTO DE INVESTIGACIONES
ELECTRICAS
Ave. Palmira s/n
Apdo. Postal 475
Cuernavaca, Mor.
Tel. 91-731- 438-11

DR. JESUS RIVERA RODRIGUEZ
PROFESOR TITULAR
DEPTO. DE INGENIERIA PETROLERA
DIVISION DE ESTUDIOS DE
POSGRADO, F.I. U.N.A.M.
TEL. 550-87-12

DR. FERNANDO SAMANIEGO VERDUZCO
COORDINADOR DE LA SECCION DE
INGENIERIA ENERGETICA
DIVISION DE ESTUDIOS DE POSGRADO
FACULTAD DE INGENIERIA
U.N.A.M.
TEL. 550-87-12

DR. CESAR SUAREZ ARRIAGA
DEPTO. DE EVALUACION DE
YACIMIENTOS
COMISION FEDERAL DE ELECTRICIDAD
GERENCIA DE PROYECTOS GEOTERMO-
ELECTRICOS
Ave. Camelinas # 3527 - 7°Piso
Morelia, Mich. C.P. 58270
TEL. 452-31

./..

ING. VICTOR ARELLANO GOMEZ
INVESTIGADOR DEPTO. DE GEOTERMIA
AREA INGENIERIA DE YACIMIENTOS
INSTITUTO DE INVESTIGACIONES
ELECTRICAS.
DEPTO. DE GEOTERMIA
Ave. Palmira s/n
Apdo. Postal 475
Cuernavaca, Mor.
TEL. 91-731-4-38-11

ING. ENRIQUE CONTRERAS LOPEZ
INVESTIGADOR DEPTO. DE GEOTERMIA
AREA INGENIERIA DE YACIMIENTOS
INSTITUTO DE INVESTIGACIONES
ELECTRICAS.
DEPTO. DE GEOTERMIA
Ave. Palmira s/n
Apdo. Postal 475
Cuernavaca, Mor.
TEL. 91-731-4-38-11

ING. CARLOS MIRANDA MOCTEZUMA
SUPERINTENDENTE DE PRODUCCION
CAMPO GEOTERMICO LOS AZUFRES
Melchor Ocampo 35 Poniente
Cd. Hidalgo, Mich
TELS. 4-09-44
4-03-52

DR. GUILLERMO DOMINGUEZ VARGAS
COORDINADOR DE LA MAESTRIA DE
EXPLORACION DE RECURSOS ENERGETICOS
DEL SUBSUELO
FACULTAD DE INGENIERIA
DIVISION DE EST. DE POSGRADO,
U.N.A.M.
TEL. 550-87-12

1/II/84

*bvr

INGENIERIA DE YACIMIENTOS GEOTERMICOS

13 DE Marzo 18 DE Mayo 1984

Nº	TEMA	SEMANA 1	2	3	4	5	6	7	8	9	10	PROFESOR	DURACION TOTAL (HORAS)
I	CONCEPTOS BASICOS Y CLASIFICACION DE YACIMIENTOS GEOTERMICOS											DR. JESUS RIVERA	30
II	FLUJO DE FLUIDOS Y CALOR EN YACIMIENTOS											DR. HEBER CINCO	30
III	PRUEBAS DE PRESION											DR. FERNANDO SAMANIEGO	30
IV	SIMULACION NUMERICA DE YACIMIENTOS GEOTERMICOS											DR. GUILLERMO DOMINGUEZ	30
V	FLUJO DE FLUIDOS Y CALOR EN POZOS GEOTERMICOS											DR. CESAR SUAREZ	30
VI	ASPECTOS PRACTICOS DE LA SIMULACION NUMERICA DE YACIMIENTOS											ING. VICTOR ARELLANO	30
VII	ASPECTOS PRACTICOS DE LA SIMULACION NUMERICA DE FLUJOS EN POZOS GEOTERMICOS											ING. VICTOR ARELLANO	30
VIII	MEDICION DE PROPIEDADES FISICAS DE ROCAS											ING. ENRIQUE CONTRERAS	30
IX	ASPECTOS PRACTICOS DE LA PRODUCCION											ING. CARLOS MIRANDA	60
X	CONFERENCIAS												15
		13-16 Marzo	19-23 Marzo	26-30 Marzo	2-6 Abril	9-13 Abril	16-18 Abril	23-27 Abril	30 Abr. 4-Mayo	7-11 Mayo	14-18 Mayo		

NOTA: 16 al 27 Abril.- Período de prácticas en el C.G. "Los Azufres", Cd. Hidalgo, Michoacán
30 Abril al 18 de Mayo - Período de prácticas en el Instituto de Investigaciones Eléctricas en Cuernavaca, Morelos

CURSO: " INGENIERIA DE YACIMIENTOS GEOTERMICOS."
13 de marzo al 18 de mayo 1984

TEMA: "THERMAL BEHAVIOR OF UNCONSOLIDATED OIL SANDS"

DR. JESUS RIVERA RODRIGUEZ
13-23 MARZO
material adicional

JER DR. JESUS RIVERA RODRIGUEZ

Thermal Behavior of Unconsolidated Oil Sands

W. H. SOMERTON
J. A. KEESE*
S. L. CHU**
MEMBERS SPE-AIME

U. OF CALIFORNIA
BERKELEY, CALIF.

ABSTRACT

Thermal conductivities of unconsolidated oil sands have been measured and the results correlated with physical properties of the sand-fluid system. Saturation of the wetting fluid has a dominant effect on thermal conductivity values. Water-saturated sands were found to have thermal conductivities six to eight times greater than values for the same sand packs air saturated. For correlation purposes, the porosity of a sand pack is an adequate indicator of matrix structure. Other quantities needed to develop a satisfactory equation for predicting thermal conductivity are the conductivities of the wetting fluid and of the rock solids.

The effects of changes in temperature on the thermal conductivity of unconsolidated oil sands are relatively small and can be evaluated with a simple linear equation. The effects of changes in pressure on the thermal conductivity of liquid-saturated unconsolidated sands are also small and for practical purposes can be ignored.

Results of the present work are believed to have direct application to calculations relating to thermal processes in underground reservoirs. Core-analysis and well-log data can be used to evaluate the thermal properties of unconsolidated oil sands required for such calculations.

INTRODUCTION

The most successful thermal recovery operations are those that have been applied to relatively shallow producing formations consisting mostly of unconsolidated sands. Necessary in designing such projects is a knowledge of the thermal properties and behavior of the sand-fluid system under reservoir conditions of saturation, pressure, and temperature. A great deal of literature has been published on the thermal properties of granular materials, and several models and correlations for predicting thermal properties have been proposed.[1-5] Unfortunately, most test data have been obtained for systems or conditions much different from those found in petroleum reservoirs. Most models or prediction equations do not cover ranges of variables of importance to subsurface applications and, in addition, often require knowledge of system parameters that normally are not readily available from common sources such as core analyses and well logs.

The purpose of this work was to establish relationships between laboratory measurements of thermal properties and other more easily measurable properties of unconsolidated sands. Simple systems consisting of uniform-grain-size quartz sands saturated with single fluids were first studied. The work then progressed to more complex systems, including actual oilfield cores containing substantial portions of their original fluids.

RELATIONSHIP OF THERMAL CONDUCTIVITY TO OTHER PHYSICAL PROPERTIES

The thermal conductivity of fluid-saturated, unconsolidated sand is strongly dependent upon the saturation and thermal conductivity of the wetting phase fluid. Air- or gas-saturated sands characteristically have low thermal conductivities. This is because the contact areas between grains, through which heat must flow, are small. Introduction of a wetting-phase liquid greatly increases the thermal conductivity by increasing the effective grain contact area and thus enlarging the effective area through which heat can flow. Present experimental results show that the thermal conductivity of brine-saturated unconsolidated sands increases sixfold to eightfold over that of the same sand packs air saturated. This effect is considerably less pronounced in consolidated sandstones; Anand's data[6] show a twofold to threefold increase between brine-saturated and air-saturated sand packs.

Other physical properties of the sand-fluid system that have important effects on thermal conductivity include porosity and conductivity of the solid phase. Grain size, shape, and size distribution have some effect, but are probably of less importance. Permeability and electrical resistivity factor are also related to thermal conductivity, but

Original manuscript received in Society of Petroleum Engineers office Aug. 3, 1973. Revised manuscript received June 12, 1974. Paper (SPE 4506) was first presented at the 48th Annual Fall Meeting, held in Las Vegas, Nev., Sept. 30-Oct. 3, 1973.

[1]References listed at end of paper.

*Now with Standard Oil Co. of California, Bakersfield, Calif.
**Now with Bechtel Corp., San Francisco, Calif.

only in that they relate to other properties such as pore size, shape, and tortuosity, which are themselves related to thermal conductivity.

THERMAL CONDUCTIVITY MODELS

A number of models have been proposed and equations developed for predicting thermal conductivity from more easily measurable properties of the system. These models have been reviewed in detail by several authors.[3,4,7] Properties of the system commonly included in the models are the conductivities of the solid and fluid phases and the porosity and bulk density of the system. The models consist of arrangements of components in series or in parallel or of intermediate configurations. Thermal conductivity is calculated on the basis of unidirectional heat flow. Packing and shape factors and other empirical factors are generally employed to make the model fit experimental data.

Krupiczka[4] has solved Laplace equations for temperature distributions in both the solid regions and the fluid regions of two models—cubic packing of spheres and square packing of cylinders. The restriction of unidirectional flow of heat is thus eliminated, and improved agreement between calculated and measured values should be expected. The resulting equations are rather complex and Krupiczka approximates the solution by the following function:

$$\lambda/\lambda_f = (\lambda_s/\lambda_f)^{A + B \log \lambda_s/\lambda_f}, \quad . (1)$$

where

λ = effective thermal conductivity of system,

λ_f = thermal conductivity of fluid,

λ_s = thermal conductivity of solid,

$A = 0.280 - 0.757 \log \phi$,

ϕ = fractional porosity;

B = constant = −0.057.

In testing the above correlation against 165 data points from the literature, it was found that 76 percent of the calculated values agreed within ± 30 percent of experimental values.

The other model that seems to be applicable to the present work is one by Kunii and Smith,[5] who developed models for loose packing and for tight packing of spheres. They considered parallel heat flow through the fluid in the pore space and the solid. However, they added a series term to the solid system to account for heat transfer between solid grains through stagnant fluid near the contact points. The final equation, neglecting radiation and convective heat transfer, is given as

$$\lambda/\lambda_f = \phi + \frac{\beta(1-\phi)}{\ell + 2/3(\lambda_f/\lambda_s)}, \quad . (2)$$

where

β = a packing factor, 1.0 for loose packing and 0.895 for close packing,

ℓ = effective thickness of stagnant fluid near grain contacts evaluated as a function of λ_s/λ_f and packing factor β.

Eq. 2 has been shown by Kunii and Smith to correlate published data within ± 20 percent.

STATISTICAL MODELS

The complexities of natural unconsolidated sand-fluid systems require empirical factors to make simplified models fit measured values of thermal conductivities. Some data required by the models — conductivity of solid phase, shape and packing factors, etc. — are not normally available from core-analysis or well-log records. Keese[7] applied a linear regression analysis program in an effort to develop a statistical model. Data used in his analysis included porosity, permeability, and electrical resistivity factor, all of which are usually available from core analyses. Other data included median grain diameter (D_{50}), a grain-size distribution parameter (D_{90}/D_{10}), conductivity of the saturating fluid and conductivity of rock solids. Measured values of these latter data are generally not available, but reasonable values can be estimated. Grain size and size distribution were found to be of minor importance in the correlation and were assigned general values such as coarse (0.025 in.), medium (0.015 in.), and fine (0.005 in.), and well sorted to poorly sorted on a scale of 1.00 to 0. The correlation would be expected to be very sensitive to the conductivity of the saturating fluid. Values of the conductivities of water, oil, and gas or air are well known, and rather precise values can be assigned for single-fluid saturation cases. Mixed-fluid saturation is a special problem that will be dealt with later. The last remaining quantity is the conductivity of the rock solids. If the quartz content is high, a value of 5.0 Btu/ft-hr-°F can be assigned. If the feldspar, mica, and clay content is high, λ_s values as low as 2.5 Btu/ft-hr-°F may have to be assigned. Intermediate values may be used for other mineral compositions.

The effects of mixed-fluid saturations on the effective thermal conductivity are currently being investigated.[8] Gomaa[9] has developed a mathematical model that seems to predict conductivities of the few rock/mixed-fluid systems he investigated. His model predicts a nearly linear increase in thermal conductivity with increase in wetting-phase saturation above connate or irreducible saturation of the wetting phase. There is a large decrease in thermal conductivity between connate saturation and 100 percent saturation of the nonwetting phase. Present measurements on mixed-fluid-saturated oil-field cores confirmed this behavior. Chu[10] added a term for saturation of the wetting-phase fluid to other data used by Keese[7] in the regression analysis program and developed an equation that gave a reasonable correlation of his data.

OBJECTIVES OF PRESENT WORK

Our purpose was to develop and test models that would permit the prediction of thermal behavior of unconsolidated sand/fluid systems from data readily available from core-analysis and well-log records.

Thermal conductivity measurements were first made on sands that were saturated with air, brine, or Stoddard solvent, and whose composition, median grain size, and grain-size distribution were known. Porosity, bulk density, formation resistivity factor, and air permeability were measured for all samples. Tests were then extended to include extracted oilfield unconsolidated sands. The mineral content, median grain size, and grain-size distribution of the oil sands varied considerably from those of the earlier prepared sand mixes. Physical properties were measured and thermal conductivity tests were run on air-saturated and solvent-saturated samples. A final series of tests was run on oilfield cores containing original fluids. Brine was added to some of the samples to give high water-saturation values.

EXPERIMENTAL INVESTIGATION

Thermal conductivities were measured with a steady-state comparator apparatus described in an earlier paper.[11] The apparatus was modified somewhat to facilitate handling of unconsolidated samples. Basically, it consists of a Vespel* holder in which the unconsolidated sand is packed. The holder (2 in. in diameter × 1¼ in. thick) is sealed by thin stainless steel discs and Viton O-rings. Holders for the standards, made of the same material and design but only half as thick, are mounted above and below the sample holder. At the top of the stack is a heat source and at the bottom is a heat sink.

Heat is provided from separate temperature-controlled baths in which silicone oil is used as the circulating fluid. To minimize radial heat flow, a cylindrical guard heater is mounted around the sample and standards holders. Ceramic fiber insulation ½ in. thick is placed between the holders and the guard heater. The guard heater is controlled to the temperature at the midpoint of the test specimen. The entire stack is mounted in a hydraulic press to provide good contact of the holders and to simulate overburden pressure on the sample. A pressure line leads from the sample holder to pore-pressure control and measuring equipment. In the centers of the thin stainless steel discs that enclose the holders are thermocouples. These are connected to a switching arrangement so that absolute temperatures and differential temperatures across the sample and standards can be recorded on a multipoint strip chart.

Sand of known composition and grain size was packed into the holder with a hydraulic press and vibrator. Bulk densities and porosities were calculated from measurements of sand-grain density, weight, and volume. Special holder end caps were provided for measuring air permeability. The thermocouple plates were then assembled and the stack was mounted in the hydraulic press. An axial stress of 350 psi was applied to the sample and was controlled to this value throughout the test. The top and bottom oil circulating baths were maintained at temperatures of 155° and 105°F, respectively. The small heat loss in the insulated lines connecting the baths with the top and bottom plates of the stack resulted in a sample midpoint temperature of 125°F.

Approximately 5 hours was required to attain temperature equilibrium in the system. When equilibrium was achieved, differential temperatures across the sample and across the two standards were recorded. The thermal conductivity of the sample was calculated by applying the steady-state linear heat-flow equation. The standards of known thermal conductivity—Pyroceram** or fired Lava†—served as heat meters. A small correction was applied to account for some radial heat flow in the finite-conductivity holders. This correction was determined experimentally by Anand[6] using test specimens of known thermal conductivity, and was checked by theoretical calculations reported by Gomaa.[9]

After the dry thermal conductivity run was completed, the sample holder was removed from the stack and the sand pack was saturated with liquid, either Stoddard solvent or brine. For brine-saturated samples, the formation resistivity factor was measured. The saturated sample was returned to the stack and the thermal conductivity was measured again. The pore-pressure system was closed to prevent loss of liquid saturant and a pressure of a few psi was allowed to build up by thermal expansion, this pressure being monitored to assure that no leaks occurred during the test.

The saturated oil sands required special handling. A punch was used to extract 2-in.-diameter samples from the center of the original 5-in.-diameter cores. The sample was carefully pressed into the holder and the top was cut off slightly above the top of the cell. A stress of 500 psi was applied to the sample to bring the end of it level with the top of the cell. These steps were done as quickly as possible and the cell was sealed immediately to prevent loss of fluids. Thermal conductivity was measured at the same temperature, axial stress, and pore pressure as other liquid-saturated samples. After the test was completed, the oil sand was removed from the cell and the water and oil contents were determined by standard extraction tests. Density, weight, and volume measurements were used to determine porosity, bulk density, and oil and water saturations. Extraction tests run before and after thermal conductivity tests showed that loss in fluid saturation during testing was less than 2 percent.

Physical properties of unconsolidated sands are

*A polyimide resin manufactured by DuPont.

**Glass-ceramic Code 9606, Corning Glass Works.

†An aluminum silicate manufactured by American Lava Corp.

given in Tables 1 and 2. Table 1 is for uniform-grain-size Ottawa and Del Monte sands consisting predominantly of quartz, and specially prepared mixtures of the same sands. The factor D_{90}/D_{10} was determined as a measure of grain-size distribution, where D_{90} is the grain size for which 90 percent of the grains by weight are coarser and D_{10} is the grain size for which 10 percent of the grains by weight are coarser. Table 2 gives the source and physical properties of extracted, unconsolidated oil sands used in the tests.

Table 3 gives the source and measured physical properties of the unextracted oil sands. These data include measured values of oil and water saturation. Note that the total fractional liquid saturation is less than 1.00 in all cases. Grain sizes of sands in each of the three depth intervals appeared to be quite uniform. Since grain size is not a very important factor in the correlation, median-grain diameters were determined for only a few selected samples. The last two tests reported for each depth interval were run on extracted oil sands, both dry

TABLE 1 — PHYSICAL PROPERTIES OF UNCONSOLIDATED QUARTZ SANDS

Sand Type and Number	Permeability (darcies)	Formation Resistivity Factor	Porosity (fraction)	Thermal Conductivity (Btu/hr-ft-°F) Air Saturated	Thermal Conductivity (Btu/hr-ft-°F) Brine Saturated	Median Grain Size (in.)	D_{90}/D_{10}
Ottawa 1	–*	–	0.35	0.281	–	0.0239	1.00
Ottawa 1	–	–	0.40	0.236	–	0.0239	1.00
Ottawa 1	3.31	4.43	0.37	0.240	1.88	0.0239	1.00
Ottawa 2	3.06	3.73	0.37	0.219	1.74	0.0182	1.00
Ottawa 2	5.47	4.26	0.40	0.228	1.74	0.0182	1.00
Ottawa 3	–	–	0.37	0.242	–	0.0145	1.00
Ottawa 3	–	–	0.38	0.205	–	0.0145	1.00
Ottawa 3	6.83	4.95	0.41	0.232	1.94	0.0145	1.00
Ottawa 4	7.33	3.87	0.40	0.216	1.73	0.0097	1.00
Ottawa 5	–	–	0.40	0.201	–	0.0060	1.00
Ottawa 5	5.51	3.62	0.46	–	1.61	0.0060	1.00
Ottawa 5	3.90	3.82	0.41	0.205	1.66	0.0060	1.00
Ottawa 5	3.86	4.75	0.39	0.218	1.68	0.0060	1.00
Ottawa 5	–	3.85	0.41	0.192	0.42**	0.0060	1.00
Ottawa 6	2.05	–	0.44	0.185	–	0.0029	1.00
Del Monte 4	6.40	3.00	0.44	0.147	1.07	0.0097	1.00
Del Monte 4	5.59	3.01	0.42	0.173	1.06	0.0097	1.00
Del Monte 4	7.00	3.00	0.44	0.167	1.08	0.0097	1.00
Del Monte 6	–	–	0.42	0.186	–	0.0029	1.00
Del Monte 6	1.05	4.74	0.50	0.152	0.91	0.0029	1.00
Del Monte 6	0.77	3.66	0.42	0.160	0.92	0.0029	1.00
Del Monte 6	1.09	4.06	0.45	0.163	0.82	0.0029	1.00
Mix 1	8.71	5.47	0.39	0.205	1.63	0.0167	0.677
Mix 2	4.32	4.80	0.37	0.278	1.68	0.0070	0.292
Mix 3	2.89	4.65	0.34	0.278	1.76	0.0075	0.244
Mix 4	1.98	–	0.31	0.283	–	0.0077	0.136
Mix 4	0.86	–	0.32	0.271	0.51**	0.0077	0.136
Mix 4	–	–	0.32	0.240	1.65	0.0077	0.136
Mix 5	2.29	4.96	0.33	0.303	1.79	0.0078	0.097
Mix 6	4.92	4.26	0.32	0.332	–	0.0175	0.136
Mix 6	2.06	5.98	0.30	0.305	2.17	0.0175	0.136
Mix 7	0.29	4.71	0.32	0.278	–	0.0039	0.136
Mix 7	0.11	5.45	0.32	0.254	1.84	0.0039	0.136

*Not measured.
**Solvent saturated.

TABLE 2 — PHYSICAL PROPERTIES OF UNCONSOLIDATED EXTRACTED OIL SANDS

Sample Number	Source	Depth (ft)	Permeability (darcies)	Porosity (fraction)	Thermal Conductivity (Btu/hr-ft-°F) Air Saturated	Thermal Conductivity (Btu/hr-ft-°F) Solvent Saturated	Median Grain Size (in.)	D_{90}/D_{10}
1	Kern River	575	1.06	0.31	0.269	–	0.0231	0.063
2	Kern River	598	–*	0.42	0.220	0.397	0.0285	0.097
2	Kern River	598	2.94	0.37	0.220	0.429	0.0285	0.185
4	Midway-Sunset	949	2.55	0.45	0.207	0.298	0.0079	0.076
6	Midway-Sunset	955	0.59	0.42	0.217	0.348	0.0070	0.076
3	Huntington Beach	2,460	2.05	0.38	0.197	0.346	0.0082	0.161
3	Huntington Beach	2,460	2.26	0.40	0.201	0.344	0.0082	0.161
3	Huntington Beach	2,460	2.33	0.41	0.207	0.363	0.0082	0.161
3	Huntington Beach	2,460	1.86	0.43	0.196	0.339	0.0072	0.161
5	Bradley Canyon	2,638	0.21	0.36	0.207	0.438	0.0072	0.100
7	Bradley Canyon	2,768	0.79	0.41	0.222	0.385	0.0064	0.192
8	Bradley Canyon	2,782	0.49	0.41	0.195	0.346	0.0057	0.103
9	Bradley Canyon	2,796	0.34	0.38	0.201	0.375	0.0052	0.103

*Not measured.

and fully saturated with brine.

EXPERIMENTAL RESULTS

Results of thermal conductivity measurements on the quartz sands are plotted against porosity in Fig. 1 for both air-saturated and brine-saturated samples. The data are segregated according to grain-size ranges to give some measure of the importance of this variable. The solid lines represent the relations predicted by Krupiczka (Eq. 1) and the broken lines represent the relations predicted by Kunii and Smith (Eq. 2). The dotted lines will be discussed later.

The increase in thermal conductivity with decrease in porosity is clearly shown for air-saturated quartz sands. The effect of median grain size on conductivity is much less clear, although there is a general tendency for coarser sands to have higher thermal conductivities. The Krupiczka equation seems to fit the experimental data quite well, with the Kunii and Smith relation not showing so good a match.

The data for brine-saturated samples in Fig. 1 show larger scatter than the air-saturated data. There is a general increase in conductivity with decreased porosity and increased grain size. The group of six data points with low conductivity and high porosity values were for crushed Del Monte sand, whereas the other points were for natural Ottawa sands. The lower conductivity of the crushed Del Monte sand may be attributed to its greater angularity and probable reduced grain-to-grain contact. It is not clear, however, why the thermal conductivity values for the air-saturated Del Monte sands were not also low. The Krupiczka curve parallels the trend of the Ottawa sand data, although the Kunii and Smith relation seems to fit the combined data better.

The extracted oil sand data are plotted against porosity in Fig. 2 for air-, solvent-, and water-saturated samples. The Krupiczka relations for the three saturations have been plotted on the figure. These relations have been calculated assuming that a value of $\lambda_s = 2.75$ applies to oil sands with their high feldspar, mica, and clay content. The dotted lines are for modified values as will be discussed later. The effects of porosity and grain size are about the same as for quartz sands.

Fig. 3 shows the thermal conductivities of oil sands containing original fluids plotted against fractional brine saturation. The data have been segregated into three porosity ranges: 0.28 to 0.30, 0.31 to 0.33, and 0.34 to 0.37. From regression analysis, including only porosity and water saturation as variables, the best fit equation is given as

$$\lambda_{SW} = 0.735 - 1.30\,\phi + S_w^{1/2} \quad . \quad . \quad . (3)$$

Fig. 4 shows the limited data available for partially water-saturated quartz sand (air was the

TABLE 3 — PHYSICAL PROPERTIES OF UNEXTRACTED KERN RIVER OIL SANDS

Depth (ft)	Porosity (fraction)	Bulk Density (lb/cu ft)	Median Grain Size (in.)	Saturations Water	Saturations Oil	Thermal Conductivity (Btu/ft-hr-°F)
374 to 380	0.30	128.	0.033	0.51	0.23	1.03
	0.29	132.		0.61	0.31	1.12
	0.30	132.		0.60	0.27	1.12
	0.32	123.		0.37	0.26	0.91
	0.33	122.		0.18	0.22	0.85
	0.31	125.		0.28	0.44	0.85
	0.31	129.		0.50	0.32	1.08
	0.30	125.		0.60	0.00	1.15
	0.29	132.		0.81	0.00	1.28
	0.30	121.		0.07	0.29	0.72
	0.28	134.		0.60	0.26	1.15
	0.31	118.		0.10	0.20	0.67
	0.28	116.		0.00	0.00	0.36
	0.26	135.		1.00	0.00	1.42
543 to 550	0.33	129.	0.0164	0.34	0.64	0.92
	0.33	129.		0.29	0.67	0.83
	0.33	129.		0.37	0.62	0.90
	0.35	131.		0.34	0.55	0.93
	0.33	130.		0.33	0.61	0.90
	0.33	125.		0.37	0.56	0.93
	0.30	129.		0.29	0.46	0.91
	0.30	127.		0.28	0.34	0.90
	0.35	121.		0.08	0.53	0.63
	0.31	128.		0.25	0.52	0.80
	0.31	129.		0.77	0.00	1.31
	0.31	128.		0.76	0.00	1.29
	0.33	127.		0.78	0.00	1.22
	0.31	130.		0.95	0.00	1.34
	0.32	112.		0.00	0.00	0.30
	0.31	132.		1.00	0.00	1.38
614 to 617	0.31	130.	0.0116	0.46	0.44	0.94
	0.32	129.		0.46	0.41	0.91
	0.35	125.		0.37	0.43	0.86
	0.36	127.		0.54	0.40	0.93
	0.32	126.		0.38	0.46	0.90
	0.34	127.		0.87	0.00	1.19
	0.33	117.		0.07	0.32	0.56
	0.32	121.		0.13	0.39	0.67
	0.32	117.		0.05	0.25	0.59
	0.33	124.		0.65	0.00	1.17
	0.30	127.		0.71	0.00	1.31
	0.35	126.		0.92	0.00	1.16
	0.34	122.		0.68	0.00	1.13
	0.37	103.		0.00	0.00	0.27
	0.34	129.		1.00	0.00	1.20

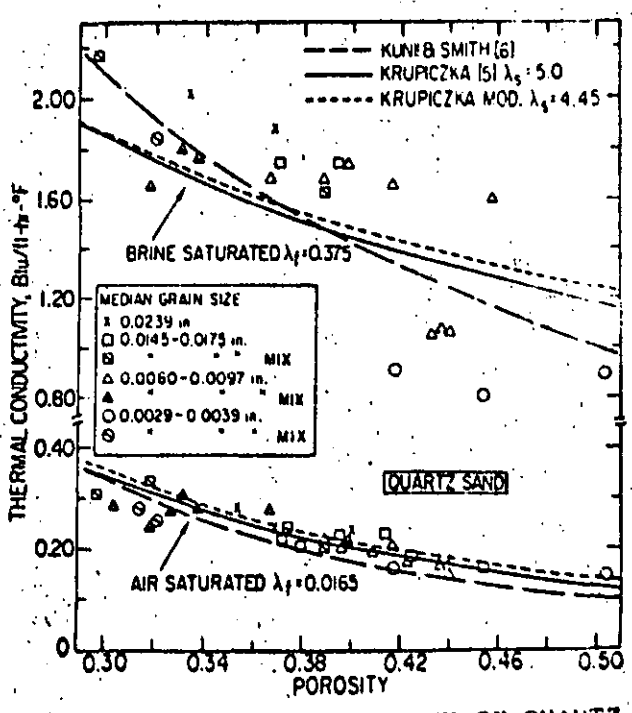

FIG. 1 — THERMAL CONDUCTIVITY OF QUARTZ SANDS.

nonwetting phase).[9] For comparison, a curve is shown for oil sands calculated from Eq. 3 at the same porosity as the quartz sand pack ($\phi = 0.335$). It is apparent that the slope for the quartz sand is greater than that for the oil sand. To fit a curve of the type given by Eq. 3, S_w must be multiplied by a numerical coefficient greater than unity. This coefficient has been assigned the value of the ratio of the thermal conductivity of quartz, $\lambda_{s(q)}$, to the conductivity value used for the oil sand, $\lambda_{s(os)}$:

$$\frac{\lambda_{s(q)}}{\lambda_{s(os)}} = \frac{5.0}{2.75} = 1.815 .$$

Eq. 3 can thus be modified to

$$\lambda_{sw} = 0.735 - 1.30\,\phi + 0.363\,\lambda_s S_w^{1/2} . \quad \ldots\ldots\ldots\ldots\ldots\ldots (4)$$

Values calculated from Eq. 4 and shown in Fig. 4 as the solid line give quite a good match to the experimental data for quartz sand with variable brine saturation.

ANALYSIS OF RESULTS

Multiple regression analysis techniques were used to evaluate the data in Tables 1 and 2 and in Table 3. For the quartz sand data and the extracted oil sand data, combinations of variables were used, including porosity, permeability, formation resistivity factor, median grain size, grain-size distribution, and conductivity of saturating fluids and of solid matrix. Results of the analysis reported by Keese[7] showed that for unconsolidated sands, the conductivity of the saturating fluid has an overwhelming effect. Grain-size distribution and formation resistivity factor have small effects, the other variables having about equal, moderate effects on thermal conductivity. Results showed a definite relationship between porosity and grain size and between porosity and permeability. It was concluded that porosity alone was an adequate correlating parameter for the matrix structure of unconsolidated sands. Thus it appears that the pertinent variables are porosity and the conductivities of the liquid and solid phases. This agrees with earlier investigations for unconsolidated sands saturated with a single fluid.

For the unextracted oil sands, an additional variable of mixed fluid saturations was included in the analysis. Results reported in detail by Chu[10] showed that oil saturation, when included with water saturation in the correlation, had little effect on thermal conductivity. In fact in the range of oil saturations for the present samples (0 to 0.67) it appeared to make no appreciable difference whether the nonwetting phase was oil or air. It should be noted that the total liquid saturation for unextracted oil sands was less than unity in all cases, the remainder being air or gas saturation. The correlation was improved when water saturation was taken to a fractional power (approximately 1/3).

In summary, it seems reasonable to assume that

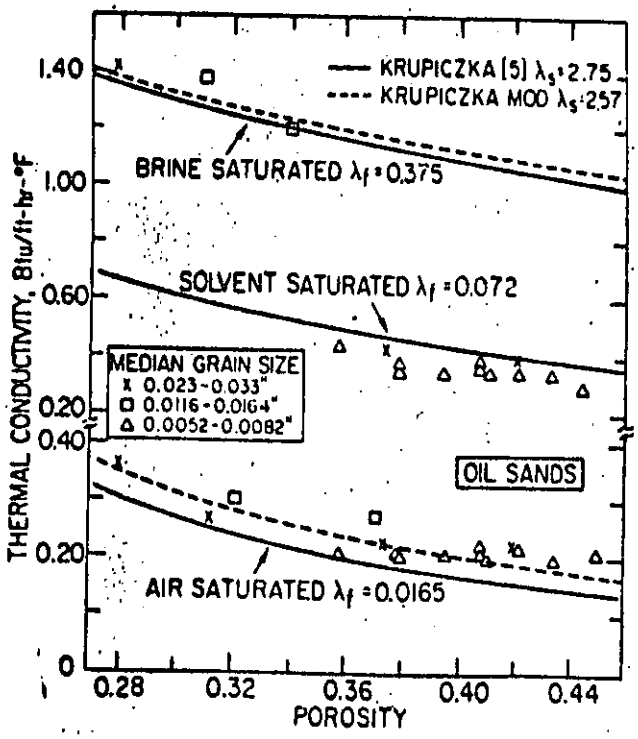

FIG. 2 — THERMAL CONDUCTIVITY OF OIL SANDS.

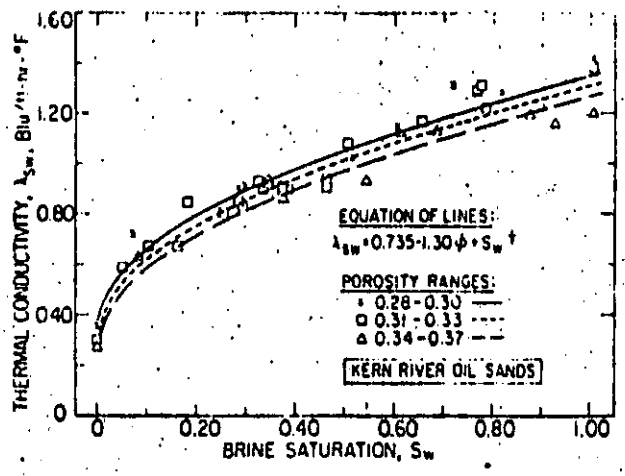

FIG. 3 — THERMAL CONDUCTIVITY OF KERN RIVER OIL SANDS.

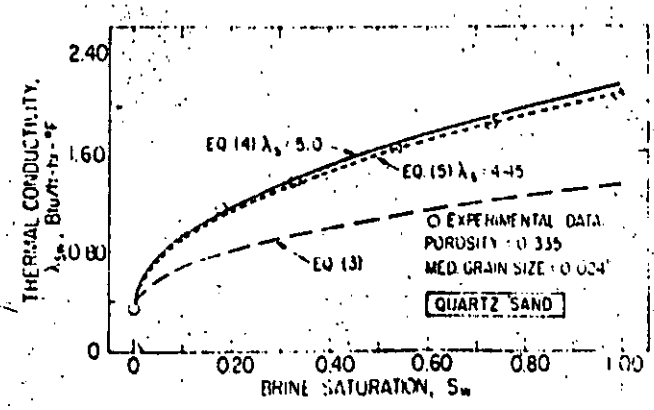

FIG. 4 — THERMAL CONDUCTIVITY OF PARTIALLY BRINE-SATURATED QUARTZ SAND.

the quantities of porosity, water saturation, and conductivities of solid and liquid phases are sufficient to obtain useful correlations.

The best fit for the data given in Figs. 3 and 4 is expressed by Eq. 4. The average error for all the data was 4 percent and three-fourths of the data points had errors of 5 percent or less. This agreement is excellent, considering that oil saturations of the samples ranged from zero in the case of quartz sands and extracted oil sands to as high as 67 percent for unextracted oil sands. The amount of oil saturation appeared to have no effect on the percent error.

If Eq. 4 is applied to data in Tables 1 and 2, a somewhat larger error results. For the air-saturated sands the average error was 9.3 percent. For brine-saturated sands the values calculated from Eq. 4 were high, averaging 16.5 percent larger than the experimental values. Since Eq. 4 also gave slightly high values for quartz sand data shown in Fig. 4, it seemed desirable to check the assumed values of solids conductivity, λ_s. Recently published data on thermal conductivity of common rock-forming minerals by Horai[12] are summarized in Table 4. The reported value for quartz is 4.45 Btu/ft-hr-°F compared with the value of 5.0 used in the present analysis. Results of mineral analysis of the oil sands are given in Table 5. From this analysis and the mineral conductivity data, λ_s was calculated for the oil sands. It was necessary to assume a value of conductivity for the alteration products, kaolinite and sericite, as 1.60 Btu/ft-hr-°F. On a weighted-average basis (parallel conductors), λ_s for the oil sands was found to be 2.57 rather than the assumed value of 2.75. On the basis of series conductors, the value dropped to 1.97, and a geometric average gave a value of 2.25 Btu/ft-hr-°F.

Use of the above values of solids conductivity will change the numerical coefficient in the third term of Eq. 4 to 0.39. This will have no effect on the correlation of oil sand data, but will improve the fit of the quartz sand data to the equation.

TABLE 4 — THERMAL CONDUCTIVITY OF ROCK-FORMING MINERALS[12]

Mineral	Density (gm/cc)	Thermal Conductivity (Cal/cm-sec-°C)	Thermal Conductivity (Btu/ft-hr-°F)
Quartz	2.647	0.01837	4.45
Orthoclase	2.583	0.00553	1.34
Plagioclase	2.618	0.00512	1.24
Calcite	2.721	0.00858	2.08
Muscovite	2.872	0.00529	1.28
Chlorite	2.763	0.00174	2.84
Hornblende	3.111	0.00735	1.78
Epidote	3.413	0.00627	1.51
Sphene	3.525	0.00558	1.35
Biotite	2.886	0.00559	1.35

TABLE 5—MINERAL ANALYSIS AND CALCULATED SOLIDS CONDUCTIVITY—OIL SANDS

Mineral	Fraction (n)	λ	n × λ
Quartz	0.34	4.45	1.513
Orthoclase	0.01	1.34	0.013
Plagioclase	0.21	1.24	0.260
Kaolinite-Sericite	0.25	1.60	0.400
Chlorite	0.07	2.84	0.197
Hornblende	0.04	1.78	0.072
Sphene	0.02	1.35	0.027
Epidote	0.02	1.51	0.030
Others	0.04	1.35	0.054
Total	1.00		2.566

APPLICATIONS OF CORRELATIONS

Eq. 3 may be used to estimate thermal conductivity of oil sands having low quartz content and porosities between 28 and 37 percent. For sands with higher quartz content, a correlation including conductivity of the solid phase is needed to improve the estimate. A relation of the form of Eq. 4 may be used with a modified numerical coefficient as

$$\lambda_{SW} = 0.735 - 1.30\,\phi + 0.390\,\lambda_s S_w^{1/2} \quad \ldots\ldots\ldots\ldots\ldots\ldots\ldots (5)$$

If a mineral analysis is available, an estimate of solids conductivity, λ_s, may be made using mineral conductivity values given in Table 5 and assuming that a weighted average value applies. If a mineral analysis is not available but the quartz content can be estimated, the solids conductivity can be estimated from the relation

$$\lambda_s = 4.45\,Q + 1.65\,(1 - Q) \quad \ldots\ldots (6)$$

where Q is the fractional quartz content.

The first two terms in Eq. 5 ($0.735 - 1.30\phi$) give an estimate of thermal conductivity of air-saturated sands. The Krupiczka equation may give more realistic values, provided the correct numerical constants are known. By modifying the constant A to

$$A' = 0.362 - 0.650 \log \phi ,$$

we obtain a better fit of Eq. 1 to the results for both the dry quartz sand and the extracted oil sand. (See dotted lines in Figs. 1 and 2.) Eqs. 1 and 5 may be combined to form the following:

$$\lambda_{SW} = \lambda_f(\lambda_s/\lambda_f)^{A'+B\,\log\lambda_s/\lambda_f} + 0.390\lambda_s S_w^{1/2} \quad \ldots\ldots\ldots\ldots\ldots\ldots\ldots (7)$$

Since the fluid is air, λ_f may be assigned a value of 0.0165 Btu/ft-hr-°F. From the trend of the data in Figs. 1 and 2, it appears likely that Eq. 7 will be valid over a porosity range of 28 to 46 percent.

Additional investigations are needed on sands of different mineral and fluid compositions before the foregoing equations can be applied generally. The effects of mixed liquid saturations and the wettability of mineral grain surfaces need further study.

EFFECT OF TEMPERATURE ON THERMAL CONDUCTIVITY

Earlier work[12] presented a method for predicting the change of thermal conductivity with temperature. With the work of Tikhomirov[13] as a guide, an equation was developed for a family of curves that defined conductivity-temperature trends for a large body of experimental data. High-conductivity materials show large decreases in conductivity with increases in temperature. Low-conductivity materials, on the other hand, may actually show small increases in thermal conductivity with increased temperatures. Unconsolidated sands fall in the low- to medium-conductivity category, in which range the change of conductivity with temperature is nearly linear. The equation developed earlier can thus be simplified to the following:

$$\lambda_t = \lambda_{125} - 1.28 \times 10^{3} (T-125) (\lambda_{125} - 0.82) \quad \ldots\ldots\ldots (8)$$

where

λ_t = conductivity at any temperature, Btu/ft-hr-°F,

λ_{125} = conductivity at a temperature of 125°F, Btu/ft-hr-°F,

T = temperature, °F.

Eq. 10 yields a family of straight lines with positive slopes for conductivity values below (λ_{125} = 0.82 Btu/ft-hr-°F) and negative slopes for higher (λ_{125}) values.

EFFECT OF PRESSURE

The effect of pressure on thermal conductivity has been found to be relatively small.[11] The following expression may be applied to highly compressible formations:

$$\frac{\Delta\lambda}{\Delta P} = 10^{-5}[0.50\rho_b\phi + 5.75\phi - 0.37k^{0.10} + 0.12F] \quad \ldots\ldots (9)$$

where

$\Delta\lambda/\Delta P$ = change in conductivity with pressure, Btu/ft-hr-°F-psi,

ρ_b = bulk density, gm/cc,

ϕ = fractional porosity,

k = permeability, md,

F = formation resistivity factor.

If typical data for brine-saturated sands are used, the change in conductivity would be less than 1 percent per 1,000-psi change in pressure. For dry sands the change would be less than 4 percent for the same change in pressure.

We did not test the above expression on unconsolidated sands because pressure changes would have had an adverse effect on the experimental technique. However, the effect of pressure changes on the thermal conductivity of liquid-saturated unconsolidated sands is considered to be small enough to ignore, except when fluid phase changes occur.

CONCLUSIONS

Equations have been presented for use in estimating the thermal conductivity of partially liquid-saturated unconsolidated sands. Knowledge of the porosity and water saturation and some notion of the quartz content of the sand is needed for estimating thermal conductivity. Although the equations are based on data obtained on quartz sands and California unconsolidated oil sands, they should have general application to unconsolidated oil sands.

A simplified equation has also been developed for estimating the effect of temperature changes on thermal conductivity. It appears that pressure changes have little effect on thermal conductivity unless phase changes occur.

Research is being continued in an effort to evaluate more quantitatively the effects of mixed liquid- and of partial liquid-saturation on thermal conductivities of sands. The wettability of sand grain surfaces may play an important role in the heat-transfer mechanism and needs to be investigated.

ACKNOWLEDGMENTS

The work was performed as part of API Research Projects 117 and 155. Core samples were provided by Chevron Oil Field Research Co. and Getty Oil Co. We wish to thank those companies and API for their support.

REFERENCES

1. Schumann, J. E., and Voss, V.: "Heat Flow Through Granulated Materials," *Fuel* (1934) Vol. 13, 249.

2. DeVries, D. A.: *Mededelingen van de Landbouwhogeschoolte Wageningen* (1952) Vol. 52, 1.

3. Woodside, W., and Messmer, J. H.: "Thermal Conductivity of Porous Media. I. Unconsolidated Sands," *J. Applied Physics* (1961) Vol. 32, No. 9, 1688.

4. Krupiczka, R.: "Analysis of Thermal Conductivity in Granular Materials," *Intl. Chem. Eng.* (1967) Vol. 7, No. 1, 122.

5. Kunii, D., and Smith, J. M.: "Heat Transfer Characteristics of Porous Rocks," *AIChE Jour.* (1960) Vol. 6, No. 1, 71.

6. Anand, J.: "Thermal Conductivity of Fluid Saturated Rocks at Elevated Pressures and Temperatures," MS thesis, U. of California, Berkeley (1971).

7. Keese, J. A.: "Thermal Conductivity of Unconsolidated Oil Sands," MS thesis, U. of California, Berkeley (1973).

8. "Thermal Properties of Partially Liquid Saturated Rocks at Elevated Temperatures and Pressures," API RP 155, U. of California, Berkeley (1972-74).

9. Gomaa, E. E.: "Thermal Behavior of Partially Liquid Saturated Porous Media," PhD dissertation, U. of California, Berkeley (1973).

10. Chu, S. L.: "Thermal Conductivity of Brine-Oil Bearing Unconsolidated Oil Sand," MS Research Report, U. of California, Berkeley (1973).

11. Anand, J., Somerton, W. H., and Gomaa, E.: "Prediction of Thermal Conductivities of Formations From Other Known Properties," *Soc. Pet. Eng. J.* (Oct. 1973) 267-273.

12. Horai, Ki-iti: "Thermal Conductivity of Rock-Forming Minerals," *J. Geophys. Research* (1971) Vol. 76, No. 5, 1278.

13. Tikhomirov, V. M.: "Conductivity of Rocks and Their Relationship with Density, Saturation and Temperature," *Neftianoe* Khoziaistra (1968) Vol. 46, No. 4, 36.

***

CURSO: "INGENIERIA DE YACIMIENTOS GEOTERMICOS "
13 DE MARZO AL 18 DE MAYO DE 1984

tema; "PREDICTING THERMAL CONDUCTIVITIES OF-
FORMATIONS FROM OTHER KNOWN PROPERTIES."

DR. JESUS RIVERA RODRIGUEZ
13-23 MARZO
MATERIAL ADICIONAL.

JRR DR. JESUS RIVERA RODRIGUEZ

Predicting Thermal Conductivities of Formations From Other Known Properties

J. ANAND*
W. H. SOMERTON
E. GOMAA**
MEMBERS AIME

U. OF CALIFORNIA AT BERKELEY
BERKELEY, CALIF.

ABSTRACT

Measuring the thermal properties of rocks and rock-fluid systems is difficult and time consuming, and the results from such measurements are of limited value unless complete descriptions of the rock and fluids are given. A need exists for a method of predicting thermal behavior from other more easily measurable properties. Presented here are correlations developed for predicting the thermal conductivity of consolidated sandstones from a knowledge of density, porosity, permeability, and formation resistivity factor. Values for all these properties are available from well logs or core analysis data. Also obtained were correlations for estimating the thermal conductivity of liquid-saturated sandstones from a knowledge of the conductivities of dry sandstones and the saturating liquid and properties of the sandstone. The thermal conductivity of most rocks decreases with increasing temperature and a method of estimating this effect is presented. The effect of pressure on conductivities is generally small, but may be predicted from a knowledge of the bulk compressibility of the rock.

INTRODUCTION

Although thermal recovery processes have been applied in the petroleum industry for many years, there is still a lack of basic thermal data with which to predict the performance of these processes. Much of the thermal conductivity work reported in the literature lacks a complete description of the physical properties of the rocks used, and in addition, most of the thermal conductivity measurements have been made at room temperature and at atmospheric pressure. The work reported in this paper deals with the thermal conductivity of typical porous rocks at simulated subsurface conditions of temperature, pressure, and saturation. Because thermal conductivity is difficult to measure, emphasis has been placed here on methods of predicting thermal conductivity from other more easily measured properties as well as on methods of predicting the effects of temperature, pressure, and liquid saturation on thermal properties.

RELATIONSHIP OF THERMAL CONDUCTIVITY TO OTHER PHYSICAL PROPERTIES

The thermal conductivities of dry rocks have been shown to be functions of density, porosity, grain size and shape, cementation, and mineral composition.[1] The first two properties are easy to measure and precise values may be assigned for correlation purposes. Grain size and shape and cementation are difficult to quantify. There are, however, other related properties that can be used to characterize these properties for use in correlations. Permeability and formation resistivity factors are probably most closely related to these properties and are readily measurable as unique values. Precise mineral composition values are generally not available, and even if they were, it would be difficult to introduce them into correlations. The high thermal conductivity of quartz seems to have a predominating influence, and thus for most sandstones containing quartz in moderate amounts, the effects of other minerals can be ignored.

Many efforts have been made to relate thermal conductivity to the physical properties of porous rocks. These efforts have been reviewed in rather complete detail by Scorer[1] and Anand.[2] Unfortunately, most of the correlations developed require a knowledge of the thermal conductivity of the rock matrix or the dry rock at some known porosity. Although some simple correlations have been obtained, these are for specific systems and are not applicable generally. Probably the most useful work in this area is that reported by Zierfuss and Van der Vliet.[3] Basing their analysis on 36 sandstones having a wide range in measured properties, they obtained a correlation between effective porosity and the product of thermal conductivity and formation resistivity factor. A fourth-order polynomial fit of thermal conductivity and fractional porosity was obtained by regression analysis. Their data also seemed to indicate that thermal conductivity increases with permeability, this being attributed to conduction in wider pores.

In the work discussed here, multiple regression

Paper (SPE 4171) was presented at SPE-AIME 43rd Annual California Regional Fall Meeting, held in Bakersfield, Nov. 8-10, 1972.

*Now at U. of Southern California, Los Angeles.

**Now with Standard Oil Co. of California, San Francisco.

[1] References given at end of paper.

analyses using all the known physical properties of rocks were employed to obtain a useful relationship for predicting thermal conductivity.

THERMAL CONDUCTIVITIES OF LIQUID-SATURATED ROCKS

The thermal conductivity of fluid-saturated rocks is dependent upon the conductivities of the dry rock and the saturating fluid and physical properties of the rock. Assad,[4] Sugawara and Yoshizawa[5] and Van der Vliet[3] have dealt with this problem; however, testing their relationships with data from the literature[3] and with the data we obtained did not yield satisfactory results. The difficulty seems to lie in the fact that, although liquid-saturated rocks have higher conductivities than dry rocks, the amount of increase is a complex function of the amount, character, and distribution of pore space, and the conductivity of the saturating fluid.

Earlier efforts[2] to develop correlations using regression analysis on common physical properties of the rock fluid system were only partially successful. In the present work, nonlinear multiple regression analysis on dimensionless groupings of properties of the system gave satisfactory relationships.

EFFECT OF TEMPERATURE ON THERMAL CONDUCTIVITY

The thermal conductivity of most materials that have crystalline structures decreases with increased temperature.[6] Theory indicates that thermal conductivity should vary with the reciprocal of temperature. In mixed crystals and highly disordered crystals, conductivity varies more slowly than T^{-1} and, in fact, may show a slight increase with temperature. The thermal conductivity of glasses and vitreous materials increases with temperature.

To predict the effect of temperature on the thermal conductivity of rocks, Tikhomirov[7] developed a correlation equation based on experimental data. A plot of this equation shows that moderate negative gradients of thermal conductivity with temperature will be predicted for high-conductivity rocks, whereas small positive gradients will be predicted for low-conductivity rocks. This agrees with theory and with the experimental results of our investigation.

For the work discussed here, we developed a modified expression of the same general form as Tikhomirov's equation. This expression predicts the thermal conductivity-temperature behavior of liquid-saturated rocks as well as of dry rocks.

EFFECT OF PRESSURE ON THERMAL CONDUCTIVITY

Several investigators have shown that thermal conductivity increases with an increase in effective stress on the rock.[8-10] This should be expected since increasing the stress improves the thermal contact between grains and increases the over-all density of the rock and, consequently, the thermal conductivity.

In measuring thermal conductivity in the laboratory a large part of the apparent increase in conductivity with pressure may actually be due to reduction in thermal contact resistances between the several contacting surfaces: heat source, heat sink, the temperature measuring devices, the standards, and the test specimen. When good thermal contact is established, the change in thermal conductivity with added stress is generally small.

A relation between the bulk compressibility of porous rocks and the change in thermal conductivity should be expected. Edmondson[9] showed that the thermal conductivities of Berea, Bandera, and Boise sandstones increase by 7.8, 9.5, and 12.3 percent/1,000 psi, respectively, in the pressure range of 900 to 3,600 psi. The compressibilities of Berea, Bandera, and Boise sandstones are reported by Lobree[11] to be 4.54×10^{-7}/psi, 6.46×10^{-7}/psi, and 9.0×10^{-7}/psi, respectively. If these data are plotted as shown in Fig. 1, a linear relation is obtained. Edmondson's values for the increase in conductivity with pressure are high compared with results obtained by Woodside and Messmer[10] and with those obtained in our work. An increase of 11.5 percent/1,000 psi in the pressure range of zero to 1,000 psi, and an increase of 2.5 percent/1,000 psi in the pressure range of 2,000 to 4,000 psi for Berea sandstone, were reported by Woodside and Messmer.

The effect of pore pressure is to reduce the effective stress on the rock. More realistically, a reduction in fluid pore pressure results in increased effective stress on the rock and thus an increase in thermal conductivity. Pore pressure may also be associated with the phase behavior of contained fluids. Reduction in pore pressure may result in the vaporization of some of the liquid components and this may cause a large reduction in thermal conductivity. This is a fluid saturation effect and should not be attributed to pore pressure *per se*.

EXPERIMENTAL WORK

APPARATUS AND PROCEDURE

Correlation equations were developed mainly from data taken from the literature.[3] To test these correlations, a new set of data was obtained and the correlations were modified slightly in some cases to fit these new data.

Thermal conductivities were measured in a steady-state comparator apparatus (described in detail in Ref. 2). The apparatus, shown schematically in Fig. 2, consists essentially of a stack containing a holder for the disc-shaped sample of unknown conductivity. The sample is sandwiched between two holders containing standards of the same geometry as the unknown sample, but for which the conductivities are accurately known. Thermocouples are mounted in the centers of sample and standard holder plates so that the temperatures across the sample and the standards may be measured. The heat source at the top of the stack is a tank in which heated silicone oil is circulated from a constant-temperature bath. The heat sink at

the bottom of the stack is a plate through which silicone oil is circulated from a second constant-temperature bath. Thus heat flows vertically downward to minimize convective heat transfer. The total temperature drop across the stack is small — about 40 to 50°F — and radiative heat transfer is considered to be negligible.

The sample and standard holders are made of Bakelite, which has a thermal conductivity about an order of magnitude less than that of most of the samples measured. To minimize radial heat losses, however, a Bakelite ring on which heating tapes are mounted surrounds the stack and is maintained at the midpoint temperature of the stack. The space between the guard heater and the stack is filled with a ceramic fiber insulation. The entire apparatus

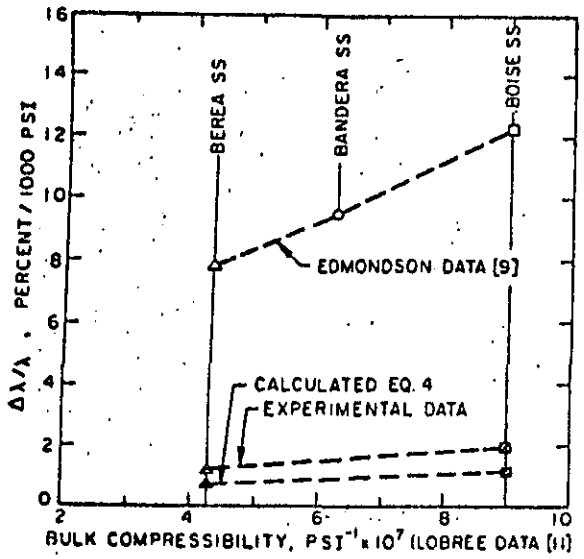

FIG. 1 — EFFECT OF PRESSURE ON THERMAL CONDUCTIVITY VS ROCK COMPRESSIBILITY.

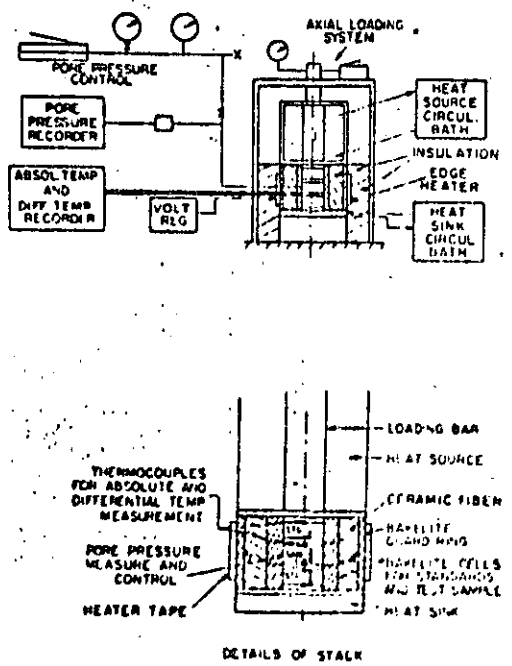

FIG. 2 — SCHEMATIC DIAGRAM OF THERMAL CONDUCTIVITY APPARATUS.

is mounted in a loading frame so that controlled axial stress may be applied. On the sample holder is a pore pressure fitting and a line that connects to a pressure recording and control system.

Pyroceram glass ceramic code 9609 was used for the standards. Its conductivity is quite close to that of sandstones; it is capable of withstanding the loads to which it must be subjected; and it is quite stable at temperatures used in the experiments.

A multipoint strip-chart recorder was used to monitor the temperatures of the six thermocouples. When the apparatus reached steady-state conditions (in 3 to 4 hours), differential temperatures across the two standards and the sample were recorded. Thermal conductivities were calculated on the basis of these data and of the known conductivities of the standards.

The test specimens and the standards were discs 2 in. in diameter and 0.625 in. thick. All samples were run dry and saturated with brine (0.1 N potassium chloride). Several samples were also run saturated with silicone oil (a dimethyl polysiloane), Stoddard solvent, and *n*-hexane. A high-temperature version of this apparatus was used to extend the temperature correlation.

Other physical properties of the sandstone samples were measured with standard laboratory equipment. These properties include density, porosity, permeability, and electrical resistivity factor.

EXPERIMENTAL RESULTS

Typical results of the thermal conductivity measurements are shown in Figs. 3 through 5. The maximum error expected in these tests is ±5 percent as calculated by error analysis.[2] In general, thermal conductivity decreases linearly with increase in temperature, the decrease being much more pronounced for liquid-saturated samples than for dry samples.

Liquid saturation increases thermal conductivity substantially. The amount of increase is related to the thermal conductivity of the saturating fluid and to the properties of the rock, including porosity and thermal conductivity in the dry state. It should be pointed out that all liquid-saturated samples were

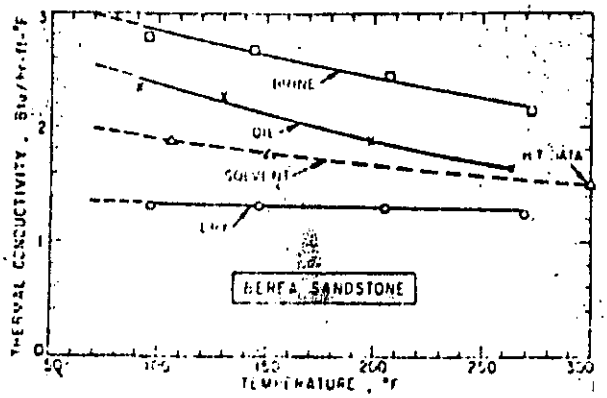

FIG. 3 — THERMAL CONDUCTIVITY OF BEREA SANDSTONE — EFFECTS OF TEMPERATURE AND FLUID SATURATION.

Sample	Density (gm/cc)	Porosity	Resistivity Factor	Permeability (md)	Thermal Conductivity at 67°F, Btu/hr-ft-°F: Dry	Brine	Silicone Oil	Stoddard Solvent
Berea	2.15	0.162	13.0	190	1.35	3.00	2.55	1.98
Bandera	2.10	0.208	13.0	38	0.98	2.06	1.90	1.57
Boise	1.84	0.292	7.9	2,513	0.85	1.78	1.22	1.19
SS No. 1	2.22	0.160	18.5	152	1.47	2.96	1.65	—
SS No. 2	2.00	0.250	10.9	557	1.10	3.26	2.24	—
SS No. 3	2.26	0.149	12.0	34	0.92	1.42	—	—
Venango	2.34	0.122	35.9	437	2.39	—	—	—
Gatchell	2.04	0.227	13.3	858	1.19	—	—	—

fully saturated and that pore pressure was maintained high enough to avoid vapor formation at the temperature of the test.

Most thermal conductivity tests were run at an axial stress of 565 psi, this stress level being high enough to minimize the effect of contact resistance. Fig. 6 shows thermal conductivities of Berea, Boise, and SS 2 for different axial stress levels. The apparent thermal conductivity increases sharply from a stress of zero to approximately 400 to 500 psi and then rises at a low and constant rate. For Berea and Boise sandstones, thermal conductivities increase by 1.25 percent/1,000 psi and 2.0 percent /1,000 psi, respectively. These values are much lower than those reported earlier by Edmondson.[9]

Other physical properties of the sandstones, including density, porosity, permeability, and formation resistivity factor, are given in Table 1.

Thermal conductivity was measured on one shale sample that was first air dried and then brine saturated (see Fig. 5). The low conductivity values and the slightly positive gradients with temperature are typical for fine-grained rocks. The air-dried and brine-saturated densities are given in Fig. 5 for comparison purposes.

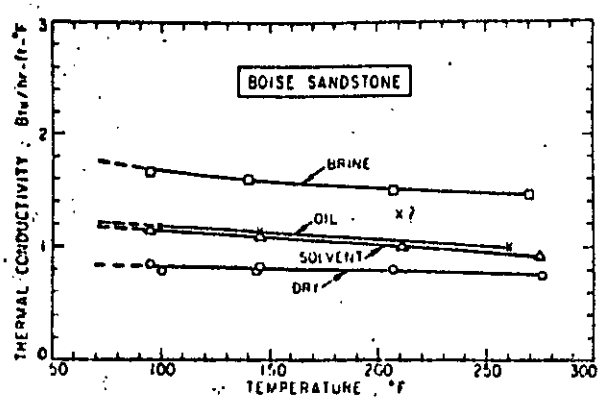

FIG. 4 — THERMAL CONDUCTIVITY OF BOISE SANDSTONE — EFFECTS OF TEMPERATURE AND FLUID SATURATION.

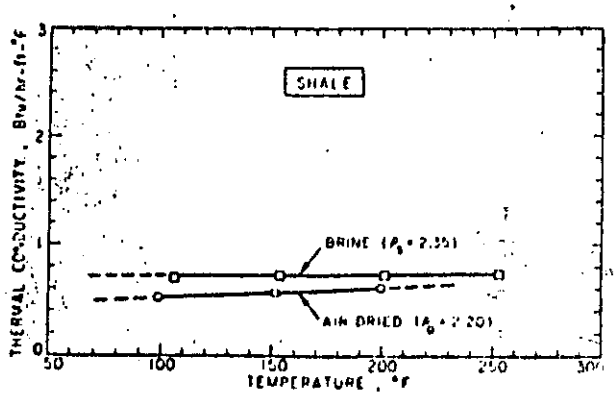

FIG. 5 — THERMAL CONDUCTIVITY OF SHALE — EFFECT OF TEMPERATURE AND FLUID SATURATION.

CORRELATIONS

It should be apparent from the foregoing that the measurement of thermal conductivity of rocks is difficult, time consuming, and of limited practical value unless some generalized relationships to other physical properties and to changes in environmental conditions can be developed. In the following section, the results of our investigation are used to test such relationships developed from literature data. Also presented are methods of predicting the thermal behavior of rocks from other more easily measured properties.

THERMAL CONDUCTIVITIES OF DRY SANDSTONES

Multiple regression analyses run on thermal conductivity and physical property data from the literature[3] and from our work yielded the following equation.

$$\lambda = 0.340\rho - 3.20\phi + 0.530k^{0.10} + 0.0130F - 0.031, \quad \ldots\ldots\ldots\ldots\ldots\ldots (1)$$

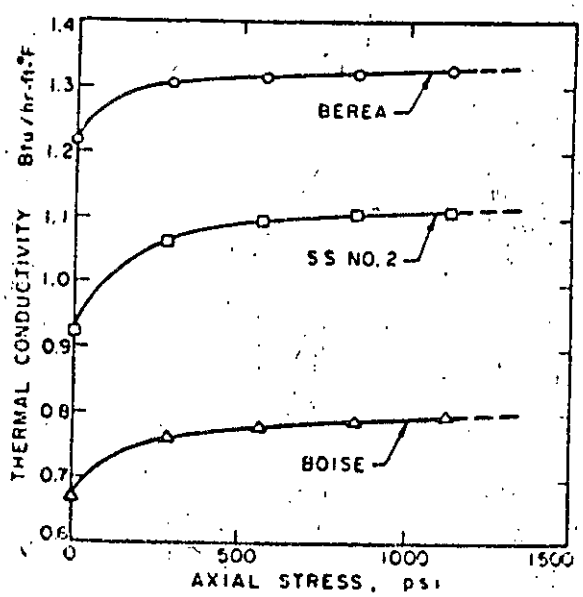

FIG. 6 — EFFECT OF AXIAL STRESS ON THERMAL CONDUCTIVITY.

where λ = thermal conductivity, Btu/hr-ft-°F
ρ = bulk density, gm/cc
ϕ = fractional porosity
k = permeability, md
F = formation resistivity factor

For 38 data points, the standard deviation was 0.139 for a conductivity range of 0.4 to 2.2 Btu/hr-ft-°F. The agreement between measured thermal conductivity values and calculated values is shown in Fig. 7. The solid line represents perfect agreement and the broken lines show the limits of one standard deviation. With one exception, data from our work were well within these limits. A deviation of less than 10 percent was obtained for 74 percent of the data points and less than 15 percent for 87 percent of the data points.

Further analysis of Eq. 1 indicates that porosity is the most important variable; density and permeability have about equal effect; and formation resistivity factor is the least important variable. The positive and negative numerical coefficients for density and porosity, respectively, are as expected. The positive coefficient for permeability is probably a reflection of the effect of grain size. Other factors being equal, permeability and thermal conductivity both increase with increased grain size. A study[2] of Zierfuss and Van der Vliet data confirms this observation. The positive coefficient for formation resistivity factor is apparently associated with its relation to bulk density and porosity.

Some question may arise as to the need for both density and porosity in the correlation equation since they are interrelated. By including both terms rather than using either terms alone, the correlation was definitely improved. This may be an expression of the effect of mineral composition since the less dense feldspars and clays are known to have lower thermal conductivities than quartz. As was pointed out earlier, we did not include matrix conductivity in our correlation because of the usual lack of knowledge of mineral composition and the difficulty of assigning conductivity values.

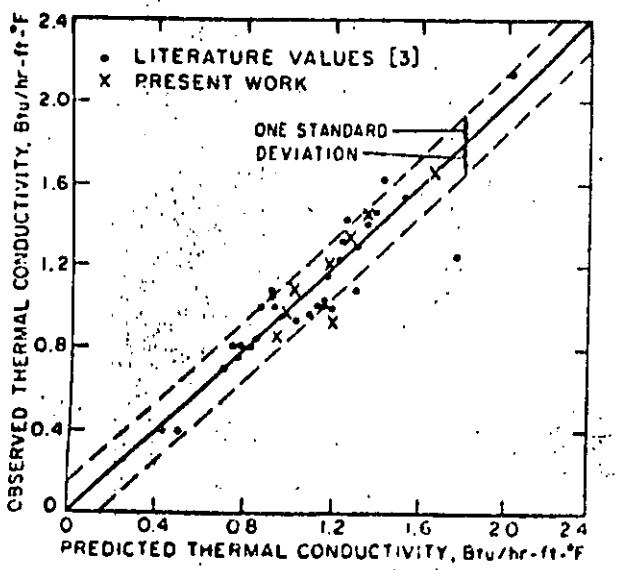

FIG. 7 — AGREEMENT BETWEEN MEASURED AND CALCULATED THERMAL CONDUCTIVITY VALUES.

THERMAL CONDUCTIVITIES OF LIQUID-SATURATED SANDSTONES

Several efforts were made to obtain correlations for predicting thermal conductivities of liquid-saturated sandstones. The most satisfactory correlation was obtained with the following dimensionless groupings or quantities.

$$\frac{\lambda_s}{\lambda_d}, \left(\frac{\lambda_l}{\lambda_a} - 1\right), \left(\frac{\phi}{1-\phi}\frac{\lambda_l}{\lambda_d}\right), \frac{\rho_s}{\rho_d}, m,$$

where λ = thermal conductivity
ϕ = fractional porosity
ρ = bulk density of rock
m = Archie's cementation factor

and where subscripts are defined as follows:

a = air
d = dry rock
l = saturation fluid
s = liquid-saturated rock.

When a nonlinear, multiple regression computer program was applied to literature data,[3] the following equation gave the best fit.

$$\frac{\lambda_s}{\lambda_d} = 1.00 + 0.30\left[\frac{\lambda_l}{\lambda_a} - 1.00\right]^{0.33} + 4.57\left[\frac{\phi}{1-\phi}\cdot\frac{\lambda_l}{\lambda_d}\right]^{0.48m}\left[\frac{\rho_s}{\rho_d}\right]^{-4.30} \quad \ldots\ldots\ldots (2)$$

For the 52 literature data points used in the correlation, the standard deviation was 0.179 for the range of λ_s/λ_d ratio values of 1.20 to 2.30. The agreement between literature values and calculated values was within 10 percent for 56 percent of the values and within 15 percent for 85 percent of the values.

The agreement between literature values of the thermal conductivity ratio and values calculated from Eq. 2 is shown in Fig. 8. The solid line represents perfect agreement and the broken lines show the limits of one standard deviation. Experimental and calculated values from our work are plotted as X's in Fig. 8. Eleven of the 14 points are within one standard deviation, one point was out of the range of the correlation, and two points showed differences greater than one standard deviation. The low experimental point may be due to incomplete saturation of the test sample with the viscous silicone oil.

Since the correlation equation is expressed in terms of dimensionless ratios, m (the exponent in Archie's equation relating porosity and formation resistivity factor) was used in the correlation rather than resistivity factor itself. The effect of m in Eq. 2 is similar to the effect of F in Eq. 1 in that

increasing both values increases the conductivity. The conductivity of the saturating liquid has the dominant effect on the conductivity of the liquid-saturated rock. It is difficult to assess the relative importance of the other parameters in Eq. 2 because of their complicated interrelationships.

In the case of saturation with two liquids or liquids and a gas, the conductivity of the wetting phase has a dominant effect on the conductivity of the rock-fluid system. Thus for water-wet sandstones, the value of liquid conductivity to be used in the correlation should be biased toward the value of conductivity for the water. This matter is the subject of current investigations.

It would, of course, be possible to combine Eqs. 1 and 2 so that the thermal conductivity of liquid-saturated samples could be estimated directly from one equation. Regression analyses run on combined data for dry and liquid-saturated samples gave poor results. Part of the reason for this is that there is a difference in the heat transfer mechanism between solid and gas and solid and liquid. Assad[4] observed a substantial difference in the thermal conductivities of the same sandstone saturated with a gas and with a liquid of equal conductivity. For this reason, Eq. 2 should not be used in estimating the thermal conductivity of gas-saturated sandstones. The dry (air-saturated) value would be more suitable for this purpose.

EFFECT OF TEMPERATURE ON THERMAL CONDUCTIVITIES

The correlations discussed above have all been based on thermal conductivity values measured at or near room temperature. Our test data were extrapolated to 68°F (20°C) to obtain values for use in testing the correlations.

The effect of temperature on the thermal conductivities of the sandstones used was tested against Tikhomirov's correlation.[7] The results were not entirely satisfactory. Guided by Tikhomirov's correlation, we obtained a new family of curves but modified them according to the conductivity-temperature trends we had obtained. The equation of this family of curves is as follows.

$$\lambda_T = \lambda_{68°} - 0.71 \times 10^{-3}(T - 528)(\lambda_{68°} - 0.80) \cdot [\lambda_{68°}(T \times 10^{-3})^{-0.55\lambda_{68°}} + 0.74], \quad . \quad . \quad (3)$$

where λ_T = thermal conductivity at temperature T

$\lambda_{68°}$ = thermal conductivity at temperature 68°F

T = temperature, °R = °F + 460°

A plot of Eq. 3 based on even values of thermal conductivities at 68°F is shown as Fig. 9. The results of our conductivity-temperature measurements are plotted on the same figure. Although there is some scatter in the data, the general agreement is quite good. Additional data are needed in the higher conductivity and higher temperature ranges. A few results from tests using the high-temperature thermal conductivity apparatus have been included in Fig. 9 as X's joined by dashed lines.

Tikhomirov's correlation was developed for dry rocks, but the present correlation seems to be equally valid for liquid-saturated sandstones. Unusual thermal properties of some liquid saturants could cause some deviation of behavior from that predicted by Eq. 3, particularly for high-porosity rocks. In addition, phase changes of saturants may result in discontinuities, but this is a fluid saturation effect rather than a temperature effect *per se*.

The conductivity-temperature equation may need to be modified if it is to be applied to a greater range of rock-fluid systems. However, it can certainly be used as a general guide for predicting the thermal conductivity-temperature behavior of most sandstones.

EFFECT OF PRESSURE ON THERMAL CONDUCTIVITY

Most of the present thermal conductivity tests were run at an axial stress high enough to minimize the effect of contact resistance and at pore pressures high enough to keep all fluid saturants in liquid phase. Limited work at higher stresses indicated that thermal conductivities increase by

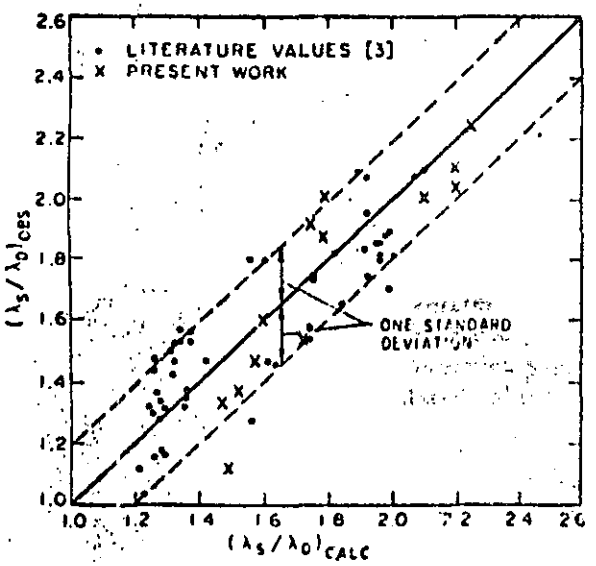

FIG. 8 — AGREEMENT BETWEEN MEASURED AND CALCULATED CONDUCTIVITY RATIOS.

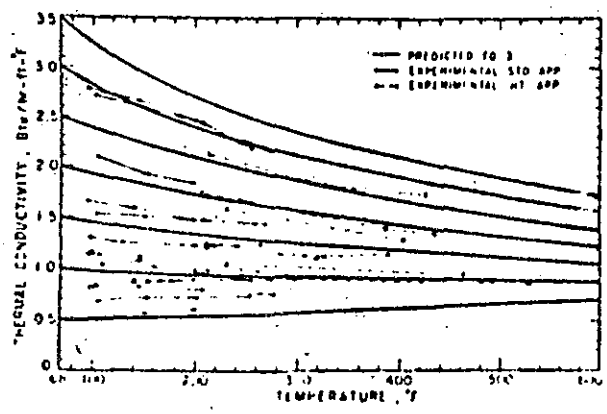

FIG. 9 — EFFECT OF TEMPERATURE ON THERMAL CONDUCTIVITY OF SANDSTONE.

only 1 to 2 percent for every 1,000 psi increase in effective stress. These values are somewhat lower than values reported in the literature.[8-10] In estimating the magnitude of the effect of stress on thermal conductivity, the known effects of stress on other properties were considered. Eq. 1 was first differentiated with respect to effective stress:

$$\frac{\partial \lambda}{\partial p} = 0.34 \frac{\lambda \rho}{\partial p} - 3.20 \frac{\partial \phi}{\partial p} + 0.053 k^{-0.90} \frac{\partial k}{\partial p} + 0.013 \frac{\partial F}{\partial p} \quad . \quad . \quad . \quad . \quad . \quad . \quad . \quad . \quad . \quad (4)$$

The derivative terms for density, porosity, permeability, and formation resistivity factor have been evaluated by Dobrynin[12] in terms of compressibilities. Assuming linear approximations, the following substitutions have been made for the derivative terms in Eq. 4.

$$\frac{1}{\rho} \frac{\partial \rho}{\partial p} = f_1 \phi, \quad \frac{1}{\phi} \frac{\partial \phi}{\partial p} = f_2, \quad \frac{1}{k} \frac{\partial k}{\partial p} = f_3,$$

$$\frac{1}{F} \frac{\partial F}{\partial p} = f_4,$$

where f_1, f_2, f_3 and f_4 are functions of compressibility. Since numerical magnitudes of the compressibility of rocks are generally not known, numerical coefficients for formations of high, medium and low compressibility may be substituted in the following general equation.

$$\frac{\partial \lambda}{\partial p} = 10^{-5} [A \rho \phi + B \phi - C k^{0.10} + DF], \quad . \quad . \quad (5)$$

where $\partial \lambda / \partial p$ = change in thermal conductivity, Btu/hr-ft-°F-psi

ρ = bulk density, gm/cc

ϕ = fractional porosity

k = permeability, md

F = formation resistivity factor

C_b	A	B	C	D
High	0.51	5.75	0.37	0.12
Medium	0.25	3.51	0.18	0.07
Low	0.13	1.44	0.09	0.034

Assuming Berea sandstone to be of medium-low compressibility and Boise sandstone to be of medium-high compressibility, 0.8 and 1.3 percent increases in thermal conductivity per 1,000 psi increase in stress, respectively, are calculated from Eq. 5. These compare with 1.25 and 2.0 percent increases obtained experimentally. (See Fig. 1.) This difference is probably due to the difference in stress levels in the two cases — about 1,000 psi average stress in the experimental determination and 2,000 psi average stress for calculated values.

SUMMARY AND CONCLUSIONS

The correlations given by Eqs. 1, 2, 3 and 5 are based on the limited amount of reliable data available and therefore must be considered as tentative. However, the general form of the relations is believed to be valid and useful for estimation purposes. And it is felt that even this step represents significant progress, considering the wide spread of thermal conductivity values appearing in the literature. These correlations will be improved and extended as more reliable data are obtained for a greater variety of rock types and over a broader range of environmental conditions.

Work is currently in progress at higher pressures and temperatures, on unconsolidated sands, and for multiple liquids and partial gas saturations.

ACKNOWLEDGMENTS

This work was performed as part of API Research Project 117. We thank API for this support. Also, for their support and encouragement, we express our sincere appreciation to the Project Guidance Committee, R. L. Bailey, Chairman, Chevron Oil Field Research Co.; E. J. Couch, Mobil Research and Development Corp.; and Vaughn Jones, Getty Oil Co. Several other students have assisted in the project — Doug Grandt, Ko Chen, and Jeff Keese — and their assistance as well as that of David White, Laboratory Mechanician, is acknowledged.

REFERENCES

1. Scorer, J. D. T.: "The Relationship Between Thermal Conductivity and Other Rock Properties," MS thesis, U. of California, Berkeley (1964).
2. Anand, J.: "Thermal Conductivity of Fluid Saturated Rocks at Elevated Pressures and Temperatures," MS thesis, U. of California, Berkeley (Sept. 1971).
3. Zierfuss, H. and Van der Vliet, G.: "Laboratory Measurements of Heat Conductivity of Sedimentary Rocks," *Bull.*, AAPG (1956) Vol. 40, No. 10, 2475.
4. Assad, Y.: "A Study of the Thermal Conductivity of Fluid Bearing Porous Rocks," PhD dissertation, U. of California, Berkeley (1955).
5. Sugawara and Yoshizawa: "An Investigation of the Thermal Conductivity of Porous Rocks," *Australian J. of Physics* (1961) Vol. 14, No. 4,469.
6. Powell, R. W., Ho, C. Y. and Liley, P. E.: *Thermal Conductivity of Selected Materials*, National Bureau of Standards, Washington (Nov. 1966).
7. Tikhomirov, V. M.: "Conductivity of Rocks and Their Relationship with Density, Saturation and Temperature," *Neftianoe Khoziaistro* (in Russian) (1968) Vol. 46, No. 4, 36.
8. Khan, A. M.: "A Thermoelectric Method for Measurement of Steady State Thermal Conductivity of Rocks," MS thesis, U. of California, Berkeley (1961).
9. Edmondson, T. A.: "Thermal Diffusivity of Sedimentary Rocks Subjected to Simulated Overburden Pressures," MS thesis, U. of California, Berkeley (1961).
10. Woodside, W. and Messmer, J. H.: "Thermal Conductivity of Porous Media," *J. Appl. Phys.* (1961) Vol. 39, No. 9, 1688.
11. Lobree, D. T.: "Measurement of Compressibilities of Reservoir Type Rock at Elevated Temperatures," MS thesis, U. of California, Berkeley (1968).
12. Dobrynin, V. M.: "Effect of Overburden Pressure on Some Properties of Sandstones," *Soc. Pet. Eng. J.* (Dec. 1962) 360-366; *Trans.*, AIME, Vol. 225.

CURSO:"INGENIERIA DE YACIMIENTOS GEOTERMICOS"
13 DE MARZO AL 18 DE MAYO 1984

tema; ADDITIONAL THERMAL DATA FOR POROUS ROCKS-THERMAL EXPANSION AND HEAT OF REACTION.

DR. JESUS RIVERA RODRIGUEZ
13-23de marzo
MATERIAL ADICIONAL.

DR. JESUS RIVERA RODRIGUEZ

(1)

Additional Thermal Data for Porous Rocks--Thermal Expansion and Heat of Reaction

W. H. SOMERTON
MEMBER AIME
M. A. SELIM

THE U. OF CALIFORNIA
BERKELEY, CALIF.

ABSTRACT

Thermal expansions and heats of reaction of three typical sandstones were measured in the temperature range of 25° to 1,000°C. The significance of these data in subsurface heat-transfer calculations is discussed.

Linear thermal expansions were measured both parallel and perpendicular to the bedding planes. Volume expansions are reported as the perpendicular expansion plus two times the parallel expansion. Expansion behavior of the sandstones was found to be controlled by the expansion characteristics of the quartz content. Differential expansion of the quartz grains and other minerals included in the sandstones caused permanent deformation of the heated samples after they were cooled to room temperature. Structural damage resulting from heating is probably an important cause of the reduction of thermal conductivity of heated samples.

Measurements of heats of reaction were based on the known heat required for α-β quartz inversion. Thermal reactions, which probably include dehydroxylation of clay minerals, and decomposition of carbonate minerals contained within the samples, were found to require more than one-fourth of the amount of heat necessary to raise the temperature of the rock alone. In shales and limestones, the reaction heat could be substantially greater than that required from specific heat considerations alone.

INTRODUCTION

In earlier work,[1-3] methods of measuring thermal properties were developed and thermal data for several sedimentary-rock types were reported. Data included thermal conductivity, specific heat and thermal diffusivity. In addition, calculations of heat transfer in subsurface formations may require data on the thermal-expansion characteristics of rock and the heats of reaction of mineral constituents.

Thermal expansion of rocks is relatively small in magnitude and, from the standpoint of change in bulk density, has only minor effects on heat-transfer characteristics. Thermal-expansion behavior, however, may have significant effects on the structure of rocks. Differential expansion of different minerals and along different crystallographic axes may result in structural damage which could effectively reduce the thermal conductivity of the rock.

Many mineral constituents of sedimentary rocks undergo phase or related changes when heated to sufficiently high temperatures. Although some of these reactions (such as the α-β quartz inversion) are reversible and the heat absorbed is returned to the system upon cooling, many of the major reactions are irreversible. Through certain temperature ranges, the additional heat energy required to complete the reactions may be nearly as great as that necessary to raise the temperature of the rock in the absence of thermal reactions. If the heat requirements for these reactions are not considered, serious errors in heat-transfer calculations may result.

Thermal-expansion and thermal-reaction data have been obtained for three typical sandstones. Methods of measurement and results obtained are reported and discussed in the following.

THERMAL EXPANSION OF SANDSTONES

The linear expansions of three outcrop sandstones (Bandera, Berea and Boise) have been measured in the temperature range of 25° to 1,000° C. Expansion measurements were made in the directions parallel and perpendicular to the bedding.

The differential expansion apparatus used is that described by Mitoff and Pask.[4] The test sample is heated in an electric furnace with a temperature rise of 6°C/minute. The lengthening of the samples upon heating is compared with the small and known expansion of a fused silica rod. The change in length is transmitted to an X-Y recorder by means of a Statham transducer. A maximum error of ± 1.5 per cent has been obtained with this apparatus

Original manuscript received in Society of Petroleum Engineers office Aug. 30, 1960. Revised manuscript received Sept. 27, 1961. Paper presented at 31st Annual California Regional Meeting of SPE, Oct. 21-22, 1960, in Pasadena, Calif.

[1]References given at end of paper.

for materials of known linear expansion. Upon reaching maximum temperature, the sample is cooled at approximately the same rate and the contraction is recorded. The final length of the sample is measured to test the reliability of the final recorded value.

The linear expansions of Berea sandstone both parallel and perpendicular to the bedding are compared in Fig. 1 with the expansion of quartz perpendicular and parallel to C-axis.[5] The most important features of Fig. 1 are: (1) the close agreement between the heating curves for Berea sandstone and the curve for quartz perpendicular to the C-axis; and (2) the lack of agreement of the Berea heating curves with the curve for quartz parallel to the C-axis. Discontinuities in the curves at 575°C are attributed to the α-β inversion of quartz. The cooling curves for Berea deviate considerably from the heating curves, the samples being permanently elongated at the conclusion of the test.

Linear expansions of the three sandstones perpendicular to the bedding are compared with the expansion of quartz in Fig. 2. Curves for expansion parallel to the bedding and cooling curves are not shown for Bandera and Boise because of their close similarity to the Berea curves. All sandstone samples showed permanent elongation upon cooling. The volume expansions shown in Fig. 3 were calculated as the sum of the perpendicular linear expansion and two times the parallel expansion.[5]

Interpretation of thermal expansion data is as follows.

1. The quartz contents of the three sandstones ranged from about 50 per cent for Boise to 90 per cent for Berea, and yet the linear thermal expansions of the three sandstones were nearly the same and about equal to that for quartz. The presence of quartz, probably above some minimum amount, appears to control the expansion behavior of sandstones.

2. Expansion of quartz in the direction perpendicular to the C-axis has a predominating effect on the expansion characteristics of the sandstones. Since the amounts of expansion of the sandstones in the directions parallel and perpendicular to the bedding were approximately the same, random orientation of the quartz crystals would be expected.

3. Permanent elongation of the samples after cooling resulted from deformation within the sample, due primarily to the differential expansion of the quartz grains. At temperatures above that for α-β quartz inversion, where the coefficient of expansion for quartz becomes negative, the role of other mineral constituents becomes important in determining expansion and deformation characteristics of the sandstones.

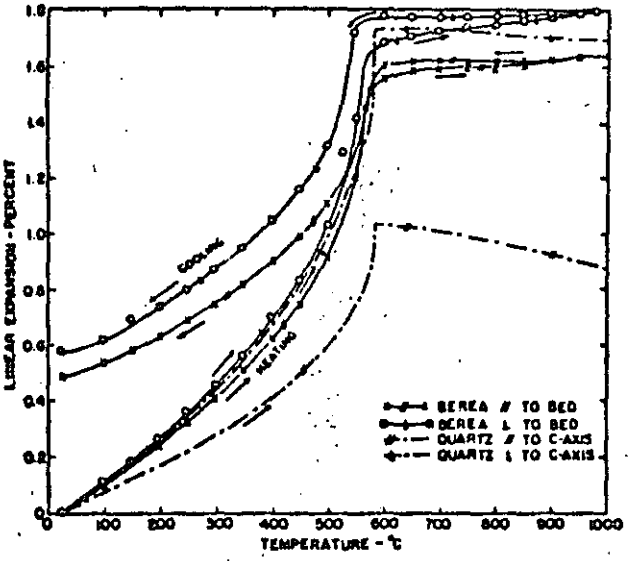

FIG. 1 – LINEAR EXPANSION OF BEREA SANDSTONE AND QUARTZ.

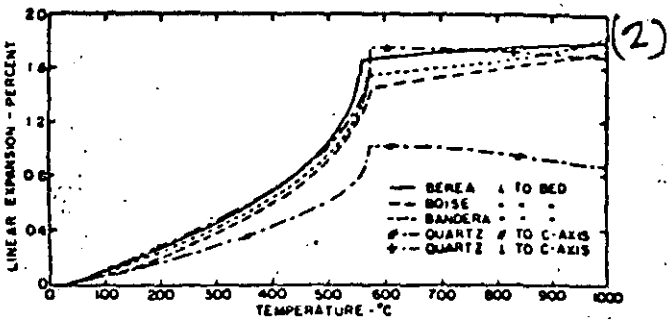

FIG. 2 – LINEAR EXPANSION OF SANDSTONES PERPENDICULAR TO BEDDING.

THERMAL REACTIONS

In measuring thermal diffusivities of rocks by the unsteady-state method,[2] anomalies were observed to occur in the differential temperature records. Similar to differential thermal analyses (DTA), these temperature anomalies may be correlated with thermal reactions which occur in certain of the mineral constituents. The most consistent reaction is the inversion of quartz from the α- to β-phase at 573°C. The amount of heat needed to complete this inversion is known to be 4.825 calories/gm.[6] The phase change is reversible, and an equivalent amount of heat is liberated upon cooling.

Other typical thermal reactions which may occur are summarized in Table 1. Most of these reactions occur over a broad temperature range and require substantially larger amounts of heat than the quartz

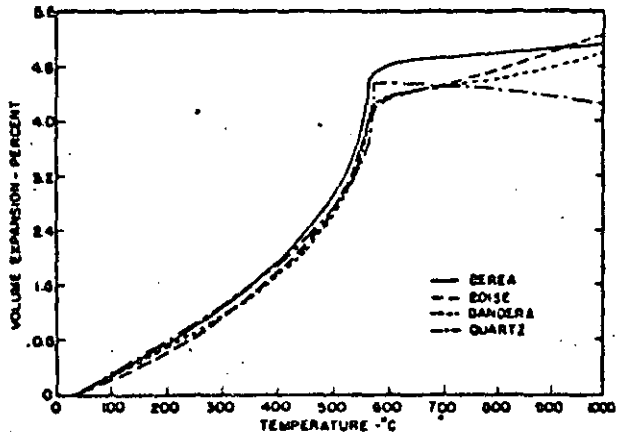

FIG. 3 – VOLUME EXPANSION OF SANDSTONES.

TABLE 1 — HEATS OF REACTION FOR SEVERAL MINERALS[7]

Temp. Range (°C)	Mineral	Heat of Reaction (Calories/gm)	Reaction
25-220	Ca-Montmorillonite	127	Desorption
25-220	Mg-Montmorillonite	135	Desorption
400-695	Mg-Illite	64	Decomposition
455-642	Kaolinite	253	Decomposition
554-723	Ca-Montmorillonite	67	Decomposition
573	Quartz	4.82	α-β Inversion
700-830	Calcium Carbonate	465	Decomposition
790-950	Mg-Illite	15	Decomposition
816-908	Ca-Montmorillonite	26	Decomposition

inversion. These reactions are normally irreversible or are only reversible under special conditions. Differential temperature records for the three sandstones shown in Fig. 4 demonstrate this point. The dashed lines show the quartz inversion starting at approximately 575° C, followed by several other temperature anomalies. The solid lines show the thermal behavior of the same sandstone samples on a repeat run. The reversible quartz reaction is the only important anomaly remaining.

The purpose of the present investigation was to estimate the magnitude of heat required to satisfy the thermal reactions and to compare this with the heat required to raise the temperature of the rock excluding thermal reactions. The known heat of reaction for quartz inversion and the known quartz content of Berea sandstone were used for standardization purposes.

The apparatus used to evaluate thermal reactions is the same as that described earlier for thermal diffusivity measurements.[3] In the earlier work, cylindrical core samples were mounted in an electric furnace and heated at a constant rate of temperature rise. At temperatures where thermal reactions were known to occur, temperature was held constant until the reaction was completed. The edge temperature of the sample and edge-to-center differential temperatures were measured with thermocouples and traced on a recorder chart. It was shown[3] that, for these conditions, thermal diffusivity is inversely proportional to the differential temperature; i.e.,

$$D_t = a^2 b/4\,\Delta T \quad \ldots\ldots\ldots\ldots \quad (1)$$

where D_t is thermal diffusivity ($D_t \equiv \alpha$ in Refs. 1 through 3), a is the distance between center and edge thermocouples, b is the heating rate and ΔT is the temperature differential.

In the present case, differential thermocouples were located at distances r/a = 1.0, 0.8, 0.6, 0.4 and 0.2 from the center of the sample. The rate of temperature rise at the sample edge was maintained constant, and temperature differentials between the center of the sample and the several r/a locations were recorded. Fig. 5 shows the thermocouple responses caused by the α-β quartz inversion. Physically, the reaction is explained as follows. When the outer surface of the core reaches reaction temperature (573°C), part of the heat supply is used to promote the reaction. The normal temperature gradient in the sample is disturbed and a slight decrease in the differential temperature is noted for the first thermocouple. As the reaction reaches and then passes the first thermocouple, a sharp increase in the temperature differential for this couple occurs. The edge temperature continues to increase at the constant input rate; but less heat reaches the unreacted portion of the sample because of the large amount of heat consumed by the reaction,

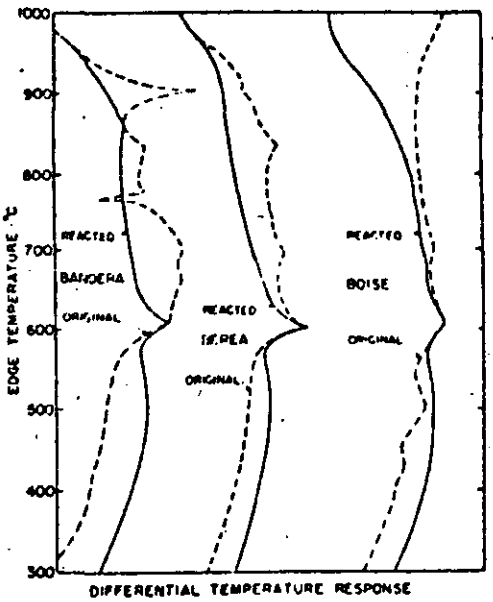

FIG. 4 — THERMAL BEHAVIOR OF SANDSTONES.

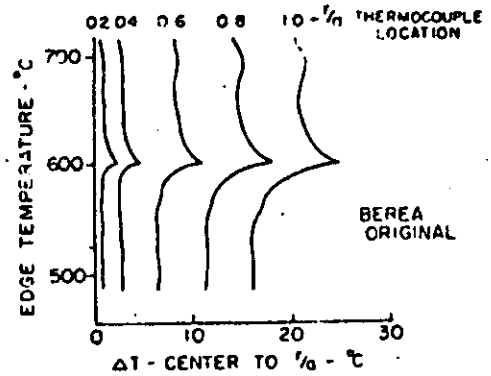

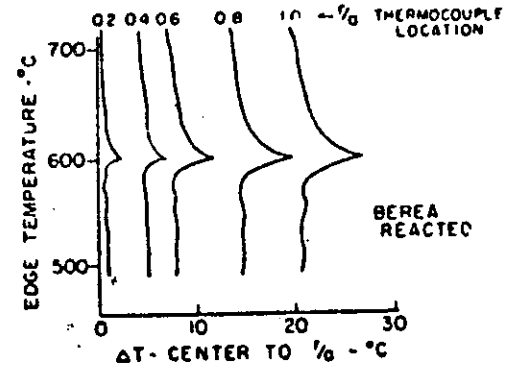

FIG. 5 — TEMPERATURE DIFFERENTIALS FOR QUARTZ INVERSION.

and the rise in center temperature lags. Thus, a sharp temperature discontinuity must exist at the reaction front. Similar response is noted as the reaction proceeds past each interior thermocouple. All curves show a maximum value when the reaction reaches the center thermocouple. The temperature differentials then decrease to re-establish the original temperature gradient in the sample.

If the supply of heat to the system is constant, a heat balance may be written as

$$\left(D_t C_p \frac{\delta T}{\delta r}\right)_\alpha - \left(D_t C_p \frac{\delta T}{\delta r}\right)_\beta = H_R \frac{\delta R}{\delta \theta} \quad . \quad . \quad . \quad (2)$$

where C_p is heat capacity, $\delta T/\delta r$ is temperature gradient, H_R is heat of reaction, $\delta R/\delta \theta$ is the rate of movement of the reaction through the sample and α and β refer to the unreacted and reacted zones, respectively. Since the change of D_t within the temperature range of the reaction is small, the assumption of constant heat supply is valid and Eq. 2 should apply to the present system. However, attempts to confirm the equation with experimental data from Fig. 5 failed. Many more thermocouples would be needed to establish reliable values of the temperature gradient ahead of and behind the reaction front, and the rate of movement of the reaction.

Resort was made to an empirical method to obtain useful information from the experimental data. The method, which is used in quantitative interpretation of DTA data,[7] involves the correlation of areas of the anomalies on the differential temperature-vs-edge temperature curves with heats of reaction. In Fig. 5 the areas between an estimated base line and the anomalies were measured for each thermocouple location. These areas were then plotted against calculated heats of reaction for a volume of unit length of sandstone contained within each thermocouple radius and the center of the sample. A reasonably good straight-line relation resulted, as shown in Fig. 6. A value of 1 calorie/unit of anomaly was used in determining the heats of unknown reactions.

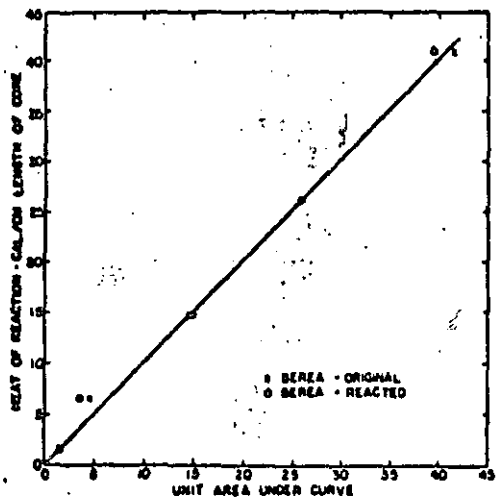

FIG. 6 — AREA-HEAT OF REACTION CORRELATION.

TABLE 2 — EXPERIMENTAL HEATS OF REACTION

Sample	Temp. Range (°C)	Heat of Reaction (Calories/gm rock)	Equiv. Heat (Calories/gm rock)
Bandera	577-615	2.9	11
	615-735	21.	34
	735-750	−0.9	4
	750-825	5.6	22
	825-920	7.9	27
		Σ 36.5	Σ 98
Berea	565-600	4.3	9
	600-725	10.	34
	725-840	14.	33
	840-925	8.7	25
		Σ 37.0	Σ 101
Boise	565-620	2.6	14
	620-725	3.9	28
	725-975	—	71

In analyzing the data of Fig. 4, the only known reactions were the α-β quartz inversions. Differences in the original and reacted curves below 573°C are due primarily to the reduction in thermal conductivities of the reacted samples. This is probably caused by the loss of free and combined water and structural damage of the cores by differential thermal expansion during the initial heating run. Reactions above 573°C include, in addition to quartz inversion, dehydroxylation of clay minerals and decomposition of calcium carbonate. It was not considered practical to attempt to separate specific mineral reactions because the purpose of the work was only to evaluate the additional heat requirements due to thermal reactions. Breaks in the curves were used to establish temperature ranges of the important reaction zones as shown in Table 2. Areas between the original and reacted curves of Fig. 4 were measured, and heats of reaction were calculated from the correlation factor and bulk densities of the samples.

In Table 2, the heats of reaction are shown and compared with the amount of heat required to raise the temperature of the rock without thermal reactions. The reaction heat is 27 per cent of the total heat requirements for both Bandera and Berea sandstones. A similar analysis was not made for Boise sandstone because of the difficulty of explaining the large thermal reaction above 725°C. This same behavior persisted in tests on several other samples of Boise.

SUMMARY AND APPLICATIONS

The results of these tests, made at atmospheric pressure on oven-dried sandstone samples, typify behavior at just one set of limiting conditions. Before such data can be applied directly to subsurface calculations, the effects of a wider range of conditions relating liquid saturation and overburden pressure needed to be investigated.

Differential thermal expansion of the mineral constituents of rocks will undoubtedly lead to structural damage under subsurface heating conditions. The magnitudes of effects on mechanical

and flow properties are unknown, but these currently are being investigated in this laboratory. It is possible that cores taken from high-temperature reservoirs may be altered by cooling as well as by the release of overburden and pore pressure.

Thermal reactions involving the release of adsorbed and combined water and the liberation of such gases as carbon dioxide will be different under subsurface conditions of liquid saturation and pressure than the same reactions observed on oven-dried cores at atmospheric pressure. Temperatures of reaction will be higher and the heats of reaction may be different. Brindley and Nakahira[8] report that the starting temperature of the endothermic kaolinite reaction is raised by 100°C under a water-vapor pressure of 6 atm. Further laboratory investigation will be necessary to evaluate these effects.

NOMENCLATURE

D_t = thermal diffusivity (= α in Refs. 1 through 3)

a = distance between center and edge thermocouples

b = heating rate

ΔT = temperature differential

r = radius of core sample

C_p = heat capacity

$\frac{\partial T}{\partial r}$ = temperature gradient

H_R = heat of reaction

$\frac{\partial R}{\partial \theta}$ = rate of reaction movement through the sample

θ = time

α, β = unreacted and reacted zones, respectively

REFERENCES

1. Somerton, W. H.: "Some Thermal Characteristics of Porous Rocks", *Trans.*, AIME (1958) Vol. 213, 61.
2. Somerton, W. H. and Boozer, G. D.: "Thermal Characteristics of Porous Rocks at Elevated Temperatures", *Trans.*, AIME (1960) Vol. 219, 77.
3. Somerton, W. H. and Boozer, G. D.: "A Method of Measuring Thermal Diffusivities at Elevated Temperatures", *AIChE Jour.* (1961) Vol. 7, 87.
4. Mitoff, S. P. and Paak, J. A.: "A Recording Differential Expansion Apparatus", *Am. Ceram. Soc. Bull.* (1956) Vol. 35, No. 10, 402.
5. Birch, F., Shairer, J. F. and Spicer, H.: editors, *Handbook of Physical Constants*, GSA (1942) 35.
6. Kelley, K. K.: "Contributions to the Data on Theoretical Metallurgy", Bull. 584, USBM (1960).
7. Barshad, I.: "Temperature and Heat of Reaction Calibration of the Differential Thermal Analysis Apparatus", *Am. Mineralogist* (1952) Vol. 37, 667.
8. Brindley, G. W. and Nakahira, M.: "Kinetics of Dehydroxylation of Kaolinite and Halloysite", *Jour. Am. Ceram. Soc.* (1957) Vol. 40, No. 10, 346.

***

CURSO: "INGENIERIA DE YACIMIENTOS GEOTERMICOS"
13 DE MARZO AL 18 DE MAYO 1984

tema; " TABLAS "

DR. JESUS RIVERA RODRIGUEZ
13-23 MARZO

MATERIAL ADICIONAL.

DR. JESUS RIVERA RODRIGUEZ

Taken from:
Geothermics with Special Reference to Applications, O. Kappelmeyer & R. Haenel
Editorial Geopublications Associates. Berlin, Stuttgard (1974).

6.3 Thermal properties of rocks from 0 – 50 °C

6.3.1 *Igneous and volcanic rocks; n = number of measured samples; 0 = temperature; "Ref." see 6.9*

Material	Density [g cm^{-3}]				Thermal conductivity [10^{-3} cal cm^{-1} s^{-1} deg^{-1}]				Specific heat [cal g^{-1} deg^{-1}]				Thermal diffusivity [10^{-3} cm^2 s^{-1}]				
	Ref.	n	range	mean	Ref.	n	0	range	mean	Ref.	n	0	range	mean	Ref.	n	0	range	mean
Albitite	8			2.61	8		25		4.84										
Anorthosite	8			2.74	8		25		4.46										
	8			2.70	8		25		4.15										
	8			2.74	8		25		4.04										
	20			2.83	20		20		5.00										
Basalt	19			2.66	80		19		3.30										
	39			2.89	78		0		3.17										
					19		20		6.72										
	8			2.59	8		25		5.45										
	19			2.92	19		25		4.00										
	19			2.60	19		25		3.45										
					11		30		4.04										
	42			2.58	42		25		5.47										
	30	3	2.84–2.89	2.86	30	3	50	3.84–4.14	4.01	30	3	50	0.211–0.212	0.211	30	3	50	0.38–6.83	6.85
					38	11	20	3.30–6.40	4.21										
					38	4	20	3.80–4.00	3.90										
					38	12	20	3.50–4.10	3.80										
Bronzitite	8			3.26	8		25		10.15										
Diabase	54			3.01	54		25		5.53	80		50		0.188					
	54			2.96	54		25		5.19										
	54			2.96	54		25		5.03						54		20		9.46
					80		0		5.26	80		0		0.167	54		20		7.37
					54		20		4.70										
Dolerite	54			3.82	54		50		3.82										
Diorite	42			2.92	42		25		4.87										
					38		25		4.97										
					54		20		4.56						54		20		9.47
Dunite	42			3.21	42		25		9.50										
					80		25		11.45										
	8			3.27	8		25		10.90										
	8			3.25	8		25		12.45										
	8			3.25	8		25		10.65										

6.3.1 *Igneous and volcanic rocks (continued)*

Material	Density [g cm^{-3}]				Thermal conductivity [10^{-3} cal cm^{-1} s^{-1} deg^{-1}]					Specific heat [cal g^{-1} deg^{-1}]					Thermal diffusivity [10^{-3} cm^2 s^{-1}]				
	Ref.	n	range	mean	Ref.	n	θ	range	mean	Ref.	n	θ	range	mean	Ref.	n	θ	range	mean
Gabbro	8			3.03	8		25		5.46										
	6			2.86	8		50		4.62										
	8			2.88	8		25		4.75										
					80	2	25		5.11										
					80	2	30		6.00										
Granite	8	4		2.62	8	4	25		6.26										
					80	2	50		6.23										
					52		50		8.16										
	30	12	2.50—2.72	2.59	30	12	50	5.19—7.35	7.06	30	8	50	0.188—0.233	0.105	30	8	50	10.29—14.31	14.23
					14	12	20		7.77										
	19	6	2.50—2.72	2.59											19	12	50	6.00—17.40	10.00
	54	13	2.60—2.65	2.62	54	13	20	3.04—6.76	5.64	54	13	20	0.21—0.33	0.270	54	13	20	5.03—15.14	8.87
Granodiorite	54	9	2.62—2.76	2.71	54	9	20	3.91—5.56	4.85	54	9	20	0.20—0.30	0.200	54	13	20	5.03—9.06	7.19
					61	14	28	6.20—8.3	7.61										
					61	5	27		6.64										
Hypersthenite				3.26	8		25		10.50										
Lava	54	5	0.95—2.64	1.58	54	5	20	0.5097—1.743	1.16	54	5	20	0.160—0.33	0.200	54	5	20	3.02—5.35	3.77
					12	9	25		7.40										
					59	13	20		7.20										
					10	27	20		5.01										
					10	10	20		6.40										
Lherzolite					43		50		8.50										
Monzonite				2.64	8		25		7.31										
Norite			2.75—3.05	2.92	51	5	20	5.5—7.3	6.42										
Obsidian	69			2.31	54		50		0.84										
					8		25		3.28										
Olivinitite					38		25		8.36										
Peridotite	42			3.05	42		50		8.60										
	42			2.95	42		25		9.50										
Syenite	8			2.80	8		50		5.25										
					80		50		5.25										
	51			2.78	51		18		7.34										
	51			2.60	51		21		7.54										
Syenite porphyry	31	31	2.51—2.80	2.69	31	31	20	6.1—9.48	7.73										
Serpentinite					38	2	20	3.1—3.2	4.30										
Tonalite				2.74	8		25		6.29										

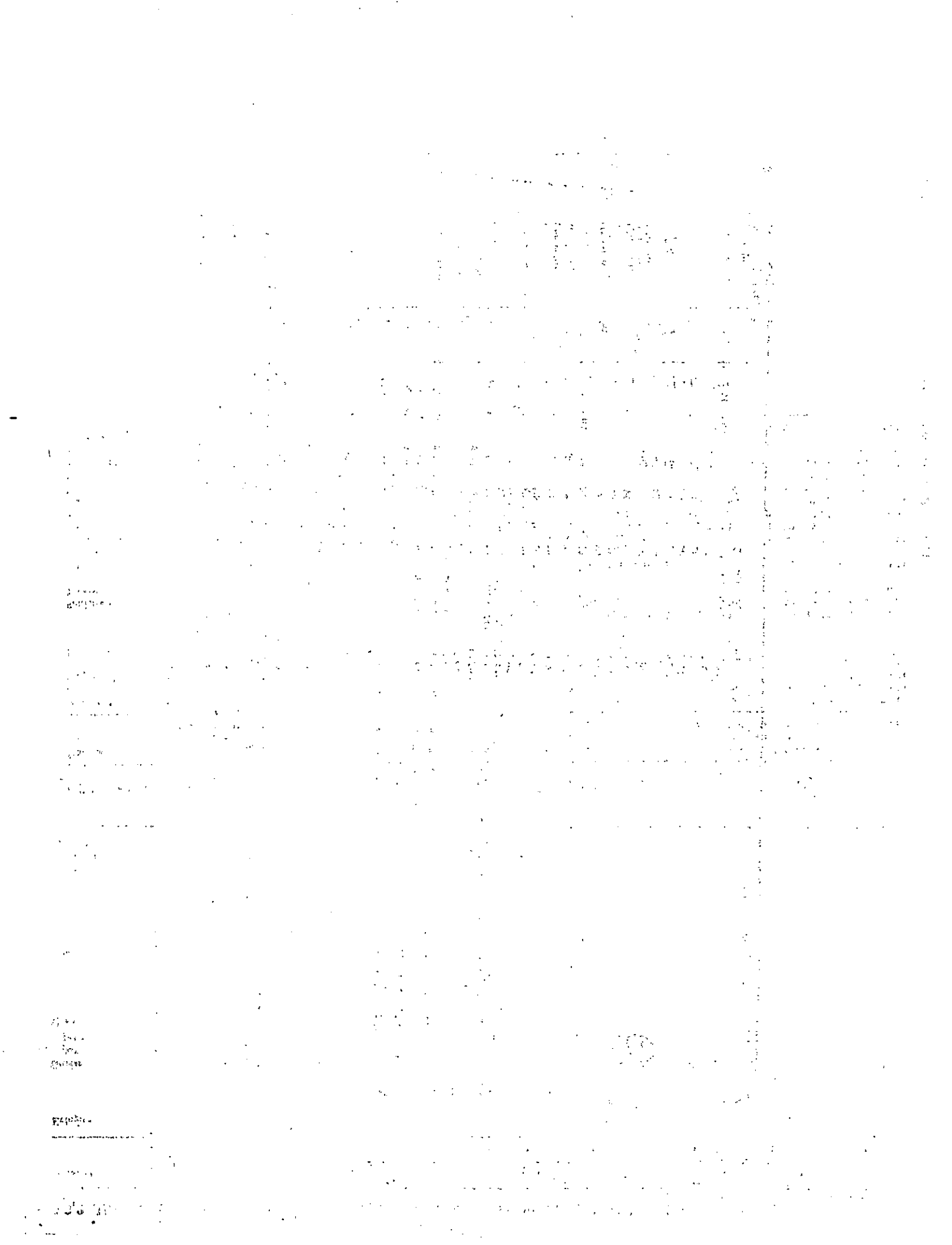

6.3.2 *Metamorphic rocks; n = number of measured samples; θ = temperature; "Ref." see 6.9*

Material	Density [g cm⁻³] Ref.	n	range	mean	Thermal conductivity [10⁻³ cal cm⁻¹ s⁻¹ deg⁻¹] Ref.	n	θ	range	mean	Specific heat [cal g⁻¹ deg⁻¹] Ref.	n	θ	range	mean	Thermal diffusivity [10⁻³ cm² s⁻¹] Ref.	n	θ	range	mean
Eclogite	68			3.25	52		25		8.00										
					54		50		7.41										
	42			3.30	42		25		8.87										
					38		25		8.12										
Gneiss	30	4	2.70–2.73	2.71	30	4	50	6.16–7.03	6.46	30	4	50	0.183–0.208	0.193	30	4	50	11.34–14.07	12.24
par.	8			2.64	8		50		7.00										
perp.	8			2.61	8		50		4.08										
Marble					80		0		7.28	80		0		0.179	80		0		10.30
	8			2.69	8		25		6.90										
	8			2.69	8		25		6.78										
	19			2.60	19		25		6.67										
	19			2.67	19		45		5.80										
Quarzite					80		50		13.90	80		50		0.185					
	19			2.80	19		25		14.45										
	30	1		2.60	30	1	50		14.76	30	1	50		0.168	30	50			29.52
					10	8	20		16.05										
					12	17	20		14.30										
					59	21	25		14.50										
					50	7	20		10.10										
Serpent. Peridotite					51	8	20	5.7–7.0	6.34										
	42			2.74	42		25		10.50										

6.3.3 *Sediments; n = number of measured samples; θ = temperature; "Ref." see 6.9*

Material	Density [g cm⁻³] Ref.	n	range	mean	Thermal conductivity [10⁻³ cal cm⁻¹ s⁻¹ deg⁻¹] Ref.	n	θ	range	mean	Specific heat [cal g⁻¹ deg⁻¹] Ref.	n	θ	range	mean	Thermal diffusivity [10⁻³ cm² s⁻¹] Ref.	n	θ	range	mean
Anhydrite	18	7	2.95–2.91	2.80	18	7	50	9.80–14.50	12.61						18	7	50	17.00–25.7	22.41
Clay	30	3	2.40–2.44	2.52	30	3	50	5.20–5.40	5.30	30	3	50	0.213–0.240	0.227	30	3	50	8.53–10.18	9.50
Clay marl	30	7	2.43–2.64	2.54	30	7	50	4.14–6.15	4.87	30	7	50	0.186–0.234	0.205	30	7	50	8.01–11.66	9.34
Claystone	30	15	2.36–2.83	2.60	30	15	50	4.17–8.18	5.68	30	9	50	0.197–0.223	0.211	30	9	50	8.24–15.80	12.18
Dolomite					80		50		10.60						80		50		8.50
	19			2.67											19		50		8.47
	8			2.83	8		25		11.10										
	30	6	2.53–2.72	2.63	30	6	50	6.01–9.06	7.98	30	6	50	0.220–0.239	0.228	30	6	50	10.73–14.97	11.17
Schistose clay	30	3	2.42–2.57	2.49	30	3	50	4.60–5.50	5.13	30	3	50	0.218–0.222	0.220	30	3	50	8.10–10.24	9.37
Limestone	30	11	2.41–2.67	2.65	30	11	50	4.05–6.40	5.28	30	11	50	0.197–0.227	0.204	30	11	50	8.24–12.15	10.54
	8			2.60	8		25		6.67										
Lime marl	30	2	2.43–2.62	2.53	30	2	50	4.40–5.74	5.07	30	2	50	0.200–0.227	0.214	30	2	50	9.04–9.64	9.34
Compact limestone	30	6	2.58–2.66	2.62	30	6	50	5.58–8.38	6.75	30	6	50	0.197–0.220	0.210	30	6	50	10.78–15.21	12.18
Marl	30	3	2.50–2.67	2.63	30	3	50	5.55–7.71	6.44	30	3	50	0.217–0.221	0.219	30	3	50	9.89–13.82	11.18
Marly clay	30	2	2.46–2.49	2.47	30	2	50	4.21–4.82	4.52	30	2	50	0.183–0.236	0.210	30	2	50	7.17–10.72	8.94
Clay slate	30	5	2.62–2.83	2.68	30	5	50	3.45–8.70	5.13	30	5	50	5 x 0.205	0.205	30	5	50	6.42–15.15	9.26
Salt	18	14	2.08–2.28	2.16	18	14	50	10.7–13.7	13.19						18	14	50	25.20–33.80	30.60
Salt slate	18	7	2.13–2.57	2.37	18	7	50	3.00–10.00	6.59						18	7	50	6.38–21.70	13.90
Sandstone	30	51	2.35–2.97	2.65	30	54	50	5.20–12.18	7.75	30	31	50	0.182–0.256	0.197	30	31	50	10.94–23.62	16.45
Slate	42			2.70	42		25		6.20										
Slate, perp.	8			2.76	8		25		4.51										
Sylvinite	18	10		2.12	18	10	30	11.00–13.80	12.63						18	10	50	26.40–32.90	29.90

6.3.4 *Minerals; n = number of measured samples; θ = temperature; "Ref." see 6.9*

Material	Density [g cm⁻³] Ref.	range	mean	Thermal conductivity [10⁻³ cal cm⁻¹ s⁻¹ deg⁻¹] Ref.	n	θ	range	mean
Calcite, par.				8		25		8.84
perp.				8		25		7.74
Halite (single cryst.)	8		2.16	8		25		13.30
Olivine	41		3.45	41		25		12.10
Quartz, par.				8		25		24.85
perp.				8		25		14.90
[010]				43		50		16.85
[001]				43		50		26.30
[010]				41		50		14.30
[001]				41		50		30.00

6.4 Temperature effect on the thermal behaviour of rocks

(5)

6.4.1 *Thermal conductivity* [10^{-3} cal cm^{-1} s^{-1} deg^{-1}]; *n = number of measured samples; "Ref." see 6.9*

Material	Density [g cm^{-3}]	0	50	100	200	300	400	500	600	700	800	900	1000	1100	1200	1300	1400 °C	n	Ref.
Igneous and volcanic rocks																			
Albitite	2.61		4.83	4.84	4.80	4.70	4.53												8
Anorthosite, I	2.71		4.43	4.49	4.54	4.69													8
, II	2.70		4.13	4.18	4.20	4.34	4.50												8
, III	2.74		4.02	4.05	4.10	4.27													8
Basalt	2.58		5.65	5.30	5.00	4.35	3.80	3.50	3.30	3.25	3.20								42
Bronzitite	3.20		11.10	9.20	8.81	7.83	7.30												8
Diabase			5.20	5.20	5.15	5.14												3	80
, I	3.01		5.62	5.44	5.35	5.37													54
, II	2.96		5.23	5.15	5.10	5.03	4.99												54
, III	2.96		5.04	5.02	5.01	5.01	5.03	5.06											54
			2.74	2.87	3.00	3.27	3.33												8
Diorite	2.92		4.05	4.80	4.70	4.40	4.20	4.00	3.80	3.75	3.70								42
				4.73	4.47	3.82	3.53	3.32	3.10	2.87	2.65	2.53	2.41	2.41	2.50	2.75			38
						3.01		3.03		3.08		3.42		3.25	3.32				52
Dolerite	3.82			3.82	3.60	3.01	3.03	3.00	3.00	3.08	3.23	3.34	3.27	3.18	3.13				54
Dunite			12.40	10.50	9.40	8.10												3	80
	3.21		10.00	9.00	8.30	7.20	6.45	5.80	5.30	4.90	4.00								42
, I	3.27		11.80	10.00	8.82	7.52													8
, II	3.25		14.30	11.40	10.10	8.77													8
, III	3.25		11.20	10.10	9.30	8.08													8
					8.92	0.70	8.46	8.40	8.48	8.54	8.60	8.75	8.38	8.35	8.20	7.80	7.05		53
Gabbro, (pyroxene)						3.11		3.37		3.56		3.30		2.68	2.63				52
, I	3.03		5.55	5.37	5.25	5.13													8
, II	2.86			4.62	4.65	4.75													8
, III	2.88		4.75	4.73	4.75	4.76	4.78	4.81											8
Granite, I	2.61		8.10	7.80	7.20	6.46	5.86												8
, II	2.61		9.09	8.30	7.06	6.80													8
, III	2.65		6.66	6.25	5.90	5.50													8
, IV	2.64		5.80	5.60	5.42	5.12													8
				4.78	4.06	3.27	2.85	2.58	2.36	2.20	2.13	2.10	2.00	2.00	2.10	2.13	2.32	2.34	54
						2.94		2.51		2.15		2.01		1.96		2.13	2.34		52
				5.18	4.61	3.08	3.22	2.94	2.72	2.57	2.44	2.36	2.34	2.34	2.30	2.56	2.77		38
Hornblende-Gabbro	3.06		7.75	7.53	7.35	6.95	6.60	6.40	6.15	5.90	5.80								42
Hypersthenite	3.26		11.00	10.00	9.32	8.70													8
Lherzolite				8.50	7.60	9.05	7.70	7.40	7.40	7.20	6.75	6.55	6.55	6.42	6.30	7.50			43

6.4.1 *Thermal conductivity (continued)*

(6)

Material	Density [g cm^{-3}]	0	50	100	200	300	400	500	600	700	800	900	1000	1100	1200	1300	1400 °C	Ref.
Monzonite	2.64	7.50	6.98	6.65	6.01													8
Obsidian		3.21	3.35	3.48	3.74	4.00	4.26	4.52										8
			0.84	1.19	1.70	1.79	1.86	2.01	2.20	2.48	2.77	2.97	2.98					54
				1.31	1.74	1.86	2.05	2.27	2.57	2.89	3.22							38
Olivinite			7.55	6.69	4.97	4.46	4.52	4.37	4.16	3.97	3.82	3.78	3.75	3.70	3.61	3.56	3.51	54
			7.05	7.16	5.87	5.49	5.20	4.99	4.82	4.66	4.51	4.48	4.39	4.32	4.25	4.22	4.20	38
Pendotite, I	3.05		8.60	8.00	7.15	6.60	6.20	5.80	5.50									42
, II	2.95	9.80	9.20	8.70	7.85	7.25	6.70	6.40	6.00									42
Syenite	2.80		5.25	5.08	4.90													8
Quartz-Diorite	2.64	8.50	8.05	7.75	7.30	7.00	6.80	6.75	6.70									42
Tonalite	2.74	6.42	6.15	5.90	5.52													8
Metamorphic rocks																		
Eclogite			7.40	6.02	4.23	3.78	3.50	3.30	3.18	3.24	2.72	2.53	2.34	2.15	1.97			38
	3.50	6.00	5.75	5.60	5.05	4.75	4.40	4.20	4.15									42
			7.11	6.21	4.30	3.77	3.63	3.27	2.94	2.89	2.74	2.56	2.27	2.13	1.96			54
					3.87		3.60		2.96		2.86		2.29		1.96			52
Gneiss, par.	2.64	2.72	7.00	6.85														8
, perp.	2.64	5.17	4.98	4.82														8
Marble, par.	2.69	7.30	6.44	5.95	5.10													8
, perp.	2.69	7.20	6.32	5.72	5.05													8
		7.28		5.85	5.15													80
Quartzite		14.00		12.50														80
Serp. Peridotite	2.74	11.00	10.00	9.25	8.05	7.35	6.60	6.15	5.75	5.40								42
Sediments																		
Dolomite	2.83	11.00	10.30	9.30	7.95													8
		11.00		9.30	8.00													80
limestone,																		
Solenhofen	2.60	7.20	6.14	5.53	4.77													8
, Pensylvanian,																		
, par.	2.60	8.24	7.55	7.04	6.54													8
, perp.	2.69	6.09	5.08	5.41														8
		7.20		5.50	4.80	3.35												80
Quartz-sandstone																		
, par.	2.64	13.60	11.80	10.80	9.00													8
, perp.	2.65	13.10	11.40	10.30	8.65													8

6.4.1 *Thermal conductivity (continued)*

Material	Density [g cm^{-3}]	0	50	100	200	300	400	500 °C
Shale			2.17	2.25	2.38	2.54	2.68	2.83
Slate		4.90	4.80	4.50	3.90	3.50		
par.	2.70	0.35	0.05	5.85	5.50	5.20	4.95	4.80
perp.	2.76	4.63	4.40	4.23	4.08			
Minerals and single crystals								
Calcite, par.		27.30	22.40	19.00	15.10	12.30	10.30	
, perp.		10.30	13.50	11.80	9.70	8.40	7.40	
Forsterite				8.69	7.67	6.67	5.90	5.30
Halite	2.16	14.60	12.00	10.05	7.45	5.95	4.98	
		16.70		11.60				
		14.60		10.10	7.50	6.00	5.00	
Olivine	3.45		11.90	11.50	10.40	9.50	9.25	9.44
Periclase	3.58			120.0	88.5	69.0	58.4	48.9
Quartz, [010]			16.85	15.4	13.3	10.9	10.75	10.62
, [001]			26.0	24.3	20.8	15.5	13.9	12.0
, [001]			30.0	33.0	16.0	12.3	9.85	8.62
, [010]			14.3	12.0	9.60	8.50	7.20	6.74
, par.		27.3	22.4	19.0	15.1	12.3	10.3	
, perp.		10.3	13.3	11.8	9.70	8.40	7.40	
Fused silica			3.70	3.45	3.33	3.74	4.14	4.70
			2.80	3.10	3.50	3.79	4.05	4.35

6.4.1

Material	600	700	800	900	1000	1100	1200	1300	1400 °C	Ref.
Shale	2.98	3.06	3.15	3.25	3.32					80
Slate										80
par.	4.80									42
, perp.										8
Minerals and single crystals										
Calcite, par.										8
, perp.										8
Forsterite	4.90	4.67	4.37	4.18	4.04	3.94	3.87	3.82	3.80	54
Halite										8
										8
										8
Olivine	9.95	11.0	12.6							41
Periclase	42.4	36.2	34.9							41
Quartz, [010]	10.10	13.05	16.50	20.46	27.00	Minimum: 8.35/573 °C				43
, [001]	8.70	10.0	11.7	13.4	16.7	20.0				43
, [001]	9.05	10.5	11.95							41
, [010]	6.59	7.70	9.20							41
, par.										3
, perp.										48
Fused silica	5.40	6.08	6.01	9.74	12.35	14.96	19.07			8
	4.80	5.40								41

6.4.2 *Specific heat* [cal g^{-1} deg^{-1}]; *"Ref." see 6.9*

Material	Density [g cm^{-3}]	0	50	100	200	300	400	500 °C
Basalt				0.208	0.228	0.243	0.251	0.259
		0.205		0.230	0.248	0.262	0.273	0.284
Diabase		0.167		0.190	0.208	0.223	0.236	0.247
Gneiss		0.177		0.209	0.242			
Granite				0.202	0.224	0.240	0.253	0.262
		0.191		0.209	0.227	0.243	0.260	0.267
Peridotite				0.240	0.263	0.277	0.290	0.300
Serpentinite				0.261	0.285	0.302	0.317	0.331
Fused silica	2.21		0.179	0.196	0.224	0.245	0.259	0.269
Quartz, [001]	2.65		0.183	0.199	0.229	0.253	0.268	0.280
, [010]	2.65		0.183	0.199	0.229	0.253	0.268	0.280
Quartzite		0.167		0.203	0.232	0.255	0.270	0.275
Olivine, [001]	3.45		0.195	0.211	0.230	0.247	0.258	0.264
Periclase, [001]	3.58				0.258	0.270	0.277	0.281
Clay, I		0.191		0.208	0.224	0.242	0.258	0.279
, II		0.179		0.202	0.224	0.247	0.270	0.292
Slate		0.169		0.216	0.239	0.252	0.263	0.270
Marble		0.179		0.214	0.239	0.256	0.270	0.280

6.4.2

Material	600	700	800	900	1000	1100	1200 °C	Ref
Basalt	0.267	0.274	0.281					47
	0.296	0.306	0.315				0.356	80
Diabase	0.259	0.262	0.264				0.325	80
Gneiss								80
Granite	0.270	0.278	0.284					47
	0.295	0.313	0.332					80
Peridotite								47
Serpentinite								47
Fused silica	0.278	0.284						41
Quartz, [001]	0.255	0.262	0.280					41
, [010]	0.255	0.262	0.280					41
Quartzite	0.275	0.277	0.280					80
Olivine, [001]	0.269	0.274	0.279					41
Periclase, [001]	0.285	0.290	0.295					41
Clay, I	0.306		0.426				0.426	80
, II	0.316	0.338	0.361					80
Slate	0.276	0.280	0.287				0.304	80
Marble								80

6.4.3 *Thermal diffusivity* [10^{-3} cm^2 s^{-1}]. *after* Kanamori, Fuji *and* Mizutani *(1968)*

Material	Density [g cm^{-3}]	50	100	200	300	400	500	600	700	800 °C
Fused silica	2.21	7.23	7.18	7.08	6.98	7.11	7.33	7.82	8.59	
Quartz, [001]	2.65	59.2	41.5	26.8	18.6	14.5	11.8	13.3	15.2	16.0
Quartz, [010]	2.65	29.4	22.6	15.8	12.05	9.95	8.90	9.60	11.05	12.6
Olivine, [001]	3.45	17.68	15.80	12.90	11.10	10.33	10.30	10.70	11.60	13.0
Periclase, [001]	3.58			96.0	71.4	57.7	48.7	41.7	36.7	33.2
Jadeite		14.80	13.46	11.55	10.10	9.09	8.45	8.30		9.35
Garnet 1		10.85	10.21	9.15	8.45	8.03	7.93	8.00	8.09	8.30
Garnet 2		10.73	10.20	9.45	8.87	8.35	8.05	8.00	8.00	8.20
Spinel				35.6	32.2	29.4	26.5	24.5	23.1	21.3
Corundum			66.0	59.2	37.2	29.6	26.0	22.5	19.1	16.8
Alkalifeldspar		7.06	6.77	6.51	6.62	6.80	7.19	7.65	8.22	8.79

6.5 Change in thermal conductivity of rocks with pressure in one direction; thermal conductivity in 10^{-3} cal cm^{-1} s^{-1} deg^{-1}, after Horai and Baugher (1970)

Material	0.4	10	20	41	82	123	164	205 kg cm^{-2}
	increasing pressure							
Anhydrite								
No 16	8.56	—	10.01	10.21	10.38	10.50	10.65	—
No 85	8.72	9.33	9.86	10.23	10.32	10.55	10.52	—
No 98	9.42	—	10.65	10.86	11.28	11.51	11.56	11.60
No 100	7.51	8.11	8.80	9.35	8.65	—	10.02	—
No 259a	8.11	—	9.65	10.00	10.26	10.30	10.40	—
No 259b	8.45	9.12	9.62	9.92	10.18	—	10.40	—
No 366	8.18	8.38	8.84	9.21	9.53	9.61	9.68	—
Sandstone								
No 172	6.84	—	7.42	7.36	7.47	—	7.56	—
No 224	5.51	—	5.80	5.93	5.99	—	6.21	—
No 234	6.69	—	7.03	7.19	7.36	—	7.50	—
No 286	7.50	—	8.12	8.47	8.63	—	8.02	—
No 313	9.44	—	10.43	10.51	10.78	—	11.26	—
No 343	8.51	—	9.45	9.72	—	—	—	—
Dolomite								
No 103	7.62	—	—	9.25	9.32	9.48	—	—
No 365	6.18	—	6.61	6.81	6.92	7.02	—	—
Limestone								
No 19	5.06	—	5.40	—	5.64	—	5.70	—
No 34	4.22	—	4.21	—	4.32	—	4.33	—
No 102	7.67	—	8.16	8.20	8.22	8.22	—	—
No 260	4.32	—	—	4.80	4.81	4.82	—	—
No 270	3.53	—	3.74	3.88	3.95	—	3.95	—
Porphyry								
No 244	4.72	—	4.80	4.92	—	—	—	—
No 245	4.10	—	4.27	4.53	4.65	—	4.74	—
Clastogene								
No 378	4.14	—	4.35	4.42	4.46	—	4.46	—

6.5

Material	246	248	287	328	410	287	246	205 kg cm^{-2}
					decreasing pressure			
Anhydrite								
No 16	—	10.69	—	10.80	10.82	—	—	—
No 85	—	10.57	—	10.65	10.64	—	10.58	—
No 98	—	—	11.08	—	—	—	—	—
No 100	—	10.30	—	10.38	10.52	—	10.41	—
No 259a	—	10.70	—	10.78	10.81	—	10.82	—
No 259b	—	10.70	—	10.60	10.70	—	—	—
No 366	—	9.74	—	9.80	9.88	—	—	9.71
Sandstone								
No 172	7.65	—	—	7.67	7.75	—	—	7.70
No 224	6.41	—	—	6.38	6.53	—	6.48	—
No 234	7.60	—	—	7.68	7.85	7.78	—	—
No 286	9.00	—	—	9.17	9.22	—	9.00	—
No 313	—	—	—	—	11.68	11.65	—	—
No 343	10.47	—	—	—	10.71	—	—	10.47

6.5 (continued)

Material	246	248	287	328	410	287	246	205 kg cm^{-2}
	decreasing pressure							
Dolomite								
No 103	9.75	—	—	9.85	9.89	9.66	—	—
No 365	7.29	—	—	7.30	7.36	—	7.35	
Limestone								
No 19	5.81	—	—	5.82	5.79	—	—	5.8
No 34	4.47	—	—	4.51	4.49	—	—	4.3
No 102	—	—	8.33	—	8.49	—	—	
No 260	—	—	—	4.85	4.86	—	—	4.9
No 270	3.96	—	—	—	3.99	—	—	
Porphyry								
No 244	4.91	—	—	—	5.01	—	—	
No 245	4.79	—	—	4.86	4.81	—	—	
Clastogene								
No 378	4.47	—	4.52	—	4.52			

Material	164	82	61	41	20	10	0.4	0.0 kg cm^{-2}
Anhydrite								
No 16	10.68	—	—	10.46	10.31	10.10	10.00	9.80
No 85	—	10.35	—	10.26	10.06	9.93	9.73	9.67
No 98	—	—	—	—	—	—	—	—
No 100	—	10.23	—	10.13	9.82	—	9.31	—
No 259a	—	10.50	—	10.30	—	—	—	7.84
No 259b	10.53	—	—	—	10.23	—	9.63	—
No 366	—	—	—	—	9.13	8.95	8.32	—
Sandstone								
No 172	—	7.61	—	7.50	7.54	—	7.35	—
No 224	—	6.38	—	6.27	6.08	—	—	—
No 234	—	7.47	—	7.43	7.36	—	6.22	—
No 286	—	9.02	—	8.76	8.59	—	7.73	—
No 313	—	10.91	—	10.80	10.47	—	9.02	—
No 343	—	—	—	—	9.61	—	8.60	—
Dolomite								
No 103	—	—	9.32	—	9.07	8.94	8.33	—
No 365	—	—	—	7.05	—	—	—	5.97
Limestone								
No 19	—	5.64	—	—	5.57	—	5.28	—
No 34	—	4.34	—	—	4.28	—	4.21	—
No 102	—	8.29	—	—	8.11	—	7.35	—
No 260	—	4.92	—	4.82	4.77	—	4.72	—
No 270	—	—	—	—	3.76	—	3.41	—
Porphyry								
No 244	4.88	—	4.70	—	4.76	—	4.61	—
No 245	4.75	4.67	—	—	4.59	—	3.59	—
Clastogene								
No 378	—	—	—	4.46	4.42	—	4.43	—

6.6 Anisotropy of thermal conductivity of rocks; k [10^{-3} cal cm^{-1} s^{-1} deg^{-1}]; Density [g cm^{-3}]; „Ref." see 6.9

Material	Location	Ref.	Density	n	k_1	n	k_0	$A = \frac{k_0}{k_1}$
Anhydrite	Germany, Thüringen	79		13	8.54	12	8.71	1.02
Clay slate	Germany, Saarland	60	2.66	4	4.00	4	7.86	1.96
	Germany, Rheinland	35	2.64	6	4.56	6	6.85	1.50
Claystone and schist	Germany, Thüringen	79		2	3.62	2	6.03	1.67
Dolomite	Germany, Thüringen	79		58	9.35	61	9.50	1.02
Gneiss	Simplon tunnel	15	2.72	23	6.33	8	8.90	1.41
Gneiss	Germ., Niedersachsen	8	2.64	1	4.98	1	7.0	1.40
Gneiss and mica schist	Arlberg tunnel	16	2.69	8	7.23	7	10.74	1.48
	Izetschberg tun.	15		13	6.27	6	9.32	1.49
	Washington D.C.	21		35	6.62	34	8.61	1.30
	Aiken, Carolina	22	2.71	10	5.51	10	7.01	1.27
Granite and granitic gneiss	Tauern tunnel	16	2.61	9	6.85	13	8.87	1.29
Injection slate and gneiss	Adams tunnel, Colorado	9		15	6.95	17	8.55	1.23
Limestone	Germ., Niedersachsen	8	2.69	1	5.68	1	7.55	1.33
Marble	Germ., Niedersachsen	8	2.69	1	6.32	1	6.44	1.02
Quartz-sandstone	Germ., Niedersachsen	8	2.64	1	11.40	1	11.80	1.03
Quartz rock and sandstone	Germany	36		17	7.14	17	7.74	1.08
Quartz rock and gneiss	Australia	69		4	7.00	4	11.80	1.68
Salt	Germ., Niedersachsen	18	2.17	1	13.70	1	13.60	0.99
Sandstone	Germany, Rheinland	60	2.57	6	8.02	6	8.97	1.12
	Germany, Saarland	35	2.73	3	8.23	3	8.73	1.06
	Germany, Thuringen	79		28	4.59	19	5.46	1.19
Schists	Bihar, Indian	75	2.70	12	7.22	12	8.28	1.17
Schiste lustrées	Simplon tunnel	15	2.71	8	5.74	6	7.50	1.30
Sylvinit	Germ., Niedersachsen	18	2.10	1	12.30	1	12.60	1.02

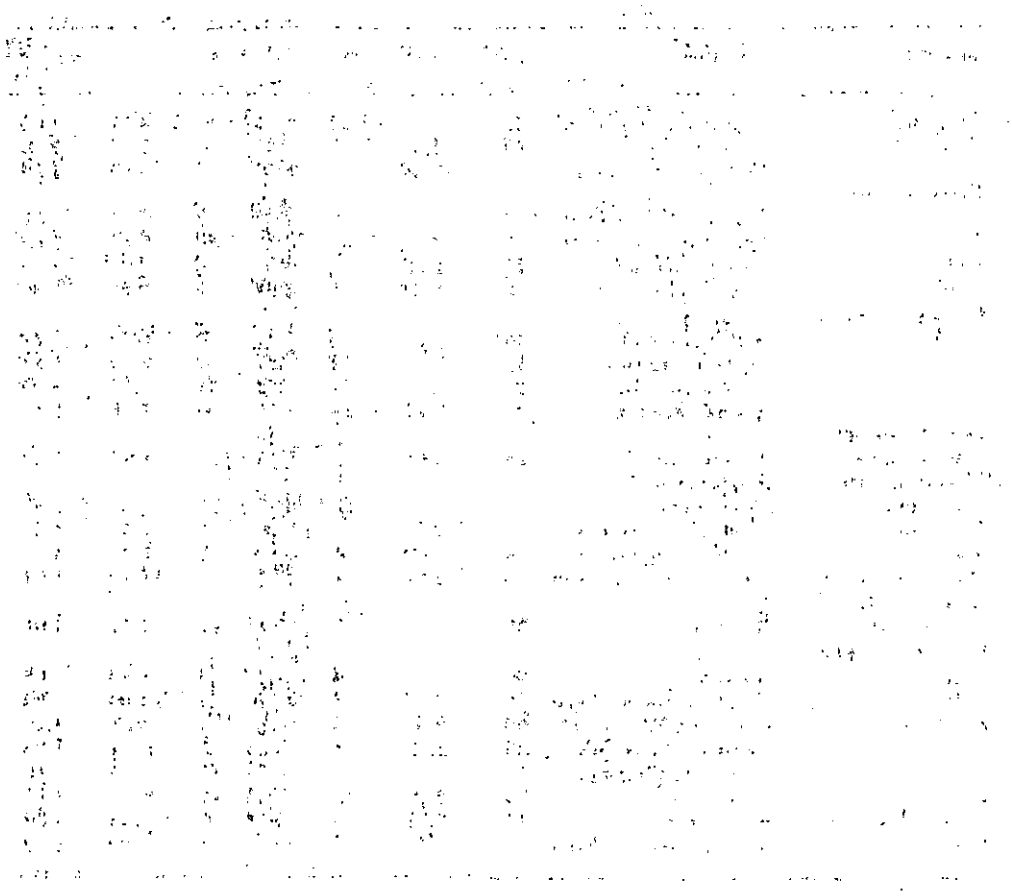

CURSO: "INGENIERIA DE RESERVORIOS GEOTERMICOS"
13 DE MARZO AL 18 de MAYO 1984

TEMA: "RESERVOIR ENGINEERING CONCEPTS"

DR. FERNANDO SAMANIEGO
13-23 MARZO
MATERIAL ADICIONAL

Fernando Samaniego V., Instituto de Investigaciones Electricas
Heber Cinco-Ley, Stanford University

9

Reservoir Engineering Concepts

Introduction

Geothermal reservoir engineering is related in many aspects to oil and gas reservoir engineering, which began receiving attention in the 1930s (Richardson, 1973). However, it wasn't until the end of the '60s, with the classic studies on the Wairakei field by Whiting and Ramey (1969) and the Geysers field by Ramey (1970) that geothermal reservoir engineering began receiving special attention. Geothermal reservoir engineering includes activities that begin with locating the wells, well logging, drilling and flow measurements, identification of the production mechanism, and performance prediction of reservoir behavior to find the optimum production conditions that would lead to maximum economic heat recovery.

The basic tasks of the reservoir engineer are the prediction of the long-term behavior of the well and the reservoir (Ramey, 1977). There are a few important questions that he or she must answer:

1. What is the optimum development plan for the reservoir?
2. How many wells and what kind of pattern will be required for optimum development of the reservoir?
3. What will be the rate of production for the wells?
4. How much heat will be recovered?
5. What will be the variation of temperature versus time?
6. Would it be feasible to implement an enhanced recovery process to recover additional heat?

To answer all these and other possible questions, the engineer must undertake a continuous and very careful work since the beginning of the life

of the reservoir. As production from the reservoir increases and more data becomes available, the reservoir engineer has more data for history matching purposes, allowing him or her to update previous studies and, consequently, to make better predictions of the reservoir behavior. Unfortunately, all data concerning the reservoir becomes available only when it is fully depleted.

It is important that the reservoir engineer quantitatively appreciates the physical processes that occur within the geothermal system, because this permits optimum exploitation of the reservoir. This "appreciation" can be divided into three main steps: first, the physical processes associated with the particular geothermal system under study must be identified and used to develop a conceptual model of the reservoir; second, a careful assessment of the physical and thermal properties of the rock and fluids must be made (these data will be extremely useful for simulation studies purposes); and third, a mathematical or physical model of the reservoir is developed, using the previously determined information about the reservoir. This model should include the properly identified initial and boundary conditions for the system. Once the model is at hand, it can be updated and refined as new production data becomes available. The reservoir response under production should be carefully matched with the model. This technique of matching the observed production history data by means of a suitable model and using the model to predict future performance is fundamental to the subject of reservoir engineering.

About the middle of the 1960s geothermal reservoir engineering relied heavily on the theory developed for oil and gas reservoir engineering. In cases where the characteristics of the geothermal and petroleum systems are alike, the oil and gas reservoir engineering techniques can be properly employed, if inherent differences in the systems are considered. Examples of successful applications of these techniques to geothermal reservoirs are available (Whiting and Ramey, 1969; Ramey, 1970; Atkinson et al., 1978). However, there are several factors that make geothermal reservoir engineering a unique subject in itself, such as very high reservoir temperatures; formations containing the fluid in many cases are highly fractured and of volcanic type; chemical deposition of solids during flow of fluids in the reservoir; and steam flashing. Due to the interest in geothermal energy, geothermal reservoir engineering has shown great advancements in the last fifteen years (Takahashi et al., 1975).

This chapter presents a review of the basic principles of geothermal reservoir engineering. The presentation includes a discussion of some of the practical aspects of reservoir engineering, such as well test analysis; and mathematical reservoir simulation.

Types of Geothermal Systems

Geothermal systems can be classified in four main types: vapor-dominated (dry steam); liquid-dominated (hot water); geopressured (hot) accumulations; and dry (hot rock) formations. Although each one of these systems has potential for exploitation, the vapor-dominated system offers the optimum conditions for electricity production. According to White (1973), technology currently available for geothermal electricity generation makes use of steam. Based on present knowledge, there are some requirements that have to be met for electricity generation from geothermal steam: (a) temperature of reservoir should be high (at least 180°C, and preferably above 200°C); (b) reservoir depth must be less than 3 km; (c) reservoir volume must be adequate; (d) the reservoir should contain natural fluids for transferring the heat to surface and power plants; (e) permeability of the formation should be adequate to ensure sustained delivery of fluids to wells at high enough rates to meet power production needs; (f) there must be no major unsolved technology problems. Unfortunately, these requirements are not easily met in the earth's crust.

Vapor-Dominated Systems

These systems are the rarest found in nature and the most desirable (Burnham, 1973), because thay provide a clean and environmentally safe energy source with minor production problems. There are a few vapor-dominated systems, among which the two most important ones are the Lardarello fields of Italy and The Geysers of California, which produce dry or superheated steam with no associated liquid (White, 1973). This is the reason why they are commonly known as "dry-steam" systems. White et al., (1971) have concluded, however, that liquid water and vapor usually coexist in the reservoir, with vapor being the continuous, pressure-controlling phase.

Vapor systems contain far less heat than the hot-water systems (Ramey et al., 1973), but, as mentioned earlier, problems related with their utilization are minor. The production mechanism of steam reservoirs is similar to that of natural-gas reservoirs, because pressure is reduced by the expansion of the gas in-place. The fractional mass production of original mass in place is usually high, being around 85-90%. The situation for energy recovery, however, is quite different, being quite low. Ramey et al. (1973) presented a table in which they compared the recovery for a hot-water and a steam reservoir. For the latter, a fractional energy recovery is 5.6%, because most of the heat is stored in the rock and, since the steam flow process in the reservoir is essentially isothermal, almost none of the heat contained in the rock is recovered. To recover heat stored in the rock, the production process should reduce the rock temperature. For these systems, additional energy can be recovered by means of an enhanced recovery process, using liquid-reinjection to the reservoir.

Hot Water Systems

In these systems, water is the continuous, pressure-controlling fluid phase. Such a system may contain some vapor, found as discrete bubbles in the shallow, low-pressure zones. Among geothermal systems discovered to date, hot liquid-dominated systems are far more common than vapor-dominated systems (White, 1973). Water in these reservoirs is a dilute aqueous solution containing sodium, potassium, lithium, calcium, chloride, bicarbonate, sulfate, borate, and high percent of silica. Some of the most important liquid-dominated systems are those located in the Imperial Valley in California, Wairakei in New Zealand, and Cerro Prieto in Mexico.

As mentioned previously, the energy content of these systems is higher than that for the vapor-dominated systems. Ramey et al. (1973) have shown that the fractional energy recovery for these kinds of systems is higher than for the vapor-dominated systems. This is caused by flashing of the water in the reservoir or by reinjection of water, which are the key factors in the recovery of geothermal energy from these systems. The problems encountered in the utilization of these systems are more difficult than those found for the vapor-dominated systems; however, current elaborate research programs may overcome these difficulties in the future.

Geopressured (Hot) Accumulations

Geopressured systems are composed of rocks that contain fluids at pressures far greater than normal (hydrostatic). Knapp et al. (1977) presented an explanation for the existence of these high-pressure zones. Briefly, these zones have a highly impermeable overlying formation that prevents the migration of fluids out of the zone and, thus, causes the fluids saturating this zone to partially bear the overburden load. This results in an increase in the fluid pressure. Pressure gradients in a geopressured zone usually approach lithostatic pressure, i.e., 1 psi/ft. The geopressured sediments have a low thermal conductivity and high heat capacity, causing the system's temperature to be high. The most important geopressured zone known to date is the Gulf Coast region of the United States, which extends on land and offshore from Texas to the Mississippi estuaries.

Fluids contained in geopressured systems are commonly saturated with methane. At the pressures and temperatures encountered, the quantity of methane associated with water saturating the system can be important. This is an additional benefit that can be obtained from the exploitation of these

accumulations. Another factor that augments the solution of methane in the water of these reservoirs is water salinity, which is lower under the geopressured conditions than at normal conditions (Burst, 1969). Low-salinity waters can hold more methane in solution than high-salinity waters.

Dry (Hot-Rock) Formations

Hot dry formations are systems that do not contain water to act as heat transport medium. The incidence of this type of geothermal resources is far greater than that of the fluid-saturated geothermal sites (Burnham and Stewart, 1973). These resources can be an important energy supply, provided that means can be found to extract and use such heat economically. The most simple, practical, and economical way to recover heat from these systems is introducing water into the formation, permitting it to circulate until it has been heated to a sufficiently high temperature, and then recovering the fluid as steam or hot water (Smith et al., 1973 and 1975).

Frequently, dry formations have very low permeability, and the problems of containing and recovering the injected water can be overcome by means of creating flow passages of sufficient surface area, through which water can flow for economically long periods of time. This would allow heat recovery through contact of the water with the surface area of the flow passages. The basic heat extraction system tested to date consists of an injector and a producer well, intercommunicated by a hydraulic fracture.

Geothermal systems saturated with fluids (convective systems) can be classified on the basis of the location of their initial conditions on a pressure-temperature diagram. Such a classification has been presented by Whiting and Ramey (1969) and by Martin (1975). Figure 9-1 presents a pressure-temperature diagram for pure water. The solid line is the boiling curve. Similar diagrams for geothermal brines should be modified to include the effect of dissolved salts. It is helpful to examine events subsequent to producing a reservoir at different assumed initial conditions.

Several points in Figure 9-1 must be considered. Point A represents the initial conditions for a single-phase (steam) reservoir that initially existed entirely within the vapor region. There is no formation of hot water because reservoir conditions prohibit it; therefore, the flow is isothermal and the boiling curve is not crossed. At the end of production, the temperature of the reservoir would be high. Thus, additional energy can be recovered by water injection. Point B represents the initial conditions for a reservoir; these conditions fall on the vapor pressure curve and, consequently, there are two phases (hot water and steam) originally present in the reservoir. The analog of this reservoir in petroleum reservoir engineering is the gas-cap reservoir. According to Whiting and Ramey (1969), for this system production is a mixture of hot water and steam that could range from saturated

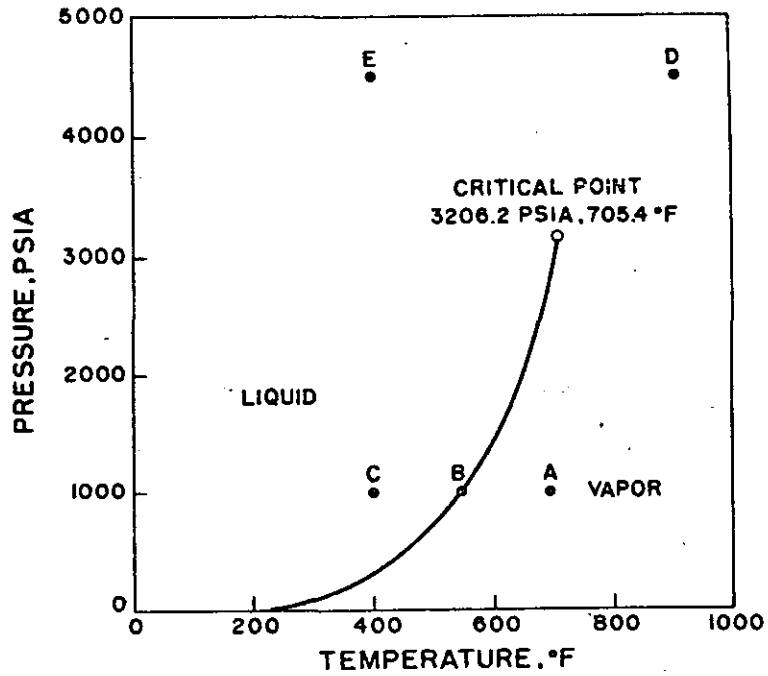

Figure 9-1. Pressure-temperature diagram for water (After Whiting and Ramey, 1969, Fig. 1, p. 894, by permission of the S.P.E. of A.I.M.E.)

liquid to saturated steam. Point C corresponds to a reservoir that originally had only hot water. The production mechanism is such that eventually, as reservoir pressure declines, the conditions of the vapor-pressure curve will be reached. From then on, production is similar to that of reservoir B previously discussed. Whereas the reservoir fluid is hot water, the flow in the reservoir is essentially isothermal and isoenthalpic. When the vapor pressure curve is reached, the pressure and temperature decline along this curve.

Point D in Figure 9-1 corresponds to a reservoir that originally existed at conditions of pressure and temperature above the critical values. As pressure declines due to production, a reservoir of this type would eventually become similar to reservoir A. These reservoirs usually do not exhibit pressure-temperature conditions that could result in crossing the vapor-pressure curve. Point E represents a reservoir whose initial condition of pressure is higher than the critical pressure. Due to production from the reservoir, pressure will decline, and the reservoir eventually will become similar to reservoirs C and B.

Table 9-1
Assessment of Geothermal Systems

Situation system	Technology	Environmental impact	Economics	Resource availability
Vapor-dominated	Established	Small	Attractive	Limited
Liquid-dominated	Partially established	Potentially large	Known but uncertain	Limited but significant in some areas
Dry (hot-rock) formations	Only partially developed	Unknown	Partially known	Potentially large
Geopressured (hot) accumulations	Only partially developed	Unknown	Partially known	Limited but significant in some areas

From the previous discussion and according to Whiting and Ramey (1969), it can be inferred that for performance prediction purposes, it is necessary to know mass production and enthalpy of the produced fluids. It has also been pointed out that the reservoir rock is an important potential source for energy recovery.

It is of interest to know in a general sense what are the state of technology development, environmental impact, economics, and availability of the different geothermal systems. Table 9-1 shows such type of information for present conditions (Davis and Golan, 1974). A striking fact drawn from this table is that our knowledge is more complete for those resources that are limited in extent. If geothermal energy is to be an important worldwide source of energy, the technology for energy recovery from dry (hot-rock) formations has to be fully developed. This will need an extensive research program to evaluate all aspects related to these systems, e.g., environmental impact, economics, and the necessary technology development. Such efforts are presently under way (Smith et al., 1973; Murphy, 1975).

Pressure Transient Analysis for Geothermal Wells

Transient pressure testing consists of recording the pressure variation versus time in the well or neighboring wells after the flow rate of the well(s)

is changed, and, subsequently, estimating the reservoir and well properties. This technique estimates these data at the *in situ* conditions of pressure, temperature, and fluid saturation prevailing in the reservoir. From the analysis of pressure transient tests, among other data, the following information can be obtained:

1. Permeability thickness product (kh) in the drainage volume of the well and permeability (k)
2. Condition of the well, represented by the skin factor (s)
3. Average pressure within the drainage volume (p)
4. Porosity of the drainage volume (ϕ)
5. Pore volume of the reservoir (v_p) and its shape
6. Reservoir and fluid discontinuities (faults, etc.).

This information would be extremely useful to help analyze, improve, and forecast reservoir performance. Ramey (1975) presented an example of practical use of this data. He stated that quantitative information on these listed items would answer questions that are usually raised, such as: Is the low productivity of a well caused by plugging of the well, low formation permeability, or a low driving force and/or formation capacity for moving fluid into the well?

Thus, transient pressure testing is an extremely useful tool for reservoir diagnosis. Transient pressure testing is sometimes referred to as a practical application of reservoir engineering (Dake, 1978). In specific situations (Earlougher, 1977), it is indispensable to have correct well or reservoir analysis; for example, in defining near-wellbore and inter-well conditions as opposed to composite properties that would be obtained from steady-state tests.

To carry out a transient pressure analysis of field data, it is important to choose or obtain an adequate mathematical expression that can be used for interpretation and design of the test. This expression can be derived by properly combining the physical laws that describe the specific fluid flow problem in the reservoir, and considering the production condition of the well.

Transient pressure tests can be classified in two main types: *single well tests*, and *multiple well tests*. Single well tests, as the name indicates, are those that involve only one well, producer or injector. These tests require measuring the well's pressure response after a rate change has taken place. On the other hand, multiple well tests directly involve more than one well. In tests like this, a rate change in a well called "active" creates a pressure response in a neighboring "observation" well. Both pressure responses for

single and multiple wells can be analyzed for reservoir properties. The most important well tests are:

1. *Single well tests*— drawdown tests, buildup tests, injectivity tests, falloff tests, and multiple-rate tests.
2. *Multiple well tests*— interference tests, and pulse tests.

Figure 9-2 shows a schematic representation of the variation of the mass flow rate w and pressure versus time during three different types of transient pressure tests. Figure 9-2a represents a drawdown test; Figure 9-2b, a buildup test; and Figure 9-2c, a two-rate test. The most simple pressure drawdown test consists of a series of bottomhole pressure measurements made over a period of time with the flow rate constant. Before the test, pressure throughout the reservoir should be uniform, i.e., static. If the constant rate production and the static pressure condition are not met, alternative methods are available (Matthews and Russell, 1967; Earlougher, 1977). Depending on the purpose for which they are performed, there are two types of drawdown tests: (a) short-term drawdown tests to estimate the formation permeability and wellbore condition; and (b) long-term or reservoir limit tests to estimate the reservoir volume.

A *pressure buildup test* consists of a series of shut-in bottomhole pressure measurements, p_{ws}, made immediately before and at times Δt after shut-in. Again, the most simple buildup test involves a well that produced with a constant flow rate, w, for a period of time before shut-in (Figure 9-2b). Buildup tests are conducted in wells for similar purposes as drawdown tests; namely to estimate the flow capacity of the formation, kh, in the drainage volume; to estimate the well condition, s; and to determine the average (static) pressure in the reservoir.

A *two-rate test* is a particular case of a multiple-rate test. It consists of a series of flowing bottomhole pressure measurements made at times Δt after a rate change of the well (Figure 9-2c). The two-rate tests provide information about formation permeability, wellbore condition, and average drainage volume pressure at the start of the test.

Whereas drawdown and buildup tests are conducted in production wells, their counterpart in injection wells are the injectivity and the falloff tests. An *injectivity test* consists of a series of bottomhole pressure measurements, p_{wf}, made over a period of time with the injection flow rate being constant. The type of information that can be obtained from the analysis of these tests is the same as from drawdown tests. A *falloff test* consists of a series of bottomhole pressure measurements made immediately before and at times Δt after stopping injection. Once more, the most simple falloff test is that where injection rate, w, is constant, until the well is shut-in at time t. The

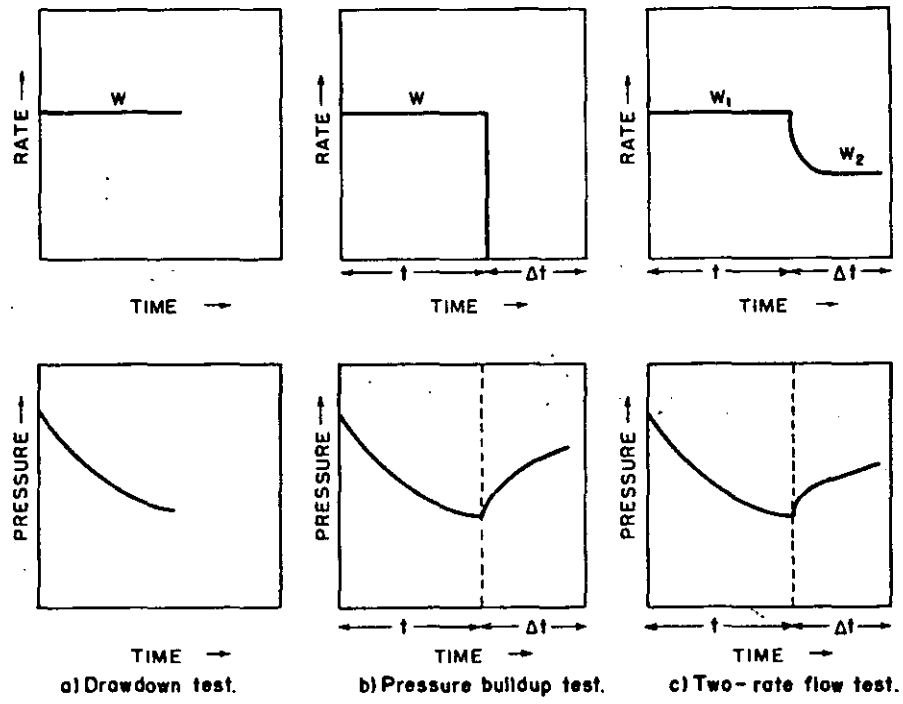

Figure 9-2. Variation of mass flow rate and bottom-hole pressure versus time for various pressure transient tests.

possible information to be obtained from these tests is the same as from pressure buildup tests.

Multiple-well transient tests consist of a series of pressure measurements of the pressure response in one or more observation wells, after a rate change on an active neighboring well. The most simple multiple-well transient test involves only one active and one observation well. Analysis could also be made of pressure response when there are more than one active and observation wells, but it will be more complicated. Figure 9-3 schematically illustrates the use of two wells in an interference or pulse test. The observation well is shut-in for pressure measuring purposes. As discussed by Matthews and Russell (1967), the name "pressure interference" comes from the fact that the pressure drop, caused by the active (producers or injectors) wells, at the shut-in observation well "interferes with" the pressure at the observation well.

In an interference test, the duration of the rate change is long, in contrast to the shorter duration of rate change in a pulse test, but the analysis

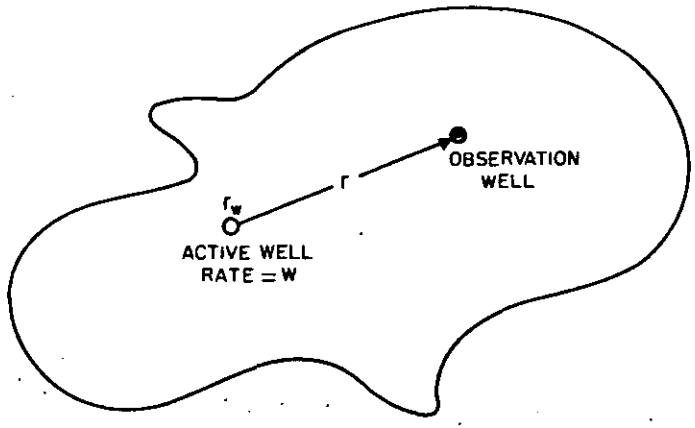

Figure 9-3. Schematic of an active and observation well in an interference test.

technique for reservoir properties is more elaborate. Multiple-well tests can give information about reservoir properties that cannot be obtained from ordinary single well tests. For instance, it is possible to estimate reservoir connectivity. A test like this may answer such questions as, Is the area of the reservoir closed to a well being drained by other wells and, if so, how fast? This test would also help to determine the preferential reservoir flow patterns. This could be accomplished by selectively opening wells that surround the shut-in well.

Because flow in a geothermal reservoir can be steam, hot water, or a mixture of steam and hot water, it is important to understand analysis techniques for these three different cases vis-á-vis some of the most used pressure transient tests.

Transient Pressure Analysis for Steam Wells

Due to the fact that single-phase (steam or hot water) flow in geothermal reservoirs is essentially isothermal (Whiting and Ramey, 1969), transient pressure analysis techniques are usually based on a strict analogy with the single-phase isothermal flow techniques developed by petroleum engineers and hydrogeologists. The laminar flow (a) of a slightly compressible fluid in a radial, horizontal, isotropic reservoir, (b) under the condition of small pressure gradients in the reservoir and applicability of Darcy's law, and (c) assuming that the rock and fluid properties are independent of pressure is expressed by the diffusivity equation (Muskat, 1938; Matthews and Russell, 1967; Earlougher, 1977). For convenience, the solution to this reservoir fluid

flow problem is usually expressed in dimensionless form. The following groups have been defined by Ramey (1975) and Ramey and Gringarten (1975), where a and B are unit constants:

Dimensionless pressure for flow of steam—

$$p_D\ (r_D\ t_D\ ) = \frac{Mkh\ (p_i^2 - p^2)}{\alpha w \mu\ Z\ T} \tag{9-1}$$

Dimensionless time—

$$t_D = \frac{\beta\ kt}{\phi\ \mu\ c_t\ r_w^2} \tag{9-2}$$

Dimensionless radial distance—

$$r_D = \frac{r}{r_w} \tag{9-3}$$

If a consistent set of units is used, then these constants will have a value equal to one. Table 9-2 shows some of the most used unit systems, and the corresponding values for a and B.

The pressure in the reservoir at any point in space and time can be estimated from Equation 9-1 if the particular p_D for the system under consideration is known. The dimensionless pressure p_D is a function of the type of system, infinite or finite, and of the boundary conditions, rate or pressure specified. For a well producing at a constant flow rate w, assuming that the conditions for the flow of a fluid of constant and small compressibility apply, and for infinite acting conditions, the p_D can be expressed by the line source solution (Earlougher, 1977):

$$p_D\ (r_D\ \ t_D) = -\frac{1}{2}\ E_i\ \left(-\frac{r_D^2}{4t_D}\right) \tag{9-4}$$

For transient pressure analysis purposes, the pressure of interest is the wellbore pressure. For this condition, $r = r_w$, and combining Equations 9-1, 9-2, 9-3, and 9-4, and using the logarithmic approximation to the exponential integral, an expression for the wellbore pressure can be obtained as follows:

$$p_{wf}^2 = p_i - 1.1513\alpha\ \frac{w\mu ZT}{Mkh}\left[\log\frac{kt}{\phi\mu\ c_t\ r_w^2} + \log\frac{4\beta}{\gamma} + 0.86859s\right] \tag{9-5}$$

Table 9-2
Absolute and Hybrid System of Units Used in Geothermal Reservoir Engineering

Variable	SI system*	Hybrid system
k	metre^2	md
h	m	m
p	Newton/metre^2 = pascal	kg$_f$/cm^2
w	kg/sec	ton/hr
ν_{sc}	metre^3/kg	cm^3/gm
B	metre$^3{}_{rc}$/metre^3 **	metre$^3{}_{rc}$/metre$^3{}_{sc}$
μ	kg/metre.sec	cp
t	sec	hours
ϕ	fraction	fraction
c_t	(Newton/metre^2)$^{-1}$	(kg/cm^2)$^{-1}$
r	metre	metre
α	26.1201	77.459×10^3
β	1	0.000348
δ	1/2 π	456.7869
ϵ	1/2 π	1/2 π
η	2.6465	27

* SI is the abbreviation for International System of Units.
** *rc* stands for reservoir conditions and *sc* for standard conditions.

where $\gamma = 1.7810724$, and log = base 10 logarithm.

This equation can be used for interpretation of a steam drawdown test. It can be observed that it describes a straight-line relationship between p^2_{wf} and log t. Theoretically, a plot of flowing bottom hole pressure data versus the logarithm of time (usually called a "semilog plot") should be a straight line with slope m, given by the following expression:

$$m = \frac{1.1513\,\alpha w\,\mu\,Z\,T}{Mkh} \tag{9-6}$$

From this equation, the capacity of the formation can be obtained:

$$k\,h = \frac{1.1513\,\alpha w\,\mu\,Z\,T}{mM} \tag{9-7}$$

By rearranging Equation 9-5, an expression for the skin factor, s, can be obtained:

$$s = 1.1513\left[\frac{p_i^2 - p^2_{1hr}}{m} - \log\frac{k}{\phi\mu\,c_t\,r_w^2} - \log\frac{4\beta}{\gamma}\right] \tag{9-8}$$

For pressure buildup testing, the bottomhole shut-in pressure of the well may be expressed by means of the principle of superposition for a well producing at a rate w until time t (Figure 9-2b), and at zero rate thereafter. Thus, at any time after shut-in, the wellbore pressure may be expressed as follows:

$$p^2_{ws} = p_i^2 - \alpha\frac{w\mu\,Z\,T}{Mkh}\left[p_D(t+\Delta t)_D - p_D\,(\Delta t_D)\right] \tag{9-9}$$

Substituting Equation 9-5 into Equation 9-9:

$$p^2_{ws} = p_i^2 - m\log\left(\frac{t+\Delta t}{\Delta t}\right) \tag{9-10}$$

This equation can be used for interpretation of a buildup test. It describes a straight-line relationship between p^2_{ws} and log $(t + \Delta t) / \Delta t$. Theoretically, a plot of flowing bottomhole pressure data versus the log $(t + \Delta t)/\Delta t$ should be a straight line with slope m given by Equation 9-6. Figure 9-4 shows a schematic Horner plot of pressure buildup data. The straight-line portion of the Horner plot can be extrapolated to $(t + \Delta t) / \Delta t = 1$, the equivalent to infinite shut-in time, to obtain an estimate of p_i. This is only valid for infinite acting systems during the flow period. After the exterior boundary affects production, the extrapolated pressure is p^*. This value can be used to estimate the average drainage volume pressure (Matthews et al., 1954). As pointed out by Matthews and Russell (1967), an equation describing the pressure behavior for an infinite acting reservoir may be immediately rewritten for the finite reservoir case by substituting p^* by p_i.

The skin factor, s, may also be estimated from pressure buildup analysis. An expression for this factor can be obtained by combining the expressions for flowing and shut-in pressures as given by Equations 9-5 and 9-10:

$$s = 1.1513\left[\frac{p^2_{1hr} - p^2_{wf}\,(\Delta t = 0)}{m} - \log\frac{k}{\phi\mu\,c_t\,r_w^2} - \log\frac{4\beta}{\gamma}\right] \tag{9-11}$$

In this equation, p^2_{wf} $(\Delta t = 0)$ is the measured flowing bottomhole pressure immediately before shut-in. The p^2_{1hr} pressure must be obtained from the straight line portion of the pressure buildup test 1 hour after shut-in, or from its extrapolation if the straight-line portion of the test has not been reached at this time. This also holds true for other types of tests, as for the drawdown test previously discussed.

The early deviation of a transient pressure test from a straight line may be caused, among other factors, by wellbore storage (van Everdingen and Hurst, 1949; Ramey, 1965; Agarwal, et al., 1970). This can be caused by expansion or compression of fluids in the wellbore and by liquid level

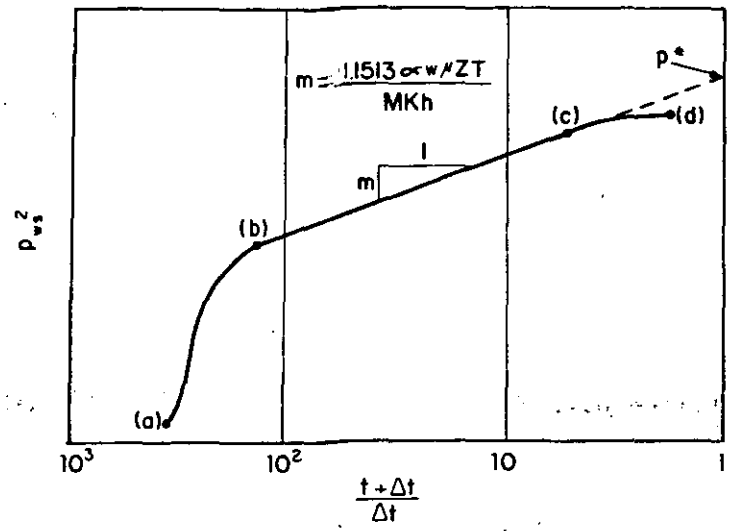

(a)–(b) Short-time data.
(b)–(c) Semilog straight line portion.
(c)–(d) Boundary effects.

Figure 9-4. Schematic representation of a Horner plot for pressure buildup data.

movements in the wellbore. This effect has to be properly considered for accurate test design and interpretation.

Example 9-1: Pressure Buildup Test Analysis—Horner Method

This example is a pressure buildup test analysis for the Geysers Steam Well C, presented by Ramey (1975). The reservoir data regarding this test were:

w = 102.3 ton/hr	T = 515°K
t = 552 hr	M = 18 g/g mole
r_w = 0.122 m	m = 210 (kg/cm²)²/log cycle
μ = 0.0225 cp	$p_{1\ hr}^2$ = 1,047 (kg/cm²)²
c = 0.037 (kg/cm²)⁻¹	p_{wf}^2 = 262 (kg/cm²)²
Z = 0.84	p^{*2} = 1,333 (kg/cm²)²

Total depth = 1,120 m; open hole is below 155 m.

Figure 9.5 shows a semilogarithmic plot of test data. As previously mentioned, wellbore storage affects transient pressure behavior and, therefore,

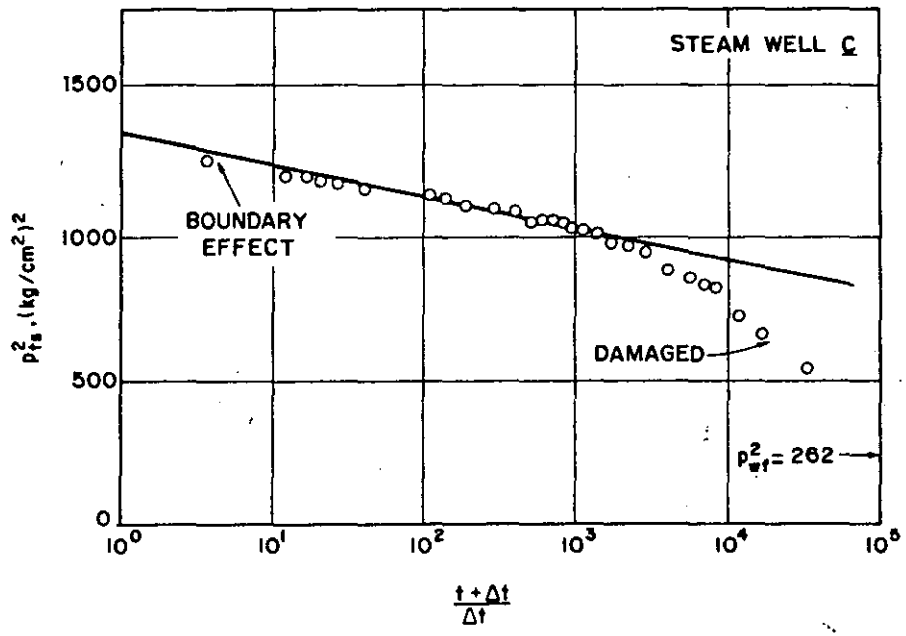

Figure 9-5. Horner buildup graph for Geysers Steam Well C. (After Ramey, 1975, Fig. 7, p. 1753)

should be considered in all transient pressure analyses. This will be considered later in this chapter. A straight line appears to start at a ratio approximately equal to 1000. This corresponds to a shut-in time of 0.55 hr. From the slope of the straight-line portion of the test pressure plot and Equation 9-7, the product kh may be estimated:

$$kh = \frac{1.1513\ (77.459 \times 10^3)\ (102.3)\ (0.0225)\ (0.84)\ (515)}{(210)\ (18)}$$

$$= 23{,}491\ \text{md-m}$$

The skin factor can be estimated by using Equation 9-11. Inasmuch as no data about the average drainage volume pressure at the start of the test, p_i, and porosity ϕ are given, it cannot be computed for this particular example.

Transient Pressure Analysis for Hot-Water Wells

As previously mentioned, the reservoir fluid flow of hot water can be described based on a strict analogy with the single-phase isothermal flow techniques. Once again, it is assumed that flow in the reservoir is approximately described by the diffusivity equation. For hot-water reservoir flow

problems, the dimensionless pressure group has been defined by Ramey (1975) as follows:

$$p_D\ (r_D\ \ t_D) \quad = \frac{kh\ (p_i - p)}{\delta\ v_{sc}\ wB\ \mu} \tag{9-12}$$

where δ is a conversion unit constant (Table 9-2).

For a well producing at a constant flow rate w, and considering that all the assumptions mentioned for the reservoir steam flow problem hold, Equation 9-12 can be combined with Equation 9-4, for conditions at the wellbore, $r = r_w$, to obtain an expression for the wellbore pressure:

$$p_{wf} = p_i - 1.1513\delta \frac{v_{sc}\ wB\mu}{kh}\left[\log\frac{kt}{\phi\ \mu\ c_t\ r_w^2} + \log\frac{4\beta}{\gamma} + 0.86859s\right] \tag{9-13}$$

This equation can be used for interpretation of a hot-water drawdown test. Theoretically, according to Equation 9-13, a plot of flowing bottomhole pressure data versus the logarithm of time should be a straight line, with slope m given by the following expression:

$$m = \frac{1.1513\delta\ v_{sc} w\ \beta\ \mu}{kh} \tag{9-14}$$

From this expression, the flow capacity of the formation can be obtained:

$$kh = \frac{1.1513\delta\ v_{sc}\ w\ \beta\ \mu}{m} \tag{9-15}$$

An expression for the skin factor, s, can be obtained by the rearrangement of Equation 9-13:

$$s = 1.1513\left[\frac{p_i - p_{1hr}}{m} - \log\frac{k}{\phi\mu\ c_t\ r_w^2} - \log\frac{4\beta}{\gamma}\right] \tag{9-16}$$

The basis for pressure buildup analysis is the principle of superposition. Following a similar procedure as for the steam reservoir flow problem, an expression for the shut-in bottomhole pressure, p_{ws} can be written as follows:

$$p_{ws} = p_i - m\log\frac{(t + \Delta t)}{\Delta t} \tag{9-17}$$

This equation can be used for interpretation of a hot-water buildup test. Theoretically, according to Equation 9-17, a plot of flowing bottomhole shut-in pressure data versus the log $(t + \Delta t)/\Delta t$ should be a straight line with slope given by Equation 9-14. A schematic Horner plot of pressure buildup data would look like that shown in Figure 9-4 for a steam well, with p_{ws}^2 being replaced by p_{ws}. With regard to the extrapolation of the straight-line portion of the buildup curve, for infinite shut-in time, $(t + \Delta t)/\Delta t = 1$), the pressure obtained is p^*. This can be used to estimate the average drainage volume pressure.

The skin factor, s, may also be estimated from pressure buildup analysis. An expression for this factor can be obtained by combining the expressions for flowing and shut-in pressures, given by Equations 9-13 and 9-17:

$$s = 1.1513\left[\frac{p_{1hr} - p_{wf}\ (\Delta t = 0)}{m} - \log\frac{k}{\phi\mu\ c_t\ r_w^2} - \log\frac{4\beta}{\gamma}\right] \tag{9-18}$$

Everything that was discussed regarding p_{wf} $(\Delta t = 0)$ and p_{1hr} for the steam flow problem, applies for this hot-water flow problem. With respect to the wellbore storage effect, it can affect a transient pressure test in much the same way as for a steam well (Gringarten, 1978).

The transient pressure analysis theory just presented for hot-water wells can be far more complex, if two-phase flow develops, either in the wellbore or in the formation. The petroleum engineering and hydrogeological methods of analysis have been shown to apply correctly to geothermal wells when no flashing occurs (Witherspoon, 1978). When flashing develops in the formation, however, they apparently cannot be used (Gulati, 1975; Garg, 1978). It was only recently (Rivera and Ramey, 1977; Gringarten, 1978) that information on flashing occurring in the wellbore became available. This is chiefly due to mechanical problems caused by the hostile, hot geothermal environment, and high flow rates of boiling fluids, making difficult the data gathering of bottomhole pressure, because the recording instruments could be easily damaged under these conditions.

Another type of test that has been successfully used in hot-water wells is *multiple-rate testing*. It is often inconvenient to shut-in a well for a pressure buildup survey because it involves loss of production and sometimes it is difficult, for a variety of reasons, to start production after the survey. Also, the previously described drawdown testing techniques of analysis require a constant flow rate. There are many cases where it is impractical or impossible to maintain a constant flow rate long enough, and this type of simplified pressure drawdown test cannot be carried out. Multiple-rate testing, therefore, appears frequently as an alternative for the determination of reservoir parameters. Multiple-rate tests may range (Earlougher, 1977) from one with

uncontrolled, variable rate, to one with a series of constant rates, to one at constant bottomhole pressure conditions with a continuously changing flow rate. This type of test has been used with great success for hot-water wells (Rivera and Ramey, 1977; Gringarten, 1978; Saltuklaroglu and Rivera, 1978). One particular case of a multiple rate is when there are only two different flow rates. This type of test, which is called two-rate (Russell, 1963) simplifies testing and analysis. Multiple-rate tests provide information about formation flow capacity and well conditions, represented by the skin factor. The average drainage volume pressure prevailing at the beginning of the test can also be estimated.

To develop a general equation, the pressure test is divided into intervals during each of which production rate can be considered constant. The flow rate-time schedule is as follows:

$$
\begin{aligned}
w &= w_1, \quad 0 \leq t \leq t_1 \\
w &= w_2, \quad t_1 \leq t \leq t_2 \\
w &= w_3, \quad t_2 \leq t \leq t_3 \\
&\vdots \\
w &= w_N, \quad t_N - 1 \leq t \leq t_N
\end{aligned}
$$

This discretization of a possible continuously changing flow rate may be improved as the time intervals become smaller. The pressure drop during the time period N can be expressed by means of the principle of superposition and Equation 9-13:

$$
p_{wf} = -1.1513\delta \frac{\nu_{sc}\beta\mu}{kh} \sum_{j=1}^{N} (w_j - w_{j-1}) \log (t - t_{j-1}) + p_i
$$

$$
- 1.1513\delta \frac{\nu_{sc} w_N \beta\mu}{kh} \left[\log \frac{k}{\phi\mu c_t r_w^2} + \log \frac{4\beta}{\gamma} + 0.86859\, s \right] \quad (9\text{-}19)
$$

This expression can be rearranged in the following form:

$$
\frac{p_i - p_{wf}}{w_N} = 1.1513\delta \frac{\nu_{sc}\beta\mu}{kh} \sum_{j=1}^{N} \left[\frac{(w_j - w_{j-1}) \log (t - t_{j-1})}{w_N} \right]
$$

$$
+ 1.1513\delta \frac{\nu_{sc}\beta\mu}{kh} \left[\log \frac{k}{\phi\mu c_t r_w^2} + \log \frac{4\beta}{\gamma} + 0.86859\, s \right] \quad (9\text{-}20)
$$

Equation 9-20 is the interpretation equation used for a general hot-water multiple-rate test. It describes a straight-line relationship of slope:

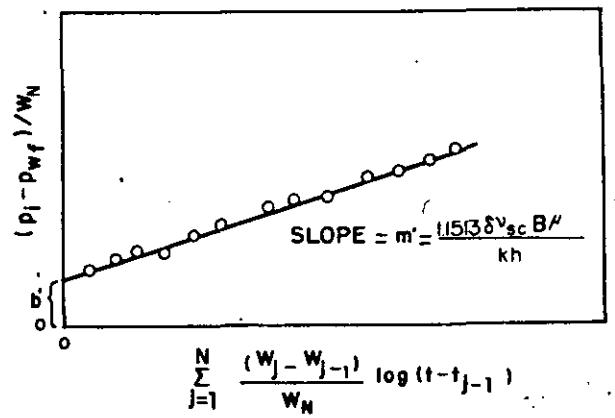

Figure 9-6. Schematic representation of a multiple-rate test.

$$
m' = 1.1513\delta \frac{\nu_{sc}\beta\mu}{kh} \quad (9\text{-}21)
$$

and intercept:

$$
b' = m' \left[\log \frac{k}{\phi\mu c_t r_w^2} + \log \frac{4\beta}{\gamma} + 0.86859\, s \right] \quad (9\text{-}22)
$$

Multiple-rate pressure transient data follow a straight line when plotted in Cartesian coordinates as shown in Figure 9-6:

$$
\frac{p_i - p_{wf}}{w_N} \quad \nu_{s-} \sum_{j=1}^{N} \frac{(w_j - w_{j-1})}{w_N} \log (t - t_{j-1}) \quad (9\text{-}23)
$$

Earlougher (1977) clearly stated that in order to plot it correctly, it is important that the rate corresponding to each plotted pressure point is w_N, the last rate that can affect that pressure. As time goes on, the number of flow rates may increase and the last rate may change; but each pressure is identified with the rate occurring when that pressure was measured. It should be clear that there may be more than one pressure reading associated with one specific rate. It is important to keep in mind that this multiple-rate theory assumes transient flow conditions throughout the whole test. This is due to the fact that the interpretation equation has been derived based on the line source solution, only valid for infinite acting systems (transient flow

conditions). Thus, the separate flow periods should be of short duration so that transient flow will prevail at each rate through the whole test.

From the slope of the multiple-rate pressure curve, given by Equation 9-21, the formation permeability may be estimated as follows:

$$k = \frac{1.1513\delta v_{sc}\ \beta\mu}{m'\ h} \tag{9-24}$$

Also, from the intercept of the pressure curve, given by Equation 9-22, the skin factor, s, can be estimated:

$$s = 1.1513\left[\frac{b'}{m'} - \log\frac{k}{\phi\mu\ c_t\ r_w^2} - \log\frac{4\beta}{\gamma}\right] \tag{9-25}$$

Example 9-2: Multiple-Rate Test Analysis

This test, which was made for a hot-water well, ASAL 1, located in the French Territory of Afars and Issas (now Republic of Djibouti), was presented by Gringarten (1978). Flashing of the hot water occurred at some depth in the wellbore. The mass rate of flow variation is shown in Figure 9-7. The pressure data measured during the second 6-in. buildup test (flow period No. 4), was graphed (Figure 9-8) in a slightly different manner than that just described. Gringarten plotted p_{wf}, instead of the group $(p_i - p_{wf})/w_N$, and the time units used were minutes instead of hours. The pressure coordinate was changed because of uncertainty of the average drainage volume pressure for this well, p_i. Otherwise, the method of analysis is the same. Figure 9-8 shows a straight-line portion of slope $m' = 3.6 \times 10^{-3}$. Other data needed to analyze the test is $\mu = 0.2$ cp and $v = 1.25 \times 10^{-3}$ m^3/kg, which is equivalent to $v_{sc}B$ in Equation 9-21. Substituting these values into Equation 9-21 and *sc* considering the change of units (Gringarten's eq. 5, p. 3) yields the following equation:

$$kh = \frac{0.228\ v\ \mu}{m'} = \frac{0.228\ (1.25\times10^{-3})\ (0.2)}{3.6\ \times\ 10^{-3}}$$

$$= \quad 15.9 \text{ darcy-meter}$$

The calculated average drainage volume pressure from the test is 76.6 bars (1 bar = 14.503 psi), which agrees reasonably with a measured value before the test of 77.4 bars.

It can be observed from Figure 9-8 that deviations from the straight line occur at short times (portion a-b, Figure 9-4) and at long times (portion c-d, Figure 9-4). It will be discussed that the short-time deviation (for buildup

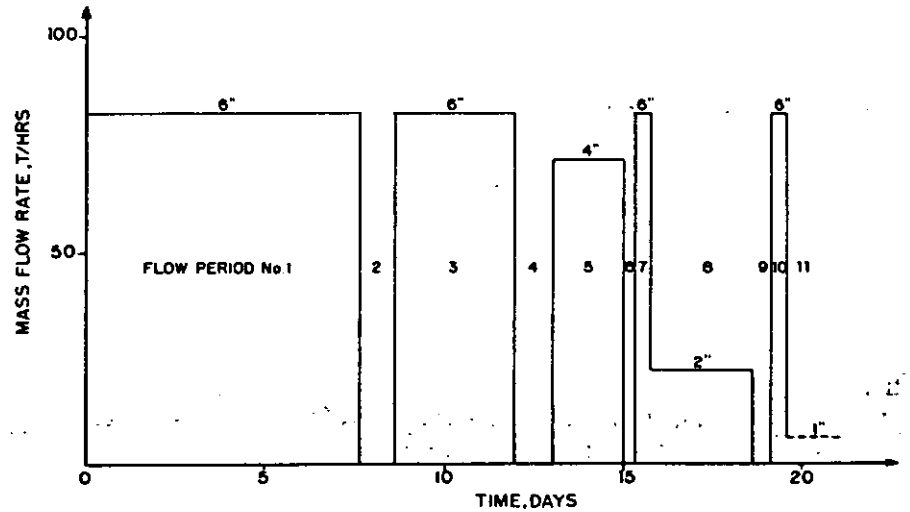

Figure 9-7. Mass flow rate changes during ASAL 1 tests. (After Gringarten, 1978, Fig. 2, p. 6, by permission of the S.P.E. of A.I.M.E.)

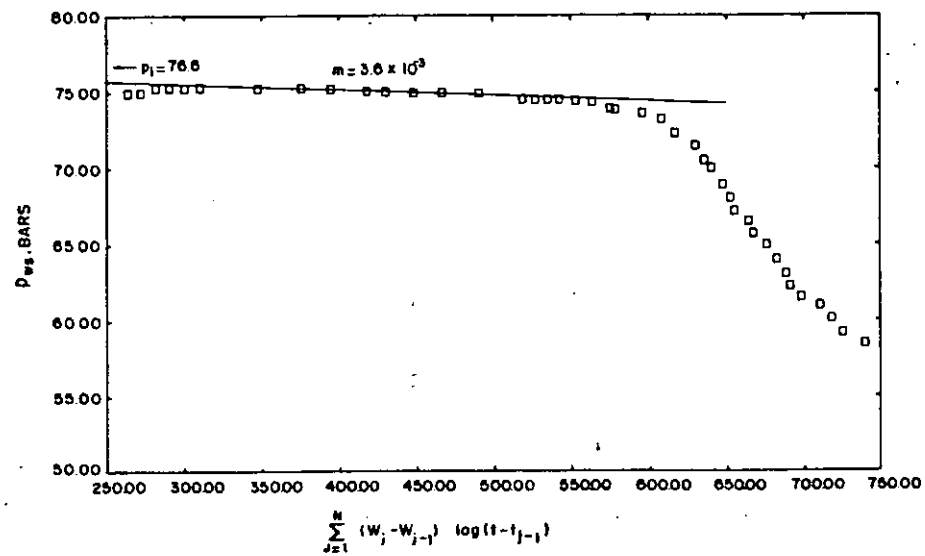

Figure 9-8. ASAL 1 pressure buildup test (6" outlet, flow period #4) (After Gringarten, 1978, Fig. 7, p. 9, by permission of the S.P.E. of A.I.M.E.)

times less than 20 minutes) is caused by wellbore storage effects. For long times (buildup times greater than 6 hours), the data points deviate from the straight-line portion of the pressure curve because of steam condensation in the wellbore.

Interference Testing for Geothermal Reservoirs

Interference testing is preferred in some instances over single well tests depending on the type of information required (Rivera et al., 1978). It has been previously mentioned that important data like reservoir connectivity and porosity can be estimated from analysis of these tests. Reservoir connectivity is an important factor because the number of wells in a reservoir usually increases, causing mutual interference of wells. The application of these tests to hot-water geothermal reservoirs has been successfully reported in the literature (Witherspoon et al., 1978; Rivera et al., 1978; and Narasimhan et al., 1978).

Interference tests are usually analyzed by a type curve matching technique. The type curve used is the line source solution, for an infinite acting system, plotted on a log-log paper in terms of p vs $t_D/r_D{}^2$ (Ramey et al., 1973; Earlougher, 1977). Figure 9-9 presents this type curve for a well located in an infinite acting system. The type curve matching technique consists of plotting the observation well pressure drop, $\Delta p_i - p$, on the ordinate versus flowing time, t, on the abscissa of a log-log paper of the same size as in Figure 9-9. Normally, a tracing paper is placed over the type curve, and the major grid lines are traced for reference. The grid lines of Figure 9-9 (not shown) are used to plot actual data on the tracing paper. Next, the data plot is moved vertically and horizontally over Figure 9-9, keeping the grids of the type-curve and those of the data plot parallel to each other until the best match is obtained with the type-curve. A convenient match point is pierced and the values of $(\Delta p)_M$ and $(t)_M$ are read from the data plot. The corresponding points lying directly under this point on Figure 9-9 are $(p_D)_M$ and $(t_D)_M$. The formation permeability is estimated from the pressure match-point data and the definition of p_D is given by Equation 9-12:

$$k = \frac{\delta v_{sc}\, w\, \beta\, \mu}{h} \frac{(p_D)_M}{(\Delta p)_M} \tag{9-26}$$

In a similar way, the porosity compressibility product is estimated from the time match-point data and the definition of t_D and r_D by Equations 9-2 and 9-3:

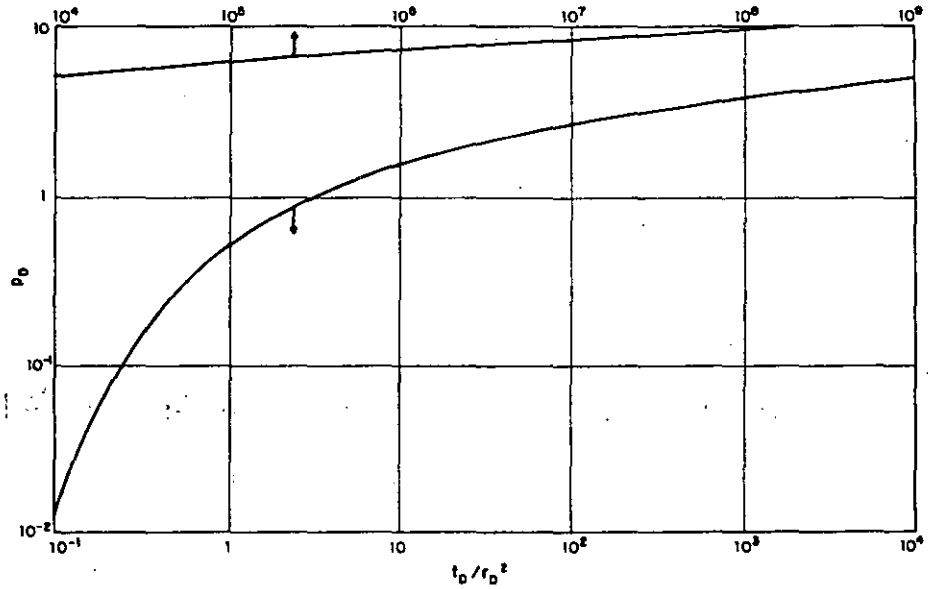

Figure 9-9. Dimensionless pressure for a single well in an infinite system, no wellbore storage, no skin. Exponential-integral solution. (After Earlougher, 1977, Fig. C.2, p. 194, by permission of S.P.E. of A.I.M.E.)

$$\phi c_t = \frac{\beta}{r^2} \frac{k}{\mu} \frac{(t)_M}{(t_D/r_D^2)_M} \tag{9-27}$$

This type of curve analysis method is simple, rapid, and accurate, provided the conditions for applicability of the line source p_D solution are met, i.e., when $r_D = r/r_w > 20$ and $t_D/r_D^2 > 0.5$ (Earlougher, 1977).

Example 9-3: Type Curve Matching Analysis of a Pressure Interference Test

This is a pressure interference test carried out in the liquid-dominated Cerro Prieto Geothermal Field, located in Mexico. These results are taken from a paper by Rivera et al. (1978), and involved one observation well (M-101) and four active wells (M-50, M-51, M-90, and M-91). The early pressure drop response at the observation well M-101 was analyzed, while the only active well was M-91 and the other three wells were shut-in. Figure

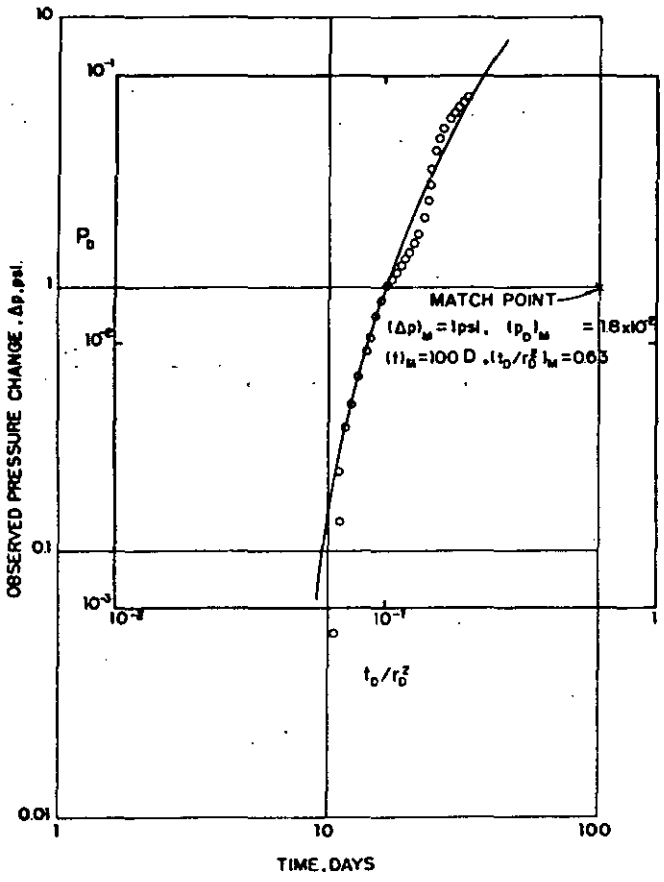

Figure 9-10. Type curve match of an interference test, active wells M-91, M-90, M-51, M-50. Observation well M-101. Cerro Prieto Geothermal Field (After Riviera et al., 1978, Fig. 5)

9-10 shows the type-curve match presented by these authors. Other related data for the test were:

w = 185.3 ton/hr
v_{sc} = 1.043 cm³/g
β = 1.185 metre³$_{rc}$/metre³$_{sc}$
μ = 0.1017 cp
r = 1550 m

From the results of the match point data and from Equations 9-26 and 9-27, the following estimates for the reservoir parameters are obtained:

$$kh = 456.7869\ (1.043)\ (185.3)\ (1.185)\ (0.1017)\ \frac{(1.8\times10^{-2})}{(1)\ (1/14.22)}$$

$$= 2{,}723 \text{ md-m}$$

and

$$\phi c_t h = \left(\frac{0.000348}{(1{,}550)^2}\right)\ \left(\frac{2{,}723}{0.1017}\right)\ \left(\frac{(100)\ (24)}{0.63}\right) = 0.0148 \text{ m/(kg/cm}^2\text{)}.$$

Pressure Transient Analysis for Two-Phase Flow

Up to now, most of the discussion has been based on single-phase isothermal reservoir flow. Sometimes, however, flow conditions in the reservoir are such that two-phase flow can occur, causing the flow to be non-isothermal. Garg (1978a, 1978b) has recently presented a theory for analysis of two-phase pressure transient data in geothermal wells. He considered two different situations: (a) a reservoir that is originally two-phase everywhere, and (b) a reservoir that originally contained hot water, but after production the pressure drop resulted in a flashing front propagation away from the wellbore. He derived a diffusivity-type equation, which resembles quite closely the diffusivity equation. This type of analogy has been found for other reservoir fluid flow problems (Martin, 1959). Based on this similarity of the equations that describe the flow problem, Garg derived an expression for the flowing bottomhole pressure for the two above mentioned reservoir situations:

(a) Two-phase flow exists everywhere in the reservoir at initial conditions:

$$p_{wf} = p_i - 1.1513\delta \frac{w}{(k/\nu)_t h}\left[\log\frac{(k/\nu)_t t}{\phi\ \rho\ c_t r_w^2} + \log\frac{4\beta}{\gamma}\right] \tag{9-28}$$

(b) Hot water is present everywhere in the reservoir at initial conditions, with a flashing-front propagating after two-phase pressure conditions are reached:

$$p_{wf} = p_s - \frac{\delta w}{2[(k/\nu)_t]_1 h} E_i(-\lambda^2) - 1.1513\delta \frac{w}{[(k/\nu)_t]_1 h}$$
$$\left[\log\frac{(k/\nu)_t t}{\phi\ \rho (c_t)_1\ r_w^2} + \log\frac{4\beta}{\gamma}\right] \tag{9-29}$$

where: $(k/\nu)_t$ = total kinematic mobility = $(k/\nu)_w + (k/\nu)_s$
$(k/\nu)_w$ = kinematic mobility for the water = $k\ k_{rw}\ \rho_w/\mu_w$
$(k/\nu)_s$ = kinematic mobility for the steam = $k\ k_{rs}\ \rho_s/\mu_s$

λ = roots of eq. 13d of Garg's (1978b) paper
1 = subscript denoting the two-phase region

Equations 9-28 and 9-29 can be used for interpretation of a two-phase flow drawdown test. Theoretically, according to these equations, a plot of flowing bottomhole pressure data versus the logarithm of time should be a straight line with slope m given by the following expression:

$$m = \frac{1.1513\delta w}{(k/\nu)_t h} \tag{9-30}$$

From this expression, the total kinematic mobility can be estimated:

$$(k/\nu)_t = \frac{1.1513\delta w}{mh} \tag{9-31}$$

Recently, a sound theoretical basis for the estimation of the kinematic mobility from pressure interference testing has been suggested (Pruess et al., 1978). This is an extension of Garg's theory of analysis for two-phase flow.

Example 9-4: Two-Phase Flow Pressure Transient Test with a Propagating Flashing Front

This is a simulated test presented by Garg (1978b). Single-phase (hot water) conditions prevail for some time after the start of production, until eventually, the pressure level declines sufficiently to reach the two-phase flow conditions, and a flashing front propagates away from the well. Figure 9-11 shows a semilog plot of the results of this test. At early times, up to about 12 seconds, hot-water flow conditions prevail in the vicinity of the well. From this time on, two-phase flow conditions start to be operative and for a period of time related to numerical approximations, the curve is relatively flat. After the numerical problem is overcome, for late times, the pressure data follow approximately a straight line. The computed value of $(k/\nu)_t'$ obtained from the slope of the straight-line portion of the pressure curve of Figure 9-11, and Equation 9-31, agrees well with the actual range of values for this parameter.

Modern Well Test Analysis

According to Ramey (1970), modern well test analysis specifies that the well be tested for a period of time long enough to reach and define a proper "straight line," when pressure transient data are plotted on semilogarithmic

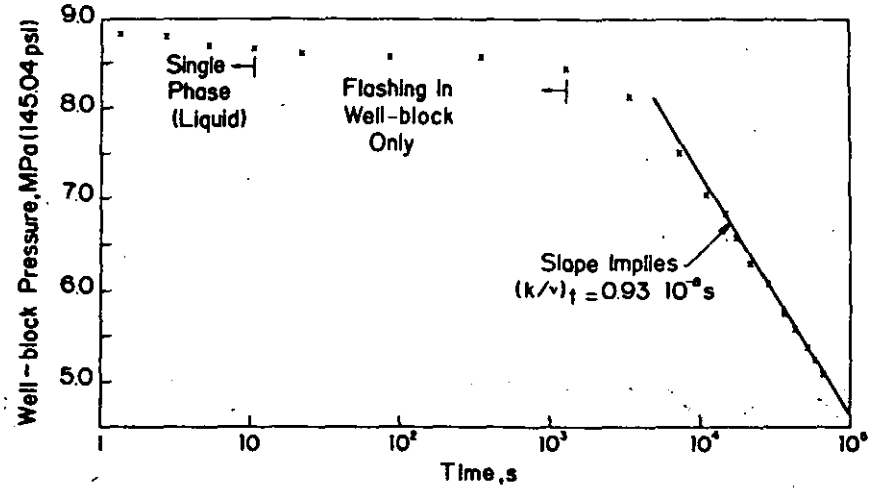

Figure 9-11. Simulated drawdown history *(g)*. Reservoir is initially single-phase everywhere ($p = 9.000$ MPa ~1,305.3 psi; $T = 573.15$K = 572°F). Absolute permeability k for this case is 0.01 μm^2 (~0.01 darcy) and the actual range of $(k/\nu)_t$ values for points lying on the straight line is $(0.93\text{-}1.15)10^{-6}$s. (After Garg, 1978b, Fig. 7, P. 12, by permission of the S.P.E. of A.I.M.E.)

graph paper. It was not until the end of the '60s that pressure data recorded before the straight-line portion was reached started to be analyzed. It has since been realized that this early time data could be extremely helpful for test interpretation purposes. The early time data, also called "short-time data," are influenced by the effects of several factors, like wellbore storage, flow through perforations, partial penetration, and well stimulation such as fracturing or acidizing.

Short-time data can usually be analyzed by a log-log type curve matching technique similar to that previously described for interference testing. The type curve is a log-log graph of the solution of a specific reservoir fluid flow problem, plotted in terms of p_D vs t_D. The type curve should be chosen in such a manner as to closely represent the field situation. Perhaps, the most commonly used type curve to date has been that presented by Agarwal et al. (1970) and Wattenbarger and Ramey (1970) for the pressure transient behavior of a well, including wellbore storage and skin damage (Figure 9-12). This type curve can be used to approximately determine the beginning of the correct semilog straight line. The curves of Figure 9-12 show an early unit slope straight-line portion, representing wellbore storage dominated flow conditions, followed by a transition to the relatively flat curves for zero wellbore storage. The point where the curves including wellbore storage

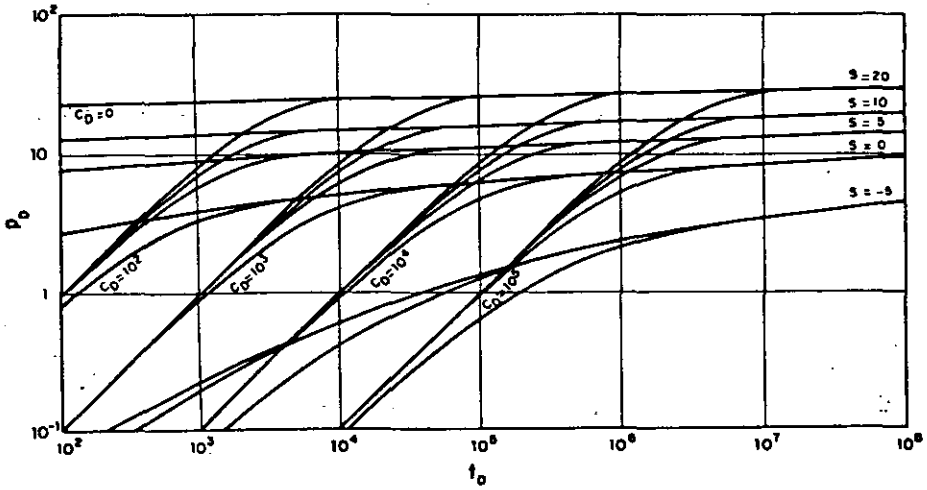

Figure 9-12. Dimensionless pressure for a single well in an infinite system, wellbore storage and skin included. (After Agarwal, Al-Hussainy, and Ramey. 1970. Graph courtesy H. J. Ramey, Jr.)

reach the zero wellbore storage curves represents the start of the correct semilog straight line. This time can be expressed (Ramey et al., 1973):

$$t_D = C_D\ (60 + 3.5\ s) \tag{9-32}$$

where:

$$C_D = \frac{\epsilon\ C\ B\ v_{sc}}{\phi\ h\ c_t\ r_w^{\ 2}} \qquad \text{for hot water} \tag{9-33}$$

and

$$C_D = \frac{\eta\ C'\ Z\ T}{M\ \phi\ h\ c_t\ r_w^{\ 2}} \qquad \text{for steam.} \tag{9-34}$$

For a good semilog analysis of the pressure transient data, the duration of the test should be at least ten times the time given by Equation 9-32. This would provide a minimum of a log cycle of pressure field data, allowing a proper tracing of the straight-line portion of the pressure curve.

There are many type curves presently available for pressure analysis of short-time data. The difference between them is the well condition that they consider, e.g., a well with a horizontal fracture (Gringarten et al., 1974), a well with a vertical fracture (Gringarten et al., 1975; Cinco et al., 1978), etc.

Type curve matching techniques can be used, in combination with other data, to identify the near wellbore conditions and, as mentioned, to determine the correct start of the semilog straight line. With a properly estimated start of the semilog straight line, the results obtained from the semilog analysis are more accurate than those coming from log-log type-curve matching. As pointed out by Gringarten et al. (1975) a combination of type-curve matching techniques with conventional semilog analytical methods permits a highly confident analysis of field data.

Example 9-5: Modern Well Test Analysis of a Pressure Transient Test in a Steam Well

Example 9-1 showed the analysis of a pressure buildup test presented by Ramey (1975). The purpose of this example is to illustrate how type-curve matching techniques can be used to identify the correct start of the semilog straight line. Figure 9-13 shows a type-curve match of the buildup data to the type curve of Figure 9-12. Field data fairly matches the curve for $c_D = 10^2$ and $s = 5$. More important than this, however, is the fact that the data reaches the type-curve for $c_D = 0$ at Δt equal to 0.3 hour. This corresponds to a $(t+\Delta t)/\Delta t$ value of 1,841. Examination of Figure 9-5 shows that, according to type-curve analysis, the start of the straight line has been correctly identified. As previously pointed out, any other information in addition to the start of the straight line, should only be taken in a qualitative sense.

Simulation of Geothermal Reservoirs

The word "simulate" has been defined by Webster as "to assume the appearance of without the reality." To the reservoir engineer, the term reservoir simulation means the process of deducing the physical behavior of a real reservoir from the performance of a model. There are two basic types of models: (a) physical (for example, a laboratory sandpack), and (b) mathematical. A mathematical model of a physical system consists of a set of partial differential equations subject to certain simplifying assumptions, together with an appropriate set of boundary conditions, which describe the physical processes active in the reservoir (Peaceman, 1978; Coats, 1969; Crichlow, 1977).

Reservoir simulation applies the concepts and techniques of mathematical modeling to the analysis of the behavior of geothermal reservoir systems. Most often, the term reservoir simulation is used with regards to the hydrodynamics of flow within the reservoir, but in a more general sense it refers to the total geothermal system, which includes mainly the reservoir itself, the tubing, and the surface facilities. A simulator can be defined as a group of

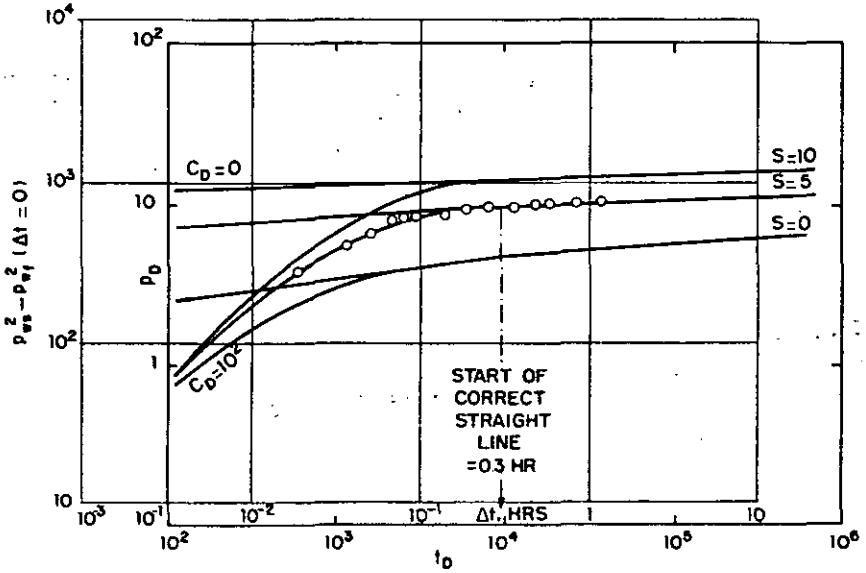

Figure 9-13. Type curve match of buildup data for steam well C to the type curve of Figure 9.12.

computer programs that implement the mathematical model in a digital computer.

The main purpose of simulation is to estimate the behavior of a geothermal reservoir under a variety of exploitation schemes. This is extremely advantageous because the reservoir can be produced only once, and the model can be produced or "run" as many times as needed at cost and over a short period of time. From observation of model performance, under a variety of producing conditions, the optimum exploitation conditions for the reservoir can be selected. Some of the information that can be obtained from reservoir simulation studies is:

1. The capability of a reservoir of producing significant quantities of energy over meaningful periods of time.
2. The number of wells and spacing required for optimum development of the reservoir.
3. The effect of the rate of production of the wells on total energy recovery.
4. Variation of fluid temperature with time.
5. Feasibility of implementation of an enhanced recovery process to recover additional heat.

Reservoir models range in complexity from simple ones for fairly homogeneous systems, where average values for reservoir properties, such as permeability and porosity, are adequate to describe their behavior, to those used for highly heterogeneous systems, where fragmentation into blocks (cells) is necessary. In order to choose a model that would represent a particular reservoir, a good understanding of the reservoir and a detailed examination of the data available (Odeh, 1969) is required. A model that fits a particular reservoir may not be appropriate for another reservoir, despite the apparent existence of similarities between them. As pointed out by Odeh (1969), a reservoir model is useful only when it reasonably matches the field situation. A general rule (Coats, 1969) that should be followed in reservoir simulation is to "select the *least* complicated model and largest reservoir description, which will allow the desired estimation of reservoir performance." In other words, the model to be used should be the simplest that duplicates reservoir behavior.

The discussion presented in this section includes a brief review of some of the simple reservoir models (zero dimension), and of the more complex (multidimensional) models, suited for numerical simulation.

Whiting and Ramey's Model (1969)

The model developed by Whiting and Ramey is zero dimensional because rock and fluid properties and pressure values are not a function of location in the reservoir. These parameters are calculated as average values for the whole reservoir. This type of models has also been called lumped-parameter models.

This model can be used for performance forecasting of reservoir behavior (Ramey et al., 1973). Where some field development already exists and production is in progress, a mathematical model for fluid flow in the reservoir can be postulated. The reservoir size and its productivity can be determined by matching measured production data (mass produced, enthalpy produced, reservoir pressure and temperature, etc.) with the corresponding parameters of the mathematical model. Once all model parameters and their relationships have been identified, the model can be used for performance production forecasting under different assumed exploitation schemes.

The model of the reservoir system developed by Whiting and Ramey is shown in Figure 9-14. The system contains rock, water, and steam. The reservoir system has a bulk volume V and a porosity of ϕ. The cumulative fluid production at any given time is W_p, whereas the cumulative heat production associated with this fluid production is Q_p. The model also considers heat loss, Q_L, and mass fluid loss, W_L, due to convection in, for

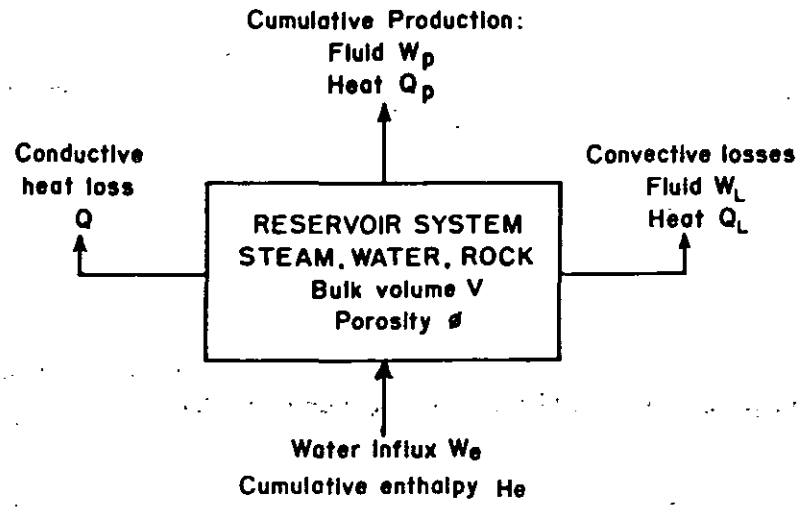

Figure 9-14. Schematic diagram of reservoir model (After Whiting and Ramey, 1969, Fig. 4, p. 895, by permission of the S.P.E. of A.I.M.E.)

example, hot springs, fumaroles, etc. The authors have discussed that heat loss, Q, at the reservoir boundary is negligible and should not significantly affect reservoir behavior. Water recharge, W_e, and its associated energy (cumulative enthalpy, H_e) are also considered.

The model of Whiting and Ramey considers the following basic assumptions (Ramey et al., 1973): (a) thermodynamic equilibrium (temperature of rock, water, and steam are equal); (b) pressure and saturation are uniform throughout the reservoir; and (c) uniform fluid production, which implies that fluid production comes from all parts of the reservoir.

A combined mass, energy, and volumetric balance gives the following expression:

$$W_p\,(H_p - E_c) + W_L\,(H_L - E_c) + Q$$
$$= W\left\{E_i - E_c + \left[(1-\phi)/\phi\right]\left[x_i\,v_{si} + (1-x_i)\,v_{wi}\right]\rho_r C_{v_r}(T_i - T_c)\right\}$$
$$+ (H_e - E_c)\,(B/v_{we})\Sigma\,Q_D\,(t_D)\,\Delta p_n \qquad (9\text{-}35)$$

where: H_p = enthalpy of produced fluids
W = initial mass of hot water and steam in reservoir bulk volume, V
E = internal energy
Q = conductive heat loss

ϕ = porosity of rock matrix
x = steam quality
v = specific volume
ρ_r = density of rock and contained fluids
C_{v_r} = specific heat at constant volume of reservoir rock and contained fluids
T = temperature
B = water recharge constant
$Q_D\,(t_D)$ = dimensionless cumulative recharge, corresponding to dimensionless time, t_D
Δp_n = pressure drop at any time n

The subscripts p, L, c, i, r, s, w, and e indicate produced, loss, current, initial, reservoir, steam, liquid water, and recharge values, respectively. The model given by Equation 9-35 can be simplified, according to the situation of a specific reservoir. For instance, for a reservoir containing only hot water, this equation reduces to:

$$(W_p + W_L)\,v_w = W\,(v_w - v_{wi}) + B\Sigma Q_D\,(t_D)\,\Delta p_n. \qquad (9\text{-}36)$$

It is common to find that reservoirs are associated with adjacent aquifers. Due to production, reservoir pressure declines, causing the aquifer to react by yielding up water. If water recharge is influencing reservoir behavior, it has to be properly considered for accurate reservoir performance predictions. One of the most useful methods for calculating water recharge is that of van Everdingen and Hurst (1949). Miller et al. (1978) presented an excellent review of water recharge into geothermal reservoirs (see also Whiting and Ramey, 1969, p. 897).

Whiting and Ramey applied the model for liquid hot water (Equation 9-36) to the Wairakei geothermal reservoir in New Zealand. A least-mean-squares fit to the production history from 1956 to 1961 was used to obtain estimates for the initial water in place and the initial pressure. Once the optimum model parameters were determined, a prediction of reservoir performance through 1965 was made, indicating excellent agreement between measured and calculated values (Figure 9-15).

Brigham and Morrow's Model (1977)

Brigham and Morrow have presented a zero-dimensional model for vapor-dominated systems. They considered three cases regarding the distribution of hot water and steam. These authors assumed that the system is closed and that energy is derived from the rock mass itself.

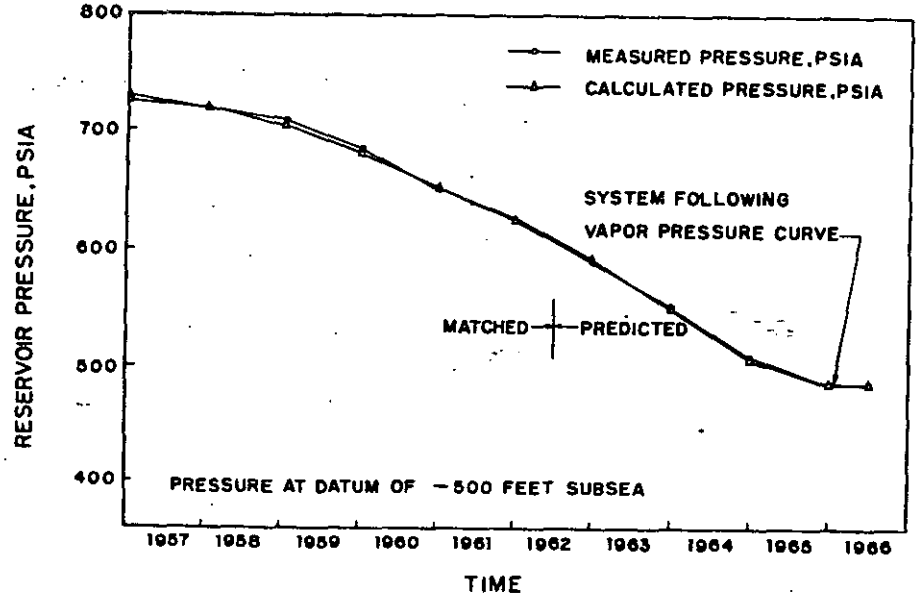

Figure 9-15. Prediction of geothermal reservoir performance. (After Whiting and Ramey, 1969, Fig. 5, p. 898, by permission of the S.P.E. of A.I.M.E.)

The first system is completely filled with steam with no water present. Flow in this system is essentially isothermal, because the heat capacity of the rock is large compared with that of steam. Then, in order to study the system's behavior only a mass balance needs to be taken. Under these reservoir flow conditions, a steam reservoir can be treated as an ordinary petroleum gas reservoir (Craft and Hawkins, 1959), where average reservoir pressure divided by the gas deviation factor, p/Z, is plotted versus cumulative production, resulting in a straight line. The intercept on the abscissa is equal to the original mass of fluid in place, m_{gi}. The equation can be presented as follows:

$$p_f/Z_f = (p_i/Z_i)\frac{(m_{gi} - \Delta m_g)}{m_{gi}} = (p_i/Z_i)\frac{(m_{gf})}{m_{gi}} \qquad (9\text{-}37)$$

where: p = reservoir pressure
m_g = mass of steam
Δm_g = mass of steam produced during a depletion step
i = subscript for the initial conditions of a depletion step
f = subscript for the end conditions of a depletion step

The reserve forecasting procedure, using Equation 9-37, will be used to compare predictions for the other two cases.

The second model considers that the steam zone is separated from an underlying liquid zone by a horizontal interface at which boiling takes place. As steam is produced, water boiling will take place, resulting in a liquid level drop; thus its name, the *falling liquid level model*. Flow in the steam zone is assumed to be isothermal, whereas on the water zone non-isothermal flow conditions would prevail. A mass and energy balance is made for the water zone.

The third model also considers that the steam zone has an underlying liquid zone, but assumes that liquid boiling takes place throughout the whole liquid zone, and that liquid level does not drop. This model is called the *constant liquid level model*. Consequently, in this system steam saturation will continuously build up within the liquid zone. The energy equation for this system resembles that of Whiting and Ramey (1969), with the exception that only steam flows out of the system. The authors have solved the falling liquid level and the constant liquid level models for three hypothetical reservoirs, having porosities of 0.05, 0.10, and 0.20. It was assumed that the volume of the steam zone was the same as the volume of the liquid zone. Calculations were also made, but not reported, for systems having a ratio of steam to liquid zone of 9, which showed results very close to those for a unity ratio.

Figure 9-16 shows the results of these authors for a steam falling liquid level system (their fig. 1). From the results of this figure and from other results shown by Brigham and Morrow, the following conclusions have been made. For low-porosity reservoirs, an extrapolation of the p/Z versus cumulative production plot will be too optimistic, whereas for high-porosity reservoirs it will be pessimistic. A porosity of about 0.10 will give approximately correct predictions. The constant liquid level model predicts higher recovery for a given reservoir pressure than the falling liquid level model. The presence of even a small water zone in the lower portion of the system is an important fraction of total system's mass, and can significantly affect the p/Z prediction procedure. Finally, they concluded that the steam zone of the reservoir remains isothermal whether or not there is a water boiling zone below the steam. This causes characterization problems, because pressure, temperature, and enthalpy measurements are not sufficient to determine the original state of the reservoir fluid system. An application of the p/Z versus cumulative production plot to actual field data has been presented by Ramey (1970a).

Other Zero-Dimensional Models

Another zero-dimensional model for the simulation of geothermal reservoirs has been presented by Martin (1975). His model is valid for single- and two-phase flows; it was derived following the logic behind solution gas drive

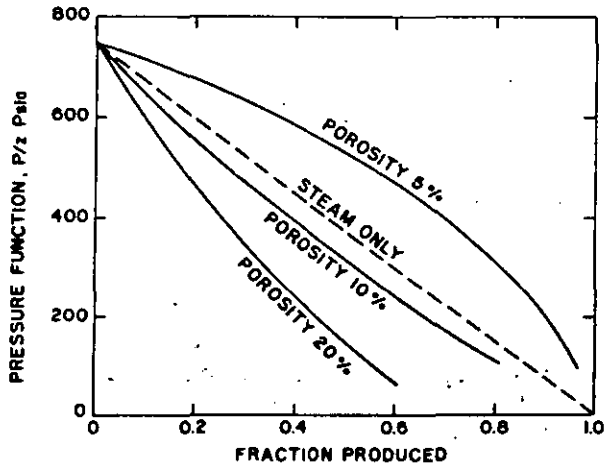

Figure 9-16. Pressure depletion vs. recovery, falling liquid level. (After Brigham and Morrow, 1977, Fig. 1, by permission of the S.P.E. of A.I.M.E.)

petroleum reservoirs. To the author's knowledge, this model has not received field application.

One more zero-dimensional model is that presented by Atkinson et al. (1978). Their model considered a steam and a water zone and the presence of carbon dioxide and other noncondensable gases in the steam zone. It also took into consideration the possibility that water could recharge the reservoir. This model was successfully evaluated, matching the production history of the Bagnore steam field in Italy.

Numerical Geothermal Reservoir Simulation

When important heterogeneities exist in the reservoir, rock and/or fluid properties (permeability, saturation, pressure, viscosity, etc.) vary in space, then simple zero-dimensional models can no longer be used for prediction of reservoir performance. A model that considers the variation of rock and fluid properties is called a distributed-parameter model. A reservoir where properties vary in space, is usually divided in blocks (cells), assigning to each one of them average values for rock and fluid properties. For a multicell model like this, the basic building block is the previously-described zero-dimensional model.

A mathematical model for describing fluid flow in a geothermal reservoir includes equations for the conservation of mass, momentum, and energy for

water and steam, and for specifying the state of the system (Faust and Mercer, 1975; Thomas and Pierson, 1978). A review of the literature shows that several such models have been presented (Faust and Mercer, 1975; Thomas and Pierson, 1978; Coats, 1977; Brownell et al., 1975; Lasseter et al., 1975). These models differ from each other according to the assumptions implied. A model for the flow of hot water and steam, written for a general coordinate system, consists of the following equations:

$$\Delta \cdot \left[\frac{k k_{rw} \rho_w}{\mu_w} (\Delta p - \rho_w g) + \frac{k k_{rs} \rho_s}{\mu_s} (\Delta p - \rho_s g) \right] - q = \frac{\partial}{\partial t} (\phi \rho_W S_w + \phi \rho_s S_s) \tag{9-38}$$

Energy balance for the water-steam-rock system can be presented as follows:

$$\Delta \cdot \left[\frac{k\, k_{rw}\, \rho_w H_w}{\mu_w} (\Delta p - \rho_w g) + \frac{k\, k_{rs}\, \rho_s H_s}{\mu_s} (\Delta p - \rho_s g) \right] + \Delta (k \Delta T) - q_{HL} - q_H = \frac{\partial}{\partial t} \left[(\phi\ \rho_w\ H_w S_w + \phi \rho_s H_s S_s) + (1-\phi) \rho_r H_r \right] \tag{9-39}$$

where:

k = absolute permeability
k_{rs} (k_{rw}) = relative permeability to steam (water)
ρ_s (ρ_w) = steam (water) density
μ_s (μ_w) = steam (water) viscosity
p = pressure
g = acceleration of gravity
q = mass (source) production rate
ϕ = porosity
S_s (S_w) = steam (water) saturation
H_s (H_w) = enthalpy of saturated steam (water)
K = thermal conductivity
T = temperature
q_{HL} = heat loss rate
q_H = enthalpy production rate
ρ_r = average rock-grain density
H_r = rock enthalpy

The pressure enthalpy approach followed in the previous mathematical model is one of the different possible avenues to be taken. Another approach followed by other authors uses density and internal energy as the unknown variables (Brownell et al., 1975; Lassater et al., 1975). The use of fluid pressure and enthalpy seems a logic approach, because they define the thermodynamic state of the system and are usually obtained in field operations.

In the derivation of Equations 9-38 and 9-39, the following assumptions have been made (Mercer et al., 1974; Faust and Mercer, 1975):

1. The reservoir is treated as a porous medium.
2. Capillary pressure effects are negligible. This means that the pressure in the water and steam phases are equal.
3. Thermal equilibrium exists among all phases: hot water, steam, and rock.
4. Validity of Darcy law for two-phase flow.
5. Thermal conductivity is a property of the medium.
6. The geothermal fluid is pure water.

Ignoring one or more of these assumptions will no doubt increase the accuracy of predictions in specific situations, but will also change the complexity and economics of the study. At the present time, there are geothermal mathematical models more complete than that given by Equations 9-38 and 9-39. An example is Coat's model (1977), where he considers capillary effects and the thermal dependence of relative permeability. Other recent models include the effect of inert gases (Zyvolski and Sullivan, 1978) and precipitation of dissolved salts on porosity and permeability (Todd et al., 1978).

In order to solve the two nonlinear partial differential equations given by Equations 9-38 and 9-39, it is necessary to assume some additional functional and algebraic relations between the variables involved. For a complete discussion of this subject, the paper by Coats (1977) should be referred to. As an example of the relations needed, the steam and water saturation must add to unity:

$$S_s + S_w = 1 \tag{9-40}$$

To solve the mathematical model given by Equations 9-38 and 9-39 and its additional relations, the proper reservoir boundary conditions should be considered. Analytical solutions can be obtained by the classical methods of

mathematical physics only for simple reservoir situations, such as homogeneous systems with regular boundaries (i.e., a single well in the center of a radial reservoir). Thus, the nonlinear partial differential Equations 9-38 and 9-39 describing the flow of fluids in geothermal reservoirs must be solved by approximation. If it is desired that approximate values of the solution to the mathematical model be obtained, then some numerical process is formulated that will produce these values after a finite number of calculations. With the advent of high-speed computers, it became increasingly desirable to produce algorithms that are applicable to a wide class of problems and simultaneously lead to increasingly more accurate approximations with an additional expenditure of computer time alone. Numerical methods have been extensively used because they meet these two criteria. These methods have proved to be highly successful for obtaining solutions to very complex reservoir situations. A numerical model (simulator), as previously defined, constitutes a group of computer programs that use numerical methods to obtain an approximate solution to the mathematical model. Further discussion of the numerical solution to the mathematical model is beyond the scope of this chapter. They include finite difference techniques, finite element methods, or a combination of the two.

Conclusions

The main purpose of this chapter was to provide a brief review of presently available techniques for prediction of geothermal reservoir behavior. It seems that predictions of reasonable accuracy can be made with actually available methods for the majority of geothermal systems saturated with fluids (convective systems). There is a lack of knowledge for other types of systems, however, such as the hot-dry formations. It is expected that geothermal reservoir engineering will continue to show advancement due to the strong research program currently under way.

Discussion of this chapter has included the practical aspects of reservoir engineering, such as well test analysis, and a brief presentation of mathematical reservoir simulation. The reservoir data obtained from pressure transient analysis best represent actual reservoir conditions, and are extremely useful as input for reservoir simulation studies. Reservoir simulation studies are initially carried out with simple models, which are continuously updated and refined as new production data becomes available. As a simple matter, the model used should be the simplest that duplicates reservoir behavior. A properly conducted reservoir engineering study would lead to the determination of the optimum exploitation conditions for the particular reservoir.

Nomenclature*

B = water-recharge constant, Reservoir Simulation Section
B = formation volume factor, $metre^3_{rc}$ /$metre^3_{sc}$
b' = intercept on semilog plot of transient-test pressure data normalized by rate, kg/cm^2/(ton/hr), Equation 9-22
c = compressibility, $(kg/cm^2)^{-1}$
C = wellbore storage constant for hot water, ton/(kg/cm^2), Equation 9-32
C' = wellbore storage constant for steam, (ton/kg/cm^2), Equation 9-33
C_D = dimensionless wellbore storage constant, Equations 9-32 and 9-33
C_{vr} = specific heat at constant volume of reservoir rock and contained fluids
E = internal energy
g = acceleration of gravity
h = formation thickness, m
H = enthalpy
k = absolute permeability
k_r = relative permeability, fraction
m = slope of linear portion of semilog plot pressure transient data, kg/cm^2/cycle
m' = slope of the data plot for a multiple-rate test, kg/cm^2/(cycle ton/hr), Equation 9-21
M = molecular weight, g/mole
p = pressure, kg/cm^2
q = mass (source) production rate
q_H = enthalpy production rate
q_{HL} = heat loss rate
Q = conductive heat loss
r = radius, m
s = van Everdingen-Hurst skin factor
t = time, hours
Δt = running testing time, hours
T = temperature, K
w = production rate, tons/hr
W = initial mass (hot water and steam in the reservoir); Equation 9-34
x = steam quality, fraction
z = real gas deviation factor
α = conversion factor, Equation 9-1
β = conversion factor, Equation 9-2
γ = constant equal to 1.7810724, Equation 9-5
δ = conversion factor, Equation 9-12
ϵ = conversion factor, Equation 9-32
η = conversion factor, Equation 9-33
μ = viscosity, cp
ν = specific volume, cm^3/g
ν_w = specific volume of saturated liquid water
ν_s = specific volume of saturated steam
ν_{wi} = initial specific volume of saturated liquid water
ν_{si} = initial specific volume of saturated steam
ρ = density
K = thermal conductivity
ϕ = porosity, fraction

*Unless otherwise stated, the units are those of the SI system. See Conversion Table 1-12.

Subscripts

c = current
D = dimensionless
e = recharge
f = flowing, force
i = initial
j = index
L = loss
M = match point in type-curve matching
N = last-rate interval in a multiple-rate flow test
p = produced
r = reservoir, rock
rc = reservoir conditions
s = shut-in, steam
t = surface
sc = standard conditions
t = total
w = wellbore, water
1hr = data from straight-line portion of semilog plot at 1 hour of test time, extrapolated if necessary

Special functions:

Exponential integral $= E_i(-x)$

$$= -\int_x^\infty \frac{e^{-u}}{u}\,du$$

References

Agarwal, R. G., Al-Hussainy, R., and Ramey, H. J., Jr., 1970. An Investigation of Wellbore Storage and Skin Effect in Unsteady Liquid Flow: I. Analytical Treatment. *Soc. Pet. Eng. J.* (Sept.), pp. 279-290.

Atkinson, P. G., Celati, R., Corsi, R., and Kucuk, F., 1978. Behavior of Two Component Vapor-Dominated Geothermal Reservoirs. Ann. California Regional Meeting, Soc. Pet. Eng., San Francisco, Ca., paper SPE No. 7132.

Brownell, D. H., Garg, S. K., and Pritchett, J. W., 1975. Computer Simulation of Geothermal Reservoirs. Ann. California Regional Meeting, Soc. Pet. Eng., Ventura, Ca., paper No. 5381.

Burnham, J. B., and Stewart, D. H., 1973. Recovery of Geothermal Energy from Hot, Dry Rock with Nuclear Explosives. In P. Kruger and K. Otte (Eds.) *Geothermal Energy Resources, Production and Stimulation*. Stanford University Press, Stanford, Ca., pp. 223-230.

Burst, J. F., 1969. Diagenesis of Gulf Coast Clayey Sediments and Its Possible Relation to Petroleum Migration. *Bull. Am. Assoc. Pet. Geologists*, 53 (1): 73-93.

Crichlow, H. B., 1977. *Modern Reservoir Engineering — A Simulation Approach*. Prentice-Hall, Englewood Cliffs, N. J.

Cinco-Ley, H., Samaniego V. F., and Domínguez, A. N., 1978. Transient Pressure Behavior for a Well with a Finite-Conductivity Vertical Fracture. *Soc. Pet. Eng. J.* (Aug.), pp. 253-264.

Coats, K. H., 1969. Use and Misuse of Reservoir Simulation Models. *J. Pet. Tech.* (Nov.), pp. 1391-1398.

Coats, K. H., 1977. Geothermal Reservoir Modelling. Ann. Fall Technical Conference, 52nd., Soc. Pet. Eng., Denver, Colo., paper No. 6892.

Craft, B. C., and Hawkins, M. F., 1959. *Applied Petroleum Reservoir Engineering*. Prentice-Hall, Englewood Cliff, N. J.

Dake, L. P., 1978. *Fundamentals of Reservoir Engineering. Developments in Petroleum Science*, 8, Elsevier, Amsterdam; 433 pp.

Davis, W. K., and Golan, S., 1974. The New Energy Sources Ind. Research. (Nov. 15), pp. 8-15.

Earlougher, R. C., Jr., 1977. *Advances in Well Test Analysis*. Monograph Series, Society of Petroleum Engineers of AIME, Dallas, Tex.: 264 pp.

Faust, C. R., and Mercer, J. W., 1975. Mathematical Modelling of Geothermal Systems. Second U. N. Symposium on the Development and Use of Geothermal Resources, San Francisco, Ca., Proc. Lawrence Berkeley Lab., University of California, Berkeley, Ca., pp. 1635-1641.

Garg, S. K., 1978a. Pressure Transient Analysis for Two-Phase Geothermal Reservoirs. *Trans. Geothermal Resources Council*, 2: pp. 203-206.

Garg, S. K., 1978b. Pressure Transient Analysis for Two-Phase (Liquid Water/Steam) Geothermal Reservoirs. Ann. Fall Technical Conference, 53rd., Soc. Pet. Eng., Houston, Tex., paper No. 7479.

Gringarten, A. C., 1978. Well Testing in Two-Phase Geothermal Wells. Ann. Fall Technical Conference, 53rd, Soc. Pet. Eng., Houston, Tex., paper No. 7480.

Gringarten, A. C., and Ramey, H. J., Jr., 1974a. Unsteady-State Pressure Distributions Created by a Well with a Single Horizontal Fracture, Partial Penetration or Restricted Entry. *Soc. Pet. Eng. J.* (Aug.), pp. 413-426.

Gringarten, A. C., Ramey, H. J., Jr., and Raghavan, R., 1974b. Unsteady-State Pressure Distributions Created by a Well with a Single Infinite Conductivity Vertical Fracture. *Soc. Pet. Eng. J.* (Aug.), pp. 347-360.

Gringarten, A. C., Ramey, H. J., Jr., and Raghavan, R., 1975. Applied Pressure Analysis for Fractured Wells. *J. Pet. Tech.* (July), pp. 887-892.

Gulati, M. S., 1975. *Pressure and Temperature Buildup in Geothermal Wells*. Stanford Geothermal Reservoir Engineering Workshop, Stanford, Ca., Proc.: Stanford University, SGP-TR-12, pp. 69-73.

Knapp, R. M., Isokrari, O. F., Garg, S. K., and Pritchett, J. W., 1977. An Analysis of Production from Geopressured Geothermal Aquifers. Ann. Fall Technical Conference, 52nd, Soc. Pet. Eng., Denver, Colo., paper No. 6825.

Lasseter, T. J., Witherspoon, P. A., and Lippmann, M. J., 1975. Multiphase Multidimensional Simulation of Geothermal Reservoirs. Second U. N. Symposium on the Development and Use of Geothermal Resources, San Francisco, Ca., Proc. Lawrence Berkeley Lab., University of California, Berkeley, Ca., pp. 1715-1723.

Martin, J. C., 1959. Simplified Equations of Flow in Gas Drive Reservoirs and the Theoretical Foundation of Multi-phase Pressure Buildup Analysis. *Trans. Am. Inst. Min. Metall. Eng.*, 216: pp. 309-311.

Martin, J. C., 1975. Analysis of Internal Steam Drive in Geothermal Reservoirs. *J. Pet. Tech.* (Dec.), pp. 1493-1499.

Matthews, C. S., Brons, F., and Hazebroeck, P., 1954. A Method for Determination of Average Pressure in a Bounded Reservoir. *Trans. Am. Inst. Min. Metall. Eng.*, 201: pp. 182-191.

Matthews, C. S., and Russell, D. G., 1967. *Pressure Buildup and Flow Tests in Wells*. Monograph Series, Society of Petroleum Engineers of AIME, Dallas, Tex.: 167 pp.

Mercer, J. W., Faust, C., and Pinder, G. F., 1974. Geothermal Reservoir Simulation. *Proc. of N.S.F.*, Conference on Research for the Development of Geothermal Energy Resources, Pasadena, Ca., pp. 256-267.

Miller, F. G., Cinco, H., Ramey, H. J., Jr., and Kucuk, F., 1978. Reservoir Engineering Aspects of Fluid Recharge and Heat Transfer in Geothermal Reservoirs. *Trans. Geothermal Resources Council*, 2: pp. 449-452.

Murphy, H. D., 1975. *Hydraulic-Fracture Geothermal Reservoir Engineering*. Stanford Geothermal Reservoir Eng. Workshop, SGP-TR-12, pp. 174-177.

Muskat, M., 1938. *The Flow of Homogeneous Fluids Through Porous Media*. McGraw-Hill Book Co., New York, N. Y.

Narasimhan, T. N., Schroader, R. C., Goranson, C. B., and Benson, S. M., 1978. Results of Reservoir Engineering Tests, 1977, East Mesa, California. Ann. Fall Technical Conference, 53rd, Soc. Pet. Eng., Houston, Tex., paper No. 7482.

Odeh, A. S., 1969. Reservoir Simulation. . . What Is It?. *J. Pet. Tech.* (Nov.), pp. 1383-1388.

Peaceman, D. W., 1977. *Fundamentals of Numerical Reservoir Simulation*. Elsevier, Amsterdam.

Pruess, K., Schroader, R. C., and Zerzan, J., 1978. *Studies of Flow Problems with the Simulator Shaft 78*. Stanford Geothermal Reservoir Engineering Workshop, Stanford, Ca., Proc.: Stanford University (in print).

Ramey, H. J., Jr., 1965. Non-Darcy Flow and Wellbore Storage Effects in Pressure Buildup and Drawdown of Gas Wells. *J. Pet. Tech.* (Feb.), pp. 223-233.

Ramey, H. J., Jr., 1970a. A Reservoir Engineering Study of the Geysers Geothermal Field. Testimony for the Trial of Reich and Reich vs Commissioner of the Internal Revenue, Tax Court of the U.S., 52 T. C. No. 74.

Ramey, H. J., Jr., 1970b. Short-Time Well Test Data Interpretation in the Presence of Skin Effect and Wellbore Storage. *J. Pet. Tech.* (Jan.), pp. 97-104.

Ramey, H. J., Jr., 1975. Pressure Transient Analysis for Geothermal Wells. Second U. N. Symposium on the Development and Use of Geothermal Resources, San Francisco, Ca., Proc. Lawrence Berkeley Lab., University of California, Berkeley, Ca., pp. 1749-1757.

Ramey, H. J., Jr., 1976. Practical Use of Modern Well Test Analysis. Ann. Fall Technical Conference, 51st, Soc. Pet. Eng., New Orleans, La., paper No. 5878.

Ramey, H. J., Jr., 1977. Petroleum Engineering Well Test Analysis-State of the Art. *Proceeding: Invitational Well Testing Symposium*, Oct. 19-21, Lawrence Berkeley Lab., Berkeley, Ca., pp. 5-9.

Ramey, H. J., Jr., Kruger, P., and Raghavan, R., 1973a. Explosive Stimulation of Geothermal Reservoirs. In P. Kruger and K. Otte (eds.), *Geothermal Energy Resources, Production and Stimulation*. Stanford University Press, Stanford, Ca., pp. 231-249.

Ramey, J. H., Jr., Kumar, A., and Gulati, M. S., 1973b. *Gas Well Test Analysis Under Water-Drive Conditions*, Amer. Gas Assoc., Arlington, Va.

Ramey, H. J., Jr., and Gringarten, A. C., 1975. Effect of High-Volume Vertical Fractures on Geothermal Steam Well Behavior. Second U. N. Symposium on the Development and Use of Geothermal Resources, San Francisco, Ca., Proc. Lawrence Berkeley Lab., University of California, Berkeley, Ca., pp. 1759-1762.

Richardson, J. G., and Stone, H. L., 1973. A Quarter Century of Progress in the Application of Reservoir Engineering. *J. Pet. Tech.* (Dec.), pp. 1371-1379.

Rivera, R. J., and Ramey, H. J., Jr., 1977. Application of Two-Rate Flow Tests to the Determination of Geothermal Reservoir Parameters. Ann. Fall Technical Conference, 52nd, Soc. Pet. Eng., Denver, Colo. paper No. 6887.

Rivera, R. J., Samaniego, V. F., and Schroader, R. C., 1978. Pressure Transient Testing at Cerro Prieto Geothermal Field. First Symposium on the Cerro Prieto Geothermal Field, San Diego, Ca., Proc.: Lawrence Berkeley Lab., University of California, Berkeley, Ca. (in print).

Russell, D. G., 1963. Determination of Formation Characteristics from Two-Rate Flow Tests. *J. Pet. Tech.* (Dec.), pp. 1347-1355.

Saltuklaroglu, M., and Rivera, R. J., 1978. *Injection Testing in Geothermal Wells*. Stanford Geothermal Reservoir Engineering Workshop, Stanford, Ca., Proc.: Stanford University (in print).

Smith, M., Potter, R., Brown, D., and Aamodt, R. L., 1973. Induction and Growth of Fractures in Hot-Rock. In P. Kruger and K. Otte (eds.), Geothermal Energy Resources, Production and Stimulation. Stanford University Press. Stanford, Ca., pp. 251-268.

Smith, M., Aamodt, R. L., Potter, R. M., and Brown, D. W., 1975. Man-Made Geothermal Reservoirs. Second U. N. Symposium on the Development and Use of Geothermal Resources, San Francisco, Ca., Proc. Lawrence Berkeley Lab., University of California, Berkeley, Ca., pp. 1781-1787.

Takahashi, P. K., Chen, B. H., Mashima, K. I., and Seki, A. S., 1975. State-of-the-Art of Geothermal Reservoir Engineering. *J. of the Power Div.*, A.S.C.E., 101 (July), pp. 111-126.

Thomas, K. K., and Pierson, R. G., 1978. Three Dimensional Geothermal Reservoir Simulation, *Soc. Pet. Eng. J.* (April), pp. 151-161.

Todd, L., Mercer, J. W., and Faust, C. R., 1978. *Simulation of Geothermal Reservoirs Including Changes in Porosity and Permeability due to Silica-Water Reactions.* Stanford Geothermal Reservoir Engineering Workshop, Stanford, Ca., Proc.: Stanford University (in print).

van Everdingen, A. F., and Hurst, W., 1949. The Application of the Laplace Transformation to Flow Problems in Reservoirs. *Trans. Am. Inst. Min. Metall. Eng.*, 186, pp. 305-324.

Wattenbarger, R. A., and Ramey, H. J., Jr., 1970. An Investigation of Wellbore Storage and Skin Effect in Unsteady Liquid Flow: II. Finite Difference Treatment. *Soc. Pet. Eng. J.* (Sept. 1970), pp. 291-297.

White, D. E., 1973. Characteristics of Geothermal Resources. In P. Kruger and K. Otte (eds.), *Geothermal Energy Resources, Production, and Stimulation.* Stanford University Press, Stanford, Ca., pp. 69-94.

White, D. E., Muffler, L. J. P., and Truesdell, A. H., 1971. Vapor Dominated Hydrothermal Systems Compared with Hot-Water Systems. Econ. Geol., V. 66, pp. 75-97.

Whitherspoon, P. A., Narasimhan, T. N., and McEdwards, D. G., 1978. Results of Interference Tests from Two Geothermal Reservoirs. *J. Pet. Tech.* (Jan.), pp. 10-16.

Whiting, R. L., and Ramey, H. J., Jr., 1969. Applications of Material and Energy Balances to Geothermal Steam Production. *J. Pet. Tech.* (July), pp. 893-900.

Zyvolski, G. A., and O'Sullivan, M. J., 1978. *Simulation of the Broadlands Geothermal Field, New Zealand.* Stanford Geothermal Reservoir Engineering Workshop, Stanford, Ca., Proc.: Stanford University (in print).

CURSO: INGENIERIA DE YACIMIENTOS GEOTERMICOS

23 DE MARZO AL 18 DE MAYO 1984

TEMA: "FLUJO LAMINAR Y PERMANENTE DE UN FLUIDO MONOFASICO INCOMPRENSIBLE EN UNA TUBERIA CIRCULAR HORIZONTAL A LA TEMPERATURA To."

DR: CESAR SUAREZ

2-13 ABRIL

MATERIAL COMPLEMENTARIO

FLUJO LAMINAR Y PERMANENTE DE UN FLUIDO MONOFÁSICO INCOMPRESIBLE EN UNA TUBERÍA CIRCULAR HORIZONTAL A LA TEMPERATURA T_0.

OBJETIVO: Empleando las leyes básicas de conservación y comportamiento, encontrar soluciones analíticas para el perfil de velocidades, de temperaturas y caída de presión del fluído a lo largo de la tubería.

DESCRIPCIÓN DEL PROBLEMA FÍSICO.-

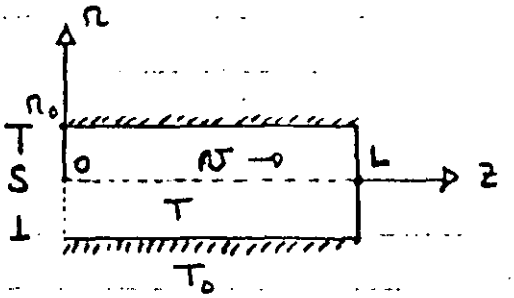

Un fluído viscoso, incompresible y conductor de calor, se desplaza en la dirección Oz horizontal, dentro de un tubo hueco de radio r_0 y de sección circular S. El estudio se hace en una zona de longitud L en la cual el fluído ocupa totalmente el volumen $L \cdot S$ y el perfil de velocidades y temperaturas se ha estabilizado completamente. La temperatura de la pared es $T_0(z)$ y la del fluído $T(r,z)$.

HIPÓTESIS GENERALES.-

Flujo laminar ($Re < 3000$); permanente ($\partial/\partial t = 0$); incompresible ($J = 1$, $\operatorname{div} \vec{v} = 0$); vector velocidad $\vec{v} = (0,0,v) = v\vec{e}_z$, $v(r)$; las propiedades del fluído son independientes de la temperatura.-

ECUACIONES DEL PROBLEMA.-

Navier-Stokes: $$\rho \vec{a} = \vec{f} - \vec{\nabla} P + (\lambda + \mu)\, \vec{\nabla}(\operatorname{div} \vec{v}) + \mu \Delta \vec{v}$$

Energía Total: $$\frac{d}{dt}(\rho e) = -\rho e \operatorname{div} \vec{v} + \vec{f} \cdot \vec{v} - \operatorname{div}(P\vec{v}) + \operatorname{div}(\tau \cdot \vec{v}) + K \Delta T$$

I.- PRIMERA PARTE : Solución del problema dinámico.

I.1.- Planteamiento de las ecuaciones resultantes que rigen el movimiento del fluído en términos de las hipótesis.

La resultante o proyección del sistema vectorial de Navier-Stokes sobre OZ se escribe en coordenadas cilíndricas :

$$\rho\frac{\partial v_z}{\partial t} + \rho\frac{\partial v_z}{\partial r}v_r + \rho\frac{\partial v_z}{\partial \theta}\frac{v_\theta}{r} + \rho\frac{\partial v_z}{\partial z}v_z = f_z - \frac{\partial P}{\partial z} +$$

$$+ (\lambda+\mu)\frac{\partial}{\partial z}\left(\frac{\partial v_r}{\partial r} + \frac{1}{r}\frac{\partial v_\theta}{\partial \theta} + \frac{\partial v_z}{\partial z}\right) + \mu\left(\frac{\partial^2 v_z}{\partial r^2} + \frac{1}{r}\frac{\partial v_z}{\partial r} + \frac{1}{r^2}\frac{\partial^2 v_z}{\partial \theta^2} + \frac{\partial^2 v_z}{\partial z^2}\right)$$

pero de acuerdo a las hipótesis : $\frac{\partial v_z}{\partial t} = 0$, $v_r = v_\theta = 0$, $v_z = v(r)$

$f_z = -\rho g \cos \pi/2 = 0$, $P(z)$. lo cual permite obtener el modelo matemático simplificado siguiente :

$$\boxed{\frac{dP}{dz} = \frac{\mu}{r}\frac{d}{dr}\left(r\frac{dv}{dr}\right) \; ; \; v(r_0) = 0 \, , \, \frac{\partial v(0)}{\partial r} = 0} \qquad (\mathcal{D})$$

I.2.- Resolución exacta del problema diferencial $(\mathcal{D})$.

Separando variables tenemos :

$$\int d\left(r\frac{dv}{dr}\right) = \int \frac{1}{\mu}\frac{dP}{dz}\, r\, dr + cte$$

es decir :

$$r\frac{dv}{dr} = \frac{1}{2\mu}\frac{dP}{dz}\, r^2 + cte.$$

pero $\frac{dv(0)}{dr} = 0 \Rightarrow$ cte. $= 0$

Integrando ahora esta ecuación:

$$\int_{v}^{0} dv = \frac{1}{2\mu}\frac{dP}{dz}\int_{R}^{R_0} R\,dR \quad \text{, de donde:}$$

$$\boxed{v = -\frac{dP}{dz}\frac{R_0^2}{4\mu}\left(1-\frac{R^2}{R_0^2}\right)} \qquad \text{---------- (1)}$$

ecuación que proporciona la velocidad de las partículas del fluido en función del radio y que corresponde a un perfil parabólica en el plano (R, z). En cada sección S de espesor ΔL, la distribución espacial de velocidades configuran un paraboloide de revolución de eje OZ.

Perfil de v en el plano (R, z).

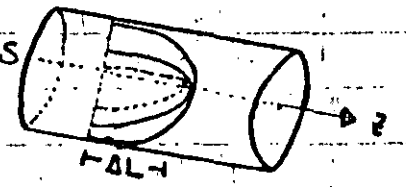

Distribución Espacial de velocidades en cada sección S·ΔL.

I.3.- Definición y cálculo de la velocidad promedio.

La velocidad promedio de las partículas que pasan por S es:

$$\bar{v} = \frac{1}{S}\int_S v\,dS = \frac{1}{\pi R_0^2}\int_0^{R_0} 2\pi v(R)\,R\,dR = \frac{2}{R_0^2}\int_0^{R_0} v\,R\,dR$$

Reemplazando el valor de v dado por la ecuación (1):

$$\bar{v} = -\frac{1}{2\mu}\frac{dP}{dz}\int_0^{R_0}\left(1-\frac{R^2}{R_0^2}\right)R\,dR = -\frac{1}{2\mu}\frac{dP}{dz}\left(\frac{R^2}{2}-\frac{R^4}{4R_0^2}\right)\Big|_0^{R_0}$$

finalmente:

$$\boxed{\bar{v} = -\frac{dP}{dz}\frac{R_0^2}{8\mu}} \qquad \text{---------- (2)}$$

I.4.- Gasto y cálculo de la caída de Presión.-

El gasto a través la sección S (gasto másico) es:

$$G_m = \frac{d}{dt}\int_V \rho\, dV = \frac{d}{dt}\int_S \rho z\, dS = \int_S \rho v\, dS = -\frac{\rho R_0^2}{4\mu}\frac{dP}{dz}\int_0^{R_0}\left(1-\frac{r^2}{R_0^2}\right)2\pi r\, dr$$

es decir:

$$\boxed{G_m = -\frac{\pi \rho R_0^4}{8\mu}\frac{dP}{dz} = S\rho\bar{v}} \qquad \text{.....(3)}$$

El gasto volumétrico es simplemente: $G_v = G_m/\rho = S\bar{v}$.
Combinando (2) y (3):

$$\boxed{-\frac{dP}{dz} = \frac{8\mu G_m}{S\rho R_0^2}} \qquad \text{.....(4)}$$

Ecuación que proporciona directamente la variación de presión a lo largo del tubo en función del gasto másico extraído, de la densidad y viscosidad del fluído y de las dimensiones de la tubería.

I.5.- Relación entre la velocidad media y la velocidad efectiva del fluído.

Reemplazando (4) en (1):

$$v = -\frac{dP}{dz}\frac{R_0^2}{4\mu}\left(1-\frac{r^2}{R_0^2}\right) = \frac{8\mu G_m}{S\rho R_0^2}\cdot\frac{R_0^2}{4\mu}\left(1-\frac{r^2}{R_0^2}\right)$$

y de (3) obtenemos:

$$\boxed{v(r) = 2\bar{v}\left(1-\frac{r^2}{R_0^2}\right)} \qquad \text{.....(5)}$$

I.6.- Distribución de Esfuerzos viscosos.

El balance de momento en la dirección del flujo dá:

$$\frac{\partial P}{\partial z} = -\rho\frac{\partial v}{\partial t} - \rho v\frac{\partial v}{\partial z} - \rho g\cos\pi/2 + \frac{\partial \tau_{rz}}{\partial r}$$

en nuestro caso presente esto se reduce a: $\frac{dP}{dz} = \frac{\partial \tau_{rz}}{\partial r}$

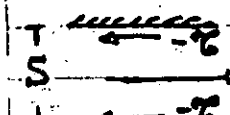

Obsérvese que en cada sección de la tubería los esfuerzos o tensiones viscosas se propagan radialmente oponiéndose al movimiento del fluído. Estos esfuerzos viscosos se originan por la fricción existente con la pared del tubo debido a su rugosidad. El efecto de esta fricción se transmite a las capas siguientes del fluído debido a la viscosidad del mismo, pero su ~~efecto~~ intensidad va decayendo en puntos alejados de la pared. Esto puede esquematizarse como:

$$\tau_{rz} = -2\tau(r) \quad \text{(el factor 2 es debido a que en cada zona, hay dos efectos iguales provocados por la pared de arriba y su opuesta).}$$

Entonces:

$$\frac{d\tau}{dr} = -\frac{1}{2}\frac{dP}{dz} \Rightarrow \int_0^{\tau} d\tau = -\frac{1}{2}\frac{dP}{dz}\int_{r=0}^{r} dr$$

Es decir:

$$\boxed{\tau(r) = -\frac{dP}{dz}\frac{r}{2}} \qquad (6)$$

En r_0 se tendrá el esfuerzo viscoso máximo que hace que $v(r_0) = 0$.

Luego: $\tau(r_0) = \tau_0 = -\frac{dP}{dz}\frac{r_0}{2}$

De donde:

$$\boxed{\tau(r) = \frac{\tau_0}{r_0}r} \qquad (7)$$

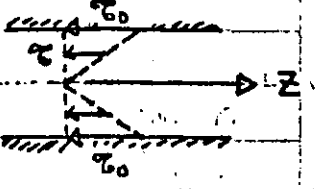

Perfil de Tensiones viscosas.

I.7.- Relación entre el número de Reynolds y los coeficientes de Fricción.

Si utilizamos directamente la definición del esfuerzo viscoso en la pared de la tubería (ley de Newton):

$$\tau_0 = \mu \frac{\partial v(r_0)}{\partial r} = 2\bar{v}\mu \frac{d}{dr}\left(1-\frac{r^2}{r_0^2}\right)_{(r_0)} = -\frac{4\bar{v}\mu}{r_0}$$

Reemplazando (4) y (3) en $\tau_0 = -\frac{dp}{dz}\frac{r_0}{2}$ obtenemos:

$$\boxed{\tau_0 = -\frac{4\mu}{r_0}\bar{v}} \qquad (8)$$

expresión idéntica a la anterior.

Comúnmente se relaciona la tensión viscosa de la pared con la energía cinética promedio del fluido:

$\tau_0 = C_f \frac{\rho \bar{v}^2}{2}$, C_f es un coeficiente complicado de proporcionalidad que puede obtenerse empíricamente.

Notese que de: $\frac{\partial \tau_{rz}}{\partial r} = -C\frac{\rho v^2}{2} = -2\frac{d\tau}{dr}$ integrando:

$$\int_0^{\tau_0} d\tau = \frac{C\rho}{4}\int_0^{r_0} v^2\, dr = C\rho\bar{v}^2 \int_0^{r_0}\left(1-\frac{r^2}{r_0^2}\right)^2 dr = \frac{8}{15} C\rho\bar{v}^2 r_0$$

es decir: $\tau_0 = \frac{16}{15} C r_0 \left(\frac{\rho\bar{v}^2}{2}\right)$ es decir que:

$\boxed{C_f = \frac{16}{15} C r_0}$ es el coeficiente de fricción de Fanning.

El número de Reynolds es: $\boxed{Re = D\rho\bar{v}/\mu = \frac{DG_m}{\mu S}}$

entonces: $\tau_0 = C_f\left(\frac{\rho\bar{v}^2}{2}\right) = \frac{4\mu\bar{v}}{r_0} \Rightarrow C_f = \frac{8\mu}{r_0\rho\bar{v}}$

De donde: $\boxed{C_f Re = 16}$, $\boxed{f_m = 4C_f}$ ——— (9)

En donde f_m es el factor de fricción de Moody.

I.8.- Ejemplo Numérico.

En una tubería horizontal de 8 pulgadas de diámetro circula agua a 150°C. Se tiene un gasto de 20 Ton/hr y se quiere calcular la pérdida total de presión a lo largo de la tubería.

Solución: Datos: $D = 8\,plg. = 0.2032\ m.$, $r_0 = 0.1016\ m.$
$S = 0.03243\ m^2.$, $G_m = 5.56\ kg/s.$

En las tablas de vapor obtenemos: a 150°C $\rightarrow P = 4.76$ bar
$\mu = 182.7 \cdot 10^{-6}\ kg/m/s.$
$\rho = 916.76\ kg/m^3$

Con estos datos: $G_m/S = 171.313\ kg/s/m^2$

Luego:

$$-\frac{dP}{dz} = \frac{8\mu G_m}{\rho r_0^2 S} = 2.646 \cdot 10^{-2}\ Pa/m$$

De donde: $$\boxed{-\Delta P = 2.646 \cdot 10^{-2} \cdot \Delta L\ (Pa)}$$

Es decir, entre dos puntos z_1, z_2 de la tubería hay una caída de presión de: $P_2 = P_1 + \Delta P$. Por ejemplo si $P_1 = 4.76$ bar y $\Delta L = 2000$ m., entonces:

$$-\Delta P = 2.646 \cdot 10^{-7} \cdot 2000\ (bar)$$

$-\Delta P = 5.292 \cdot 10^{-4}$ bar $\Rightarrow$ $$\boxed{P_2 = 4.759\ bar}$$

Nótese sin embargo que no se ha hecho referencia al régimen de flujo existente en el interior de la tubería. Calculando el número de Reynolds:

$$Re = \frac{D G_m}{\mu S} = 190,535.3$$

de donde: $C_f = \frac{16}{Re} = 8.3974 \cdot 10^{-5}$ que correspondería a una tubería prácticamente lisa con rugosidad mínima. El flujo es entonces turbulento y hay que aplicar otras técnicas de análisis.

Obsérvese finalmente que la velocidad media es:

$$\bar{v} = \frac{G_m}{\rho S} = 0.187 \text{ m/s}.$$

La cual nos permite calcular (si el flujo fuera laminar) la ~~transferencia~~ tensión viscosa de la pared del tubo sobre el fluído:

$$\tau_0 = -\frac{4\mu}{R_0}\bar{v} = 1.344 \cdot 10^{-3} \text{ Pa}$$

que en efecto corresponde a una tensión muy pequeña.

II.- SEGUNDA PARTE: Solución del Problema Térmico.

II.1.- Planteamiento de la ecuación de la Energía resultante.

Con la ecuación de la energía hacemos $\frac{\partial(\rho e)}{\partial t} = 0$, $\operatorname{div}\vec{v} = 0$:

$$\vec{v}\cdot\vec{\nabla}(\rho e) = -\operatorname{div}(p\vec{v}) + K\Delta T$$

Sea $\rho e = \rho h - p$, h entalpía específica, y $dh = c\,dT$ con c calor específico a presión constante, obtenemos:

$$\rho c v_r \frac{\partial T}{\partial r} + \rho c v \frac{\partial T}{\partial z} = \frac{K}{r}\frac{\partial}{\partial r}\left(r\frac{\partial T}{\partial r}\right) + \frac{K}{r^2}\frac{\partial^2 T}{\partial \theta^2} + K\frac{\partial^2 T}{\partial z^2}$$

con $T(r,z)$ la temperatura del fluido, K la conductividad térmica del fluido. Como $v_r = 0$, $\frac{\partial^2 T}{\partial \theta^2} = 0$, supondremos además que la conducción axial de la temperatura es mucho menor que la radial: $\frac{\partial^2 T}{\partial r^2} >> \frac{\partial^2 T}{\partial z^2} \sim 0$. Y definiendo $\delta = \frac{K}{\rho c}$ la difusividad térmica del fluido obtenemos la ecuación:

$$\boxed{\frac{1}{r}\frac{\partial}{\partial r}\left(r\frac{\partial T}{\partial r}\right) = \frac{v}{\delta}\frac{\partial T}{\partial z}} \qquad \text{..... (E)}$$

Unidades de los coeficientes térmicos:

$$c \to \frac{J}{Kg\,^\circ C}\ ;\quad K \to \frac{W}{m\,^\circ C}\ ;\quad \delta \to \frac{m^2}{s}\ .$$

II.2.- Resolución Exacta del problema diferencial (E).-

Suponemos que existe un perfil de temperaturas completamente desarrollado en el fluido, y que éste es invariante con la posición z. Definimos:

$$t = \frac{T_0 - T}{T_0 - T_m}$$

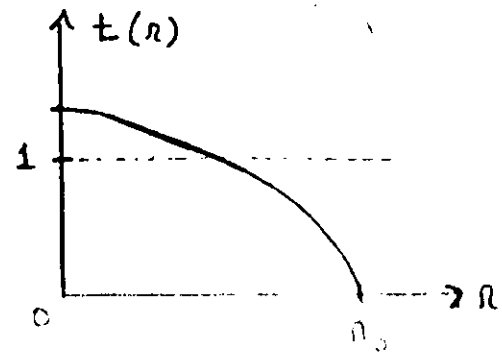

t es una temperatura adimensional que depende únicamente del radio, en donde:

$T_0(z) \equiv$ temperatura de la pared del tubo.

$T_m(z) \equiv$ " " promedio del fluido.

La temperatura promedio T_m caracteriza a la energía térmica media del fluido en movimiento:

tasa de energía térmica convectiva en z = $G_m \cdot h_m = G_m C T_m$

pero: $G_m C T_m = (S \bar{v} \rho) C T_m$

Podemos entonces definir: $T_m = \frac{1}{S\bar{v}} \int_S v T \, dS$

Promedio ponderado que toma en cuenta el movimiento del fluido. Obsérvese entonces que:

$\frac{dt}{dr} = \frac{-1}{T_0 - T_m} \frac{\partial T}{\partial r}$, es una expresión

que no depende de z (pues $t(r)$), entonces en la pared del tubo cuando $r = r_0$:

$$\text{cte} = \frac{dt(r_0)}{dr} = -\frac{1}{T_0 - T_m} \frac{\partial T(r_0)}{\partial r} \quad \ldots\ldots (1)$$

En la vecindad inmediata de la pared, el fluido recibe (o da) energía térmica. Este calor es arrastrado por las partículas del fluido en movimiento, lo cual se denomina transferencia de calor por convección. Esta convección se esquematiza por la ecuación:

$$\dot{q}_0 = \gamma (T_0 - T_m) \quad \ldots\ldots (2)$$

En donde: $\dot{q}_0$ es el flujo de calor instantáneo por unidad de área, de la pared al fluido. γ es la conductancia convectiva o coficiente de transferencia de calor por convección, cuyas unidades son: $\gamma \rightarrow W/m^2/{}^\circ C$

Por otra parte la conducción del calor en la capa de fluido vecina a la pared es dada por:

$$\dot{q}_0 = -K \frac{\partial T(r_0)}{\partial r} \quad \ldots\ldots (3)$$

Combinando (1), (2) y (3) obtenemos:

$$\gamma = K \cdot cte. = \text{constante} \quad \ldots\ldots (4)$$

En casos reales, se ha verificado que esto es aproximadamente cierto, al menos en ciertas regiones.

Por otra parte, como $t(r)$:

$$0 = \frac{dt}{dz} = \frac{1}{T_0 - T_m}\left(\frac{dT_0}{dz} - \frac{\partial T}{\partial z}\right) - \frac{(T_0 - T)}{(T_0 - T_m)^2}\left(\frac{dT_0}{dz} - \frac{dT_m}{dz}\right)$$

es decir:

$$\frac{\partial T}{\partial z} = \frac{dT_0}{dz} - t\left(\frac{dT_0}{dz} - \frac{dT_m}{dz}\right) \quad \ldots\ldots (5)$$

Reemplazando (5) en la ecuación de la energía (6):

$$\frac{1}{r}\frac{\partial}{\partial r}\left(r \frac{\partial T}{\partial r}\right) = \frac{v}{\delta}\left[\frac{dT_0}{dz} - t\left(\frac{dT_0}{dz} - \frac{dT_m}{dz}\right)\right] \quad \ldots\ldots (6)$$

Esta ecuación diferencial puede integrarse exactamente en dos circunstancias importantes que enseguida analizamos.

II.2.1 .- Primer caso: Flujo de calor constante.

Tenemos: $\dot{q}_0 = \text{constante} \Rightarrow T_0 - T_m = \text{constante}$.

Es decir: $\frac{dT_0}{dz} - \frac{dT_m}{dz} = 0$

Situación que corresponde a la gráfica →

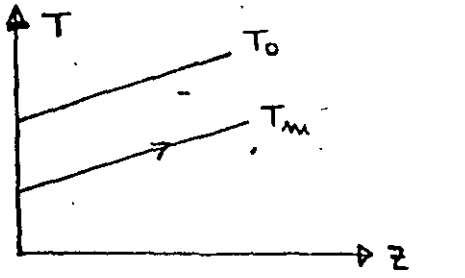

Sustituyendo en (6) obtenemos el siguiente problema diferencial:

$$\frac{1}{r}\frac{\partial}{\partial r}\left(r\frac{\partial T}{\partial r}\right) = \frac{v}{\delta}\frac{dT_m}{dz} \quad ; \quad \begin{cases} T(r_0) = T_0 \\ \dfrac{\partial T(0)}{\partial r} = 0 \end{cases} \qquad \text{---- (7)}$$

Este problema es resoluble exactamente pues de un lado se tiene una E.D.P en función del radio y de z, mientras que el lado derecho al quitar $v(r)$, depende únicamente de z; manteniendo z fijo se integra parcialmente en r:

Sustituyendo el perfil de velocidades $v(r)$ dado por I.5:

$$\frac{1}{r}\frac{\partial}{\partial r}\left(r\frac{\partial T}{\partial r}\right) = \frac{2\bar{v}}{\delta}\left(1-\frac{r^2}{r_0^2}\right)\frac{dT_m}{dz}$$, resolviendo:

$$T = T_0 - \frac{2\bar{v}}{\delta}\frac{dT_m}{dz}\left(\frac{3}{16}r_0^2 + \frac{r^4}{16\,r_0^2} - \frac{r^2}{4}\right) \qquad \text{--- (8)}$$

Esta ecuación proporciona la distribución $T(r,z)$ de temperaturas del fluido. Si la temperatura media decrece es decir si $dT_m/dz < 0$, el fluido se está enfriando, o sea, cede calor al tubo y $T \geq T_0$. En cambio si T_m aumenta entonces $dT_m/dz > 0$, y el fluido se calienta recibiendo calor de la tubería, entonces $T \leq T_0$ a lo largo de su recorrido.

El perfil de temperaturas en r, también será parabólico pero mucho más pronunciado debido al término r^4.

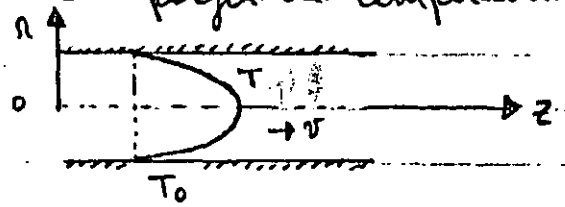

(enfriamiento)

En el centro del tubo, la temperatura es máxima para el caso en que el fluido ceda energía térmica al tubo y:

($T > T_0$)

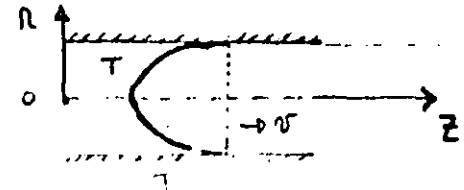

$$T(0,z) = T_0 - \frac{2\bar{v}}{\delta}\frac{dT_m}{dz}\cdot\frac{3r_0^2}{16}$$

Como $T_m = \frac{1}{S\bar{v}} \int_S v\,T\,dS$, reemplazando las ecuaciones I.5 para $v(r)$ y II.8 para $T(r,z)$ obtenemos por integración:

$$\boxed{T_m = \frac{2}{r_0^2 \bar{v}} \int_0^{r_0} v\,T\,r\,dr = T_0 - \frac{11}{96} \frac{2\bar{v}}{\delta} \frac{dT_m}{dz} r_0^2} \quad \ldots (9)$$

De donde:

$$\boxed{\dot{q}_0 = \gamma (T_0 - T_m) = \gamma \frac{11}{96} \frac{2\bar{v} r_0^2}{\delta} \frac{dT_m}{dz}} \quad \ldots (10)$$

Planteando la conservación de la energía interna sobre un sector de espesor dz del fluído tendremos:

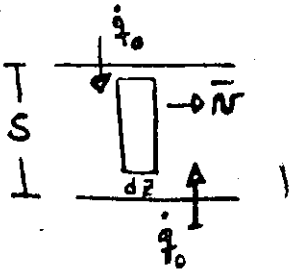

$$\rho\,\bar{v} \cdot \vec{\nabla}(h) = -\operatorname{div} \vec{q} \qquad (\text{con } \rho e = \rho h + P)$$

es decir:

$$\rho\,(0,0,v) \cdot \left(\frac{\partial h}{\partial r}, 0, \frac{\partial h}{\partial z}\right) = -\left(-\frac{\partial q}{\partial r} + \frac{\partial q}{\partial z}\right)$$

es decir, como $\frac{\partial h}{\partial z} = c \frac{\partial T}{\partial z} \Rightarrow \rho\,v\,c \frac{\partial T}{\partial z} = \frac{\partial q}{\partial r}$, $\frac{\partial q(0)}{\partial r} = 0$

sobre el volumen $S\,dz$ empleamos los parámetros promedio $\bar{v}$ y T_m luego integrando:

$$\int_0^{r_0} \rho\,\bar{v}\,c \frac{dT_m}{dz} dr = \int_0^{\dot{q}_{01}} dq$$

por lo tanto: $\rho\,\bar{v}\,c \frac{dT_m}{dz} r_0 = \dot{q}_{01}$, para una pared. Lo mismo ocurre con la pared opuesta en cada sección del plano (r,z) por tanto en total: $\dot{q}_{01} + \dot{q}_{01} = 2\dot{q}_0$, de donde:

$$\boxed{\dot{q}_0 = \frac{\rho\,\bar{v}\,c\,r_0}{2} \frac{dT_m}{dz}} \quad \ldots (11)$$

Combinando con (10):

$$\boxed{\gamma = \frac{48}{11} \frac{K}{D}} \quad \ldots (12)$$

El número de Nusselt es:

$$\boxed{Nu = \frac{\gamma D}{K} = 4.364} \quad \ldots (13)$$

El número de Nusselt es tan importante como, equivalentemente, el número de Reynolds en problemas de convección. Otros números adimensionales igualmente importantes son:

el número de Prandtl : $P_n = \mu C / K$

" " Stanton : $S_t = \frac{\gamma}{\bar{v} \rho C}$

Combinándolos con el número de Reynolds : $Re = \frac{D \bar{v} \rho}{\mu}$ obtendremos :

$$\boxed{S_t P_n Re = N_u = 4.364} \quad \ldots\ldots (14)$$

Nótese que la conductancia γ resulta independiente de N, C, ρ, T. Esto solo es cierto para flujo laminar.

II.2.2.- Segundo Caso: Temperatura del tubo constante.

Tendremos entonces : $T_0 = cte \Rightarrow \frac{dT_0}{dz} = 0 \Rightarrow \frac{\partial T}{\partial z} = + \frac{dT_m}{dz}$

de donde :

$$\boxed{\frac{1}{r} \frac{\partial}{\partial r}\left(r \frac{\partial T}{\partial r}\right) = \frac{v}{\delta} + \frac{dT_m}{dz}} \quad \ldots\ldots (15)$$

$$\boxed{T(r_0) = T_0 \;,\; \frac{\partial T}{\partial r}(0) = 0}$$

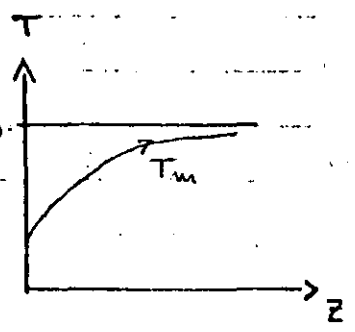

La técnica de solución de este problema es un poco más complicada y elaborada. El problema planteado en términos de una temperatura adimensional es del tipo Sturm-Liouville, cuya solución se presenta en términos de un cociente de dos series infinitas exponenciales. El resultado final es el número de Nusselt :

$$\boxed{N_u = 3.658}$$

Es posible sin embargo, intentar hallar una solución por aproximaciones sucesivas de la siguiente manera:

Reemplazando el perfil de velocidades I.5 y el de temperaturas dado por II.8 en (15) obtenemos:

$$\frac{1}{\Lambda}\frac{\partial}{\partial\Lambda}\left(\Lambda\frac{\partial T}{\partial\Lambda}\right)=\left(\frac{2\bar{v}}{\delta}\frac{dT_m}{dz}\right)^2\cdot\frac{1}{T_0-T_m}\cdot\left(1-\frac{\Lambda^2}{\Lambda_0^2}\right)\left(\frac{3}{16}\Lambda_0^2+\frac{\Lambda^4}{16\Lambda_0^2}-\frac{\Lambda^2}{4}\right)$$

Esta ecuación puede integrarse directamente con respecto a Λ:

$$T-T_0=\left(\frac{2\bar{v}}{\delta}\frac{dT_m}{dz}\right)^2\frac{1}{T_0-T_m}\left[\frac{3}{64}\Lambda_0^2\Lambda^2-\frac{7\Lambda^4}{256}+\frac{5\Lambda^6}{576\Lambda_0^2}-\frac{\Lambda^8}{128\Lambda_0^4}\right]_{\Lambda_0}^{\Lambda}$$

obtenemos un primer perfil:

$$T_{(1)}(\Lambda,z)=T_0+\left(\frac{2\bar{v}}{\delta}\frac{dT_m}{dz}\right)^2\frac{1}{T_0-T_m}\left[\frac{3\Lambda_0^2}{64}\Lambda^2-\frac{7\Lambda^4}{256}+\right.$$

$$\left.+\frac{5\Lambda^6}{576\Lambda_0^2}-\frac{\Lambda^8}{128\Lambda_0^4}-\frac{47}{2304}\Lambda_0^4\right]$$

Esta temperatura se reemplaza a su vez en (15), se vuelve a integrar obteniendo otro perfil $T_{(2)}$. Se repite de esta forma el proceso hasta llegar a un cierto límite T. En cada paso es posible calcular una temperatura media T_{m_j}, una conductancia δ_j y un número de Nusselt correspondiente Nu_j.

Es obvio entonces que en el límite, este proceso converje hasta:

$$T_{(j)}\to T \quad y \quad Nu_j\to Nu=3.658$$

Debido a lo tedioso de los cálculos, es recomendable efectuar efectuar las integraciones de los polinomios sucesivos en Λ mediante un procedimiento numérico con ayuda de una calculadora ~~programa~~ programable.

El resultado final es el perfil mostrado en la figura:

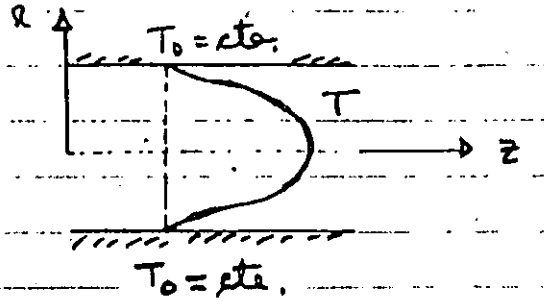

II.3 Ejemplo Numérico.-

Un tubo de 0.6 cm. de diámetro y de 1.2 m de largo es calentado por una resistencia eléctrica. La función del tubo es calentar un fluido que circula a su interior de la temperatura T_1 a la temperatura T_2 ($T_1 < T_2$). El gasto másico es de $1.26 \cdot 10^{-4}$ Kg/s, $\rho = 753$ Kg/m^3, $\mu = 0.022 \frac{Kg}{m\,s}$ $c = 2.092$ Kg/Kg/°C, $k = 0.137$ W/m/°C.

Calcular $T_0(z)$ y $T_m(z)$. ¿Cuál es la máxima temperatura experimentada por el fluido?

CURSO: INGENIERIA DE YACIMIENTOS GEOTERMICOS"
13 DE MARZO AL 18 de MAYO 1984

TEMA: "THE PSEUDOPRESSURE OF SATURATED STEAM"
"THE REAL GAS PSEUDO"

DR. HEBER CINCO LEY
26-30 MARZO
MATERIAL COMPLEMENTARIO

THE REAL GAS PSEUDO

PRESSURE FOR GEOTHERMAL STEAM -- SUMMARY REPORT

L. S. Mannon
Atlantic Richfield Co.
1860 Lincoln Suite 501
Denver, Colorado 80295

and

P. G. Atkinson
Union Oil Co.
P. O. Box 6854
2099 Range Ave.
Santa Rosa, California 95406

INTRODUCTION

The producing characteristics of vapor-dominated geothermal steam reservoirs bear some strong resemblances to those observed in hydrocarbon natural gas reservoirs. Consequently, many geothermal steam well tests are commonly analyzed using flow theory developed for the isothermal flow of hydrocarbon natural gases. Such analysis is most often made using the idealization of perfect gas fluid flow behavior in the reservoir.

This study investigated the real gas flow characteristics of geothermal steam over the ranges of pressure, temperature, and noncondensable gas content commonly found in vapor dominated geothermal systems. Details of this study are available elsewhere (Mannon, 1977).

THEORY

The transient flow of a real gas in an incompressible porous medium is described by a highly nonlinear partial differential equation. For the case of an ideal gas, this equation, while still nonlinear is similar in form to the classical diffusivity equation which describes transient liquid flow in porous media. Aronofsky and Jenkins (1953) provided numerical solutions to this equation which demonstrated that transient ideal gas flow could be analyzed using some of the techniques developed for transient liquid flow.

Al-Hussainy et al. (1966) proposed an integral transformation which converts the form of the nonlinear flow equation for a real gas into one, which, while still nonlinear, is also similar in form to the diffusivity equation. Thus, there exists the possibility that real gas transient fluid flow can be analyzed in terms of the transformed pressure variable using techniques developed for transient liquid flow. This possibility was verified for hydrocarbon natural gases in radial flow systems by Al-Hussainy and Ramey (1966) and Wattenbarger and Ramey (1968).

RESULTS

The integral transformation proposed by Al-Hussainy et al, has been called the "real gas pseudo pressure" and is:

$$m(p) = \int_{p_o}^{p} \frac{p\, dp}{\mu(p)\, z(p)} \quad ;$$

where; m = real gas pseudo pressure
p = pressure
p_o = arbitrary base pressure
μ = viscosity of the gas
z = compressibility factor for the gas

In this study, the real gas pseudo-pressure, m(p), was evaluated for geothermal steams over the range 20 to 1000 psia (2-75 bars), temperature range 300 to 600°F (150-325°C) and various noncondensable gas contents. Other physical properties relevant to single-phase isothermal gas flow in porous media were also evaluated and compiled.

The m(p) function was found to be linear in p^2 for low pressures (up to approximately 150 psia or 10 bars). This is depicted in Fig. 1. This behavior is described by a relationship of the form:

$$m(p) = a_1 p^2 + b_1 \qquad (1)$$

At higher pressures a graph of log m(p) vs. log p produced straight lines of the form:

$$m(p) = a_2 p^{b_2} \qquad (2)$$

where b_2 varied between 2.045 and 2.099 (Fig. 2). High accuracy curve fits of Figs. 1 and 2 are presented in Tables 1 (Engineering Units) and 2 (International Units). Varying the mole fraction of carbon dioxide in the gas up to a mole fraction of 60% did not change the basic shape of the curves in Figs. 1 and 2, and tended to increase the value of m(p) by a factor of less than 2.

DISCUSSION

These results will allow the reservoir engineer to more accurately analyze transient flow of superheated geothermal steams. Geothermal steam wells have traditionally been analyzed using the ideal gas flow model, described by Eq. 1, without quantitative justification. The results of this study will allow for quantitative justification of the ideal gas flow assumption, where possible. Alternatively, they will facilitate use of the more correct pseudo-pressure function when analyzing geothermal steam wells.

REFERENCES

Al-Hussainy, R., and Ramey, H.J., Jr.: "Application of Real Gas Flow Theory to Well Testing and Deliverability Forecasting," Jour. Petroleum Technology, May 1966, 637

Al-Hussainy, R., Ramey, H.J., Jr., and Crawford, P.B.: "The Flow of Real Gases Through Porous Media." Jour. Petroleum Technology, May 1966, 624

Aronofsky, J., and Jenkins, R.: "Unsteady Radial Flow of Gas Through Porous Media," Jour. Applied Mechanics, Vol. 20, 1953, 210

Mannon, L.S.: "The Real Gas Pseudo Pressure for Geothermal Steam," M.Sc. Report, Department of Petroleum Engineering, Stanford University, September 1977; to be issued as a Stanford Geothermal Program Technical Report.

Wattenbarger, R.A., and Ramey, H.J., Jr.: "Gas Well Testing with Turbulence, Damage, and Wellbore Storage," Jour. Petroleum Technology, May 1966, 637.

TABLE 1

ANALYTICAL EQUATIONS FOR APPROXIMATING

THE REAL GAS PSEUDO-PRESSURE

(Engineering Units)

Temperature	Limits	Curve Fit Equation
300°F	$p \leq 60$ psia	$m(p) = 36.88p^2 - 8396$
350°F	$p \leq 70$ psia*	$m(p) = 33.93p^2 - 7819$
	$p \geq 70$ psia	$m(p) = 21.60p^{2.095}$
400°F	$p \leq 80$ psia	$m(p) = 31.41p^2 - 7248$
	$p \geq 80$ psia	$m(p) = 21.33p^{2.080}$
450°F	$p \leq 100$ psia	$m(p) = 29.25p^2 - 6769$
	$p \geq 100$ psia	$m(p) = 19.94p^{2.078}$
500°F	$p \leq 140$ psia	$m(p) = 27.36p^2 - 6336$
	$p \geq 140$ psia	$m(p) = 18.65p^{2.075}$
550°F	$p \leq 160$ psia	$m(p) = 25.71p^2 - 5946$
	$p \geq 160$ psia	$m(p) = 18.02p^{2.068}$
600°F	$p \leq 190$ psia	$m(p) = 24.31p^2 - 5916$
	$p \geq 190$ psia	$m(p) = 18.25p^{2.053}$

* At the meeting point, the upper and lower equations agree to 3 or more significant figures.

TABLE 2

ANALYTICAL EQUATIONS FOR APPROXIMATING

THE REAL GAS PSEUDO-PRESSURE

(International Units)

Temperature	Limits	Curve Fit Equation
150°C	$p \leq 4$ bars	$m(p) = 36.80p^2 - 40.65$
175°C	$p \leq 5$ bars *	$m(p) = 34.20p^2 - 38.60$
	$p \geq 5$ bars	$m(p) = 27.89p^{2.099}$
200°C	$p \leq 6$ bars	$m(p) = 31.93p^2 - 36.74$
	$p \geq 6$ bars	$m(p) = 26.78p^{2.081}$
225°C	$p \leq 7$ bars	$m(p) = 29.93p^2 - 34.94$
	$p \geq 7$ bars	$m(p) = 24.96p^{2.079}$
250°C	$p \leq 10$ bars	$m(p) = 28.31p^2 - 37.04$
	$p \geq 10$ bars	$m(p) = 23.35p^{2.076}$
275°C	$p \leq 10$ bars	$m(p) = 26.62p^2 - 33.09$
	$p \geq 10$ bars	$m(p) = 22.25p^{2.069}$
300°C	$p \leq 12$ bars	$m(p) = 25.23p^2 - 32.74$
	$p \geq 12$ bars	$m(p) = 21.66p^{2.056}$
325°C	$p \leq 13$ bars	$m(p) = 23.93p^2 - 30.66$
	$p \geq 13$ bars	$m(p) = 21.11p^{2.045}$

* At the meeting point, the upper and lower equations agree to 3 or more significant figures.

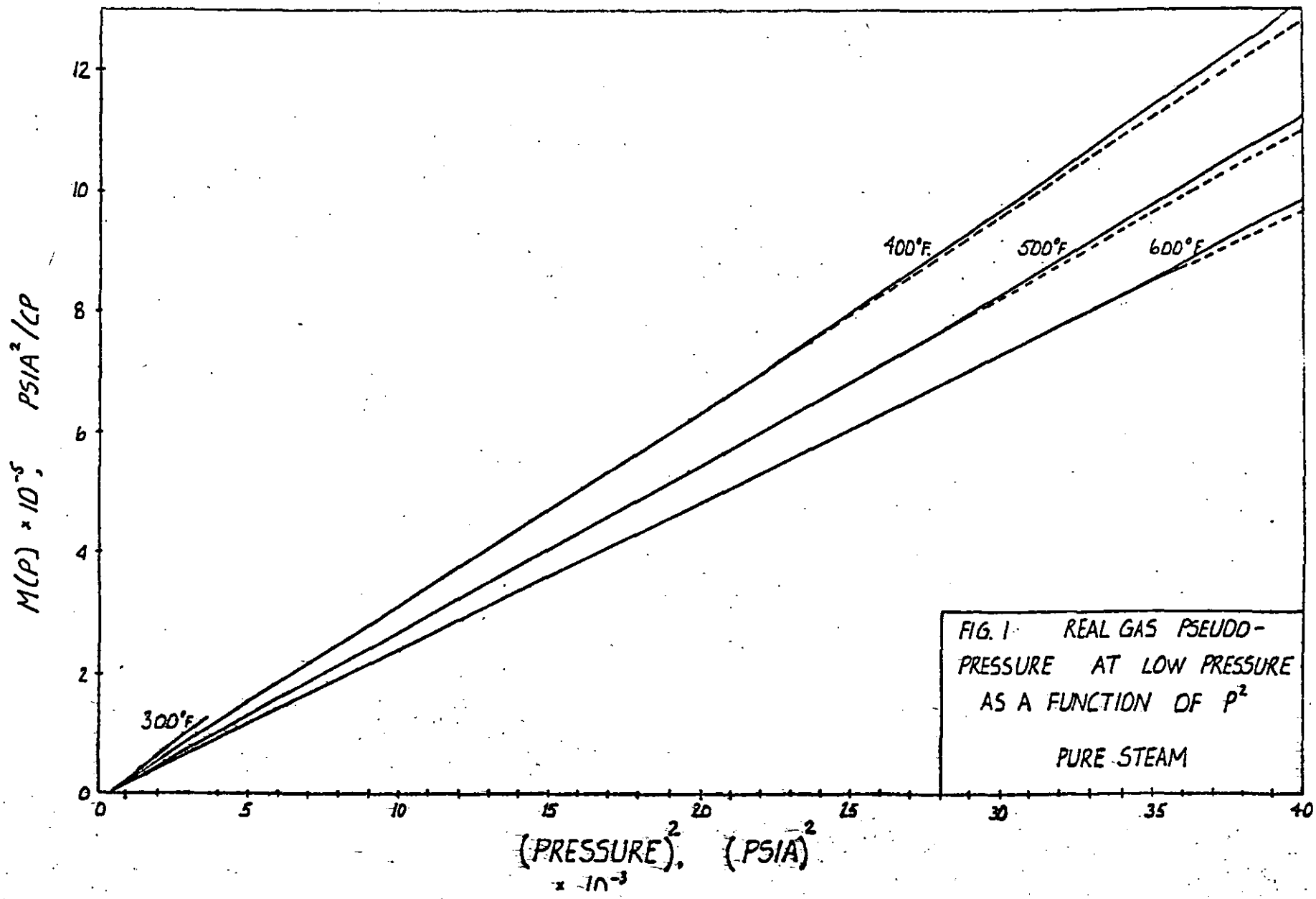
M(P) × 10⁻⁵, PSIA²/CP
12
10
8
6
4
2
0
0
5
10
15
20
25
30
35
40
(PRESSURE)², (PSIA)²
× 10⁻³
300°F.
400°F.
500°F
600°F
FIG. 1 REAL GAS PSEUDO-PRESSURE AT LOW PRESSURE AS A FUNCTION OF P²
PURE STEAM

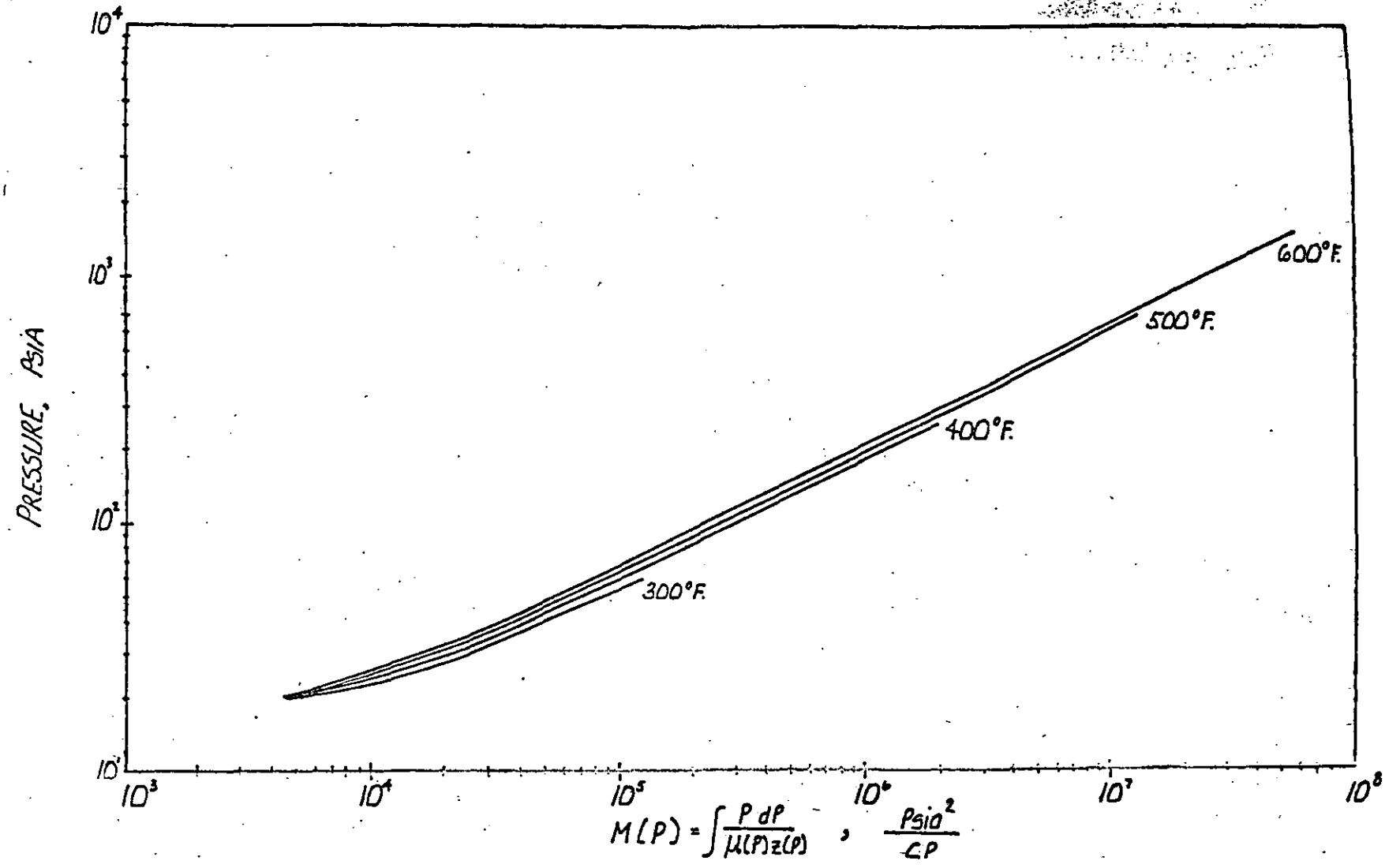

FIG. 2 REAL GAS PSEUDO-PRESSURE M(P) FOR PURE STEAM

Postal address:

APPLIED MATHEMATICS DIVISION,
D.S.I.R.,
P.O. BOX 1335,
WELLINGTON.

Location:

APPLIED MATHEMATICS DIVISION, D.S.I.R.,
7th FLOOR RANKINE BROWN BUILDING,
VICTORIA UNIVERSITY OF WELLINGTON,
KELBURN,
WELLINGTON.

THE PSEUDOPRESSURE OF SATURATED STEAM

MALCOLM A. GRANT

TECHNICAL REPORT NO. 77
JULY 1978.

THE PSEUDOPRESSURE OF SATURATED STEAM

1. Definition and use of the pseudopressure

In a porous medium containing steam and immobile water, the equation for the flow of (saturated) steam is (Grant 1978):

$$(H_s - H_w)\frac{dp_s}{dT} k \nabla \cdot \left[\frac{\rho}{\mu}\nabla p\right] + \rho_m C_m \frac{\partial p}{\partial t} = 0 \qquad (1)$$

and $p = p(T)$.

This is a nonlinear diffusion equation, nonlinear because of the $\frac{\rho}{\mu}$ multiplying $\nabla\rho$, and because the coefficient of $\frac{\partial p}{\partial t}$ is also a function of T and hence P. It can be linearised in P, to obtain

$$\nabla^2 p = \frac{1}{\kappa_o}\frac{\partial p}{\partial t} \qquad (2)$$

where $$\kappa_o = \frac{k}{\rho_m C_m}\left[\frac{\rho_s}{\mu_s}\frac{dp_s}{dT}(H_s - H_w)\right]_o$$

is evaluated at the assumed initial uniform state.

We can also write

$$m^* = \int \frac{\rho}{\mu}\, dp = \int \frac{dp}{\nu} \qquad (3)$$

so that

$$\nabla^2 m^* = \frac{1}{\kappa}\frac{\partial m^*}{\partial t} \qquad (4)$$

This can again be linearised by setting κ equal to its initial value κ_o:

$$\nabla^2 m^* = \frac{1}{\kappa_o}\frac{\partial m^*}{\partial t} \qquad (5)$$

removed, but the variation in κ has not been accounted for. However, it is nearly always better practice, with nonlinear diffusion equations, to represent the divergence terms exactly (here $\nabla^2 m$). The errors incurred by ignoring the variations in κ seem less important. A rough reason can be advanced. Both (5) and (2) are valid if the pressure changes are small. But (5) is also valid for steady pressure changes of any magnitude. If a bore is running for a long time, there is a quasi-steady region near the bore. The approximation (5) may better represent this, for large drawdowns, than (2).

It should be noted that the pseudopressure defined here does not have the dimensions of pressure, but $\rho p/\mu$ (= $kg/m^3 s$). Conventional gas pseudopressures are differently defined. Such a pseudopressure for superheated steam is given by Atkinson and Mannon (1977).

The boundary conditions are also scaled. If we have two-dimensional flow to a bore producing at a rate q (m^3/sec) = W^* (kg/sec), the condition is

$$2\pi r\left(\frac{\kappa}{\mu}\frac{\partial p}{\partial r}\right)_{r=a} = q \qquad (7)$$

this is $$2\pi r\left(k\frac{\partial m^*}{\partial r}\right)_{r=a} = W^* \qquad (8)$$

Thus, where the expression $q\mu$ occurs, it is replaced by W^*. For example, in the standard 2-d solution

$$\Delta p = p - p_o = \frac{q\mu}{4\pi kh} E_1\left(\frac{a^2}{4\kappa t}\right) \qquad (9)$$

we have, using the pseudopressure,

$$\Delta m^* = m^* - m_o^* = \frac{W^*}{4\pi kh} E_1\left(\frac{a^2}{4\kappa t}\right) . \qquad (10)$$

Since it is usually mass flow rates that are specified, use of the pseudopressure usually makes some small saving of effort in looking up densities and viscosities.

2. Formulae for $m^*(p)$

Use of the pseudopressure is convenient only if there is a simple expression for it as a function of pressure. Fortunately this is so. In any approximate formula for pseudo pressure, we need its derivative dm^*/dp represented to some order of accuracy, for we always use differences $m^*(p_1) - m^*(p_2)$, Thus we approximate ρ/μ to some order of accuracy, and integrate to get m^*.

The following expression is accurate to 1% (130-240°C) 2% (100-260°C).

$$\frac{1}{\nu} = \frac{\rho}{\mu} = 4.793 \times 10^4 \, p^{6/7} \qquad (11)$$

where p is in bars. Keeping p in bars from now on;

$$\frac{dm^*}{dp} = 10^5 \frac{\rho}{\mu} = 4.793 \times 10^4 \, p^{6/7}$$

$$m^* = 2.58 \times 10^9 \, p^{13/7} \qquad (12)$$

For convenience, define

$$\boxed{m(p) = p^{13/7}} \qquad (13)$$

$$= m^*/(2.58 \times 10^9) \qquad (14)$$

3. Equations in field units

3.1. Units bar, tonne/hr, darcy-metre

It is simplest to work with these units, and the function

$$\boxed{m(p) = p^{13/7}} \quad .$$

The standard drawdown formula (10) now becomes:

$$m' = 2.58 \times 10^9 \, p^{13/7} = 2.58 \times 10^9 \, m$$

$$W' = W/3.6$$

$$kh \rightarrow 10^{-12} \, kh$$

$$2.58 \times 10^9 \, \Delta m = \frac{W}{3.6} \frac{1}{4\pi \, 10^{-12} \, kh} E_1 \left(\frac{a^2}{4\kappa t}\right)$$

or $$\boxed{\Delta m = 8.57 \frac{W}{kh} E_1 \left(\frac{a^2}{4\kappa t}\right)} \qquad (15)$$

If a bore is running for time t, and then switched off for time Δt,

$$\Delta m = -8.57 \frac{W}{kh} \left\{ E_1 \left(\frac{a^2}{4\kappa \Delta t}\right) - E_1 \left(\frac{a^2}{4\kappa (t+\Delta t)}\right) \right\}$$

$$= 8.57 \frac{W}{kh} \ln \left(\frac{t + \Delta t}{\Delta t}\right)$$

$$= 19.7 \frac{W}{kh} \log_{10} \left(\frac{t + \Delta t}{\Delta t}\right) \qquad (16)$$

Then, if M is the slope of a plot of $p^{13/7}$ vs t, or $\frac{t+\Delta t}{\Delta t}$, on semilog paper (slope of M per cycle),

$$M = 19.7 \, W/kh$$

or $$\boxed{kh = 19.7 \, W/M} \quad . \qquad (17)$$

Summary

$$m(p) = p^{13/7}$$

$$\Delta m = m - m_o = 8.57 \frac{W}{kh} E_1 \left(\frac{a^2}{4\kappa t}\right)$$

$$kh = 19.7 \, W/M \qquad (M = \text{slope of } m \text{ per cycle.})$$

3.2. Units kg/cm^2, tonne/hr, darcy-metre

It is simplest to redefine

$$\boxed{m(p) = p^{13/7}} \quad . \tag{18}$$

Since 1 kg/cm^2 = 0.981 bar, a factor of $(0,981)^{13/7}$ multiplies the formula for m^4

$$m^4 = 2.49 \times 10^9 \, p^{13/7} = 2.49 \times 10^9 \, m \, .$$

Then the drawdown formula is

$$\boxed{\Delta m = 8,88 \, \frac{W}{kh} \, E_1 \left(\frac{a^2}{4\kappa t}\right)} \tag{19}$$

and

$$\boxed{kh = 20.4 \, W/M} \quad . \tag{20}$$

M = slope of a plot of $p^{13/7}$ vs t or $(t + \Delta t)/\Delta t$ on semilog paper (slope of M per cycle).

NOTATION

SI units are used unless otherwise specified.

t	time
μ	dynamic viscosity
ν	kinematic viscosity
ρ	density
T	temperature
p	pressure (also bar and ksc)
p_s	saturation pressure of steam
H	specific enthalpy
C	specific heat
ϕ	porosity
k	permeability (also darcy)
h	aquifer thickness
m^*	pseudopressure
m	$= p^{13/27}$ = scaled pseudopressure
W^*	mass flow
W	mass flow, tonne/hr
κ	diffusivity
M	slope of m vs $\log_{10} t$

$$E_1(x) = \int_x^\infty \frac{1}{u} e^{-u}\, du$$ (Abramowitz & Stegun 1965)

a	bore radius
r	radial distance

Suffices:

o	initial state
m	medium
s	steam

References

1. U.K. Steam Tables in S.I. Units, 1970.

2. Abramowitz & Stegun, "Handbook of Mathematical Functions", Dover, 1965.

3. Grant, "Two-phase Linear Geothermal Pressure Transients - A Comparison with Single-Phase Transients", N.Z. Jl. Sci., Sept. 1978.

4. Mannon & Atkinson, "The Real Gas Pseudo-Pressure for Geothermal Steam", Third Workshop on Geothermal Reservoir Engineering, Stanford, 1977.

CURSO: INGENIERIA DE YACIMIENTOS GEOTERMICOS
13 DE MARZO AL 18 DE MAYO 1984

TEMA: "AN ANALYSIS OF HIGH VELOCITY
GAS FLOW THROUGH POROUS MEDIA"

DR. HEBER CINCO LEY
26-30 MARZO
MATERIAL COMPLEMENTARIO

SPE 6827

AN ANALYSIS OF HIGH VELOCITY GAS FLOW THROUGH POROUS MEDIA

by Abbas Firoozabadi, Member SPE-AIME, Abadan Institute of Technology, and Donald L. Katz, U. of Michigan

This paper was presented at the 52nd Annual Fall Technical Conference and Exhibition of the Society of Petroleum Engineers of AIME, held in Denver, Colorado, Oct. 9-12, 1977. The material is subject to correction by the author. Permission to copy is restricted to an abstract of not more than 300 words. Write: 6200 N. Central Expy. Dallas, Texas 75206.

ABSTRACT

Darcy's law is known to be inadequate to represent high velocity gas flow in porous media, such as near the wellbore. An updated correlation is presented for the coefficient (β) of the velocity squared term in the expanded flow equation. An analysis of the pressure loss during flow through conduits of alternating cross-sections is used to suggest more appropriate words for describing the mechanism for energy loss and terms in the flow equation.

INTRODUCTION

Much work has been done to understood flow through porous media. In the area of high velocity, suitable correlations and nomenclature are the subject of controversy due to alternate views on the mechanism causing pressure drop.[1-14]

The object of this study is to improve the understanding of high-velocity flow through porous media. Using data available and this understanding, the best correlation is sought to permit calculation of high-velocity flow based on permeability, porosity, and character of the rock. Hopefully, a nomenclature can be suggested that is acceptable to both reservoir engineers and fluid mechanics research scientists. The results should be useful in improving correlations of gas well flow data and in predicting well flow from core data, fluid properties, and specified conditions.

EARLY WORK ON HIGH-VELOCITY FLOW

Fancher et al.[1] measured pressure drop during flow through a large number of unconsolidated and consolidated porous media. Their correlation of the data was by the use of friction factor and Reynolds number using grain diameter as a characteristic length. It showed for flow through porous media an increased pressure drop at high velocity beyond that proportional to velocity. Data taken at the USBM[2] was correlated using a quadratic equation of pressure drop with the second term of velocity to the n power. Green and Duwez[4] added to the understanding of high-velocity gas flow data when studying sintered metals. They adapted the equation with a velocity term squared that Forchheimer[15] had developed.

$$-\frac{dP}{dL} = \frac{\mu u}{k} + \beta \rho u^2 \quad \ldots\ldots\ldots\ldots (1)$$

Cornell and Katz[5] measured the porosity, permeability, and β factors for cores, resulting in a correlation of β with permeability.[16] The term β was called a turbulence factor, but the expression was unacceptable to several workers.[14]

LANGUAGE USED IN LITERATURE

Space forbids a full quoting of the language used in describing the mechanism that consumes energy at more than a linear rate with velocity. The term used in flow equations (generally, the β in a quadratic flow equation) also has been given a variety of names in accord with the author's view of the flow mechanism.

Table A in the Appendix assembles selected typical titles and statements quoted from published works. After the flow mechanism has been reviewed, a more appropriate language will be submitted in accordance with the concepts developed herein.

MECHANISM FOR CONSUMPTION OF PRESSURE DROP ENERGY

The purpose here is to understand the mechanism by which increased velocity results in pressure drop greater than that proportional to velocity increase. The mechanism of consuming pressure drop energy in pipe flow is well understood. In Fig. 1, the cylinders of fluid are flowing at different velocities as shown. Work energy overcomes the longitudinal shear stresses between the cylinders flowing at different velocities. In the case of unidirectional flow for a constant cross-section, there is a single term in the resistance equation including the velocity of the fluid. The increased energy consumed at higher velocities is directly proportional to

*Visiting scholar, U. of Michigan, 1976.

References and illustrations at end of paper.

velocity increase for streamline flow as shown by Poiseuille's Law.

Now consider the flow in the interstices of a porous solid, as idealized in Fig. 2. In flow through pores, there are two variations from the horizontal cylindrical flow. First, the cross-section of the flow channel is increasing and decreasing alternately. Then there is the displacement from a straight line in moving through a network of pores. Each deviation from the direction of fluid movement now has two components of the viscous resistance; longitudinal shear e-f in the direction of flow and a longitudinal tension or normal stress component f-g during the expansion and correspondingly i-j and h-i during contractions, commonly written as Eqs. 2 and 3.[19]

$$\tau_{xy} = \mu\left(\frac{\partial u}{\partial y} + \frac{\partial v}{\partial x}\right) \quad \text{Longitudinal shear} \quad \ldots\ldots\ldots\ldots\ldots\ldots\ldots\ldots (2)$$

$$\sigma_{xx} = u\left(\frac{\partial u}{\partial x} + \frac{\partial v}{\partial y}\right) \quad \text{Longitudinal tension} \quad \ldots\ldots\ldots\ldots\ldots\ldots\ldots\ldots (3)$$

Now consider the effect of velocity on the resistances. The flowlines with increased velocity are no longer constant in length and are believed to increase the shear and tension area with increased velocity as shown in Figs. 3a and 3b. At still higher velocities, separation or reversed flow occurs in the enlarged cross-sections to increase the viscous resistance as shown in Fig. 3c. Here, the recirculating portion may be considered laminar. All of these transverse effects are characteristics of irregular alternating cross-section flow paths and not present in cylinders.

Porous media like sandstones or carbonates with only matrix porosity and free from irregular solution processes no doubt are always in regimes 3a and 3b. In some porous solids such as vugular carbonates, reefs, and conglomerates, there are interstices large enough to permit the regimes of Fig. 3c and even Fig. 3d described as turbulence. This turbulence was observed by a student working with the second author to occur like in pipes when an ink filament was used in a liquid flowing at increasing velocities through a bed of glass beads about 3/16-in. diameter. It is with regard to porous solids characterized by Figs. 3a and 3b that the term turbulence is unacceptable. However, flow through such solids have a continuous function between pressure drop and flow rate since there is no change in mechanism between low and high flow rates.

MATHEMATICAL REPRESENTATION OF HIGH VELOCITY FLOW

Forchheimer[15] in correlating the data for the high velocity of water through porous media found that a relationship of the type presented by Eq. 1 described his data best. In some cases another velocity term seemed better:

$$-\frac{dP}{dL} = \frac{\mu u}{k} + \beta\rho u^2 + \gamma\rho^2 u^3 \quad \ldots\ldots\ldots (6)$$

In order to use Eq. 1 for gases, it should be transferred into the following form.[8]

$$\frac{(P_1^2 - P_2^2)Mg_c}{2\mu ZRTG} = \frac{1}{k} + \frac{\beta G}{\mu} \quad \ldots\ldots\ldots (7)$$

A plot of $\frac{(P_1^2 - P_2^2)Mg_c}{2\mu ZRTG}$ vs G/μ results in a straight line for many cores. The slope of the straight line is β and the inverse of the intercept with the Y axis, the permeability k. In many cases, Eq. 7 deviates from that of a straight line. The deviation is attributed to two different factors.

One factor that appears predominantly in the lower portion of the line for flow of gases is due to the slip effect.[21] The slip could be interpreted as the bouncing of the gas molecules on the wall at low pressures as the mean free path of the molecules become the same order of magnitude as the pore diameter. In low-velocity gas flow, where the Darcy equation describes the flow behavior, Klinkenberg[21] demonstrated that the slip effect can be taken into the Darcy equation by Eq. 8:

$$k_a = k\left(1 + \frac{b}{P}\right) \quad \ldots\ldots\ldots\ldots (8)$$

The other factor causing the deviation from the straight-line behavior is due to the inadequacy of Eq. 6 to represent high-velocity gas flow. In other words, in addition to the u^2 quadratic term, a third term of the form "$\gamma\rho^2u^3$" is necessary, as noted by Forchheimer, for high-velocity water flow. One might also represent this kind of deviation by substituting an exponent n instead of 2 for u in the second term as was done by the USBM.[2]

PERMEABILITY A LIMIT AT ZERO OR LOW VELOCITY

From the analysis of the mechanism of energy consumption for fluid flowing in alternating size conduits and Eq. 6, one would expect that the high-velocity term, i.e., $\beta\rho u^2$, should apply over the full range of velocity. To illustrate that data do not deny this statement, the data are plotted to demonstrate that a constant value of permeability is in reality a limiting value.

Fig. 4 shows data on a consolidated sandstone with nitrogen flowing at high pressure at both outlet and inlet, plotted by Iffly[22] according to an equation similar to Eq. 7. The straight line represents the prior concept of Darcy law and the curve represents measured values. Accepting that the curve becomes tangent to the line at zero flow rate is a demonstration that the constant value of k applied at the limit of zero velocity. The data on water by Forchheimer give a similar relationship.[15] This behavior would be expected when the velocity is the variable that changes the flowline length as shown on Figs. 2 and 3.

In normal measurements of core permeability, in millidarcies the results are valid as the limiting value since the $\beta\rho u^2$ term is less than the experimental error in measuring the flow rate and/or pressure drop. When gases near the atmospheric pressure are used to measure permeability, the slip may give a greater error than neglecting the velocity effect.

NOMENCLATURE

The introduction of the β factor by Cornell and

Katz[5] as the turbulence factor, though defined as "extra fluid motion consuming extra energy," was unacceptable to many workers. This concept overlooked the stages of progress in the growth of shear and tension components in laminar mode prior to random movement typical of turbulence. Equally valid objections are made now to the terms non-Darcy and inertial flow.

Since there is a continuous function between pressure drop and flow rate for porous media with alternating cross-sections in the flow path, the term non-Darcy flow is out of place since it implies there are two different flow mechanisms. The same can be said for using Darcy flow at low velocities and inertia regime for higher velocities, the inertia effects are always present. There is a spectrum of velocities in the various flow channels at a given flow rate. Any implication that at low velocities, there is one type of flow mechanism and at high velocities, short of true turbulence, there is another regime disregards the nature of the mechanism by which the pressure-loss energy is consumed in porous dia.

A simple concept is to characterize the flows as "low velocity" and "high velocity" to distinguish conditions for which the $\beta\rho v^2$ term may be ignored and where it should be employed. High velocity becomes the velocity for which neglecting $\beta\rho v^2$ gives an error in computed pressure drop more than the unrealiability of the permeability measurement.

Continued use of Darcy flow to characterize the condition of low velocity is recommended. This concept is ingrained in our past and implies the permeability is constant with a range of pressure drops.

For flow rates where the neglecting of the $\beta\rho v^2$ term calculates significantly less pressure drop than would occur, high-velocity flow would be used to describe the condition.

WHAT TO CALL β

The term β is used in flow equations for gas wells and even for high flow rate oil wells. The objections to turbulence factor and inertial coefficient are clear; they denote changes in flow regimes.

The term velocity coefficient seems appropriate for β and is used in this paper. When the flow rate or velocity reaches a magnitude that accuracy in the prediction process requires the use of the velocity squared term, the velocity coefficient is required. Should high velocity cause the data plotted according to Eq. 7 to be a curve, Eq. 6 applies and a value of γ is found.

CORRELATION OF DATA FOR VELOCITY COEFFICIENT (β)

Seven sets of data were selected for correlating the velocity coefficient with permeability and/or porosity. The data were on dry cores with gas flow measurements that were believed to eliminate the Klinkenberg slip interference. Table 1 presents the relationships used in regression analysis of the data. The constants in the equations are given and the standard error of deviation for predicting β is listed. From this analysis, the data were plotted following the preferred relationships on Figs. 5 and 6. The difference between the correlation for sandstones only and all the data including carbonates were nominal, and so only one relationship is given for all the data.

The data for nonconsolidated sands are plotted on Fig. 5, the k vs β chart. The correlation lines with porosity as parameters definitely are of slope quite different than for consolidated data. The correlating curve of Fig. 5 is similar to that presented earlier without the porosity parameter.[8] If porosity is to be a parameter, Fig. 6 is preferred over the porosity lines of Janicek and Katz.[16]

Casse and Ramey[24] note the absence of temperature effect on for a Berea sandstone. Wong[13] took data on limestone cores and found curvature using Eq. 7, the cores contained connate liquid. Johnson and Taleaferro of USBM[2] also obtained curvature for data on a dry limestone core (Fig. 8). To represent such data, a second term is needed such as $\gamma\rho^2v^3$, as shown in Eq. 7, to represent pressure drop. Then β could be the first velocity coefficient and the second velocity coefficient.

COMPLEXITY OF RESERVOIR FLOW

It is appreciated that the influence of reservoir heterogeneity, fractures, infiltration at the wellbore, and presence of liquids all go to the discounting of the value of simple flow calculations with Eq. 1. However, such calculations are valuable in designing aquifer gas storage reservoirs. Also, well flow data may be used to obtain in-situ β values. Such data provide some measure of reservoir deviations from the model using core data alone, and permits evaluation of the reservoir condition.

CONCLUSION

A greater variety of high-velocity flow data on oil and gas reservoir rocks would be helpful. The range of predictions could be evaluated better and related to well flow characteristics.

Hopefully, a nomenclature can be devised that is acceptable to both practicing engineers and fluid flow specialists. The assistance of the Society of Petroleum Engineers is sought to establish language and terms that will eliminate misunderstanding in the future.

The correlation of β used during the past 20 years has been shown to be generally representative of the character of reservoir rocks. More data should give further improvement, and perhaps differentiate between rock types.

NOMENCLATURE

A = cross-sectional area, ℓ^2
b = slip coefficient, $m/\ell t^2$
g_c = unit conversion factor
G = mass flux, $m/t\ell^2$
k = absolute permeability, ℓ^2
k_a = apparent permeability, ℓ^2
L = length, ℓ
ℓw = work energy lost in overcoming friction, ℓ^2/t
M = molecular weight
P = pressure, $m/\ell t^2$
P_1 = inlet pressure, $m/\ell t^2$

P_2 = outlet pressure, $m/\ell t^2$
$\bar{P}$ = arithmetic average pressure, $m/\ell t^2$
Q_m = mass flow rate, the same as w, m/t
R = universal gas constant
T = absolute temperature
u = velocity in the x direction, ℓ/t
v = velocity in the y direction, ℓ/t
Z = supercompressibility factor
β = first velocity coefficient, $1/\ell$
γ = second velocity coefficient, $\ell t/m$
μ = viscosity, $m/\ell t$
ρ = density, m/ℓ^3
τ = longitudinal shear, $m/\ell t^2$
σ = longitudinal tension, $m/\ell t^2$

ACKNOWLEDGMENT

The assistance of C. S. Yih of the U. of Michigan Mechanics Dept. in clarifying and understanding pressure losses during flow through porous media is appreciated. The correlations of β were performed by J. Azuonye Ironkwe.

REFERENCES

1. Fancher, G. H., Lewis, J. A., and Barnes, K. B.: "Some Physical Characteristics of Oil Sands," The Pennsylvania State College, Bull. 12, Minerals Industries Experiment Station (1933) 65.
2. Johnson, T. W. and Taliaferro, D. B.: "Flow of Air and Natural Gas Through Porous Media," Technical Paper 592, USBM (1938).
3. Elenbaas, J. R. and Katz, D. L.: "A Radial Turbulent Flow Formula," Technical Publication No. 2304, AIME (Jan. 1948).
4. Green, L. and Duwez, P.: "Fluid Flow Through Porous Metals," J. Appl. Mech. (March 1951) 18, 39.
5. Cornell, D. and Katz, D. L.: "Flow of Gases Through Consolidated Porous Media," Ind. and Eng. Chem. (Oct. 1953) 45, 2145.
6. Tek, M. R.: "Development of a Generalized Darcy Equation," Trans., AIME (1957) 210, 376.
7. Houpeurt, A.: "On the Flow of Gases in Porous Media," Revue de l'Institut Francais du Petrole (Nov. 1959) XIV, 11, 1468.
8. Katz, D. L., Cornell, D., Kobayashi, R., Poettman, F. H., Vary, J. A., Elenbaas, J. R., and Weinaug, C. F.: Handbook of Natural Gas Engineering, McGraw-Hill Book Co., Inc., New York (1959).
9. Tek, M. R., Coats, K. H., and Katz, D. L.: "The Effect of Turbulence on Flow of Natural Gas Through Porous Reservoirs," Trans., AIME (July 1962) 225, 799.
10. Wright, D. E.: "Non-Linear Flow Through Granular Media," J. Hydraulic Div., Proc., ASCE (1968) 94, 851.
11. Dranchuk, P. M. and Kolada, L. J.: "Interpretation of Steady Linear Visco-Inertial Gas Flow Data," J. Cdn. Pet. Tech. (Jan.-March 1968) 36.
12. Gewers, C. W. W. and Nichol, L. R.: "Gas Turbulence Factor in a Microvugular Carbonate," J. Cdn. Pet. Tech. (April-June 1969) 51.
13. Wong, S. W.: "Effect of Liquid Saturation on Turbulence Factors for Gas-Liquid Systems," J. Cdn. Pet. Tech. (Oct.-Dec. 1970) 274.
14. Geertsma, J.: "Estimating the Coefficient of Inertial Resistance in Fluid Flow Through Porous Media," Soc. Pet. Eng. J. (Oct. 1974) 445.
15. Forchheimer, P.: "Wasserbewegung durch Boden," Zeitz, ver deutsch, Ing. (1901) 45, 1731.
16. Janicek, J. D. and Katz, D. L.: "Application of Unsteady State Gas Flow Calculations," Preprint from Research Conference, U. of Michigan, June 20, 1955.
17. Hubbert, M. K.: "Darcy's Law and the Field Equations of the Flow of Underground Fluids," Trans., AIME (1956) 207, 22.
18. Swift, G. W. and Kiel, O. G.: "The Prediction of Gas-Well Performance Including the Effect of Non-Darcy Flow," J. Pet. Tech. (July 1962) 791.
19. Yih, C. S.: Fluid Mechanics: A Concise Introduction to the Theory, McGraw-Hill Book Co., Inc., New York (1969).
20. Cornell, D.: "Flow of Gases Through Consolidated Porous Media," PhD thesis, The U. of Michigan (1952).
21. Klinkenberg, L. J.: "The Permeability of Porous Media to Liquids and Gases," Drill. and Prod. Prac., API (1941) 230.
22. Iffly, R.: "Etude de l'Ecoulement des Gas dans les Milieux Poreux - Application à la Determination de la Morphologie des Roches," A la Faculté des Sciences de l'Université de Paris (March 1956).
23. Tek, M. R., Coats, K. H., and Katz, D. L.: "The Effect of Turbulence on Flow of Natural Gas Through Porous Reservoirs," J. Pet. Tech. (1962) 799.
24. Casse, F. S. and Ramey, H. J.: "The Effect of Temperature and Confining Pressure on Single Phase Flow in Consolidated Rocks," paper SPE 5877 (1976).

APPENDIX

Table A. Language Used in Literature for the High Velocity Gas Flow.

Fancher, Lewis and Barnes[1]	(1933)	"...the flow of fluids through these porous materials closely resembles that through pipes; that there is a condition of flow in porous systems which resembles viscous flow, another which corresponds to turbulence."
Elenbaas and Katz[3]	(1948)	"Radial Turbulent Flow Formula"
Green and Duwez[4]	(1951)	"The inertial coefficient β... may be interpreted as a measure of the tortuosity of the flow channels, perhaps as an average curvature of the streamline determining the acceleration experienced by the fluid."
Hubbert[17]	(1956)	"...we have seen that the cause of the failure of Darcy's Law is the distortion that results in the flow lines when the velocity is great enough that the inertial force becomes significant."
Tek[6]	(1957)	"The generalized Darcy equation may be referred to as the

		'non-Darcy flow' regime. The transition from Darcy to non-Darcy flow is a gradual one."
Katz et al.[8]	(1959)	"If one includes extra motion of the fluid to consume the extra pressure loss, then the term 'turbulent flow' here is justified."
Houpeurt[7]	(1959)	"...we do not think, the flow can be really turbulent..., we consider the kinetic energy losses are responsible for the deviation...from Darcy's Law."
Tek, Coats and Katz[23]	(1962)	"The Effect of Turbulence on Flow of Natural Gas...."
Swift and Kiel[18]	(1962)	"Prediction of Gas-Well Performance including the effect of Non-Darcy Flow...Analysis of data...to give direct "in situ" information for...turbulence or non-Darcy coefficients."
Wright[10]	(1968)	"...Four regimes of flow for water in an unconsolidated bed. 1) a laminar regime 2) a steady inertia regime 3) a turbulent transition regime 4) a fully turbulent regime."
Gewers and Nichol[12]	(1969)	"Gas Turbulence Factor in a Microvugular Carbonate."
Greetsma[14]	(1974)	"Coefficient of Inertial Resistance. ...The flow regime of concern is usually fully laminar. The observed departure from Darcy's Law is the result of convective accelerations and decelerations of the fluid particles on their way through the pore space."

TABLE I. CORRELATIONS OF VELOCITY COEFFICIENTS (β).

Correlation Equation Tested	Standard Error of Estimate For β	
$\log\beta = m \log k + b$		Eq. 9
$m = -1.101;\ b = 23.33$	± 0.85*	
$m = -1.201;\ b = 23.83$	± 0.89	
$\log\beta = m \log(k^{0.5}\phi^{1.5}) + b$		Eq. 10
$m = -1.695;\ b = 17.89$	± 0.99	
$\log\beta = m \log\left(\frac{1}{k^{0.5}\phi^{5.5}}\right) + b$		Eq. 11
$m = 0.810;\ b = 12.66$	± 2.30	
$\log\beta = m \log(k^{0.1}\phi) + b$		Eq. 12
$m = 0.991;\ b = 19.92$	± 3.07	
$\log\beta = m \log(k\phi) + b$		Eq. 13
$m = -1.074;\ b = 21.42$	± 0.87	
$m = -1.01;\ b = 21.2$	± 0.85*	
$\log\beta = m \log\phi + b$		Eq. 14
$m = -5.148;\ b = 9.70$	± 1.91	

*Sandstones only, rest all data.

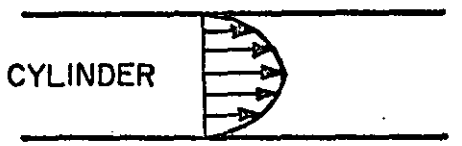

Fig. 1 - Flow in a cylindrical conduit.

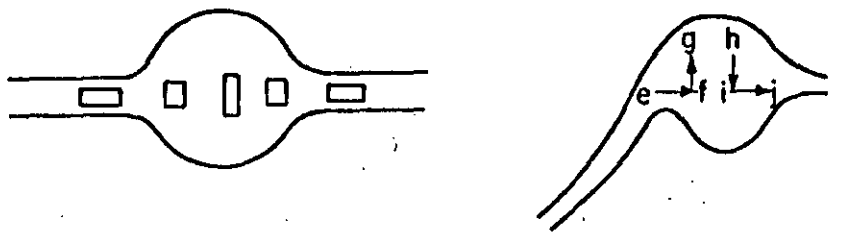

(a) Change of shape of fluid element.

(b) Longitudinal shear and longitudinal tension forces.

Fig. 2 - Flow in an idealized pore.

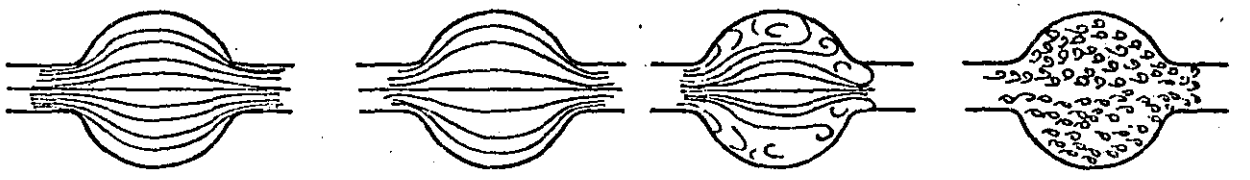

(a) Low velocity

(b) Velocity higher

(c) Intermediate, transition

(d) High velocity, turbulent

Fig. 3 - Idealized flow through alternating cross sections.

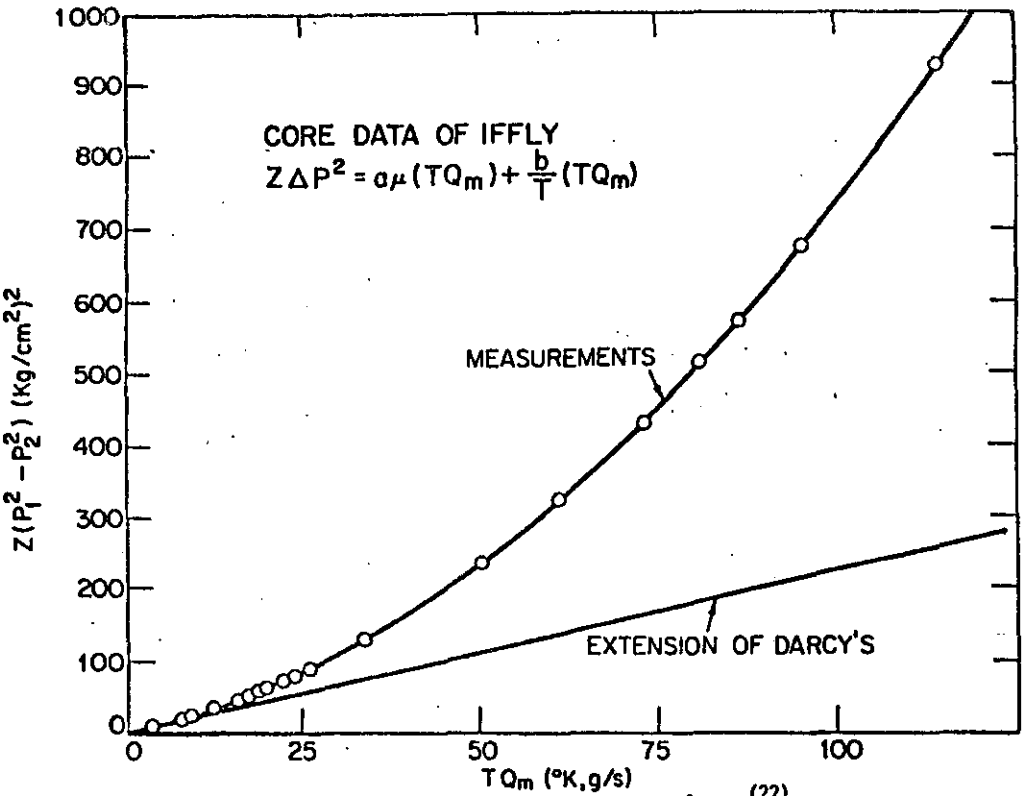

FIG. 4 - PRESSURE DROP AND FLOW RATE DATA OF IFFLY [22] ILLUSTRATING THAT DARCY'S LAW APPLIES AS A LIMIT. NITROGEN FLOW THROUGH SANDSTONE 21.4% POROSITY, 73.5 MD.

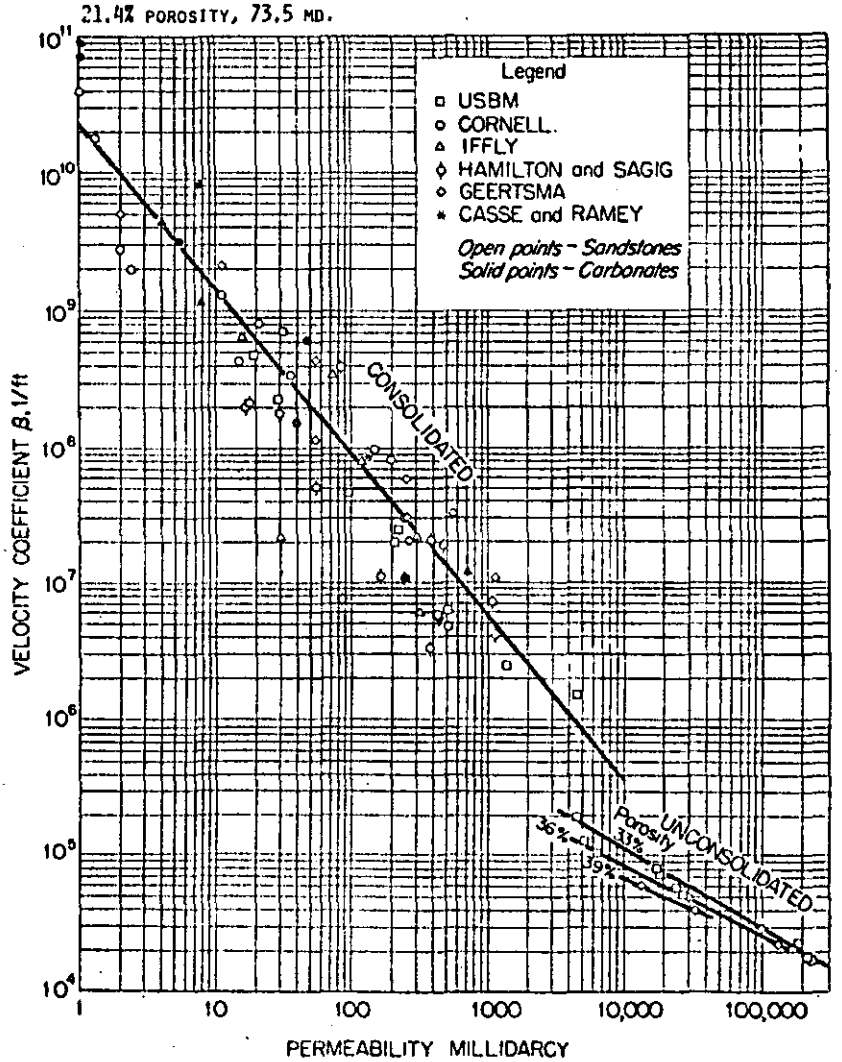

FIG. 5 - CORRELATION OF β, EQUATION 9.

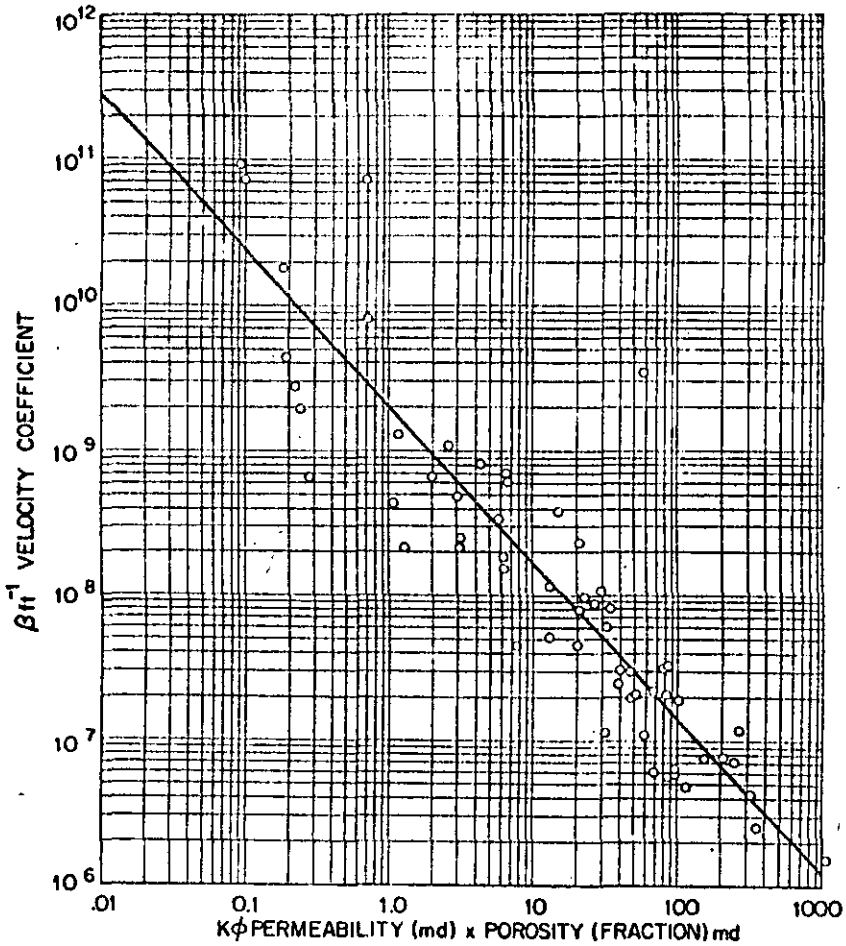

FIG. 6 - CORRELATION OF β, EQUATION 13.

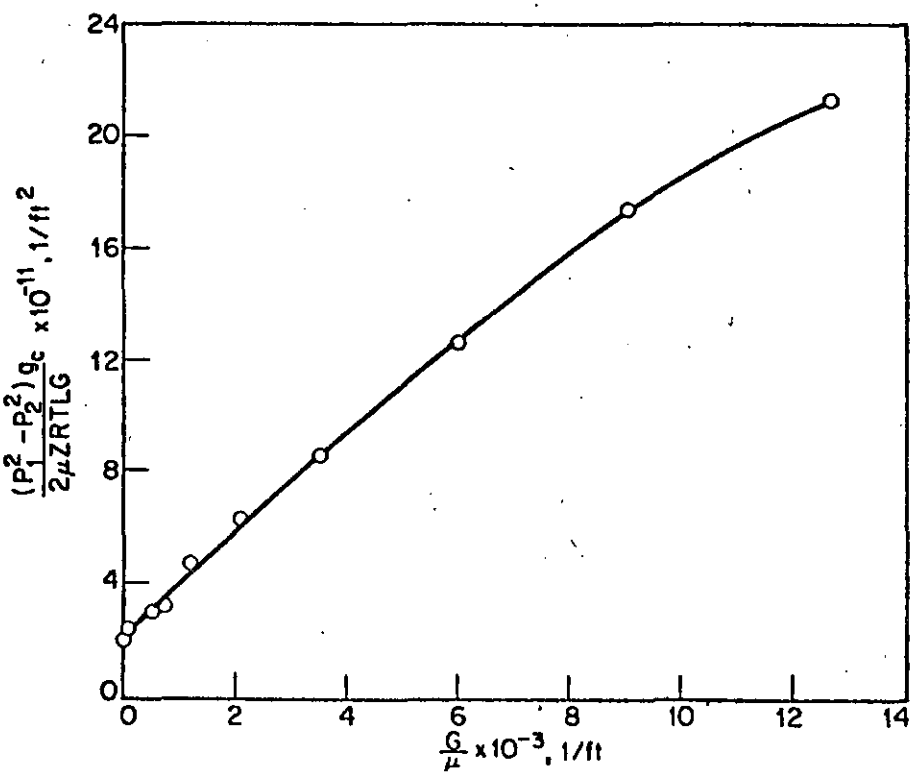

FIG. 7 - PLOT ACCORDING TO EQUATION 7 OF USBM DATA (2) FOR A LIMESTONE CORE.

SEMINARIO LATINOAMERICANO SOBRE EXPLORACION GEOTERMICA

QUITO, ECUADOR

5 - 9 SEPTIEMBRE DE 1983

olade

BID

APLICACIONES DE LA INGENIERIA DE YACIMIENTOS EN LA EVALUACION DE UN CAMPO GEOTERMICO

Jesús Rivera Rodríguez
División de Estudios de Posgrado
Facultad de Ingeniería
Universidad Nacional Autónoma de México
México, D.F.

INTRODUCCION

Una vez descubierto un campo geotérmico mediante una o más perforaciones profundas, el papel de ingeniero de yacimientos es fundamental en la determinación del tamaño del recurso, su contenido energético y de fluidos, así como de la definición de la capacidad de extracción, tanto por pozo, como a nivel campo. Toda esta información aunada con la obtenida de disciplinas afines, tales como la Geología, Geofísica y Geoquímica, traerá como consecuencia la definición adecuada del tamaño y número de unidades de generación eléctrica que se instalará en el campo geotérmico bajo estudio.

LA INGENIERIA DE YACIMIENTOS EN LA EVALUACION DE RECURSOS GEOTERMICOS

La Fig. 1 describe en forma resumida los objetivos, que desde el punto de vista de la ingeniería de yacimientos se tendrían que alcanzar con objeto de llegar a establecer una evaluación realística y fundamentada de los recursos geotérmicos aprovechables para la generación de electricidad. Con este fín, es necesario establecer una serie de parámetros básicos, que permitan caracterizar en forma adecuada, tanto las propiedades básicas de la roca, como también de los fluidos contenidos en espacio poroso y permeable del yacimiento.

Es conveniente establecer que la evaluación del potencial de un campo geotérmico es un proceso dinámico; ya que será necesario efectuar revisiones y afinaciones periódicas del mismo, a medida que nuevos datos provenientes

tanto de pozos adicionales, como de estudios más detallados en los ya existentes, vayan siendo incorporados, lo que producirá como resultado magnitudes cada vez más cercanas a la realidad. La incertidumbre que se tiene con la evaluación del potencial de un campo en cualquiera de sus etapas de desarrollo, está directamente relacionada con la cantidad y calidad de los datos disponibles.

Cuando se ha localizado y comprobado la presencia de un recurso geotérmico que pueda ser explotable a nivel comercial, para proceder a su evaluación, es necesario definir en forma clara y precisa varios términos, tales como "recurso geotérmico" y "reserva geotérmica", con objeto de establecer en forma inequívoca la porción de la energía contenida en el yacimiento que pueda ser transportada a la superficie y posteriormente convertida en electricidad.

En 1975 Nathenson y Muffler (1) y, porteriormente Muffler y Cataldi (2), establecieron una serie de difiniciones que son de gran utilidad para formar un marco adecuado de referencia y estandarizar la terminología utilizada en la evaluación de reservas. Utilizando sus definiciones como base y complementándolas con las que son de uso comun en otros campos como la minería y la explotación del petróleo, se proponen las siguientes definiciones, las cuales se sintetizan en la Fig. 2:

1. Recurso geotérmico base

Es el calor contenido en la parte de la corteza terrestre localizada bajo una cierta área y que se mide a partir de la temperatura media anual.

En esta definición se considera todo el calor contenido bajo una cierta área, sea esto recuperable o no e independientemente de cualquier consideración técnico-económica.

Dependiendo de la profundidad a que se localiza el recurso geotérmico base, éste podría dividirse en dos porciones (2); el Recurso Geotérmico Base Accesible, será aquella porción que puede alcanzarse mediante perforaciones profundas, de acuerdo con el estado de la tecnología respectiva a un tiempo dado. Aquella parte del recurso que no puede alcanzarse por limitaciones en las técnicas de perforación sería el Recurso Geotérmico Base Inaccesible.

Por otra parte, el recurso geotérmico base accesible puede a su vez ser subdividido en dos partes, a la porción útil del mismo que puede ser extraída y transportada hasta la superficie en forma competitiva con otras formas de energía, se le denomina Recurso Geotérmico. La porción del recurso geotérmico base accesible que no cumple con estos requisitos será la parte Residual del mismo.

Dentro del concepto de recurso geotérmico es conveniente considerar dos partes atendiendo a los criterios económicos prevalecientes al momento de efectuar la evaluación. La parte que pueda ser producida de acuerdo con los criterios económicos prevalecientes a un tiempo determinado, de forma tal que resulte competitiva con otras formas de energía, será el Recurso Geotérmico Económico. El resto será el Recurso Geotérmico Marginal.

Siguiendo con este procedimiento, el recurso geotérmico económico puede dividirser de acuerdo con el grado del conocimiento que del mismo se tiene. Como sugieren Muffler y Cataldi (2), cuando una porción de este recurso ha sido comprobada mediante perforaciones profundas y su magnitud ha sido sustentada mediante datos de geología, geofísica, geoquímica e ingeniería de yacimientos, dicha porción será la Reserva Geotérmica. La parte restante, cuya magnitud puede inferirse de estudios geológicos y geofísicos generales, será el Recurso Geotérmico Económico por Descubrir.

Con objeto de complementar esta clasificación, la reserva geotérmica puede a su vez subdividirse en varias categorías:

1. Reserva Geotérmica Demostrada.- Es la porción de la reserva geotérmica que ha sido comprobada mediente varias perforaciones profundas y cuya magnitud ha sido corroborada mediante estudios de geología, geofísica y geoquímica, así como de ingeniería de yacimientos.

Atendiendo el grado de conocimientos que de un área se tiene, así como también a la cantidad y calidad de la información que de la misma se dispone, la reserva geotérmica demostrada puede, a su vez, ser subdividida en dos categorías:

a) Reserva Geotérmica Probada.- Es la parte de la reserva que puede estimarse con base en datos confiables provenientes de varias perforaciones profundas, las cuales han permitido ampliar y afinar la información pre-

viamente disponible a partir de estudios geológicos, geofísicos y geoquímicos. Además, la estimación está firmemente apoyada por conrrelaciones que a través del campo se han realizado mediante estudios de ingeniería de yacimientos con los cuales se incorporan datos de la productividad de los pozos.

b) Reserva Geotérmica Demostrada Probable.- Es la porción remanente de la reserva demostrada, cuya estimación se basa en información de alguna perforación profunda, así como datos escasos de geología, geofísica y geoquímica. También pueden tenerse estudios preliminares de ingeniería de yacimientos.

2. Reserva Geotermica Posible.- Es la parte de la reserva que puede estimarse a partir de información preliminar de geología, geosífica y geoquímica, pero que no puede ser confirmada mediante los datos de alguna perforación profunda.

Esta categorización de la reserva geotérmica es consistente con la clasificación de reservas que se emplea en la industria petrolera y proporciona, a juicio del autor, una de las formas más convenientes y lógicas para establecer un marco de referencia que permita evaluar, tanto el grado de desarrollo que guardan los recursos geotérmicos de un país o región, así como también la evolución que siguen los recursos de un campo específico.

Con objeto de asegurar un nivel de referencia común, es conveniente calcular las reservas con base en la cantidad de calor disponible en la boca del pozo, antes de que ocurra cualquier transformación o transporte del mismo.

Por otra parte, debe reconocerse que no todo el calor presente en el yacimiento puede ser conducido a la boca del pozo. En efecto, solo una pequeña parte del mismo puede ser transportado a la superficie. Para tomar en cuenta este hecho, es conveniente introducir un factor de corrección a la cantidad de calor presente en el yacimiento. Definiendo este factor como Factor de Recuperación Geotérmico, R, es posible establecerlo en la siguiente forma (2):

$$\text{Factor de Recuperación Geotérmico} = \frac{\text{Calor extraído Medido en la cabeza del pozo}}{\text{Calor total originalmente contenido en un volumen determinado del yacimiento (fluídos + roca)}}$$

Adicionalmente a lo anterior, se debe considerar que para determinar la cantidad de electricidad que se producirá con el calor recuperable disponible a boca de pozo, será necesario aplicar al anterior un factor de eficiencia de conversión, el cual dependerá, entre otros factores, de las condiciones específicas de cada yacimiento, así como del tipo de proceso que se elija para la conversión de energía térmica a eléctrica.

Se considera que la terminología definida con anterioridad proporciona un marco de referencia adecuado cuando se manejan los términos "recurso geotérmico" o "reserva geotérmica"; sinembargo, persiste todavía cierta ambiguedad y vaguedad cuando se habla en términos del "potencial geotérmico de generación" (o sólo "potencial") de un campo determinado. Por tanto, y tomando como base la metodología ya establecida por OLADE para las diferentes fases de un proyecto como son: reconocimiento y prefactibilidad, factibilidad y por último desarrollo, se propone el empleo de las siguientes definiciones:

1. Potencial Geotérmico Preliminar.- Es la capacidad de generación eléctrica, expresada en MW_e por 20 años, que puede definirse para un campo geotérmico, tomando en cuenta el estado de su conocimiento al final de la fase de reconocimiento y prefactibilidad.

2. Potencial Geotérmico.- Es la capacidad de generación eléctrica, expresada en MW_e por 20 años, que puede definirse para un campo geotérmico, tomando en cuenta el estado de su conocimiento al final de la fase de factibilidad o de cualquier estapa ulterior de desarrollo.

Con objeto de cuantificar en forma adecuada la porción del potencial cuyo monto está mejor definido, se sugiere establecer una subdivision del potencial geotérmico similar a la establecida para las reservas. Así, se puede establecer la siguiente subdivisión:

a) Potencial Geotérmico Probado.- Es aquella parte del potencial que puede ser calculado con base en datos confiables de estudios geológicos, geofísicos, geoquímicos y de ingeniería de yacimientos, los cuales han sido corroborados mediante perforaciones profundas. Además, se debe tener un factor de recuperación geotérmico razonablemente estimado para el campo, así como un factor de conversión de energía térmica a eléctrica comprobado para el esquema elegido.

b) Potencial Geotérmico Probable.- Es la parte del potencial geotérmico que puede calcularse para la parte de un campo en el cual no existen perforaciones profundas, o bien éstas son escasas y distantes de la parte conocida del campo; pero de la que sí se dispone de datos de geología, geofísica y geoquímica.

c) Potencial Geotérmico Posible.- Es la parte del potencial de un campo que puede establecerse con base en datos preliminares y aislados, de alguna o varias disciplinas, tales como la geología, geoquímica y geofísica, pero los cuales no pueden ser comprobados, ya que no exite ninguna perforación profunda.

Esta clasificación del potencial geotérmico presenta la ventaja de que al referirse a cada uno de ellos en forma específica, queda sobreentendido tanto la fase en que se encuentra un proyecto en particular, así como el grado de certidumbre o incertidumbre que la cifra asociada al concepto representa.

Por otra parte, al definir el potencial de un campo, utilizando la subdivisión recomendada anteriormente, es posible ir incorporando al potencial geotérmico probado las reservas probables contenidas con las partes del yacimiento que van siendo desarrolladas, a medida que la etapa de desarrollo del campo avanza. Así mismo, al avanzar este proceso, la parte del potencial que era considerado posible, pasa a incorporarse al potencial probable, con lo cual se establece un esquema dinámico de evaluación y

conceptualmente consistente con la característica siempre evolutiva de un sistema geotérmico.

La ingeniería de yacimientos juega un papel preponderante en el establecimiento de las reservas o el potencial de un campo geotérmico, ya que reune la información proporcionada por disciplinas afines, tales como la geología, geofísica y geoquímica, complentándolos con técnicas específicas, con las cuales puede ser estimado el potencial geotérmico, sea esta preliminar, probada, probable o posible.

Alguna de la información básica adicional necesaria para la evaluación de un recurso geotérmico, se refiere a propiedades del yacimiento tales como: la permeabilidad, porosidad, tipo de fronteras externas, recarga; tanto hidráulica como térmica, correlaciones de zonas productoras, etc. Parte de esta información puede obtenerse con base en pruebas de presión que se realizan en los pozos del campo. Una clasificación simplificada de los tipos de pruebas que pueden utilizarse es la siguiente:

I. Pruebas que se realizan utilizando un solo pozo.
   1) Pruebas de decremento de presión
   2) Pruebas de incremento de presión
   3) Pruebas de inyectividad - recuperación
   4) Pruebas de ritmo de extracción variable

II. Pruebas en que se utilizan 2 o más pozos en forma simultánea.
   a) Pruebas de interferencia

La información que puede obtenerse de las pruebas de presión es la siguiente:

a) Capacidad de la formación (espesor X permeabilidad)
b) Condiciones de producción del pozo (factor de daño)
c) Presión promedio del yacimiento
d) Porosidad
e) Volumen poroso y permeable del yacimiento
f) Presencia de heterogeneidades
g) Condiciones de frontera del yacimiento

INGENIERIA DE YACIMIENTOS GEOTERMICOS

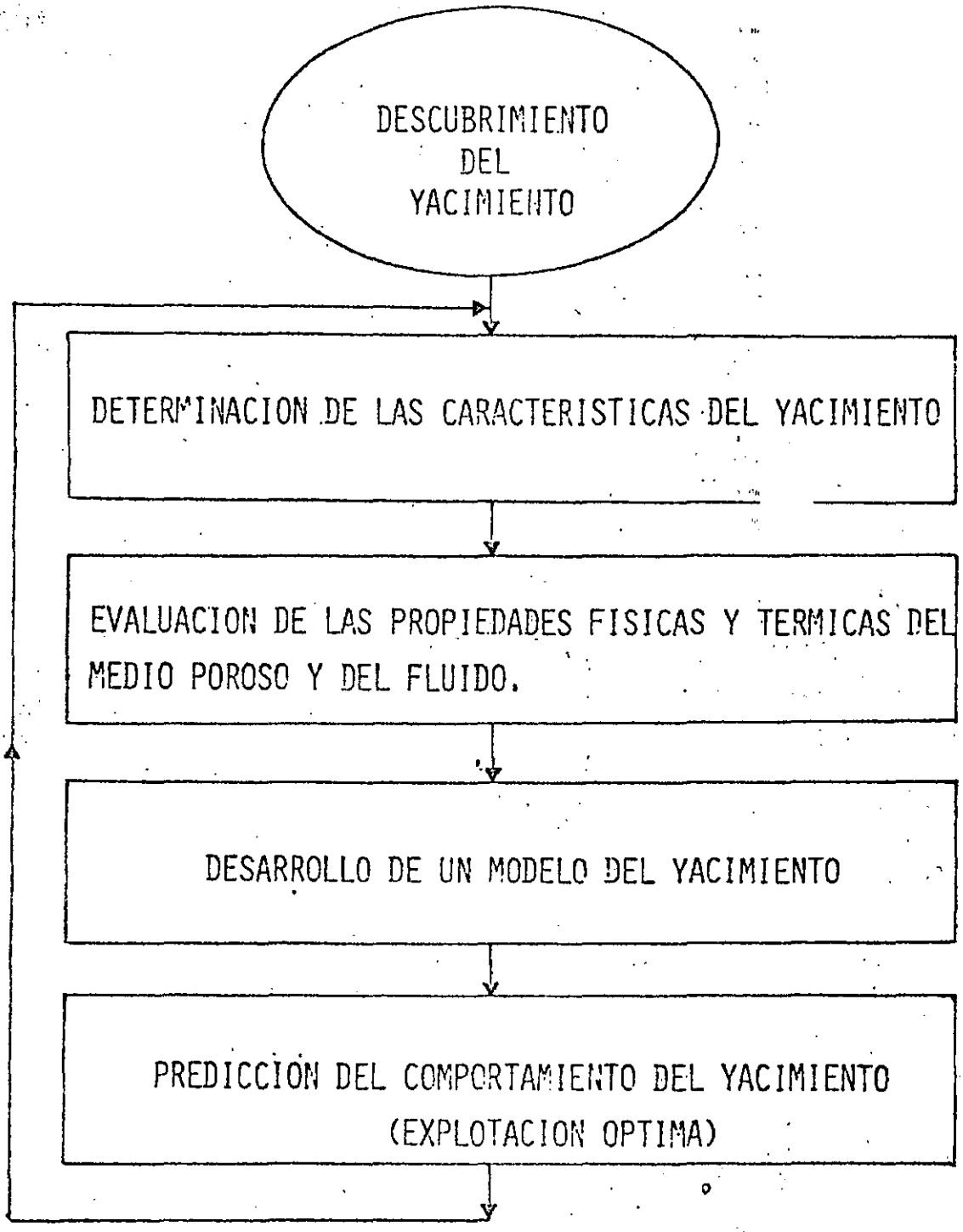

FIGURA No. 1

Principales objetivos perseguidos por la Ingeniería de Yacimientos.

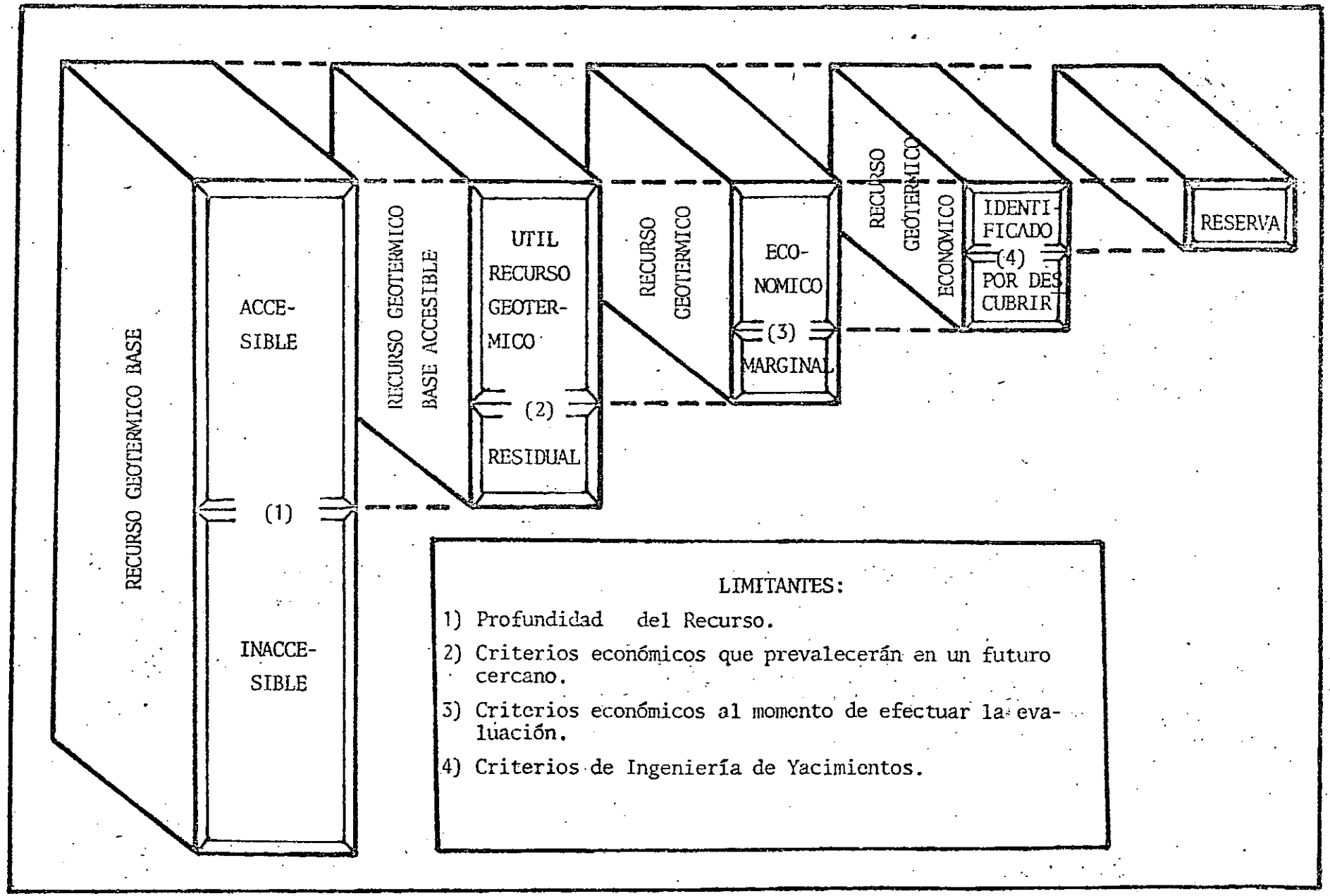

FIGURA No. 2

Concepto de Reserva Geotérmica de acuerdo con limitantes tecnológicas y económicas.

DIRECTORIO DE ALUMNOS DEL CURSO
INGENIERIA DE YACIMIENTOS GEOTERMICOS.

ING. JAIME ACOSTA SILVA (MEXICO)
INGENIERO EN EL DEPTO. DE EVA-
LUACION Y YACIMIENTOS
AV. LAS CAMELINAS
CENTRO FINANCIERO 7° PISO
COL. LAS AMERICAS
MORELIA, MICH.
TEL. 452-31

ING. OSCAR ASCH ROGER (COSTA RICA)
INGENIERO MECANICO V
SAN JOSE SABANA NORTE
APARTADO 10032
SAN JOSE COSTA RICA
INST. COSTARRICENSE DE
ELECTRICIDAD
TEL. 32-74-13

ING. FERNANDO ASCENCIO CENDEJAS (MEXICO)
INGENIERO EN EL DEPTO. DE
EVALUACION Y YACIMIENTOS
AVE. DE LAS CAMELINAS
CENTRO FINANCIERO 7° PISO
COL. LAS AMERICAS
MORELIA, MICH.
TEL. 452-31

ING.GUILLERMO ALVARADO SANCHEZ (ECUADOR)
PROFESOR AGREGADO PETROGRAFIA
PRACTICA
UNIVERSIDAD CENTRAL DEL ECUADOR
CIUDADELA UNIVERSITARIA
AMERICA Y AV. UNIVERSITARIA
QUITO, ECUADOR

ING. TOMAS ANTONIO CAMPOS
VILLAFUERTE (EL SALVADOR)
JEFE SUBSECCION DE INVESTIGACIONES
GEOTERMICAS
CENTRO DE GOBIERNO 9a. CALLE PTE.
SAN SALVADOR, EL SALVADOR

./..

ING. DAVID ESCOBAR CORDOVA (EL SALVADOR)
ING. DE RESERVORIOS
C.E.L.
CENTRO DE GOBIERNO
SAN SALVADOR.EL SALVADOR
TEL. 22-08-55

ING. RENE ALFONSO GONZALEZ ORIAS (BOLIVIA)
JEFE DIVISION DE GEOFISICA
SERVICIO GEOLOGICO DE BOLIVIA
CALLE FEDERICO ZUAZO 1673
CASILLA 2729
LA PAZ, BOLIVIA
TEL. 36 92 33

ING. EDUARDO GALVAN GARCIA (MEXICO)
PROFESIONAL ESPECIALIZADO A.
INSTITUTO MEXICANO DEL PETROLEO
EJE CENTRAL LAZARO CARDENAS 152
MEXICO, D.F.
TEL. 567-66-00 EXT. 20657

ING. DEREK IRVING RAMDEEN (PANAMA)
GEOLOGO
INSTITUTO DE RECURSOS HIDRAULICOS
Y ELECTRIFICACION (IRHE)
TEL. DOM. 21 62 29

SR. CARLOS ARMANDO JASSO PEÑA (MEXICO)
COMISION FEDERAL DE ELECTRICIDAD
JEFE DE OFICINA
CAMPO GEOTERMICO DE CERRO PRIETO
MEXICALI, B.C.

ING. ERASMO LOPEZ DAVILA (MEXICO)
INTERPRETACION DE PRUEBAS DE PRESION
COMISION FEDERAL DE ELECTRICIDAD
CAMPO GEOTERMICO CERRO PRIETO
MEXICALI, BAJA CALIFORNIA NORTE
TEL.- 768-01 EXT. 417

ING. JULIO CESAR PALMA AYALA (GUATEMALA)
INGENIERO GEOFISICO
INSTITUTO NACIONAL DE
ELECTRIFICACION INDE
SAN JOSE VILLANUEVA, GUATEMALA
SUR
GUATEMALA, C.A.
TEL. 0310321

ING. VICTOR PIMENTEL SANTANA (R. DOMINICANA)
COORDINADOR DEL PROYECTO GEOTERMICO
AUTOPISTA
KM. 6 1/2 EDIFICIO
PLAZA COMPOSTELA
STO. DOMINGO, R.D.
TEL. 565-50-90

ING. ANGEL M. QUINTERO BARRERA (COLOMBIA)
INGENIERO DIVISION DE ENERGIA ELECTRICA
MINISTERIO DE MINAS Y ENERGIA
AVENIDA EL DORADO CAN-COLOMBIA
TEL. 44-53-04

ING. ORLANDO RECARTE BUITRAGO (HONDURAS)
INGENIERO DE DISEÑO
EMPRESA NACIONAL DE ENERGIA ELECTRICA
APDO. POSTAL 99
TEGUCIGALPA, D.C. HONDURAS
TEL. 22-84-74

ING. JETZABETH RAMIREZ SABAG (MEXICO)
INVESTIGADORA
INSTITUTO DE INVESTIGACIONES ELECTRICAS
INTERIOR INTERNADO PALMIRA,
CUERNAVACA
TEL. 438-11 EXT. 2095

ING. JOSE ROSAS ELGUERA (MEXICO)
INGENIERO GEOLOGO
COLEGIO MILITAR 14- F - 7
COL. POPOTLA
DELEG. MIGUEL HIDALGO
C.P. 11400
MEXICO, D.F.
TEL. 399-65-27

SR. PEDRO SANCHEZ UPTON
INGENIERO MECANICO
COMISION FEDERAL DE ELECTRICIDAD
AV. CAMELINAS
FRACC. CAMELINAS

./..

ING. MARCO P. TORRES MERIZALDE
JEFE DE DEPARTAMENTO
INSTITUTO ECUATORIANO DE
ELECTRIFICACIÖN
AV. 12 DE OCTUBRE Y MADRID
QUITO, ECUADOR
TEL. 547-721

ING. DARIO VERASTEGUI TOCRE (PERU)
JEFE DE SERVICIO PROYECTO
GEOTERMICO CENTRO NORTE
ELECTROPERU, S.A.
EDIF. LA TORRE OF 903
CENTRO CIVICO
LIMA, PERU
TEL. 325280-516

SR. GERARDO CARRASCO NUÑEZ
AYUDANTE DE PROFESOR
UNAM FACULTAD DE INGENIERIA
CD. UNIVERSITARIA
TEL. 557-73-36

29-03-84

'bvr